Copper carbazolides in photoinduced C–N couplings

Thesis by

Jun Myun Ahn

In Partial Fulfillment of the Requirements for the Degree

of

Doctor of Philosophy

CALIFORNIA INSTITUTE OF TECHNOLOGY

Pasadena, California

2018

(Defended May 18, 2018)

Jun Myun Ahn
ORCID: 0000-0002-8181-908X

ACKNOWLEDGEMENTS

The current thesis template offered by Caltech permits a blank acknowledgements page. It is believed by many that this section is the most, if not the only, visited section of the thesis. Therefore, I wish to take full advantage of this possibility and provide my narrative on the people and moments that have shaped my five-year journey.

I conform to the norm and first thank my two advisors, Prof. Gregory C. Fu and Prof. Jonas C. Peters, who have provided irreplaceable support and mentorship throughout the years. I truly believe that they represent the optimal conditions and any other combinations would not have resulted in the completion of my degree. They are truly the dynamic duo, KC_8 and $HBAr^F$, copper and light, or copper and carbazole, and I have benefited the most from the symbiosis between the two experts in synthetic chemistry more than anybody who has set foot on the copper project. I have received blunt criticisms and occasional encouragements from both of them over the years that have propelled me to become the "harshest critic" of my own research. They have given me an incredible amount of scientific freedom and intellectual independence and allowed me to work on chemistry that excites me the most. They are the key reasons for the periods in which I proclaimed to be the happiest graduate student at Caltech and why my initial career aspirations remain unfazed. There are invaluable traits I am honored to have acquired from them and many more that I hope one day to possess. I am extremely proud to be able to say that I was jointly advised by Prof. Gregory C. Fu and Prof. Jonas C. Peters. Would I do it again if I could go back in time, knowing all the things that would happen? Even at the toughest times, my answer to this cliché question remains the same.

Apart from the increased number of meetings and presentations, one of the less desirable aspects of a joint supervision is the requirement of inviting an additional member to the candidacy and thesis committees. I am extremely fortunate, however, to have Prof. Theodor Agapie, Prof. Sarah E. Reisman, and Prof. Brian M. Stoltz in my committee; they have provided a tremendous amount of input and feedback at various meetings held in 218 Schlinger. The most desirable committee members are those who truly care about the student and their professional development, and every member of my committee belongs to that category.

Research in synthetic chemistry relies heavily on spectroscopic and analytical techniques. Without competent personnel to maintain shared instruments, my research projects would not have been completed. Acknowledgements are made to Dr. David Vander Velde for the NMR facility, Drs. Angel Di Bilio and Paul Oyala for EPR facility, Dr. Mona Shahgoli for MS facility, Dr. Scott Virgil

for the Caltech Center for Catalysis and Chemical Synthesis, Drs. Brian Sanders and Jay Winkler for the Beckman Institute Laser Resource Center, and Dr. Michael Takase and Lawrence Henling for the X-ray Crystallography Facility. The following supporting staff are also thanked: Margarita Davis, Paige Johnson, Julianne Just, Lynne Martinez, Alison Ross, and Agnes Tong.

Further acknowledgments are made to the following members, with whom I temporally overlapped, of the Fu group:

Saaket Agrawal, Arianna Ayonon, Shoshana Bachman, Dr. Agnieszka Bartoszewicz, Dr. Suzanne Batiste, Dr. Caiyou Chen, Junwon Choi, Crystal Chu, Dr. Huan Cong, Dr. Hien Do, Dr. Jaika Doerfler, Dylan Freas, Bradley Gorsline, Gregory Harlow, Dr. Haohua Huo, Dr. Stefan Jungbauer, Dr. Quirin Kainz, Dr. Marcin Kalek, William Kayitare, Dr. Soren Kramer, James Lawniczak, Dr. Hanju Lee, Sarah Lee, Yufan Liang, Albert Liu, Marc Montesinos Magraner, Dr. Yusuke Makida, Dr. Yusuke Masuda, Carson Matier, Dr. Xin Mu, William Reichard, Holt Sakai, Dr. Nathan Schley, Dr. Jens Schmidt, Joseph Schneider, Dr. Jonas Schwaben, Dr. Gregg Schwarzwalder, Dr. Yu Shibata, Martin Slusarczyk, Dr. Hidehiro Suematsu, Dr. Xingwen Sun, Dr. Hendrik Wagner, Dr. Zhaobin Wang, Felicia Weber, Dr. Linglin Wu, Dr. Zepeng Yang, Dr. Haolin Yin, Daniel Ziegler, Dr. Yasushi Yoshida, Wanji Zhang, and Dr. Wei Zhao.

and the Peters group:

Saaket Agrawal, Pablo Barros, Trixia Buscagan, Matthew Chalkley, Dr. Hsiang-Yun Chen, Dr. Cooper Citek, Bridget Connor, Sidney Creutz, Meaghan Deegan, Trevor Del Castillo, Theodore Donnell, Dr. Marcus Drover, Javier Fajardo Jr., Henry Fong, Nina Gu, Dr. Shabnam Hematian, Kareem Hannoun, Dr. Jian He, Christian Johansen, Dr. Miles Johnson, Dr. David Lacy, Dr. Heejun Lee, Dr. Tzu-Pin Lin, Ben Matson, Dr. Koichi Nagata, Patricia Nance, Mark Nesbit, Tanvi Ratani, Ryan Ribson, Jonathan Rittle, Gerri Roberts, Joseph Roddy, Dr. Alonso Rosas, Dirk Schild, Dr. Yichen Tan, Niklas Thompson, Dr. Gael Ung, Dr. Kumiko Yamamoto, and Dr. Wei Zhao.

I would also like to thank the following people for the memorable outings, company at meals, or friendly support: Tonia Ahmed, Dr. Dinesh Aluthge, Shoshana Bachman, Trixia Buscagan, Ruiyuan “Ronnie” Chen, Jaebum “Albert” Chung, Dylan Freas, Gregory Harlow, William Kayitare, Dr. Hanju Lee, Heui Beom Lee, Dr. Miles Johnson, Carson Matier, Dr. Yusuke Makida, Dr. Yusuke Masuda, Jaeyun Moon, Dr. Xin Mu, Holt Sakai, Dr. Haolin Yin, and Dr. Daniel Ziegler.

Someone once said, “You may not be a superstar, but you may be sitting next to a superstar.” There is no doubt that many epiphany-eliciting scientific discussions and chemistry advice came from many colleagues. Acknowledgements are made to the following: Dr. Marcin Kalek for his input on mechanistic studies and for introducing me to COPASI, Dr. Jonas Schwaben for encouraging the examination of carbamate nucleophiles, Drs. Caiyou Chen, Haohua Huo, Yusuke Makida, Gregg Schwarzwalder, and Zhaobin Wang for addressing my organic chemistry deficiencies, and Kareem Hannoun and Dr. Haolin Yin for their computational analyses and general discussions on photochemistry and mechanistic studies.

There are two copper(II)–carbazolides that have eluded structural confirmation for a long time: the homoleptic anion $[Cu^{II}(carb)_3]^-$ and the neutral heteroleptic complex consisting of the $[Cu^{II}(carb)_2(phosphine)]$ core. Neither words nor my generally stoic facial expressions can capture the feeling of elation I experienced when the structures were confirmed. Larry played an instrumental role in the process and I cannot thank him enough. Perseverance paid dividends.

A Ph.D. costs a lot of money. For the first four years of my graduate studies, I had graciously received financial support from the Canadian government through NSERC PGS M and PGS D programs. I send my sincere gratitude to my undergraduate mentors and advisors who allowed me to compile strong fellowship applications: Dr. Truman Wambach and Prof. Michael Fryzuk, Dr. Joel Kelly and Prof. Mark MacLachlan, Dr. Dinesh Aluthge and Prof. Parisa Mehrkhodavandi, and Dr. Claire Chatalova Sazepin and Prof. Glenn Sammis. I am also thankful for the CCE division for paying me to serve as a Teaching Assistant for Ch 1a (2013), Ch 1b (2014), Ch 1a (2014), Ch 1a (2015), Ch 1a (2016), and Ch 154a (2018), and once again Greg and Jonas for letting me allocate my time in teaching.

Last, but foremost, I express my love and gratitude to my family for their unwavering love and support.

JMA

ABSTRACT

Photoinduced, copper-catalyzed reactions of organohalides have emerged in recent years as a powerful tool to construct a wide array of C–N bonds, which are prevalent in organic materials and polymers, pharmaceuticals, natural products, and ligands in transition metal catalysts. Described herein is the study and applications of copper complexes ligated by carbazole and its derivatives in photoinduced, copper-catalyzed C–N bond-constructing transformations. Various areas of synthetic inorganic and organic chemistry are explored, including in-depth mechanistic elucidation, ligand and catalyst design, reaction development, as well as spectroscopic and structural characterization of reactive copper complexes.

Chapter 2 describes the mechanistic investigation on photoinduced, copper-catalyzed couplings of carbazoles with unactivated alkyl halides. A wide array of mechanistic tools suggests the viability of an out-of-cage C_{sp^3}–N coupling pathway. Spectroscopic and structural characterization data of the key intermediates are detailed.

Chapter 3 outlines the design and preparation of a new copper-based photoredox catalyst supported by a tridentate bis(phosphino)carbazole ligands. The ground- and excited-state properties of the new photocatalyst are examined.

Chapter 4 details the development of photoinduced, copper-catalyzed C_{sp^3}–N couplings of carbamates with unactivated alkyl bromides using the new copper photoredox system. The scope with respect to the nucleophile and the electrophile and mechanistic investigations are communicated.

Chapter 5 illustrates the chemistry of copper complexes supported by bidentate (phosphino)carbazole ligands. A diverse array of copper complexes in both the $S = 0$ and $S = 1/2$ states are reported, including a rare, paramagnetic copper–phosphine complex that may serve as a structural model for key copper intermediates of the enantioselective C_{sp^3}–N couplings of carbazoles.

PUBLISHED CONTENT AND CONTRIBUTIONS

This dissertation contains materials adapted with permission from the following publications.

1. Ahn, J. M.; Ratani, T. S.; Hannoun, K. I.; Fu, G. C.; Peters. J. C. Photoinduced, Copper-Catalyzed Alkylation of Amines: A Mechanistic Study of the Cross-Coupling of Carbazole with Alkyl Bromides. *J. Am. Chem. Soc.* **2017**, *139*, 12716–12723. DOI: 10.1021/jacs.7b07052.

J.M.A. participated in the conception of the project, designed the research, performed EPR, NMR, UV-vis, ESI-MS, X-ray crystallography, reactivity, stereochemical, and product studies, proposed a new reaction mechanism, and participated in the writing of the manuscript.

2. Ahn, J. M.; Peters, J. C.; Fu, G. C. Design of a Photoredox Catalyst that Enables the Direct Synthesis of Carbamate-Protected Primary Amines via Photoinduced, Copper-Catalyzed N-Alkylation Reactions of Unactivated Secondary Halides. *J. Am. Chem. Soc.* **2017**, *139*, 18101–18106. DOI: 10.1021/jacs.7b10907.

J.M.A. conceived the project, designed the research, performed all experiments, and participated in the writing of the manuscript.

TABLE OF CONTENTS

LIST OF FIGURES

LIST OF SCHEMES

LIST OF TABLES

LIST OF ABBREVIATIONS

A	hyperfine coupling constant
Å	angstrom(s)
Ac	acetyl
Ad	1-adamantyl
Aq	aqueous
Anal	analysis
Ar	aryl group
atm	atmosphere(s)
avg	average
Boc	*tert*-butoxycarbonyl
br	broad
Bu	butyl
i-Bu	*iso*-butyl
n-Bu	butyl or *norm*-butyl
s-Bu	*sec*-butyl
t-Bu	*tert*-butyl
Bn	benzyl
Bz	benzoyl
B3LYP	a DFT functional
B(38HF)P86	a DFT functional
°C	degrees Celsius
calcd	calculated
carb	carbazolide or carbazolyl
$carb_{tBu}$	3,6-di-*t*-butylcarbazolide or 3,6-di-*t*-butylcarbazolyl
Cbz	benzyloxycarbonyl
cf.	consult or compare to (Latin: confer)
CFL	compact fluorescent light
cm^{-1}	wavenumber(s)
cod	1,5-cyclooctadiene
conc.	Concentrated
CV	cyclic voltammogram or cyclic voltammetry
Cy	cyclohexyl
d	doublet
DCM	dichloromethane
def2-TZVP	basis sets for DFT
DFT	density functional theory
DME	1,2-dimethoxyethane
DMF	N,N-dimethylformamide
DMSO	dimethylsulfoxide
dr	diastereomeric ratio
e	electron

ee	enantiomeric excess
E	trans (entgegen) olefin geometry
e.g.	for example (Latin: exempli gratia)
EI	electron impact
EPR	electron paramagnetic resonance
ESI	electrospray ionization
Et	ethyl
et al.	and others (Latin: et alii)
equiv	equivalent
eV	electron volt
EWG	electron withdrawing group
E^0	reduction or oxidation potential
F	structure factor
Fc	ferrocene
FDA	food and drug administration
G	Gauss
g	gram(s)
GC	gas chromatography
GHz	gigahertz
GT 6-311	basis sets for DFT
G(d)	basis sets for DFT
h	hour(s)
n-Hex	hexyl or *norm*-hexyl group
HMDS	hexamethyldisilamide or hexamethyldisilazide
hv	light
HOMO	highest-occupied molecular orbital
HPLC	high performance liquid chromatography
Hz	hertz
I	intensity
I_0	initial intensity
IC	CHIRALPAK IC column for HPLC
i.e.	that is (Latin: id est)
IPA	isopropanol
IR	infrared spectroscopy
J	coupling constant
K	Kelvin or equilibrium constant
k	rate constant
kcal	kilocalorie(s)
kg	kilogram(s)
L	liter or neutral ligand
LED	light-emitting diode
LUMO	lowest-unoccupied molecular orbital
lw	linewidth

m	multiplet or meter(s)
M	molar or molecular ion
m	meta
μ	micro
max	maximum
Me	methyl
Mes	mesityl
mg	milligram(s)
MHz	megahertz
min	minute(s)
mL	milliliter(s)
mM	millimolar
mm	millimeter
mmol	millimole
MO	molecular orbital
mol	mole(s)
MS	mass spectrometry
mV	millivolt
m/z	mass-to-charge ratio
M06-L	a DFT functional
N	normal or molar
n	generic number
nm	nanometer(s)
NMR	nuclear magnetic resonance
NOE	nuclear Overhauser effect
NOESY	nuclear Overhauser enhancement spectroscopy
Nu	nucleophile
o	ortho
OD	optical density
p	para
n-pent	pentyl or *norm*-pentyl
Ph	phenyl
PG	protecting group
PNP	tridentate pincer ligand featuring carbazolide and phosphines
ppm	parts per million
Pr	propyl
i-Pr	*iso*-propyl
n-Pr	propyl or *norm*-propyl
py	pyridine
q	quartet
R	alkyl group
R	rectus
ref	reference

Rf	retention factor
rt	room temperature
s	singlet or seconds
S	sinister
sat.	saturated
SCE	saturated calomel electrode
SET	single electron transfer
S_N2	bimolecular nucleophilic substitution
t	triplet
TBS	*tert*-butyldimethylsilyl
temp	temperature
TEMPO	2,2,6,6-tetramethylpiperidine 1-oxyl
Tf	trifluoromethanesulfonyl
THF	tetrahydrofuran
TIPS	triisopropylsilyl
TLC	thin layer chromatography
TMS	trimethylsilyl
tol	tolyl
Ts	*para*-toluenesulfonyl (tosyl)
UV	ultraviolet
V	volt
vis	visible
W	watt
wR	weighted R-factor
X	anionic ligand or halide
xs	excess
XRD	X-ray diffraction
Z	cis (zusammen) olefin geometry
*	excited state
ε	extinction coefficient
λ	wavelength
λ_{max}	wavelength of local maximum intensity
Σ	summation
^1H	proton
^2H	deuterium or hydrogen-2
^{13}C	carbon-13
^{15}N	nitrogen-15
^{31}P	phosphorus-31
$\{^1H\}$	proton-decoupled
2-MeTHF	2-methyl-tetrahydrofuran
6-31G	basis sets for DFT

Chapter 1. Introduction

1.1. Transition metal-catalyzed coupling reactions of organohalides

One of the first chemical reactions taught in a classroom setting is the double displacement reaction between two generic species A–X and B–Y to form products A–Y and B–X.[1] Perhaps the most broadly executed class of a double displacement reaction in practice is the coupling of an organic electrophile (e.g. organohalides) with a carbon, or heteroatom, nucleophile on a catalytic platform constructed by a transition metal complex (**Scheme 1.1**).[2] Due to the possibility of building molecular complexity in a modular manner, transition metal-catalyzed couplings have revolutionized not only the field of synthetic chemistry, but also many other disciplines of physical science and engineering.[3] For this reason, the Nobel Prize in Chemistry was awarded for the development of Pd-catalyzed cross-coupling reactions in 2010.[4]

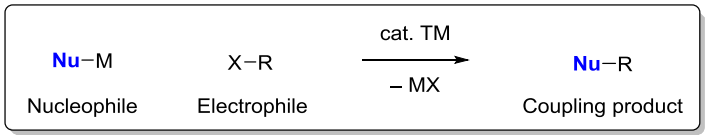

Scheme 1.1. General outline of the coupling of a nucleophile and an electrophile catalyzed by a transition metal. Nu: carbon- or heteroatom-based group; M: metal (e.g. Li); X: leaving group (e.g. halide); R: carbon-based group; TM: transition metal (e.g. Cu).

In addition to thermally-driven counterparts, photoinduced approaches to transition metal-catalyzed coupling reactions emerged as a powerful synthetic tool in the past decade.[5] The renaissance of light-driven synthetic transformations may be largely attributed to the increased diversity of photoresponsive molecules (photoredox catalysts) that can mediate the

transfer of energy or electrons between two, otherwise inert compounds. Although the synthetic community has mostly utilized photoredox catalysts based on ruthenium and iridium,[5a–c] several research groups have recognized the synthetic potential of copper in photocatalysis (**Figure 1.1**).[5d]

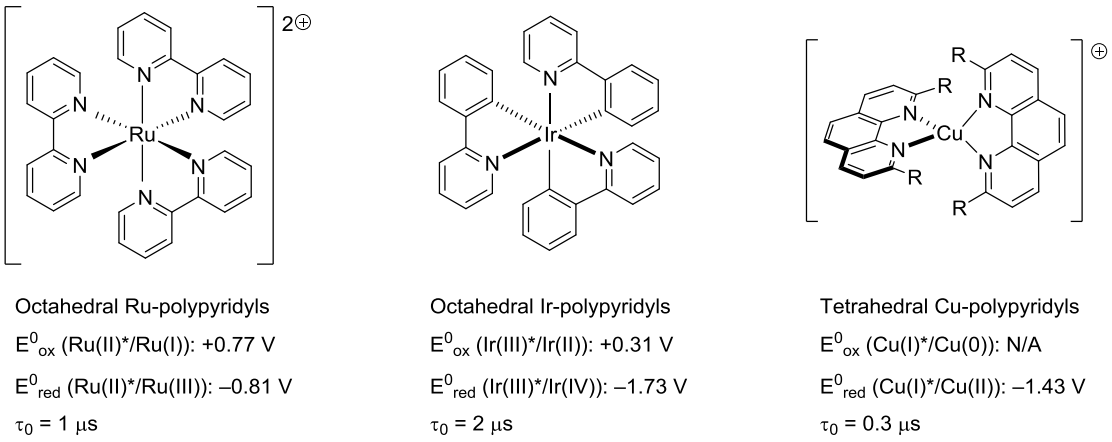

Octahedral Ru-polypyridyls
E^0_{ox} (Ru(II)*/Ru(I)): +0.77 V
E^0_{red} (Ru(II)*/Ru(III)): –0.81 V
τ_0 = 1 μs

Octahedral Ir-polypyridyls
E^0_{ox} (Ir(III)*/Ir(II)): +0.31 V
E^0_{red} (Ir(III)*/Ir(IV)): –1.73 V
τ_0 = 2 μs

Tetrahedral Cu-polypyridyls
E^0_{ox} (Cu(I)*/Cu(0)): N/A
E^0_{red} (Cu(I)*/Cu(II)): –1.43 V
τ_0 = 0.3 μs

Figure 1.1. Examples of photoredox catalysts and their excited-state properties. Potentials are reported against saturated calomel electrode in CH_3CN. R = 4-methoxyphenyl. τ_0 = lifetime.

A general outcome of the irradiation of the organohalide electrophiles is the formation of radicals (•R, **Scheme 1.2**).[6] Under the conditions of photolysis, radicals may be generated via the direct homolysis of the electrophile, halogen atom abstraction (inner-sphere electron transfer), or outer-sphere electron transfer. The resulting radicals may then traverse reaction pathways that complement even-electron elementary steps commonly observed in thermally-driven coupling reactions of organohalides.[2,7]

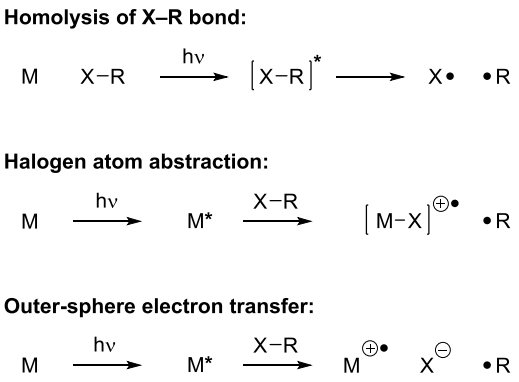

Scheme 1.2. Examples of pathways by which the formation of a radical (•R) from an organohalide (X–R) occurs in the presence of light and a hypothetical photocatalyst (M).

1.2. Photoinduced, copper-catalyzed C–N couplings

One representative proof-of-principle study that demonstrated the viability of a radical pathway in the copper-catalyzed C_{sp^2}–N coupling of an aryl halide with an amine (also known as the Ullmann coupling) was communicated by the Peters and Fu laboratories in 2012.[8] Prior to this report, the Peters group had been examining the use of their luminescent copper complexes to facilitate light-initiated multi-electron processes,[9] and observed that the irradiation of complex **1.1** and iodobenzene yields N-phenyl carbazole (**Scheme 1.3**, top).[8] In the 2012 study, the Fu and Peters groups showed that a wide array of mechanistic data is consistent with a radical pathway,[10] in contrast to the even-electron pathways that had been suggested in thermal Ullmann couplings, [11] en route to the C_{sp^2}–N bond-formation. Furthermore, they demonstrated that N–phenyl carbazole can be detected in 64% yield when lithium carbazolide is irradiated in the presence of iodobenzene and a substoichiometric quantity (10 mol%) of CuI (**Scheme 1.3**, bottom).

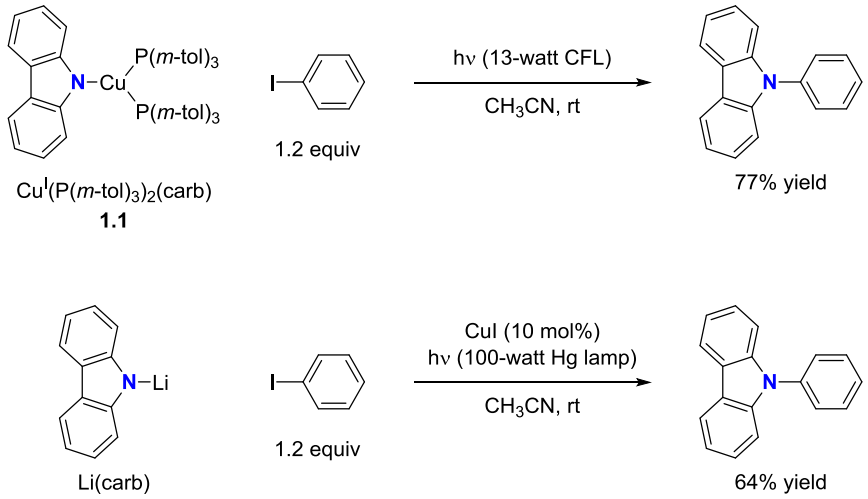

Scheme 1.3. Photoinduced Ullmann coupling reported in 2012 by the Fu and Peters laboratories.

The demonstration of the catalytic C_{sp^2}–N coupling in the absence of exogenous ligands led to the proliferation of photoinduced, copper-catalyzed coupling reactions of organohalides, all of which proceeded under the general conditions described in **Figure 1.2**.[12] By 2015, the scope had been expanded to include a variety of C-, N-, O-, and S-based nucleophiles and aryl and alkyl (C_{sp^3}) halide electrophiles.[13]

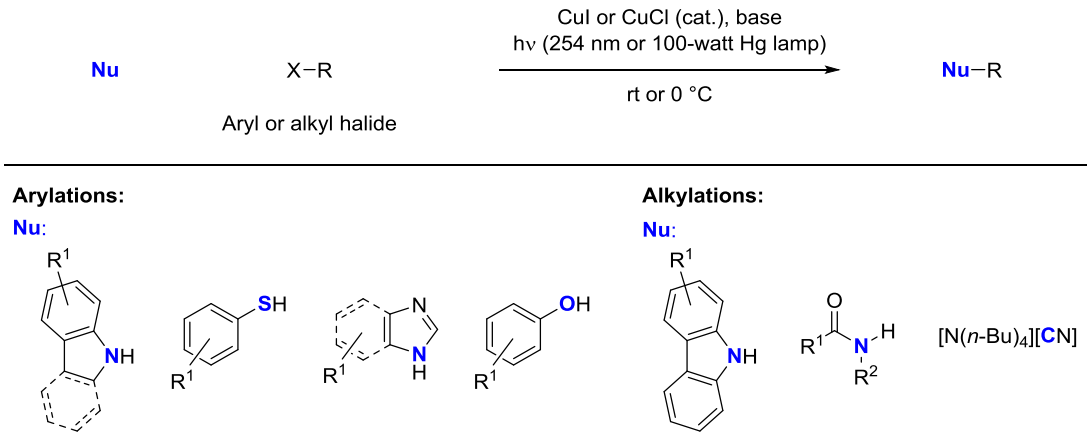

Figure 1.2. Selected examples of nucleophiles employed in photoinduced, copper-catalyzed couplings in the absence of exogenous ligands.

The possibility to construct C–N bonds under thermally mild conditions is particularly attractive in view of the prevalence C–N bonds in biologically-active natural products and pharmaceuticals. A 2014 study reported that more than 80% of U.S. FDA-approved pharmaceuticals contain one or more C–N bonds.[14] In 2011, it was estimated that 6 out of the top 10 most frequently employed reactions in medicinal chemistry forge C–N bonds, accounting for 40% of all reactions in medicinal chemistry.[15] Modern reviews and perspectives continue to echo the importance of the discovery of efficient and versatile methods to accomplish the construction of C–N bonds.[16] For example, a 2016 survey had found that 8 out of the top 10 worst-performing reaction types in terms of yield involve N–arylation or N–alkylations reactions.[16b]

1.3. Chemistry of carbazole

By far the most versatile nucleophile explored by the Fu and Peters groups is carbazole. To date, carbazole remains the only coupling partner that can participate in N–substitution reactions with any organohalide under the conditions of photoinduced copper catalysis. Specifically, the Fu and Peters laboratories observed that carbazole undergoes alkynylation (C_{sp}),[13c] alkenylation (C_{sp^2}),[13c] arylation (C_{sp^2}),[13c] and alkylation (C_{sp^3}) with primary,[13a] secondary,[13a] and tertiary alkyl halides.[17] The coupling of carbazole with tertiary alkyl halides (α-chloroamides) even proceeds in a stereoconvergent manner, providing access to enantioenriched, N–alkylated carbazoles.

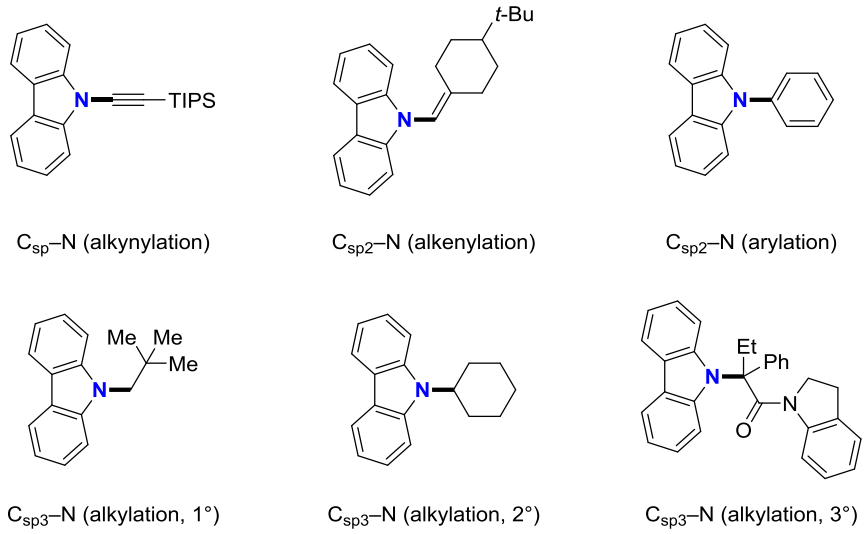

Figure 1.3. Examples of N–substituted carbazoles accessible via photoinduced methods.

Applications of N–substituted carbazoles in synthetic organic chemistry are rather limited although molecules containing the carbazole scaffold have been reported to display a wide range of biological activities,[18,19] including antibacterial and anticancer activities.[20]

N–substituted carbazoles are of particular interest, instead, in materials and polymer sciences.[21,22] Carbazole is available readily from the distillation of coal tar and can be inexpensively purchased from more than 100 commercial suppliers.[23] Its versatility to participate in a variety of N–substitution has enabled the preparation of a library of light-responsive organic small molecules and polymers with tunable photoproperties.[21, 24] Summarized in **Figure 1.4** are selected examples of compounds that contain the carbazole scaffold and their applications.

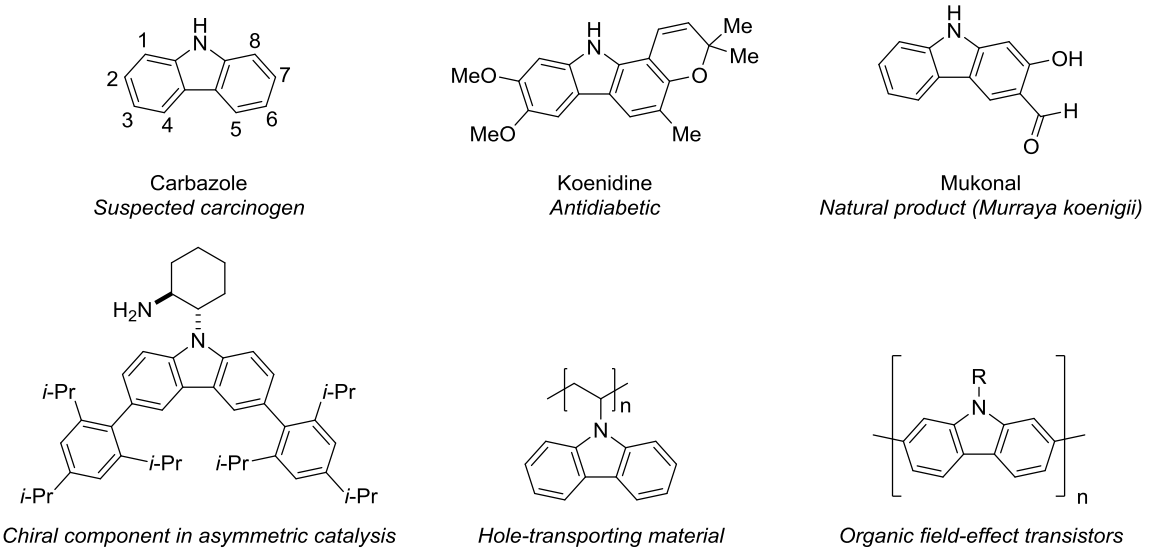

Figure 1.4. Representative structures and applications of carbazole and its derivatives.

In addition to the central N atom, the carbazole ring can also be expediently functionalized at 1- and 8- positions. As a result, an array of multidentate pincer ligands containing the carbazole scaffold had been prepared and shown to coordinate to various transition metal centers, including early[25] and late d-block metals[26]. Several complexes display catalytic activity in challenging synthetic transformations, including nitrogen

fixation,[27] alkane dehydrogenation,[28] and asymmetric epoxidation (**Figure 1.5**).[29] However, their applications in coupling reactions of organohalides have largely been underexplored.[30]

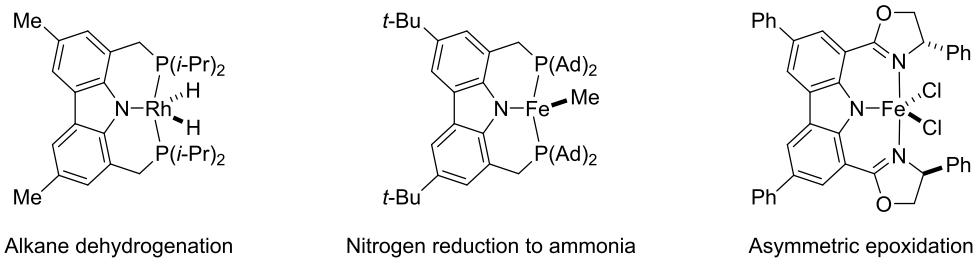

Figure 1.5. Transition metal catalysts supported by carbazole-based multidentate ligands and their applications. Ad = 1-adamantyl.

1.4. Overview of individual chapters

This Thesis recapitulates our endeavors since the autumn of 2013 to explore the chemistry of copper–carbazolide complexes in photoinduced, copper-catalyzed coupling reactions of alkyl halides, with particular emphasis on C_{sp^3}–N bond-constructing transformations.[31] At the time, the Fu and Peters groups had been continuously expanding the scope with respect to the nucleophiles and electrophiles under the general conditions of photoinduced, copper-catalyzed coupling reactions in the absence of exogenous ligands (**Figure 1.2**). However, despite the simplicity of the conditions of catalysis, mechanistic understandings had remained elusive.

We begin our narrative in **Chapter 2** by presenting an in-depth mechanistic investigation on photoinduced, copper-catalyzed couplings of carbazoles with unactivated alkyl halides (**Scheme 1.4**). We demonstrate that the nucleophile (Li(carb)) itself can be

responsible for photoinduced single electron transfer events to generate carboradicals from unactivated alkyl bromides. As part of this mechanistic study, we report the first example of structurally-characterized, homoleptic, 3-coordinate copper(II)–amide anion and elucidate its role in the key, out-of-cage C_{sp^3}–N bond-forming step.

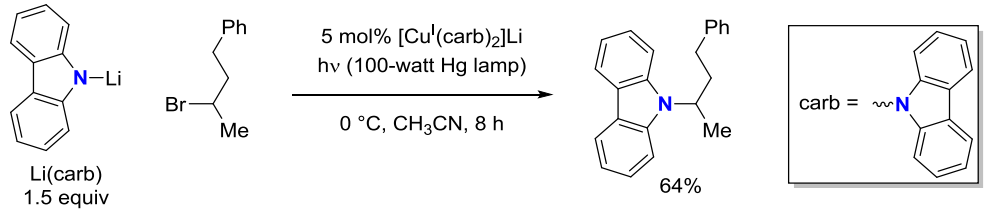

Scheme 1.4. Optimized reaction conditions for an in-depth mechanistic study on photoinduced, copper-catalyzed couplings of carbazoles with unactivated alkyl halides described in **Chapter 2**.

Inspired by the viability of an out-of-cage C_{sp^3}–N coupling mechanism, we report in **Chapter 3** a new, copper-based photoredox catalyst designed to effect the formation of C_{sp^3}–N bonds with non-photoactive nucleophiles. We share the design principles behind bis(phosphino)carbazole ligands for the preparation of photoactive copper complexes. We demonstrate that complex **3.1** is a potent excited-state photoreductant and show the viability of copper-catalyzed C_{sp^3}–N couplings induced by blue-LED irradiation (**Scheme 1.5**).

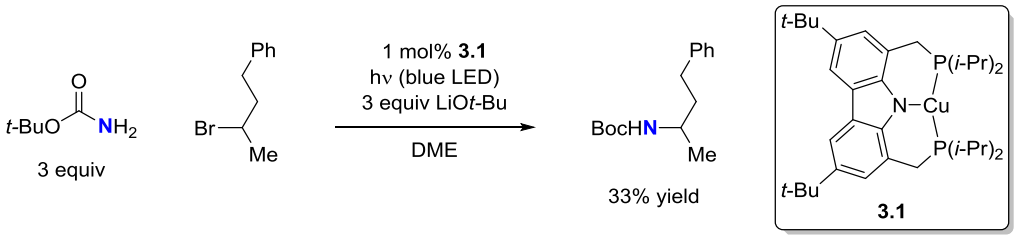

Scheme 1.5. Application of a newly-designed copper-based photoredox catalyst **3.1** ligated by a tridentate bis(phosphino)carbazole discussed in **Chapter 3**.

In **Chapter 4**, we build upon the results described in **Chapter 3** and communicate the development of the photoinduced, copper-catalyzed couplings of carbamates with unactivated alkyl bromides (**Scheme 1.6**). We establish that our reaction provides direct and expedient access to carbamate-protected primary amines, which are valuable synthetic intermediates. We share our mechanistic insights on the role of the bis(phosphino)carbazole ligand **L4.1** and confirm the viability of an out-of-cage C_{sp^3}–N bond-forming step in the N–alkylation of carbamates, akin to our findings in **Chapter 2**.

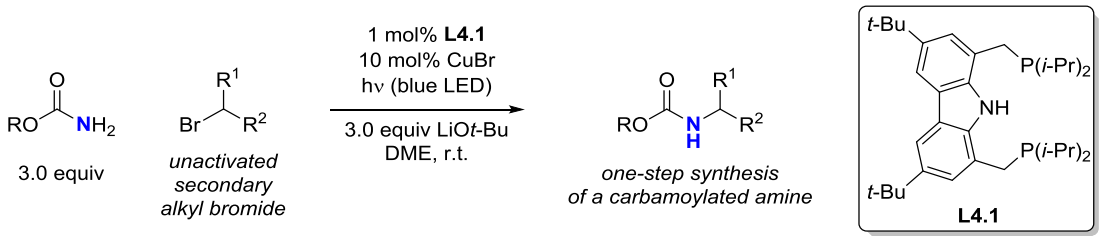

Scheme 1.6. Photoinduced, copper-catalyzed couplings of carbamates with unactivated alkyl bromides detailed in **Chapter 4**.

We examine another class of copper–carbazolide complexes in **Chapter 5** using bidentate (phosphino)carbazole ligands. We establish that a diverse array of copper complexes can be generated on bidentate ligand platforms, both in the $S = 0$ and $S = 1/2$ states. In the latter electronic state, we structurally confirm a rare example of a mononuclear, monophosphine complex of copper (**5.15**, **Figure 1.6**). We suggest that it may serve as a model complex for understanding the chemistry of key intermediates in photoinduced, copper-catalyzed enantioconvergent C_{sp^3}–N couplings of carbazoles.[17]

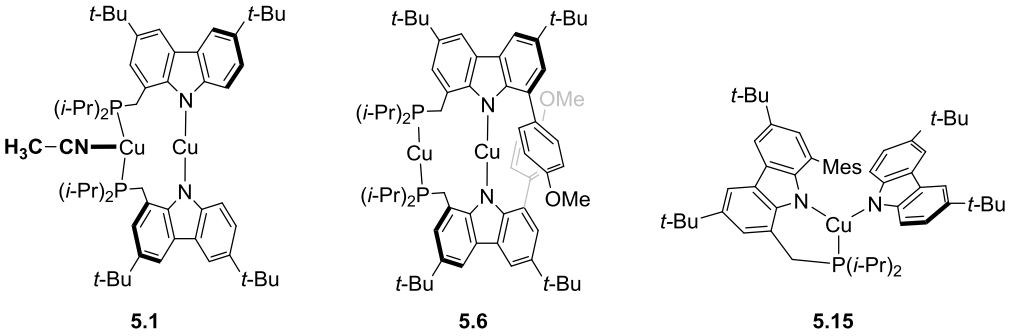

Figure 1.6. Selected structures of copper complexes supported by bidentate (phosphino)carbazole ligands reported in **Chapter 5**.

1.5. Notes and references

[1] Martin, R. B. *J. Chem. Educ.* **1999**, *76*, 133.

[2] Crabtree, R. H. *The Organometallic Chemistry of the Transition Metals*, John Wiley & Sons: Hoboken, NJ, **2009**.

[3] *Metal-Catalyzed Cross-Coupling Reactions and More*; de Meijere, A., Bräse, S., Oestreich, M., Eds.; Wiley-VCH: Weinheim, Germany, **2014**.

[4] For representative accounts and reviews, see (a) Beletskaya, I. P.; Cheprakov, A. V. *Chem. Rev.* **2000**, *100*, 3009–3066. (b) Suzuki, A. *Angew. Chem., Int. Ed.* **2011**, 50, 6722–6737. (c) Negishi, E. *Angew. Chem., Int. Ed.* **2011**, 50, 6738–6764.

[5] For recent overviews, see (a) Prier, C. K.; Rankic, D. A.; MacMillan, D. W. C. *Chem. Rev.* **2013**, *113*, 5322–5363. (b) Schultz, D. M.; Yoon, T. P. *Science* **2014**, *343*, 1239176. (c) Twilton, J.; Le, C.; Zhang, P.; Shaw, M. H.; Evans, R. W.; MacMillan, D. W. C. *Nat. Rev. Chem.* **2017**, *1*, 0052. (d) Paria, S.; Reiser, O. *ChemCatChem.* **2014**, *6*, 2477–2483.

[6] Klan, P.; Wirz, J. *Photochemistry of organic compounds: From concepts to practice*; Wiley: Chichester, U.K., **2009**.

[7] Fu, G. C. *ACS Cent. Sci.* **2017**, *3*, 692–700.

[8] Creutz, S. E.; Lotito, K. J.; Fu, G. C.; Peters, J. C. *Science* **2012**, *338*, 647–651.

[9] (a) Harkins, S. B.; Peters, J. C. *J. Am. Chem. Soc.* **2005**, *127*, 2030–2031. (b) Mankad, N. P.; Rivard, E.; Harkins, S. B.; Peters, J. C. *J. Am. Chem. Soc.* **2005**, *127*, 16032–16033. (c) Miller, A. J. M.; Dempsey, J. L.; Peters, J. C. *Inorg. Chem.* **2007**, *46*, 7244–7246. (d) Harkins, S. B.; Mankad, N. P.; Miller, A. J. M.; Szilagyi, R. K.; Peters, J. C. *J. Am. Chem. Soc.* **2008**, *130*, 3478–3485. (e) Mankad, N. P.; Harkins, S. B.; Antholine, W. E.; Peters, J. C. *Inorg. Chem.* **2009**, *48*, 7026–7032. (f) Lotito, K. J.; Peters, J. C. *Chem. Comm.* **2010**, *46*, 3690–3692. (g) Deaton, J.; Switalski, S.; Kondakov, D.; Young, R.; Pawlik, T.; Giesen, D.; Harkins, S.; Miller, A.; Mickenberg, S.; Peters, J. C. *J. Am. Chem.* Soc. **2010**, *132*, 9499–9508.

[10] Jones, G. O.; Liu, P.; Houk, K. N.; Buchwald, S. L. *J. Am. Chem. Soc.* **2010**, *132*, 6205–6213.

[11] (a) Tye, J. W.; Weng, Z.; Johns, A. M.; Incarvito, C. D.; Hartwig, J. F. *J. Am. Chem. Soc.* **2008**, *130*, 9971–9983. (b) Giri, R.; Hartwig, J. F. *J. Am. Chem. Soc.* **2010**, *132*, 15860–15863.

[12] For an independent study using a related approach, see Sagadevan, A.; Hwang, K. C. *Adv. Synth. Catal.* **2012**, *354*, 3421–3427.

[13] (a) Bissember, A. C.; Lundgren, R. J.; Creutz, S. E.; Peters, J. C.; Fu, G. C. *Angew. Chem., Int. Ed.* **2013**, *52*, 5129–5133. (b) Uyeda, C.; Tan, Y.; Fu, G. C.; Peters, J. C. *J. Am. Chem.*

Soc. **2013**, *135*, 9548–9552. (c) Ziegler, D. T.; Choi, J.; Muñoz-Molina, J. M.; Bissember, A. C.; Peters, J. C.; Fu, G. C. *J. Am. Chem. Soc.* **2013**, *135*, 13107–13112. (d) Do, H.-Q.; Bachman, S.; Bissember, A. C.; Peters, J. C.; Fu, G. C. *J. Am. Chem. Soc.* **2014**, *136*, 2162–2167. (e) Tan, Y.; Muñoz-Molina, J. M.; Fu, G. C.; Peters, J. C. *Chem. Sci.* **2014**, *5*, 2831–2835. (f) Ratani, T. S.; Bachman, S.; Fu, G. C.; Peters, J. C. *J. Am. Chem. Soc.* **2015**, *137*, 13902–13907.

[14] Vitaku, E.; Smith, D. T.; Njardarson, J. T. *J. Med. Chem.* **2014**, *57*, 10257–10274.

[15] Roughley, S. D.; Jordan, A. M. *J. Med. Chem.* **2011**, *54*, 3451–3479.

[16] (a) Brown, D. G.; Boström, J. *J. Med. Chem.* **2016**, *59*, 4443–4458. (b) Schneider, N.; Lowe, D. M.; Sayle, R. A.; Tarselli, M. A.; Landrum, G. A. *J. Med. Chem.* **2016**, *54*, 4385–4402.

[17] Kainz, Q. M.; Matier, C. M.; Bartoszewicz, A.; Zultanski, S. L.; Peters, J. C.; Fu, G. C. *Science* **2016**, *351*, 681−684.

[18] Carbazole is a suspected carcinogen according to the following study: Talhout, R.; Schulz, T.; Florek, E.; Benthem, J. V.; Wester, P.; Opperhuizen, A. *Int. J. Environ. Res. Publ. Health.* **2011**, *8*, 613–628.

[19] (a) Patel, O. P. S.; Mishra, A.; Maurya, R.; Saini, D.; Pandey, J.; Taneja, I.; Raju, K. S. R.; Kanojiya, S.; Shukla, S. K.; Srivastava, M. N.; Wahajuddin, M.; Tamrakar, A. K.; Srivastava, A, K.; Yadav, P. P. *J. Nat. Prod.* **2016**, *79*, 1276–1284. (b) Knölker, H.-J.; Reddy, K. R. *Chem. Rev.* **2002**, *102*, 4303–4427. (c) Schmidt, A. W.; Reddy, K. R. Knölker, H.-J. *Chem. Rev.* **2012**, *112*, 3193–3328.

[20] Tsutsumi, L. S.; Gundisch, D.; Sun, D. *Curr. Top. Med. Chem.* **2016**, *16*, 1290–1313.

[21] (a) Morin, J.-F.; Leclerc, M.; Adès, D.; Slove, A. *Macromol. Rapid Commun.* **2007**, *28*, 1761–1775. (b) Wang, H.; Sheikh, A. D.; Feng, Q.; Li, F.; Chen, Y.; Yu, W.; Alarousu, E.; Ma, C.; Haque, M.; Shi, D.; Wang, Z.-S.; Mohammed, O. F.; Bakr, O. M.; Wu, T. *ACS Photonics*, **2015**, *2*, 849–855.

[22] Grazulevicius, J. V.; Strohriegl, P.; Pielichowski, J.; Pielichowski, K. *Prog. Polym. Sci.* **2003**, *28*, 1297–1353.

[23] Graebe, C.; Glaser, C. *Ber. Dtsch. Chem. Ges.* **1872**, *5*, 12.

[24] Murphy, J. J.; Bastida, D.; Paria, S.; Fagnoni, M.; Melchiorre, P. *Nature* **2016**, *532*, 218–222.

[25] For select examples, refer to (a) Plundrich, G. T.; Wadepohl, H. Gade, L. H. *Inorg. Chem.* **2016**, *55*, 353–365. (b) Plundrich, G. T.; Wadepohl, H.; Clot, E.; Gade, L. H. *Chem. –Eur. J.* **2016**, *22*, 9283–9292.

[26] For representative examples, see (a) Bezuidenhout, D. I.; Kleinhans, G.; Guisado-Barrios, G.; Liles, D. C.; Ung, G.; Bertrand, G. *Chem*. *Commun*. **2014**, *50*, 2431–2433. (b) Gee, H.-C.; Lee, C.-H.; Jeong, Y.-H.; Jang, W.-D. *Chem*. *Commun*. **2011**, *47*, 11963–11965. (c) Grüger, N.; Rodriguez, L.-I.; Wadepohl, H.; Gade, L. H. *Inorg*. *Chem*. **2013**, *52*, 2050–2059.

[27] Higuchi, J.; Kuriyama, S.; Eizawa, A.; Arashiba, K.; Nakajima, K.; Nishibayashi, Y. *Dalton Trans*. **2018**, *47*, 1117–1121.

[28] Bézier, D.; Guan, C.; Krogh-Jespersen, K.; Goldman, A. S.; Brookhart, M. *Chem*. *Sci*. **2016**, *7*, 2579–2586.

[29] Niwa, T.; Nakada, M. *J*. *Am*. *Chem*. *Soc*. **2012**, *134*, 13538–13541.

[30] Several transformations have relied on tridentate, carbazole-based chiral ligands for the asymmetric three-component coupling reactions of organohalides in the presence of transition metal catalysts. For representative examples, see (a) Chen, W.; Yang, Q.; Zhou, T.; Tian, Q.; Zhang, G. *Org Lett*. **2015**, *17*, 5236–5239. (b) Xiong, Y.; Zhang, G. *J*. *Am*. *Chem*. *Soc*. **2018**, *140*, 2735–2738. (c) Inoue, M.; Suzuki, T.; Nakada, M. *J*. *Am*. *Chem*. *Soc*. **2003**, *125*, 1140–1141.

[31] For other reports by the Fu and Peters groups on photoinduced copper catalysis, see (a) Zhao, W.; Wurz, R. P.; Peters, J. C.; Fu, G. C. *J*. *Am*. *Chem*. *Soc*. **2017**, *139*, 12153–12156. (b) Matier, C. D.; Schwaben, J.; Peters, J. C.; Fu, G. C. *J*. *Am*. *Chem*. *Soc*. **2017**, *139*, 17707–17710.

Chapter 2. Mechanistic insights on copper-catalyzed alkylations of amines: photoinduced couplings of carbazoles and unactivated alkyl halides

Reproduced in part with permission from:

Ahn, J. M.; Ratani, T. S.; Hannoun, K. I.; Fu, G. C.; Peters. J. C. *J. Am. Chem. Soc*. **2017**, *139*, 12716–12723.

2.1. Introduction

As part of the 2012 study on the viability of radical pathways in the Ullmann couplings of carbazole and aryl (C_{sp^2}) halides, the Fu and Peters laboratories also observed the formation of C_{sp^3}–N bonds. Specifically, 1-(allyloxy)-2-iodobenzene was shown to produce exclusively the ring-closed compound under photoinduced N–arylation conditions (**Scheme 2.1**a).[1] The product was proposed to have resulted from the rapid, 5-*exo-trig* carboradical cyclization, resulting in the formation of a C_{sp^3} radical from the C_{sp^2} radical prior to the construction of the C_{sp^3}–N bond. This key observation inspired the development of general, photoinduced, copper-catalyzed couplings of carbazoles and alkyl halides (**Scheme 2.1**b).[2]

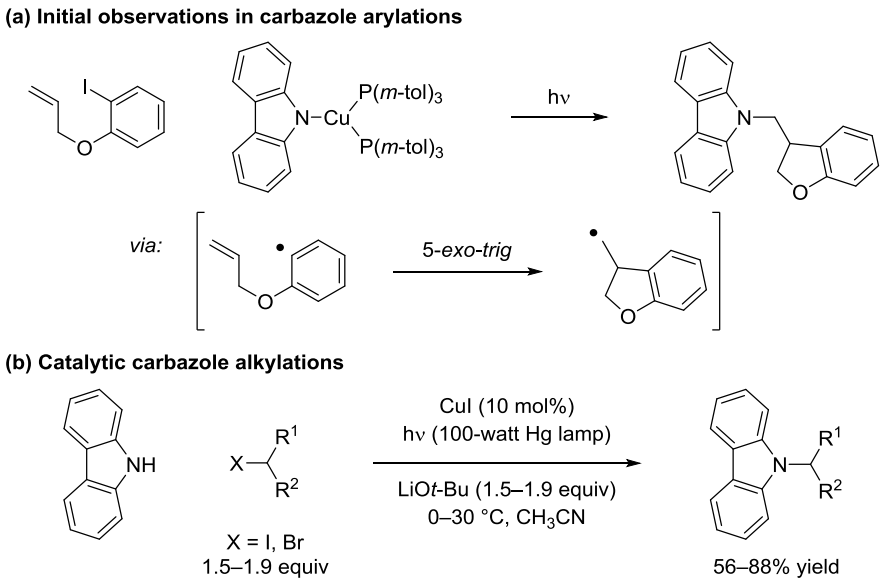

Scheme 2.1. Evolution of N–functionalizations of carbazole. (a) Formation of C_{sp^3}–N bond under carbazole arylation conditions. (b) General conditions for the photoinduced, copper-catalyzed couplings of carbazole with alkyl halides.

Under related conditions, a variety of carbon- and heteroatom-based nucleophiles (nitrogen, sulfur, and oxygen) were coupled with alkyl (C_{sp^3}), aryl (C_{sp^2}), and alkenyl (C_{sp^2}) halides.[3] Preliminary mechanistic investigations provided support for the simplified mechanistic cycle shown in **Figure 2.1**; the irradiation of a copper(I)–nucleophile complex **a** yields an excited-state complex **b**, which delivers an electron to the electrophile to generate an organic radical and a copper(II)–nucleophile complex **c**, which then combine to forge a carbon–nucleophile bond. This pathway, wherein a copper complex serves both as a photoreductant and as a participant in the key bond-constructing step, is different from that suggested for most photoredox reactions, wherein a photosensitizer (e.g., Ru^{2+} or Ir^{+}) generates a radical via reduction or oxidation, but is not itself engaged in the resulting bond-formation.[4,5]

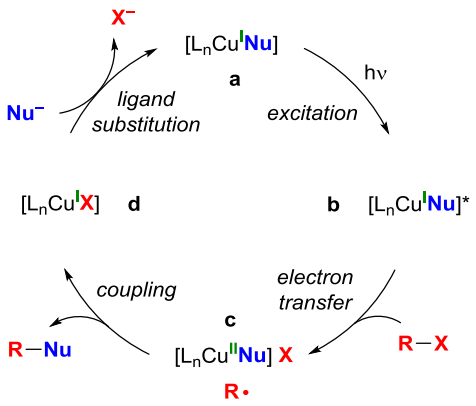

Figure 2.1. Early outline of a possible pathway for photoinduced, copper-catalyzed cross-couplings. For simplicity, all copper complexes are depicted as neutral species, and all processes are illustrated as unidirectional. X may be an inner- or an outer-sphere group, and L_n represents additional ligand(s) coordinated to copper.

Implicated in **Figure 2.1** is an in-cage coupling step, akin to the radical rebound mechanism performed by cytochrome P-450 enzymes.[6] Under this scenario, the photo-excited complex **b** generates an organic radical, and the resulting oxidized copper complex **c** couples with the formed organic radical rapidly within the solvent cage prior to diffusion. A follow-up study on the mechanism of photoinduced, copper-mediated S–arylations of aryl thiols and aryl iodides further provided support for the simplified mechanistic scheme in **Figure 2.1**.[7]

An alternate mechanistic scenario is an out-of-cage coupling pathway in which the organic radical escapes the solvent cage via diffusion and exists as a free alkyl radical before it is captured by a new copper species in solution. A related pathway (the coupling of free alkyl radicals and copper(II)–nucleophile species) had been proposed as the key bond-forming step in several copper-catalyzed C_{sp^3}–H amination reactions.[8,9]

The mechanistic understanding of transition metal-catalyzed C_{sp^3}–N bond-forming reactions is of substantial interest due to the importance of amines in a variety of disciplines, including biology, chemistry and materials science.[10] Recognizing that operating pathways may be largely dependent on the nucleophile, the electrophile, and the reaction conditions, we have chosen to elucidate the mechanism of the photoinduced, copper-catalyzed coupling of carbazole with alkyl halides. This study differs from the mechanistic investigation of photoinduced reactions of aryl iodides with copper(I)–thiolates under related reaction conditions with respect to nucleophile (sulfur vs nitrogen), electrophile (aryl vs alkyl halide), and the quantity of copper (stoichiometric vs catalytic) (**Figure 2.2**). Herein, we demonstrate

that photoinduced, copper-catalyzed couplings of carbazole with alkyl halides proceed via a predominantly out-of-cage process.

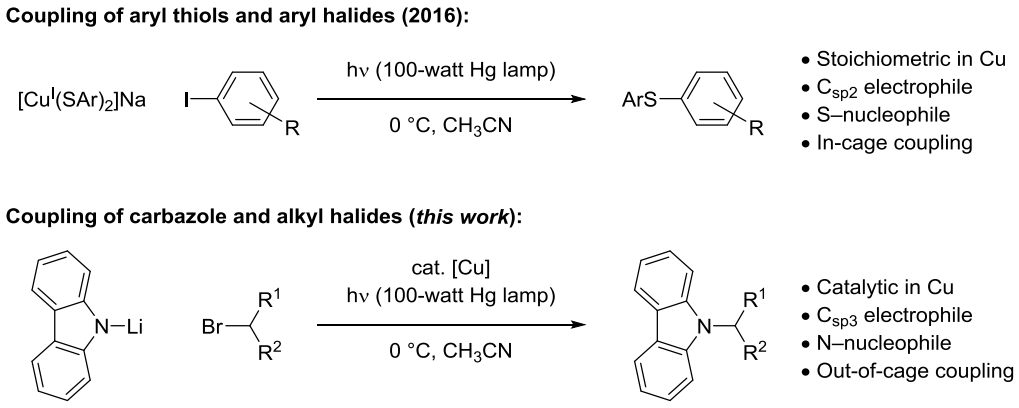

Figure 2.2. Key differences in mechanistic examinations of photoinduced, copper-catalyzed couplings.

2.2. Results and Discussions

2.2.1. Optimization of conditions for mechanistic studies

Initial studies on photoinduced, copper-catalyzed alkylations of carbazoles focused on the use of alkyl iodides as electrophiles. However, we observed unexpected side reactions of alkyl iodides during the course of the present study (**Scheme 2.2**). Secondary unactivated alkyl iodides such as 6-iodo-1-heptene can be nearly quantitatively recovered upon extended irradiation in CH_3CN at or below ambient temperature. In the absence of light, 6-iodo-1-heptene does not react with LiO*t*-Bu. In contrast, the irradiation of 6-iodo-1-heptene in the presence of LiO*t*-Bu leads to a consumption of the electrophile as determined by GC analysis of the crude mixture; the decrease in the signal corresponding to 6-iodo-1-heptene is

accompanied by the growth of a new set of peaks with roughly 4:1 ratio of signal intensities. The m/z values of the new signals are 224, consistent with those expected of cyclized isomers of 6-iodo-1-heptene. In contrast, 6-bromo-1-heptene remains stable under otherwise identical conditions; consequently, alkyl bromides were chosen as model electrophiles to minimize mechanistic complications.

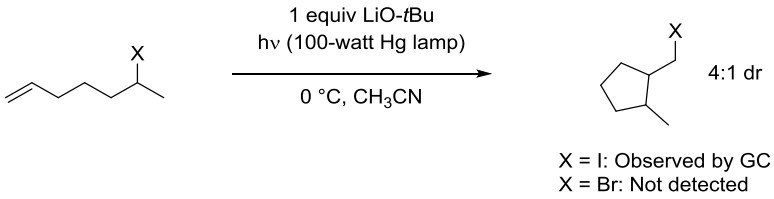

Scheme 2.2. Photostability of 6-halo-1-heptenes. 50% of the starting material is consumed after 30 min of irradiation in the case of 6-iodo-1-heptene. No isomerization is observed with 6-bromo-1-heptene even after hours of irradiation.

To further simplify the reaction conditions for mechanistic investigations, discrete reaction components were utilized ($[Cu^{I}(carb)_2]Li$ as the catalyst and Li(carb) as the nucleophile; carb = carbazolide),[11] rather than the mixture of CuI, carbazole, and LiO*t*-Bu that had been described in the earlier study. Under the new conditions, carbazole undergoes alkylation with 2-bromo-4-phenylbutane in 64% yield at 0 °C in the presence of 5 mol% of catalyst (**Scheme 2.3**). In the absence of light, no coupling (< 1%) is observed.

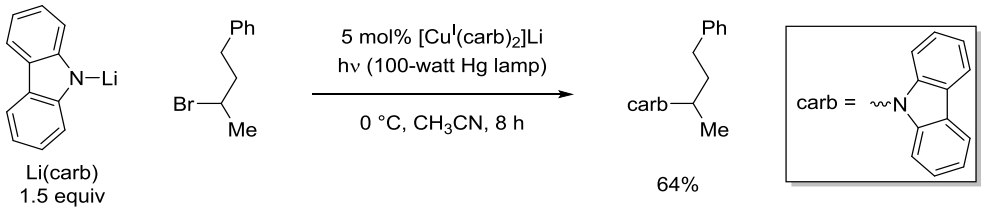

Scheme 2.3. New conditions for the mechanistic studies.

2.2.2. Stoichiometric reactivity of $[Cu^{I}(carb)_2]Li$

The irradiation of the stoichiometric mixture of $[Cu^{I}(carb)_2]Li$ with 2-bromo-4-phenylbutane leads to the generation of N–alkylation product in 96% yield (**Scheme 2.4**). This observation suggests that $[Cu^{I}(carb)_2]Li$ is both stoichiometrically and catalytically competent in the coupling of carbazole with alkyl bromides. These combined observations are consistent with the general mechanistic pathway shown in **Figure 2.1**.

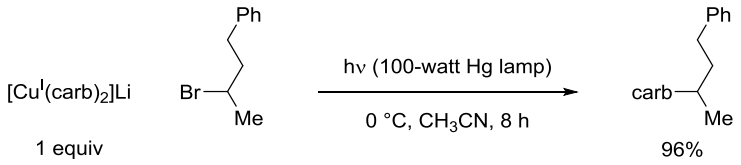

Scheme 2.4. Stoichiometric reaction between $[Cu^{I}(carb)_2]Li$ and 2-bromo-4-phenylbutane.

Because single electron transfer (SET) from the excited-state copper complex, $[Cu^{I}(carb)_2]Li^*$, to an alkyl bromide should lead to the formation of a paramagnetic copper(II) complex, we employed electron paramagnetic resonance (EPR) spectroscopy to probe for an $S = 1/2$ copper photoproduct. When a freezing mixture of $[Cu^{I}(carb)_2]Li$ and 2-bromo-4-phenylbutane (5 equiv) in butyronitrile is irradiated at 350 nm, a pseudoaxial EPR

signal is observed (**Figure 2.3**, black trace). A similar spectrum is obtained by treating $[Cu^{I}(carb)_2]Li$ with tris(4-bromophenyl)ammoniumyl hexachloroantimonate (Magic Blue; 0.2 equiv) in butyronitrile at –80 °C (**Figure 2.3**, blue trace). Although hyperfine coupling is unresolved in these spectra, strong *g* anisotropy indicates the presence of a copper-containing metalloradical.

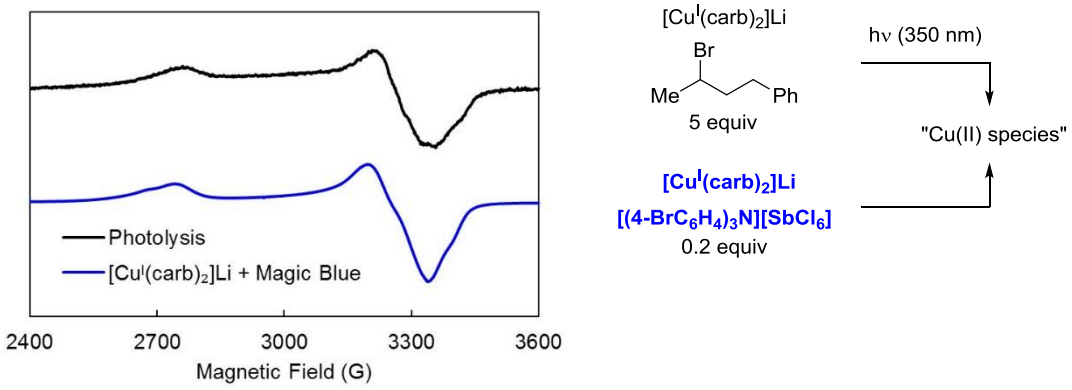

Figure 2.3. EPR spectra in the absence of exogenous Li(carb) (9.4 GHz, 77 K, butyronitrile). Black trace: mixture of $[Cu^{I}(carb)_2]Li$ and 2-bromo-4-phenylbutane (5 equiv) in freezing butyronitrile upon irradiation at 350 nm; blue trace: mixture of $[Cu^{I}(carb)_2]Li$ and Magic Blue (0.2 equiv) at –80 °C. Simulated *g* values: g = [2.445, 2.060, 1.994].

The likelihood of the photoinduced single electron oxidation of copper is further corroborated by the decrease in the lifetime of $[Cu^{I}(carb)_2]Li^*$ in the presence of an alkyl bromide. Because $[Cu^{I}(carb)_2]Li$ in CH_3CN absorbs in the UV-A, (ε_{365nm} = 4300 M^{-1} cm^{-1}), we probed the excited-state properties by transient absorption spectroscopy. The excitation using a ND:YAG laser source of a sample of $[Cu^{I}(carb)_2]Li$ yields a non-emissive excited

state with an absorption maximum at 580 nm and a lifetime of 910 ns. The quenching of the excited state by 2-bromo-4-phenylbutane occurs with a rate constant of 4.8×10^6 M^{-1} s^{-1}. In view of the EPR data, electron transfer instead of energy transfer is the more likely mechanism of quenching.[12]

2.2.3. Single electron transfer from [Li(carb)]*

Although stoichiometric reactivity patterns of $[Cu^{I}(carb)_2]Li$ with an alkyl bromide demonstrate the viability of elementary steps outlined in **Figure 2.1**, they do not necessitate the relevance of individual steps under catalytic conditions. Under the conditions of catalysis, Li(carb) rather than $[Cu^{I}(carb)_2]Li$ is present in a much larger quantity. This stoichiometry is noteworthy in view of the optical spectra of the two species. Although Li(carb) shows concentration-dependent molar absorptivity in CH_3CN, its molar absorptivity above 13 mM concentrations at 365 nm reaches 2200 M^{-1} cm^{-1}, which is approximately 50% of the molar absorptivity of $[Cu^{I}(carb)_2]Li$ at the same wavelength (**Figure 2.4**).

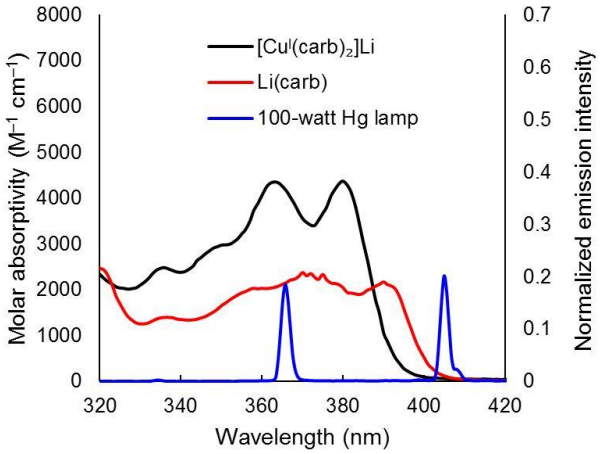

Figure 2.4. Optical spectra. Black trace: absorption of 0.094 mM solution of $[Cu^{I}(carb)_2]Li$ in CH_3CN; red trace: absorption of 1.3 mM solution of Li(carb) in CH_3CN; blue trace: emission of the 100-watt medium pressure Hg lamp normalized to its maximum intensity.

The competitive light absorption by Li(carb) has a substantial chemical consequence. In the absence of light, stirring a mixture of Li(carb) and the alkyl bromide does not result in the consumption of the electrophile. However, a small amount of the C–N coupling product is generated (5% yield) along with considerable side products (**e**, **f**, and **g**) when the mixture is irradiated with a 100-watt Hg lamp (**Scheme 2.5**). While metal-free background reactions are not uncommon in transition metal-catalyzed transformations, this observation is suggestive of the presence of both carbazyl and alkyl radicals upon irradiation.[13]

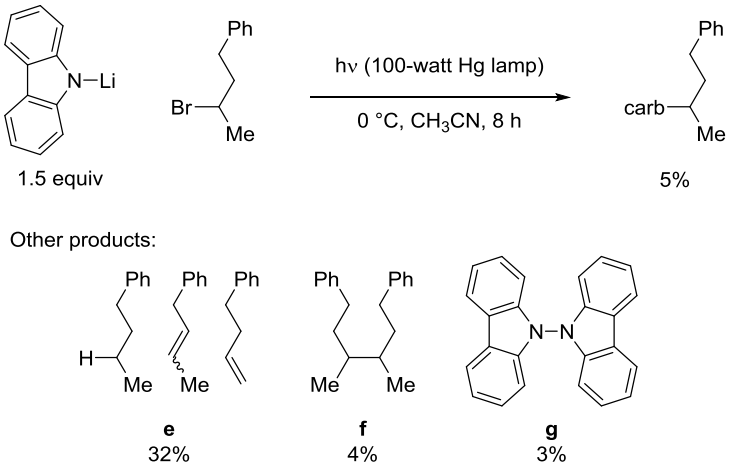

Scheme 2.5. Outcome of the irradiation of a mixture of Li(carb) and 2-bromo-4-phenylbutane in the absence of copper.

The feasibility of photoinduced SET from the excited state, [Li(carb)]*, to the alkyl bromide is further corroborated by the Stern-Volmer analysis. The absorption of 355 nm Nd:YAG laser pulse by a 49 mM (catalytic concentration) solution of Li(carb) produces a luminescent excited state with a lifetime of 31 ns. This excited state is quenched by 2-bromo-4-phenylbutane with a second-order rate constant of 4.9×10^8 M^{-1} s^{-1}.

Under turnover conditions, the copper precatalyst persists in solution. For example, ESI-MS trace of the reaction after 1 h of irradiation shows m/z signals of 395 and 397 which correspond to the masses of $[^{63}Cu^{I}(carb)_2]^-$ and $[^{65}Cu^{I}(carb)_2]^-$, respectively. However, the relative molar absorptivity values and concentrations of $[Cu^{I}(carb)_2]Li$ and Li(carb) indicate that Li(carb) serves as the dominant light absorber and reacts with the alkyl halide. Therefore, we propose that the excitation to Li(carb)* is the major photophysical event that leads to the formation of an alkyl radical under the catalytic conditions (**Figure 2.5**).

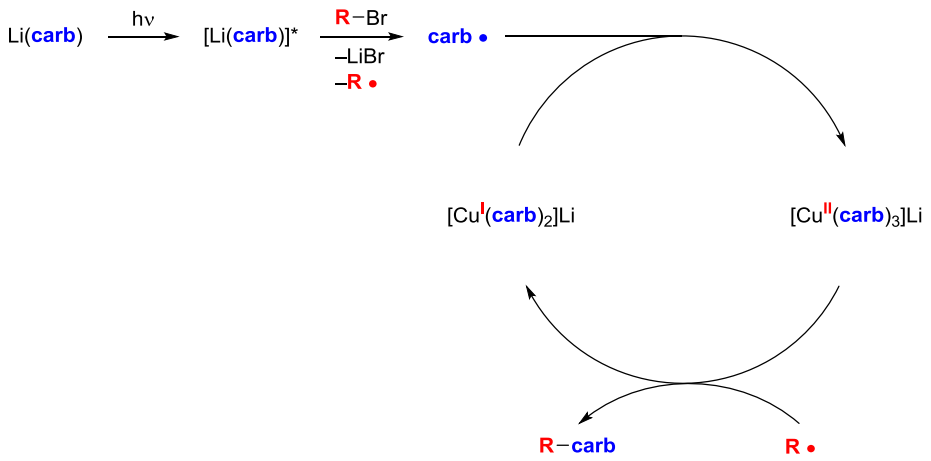

Figure 2.5. Outline of a new possible pathway for the photoinduced, copper-catalyzed coupling of Li(carb) with an alkyl bromide.

In this mechanistic model, photoinduced SET generates two organic radicals: carbazyl and alkyl radicals. The two radicals then diffuse away from one another faster than they couple and exist as free radicals in solution. Thus, an out-of-cage C–N coupling pathway is demanded under this mechanistic scenario. We propose that the carbazyl radical reacts with $[Cu^{I}(carb)_2]Li$ to generate a new copper(II) complex, $[Cu^{II}(carb)_3]Li$, which then couples with an alkyl radical to afford the N–alkylation product. As in the case of the original mechanism (**Figure 2.1**), the key C–N bond-forming step is still the reaction of an alkyl radical with a copper(II)–carbazolide complex, but the pathway for forming these intermediates is different.

2.2.4. Characterization of $[Cu^{II}(carb)_3]^-$

Because metalloradicals are generally more stable than organic radicals, we sought to detect $[Cu^{II}(carb)_3]Li$, which is the copper(II)–nucleophile intermediate proposed in

Figure 2.5. Specifically, the reaction mixture under the model conditions (**Scheme 2.3**) was irradiated at 0 °C for 60 min and subsequently freeze-quenched at –196 °C, which led to the appearance of a strong, pseudoaxial EPR signal that shows an unpaired spin coupled to $^{63/65}$Cu (I = 3/2) (**Figure 2.6**, black trace). This EPR spectrum is different from that observed upon the irradiation of a mixture of [Cu^{I}(carb)$_2$]Li and the same alkyl bromide in the absence of exogenous Li(carb) (**Figure 2.3**).

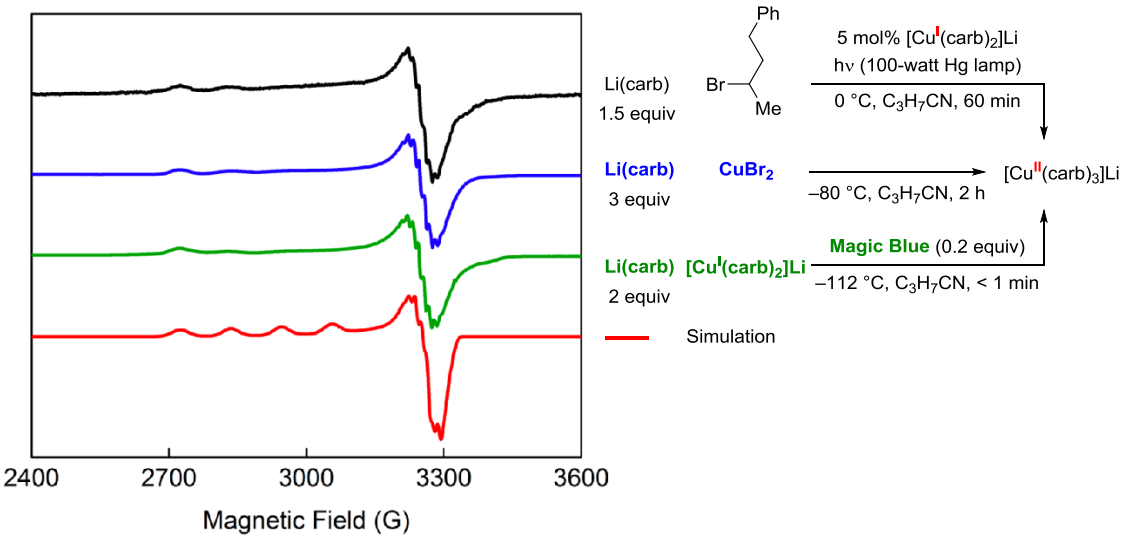

Figure 2.6. Simulated and experimental (9.4 GHz, 77 K, C_3H_7CN) EPR spectra of [Cu^{II}(carb)$_3$]Li, generated through three independent pathways. Black trace: freeze-quenched sample of an irradiated mixture of standard reactions; blue trace: mixture of Li(carb) and $CuBr_2$; green trace: mixture of Li(carb), [Cu^{I}(carb)$_2$]Li, and Magic Blue; red trace: simulated EPR spectrum (g = [2.318, 2.058, 2.050]), displaying hyperfine couplings to one $^{63/65}$Cu and three ^{14}N atoms.

The EPR-active compound observed under turnover conditions can also be generated through the treatment of $CuBr_2$ with 3 equiv of Li(carb) at low temperature (**Figure 2.6**, blue trace), and through the reaction of $[Cu^{I}(carb)_2]Li$ with Li(carb) and Magic Blue (**Figure 2.6**, green trace). These EPR signals are modeled well as a monomeric copper(II) species coordinated by three equivalent ^{14}N ($I = 1$) nuclei (**Figure 2.6**, red trace), consistent with its assignment as the homoleptic $[Cu^{II}(carb)_3]Li$ complex.

Although we have been unable to crystallographically characterize a lithium salt of $[Cu^{II}(carb)_3]^-$, due in part to its thermal instability, crystals of two potassium salts, $[Cu^{II}(carb)_3][K(THF)_6]$ and $[Cu^{II}(carb)_3][K(benzo\text{-}15\text{-}crown\text{-}5)_2]$, have been obtained by layering Et_2O onto a solution that contained a mixture of $Cu(OTf)_2$, K(carb), and benzo-15-crown-5 in THF at –78 °C (**Figure 2.7**, left). When an analogous reaction is performed using 18-crown-6 in place of benzo-15-crown-5, single crystals of $[Cu^{II}(carb)_3][K(18\text{-}crown\text{-}6)(THF)]$ is also obtained.[14] The powder and glass EPR spectra of $[Cu^{II}(carb)_3][K(benzo\text{-}15\text{-}crown\text{-}5)_2]$ are consistent with the spectra of $[Cu^{II}(carb)_3]Li$ (**Figure 2.7**, right). Both in solid and solution states, $[Cu^{II}(carb)_3][K(benzo\text{-}15\text{-}crown\text{-}5)_2]$ is deep-blue; $[Cu^{II}(carb)_3]^-$ shows an absorption band at 580 nm with an approximate molar absorptivity of 1100 M^{-1} cm^{-1}.

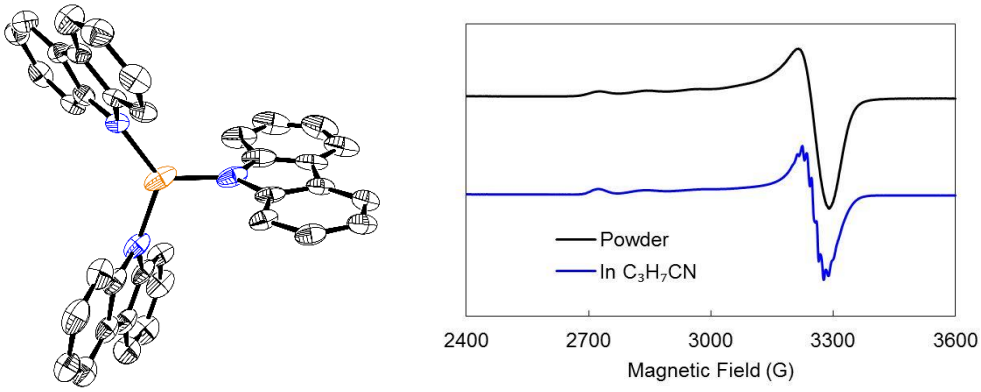

Figure 2.7. Characterization of the copper(II) intermediate. Left: solid-state molecular structure of $[Cu^{II}(carb)_3][K(THF)_6]$ as determined by single crystal X-ray diffraction (countercation and H atoms are omitted for clarity). Right: EPR spectra (9.4 GHz, 77 K); black trace: powder spectrum of $[Cu^{II}(carb)_3][K(benzo\text{-}15\text{-}crown\text{-}5)_2]$; blue trace: frozen solution of $[Cu^{II}(carb)_3][K(benzo\text{-}15\text{-}crown\text{-}5)_2]$ in C_3H_7CN.

The distinct color of $[Cu^{II}(carb)_3]^-$ allowed us to detect its presence also by optical spectroscopy. When a reaction mixture is irradiated under the standard catalysis conditions (**Scheme 2.3**), the solution turns deep-blue; this color diminishes when irradiation is discontinued and the solution is allowed to warm to room temperature. When a model reaction mixture is irradiated in a quartz cuvette at 0 °C, the absorption band at 580 nm of $[Cu^{II}(carb)_3]Li$ is observed within a few seconds (**Figure 2.8**, left, black trace). This absorption feature can also be generated through the treatment of $CuBr_2$ with 3 equiv of Li(carb) at low temperature (**Figure 2.8**, left, blue trace), and through the reaction of $[Cu^{I}(carb)_2]Li$ with Li(carb) and Magic Blue (**Figure 2.8**, left, green trace).

Within 3 min of irradiation, a concentration of $[Cu^{II}(carb)_3]Li$ accounting for ~50% of the original amount of copper is reached (**Figure 2.8**, right). Our observations indicate that the concentration of two radical species outlined in (**Figure 2.5**) diverges rapidly from the initial 1:1 stoichiometry. Derived mostly from the carbazyl radical, $[Cu^{II}(carb)_3]Li$, is a persistent radical that builds up in concentration upon irradiation of the catalysis mixture and observable by various spectroscopic techniques, while the alkyl radical is a transient radical present in low concentrations.[15]

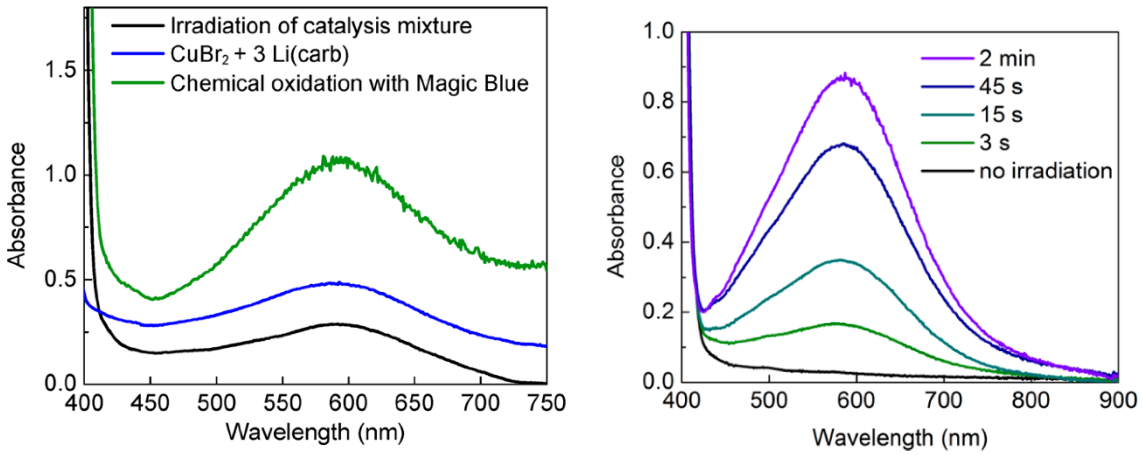

Figure 2.8. UV–vis spectra. Left: generation of $[Cu^{II}(carb)_3]Li$ through three independent ways; black trace: catalyzed reaction mixture after irradiation; blue trace: mixture of $CuBr_2$ and Li(carb) (3 equiv) in butyronitrile at –80 °C; green trace: mixture of $[Cu^{I}(carb)_2]Li$ (1 equiv) and Li(carb) (2 equiv) treated with Magic Blue (0.3 equiv) in butyronitrile at –80 °C. Right: appearance of an absorption peak at 580 nm of $[Cu^{II}(carb)_3]Li$ upon the irradiation of a reaction mixture containing $[Cu^{I}(carb)_2]Li$ (5 mol%), Li(carb) (1.5 equiv), and 2-bromo-4-phenylbutane in CH_3CN in a quartz cuvette at 0 °C.

The metalloradical $[Cu^{II}(carb)_3]^-$ unit represents a rare example of structurally characterized homoleptic three-coordinate copper(II) complex.[16] The quality of the X-ray diffraction data for $[Cu^{II}(carb)_3][K(THF)_6]$ is modest, and structural metrics should therefore be viewed with caution (**Figure 2.7**, left).[17] Nevertheless, the N–Cu–N bond angles (two large and one small: 126.7(2), 124.4(2), 108.8(2)°) indicate a structural departure from a trigonal planar geometry, as anticipated for an ^2E electronic state that is Jahn-Teller active.

DFT computations on the $[Cu^{II}(carb)_3]^-$ core show a significant delocalization of the unpaired spin, with 0.43 e^- on Cu atom and 0.27 e^- distributed between the three N atoms of the carbazolide ligands (**Figure 2.9**, left).[18] This spin-delocalization is also apparent in the experimental EPR spectrum of $[Cu^{II}(carb)_3]^-$ (**Figure 2.7**, right). Consistent with the new mechanistic hypothesis (**Figure 2.5**), DFT-predicted formation of $[Cu^{II}(carb)_3]^-$ via the coupling of carb• with $[Cu^{I}(carb)_2]^-$ is exergonic by ~9 kcal mol^{-1}. In contrast, the hypothetical coupling of a secondary unactivated alkyl radical (•R) with $[Cu^{I}(carb)_2]^-$ to generate a $[Cu^{II}(carb)_2R]^-$ unit is endergonic by ~3 kcal mol^{-1}. Thus, DFT predictions are in line with the observation of $[Cu^{II}(carb)_3]^-$ under the conditions of catalysis.

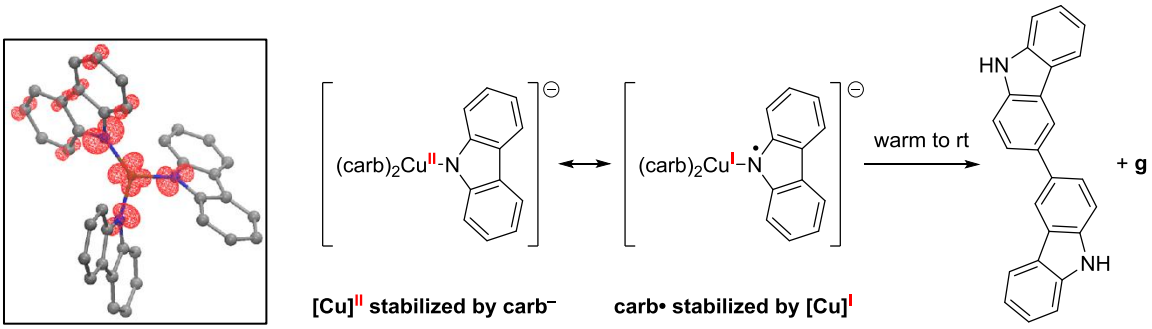

Figure 2.9. Carbazyl-radical character in $[Cu^{II}(carb)_3]^-$. Left: DFT-computed spin-density plot of $[Cu^{II}(carb)_3]^-$ in which 27% of the total spin resides on the three N nuclei. Right: resonance contributors to $[Cu^{II}(carb)_3]^-$ consistent with its thermal decomposition products; **g** is 9,9′-bicarbazyl.

Given the appreciable predicted spin density on nitrogen, $[Cu^{II}(carb)_3]^-$ might display reactivity characteristic of a carbazyl radical.[19] The observation of products of formal carbazyl radical dimerization (3,3′-bicarbazole, and 9,9′-bicarbazyl) upon warming a solution of $[Cu^{II}(carb)_3]^-$ is consistent with this view. Thus, the key bond-forming step in these photoinduced, copper-catalyzed reactions might occur through the direct C_{sp^3}–N coupling, rather than through a copper(III)–nucleophile intermediate.

Previously, a reaction between a trityl radical (Ph_3C•) and a copper(II)–anilide complex to furnish a C–N bond (Ph_3C–NHAr) and a copper(I) species had been illustrated in the literature.[8] While the addition of trityl radical did not yield the C–N coupled product, the addition of TEMPO–H to a freshly prepared solution of $[Cu^{II}(carb)_3]$Li generates TEMPO• as the only EPR-active species (TEMPO• = 2,2,6,6-tetramethylpiperidine 1-oxyl), as well as $[Cu^{I}(carb)_2]$Li (**Scheme 2.6**). The observed reactivity is consistent with hydrogen

atom abstraction from TEMPO–H by $[Cu^{II}(carb)_3]Li$, rather than a proton transfer which is expected to yield an EPR spectrum.

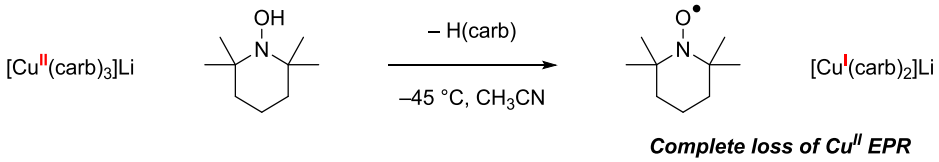

Scheme 2.6. Hydrogen atom transfer by TEMPO–H to $[Cu^{II}(carb)_3]Li$, resulting in the full consumption of $[Cu^{II}(carb)_3]Li$ and the formation of TEMPO• and $[Cu^{I}(carb)_2]Li$

Thus, the mechanistic scheme outlined in **Figure 2.5** is in essence the coupling of an alkyl radical and a carbazyl radical in an out-of-cage process mediated by copper. Copper truly provides a platform for bond-construction of two organic radicals. This mechanistic model remains conceptually different from common photoredox transformations which can be prone to radical chain processes involving free radicals.[20] While complex photochemistry of $[Cu^{I}(carb)_2]Li$ and Li(carb) does not permit an unequivocal evaluation of chain processes in the present study, the standard reaction (**Scheme 2.3**) is estimated to have a chain length of 0.3, which is suggestive of a non-chain pathway.

2.2.5. Evidence for out-of-cage coupling via free radical intermediate

Because unactivated secondary alkyl radicals are unstable, transient species, standard spectroscopic techniques that have been useful in the detection of the copper(II) intermediate were not applicable to the direct observation of free alkyl radicals. Instead, we designed and

performed independent reactivity, stereochemical, and product studies to probe for the involvement of free alkyl radicals.

Alkyl radicals with pendant olefins can undergo intramolecular cyclizations.[21] For example, the derived secondary alkyl radical of 6-bromo-1-heptene isomerizes with a rate constant of 1.0×10^5 s^{-1} at 25 °C, furnishing a primary alkyl radical with ~4:1 cis/trans diastereoselectivity.[22] When 6-bromo-1-heptene is subjected to our standard reaction conditions, the cyclized coupling product (**h**) is formed in 62% yield with 4:1 diastereoselectivity, along with 10% of the direct-coupling product (**i**) (**Scheme 2.7**). Because the rate of diffusion (typically exceeding 10^8 s^{-1}) is significantly higher than the rate of cyclization of the derived secondary radical, the predominant generation of the cyclized products **h** suggests that if ring formation is occurring through radical cyclization, then the C–N bond-construction is proceeding primarily through an out-of-cage pathway.

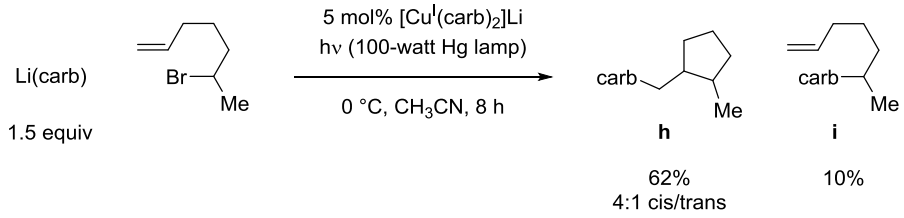

Scheme 2.7. The coupling of 6-bromo-1-heptene, yielding the cyclization product predominantly.

The 4:1 cis/trans stereoselectivity that we observed is essentially the dr previously reported for the cyclization of this putative secondary alkyl radical at 0 °C.[22] To provide further support for a radical rather than an organometallic pathway for ring formation, we

examined the photoinduced, copper-catalyzed coupling of the deuterium-labeled analogue of 6-bromo-1-heptene (**Scheme 2.8**). The analysis via NMR spectroscopy revealed a 1:1 mixture at the indicated stereocenter, which is inconsistent with a radical-free organometallic mechanism that involves an uninterrupted sequence of oxidative addition, β-migratory insertion, and reductive elimination.

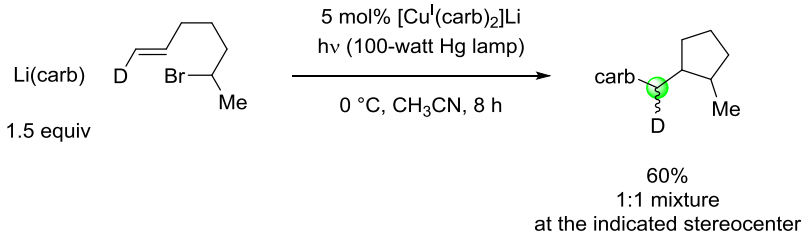

Scheme 2.8. Trans-deuterium-labeled analogue of 6-bromo-1-heptene resulting in the loss of stereochemical information upon coupling under the standard conditions.

To further explore the question of out-of-cage coupling, we investigated the effect of the concentration of the reaction on the resulting ratio of the amount of cyclized (**h**) to uncyclized (**i**) product (**Scheme 2.9**). In dilute solutions, the intramolecular isomerization takes place prior to the intermolecular coupling step. As the reaction concentrations are increased, the extent of intermolecular coupling event is increased. If all of the cross-coupling is occurring in-cage, then the ratio should not depend on concentration since the quantity of reactive species within the solvent cage remains constant. The trend that we observe–a greater preference for cyclization at lower concentration–is that expected if out-of-cage coupling is occurring. The observation of a considerable amount of TEMPO adducts derived from the trapping of the uncyclized secondary radical or the cyclized primary radicals, when

a photoinduced, copper-catalyzed cross-coupling is run in the presence of TEMPO, further supports the possibility of out-of-cage coupling.

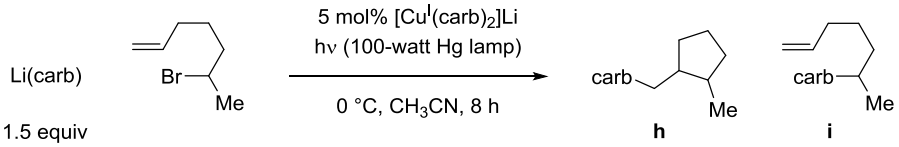

[alkyl bromide] (mM)	ratio of products (**h**/**i**)
11	11
22	7.6
33	6.1
44	5.5
55	5.1

Scheme 2.9. The effect of overall reaction concentrations on the extent of cyclization.

In thermally-driven, nickel-catalyzed transformations, the effect of the variation in the quantity of nickel catalyst on the amount of cyclization of the alkyl radical had been frequently examined.[23] A linear correlation between the quantity of the catalyst and the extent of direct coupling is often used to support the involvement of free radicals, since the concentration of reactive metal species is presumed to increase linearly with the amount introduced to the reaction mixture. When the analogous study is performed using 6-bromo-1-heptene, the effect of added [Cu^{I}(carb)$_2$]Li is not pronounced, and the ratio of cyclized-to-uncyclized product plateaus at a value of 6 past a catalyst loading of 5 mol% (**Figure 2.10**).

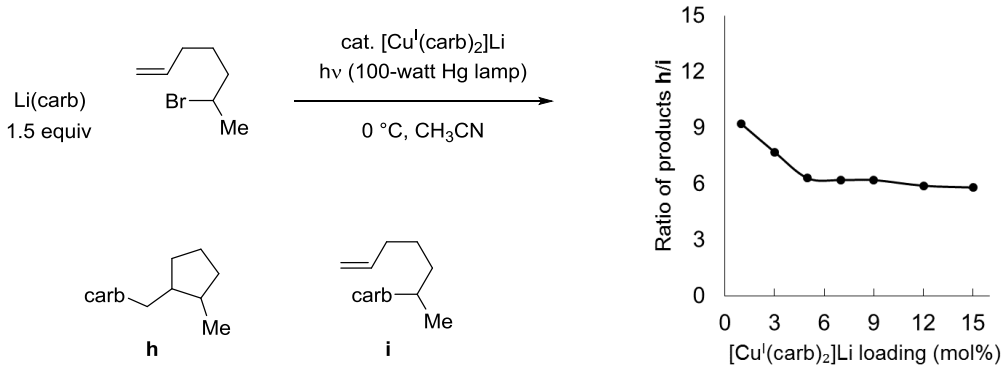

Figure 2.10. The extent of cyclization as a function of the initial catalyst concentration.

At first glance, the observed trend may appear to suggest that $[Cu^{I}(carb)_2]Li$ does not lead to the formation of an active, bond-constructing catalyst. We performed kinetic simulations to gain insight into the reduced effect of the catalyst loading on the outcome of alkyl radical cyclization. Assuming irreversibility, a simplified kinetic model involving a metal-mediated bond-formation shows the expected linear trend (**Figure 2.11**, bottom left). In contrast, under photochemical conditions, wherein the rate of radical generation is inherently gated by the photon flux, the intensity of the light source becomes a critical parameter that is invariable even when the amount of catalyst is increased. This fixed rate in photochemical settings in turn leads to a less pronounced effect on the degree of direct coupling (**Figure 2.11**, bottom right) and is the key factor that induces the observed saturation behavior in the experimental plot shown in **Figure 2.10**.

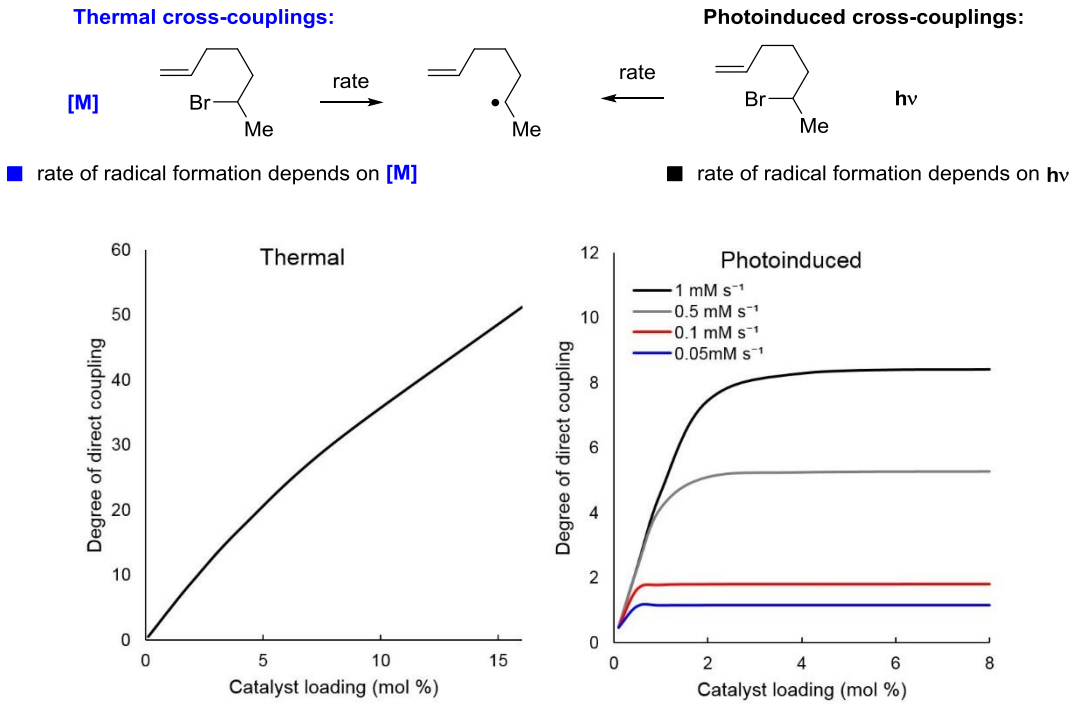

Figure 2.11. Differences in the rate-influencing steps for the formation of free radicals between thermal and photoinduced cross-couplings. Bottom left: simulated degree of direct coupling assuming linear correlation between the rate of radical generation and catalyst loading (thermal reactions). Bottom right: simulated degree of direct coupling at fixed rates of radical generation (photoinduced reactions); degree of direct coupling is determined by taking the ratio of the amount of direct coupling product to the amount of cyclized product.

Further evidence for the involvement of free alkyl radicals is provided by the product analysis of the crude reaction mixtures over time (**Figure 2.12**). Side products formed from bimolecular reactions of alkyl radicals in the absence of the catalyst are also detected in the presence of the catalyst but in much smaller amounts. In the absence of $[Cu^{I}(carb)_2]Li$, alkyl radicals undergo fast, uncontrolled bimolecular decomposition reactions, while the formation of C–N coupling product stalls at <5% yield. In the presence of $[Cu^{I}(carb)_2]Li$, the

unproductive radical decomposition products are minimized; instead, the alkyl radical is selectively captured by the persistent radical, $[Cu^{II}(carb)_3]Li$, and converted to the C–N coupling product. This observation is fully consistent with the new mechanistic proposal illustrated in **Figure 2.5** and underscores the importance of copper in photoinduced cross-couplings that occur via an SET process.

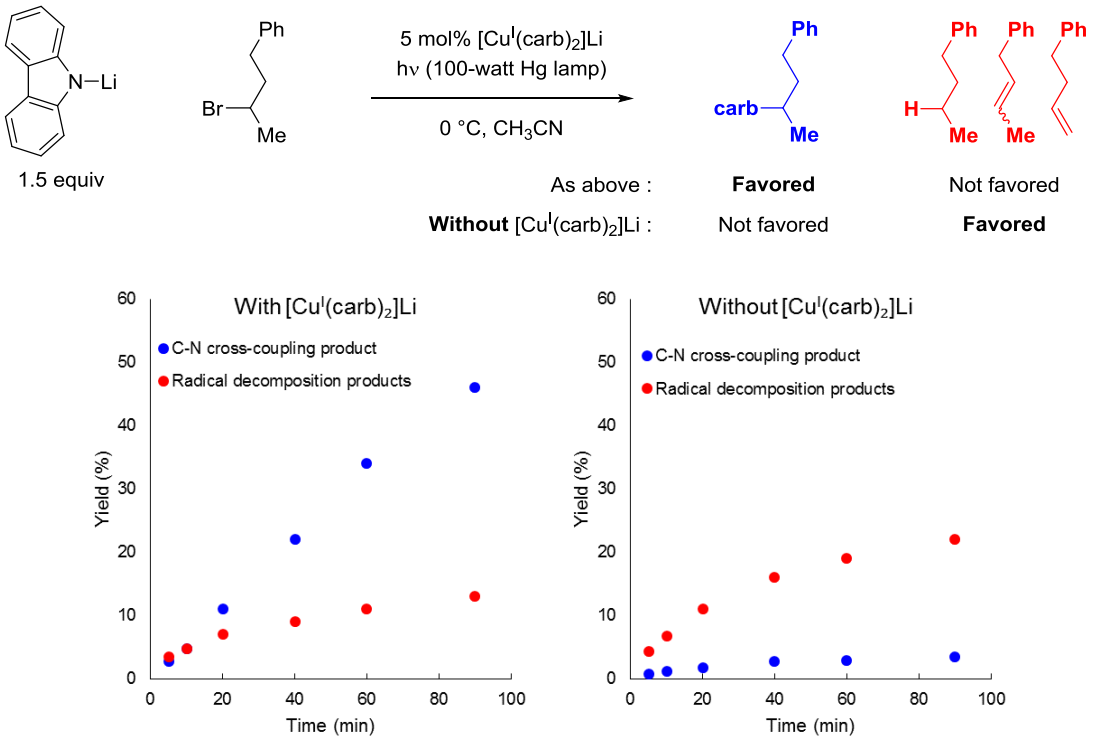

Figure 2.12. Formation of products over time. Left: yields in the presence of $[Cu^{I}(carb)_2]Li$; right: yields in the absence of $[Cu^{I}(carb)_2]Li$.

2.3. Conclusions

Using a wide range of tools, we have investigated the mechanism of the photoinduced, copper-catalyzed coupling of carbazole with an alkyl bromide, which is one

of the first examples of transition metal catalysis of the alkylation of an amine by an alkyl halide. In addition to the originally proposed pathway, we suggest that a second mechanism is operative and dominant, wherein photoexcited Li(carb) serves as a reductant of the alkyl bromide, generating an alkyl radical and a carbazyl radical, which combine via an out-of-cage, copper-catalyzed pathway in which $[Cu^{I}(carb)_2]Li$ and $[Cu^{II}(carb)_3]Li$ are key intermediates (**Figure 2.5**). Using ESI-MS, we have obtained evidence for the presence of $[Cu^{I}(carb)_2]^-$ under catalysis conditions. With the aid of UV–vis and luminescence spectroscopy, we have established that upon irradiation, Li(carb) can undergo excitation and then electron transfer to an alkyl bromide, thereby affording a carbazyl radical and an alkyl radical. Using EPR spectroscopy, we have obtained evidence for the formation of a copper(II) complex during catalysis; we had postulated this intermediate to be $[Cu^{II}(carb)_3]^-$ (generated by the reaction of a carbazyl radical with $[Cu^{I}(carb)_2]^-$), which we then independently synthesized and structurally characterized. Through the use of UV–vis spectroscopy, we have monitored the buildup of this complex, the persistent radical that is responsible for effective cross-coupling, during a reaction. Radical cyclization, stereochemical, and reactivity probes are consistent with the generation of an alkyl radical, which engages in an out-of-cage coupling with $[Cu^{II}(carb)_3]^-$. The chain length for the coupling reaction is relatively low (0.3), as expected for a non-chain process. The additional pathway illustrated in **Figure 2.5** highlights the opportunity to achieve photoinduced, copper-catalyzed coupling reactions not only through excitation of copper–nucleophile complexes but also of nucleophiles themselves. Regardless of the photoreductant under catalytic conditions, copper appears to play a critical role in the key bond construction step via coupling of a copper(II)–nucleophile complex with an organic radical.

2.4. Experimental section

2.4.1. General information

Unless otherwise noted, materials were either purchased from commercial suppliers and used as received, or prepared via literature procedures. Solvents were deoxygenated and dried by thoroughly sparging with argon followed by passage through an activated column in a solvent purification system. All manipulations of air-sensitive materials were carried out in oven-dried glassware using standard Schlenk, or glovebox techniques, under an N_2 atmosphere. Silicycle *Silia*FlashR P60 silica gel (particle size 40–63 μm) was used for flash chromatography. Analytical thin layer chromatography was conducted with glass TLC plates (silica gel 60 F254), and spots were visualized under UV light or after treatment with standard TLC stains. X-band EPR measurements were made with a Bruker EMX spectrometer at 77 K. Simulation of EPR data was conducted using the software EasySpin.2.

^{1}H, ^{13}C, and ^{31}P NMR spectra were recorded on a Bruker Ascend 400 MHz, a Varian 300 MHz, a Varian 400 MHz, a Varian 500 MHz, or a Varian 600 MHz spectrometer with $CHCl_3$ (^{1}H, δ = 7.26) and $CDCl_3$ (^{13}C, δ = 77.0) as internal references and with 85% H_3PO_4 (^{31}P) as an external reference. Multiplicity and qualifier abbreviations are as follows: s = singlet, d = doublet, t = triplet, q = quartet, m = multiplet, br = broad, app = apparent). GC analyses were carried out on an Agilent 6890 Series system with an HP-5 column (length 30 m, I.D. 0.25 mm).

X-ray crystallography studies were carried out at the Beckman Institute Crystallography Facility on a Bruker D8 Venture kappa duo photon 100 CMOS instrument

(Mo Kα radiation). Structures were solved using SHELXT and refined against F2 by full-matrix least squares with SHELXL and OLEX2. Hydrogen atoms were added at calculated positions and refined using a riding model. The crystals were mounted on a glass fiber, or a nylon loop, with Paratone N oil. Steady-state fluorimetry was performed in the Beckman Institute Laser Resource Center (BILRC; California Institute of Technology). Steady-state emission spectra were collected on a Jobin S4 Yvon Spec Fluorolog-3-11 with a Hamamatsu R928P photomultiplier tube detector with photon counting. Absorbance spectra were acquired on a Cary 50 UV-Vis spectrophotometer with a Unisoku Scientific Instruments cryostat to maintain temperature.

Mass spectral data were collected on a Thermo LCQ or LTQ ion trap mass spectrometer, or on an Agilent 5973 mass spectrometer.

Photolytic reactions were performed using a 100 W Blak- Ray Long Wave Ultraviolet Lamp (Hg), a 100-W Blak-Ray B-100Y High Intensity Inspection Lamp (Hg), or a Luzchem LZC-4V photoreactor equipped with LZC-UVA lamps centered at 350 nm. If required, the temperature was maintained with an isopropanol bath cooled by an SP Scientific cryostat.

2.4.2. Procedures for photoinduced cross-couplings

Determination of photoinstability of 6-iodo-1-heptene

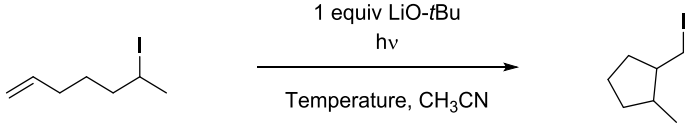

An equimolar mixture of 6-iodo-1-heptene (0.2 mmol) and LiO-*t*Bu (0.2 mmol) in CH_3CN (1 mL) was prepared in an 8 mL borosilicate vial equipped with a magnetic stir bar. The mixture was capped and stirred for 5 minutes and the reaction vessel was fully submerged in an isopropanol bath kept at 0 °C with a cryostat. The mixture was irradiated with a 100-watt Hg lamp before it was diluted with a solution of dodecane in Et_2O or EtOAc. An aliquot was filtered through a short pad of silica gel (EtOAc eluent) and the sample was injected for GC analysis.

Alternatively, a 10 mL quartz tube was used to prepare the mixture of 6-iodo-1-heptene and LiO-*t*Bu in CH_3CN. A small, measured quantity of *n*-dodecane was added as the internal standard, followed by a magnetic stir bar. The quartz tube was capped with a rubber septum, stirred for 5 minutes and placed in a Luzchem photoreactor at room temperature for irradiation under 350 nm. After irradiation, the quartz tube was shaken vigorously and an aliquot was immediately taken via syringe. The sample was filtered through a short pad of silica gel (EtOAc eluent) and the sample was injected for GC analysis. The data are summarized below for the irradiation under 350 nm.

Table 2.1. Conversion of 6-iodo-1-heptene at room temperature under 350 nm irradiation in CH_3CN in the presence of an equivalent of LiO*t*-Bu.

Time (h)	Remaining 6-iodo-1-heptene (%)*	Major isomer**	Minor isomer*	dr
0.25	67	0.29	0.08	3.5:1
0.50	50	0.41	0.12	3.5:1
0.75	39	0.45	0.13	3.5:1
1.00	32	0.49	0.14	3.5:1
2.00	26	0.57	0.16	3.5:1
3.00	17	0.59	0.17	3.4:1

* Determined by calibrated GC analysis using n-dodecane as internal standard
** Ratio of signal intensities corresponding to m/z = 224 to n-dodecane standard

General procedure for the coupling of alkyl bromides

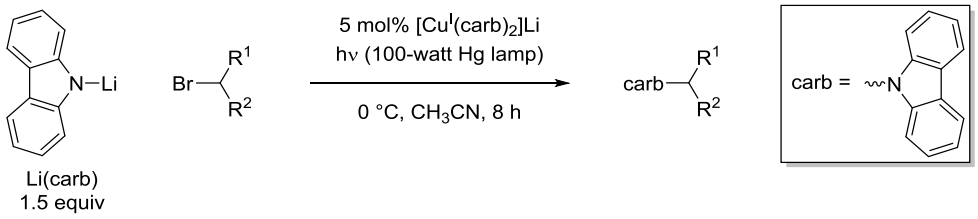

$[Li(CH_3CN)_n][Cu(carb)_2]$ (0.007 mmol), Li(carb) (0.2 mmol), and alkyl bromide (0.13 mmol) were added to a 4 mL borosilicate vial in the glovebox under a nitrogen atmosphere. A magnetic stir bar and 4 mL CH_3CN were added to the vial. The mixture was capped and stirred for 5 minutes and the reaction vessel was fully submerged in an isopropanol bath kept at 0 °C with a cryostat. The mixture was irradiated with a 100-watt Hg lamp while stirring for 8 hours, after which time it was diluted with a solution of dodecane in Et_2O or EtOAc. An aliquot was filtered through a short pad of silica gel (EtOAc eluent) and the sample was injected for GC analysis. Products were isolated after removing the solvent in vacuo and loading the crude mixture on silica gel and eluting with hexanes.

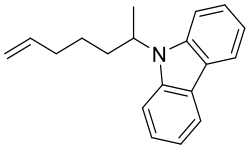

i

9-(hept-6-en-2-yl)-9H-carbazole (compound i). Following the general coupling procedure using 6-bromo-1-heptene, the title compound can be obtained after column chromatography (hexanes→1% EtOAc/hexanes) as colorless oil. A typical run produces 10% of the coupling product according to calibrated GC analysis.

^{1}H NMR (400 MHz, $CDCl_3$) δ 8.12 (d, J = 7.8 Hz, 2H), 7.51 (d, J = 8.1 Hz, 2H), 7.44 (t, J = 7.6 Hz, 2H), 7.22 (t, J = 7.0 Hz, 2H), 5.66 (ddt, J = 16.9, 10.2, 6.7 Hz, 1H), 4.96–4.84 (m, 2H), 4.85–4.66 (m, 1H), 2.40–2.22 (m, 1H), 2.13–1.88 (m, 3H), 1.68 (d, J = 7.0 Hz, 3H), 1.47–1.28 (m, 1H), 1.24–1.09 (m, 1H).

^{13}C NMR (101 MHz, $CDCl_3$) δ 139.9, 138.4, 125.5, 123.3, 120.4, 118.7, 115.0, 110.2, 51.3, 34.4, 33.5, 26.3, 19.5.

FT-IR (film): 2931, 1640, 1625, 1594, 1482, 1451, 1331, 1316, 1223, 1157, 746, 721 cm^{-1}.

MS (ESI) m/z $(M)^+$ calcd for $C_{19}H_{21}N$: 263.2, found: 263.3.

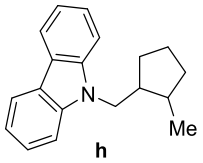

h

4:1 cis/trans

9-((2-methylcyclopentyl)methyl)-9H-carbazole (compound h). Following the general coupling procedure using 6-bromo-1-heptene, the title compound can be obtained as the mixture of diastereomers after column chromatography (hexanes→1% EtOAc/hexanes) as a colorless solid. A typical run produces 60% of the coupling product according to calibrated GC analysis. ^{1}H NMR resonances were assigned for major and minor diastereomers based on COSY data. The stereochemistry of the major diastereomer was analyzed by NOESY. NMR resonances of the major diastereomer are as follows.

^{1}H NMR (400 MHz, $CDCl_3$) δ 8.10 (d, J = 7.7 Hz, 2H), 7.48–7.41 (m, 4H), 7.24–7.20 (m, 2H), 4.37 (dd, J = 14.6, 4.6 Hz, 1H), 4.17 (dd, J = 14.6, 10.9 Hz, 1H), 2.69–2.44 (m, 1H), 2.26–2.19k (m, 1H), 1.96–1.75 (m, 2H), 1.53–1.38 (m, 4H), 1.13 (d, J = 7.1 Hz, 3H).

^{13}C NMR (126 MHz, $CDCl_3$) δ 140.8, 125.6, 123.0, 120.4, 118.8, 109.0, 44.0, 43.1, 36.2, 33.3, 29.0, 22.7, 15.6.

FT-IR (film): 2954, 2870, 1597, 1484, 1461, 1452, 1326, 1218, 1153, 748, 722 cm^{-1}.

MS (ESI) m/z $(M)^+$ calcd for $C_{19}H_{21}N$: 263.2, found: 263.3.

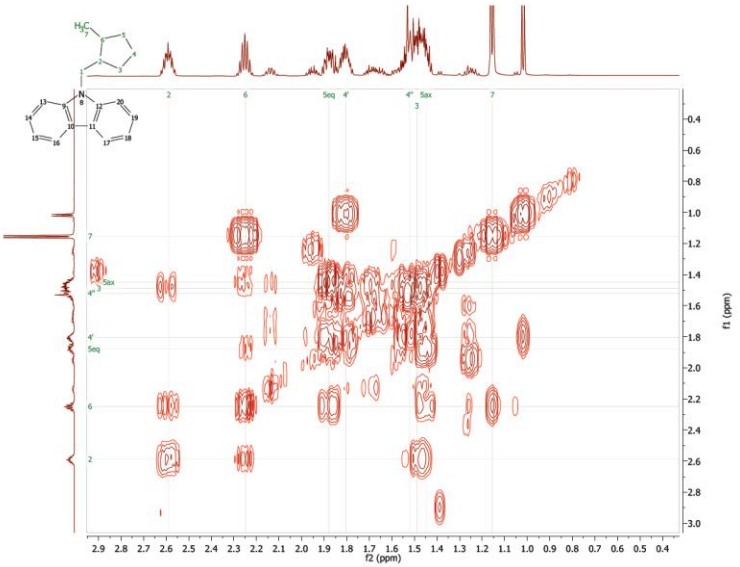

Figure 2.13. ^{1}H-^{1}H COSY trace of the major diastereomer ($CDCl_3$, rt, 600 MHz)

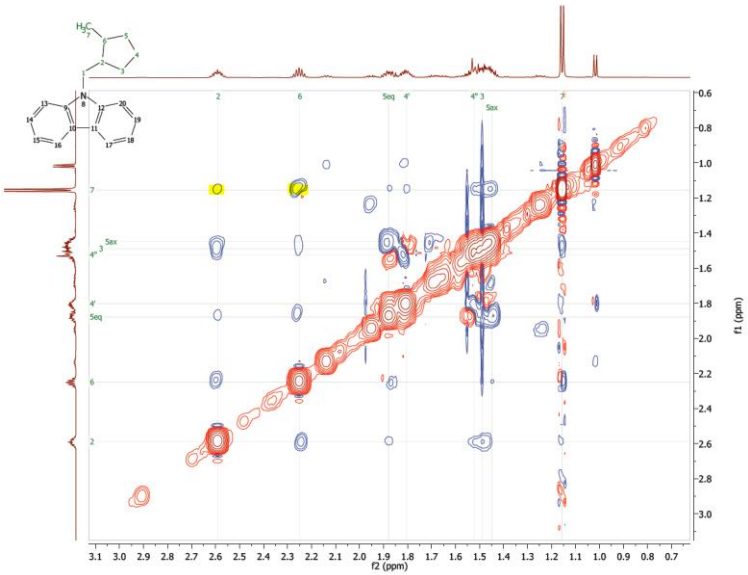

Figure 2.14. ^{1}H-^{1}H NOESY trace of the major (cis) diastereomer ($CDCl_3$, rt, 600 MHz). Couplings of the methyl resonances to the methine resonances are highlighted in yellow. The difference in the magnitude of correlation is consistent with the cis configuration in a 5-membered ring.

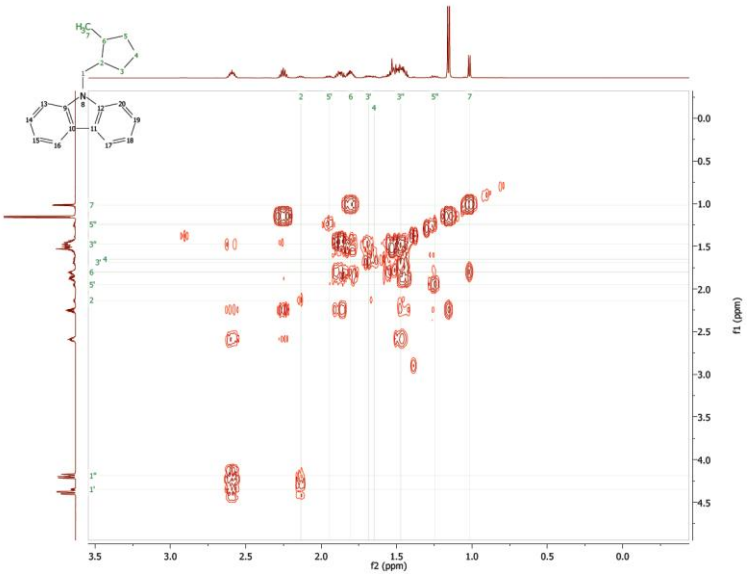

Figure 2.15. ^{1}H-^{1}H COSY trace of the minor diastereomer ($CDCl_3$, rt, 600 MHz).

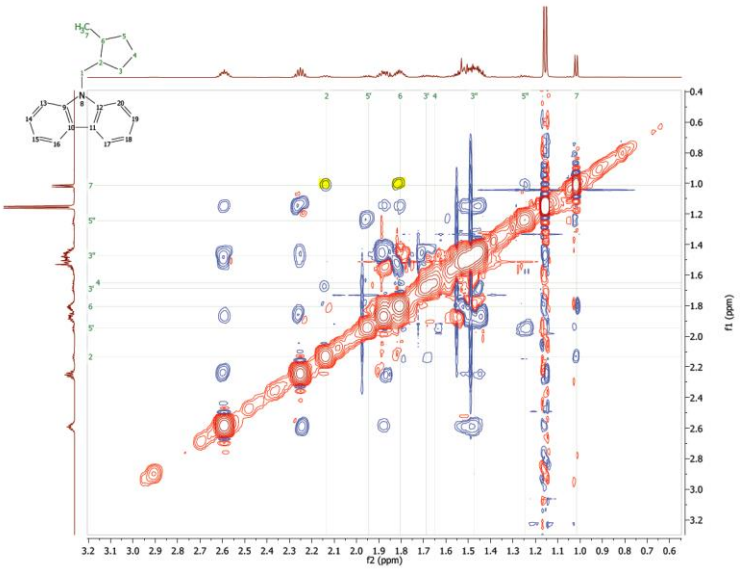

Figure 2.16. ^{1}H-^{1}H NOESY trace of the minor (trans) diastereomer ($CDCl_3$, rt, 600 MHz). Couplings of the methyl resonances to the methine resonances are highlighted in yellow. Approximately equal magnitude of correlation is consistent with the trans configuration in a 5-membered ring.

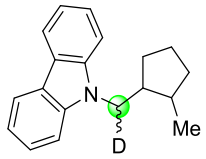

1:1 mixture at the indicated stereocenter

9-((2-methylcyclopentyl)methyl-d)-9H-carbazole. Following general coupling procedure with (*E*)-6-bromo-1-heptene-1-*d*, the title compound can be obtained as the mixture of diastereomers after column chromatography (hexanes→1% EtOAc/hexanes) as colorless solid. A typical run produces 60% of the coupling product according to calibrated GC analysis. NMR resonances of the major diastereomer are as follows.

^{1}H NMR (400 MHz, C_6D_6) δ 8.22–8.02 (m, 2H), 7.50–7.38 (m, 2H), 7.30–7.21 (m, 4H), 3.96–3.79 (m, 0.5H), 3.80–3.65 (m, 0.5H), 2.41–2.16 (m, 1H), 1.89–1.79 (m, 1H), 1.59–1.50 (m, 2H), 1.27–1.21 (m, 2H), 1.20–1.13 (m, 2H), 0.81 (d, J = 7.1 Hz, 3H).

^{13}C NMR (126 MHz, C_6D_6) δ 141.1, 125.8, 123.6, 120.8, 119.2, 109.3, 43.6 (t, J = 20.4 Hz), 43.0, 36.2, 33.3, 28.9, 22.7, 15.4.

^{2}H NMR (61 MHz, C_6D_6) δ 3.86, 3.70.

MS (ESI) m/z $(M)^+$ calcd for $C_{19}H_{20}DN$: 264.2, found: 264.1.

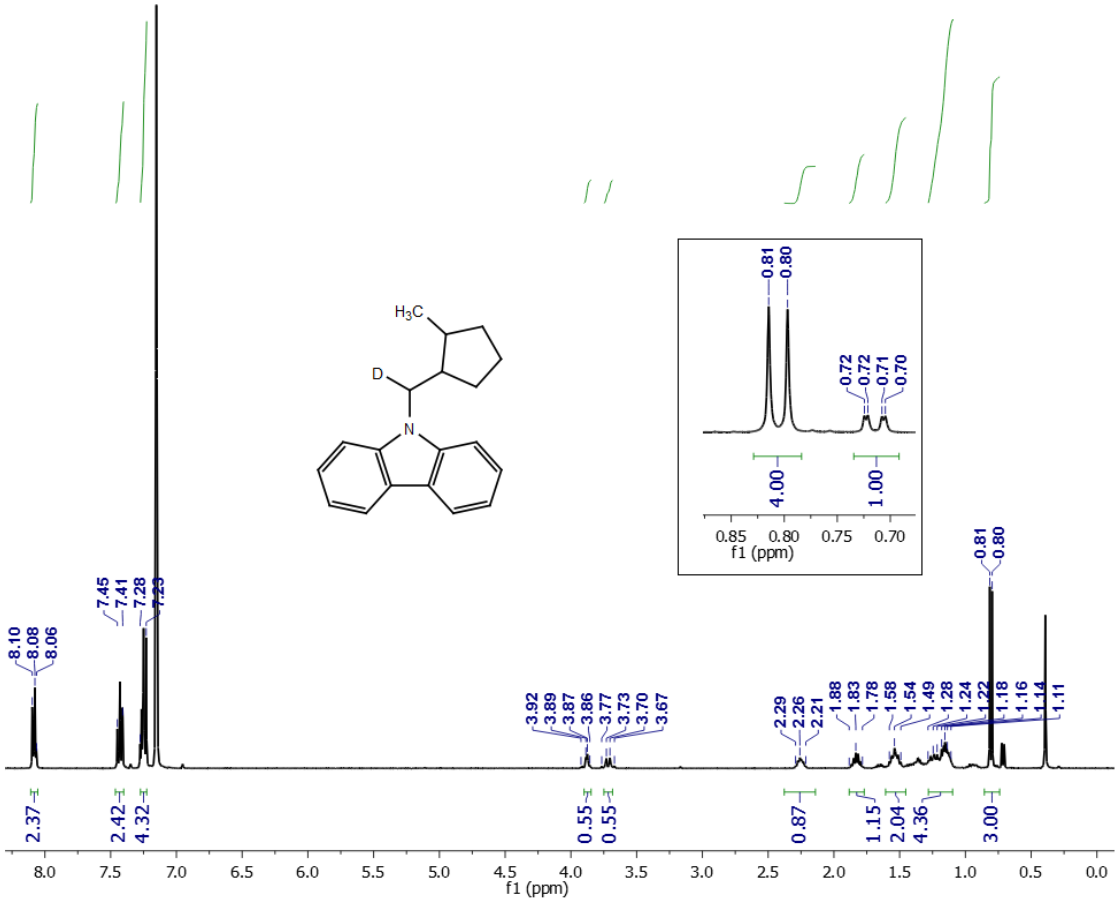

Figure 2.17. ^{1}H NMR spectrum of 9-((2-methylcyclopentyl)methyl-d)-9H-carbazole (C_6D_6, 400 MHz, rt).

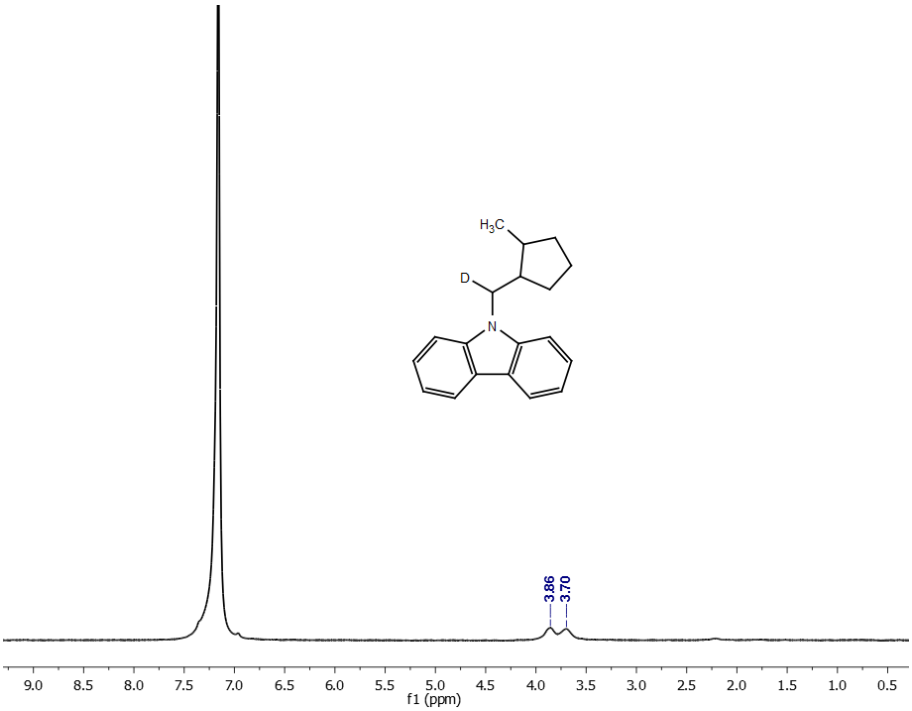

Figure 2.18. ^{2}H NMR spectrum of 9-((2-methylcyclopentyl)methyl-d)-9H-carbazole (C_6H_6, 61 MHz, rt).

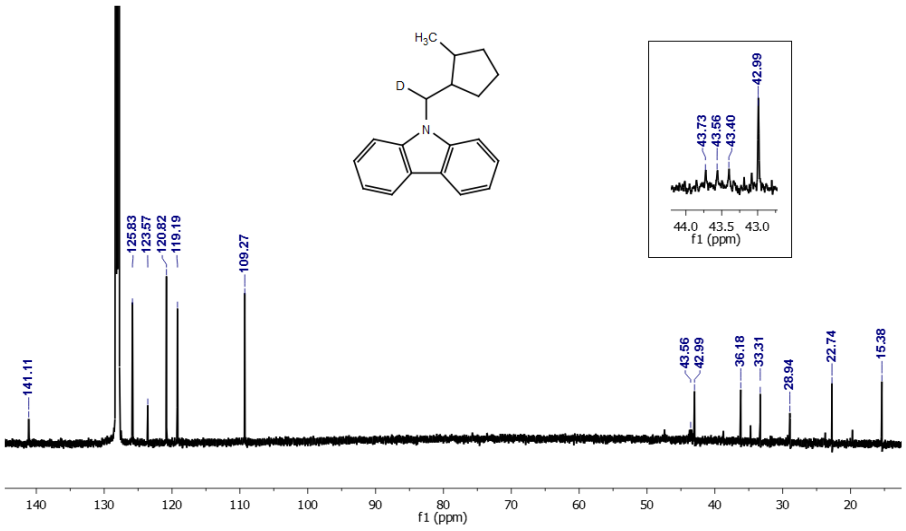

Figure 2.19. $^{13}C\{^{1}H\}$ NMR spectrum of 9-((2-methylcyclopentyl)methyl-d)-9H-carbazole (C_6D_6, 126 MHz, rt).

Procedure for the coupling of alkyl bromides in the absence of $[Cu(carb)_2]^-$

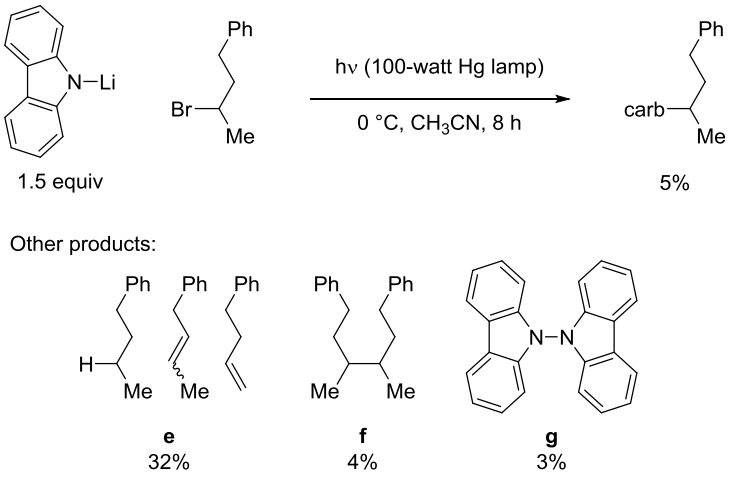

Li(carb) (0.2 mmol) and alkyl bromide (0.13 mmol) were added to a 4 mL borosilicate vial in the glovebox under nitrogen atmosphere. A magnetic stir bar and 4 mL CH_3CN were added to the vial. The mixture was capped and stirred for 5 minutes and the reaction vessel was fully submerged in an isopropanol bath kept at 0 °C with a cryostat. The mixture was irradiated with 100-watt Hg lamp while stirring for 8 hours, after which time it was diluted with a solution of dodecane in Et_2O or EtOAc. An aliquot was filtered through a short pad of silica gel (EtOAc eluent) and the sample was analyzed by GC. 9,9′-bicarbazyl (1.2 mg, 3% yield) was quantified by preparative TLC with hexanes.

Procedure for standard photolytic reactions at varying reaction concentrations

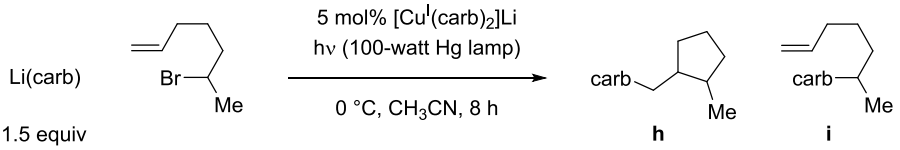

Stock solutions of $[Li(CH_3CN)_n][Cu(carb)_2]$, Li(carb), and 6-bromo-1-heptene were prepared in CH_3CN. Desired amounts of each were transferred to a 4 mL borosilicate vial,

and the mixture was diluted to a total volume of 4 mL with CH_3CN. The vial was subjected to the standard photolytic conditions, and the products were analyzed by GC. Five reaction concentrations were tested: 0.011 M, 0.022 M, 0.033 M, 0.044 M, and 0.055 M in a total of 4 mL of CH_3CN using 6-bromo-1-heptene as the limiting reagent. The data are summarized in **Table 2.2**; **h/i** values were calculated prior to rounding of yields of products **h** and **i**.

Table 2.2. Variation of yields of products **h** and **i** as a function of reaction concentrations.

[alkyl bromide] (mM)	Product **h** (dr)	Product **i**	**h/i**
11	70% (4:1)	6.7%	11
22	68% (4:1)	9.1%	7.6
33	62% (4:1)	10%	6.1
44	55% (4:1)	10%	5.5
55	51% (4:1)	10%	5.1

Procedure for stoichiometric coupling of $[Cu(carb)_2]^-$ with 2-bromo-4-phenylbutane

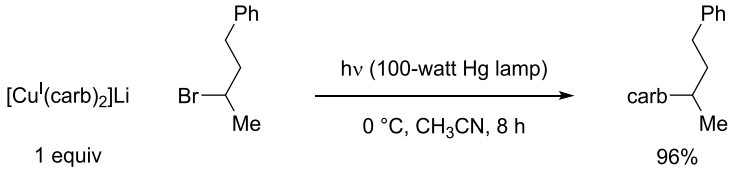

Stock solutions (0.0067 mmol mL^{-1}) of $[Li(CH_3CN)_n][Cu(carb)_2]$ and 2-bromo-4-phenylbutane were prepared in CH_3CN. Then, 0.0067 mmol of each reactant was added to a 4 mL vial containing a magnetic stir bar. The mixture was diluted to a total of 4 mL with CH_3CN. The mixture was capped and stirred for 5 minutes and the reaction vessel was fully submerged in an isopropanol bath kept at 0 °C with a cryostat. The mixture was irradiated with 100-watt Hg lamp while stirring for 8 hours, after which time it was diluted with a solution of dodecane in Et_2O or EtOAc. An aliquot was filtered through a short pad of silica

gel (EtOAc eluent) and the sample was analyzed by GC. Run 1: 95% yield. Run 2: 96% yield.

Procedure for the time-course analysis of reactions with and without [Cu(carb)$_2$]Li

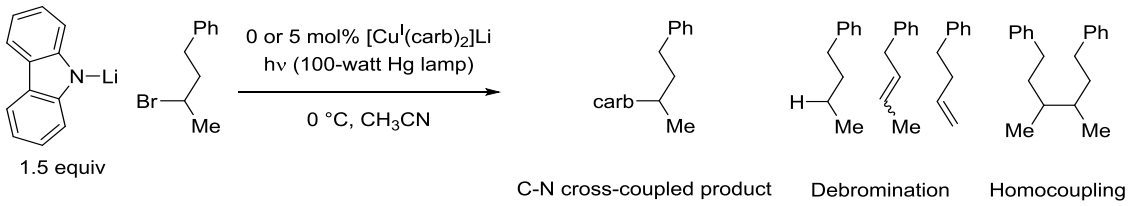

Stock solutions of [Li(CH$_3$CN)$_n$][Cu(carb)$_2$], Li(carb), and 2-bromo-4- phenylbutane were prepared in CH$_3$CN. Desired amounts of each were transferred to a 4 mL borosilicate vial as outlined in the general procedure, and the vial was diluted to a total of 4 mL with CH$_3$CN. The vial was subjected to the standard photolytic conditions for the specified amount of time, and the products were analyzed by GC. The data are summarized in **Table 2.3** and **Table 2.4**.

Table 2.3. Yields of debromination, homocoupling, and C–N cross-coupled product over time under catalysis conditions.

Time (min)	C-N cross-coupled product **(%)**	Debromination (%)	Homocoupling (%)
5	2.8	3.4	0.2
10	4.8	4.8	0.4
20	11	7.1	0.5
40	22	9	0.6
60	34	11	0.6
90	46	13	0.7

Table 2.4. Yields of debromination, homocoupling, and C–N cross-coupled product over time in the absence of copper.

Time (min)	C-N cross-coupled product **(%)**	Debromination (%)	Homocoupling (%)
5	0.7	4.3	1.1
10	1.2	6.8	1.3
20	1.7	11	1.9
40	2.7	16	2.1
60	2.9	19	2.4
90	3.4	22	3.6

2.4.3. Preparation of metal carbazolides

Preparation of $[Li(CH_3CN)_n][Cu(carb)_2]$

Mesitylcopper (183 mg, 1 mmol), carbazole (167 mg, 1 mmol), and Li(carb) (1 mmol) were added to a 20 mL scintillation vial in a nitrogen atmosphere glovebox. 10 mL of CH_3CN was added to the vial, and the mixture was stirred overnight at ambient temperature. The solution was filtered through a pad of Celite and the volatiles were removed in vacuo. Benzene (1 mL) was added to dissolve the oil and the residue was triturated with pentane (5 mL). The supernatant was decanted and benzene was added again. Benzene (1 mL) was added to the solid residue followed by pentane (5 mL) to precipitate the product. This process was repeated until a free-flowing, off-white powder was obtained. This powder was isolated atop a sintered glass frit and washed with benzene (3 × 5 mL) and pentane (3 × 5 mL). The solid can be further dried under vacuum overnight to yield the 400 mg of the title compound as one CH_3CN adduct as determined by ^1H NMR analysis. Spectroscopic data match the literature report.[2]

Preparation of Li(carb)

Carbazole (3.6 g, 22 mmol) was suspended in 150 mL of Et_2O in a 250 mL flask in a nitrogen-atmosphere glovebox. After cooling to –78 °C, *n*-butyllithium (1.6 M in hexanes, 15 mL) was added dropwise. The mixture was stirred at –78 °C for 3 h and allowed to warm to room temperature overnight. The white solid was collected atop a sintered glass frit, washed with cold Et_2O and pentane and then recrystallized in cold THF. The crystals were then dissolved in minimal acetonitrile and the solution was dried in vacuo to afford the title compound (2.9 g, 76% yield). Spectroscopic data match those reported in the literature.[24]

Preparation of $[Cu^{II}(carb)_3][K(benzo\text{-}15\text{-}crown\text{-}5)_2]$

A –70 °C suspension of $Cu(OTf)_2$ (36 mg, 0.05 mmol) in 2 mL THF was added dropwise to a pre-chilled stirring solution of K(carb) (3 equiv, 64 mg, 0.15 mmol) in 2 mL at –70 °C (temperature of coldwell when cooled by dry ice and acetone). The blue solution was allowed to stir for 5 h. The EPR spectrum of the crude mixture showed complete to the $[Cu^{II}(carb)_3]^-$. The solution was then filtered through a PTFE syringe filter, and a THF solution of benzo-15-crown-5 (2 equiv, 26 mg, 0.1 mmol) in 1 mL THF was added at –70 °C. The mixture was allowed to stand overnight at –70 °C to give a deep blue suspension containing a deep blue precipitate. The precipitate was collected while cold atop a sintered glass frit and washed with cold Et_2O to yield $[K(benzo\text{-}15\text{-}crown\text{-}5)_2][Cu^{II}(carb)_3]$ (30 mg, 26% yield). Crystals were grown by layering Et_2O onto the solution in THF at –70 °C. The blue solid was stored at -30 °C.

2.4.4. Procedures for freeze-quench EPR studies

Irradiation of $[Cu^{I}(carb)_2]Li$ and 2-bromo-4-phenylbutane in an EPR tube

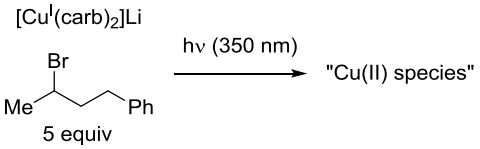

$[Li(CH_3CN)][Cu(carb)_2]$ (4.4 mg, 0.01 mmol) and 2-bromo-4-phenylbutane (10 mg, 0.05 mmol) were added to a 4 mL vial. The mixture was dissolved in 0.3 mL butyronitrile, and the resulting solution was transferred to an EPR tube. The EPR tube was sealed and cooled to –78 °C. The EPR tube was irradiated in the Luzchem photoreactor (350 nm) while being introduced to a quartz Dewar filled with liquid nitrogen. Irradiation of the freezing solution proceeded for approximately 15 seconds. Simulated parameters are as follows: g = [2.445, 2.060, 1.994], isotropic linewidth (Gaussian line shape, FWHM = 10 mT), A_{Cu} (MHz) = [75, 1, 1].

Detection of $[Cu^{II}(carb)_3]Li$ in a catalytic reaction mixture

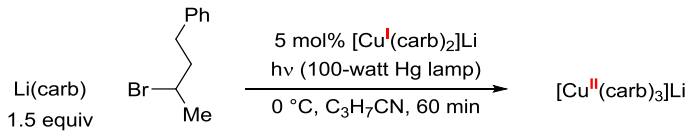

A 4 mL solution of the standard reaction mixture containing $[Li(CH_3CN)][Cu(carb)_2]$ (0.0067 mmol), Li(carb) (0.2 mmol), and the alkyl bromide (0.13 mmol) was prepared in a 4 mL borosilicate glass vial according to the standard procedure using butyronitrile as the solvent. A portion of the resulting solution (300 μL) was transferred to an EPR tube. The tube was sealed and cooled to 0 °C, and irradiated with a 100-watt Hg lamp at 0 °C.

Alternatively, an aliquot (0.1 mL) of the standard reaction mixture in CH_3CN in a 4 mL borosilicate vial that was irradiated for 1 h was transferred to a pre-cooled EPR tube containing butyronitrile (0.2 mL) under N_2. The EPR tube was briefly shaken and cooled to 77 K. Simulation parameters are as follows: g = [2.318, 2.058, 2.050]; HStrain (MHz) = [120, 5, 5]; A_{Cu} (MHz) = [350, 25, 21] A_{3N} (MHz) = [50, 35, 35].

Generation and detection of $[Cu^{II}(carb)_3]Li$ via metallation

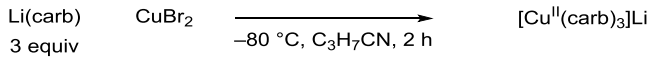

A pre-chilled solution of $CuBr_2$ (2.2 mg, 0.01 mmol) in 1 mL acetonitrile was added dropwise to a pre-chilled slurry of Li(carb) (5.3 mg, 0.03 mmol) in the glovebox. The deep blue solution was allowed to stir for 5 min before transferring an aliquot to a solution of butyronitrile in dry ice and acetone bath. The solution was then transferred to an EPR tube.

Detection of $[Cu^{II}(carb)_3]Li$ via chemical oxidation of $[Cu^{I}(carb)_2]Li$

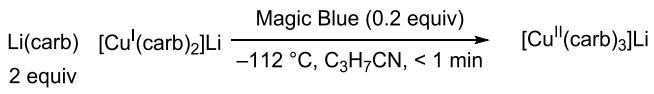

$[Li(CH_3CN)][Cu(carb)_2]$ (10.0 mg, 0.023 mmol) and Li(carb) (8 mg, 0.046 mmol) were mixed in 200 μL of butyronitrile, added to an EPR tube, and frozen at 77 K. To this frozen layer was added a 200 μL solution of tris(4-bromophenyl)ammoniumyl hexachloroantimonate ("Magic Blue", 3.4 mg, 0.0042 mmol) in butyronitrile. The solutions were allowed to mix briefly (~5 s) in thawing butyronitrile and frozen again.

2.4.5. Procedures for UV-vis studies

Determination of molar absorptivity of $[Cu^{II}(carb)_3]Li$ at 580 nm

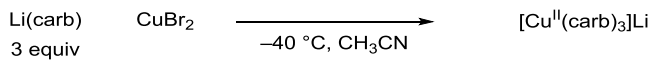

A 20 mL vial was charged with Li(carb) (5.5 mg, 0.030 mmol) and a magnetic stir bar. Next, CH_3CN (9.0 mL) was added to the vial, and the solution was cooled to thawing CH_3CN temperature. A separate vial was charged with $CuBr_2$ (6.6 mg, 0.030 mmol) and CH_3CN (3.0 mL). Then, 1 mL of the resulting green solution of $CuBr_2$ (0.010 mmol) was added dropwise to the thawing CH_3CN solution of Li(carb). After completed addition, the deep blue solution was stirred vigorously at thawing CH_3CN temperature for approximately 30 minutes. The solution was transferred into a pre-chilled 1 cm pathlength quartz cuvette. The cuvette was capped and quickly inserted into the –40 °C UV-vis sample holder. The molar absorptivity at 580 nm was found to be approximately 1100 M^{-1} cm^{-1}.

Table 2.5. Measured molar absorptivity at 580 nm of $[Cu^{II}(carb)_3]Li$ in CH_3CN.

Concentration (mM)	Absorbance	Molar absorptivity (M^{-1} cm^{-1})
0.103	1.170	1140
0.100	1.092	1092
0.083	1.028	1233
0.050	0.608	1216

Detection of $[Cu^{II}(carb)_3]Li$ during catalysis

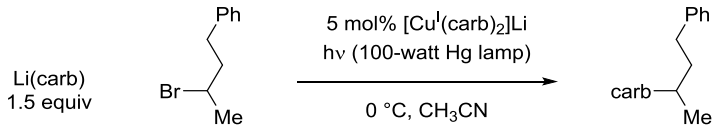

A 4 mL CH_3CN solution of the standard reaction mixture containing $[Li(CH_3CN)][Cu(carb)_2]$ (2.9 mg, 0.0067 mmol), Li(carb) (34 mg, 0.19 mmol), and 2-bromo-4-phenylbutane (28 mg, 0.13 mmol) was prepared in a quartz cuvette containing a magnetic stir bar. The reaction mixture was allowed to cool for 10 minutes in the dark at 0 °C in an ice bath. Then the mixture was irradiated with a 100-watt Hg lamp while stirring, and UV-vis spectra were collected at 0 °C at various times after irradiation.

Detection of $[Cu^{II}(carb)_3]Li$ via chemical oxidation of $[Cu^{I}(carb)_2]Li$

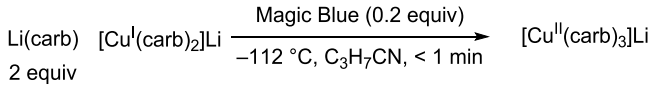

In a glovebox, a 4 mL butyronitrile solution containing $[Li(CH_3CN)][Cu(carb)_2]$ (0.037 mmol) and Li(carb) (0.074 mmol) was prepared in a quartz cuvette containing a magnetic stir bar. The cuvette was then sealed with a septum. Another solution containing tris(4-bromophenyl)ammoniumyl hexachloroantimonate ("Magic Blue", 0.012 mmol) was dissolved in 0.2 mL butyronitrile and taken up into a 1 mL Hamilton sample locked syringe, and the needle was pierced through a septum to prevent the introduction of air. The cuvette was cooled to –80 °C in the UV-vis sample holder. Next, the sample lock was opened and the solution of Magic Blue was introduced into the mixture with vigorous stirring. The stirring was stopped and the sample was allowed to stabilize before a spectrum was acquired.

Determination of the molar absorptivity of Li(carb)

A 10 mM solution of Li(carb) in CH_3CN was made, and this solution was used as a stock to generate lower concentration solutions of Li(carb). Each solution was transferred via pipette into a 1 mm path length cuvette and absorption spectra were acquired at room

temperature for each concentration. Below 0.4 mM, a solution of Li(carb) in CH_3CN does not absorb 365 nm. The molar absorptivity at 365 nm for concentrations of Li(carb) greater than 0.4 mM was found to be 2200 M^{-1} cm^{-1}.

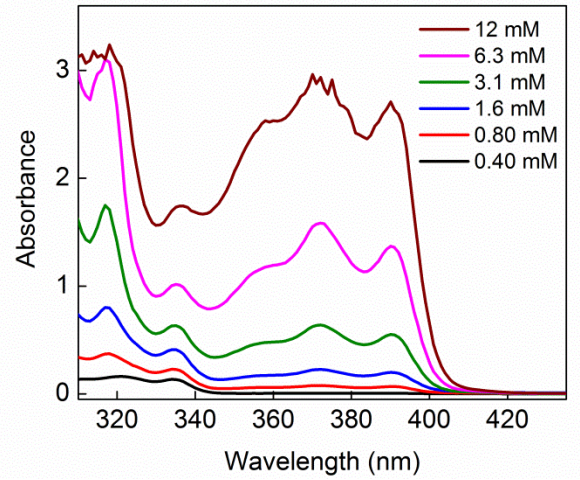

Figure 2.20. UV-vis spectra of Li(carb) in a 1 mm cuvette.

2.4.6. Actinometry

Calibration of light intensity

The Hatchard-Parker method was used to make a 0.006 M potassium ferrioxalate solution in 0.1 N H_2SO_4.[25] A 4 mL ferrioxalate solution in a quartz cuvette was then irradiated at 0 °C for 40 s in three separate runs using a 365 nm LED (Thorlabs, M365L2) and a focusing lens. A photon flux of 1.7×10^{-6} einstein min^{-1} was calculated.

Determination of quantum yield of model reaction.

A 4 mL CH_3CN solution of the standard mixture containing $[Li(CH_3CN)][Cu(carb)_2]$ (0.0067 mmol), Li(carb) (0.2 mmol), 2-bromo-4-phenylbutane (0.13 mmol) was prepared in

a 1 cm path length quartz cuvette containing a magnetic stir bar. The reaction mixture was allowed to cool to 0 °C with an internal cooling loop in a cuvette holder. Then, the mixture was irradiated with the 365 nm LED while stirring. After irradiation, the reaction mixture was diluted with Et_2O and dodecane as an internal standard. An aliquot was filtered through a short pad of silica gel (EtOAc eluent) and the sample was injected for GC analysis. The quantum yield (Φ) was, by dividing the amount of electrophile consumed by the total amount of photons absorbed by the mixture, to be 0.099.

2.4.7. Procedures for Stern-Volmer analysis

Quenching of $[Cu^{I}(carb)_2]Li^*$ by an alkyl bromide

$[Li(CH_3CN)][Cu(carb)_2]$ was diluted in CH_3CN to make a 0.00335 M solution. Also, 2-bromo-4-phenylbutane was diluted in CH_3CN to make 100, 200, 400, 600, 700, and 800 mM solutions. In 4 mL vials, a 250 μL aliquot of the solution containing $[Li(CH_3CN)][Cu(carb)_2]$ was mixed with a 250 μL aliquot of either CH_3CN or one of the solutions containing the alkyl bromide, such that the concentration of $[Li(CH_3CN)][Cu(carb)_2]$ in each solution was equal to the standard reaction concentration, 0.0017 M. The solutions were pipetted into cuvettes (1 mm path length). The lifetime of a non-emissive excited state of $[Li(CH_3CN)][Cu(carb)_2]$ as a function of electrophile concentration was measured by transient absorbance spectroscopy (λ_{pump} = 355 nm, λ_{probe} = 580 nm); the data are summarized in **Table 2.6**. The lifetime of the short-lived, emissive excited state of $[Li(CH_3CN)][Cu(carb)_2]$ was measured at the picosecond (ps) time scale using luminescence spectroscopy, and was found to be 590 ps. Data were analyzed using Matlab R2014A with the default curve fitting function.

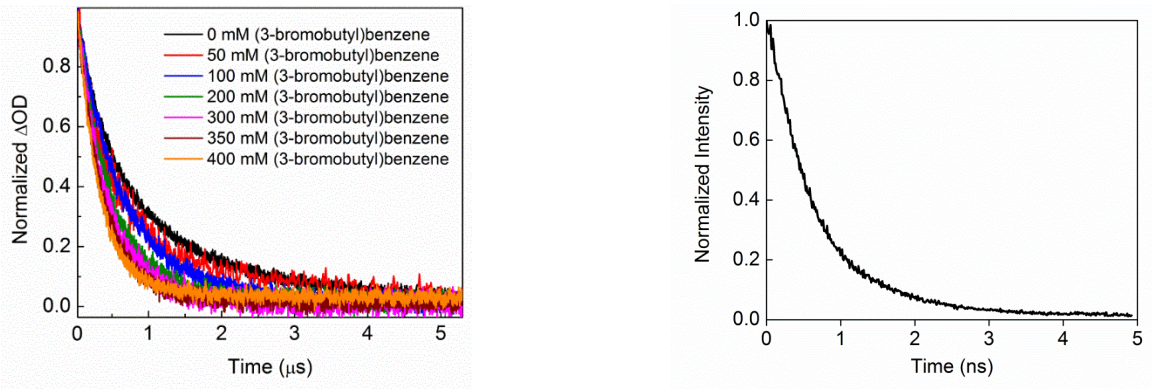

Figure 2.21. Excited state properties of [Cu(carb)$_2$]Li. Left: Transient absorbance decays in the presence of varying amounts of (3-bromobutyl)benzene (synonymous with 2-bromo-4-phenylbutane); right: luminescence decay of the emissive excited state of [Cu(carb)$_2$]Li.

Table 2.6. The lifetime of [Cu^{I}(carb)$_2$]Li* in the presence of 2-bromo-4-phenylbutane.

2-bromo-4-phenylbutane (mM)	Lifetime (ns)
0	910
50	760
100	660
200	481
300	410
350	370
400	320

Quenching of Li(carb)* by an alkyl bromide

Li(carb) (86.6 mg, 0.5 mmol) was diluted in a 10 mL volumetric flask with acetonitrile to make 10 mL of a 0.05 M solution (the concentration in the catalytic reactions). In four other volumetric flasks, the same amount of Li(carb) was weighed out, but only ~5 mL of CH_3CN was added. Then, 2-bromo-4-phenybutane was added to the Li(carb) solutions *via* syringe to make 50, 100, 200, or 400 mM solutions of 2-bromo-4-phenybutane in 10 mL CH_3CN, and CH_3CN was added to the mark. For each run, one of these solutions was

syringed into the Harrick flow cell (100 μm path length) until there were no gas bubbles, and flowed through with a syringe pump while fluorescence measurements were being collected. After each run, the flow cell was cleaned and dried under vacuum, and the next solution was syringed into the cell.

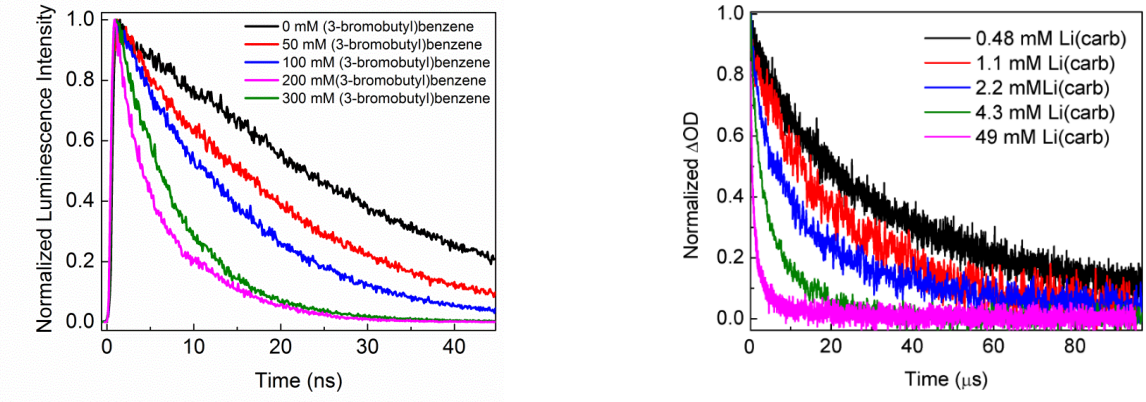

Figure 2.22. Excited state properties of Li(carb). Left: Luminescence decays of Li(carb) in the presence of varying amounts of (3-bromobutyl)benzene (synonymous with 2-bromo-4-phenylbutane); right: transient absorbance decays of Li(carb) at varying concentrations.

Table 2.7. The lifetime of Li(carb)* in the presence of 2-bromo-4-phenylbutane.

2-bromo-4-phenylbutane (mM)	Lifetime (ns)
0	31
50	19
100	14
200	7.1
300	5.8

Self-quenching of Li(carb)*

Li(carb) (43.3 mg, 0.25 mmol) was dissolved in 5 mL of CH_3CN to make a 0.05 M solution (the concentration in the catalytic reactions). This solution was serially diluted to

make 4.3, 2.2, 1.1, and 0.50 mM solutions. The solutions were pipetted into cuvettes with a path length of 1 mm. The excited state lifetime of Li(carb) was measured by transient absorbance spectroscopy (λ_{pump} = 355 nm, λ_{probe} = 580 nm). Data were analyzed using Matlab R2014A with the default curve fitting function. The rate constant of self-quenching was found to be 2.0×10^7 M^{-1} s^{-1}. It is important to note that in the presence of electrophile quencher, this long-lived, non-emissive excited state was not observed, and SET appears to proceed from the fluorescent state at a rate faster than that of intersystem crossing.

Determination of chain length

The quenching fraction (*Q*) can be defined as the ratio of the rate at which the excited state species (Li(carb)) is quenched productively (by 2-bromo-4-phenybutane) to the sum of the rates of all the other relaxation processes which are available to the excited state. However, the unusual self-quenching behavior of Li(carb) permits only the estimation of the upper limit for *Q*. Thus,

$$Q \leq \frac{k_q[\mathrm{RBr}]}{\tau_0^{-1} + k_q[\mathrm{RBr}]} = \frac{(4.9 \times 10^8 \mathrm{M^{-1}s^{-1}})(0.0325\ \mathrm{M})}{(3.1 \times 10^{-8}\mathrm{s}) + (4.9 \times 10^8 \mathrm{M^{-1}s^{-1}})(0.0325\ \mathrm{M})} = 0.33$$

The chain length is the ratio of the quantum yield to the quenching fraction. From our calculated values, a lower limit can be determined.

$$Chain\ length\ \geq \frac{\Phi}{Q} = \frac{0.099}{0.33} = 0.30$$

2.4.8. Reactivity of $[Cu^{II}(carb)_3]Li$

Thermal decomposition of $[Cu^{II}(carb)_3]Li$

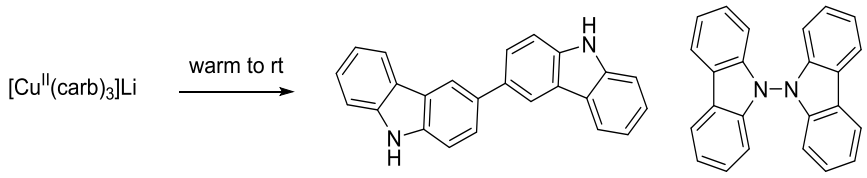

A freshly prepared CH_3CN solution of $Li[Cu^{II}(carb)_3]$ in acetone and dry ice bath was allowed to warm to room temperature overnight. The mixture was then concentrated in vacuo and the residue was loaded on a 20 cm × 20 cm Merck TLC plate. Two of many UV-active bands after developing the TLC in hexanes were identified as the commercially available 9,9′-bicarbazyl and 3,3′-bicarbazole by co-spotting and ^1H NMR spectroscopy.

Hydrogen atom transfer from TEMPO–H to $[Cu^{II}(carb)_3]Li$

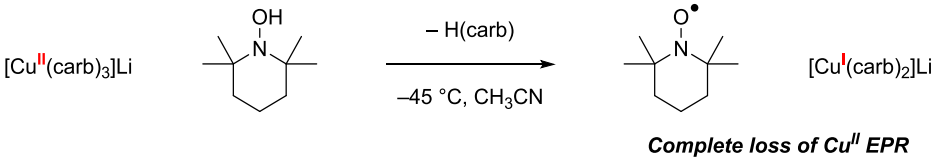

A freshly prepared solution of $[Cu^{II}(carb)_3]Li$ was prepared in thawing CH_3CN. A cold solution of 2,2,6,6-tetramethylpiperidin-1-ol[26] (TEMPO–H, 1 equiv) in CH_3CN was added to the cold solution of $[Cu^{II}(carb)_3]Li$, and the mixture was allowed to stir in thawing CH_3CN temperature for 30 min. A portion of the reaction mixture was transferred to an EPR tube and diluted with butyronitrile for X-band EPR measurement at 77 K. The only EPR active signal was that of 2,2,6,6-tetramethylpiperidine-1-oxyl (TEMPO•), and signals

corresponding to a Cu^{II} species were absent (**Figure 2.23**, left). The analogous reaction conducted in CD_3CN at –45 °C shows the appearance of $[Cu^{I}(carb)_2]^-$ signals by ^1H NMR spectroscopy, consistent with the delivery of an H atom (**Figure 2.23**, right).

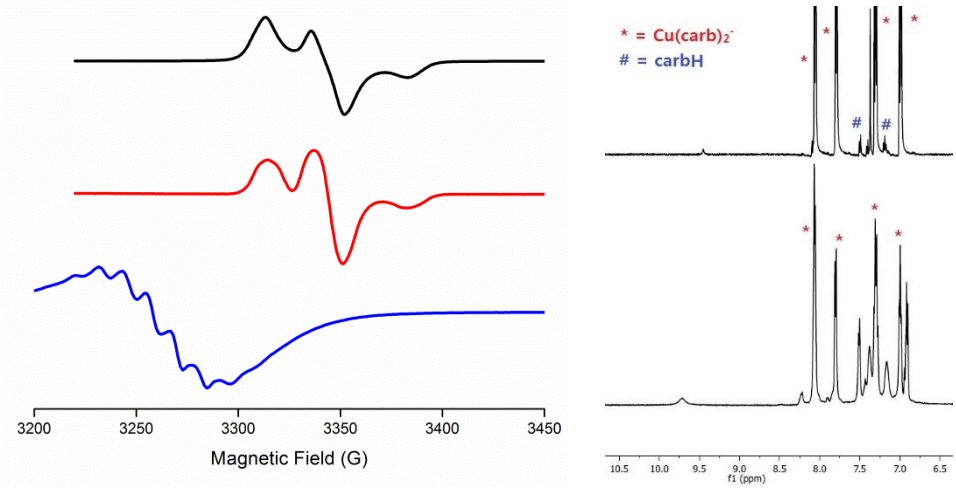

Figure 2.23. Hydrogen atom transfer to $[Cu^{II}(carb)_3]Li$. Left: EPR spectra (9.4 GHz, 77 K, butyronitrile); black trace: TEMPO•; red trace: a mixture of $[Cu^{II}(carb)_3]Li$ and TEMPO•; blue trace: freshly prepared $[Cu^{II}(carb)_3]Li$. Right: ^1H NMR spectra (500 MHz, –40 °C, CD_3CN); top: mixture of carbH and $[Cu^{I}(carb)_2]Li$; bottom: mixture of $[Cu^{II}(carb)_3]Li$ and TEMPO–H.

2.4.9. Computational methods

The Orca 3.0.1 program was used for all calculations.[27] All optimizations and energy calculations were conducted with tight convergence criteria using the M06-L functional[28] and def2-TZVP basis set.[29] Open- and closed-shell species were modeled within the unrestricted and restricted Kohn-Sham formalisms, respectively. All geometry optimizations were conducted without symmetry constraints using gradient methods. Ground state

geometries were verified as true minima by the absence of imaginary frequencies. All energies reported are Gibbs free energies at 298.15 K and include translational, rotational, vibrational, and solvation energy contributions. Solvation was treated with the conductor-like screening model, using default parameters for acetonitrile in all cases.[30] For $[Cu^{II}(carb)_3]^-$, the Loewdin spin density was derived from a constrained optimization where the N–Cu–N angles and the C(1)–C(9a)–N–Cu dihedrals along each carbazole were constrained to match that of the experimentally determined solid-state crystal structure. The energy was derived from an unconstrained optimization. Solvation was treated with the conductor-like screening model, using values of $\varepsilon = 20$ and $\eta = 1.38$ for butyronitrile.

Table 2.8. Free energies of computed molecules.

Compound	Gibbs free energy (Hartree)
$[Cu^{I}(carb)_2]^-$	-2674.3593
$Cu^{II}(carb)_2$	-2674.2012
$[Cu^{II}(carb)_2]^-$	-3191.1839
$[Cu^{II}(carb)_2(i\text{-Pr})]^-$	-2792.7926
$[carb]^-$	-516.9644
(carb)•	-516.8096
(*i*-Pr)•	-118.4381

Kinetic simulations

All simulations were performed using COPASI software using a unicompartmental biochemical model. The following table summarizes the parameters used for the kinetic simulations.

Table 2.9. Input parameters for the cyclization under photochemical conditions.

Description	Reaction	Rate
Generation of radical pairs	$\xrightarrow{h\nu}$ • R + • carb	Variable
Carbazole dimerization	• carb + • carb $\longrightarrow$ carb−carb	10^{10} $M^{-1}s^{-1}$
Uncyclized alkyl radical homocoupling	• R + • R $\longrightarrow$ R−R	10^{10} $M^{-1}s^{-1}$
Uncyclized product formation without copper	• R + • carb $\longrightarrow$ R−carb	10^{10} $M^{-1}s^{-1}$
Carbazole radical scavenging by Cu^{I}	• carb + $[Cu^{I}(carb)_2]Li$ $\longrightarrow$ $[Cu^{II}(carb)_3]Li$	10^{9} $M^{-1}s^{-1}$
Uncyclized product formation with Cu^{II}	• R + $[Cu^{II}(carb)_3]Li$ $\longrightarrow$ R−carb + $[Cu^{I}(carb)_2]Li$	10^{9} $M^{-1}s^{-1}$
Cyclization	• R $\longrightarrow$ • R^1	10^{5} s^{-1}
Cyclized product formation with Cu^{II}	• R^1 + $[Cu^{II}(carb)_3]Li$ $\longrightarrow$ R^1−carb + $[Cu^{I}(carb)_2]Li$	10^{9} $M^{-1}s^{-1}$
Cyclized product formation without Cu	• R^1 + • carb $\longrightarrow$ R^1−carb	10^{10} $M^{-1}s^{-1}$
Cyclized alkyl radical homocoupling	• R^1 + • R^1 $\longrightarrow$ R^1−R^1	10^{10} $M^{-1}s^{-1}$
Cyclized and uncyclized radical homocoupling	• R^1 + • R $\longrightarrow$ R−R^1	10^{10} $M^{-1}s^{-1}$

2.4.10. X-ray crystallographic data

$[Cu^{II}(carb)_3][K(18\text{-crown-6})(THF)]$

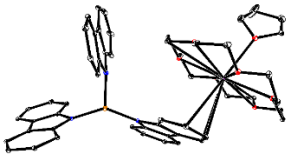

The X-ray diffraction data were of poor quality and hence only sufficient for establishing overall atomic connectivity. Only unit cell parameters are shown below.

Table 2.10. Crystal data for $[Cu^{II}(carb)_3][K(18\text{-crown-6})(THF)]$.

Identification code	$[Cu^{II}(carb)_3][K(18\text{-crown-6})(THF)]$
Empirical formula	$C_{52}H_{56}N_3O_7KCu$
Formula weight	937.63
Temperature/K	100.01
Crystal system	monoclinic
Space group	$P2_1/n$
a/Å	13.2219(5)
b/Å	18.0111(6)
c/Å	19.3667(8)
α/°	90
β/°	96.1241(14)
γ/°	90
Volume/Å^3	4585.7(3)
Z	4
ρ_{calc}g/cm^3	1.358
μ/mm^{-1}	0.624
F(000)	1972.0
Radiation	MoKα (λ = 0.71073)
2Θ range for data collection/°	4.524 to 63.522
Index ranges	$-19 \leq h \leq 19$, $-26 \leq k \leq 26$, $-28 \leq l \leq 27$
Reflections collected	136556
Independent reflections	14447 [R_{int} = 0.0742, R_{sigma} = 0.0733]

$[Cu^{II}(carb)_3][K(benzo\text{-}15\text{-}crown\text{-}5)_2]$

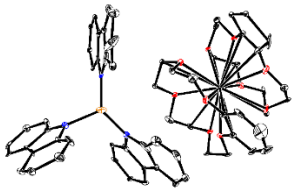

The X-ray diffraction data were of poor quality and hence only sufficient for establishing overall atomic connectivity. Only unit cell parameters are shown below.

Table 2.11. Crystal data for $[Cu^{II}(carb)_3][K(benzo\text{-}15\text{-}crown\text{-}5)_2]$.

Identification code	$[Cu^{II}(carb)_3][K(benzo\text{-}15\text{-}crown\text{-}5)_2]$
Empirical formula	$C_{64}H_{64}CuKN_3O_{10}$
Formula weight	1137.87
Temperature/K	100.0
Crystal system	monoclinic
Space group	P2/c
a/Å	22.677(3)
b/Å	13.8859(14)
c/Å	20.631(2)
α/°	90
β/°	102.949(7)
γ/°	90
Volume/Å^3	6331.2(12)
Z	15
ρ_{calc}g/cm^3	1.554
μ/mm^{-1}	2.223
F(000)	3076.0
Radiation	CuKα (λ = 1.54178)
2Θ range for data collection/°	6.364 to 160.548
Index ranges	$-27 \leq h \leq 27$, $-17 \leq k \leq 16$, $-25 \leq l \leq 22$
Reflections collected	177608
Independent reflections	12678 [R_{int} = 0.2899, R_{sigma} = 0.1706]

$[Cu^{II}(carb)_4][K(15\text{-}crown\text{-}5)_2]_2[C_4H_{10}O]_4$

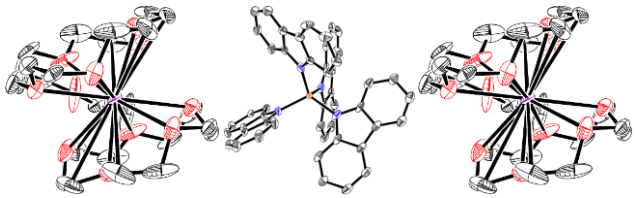

The X-ray diffraction data were of poor quality and hence only sufficient for establishing overall atomic connectivity. Solvent molecules are omitted for clarity. Only unit cell parameters are shown below.

Table 2.12. Crystal data for $[Cu^{II}(carb)_4][K(15\text{-crown-}5)_2]_2[C_4H_{10}O]_4$.

Identification code	$[Cu^{II}(carb)_4][K(15\text{-crown-}5)_2]_2[C_4H_{10}O]_4$
Empirical formula	$C_{104}H_{152}CuK_2N_4O_{24}$
Formula weight	1984.11
Temperature/K	99.98
Crystal system	tetragonal
Space group	$I4_1/acd$
a/Å	23.8760(8)
b/Å	23.8760(8)
c/Å	32.8852(12)
α/°	90
β/°	90
γ/°	90
Volume/$Å^3$	18746.6(11)
Z	24
$\rho_{calc}g/cm^3$	1.2866
μ/mm^{-1}	1.722
F(000)	7686.9
Radiation	Cu Kα (λ = 1.54178)
2Θ range for data collection/°	7.4 to 158.5
Index ranges	$-28 \leq h \leq 28$, $-28 \leq k \leq 30$, $-39 \leq l \leq 38$
Reflections collected	143587
Independent reflections	4528 [R_{int} = 0.1708, R_{sigma} = 0.0477]

$[Cu^{II}(carb)_3][K(THF)_6]$

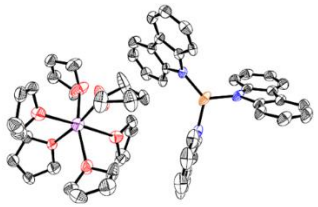

Table 2.13. Crystal data and structure refinements for $[Cu^{II}(carb)_3][K(THF)_6]$.

Identification code	$[Cu^{II}(carb)_3][K(THF)_6]$
Empirical formula	$C_{60}H_{72}CuKN_3O_6$
Formula weight	1033.9

Temperature/K	100.05
Crystal system	monoclinic
Space group	$P2_1/n$
a/Å	12.9317(5)
b/Å	22.3762(9)
c/Å	18.9484(6)
α/°	90
β/°	104.763(2)
γ/°	90
Volume/Å^3	5301.9(3)
Z	6
ρ_{calc}g/cm^3	1.288
μ/mm^{-1}	1.709
F(000)	2172.0
Radiation	CuKα (λ = 1.54178)
2Θ range for data collection/°	6.234 to 136.854
Index ranges	$-15 \leq h \leq 14$, $-26 \leq k \leq 26$, $-22 \leq l \leq 22$
Reflections collected	57323
Independent reflections	9697 [R_{int} = 0.1553, R_{sigma} = 0.1076]
Data/restraints/parameters	9697/0/650
Goodness-of-fit on F^2	1.043
Final R indexes [I>=2σ (I)]	R_1 = 0.1065, wR_2 = 0.2568
Final R indexes [all data]	R_1 = 0.1845, wR_2 = 0.3014
Largest diff. peak/hole / e Å^{-3}	1.19/-0.99

Table 2.14. Fractional Atomic Coordinates (×10^4) and Equivalent Isotropic Displacement Parameters (Å^2×10^3) for [Cu^{II}(carb)$_3$][K(THF)$_6$]. U_{eq} is defined as 1/3 of the trace of the orthogonalized U_{IJ} tensor.

Atom	*x*	*y*	*z*	U(eq)	Atom	*x*	*y*	*z*	U(eq)
Cu01	4786.3(8)	5173.8(6)	2403.2(5)	46.4(4)	C019	7544(7)	4032(4)	3943(4)	53(2)
K002	155.6(14)	6827.8(8)	2586.4(10)	56.2(5)	C01A	-273(6)	8494(3)	3917(5)	56(2)
N003	3640(4)	4749(2)	2613(2)	27.6(12)	C01B	3448(6)	6519(3)	4137(4)	49.0(19)
O004	2166(4)	6796(2)	3057(3)	48.4(13)	C01C	-1312(6)	8185(3)	3617(4)	50(2)
O005	-1816(4)	6897(2)	1959(3)	53.1(14)	C01D	-3206(6)	6635(4)	921(4)	51(2)
O006	724(4)	7682(2)	1949(3)	55.6(15)	C01E	3795(6)	6253(5)	1082(4)	58(2)
N007	4909(4)	6011(3)	2337(3)	43.7(16)	C01F	4340(6)	7451(4)	1465(4)	57(2)
O008	-10(4)	7497(2)	3587(4)	72.9(19)	C01G	7615(7)	4828(4)	625(4)	59(2)
N009	6048(4)	4818(3)	2281(3)	38.9(14)	C01H	310(7)	8261(4)	1768(4)	52(2)
O00A	213(5)	5984(3)	3441(3)	75(2)	C01I	-2981(7)	7298(4)	924(5)	64(2)
C00B	3364(5)	4737(3)	3280(3)	28.4(14)	C01J	3402(7)	7182(4)	4060(4)	57(2)
C00C	2868(5)	4412(3)	2140(3)	29.5(14)	C01K	538(7)	8046(4)	3803(5)	58(2)
C00D	5478(5)	6373(3)	2893(3)	37.1(17)	C01L	3700(7)	7298(5)	781(4)	64(3)
C00E	2100(5)	4189(3)	2483(3)	30.7(14)	C01M	3441(7)	6724(5)	600(4)	65(3)
O00F	158(6)	6072(3)	1667(3)	91(2)	C01N	-460(7)	5480(4)	3290(5)	68(3)
C00G	2432(5)	4405(3)	3231(3)	32.1(15)	C01O	-1150(7)	5547(4)	3839(5)	59(2)
C00H	6513(5)	4868(3)	1692(3)	38.1(17)	C01P	174(7)	8314(4)	953(4)	59(2)
C00I	6795(6)	4508(3)	2805(4)	38.6(17)	C01Q	-471(7)	5874(4)	4459(4)	60(2)
C00J	2802(5)	4274(3)	1414(3)	34.4(16)	C01R	-1045(6)	7537(4)	3727(5)	58(2)

C00K	6090(5)	6201(3)	3587(3)	36.5(16)	C01S	-2412(7)	7433(4)	1704(4)	61(2)
C00L	6561(5)	6641(3)	4072(4)	39.3(17)	C01T	1012(8)	7904(5)	813(4)	69(3)
C00M	5390(5)	6980(3)	2709(4)	37.2(17)	C01U	546(7)	5956(5)	555(4)	70(3)
C00N	6450(5)	7238(4)	3895(4)	41.1(18)	C01V	-285(7)	6185(5)	905(4)	69(3)
C00O	7509(6)	4587(3)	1832(4)	40.1(18)	C01W	1496(7)	7605(5)	1518(4)	73(3)
C00P	4714(5)	7000(4)	1960(3)	42.6(19)	C01X	526(7)	6049(5)	4223(4)	69(3)
C00Q	7705(6)	4357(3)	2562(4)	39.4(17)	C01Y	925(10)	5623(6)	1747(5)	107(5)
C00R	4451(5)	6403(4)	1776(4)	49(2)	C01Z	963(18)	5441(9)	1012(7)	54(6)
C00S	3891(5)	5008(3)	3936(3)	33.5(16)	C01{	1510(30)	5740(18)	1300(20)	64(12)
C00T	1966(6)	3931(3)	1042(4)	43.2(18)	C00Z	2561(6)	4608(4)	4480(4)	48(2)
C00U	5877(5)	7407(3)	3205(4)	40.4(17)	C010	8071(7)	4574(4)	1294(4)	50(2)
C00V	3472(6)	4940(3)	4531(4)	42.9(18)	C011	8445(6)	3869(3)	3700(4)	48.9(19)
C00W	1264(5)	3840(3)	2100(4)	41.3(17)	C012	1198(6)	3711(3)	1378(4)	43.5(18)
C00X	6067(6)	5129(4)	1004(3)	41.9(18)	C013	6630(7)	5103(4)	489(4)	53(2)
C00Y	2023(6)	4343(3)	3844(4)	46.3(19)	C014	8528(6)	4036(3)	3013(4)	49.1(19)
C017	-2539(6)	6409(3)	1671(4)	46.6(19)	C015	2794(6)	6294(3)	3376(4)	43.3(18)
C018	2827(6)	7310(4)	3272(4)	46.6(19)	C016	6724(6)	4345(3)	3504(4)	45.4(19)

Table 2.15. Anisotropic Displacement Parameters ($Å^2×10^3$) for $[Cu^{II}(carb)_3][K(THF)_6]$. The anisotropic displacement factor exponent takes the form: $-2\pi^2[h^2a^{*2}U_{11}+2hka^*b^*U_{12}+\ldots]$.

Atom	U_{11}	U_{22}	U_{33}	U_{23}	U_{13}	U_{12}	Atom	U_{11}	U_{22}	U_{33}	U_{23}	U_{13}	U_{12}
Cu01	38.7(6)	79.6(9)	24.3(5)	-9.1(5)	13.8(4)	-23.1(6)	C01B	41(4)	51(5)	51(5)	0(4)	4(4)	-12(4)
K002	48.5(10)	57.0(11)	63.9(12)	1.4(9)	15.6(9)	0.1(8)	C01C	50(5)	48(5)	54(5)	6(4)	17(4)	7(4)
N003	26(3)	38(3)	19(2)	0(2)	7(2)	1(2)	C01D	40(4)	60(5)	58(5)	4(4)	21(4)	6(4)
O004	44(3)	52(3)	43(3)	-2(3)	-2(2)	-7(2)	C01E	35(4)	105(7)	32(4)	-22(5)	5(3)	-1(4)
O005	56(3)	50(3)	53(3)	-1(3)	12(3)	0(3)	C01F	37(4)	94(7)	39(4)	-1(5)	11(4)	21(4)
O006	57(3)	61(4)	59(3)	19(3)	34(3)	14(3)	C01G	70(6)	82(6)	37(4)	-18(4)	34(4)	-16(5)
N007	28(3)	74(5)	29(3)	-15(3)	7(2)	-13(3)	C01H	58(5)	51(5)	48(5)	2(4)	15(4)	-5(4)
O008	52(3)	37(3)	147(6)	-23(3)	56(4)	-6(3)	C01I	76(6)	58(6)	61(6)	8(4)	20(5)	10(5)
N009	43(3)	53(4)	25(3)	-6(3)	16(3)	-20(3)	C01J	66(5)	55(5)	42(4)	-3(4)	0(4)	3(4)
O00A	92(5)	96(5)	50(3)	-21(3)	39(3)	-49(4)	C01K	54(5)	56(5)	64(5)	-4(4)	16(4)	-4(4)
C00B	25(3)	35(4)	26(3)	4(3)	8(3)	9(3)	C01L	51(5)	107(8)	30(4)	4(5)	2(4)	29(5)
C00C	29(3)	33(4)	24(3)	3(3)	2(3)	6(3)	C01M	45(5)	122(9)	26(4)	0(5)	4(4)	24(5)
C00D	20(3)	66(5)	29(3)	-5(3)	14(3)	-2(3)	C01N	76(6)	74(6)	62(5)	-41(5)	32(5)	-39(5)
C00E	26(3)	37(4)	28(3)	7(3)	3(3)	2(3)	C01O	52(5)	62(5)	71(6)	-16(5)	32(4)	-13(4)
O00F	113(5)	126(6)	36(3)	5(3)	23(3)	73(5)	C01P	79(6)	48(5)	42(5)	3(4)	-1(4)	6(4)
C00G	26(3)	39(4)	30(3)	4(3)	6(3)	5(3)	C01Q	67(6)	66(6)	57(5)	-5(4)	31(4)	-9(5)
C00H	43(4)	46(4)	29(4)	-14(3)	16(3)	-23(4)	C01R	51(5)	55(5)	79(6)	12(5)	37(4)	6(4)
C00I	44(4)	41(4)	33(4)	-12(3)	14(3)	-19(3)	C01S	73(6)	55(5)	60(5)	-12(4)	25(5)	-3(5)
C00J	31(4)	43(4)	28(3)	1(3)	7(3)	13(3)	C01T	84(7)	83(7)	46(5)	18(5)	28(5)	6(5)
C00K	26(3)	56(5)	29(3)	-5(3)	9(3)	-8(3)	C01U	79(6)	100(8)	37(4)	-2(5)	24(4)	28(6)
C00L	26(4)	61(5)	29(4)	2(3)	3(3)	-1(3)	C01V	53(5)	121(9)	34(4)	2(5)	9(4)	14(5)
C00M	21(3)	57(5)	34(4)	-5(4)	8(3)	6(3)	C01W	49(5)	132(9)	47(5)	29(5)	27(4)	17(5)
C00N	26(4)	60(5)	37(4)	-12(4)	6(3)	5(3)	C01X	48(5)	116(9)	45(5)	-17(5)	13(4)	-17(5)
C00O	46(4)	45(4)	33(4)	-19(3)	18(3)	-20(3)	C01Y	142(10)	140(11)	38(5)	12(6)	23(6)	111(9)
C00P	21(3)	82(6)	24(4)	-6(4)	5(3)	12(4)	C01Z	71(12)	55(10)	37(8)	-3(7)	17(7)	22(9)
C00Q	46(4)	41(4)	32(4)	-16(3)	12(3)	-15(4)	C01{	48(19)	50(20)	100(30)	10(20)	31(19)	25(15)
C00R	28(4)	91(7)	30(4)	4(4)	11(3)	6(4)	C01B	41(4)	51(5)	51(5)	0(4)	4(4)	-12(4)
C00S	26(3)	45(4)	27(3)	2(3)	3(3)	7(3)	C01C	50(5)	48(5)	54(5)	6(4)	17(4)	7(4)
C00T	49(4)	44(4)	31(4)	-7(3)	-1(3)	10(4)	C01D	40(4)	60(5)	58(5)	4(4)	21(4)	6(4)
C00U	31(4)	49(4)	43(4)	0(4)	11(3)	9(3)	C01E	35(4)	105(7)	32(4)	-22(5)	5(3)	-1(4)
C00V	49(4)	55(5)	23(3)	-1(3)	6(3)	9(4)	C01F	37(4)	94(7)	39(4)	-1(5)	11(4)	21(4)
C00W	33(4)	48(5)	44(4)	0(4)	11(3)	-1(3)	C01G	70(6)	82(6)	37(4)	-18(4)	34(4)	-16(5)
C00X	39(4)	63(5)	25(3)	-8(3)	12(3)	-13(4)	C01H	58(5)	51(5)	48(5)	2(4)	15(4)	-5(4)
C00Y	55(5)	55(5)	32(4)	5(4)	18(3)	-9(4)	C01I	76(6)	58(6)	61(6)	8(4)	20(5)	10(5)
C00Z	50(5)	60(5)	41(4)	13(4)	22(4)	6(4)	C01J	66(5)	55(5)	42(4)	-3(4)	0(4)	3(4)

C010	58(5)	59(5)	39(4)	-11(4)	25(4)	-3(4)	C01K	54(5)	56(5)	64(5)	-4(4)	16(4)	-4(4)
C011	51(5)	45(5)	50(5)	-6(4)	10(4)	-11(4)	C01L	51(5)	107(8)	30(4)	4(5)	2(4)	29(5)
C012	35(4)	43(4)	46(4)	-3(4)	-1(3)	3(3)	C01M	45(5)	122(9)	26(4)	0(5)	4(4)	24(5)
C013	60(5)	72(6)	28(4)	-8(4)	15(4)	-23(5)	C01N	76(6)	74(6)	62(5)	-41(5)	32(5)	-39(5)
C014	57(5)	47(5)	49(5)	-13(4)	23(4)	-8(4)	C01O	52(5)	62(5)	71(6)	-16(5)	32(4)	-13(4)
C015	42(4)	46(4)	41(4)	1(4)	7(3)	11(3)	C01P	79(6)	48(5)	42(5)	3(4)	-1(4)	6(4)
C016	60(5)	47(5)	34(4)	-5(4)	22(4)	-10(4)	C01Q	67(6)	66(6)	57(5)	-5(4)	31(4)	-9(5)
C017	48(4)	47(5)	50(4)	-4(4)	23(4)	-5(4)	C01R	51(5)	55(5)	79(6)	12(5)	37(4)	6(4)
C018	35(4)	57(5)	49(4)	5(4)	13(3)	-8(4)	C01S	73(6)	55(5)	60(5)	-12(4)	25(5)	-3(5)
C019	71(6)	54(5)	38(4)	-4(4)	18(4)	-23(4)	C01T	84(7)	83(7)	46(5)	18(5)	28(5)	6(5)
C01A	53(5)	36(4)	80(6)	-10(4)	19(4)	7(4)	C01U	79(6)	100(8)	37(4)	-2(5)	24(4)	28(6)
C01Y	142(10)	140(11)	38(5)	12(6)	23(6)	111(9)	C01V	53(5)	121(9)	34(4)	2(5)	9(4)	14(5)
C01Z	71(12)	55(10)	37(8)	-3(7)	17(7)	22(9)	C01W	49(5)	132(9)	47(5)	29(5)	27(4)	17(5)
C01{	48(19)	50(20)	100(30)	10(20)	31(19)	25(15)	C01X	48(5)	116(9)	45(5)	-17(5)	13(4)	-17(5)

Table 2.16. Bond lengths for $[Cu^{II}(carb)_3][K(THF)_6]$.

Atom	Atom	Length/Å	Atom	Atom	Length/Å	Atom	Atom	Length/Å	Atom	Atom	Length/Å
Cu01	N003	1.887(5)	C00J	C00T	1.367(9)	N007	C00D	1.384(9)	C016	C019	1.364(11)
Cu01	N007	1.886(7)	C00K	C00L	1.378(9)	N007	C00R	1.389(10)	C017	C01D	1.548(10)
Cu01	N009	1.882(6)	C00L	C00N	1.376(10)	O008	C01K	1.426(9)	C018	C01J	1.516(10)
K002	O004	2.525(5)	C00M	C00P	1.466(9)	O008	C01R	1.432(9)	C01A	C01C	1.489(11)
K002	O005	2.528(5)	C00M	C00U	1.374(10)	N009	C00H	1.401(8)	C01A	C01K	1.506(11)
K002	O006	2.471(5)	C00N	C00U	1.382(9)	N009	C00I	1.383(9)	C01B	C01J	1.489(11)
K002	O008	2.468(6)	C00O	C00Q	1.438(10)	O00A	C01N	1.408(10)	C01C	C01R	1.494(11)
K002	O00A	2.476(7)	C00O	C010	1.394(9)	O00A	C01X	1.441(9)	C01D	C01I	1.510(11)
K002	O00F	2.428(6)	C00P	C00R	1.401(11)	C00B	C00G	1.399(9)	C01E	C01M	1.393(13)
K002	C01N	3.471(10)	C00P	C01F	1.379(11)	C00B	C00S	1.394(9)	C01F	C01L	1.390(11)
K002	C01R	3.363(8)	C00Q	C014	1.383(10)	C00C	C00E	1.409(9)	C01H	C01P	1.513(10)
K002	C01V	3.408(8)	C00R	C01E	1.411(10)	C00C	C00J	1.390(8)	C01I	C01S	1.505(11)
K002	C01W	3.453(8)	C00S	C00V	1.379(9)	C00D	C00K	1.405(9)	C01L	C01M	1.348(13)
K002	C01X	3.483(9)	C00T	C012	1.398(10)	C00D	C00M	1.400(10)	C01N	C01O	1.541(11)
K002	C01Y	3.406(10)	C00V	C00Z	1.376(10)	C00E	C00G	1.455(9)	C01O	C01Q	1.469(11)
N003	C00B	1.397(7)	C00W	C012	1.380(10)	C00E	C00W	1.380(9)	C01P	C01T	1.494(12)
N003	C00C	1.384(8)	C00X	C013	1.359(9)	O00F	C01V	1.435(9)	C01Q	C01X	1.521(11)
O004	C015	1.428(8)	C00Y	C00Z	1.364(10)	O00F	C01Y	1.394(10)	C01T	C01W	1.483(11)
O004	C018	1.428(8)	C010	C01G	1.377(11)	C00G	C00Y	1.399(9)	C01U	C01V	1.490(11)
O005	C017	1.451(9)	C011	C014	1.384(10)	C00H	C00O	1.396(10)	C01U	C01Z	1.461(16)
O005	C01S	1.442(10)	C011	C019	1.405(11)	C00H	C00X	1.410(10)	C01U	C01{	1.69(4)
O006	C01H	1.411(9)	C013	C01G	1.378(12)	C00I	C00Q	1.410(10)	C01Y	C01Z	1.463(16)
O006	C01W	1.453(9)	C015	C01B	1.558(10)	C00I	C016	1.399(9)	C01Y	C01{	1.30(3)

Table 2.17. Bond angles for $[Cu^{II}(carb)_3][K(THF)_6]$.

Atom	Atom	Atom	Angle/°	Atom	Atom	Atom	Angle/°	Atom	Atom	Atom	Angle/°	Atom	Atom	Atom	Angle/°
N007	Cu01	N003	126.7(2)	N007	C00D	C00M	112.7(6)	C01V	K002	C01N	89.6(2)	C01M	C01E	C00R	116.7(9)
N009	Cu01	N003	124.4(2)	C00M	C00D	C00K	119.4(6)	C01V	K002	C01W	69.7(2)	C00P	C01F	C01L	118.4(9)
N009	Cu01	N007	108.8(2)	C00C	C00E	C00G	105.4(5)	C01V	K002	C01X	125.0(3)	C010	C01G	C013	121.1(7)
O004	K002	O005	172.63(17)	C00W	C00E	C00C	120.4(6)	C01W	K002	C01N	149.5(2)	O006	C01H	C01P	105.0(6)
O004	K002	C01N	99.0(2)	C00W	C00E	C00G	134.2(6)	C01W	K002	C01X	143.0(2)	C01S	C01I	C01D	104.3(7)
O004	K002	C01R	112.86(19)	C01V	O00F	K002	121.7(6)	C01Y	K002	C01N	67.3(3)	C01B	C01J	C018	106.4(6)
O004	K002	C01V	103.31(19)	C01Y	O00F	K002	123.8(6)	C01Y	K002	C01V	39.5(2)	O008	C01K	K002	33.8(3)
O004	K002	C01W	66.16(18)	C01Y	O00F	C01V	109.1(6)	C01Y	K002	C01W	82.8(3)	O008	C01K	C01A	107.6(6)

O004	K002	C01X	77.03(18)	C00B	C00G	C00E	106.0(5)	C01Y	K002	C01X	91.7(2)	C01A	C01K	K002	128.5(5)
O004	K002	C01Y	75.3(3)	C00B	C00G	C00Y	119.9(6)	C00B	N003	Cu01	126.6(4)	C01M	C01L	C01F	121.5(9)
O005	K002	C01N	86.1(2)	C00Y	C00G	C00E	134.1(6)	C00C	N003	Cu01	127.9(4)	C01L	C01M	C01E	122.3(8)
O005	K002	C01R	72.44(19)	N009	C00H	C00X	127.7(7)	C00C	N003	C00B	105.5(5)	O00A	C01N	K002	36.1(4)
O005	K002	C01V	71.19(19)	C00O	C00H	N009	112.0(6)	C015	O004	K002	126.5(4)	O00A	C01N	C01O	102.6(6)
O005	K002	C01W	106.87(19)	C00O	C00H	C00X	120.1(6)	C015	O004	C018	106.2(5)	C01O	C01N	K002	113.8(6)
O005	K002	C01X	110.06(19)	N009	C00I	C00Q	112.0(6)	C018	O004	K002	124.4(4)	C01Q	C01O	C01N	105.0(6)
O005	K002	C01Y	102.0(2)	N009	C00I	C016	127.4(7)	C017	O005	K002	127.4(4)	C01T	C01P	C01H	103.5(6)
O006	K002	O004	77.68(18)	C016	C00I	C00Q	120.6(7)	C01S	O005	K002	126.7(5)	C01O	C01Q	C01X	105.7(6)
O006	K002	O005	96.48(18)	C00T	C00J	C00C	118.4(6)	C01S	O005	C017	105.2(6)	O008	C01R	K002	41.0(4)
O006	K002	O00A	161.2(2)	C00L	C00K	C00D	118.4(7)	C01H	O006	K002	133.5(4)	O008	C01R	C01C	103.2(6)
O006	K002	C01N	170.4(2)	C00N	C00L	C00K	122.0(7)	C01H	O006	C01W	104.1(6)	C01C	C01R	K002	119.7(5)
O006	K002	C01R	101.11(19)	C00D	C00M	C00P	105.2(6)	C01W	O006	K002	121.1(5)	O005	C01S	C01I	104.3(6)
O006	K002	C01V	82.5(2)	C00U	C00M	C00D	120.7(6)	C00D	N007	Cu01	124.7(5)	C01W	C01T	C01P	106.0(7)
O006	K002	C01W	21.1(2)	C00U	C00M	C00P	134.2(7)	C00D	N007	C00R	104.6(7)	C01V	C01U	C01{	101.0(11)
O006	K002	C01X	146.3(2)	C00L	C00N	C00U	119.6(7)	C00R	N007	Cu01	130.7(5)	C01Z	C01U	C01V	101.9(9)
O006	K002	C01Y	103.0(3)	C00H	C00O	C00Q	105.8(6)	C01K	O008	K002	127.5(5)	O00F	C01V	K002	37.3(4)
O008	K002	O004	91.64(18)	C010	C00O	C00H	119.9(7)	C01K	O008	C01R	108.2(6)	O00F	C01V	C01U	103.9(7)
O008	K002	O005	92.87(19)	C010	C00O	C00Q	134.3(7)	C01R	O008	K002	116.6(5)	C01U	C01V	K002	126.4(6)
O008	K002	O006	90.1(2)	C00R	C00P	C00M	105.0(7)	C00H	N009	Cu01	128.7(5)	O006	C01W	K002	37.8(4)
O008	K002	O00A	87.3(2)	C01F	C00P	C00M	134.5(8)	C00I	N009	Cu01	126.3(4)	O006	C01W	C01T	105.1(7)
O008	K002	C01N	99.1(2)	C01F	C00P	C00R	120.5(7)	C00I	N009	C00H	104.4(6)	C01T	C01W	K002	126.6(6)
O008	K002	C01R	22.38(19)	C00I	C00Q	C00O	105.7(6)	C01N	O00A	K002	124.3(5)	O00A	C01X	K002	36.4(4)
O008	K002	C01V	161.4(2)	C014	C00Q	C00I	119.8(7)	C01N	O00A	C01X	106.7(6)	O00A	C01X	C01Q	103.8(6)
O008	K002	C01W	107.5(2)	C014	C00Q	C00O	134.4(7)	C01X	O00A	K002	123.4(5)	C01Q	C01X	K002	117.2(6)
O008	K002	C01X	68.8(2)	N007	C00R	C00P	112.6(6)	N003	C00B	C00G	111.4(5)	O00F	C01Y	K002	36.3(4)
O008	K002	C01Y	158.8(2)	N007	C00R	C01E	126.9(9)	C00S	C00B	N003	128.1(6)	O00F	C01Y	C01Z	107.1(8)
O00A	K002	O004	83.75(19)	C00P	C00R	C01E	120.6(8)	C00S	C00B	C00G	120.4(6)	C01Z	C01Y	K002	138.5(8)
O00A	K002	O005	102.3(2)	C00V	C00S	C00B	118.4(6)	N003	C00C	C00E	111.7(5)	C01{	C01Y	K002	116(2)
O00A	K002	C01N	19.58(19)	C00J	C00T	C012	121.5(7)	N003	C00C	C00J	127.9(6)	C01{	C01Y	O00F	107.5(14)
O00A	K002	C01R	83.2(2)	C00M	C00U	C00N	119.9(7)	C00J	C00C	C00E	120.3(6)	C01U	C01Z	C01Y	104.4(11)
O00A	K002	C01V	105.1(2)	C00Z	C00V	C00S	120.7(7)	N007	C00D	C00K	127.9(7)	C01Y	C01{	C01U	100(2)
O00A	K002	C01W	146.3(2)	C012	C00W	C00E	118.8(7)	O00F	K002	C01N	73.3(2)	C00Q	C014	C011	119.3(7)
O00A	K002	C01X	20.2(2)	C013	C00X	C00H	118.6(7)	O00F	K002	C01R	151.0(2)	O004	C015	C01B	104.6(6)
O00A	K002	C01Y	74.8(2)	C00Z	C00Y	C00G	118.4(7)	O00F	K002	C01V	21.0(2)	C019	C016	C00I	118.9(7)
O00F	K002	O004	92.6(2)	C00Y	C00Z	C00V	122.0(7)	O00F	K002	C01W	80.7(3)	O005	C017	C01D	104.6(6)
O00F	K002	O005	83.7(2)	C01G	C010	C00O	118.8(8)	O00F	K002	C01X	105.4(2)	O004	C018	K002	36.1(3)
O00F	K002	O006	97.7(2)	C014	C011	C019	120.5(8)	O00F	K002	C01Y	19.9(2)	O004	C018	C01J	103.7(6)
O00F	K002	O008	171.8(2)	C00W	C012	C00T	120.4(7)	C01N	K002	C01X	38.4(2)	C01J	C018	K002	119.5(5)
O00F	K002	O00A	86.1(2)	C00X	C013	C01G	121.5(7)	C01R	K002	C01N	88.5(2)	C016	C019	C011	120.9(7)
C01R	K002	C01X	69.2(2)	C01A	C01C	C01R	104.2(6)	C01R	K002	C01V	143.6(2)	C01C	C01A	C01K	103.2(6)
C01R	K002	C01Y	155.7(3)	C01I	C01D	C017	104.9(6)	C01R	K002	C01W	121.5(2)	C01J	C01B	C015	103.5(6)

2.5 Notes and References

[1] Creutz, S. E.; Lotito, K. J.; Fu, G. C.; Peters, J. C. *Science* **2012**, *338*, 647–651.

[2] Bissember, A. C.; Lundgren, R. J.; Creutz, S. E.; Peters, J. C.; Fu, G. C. *Angew. Chem., Int. Ed.* **2013**, *52*, 5129–5133.

[3] (a) Uyeda, C.; Tan, Y.; Fu, G. C.; Peters, J. C. *J. Am. Chem. Soc.* **2013**, *135*, 9548–9552. (b) Ziegler, D. T.; Choi, J.; Muñoz-Molina, J. M.; Bissember, A. C.; Peters, J. C.; Fu, G. C. *J. Am. Chem. Soc.* **2013**, *135*, 13107–13112. (c) Do, H.-Q.; Bachman, S.; Bissember, A. C.; Peters, J. C.; Fu, G. C. *J. Am. Chem. Soc.* **2014**, *136*, 2162–2167. (d) Tan, Y.;

Muñoz-Molina, J. M.; Fu, G. C.; Peters, J. C. *Chem. Sci.* **2014**, *5*, 2831–2835. (e) Ratani, T. S.; Bachman, S.; Fu, G. C.; Peters, J. C. *J. Am. Chem. Soc.* **2015**, *137*, 13902–13907.

[4] Twilton, J.; Le, C.; Zhang, P.; Shaw, M. H.; Evans, R. W.; MacMillan, D. W. C. *Nat. Rev. Chem.* **2017**, *1*, 0052.

[5] Skubi, K. L.; Blum, T. R.; Yoon, T. P. *Chem. Rev.* **2016**, *116*, 10035–10074.

[6] For a recent overview, see: Huang, X.; Groves, J. T. *J. Biol. Inorg. Chem.* **2017,** *22*, 185–207.

[7] Johnson, M. W.; Hannoun, K. I.; Tan, Y.; Fu, G. C.; Peters, J. C. *Chem. Sci.* **2016**, *7*, 4091–4100.

[8] Jang, E. S.; McMullin, C. L.; Käß, M.; Meyer, K.; Cundari, T. R.; Warren, T. H. *J. Am. Chem. Soc.* **2014**, *136*, 10930–10940.

[9] Wiese, S.; Badiei, Y. M.; Gephart, R. T.; Mossin, S.; Varonka, M. S.; Melzer, M. M.; Meyer, K.; Cundari, T. R.; Warren, T. H. *Angew. Chem., Int. Ed.* **2010**, *49*, 8850–8855.

[10] For example, see Lawrence, S. A. *Amines: Synthesis, Properties, and Applications*; Cambridge University Press: Cambridge, U.K., **2004**.

[11] For simplicity, we write "$[Cu^{I}(carb)_2]Li$", although the lithium may in fact be solvated by CH_3CN. For example, see ref 2.

[12] Moreover, a concentrated sample of the alkyl bromide in CH_3CN shows no absorption beyond 300 nm, whereas the Nd:YAG laser is irradiating the sample at 355 nm.

[13] Alfassi, Z. B. In *General Aspects of the Chemistry of Radicals*; Alfassi, Z. B., Ed.; Wiley: Chichester, U.K., **1999**; pp 139−173.

[14] If the 15-crown-5 is used in the reaction in place of 18-crown-6, crystals of $[Cu^{II}(carb)_4][K(15\text{-crown-}5)_2]_2$ were also detected.

[15] For a review on the persistent radical effect, see Fischer, H. *Chem. Rev.* **2001**, *101*, 3581–3610.

[16] Homoleptic, monomeric, three-coordinate copper(II) anions have only been crystallographically characterized in the case of alkoxide ligands: (a) Purdy, A. P.; George, C. F. *Inorg. Chem.* **1991**, *30*, 1969–1970. (b) Hannigan, S. F.; Lum, J. S.; Bacon, J. W.; Moore, C.; Golen, J. A.; Rheingold, A. L.; Doerrer, L. H. *Organometallics* **2013**, *32*, 3429–3436.

[17] X-ray diffraction data for $[Cu^{II}(carb)_3][K(18\text{-crown-}6)(THF)]$ and $[Cu^{II}(carb)_3][K(benzo\text{-}15\text{-crown-}5)_2]$ were of poor quality and hence only sufficient for establishing the overall atomic connectivity.

[18] For examples of other copper(II)−amido complexes wherein significant spin density is believed to reside on nitrogen, see (a) ref 9. (b) Mankad, N. P.; Antholine, W. E.; Szilagyi, R. K.; Peters, J. C. *J. Am. Chem. Soc.* **2009**, *131*, 3878−3880. (c) Wagner, C. L.; Tao, L.; Thompson, E. J.; Stich, T. A.; Guo, J.; Fettinger, J. C.; Berben, L. A.; Britt, R. D.; Nagase, S.; Power, P. P. *Angew. Chem., Int. Ed.* **2016**, *55*, 10444−10447.

[19] For examples of other copper(II)–amido complexes that abstract hydrogen atoms, see refs 8 and 18b.

[20] Cismesia, M. A.; Yoon, T. P. *Chem. Sci.* **2015**, *6*, 5426−5434.

[21] For leading references on radical clocks, see Newcomb, M. In *Encyclopedia of Radicals in Chemistry, Biology and Materials*; Chatgilialoglu, C., Studer, A., Eds.; John Wiley & Sons, Chichester, U.K., **2012**; Vol 1, pp 107−124.

[22] Lusztyuk, J.; Maillard, B.; Deycard, S.; Lindsay, D. A.; Ingold, K. U. *J. Org. Chem.* **1987**, *52*, 3509−3514.

[23] For early examples, see: (a) Biswas, S.; Weix, D. J. *J. Am. Chem. Soc.* **2013**, *135*, 16192–16197. (b) Choi, J.; Martín-Gago, P.; Fu, G. C. *J. Am. Chem. Soc.* **2014**, *136*, 12161–12165.

[24] Dinnebier, R.; Esbak, H.; Olbrich, F.; Behrens, U. *Organometallics* **2007**, 26, 2604–2608.

[25] Bolton, J. R.; Stefan, M. I.; Shaw, P.-S.; Lykke, K. R. *J. Photochem. Photobiol., A* **2011**, *222*, 166−169. Note the procedure is off by a factor of 1000, which was correctly adjusted in the present study.

[26] Wu, A.; Mader, E. A.; Datta, A.; Hrovat, D. A.; Borden, W. T.; Mayer, J. M. *J. Am. Chem. Soc.* **2009**, *131*, 11985–11997.

[27] Neese, F. *Wiley Interdiscip. Rev. Comput. Mol. Sci.* **2012**, *2*, 73–78.

[28] Zhao, Y.; Truhlar, D.G. *J. Chem. Phys.* **2006**, *125*, 194101.

[29] Weigend, F.; Furche, F.; Ahlrichs, R. *J. Chem. Phys.* **2003**, *119*, 12753.

[30] Klamt, A; Schüürmann, G. *J. Chem. Soc. Perkin Trans. 2* **1993**, *2*, 799–805.

Chapter 3. Copper complexes supported by tridentate bis(phosphino)carbazole ligands

Reproduced in part with permission from:

Ahn, J. M.; Peters, J. C.; Fu, G. C. *J. Am. Chem. Soc.* **2017**, *139*, 18101–18106.

3.1. Introduction

The out-of-cage C_{sp^3}–N coupling mechanism proposed in **Chapter 2** (**Figure 2.5**) suggests that the generation of alkyl radicals does not strictly require a photoactive copper(I)–nucleophile complex. Instead, photoinduced, copper-catalyzed coupling reactions may follow a generalized mechanistic pathway illustrated in **Figure 3.1**, in which the photoinduced radical generation (photocatalysis) is separated from the bond-forming (cross-coupling) cycle. In theory, lithium carbazolide may serve as a stoichiometric photoreductant for the hypothetical coupling of non-photoactive nucleophiles while cross-coupling is enabled by an in situ formed copper(II)–nucleophile complex. However, the N–substitution of carbazole and competing ligand substitution reactions can pose a significant challenge in the selective coupling of the desired nucleophile under this hypothetical reaction condition.

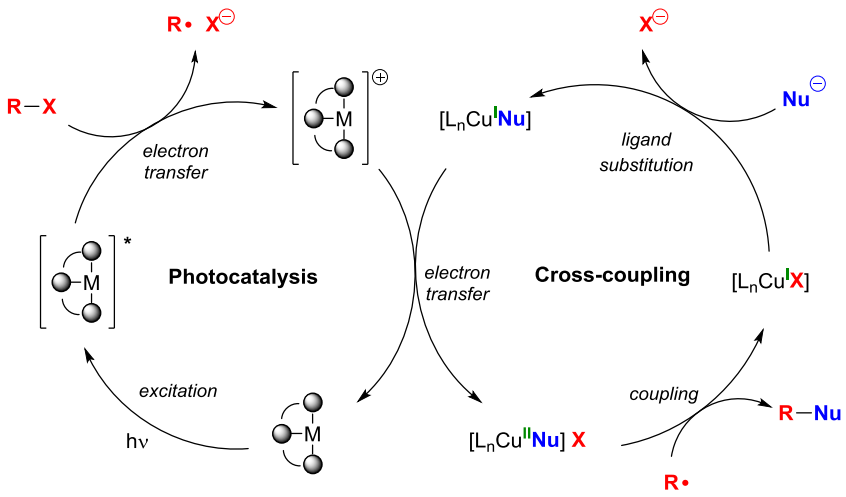

Figure 3.1. Generalized coupling of photoinduced copper catalysis. For simplicity, all copper complexes are depicted as neutral species, and all processes are illustrated as unidirectional. X may be an inner- or an outer-sphere group, and L_n represents additional ligand(s) coordinated to copper.

Although many examples of excited-state photoreductants have emerged within the past decade (e.g. **Figure 1.1**), very few have the appropriate thermodynamic driving force to react with unactivated alkyl halides other than alkyl iodides.[1] Alkyl iodides tend to exhibit promiscuous reactivity patterns which allow them to be employed in a variety of photoinduced transformations, but high reactivity can also present problems with regard to selectivity due to the prevalence of uncontrolled radical decomposition pathways.[2]

Very few systems are able to utilize unactivated alkyl bromides under photoinduced conditions. Both in terms of thermodynamics and kinetics, alkyl bromides are less likely to engage in single electron transfer (SET) pathways than the heavier congeners. The few known examples tend to require high-energy UVC light (254 nm),[3] which is less desirable in the context of functional group compatibility and safety. In fact, even the solar ultraviolet radiation does not contain wavelengths in the UVC region when measured at the surface of Earth.[4]

Since lithium carbazolide is able to engage in SET with unactivated alkyl bromides, we envisioned that the inherent photoproperties of the carbazole scaffold may be used advantageously in the design of a new photocatalyst that could initiate copper-catalyzed cross-coupling reactions of non-photoactive nucleophiles. Lending credence to the viability of this approach is the observation of an unexpected photosensitization elicited by added carbazole in photoinduced, copper-catalyzed N–arylations. Specifically, carbazole enables the N–phenylation of benzimidazole with iodobenzene under 350 nm irradiation when the otherwise identical reaction condition does not lead to an effective coupling of benzimidazole in the absence of carbazole (**Scheme 3.1**)[5]

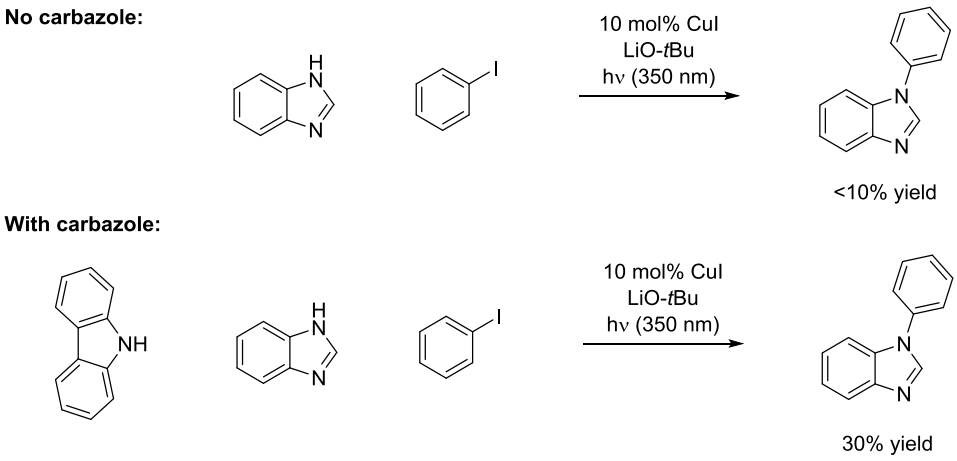

Scheme 3.1. Photosensitization by carbazole of the coupling of benzimidazole and iodobenzene observed by previous members of the Fu laboratory.

Carbazolide complexes of copper have also been shown to harness visible light irradition. The Fu and Peters laboratories have previously reported that three-coordinate copper complexes bearing two monodentate phosphines and one carbazolide ligand (complexes **3.a** and **3.b**) react with aryl and alkyl halides to form C–N bonds upon irradiation with CFL or blue LED lamps (**Figure 3.2**).[6,7] Importantly, **3.a** has an estimated reduction potential of –2.6 V vs SCE and reacts with alkyl bromides in addition to alkyl iodides.

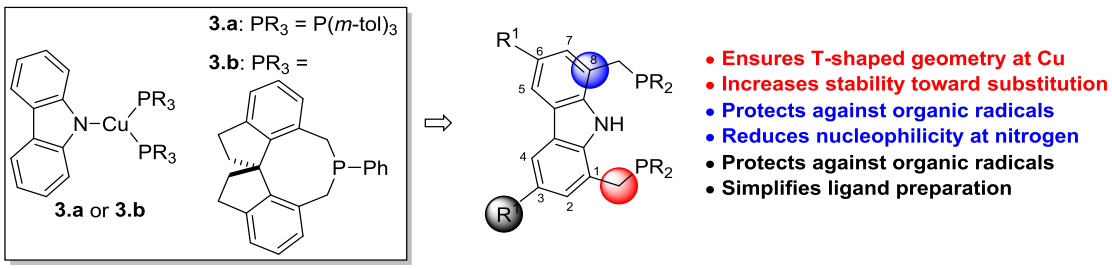

Figure 3.2. Design of visible-light photocatalyst inspired by existing examples of copper(I)-carbazolides in photoinduced copper catalysis.

We hypothesized that, by linking these monodentate ligands into a tridentate ligand, we may be able to access a copper complex that is stable to ligand substitutions (e.g. with respect to nucleophiles under cross-coupling conditions). Owing to its electronic properties, the target complex may then serve as an effective photocatalyst that can initiate new copper-catalyzed reactions upon exposure to visible light, independent of the nucleophile.

We anticipated that the design principles embodied in the tridentate bis(phosphino)carbazole ligand would minimize deleterious side reactions. The substitution at the 1- and 8-positions of the carbazole would impede the functionalization at nitrogen,[8] and the substitution at the 3- and 6-positions would preclude the addition of radicals at these sites (**Figure 3.2**).[9] Although several bis(phosphino)carbazole ligands were known when we began this investigation, we targeted the ligand bearing methylene bridges in the 1- and 8-positions to best accomplish the trigonal planar geometry in previously observed in complexes **3.a** and **3.b**.

3.2. Results and Discussions

3.2.1. Synthesis and characterization of copper(I) complexes supported by tridentate bis(phosphino)carbazole ligands

The S_N2 substitution of 1,8-bis(bromomethyl)-3,6-di-*t*-butylcarbazole with a secondary phosphine leads to a complete and clean conversion of the electrophile, and the subsequent workup forges the desired bis(phosphino)carbazole ligands (**Scheme 3.2**). Thus, a wide range of ligands containing aryl, small alkyl, sterically hindered alkyl, and chiral and achiral cyclic alkyl groups on the phosphines can be prepared.

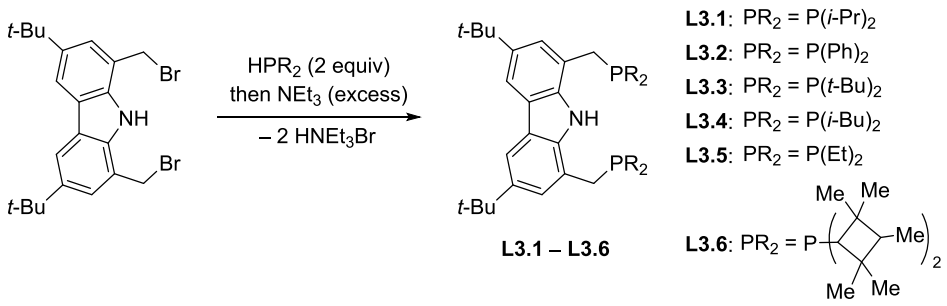

Scheme 3.2. Preparation of PNP ligands.

When ligands **L3.1**–**L3.6** are treated with mesitylcopper or with a mixture of CuCl and LiO*t*-Bu in benzene, the crude ^{1}H NMR spectra of the resulting solutions show the disappearance of N–H resonances of free ligands (**Scheme 3.3**). The ^{31}P NMR spectra also reveal the downfield shift and broadening of the phosphorous resonances, consistent with the ligation to the copper center.

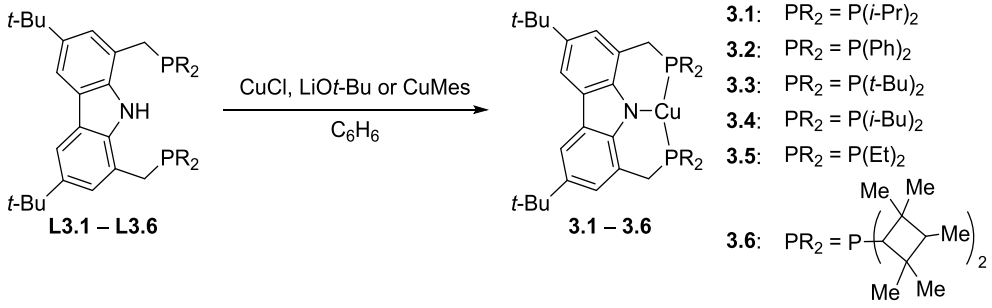

Scheme 3.3. Synthesis of mononuclear, three-coordinate copper complexes.

The formation of the copper complexes **3.1**–**3.6** is further confirmed by the analysis of their single-crystal X-ray diffraction data. All complexes feature a three-coordinate, trigonal planar copper(I) center akin to complexes **3.a** and **3.b**. The lack of counteranion and

the Cu–N distances which range from 1.96 to 2.00 Å, are consistent with the assignment of neutral copper(I) complexes. Complexes **3.1**–**3.6** are colorless in pure form, similar to **3.a** and **3.b**. Considering the availability and cost of di-*i*-propyl-substituted phosphine precursors, extensive studies and characterizations have been performed using **CuPNP-*i*Pr** (complex **3.1**) which can be recrystallized from a saturated mixture of benzene and pentane or by slow evaporation of a saturated Et_2O solution (**Figure 3.3**, left).

Complex **3.1** is poorly soluble in CH_3CN but very soluble in THF, Et_2O, or benzene. The cyclic voltammogram of **3.1** in THF shows a reversible redox behavior attributable to the $Cu^{I/II}$ couple appearing at 0.6 V vs SCE (**Figure 3.3**, right). The observed reversibility is likely a result of the improved stability provided by the chelating ligand since the oxidation of **3.a** (estimated to occur at 0.5 V vs SCE) does not display a reversible redox feature.[6]

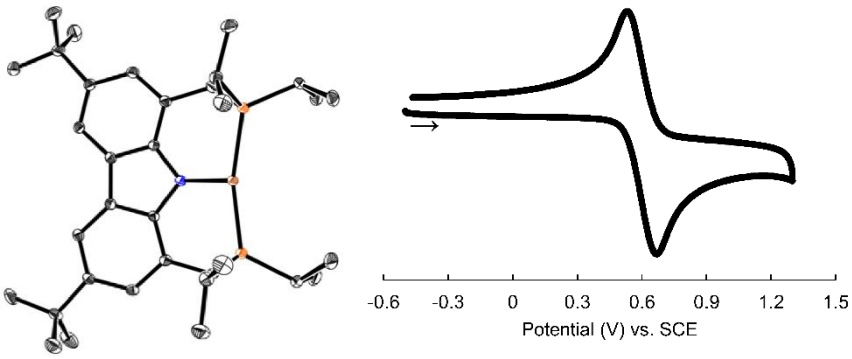

Figure 3.3. Characterization of **3.1**. Left: solid-state molecular structure (50% probability thermal ellipsoids) by X-ray diffraction of a single crystal grown from the evaporation of Et_2O; hydrogen atoms are omitted for clarity. Right: cyclic voltammogram in THF (0.1 M [TBA][PF_6]).

The UV-vis spectrum of **3.1** shows strong absorptions in the UV-A region that tail into the visible range (**Figure 3.4**, left). Importantly, the absorption overlaps with the emission spectra of 100-watt Hg lamp as well as blue LEDs. These transitions allow access to an emissive excited state, which has a lifetime of 8.1 ns. The relatively short lifetime is suggestive of a mostly ligand-centered excitation. Time-dependent density functional theory calculations indicate that a π-to-π* transition based essentially on the carbazolide core leads to the observed excited state (see section 3.4.6). On the basis of the cross section of the excitation and the emission profiles[10] (**Figure 3.4**, right) and the electrochemical data, we estimate that complex **3.1** has an excited-state reduction potential of –2.5 V vs SCE. This value is on par with strong photoreductants that are based on cerium and tungsten.[11,12]

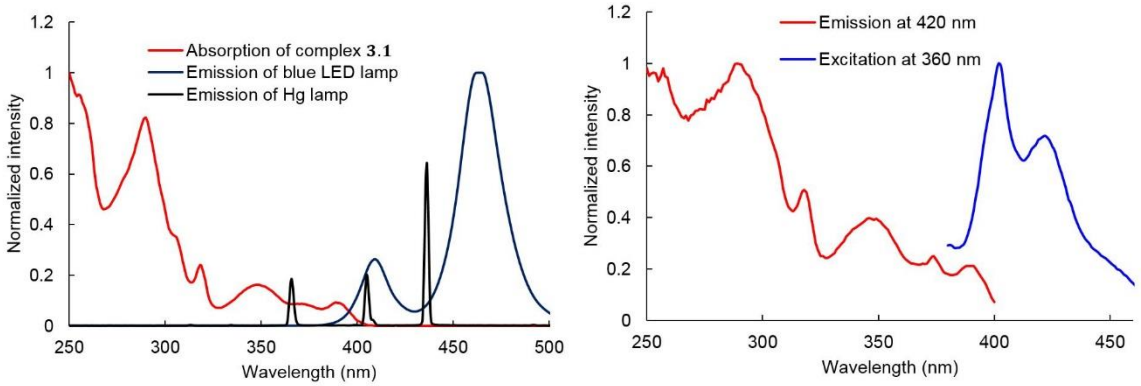

Figure 3.4. Photoproperties of **3.1**. Left: normalized absorption spectrum showing overlap with the emission spectra of common light sources. Right: excitation (emission at 420 nm) and emission spectra (excitation at 360 nm).

3.2.2. Reactivity of complex 3.1

We performed Stern-Volmer analysis using complex **3.1** to assess the viability of photoinduced single electron transfer to an unactivated secondary alkyl bromide. Quenching of the luminescence of the excited-state of complex **3.1** (**3.1***) is observed in the presence of 2-bromo-4-phenylbutane with a rate constant of 2.0×10^9 M^{-1} s^{-1}. On the basis of the estimated excited-state reduction potential of complex **3.1**, we postulate that this quenching is likely due to single electron transfer from the **3.1*** to the alkyl bromide.

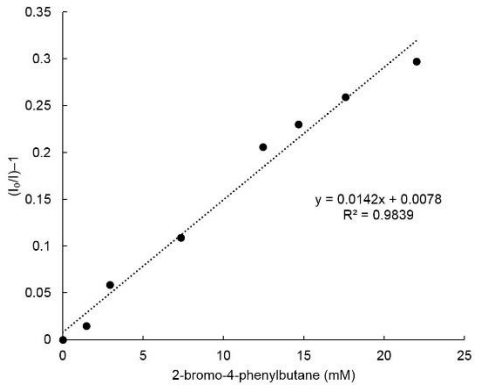

Figure 3.5. Quenching of the luminescence of **3.1*** at 427 nm in the presence of 2-bromo-4-phenylbutane.

Although the one-electron oxidation of **3.1** is reversible in the electrochemical time scale, the treatment of **3.1** with acetylferrocenium tetrafluoroborate ([FcAc][BF_4]) at –78 °C produces a dark purple solution which discolors upon warming to ambient temperature. The EPR spectrum of this purple solution shows an almost isotropic signal centered near the *g*-value of the free electron. In the presence of Na[BAr^F_{24}], single crystals suitable for XRD are obtained ([BAr^F_{24}]$^-$ = [B(3,5-(CF_3)$_2$-C_6H_3)$_4$]$^-$). Although the quality of the diffraction data is

modest, the structure confirms the atomic connectivity of the complex, [**CuPNP-*i*Pr**][BAr^F_{24}] (**3.7-BAr^F_{24}**). The cation **3.7** is a rare example of a monomeric, formally copper(II) complex ligated by phosphines. On the basis of its EPR spectrum (**Figure 3.6**), however, **3.7** may be better described as a copper(I) adduct of an organic radical cation, analogous to the only reported example of a monomeric, formally copper(II) complex supported by a bis(phosphine) ligand.[13] More discussions on paramagnetic copper complexes containing Cu–P unit are presented in **Chapter 5**.

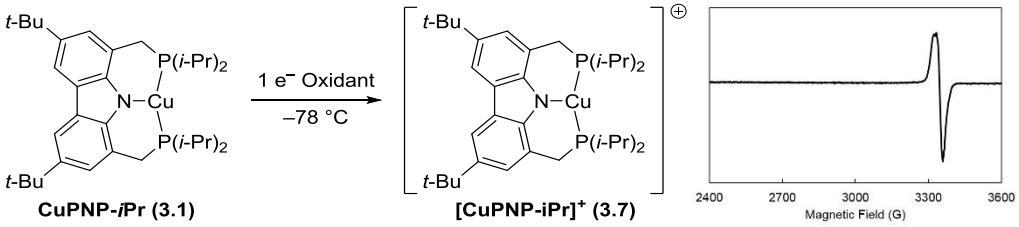

Figure 3.6. Oxidation of complex **3.1**. Inset: EPR spectrum (9.4 GHz, 77 K, THF/2-MeTHF) of **3.7-BF_4** produced by the reaction of **3.1** with [FcAc][BF_4].

Even at –35 °C, a solution of **3.7-BF_4** in THF eventually discolors. When the solution is allowed to stand for several days at –35 °C, colorless crystals are observed. Although the obtained crystals are twinned, the structure confirms the atomic connectivity of the decomposition product, which is the product of a formal hydrogen atom transfer, [**CuPNHP-*i*Pr**][BF_4] (**3.8-BF_4**; **Scheme 3.4**).

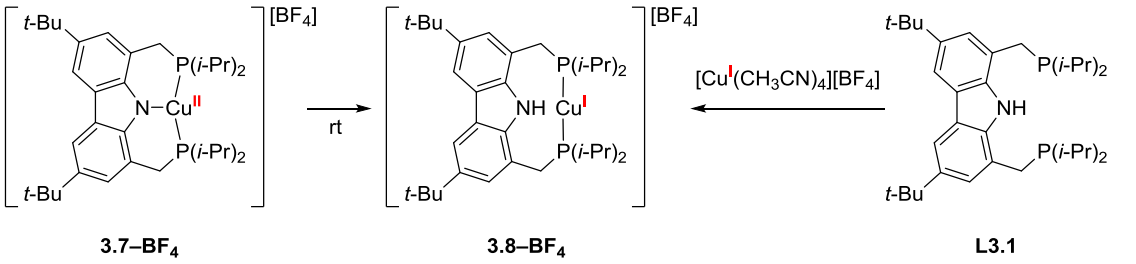

Scheme 3.4. Formation of complex **3.8–BF$_4$**.

Complex **3.8-BF$_4$** can also be prepared independently by treating ligand **L3.1** with a cationic copper(I) precursor such as [Cu(CH$_3$CN)$_4$][BF$_4$] in THF. The ^{1}H NMR spectrum of the reaction mixture shows the intact N–H resonance, unlike in the preparation of **3.1** (**Scheme 3.3**). Higher-quality single crystals suitable for XRD are obtained when [Cu(CH$_3$CN)$_4$][PF$_6$] is used. Consistent with its ^{1}H NMR spectrum, the Cu–N distance in **3.8-PF$_6$** (2.251(3) Å) is increased by more than 10% from that in **3.1**. The loss of covalent interaction in the Cu–N unit is also accompanied by the increased linearity of P–Cu–P angle, which reaches 170.4°, from the three-coordinate counterpart, which has a P–Cu–P angle of 160.2°. The Cu–N bond can be restored by the treatment of **3.8-PF$_6$** with an equivalent of LiO*t*-Bu, resulting in the formation of **3.1**.

3.2.3. Catalytic C–N coupling enabled by complex 3.1 and light

The viability to transform the decomposition product of the one-electron oxidation of **3.1** (e.g. **3.8**) back to **3.1** is advantageous in the context of developing catalytic transformations using **3.1**. Specifically, we envisioned that upon photoexcitation, the excited-state complex (**3.1***) can deliver an electron to the alkyl bromide substrate, releasing an alkyl

radical and the oxidized copper complex (**3.7**; **Figure 3.7**). Complex **3.7** may then be trapped by an external nucleophile (Nu) in solution, or participate in an electron transfer event with copper(I)–nucleophile species ([L_nCu^INu]) to enter a productive bond-forming cycle.[14] Albeit at a slow rate, **3.7** may decompose in solution to **3.8** as observed in the attempted isolation, but **3.8** can re-enter the productive cycle in the presence of an external base to form **3.1**.

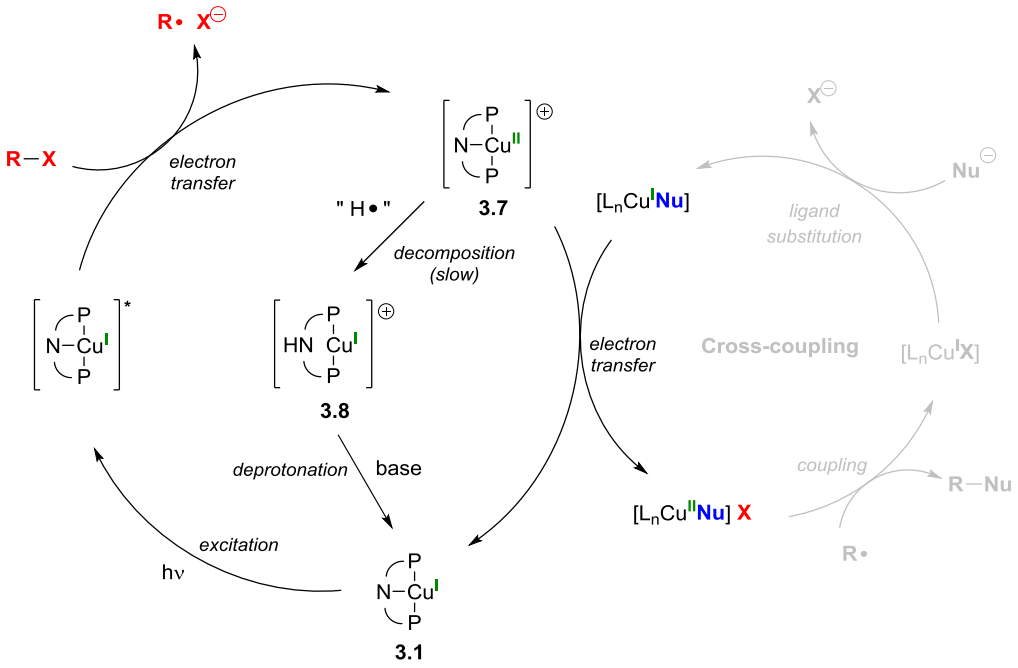

Figure 3.7. Potential photocatalytic cycle (e.g. left half of the full cycle shown in **Figure 3.1**) that involves complex **3.1**.

Gratifyingly, we found that **3.1** can be used as an effective catalyst for the photoinduced copper-catalyzed couplings of carboxamide-type nucleophiles with unactivated alkyl halides. In particular, the coupling of *t*-butyl carbamate with an unactivated

secondary bromide using blue LED lamps as the light source can be achieved in the presence of **3.1** although the yield of the observed C–N coupling is modest (33%, **Scheme 3.5**). Similar reactivity is observed when the same reaction is performed using ligand **L3.1** and CuBr (34%). In the absence of light, no reaction is observed, and the alkyl bromide can be recovered quantitatively.

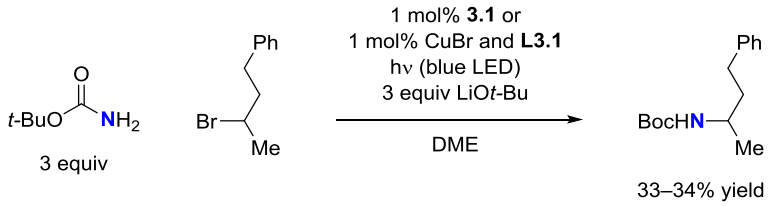

Scheme 3.5. Catalytic C–N coupling of *t*-butyl carbamate with 2-bromo-4-phenylbutane. Ar = 4-*t*-Bu-phenyl.

To further confirm the importance of the design principles embodied in **L3.1**, related tridentate ligands featuring a carbazole backbone have also been prepared (**Figure 3.8**). When ligand **SNS-Ar** (**L3.7**) or **NNN-*i*Pr** (**L3.8**) is employed instead of **L3.1** under related conditions, carbamate alkylation does not proceed. The use of 3,6-di-*t*-butyl-carbazole and tri-*t*-butylphosphine in place of **L3.1** also fails to yield substantial amount of the C–N coupled product (<5 % yield).

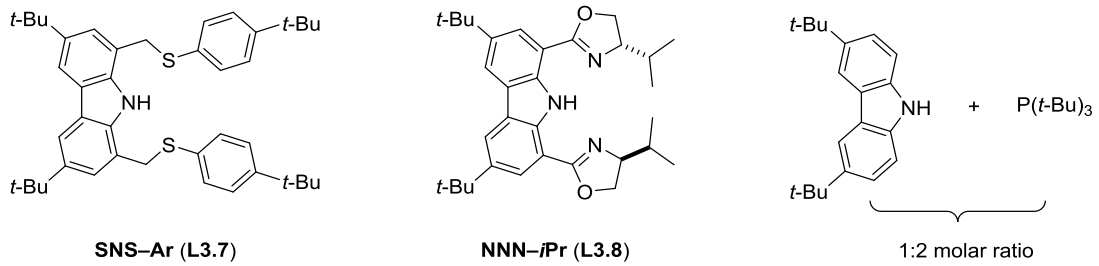

Figure 3.8. Ligand structures and combinations that are ineffective for the coupling of *t*-butyl carbamate with 2-bromo-4-phenylbutane under conditions related to that shown in **Scheme 3.5**.

The observed catalytic C–N coupling is also unique to copper. If CuBr is replaced by other transition metals commonly utilized in cross-couplings, no photocatalysis is observed. For example, even at 10 mol% loadings, carbamate alkylation is not observed using $CoBr_2$, $NiCl_2$(glyme), $PdCl_2$(cod), or Au(PPh_3)Cl in place of CuBr. Thus, the original design principles outlined in **Figure 3.2** remain appropriate for the development of photocatalysts for the C–N couplings of alkyl bromides.

3.3. Conclusions

Inspired by the mechanistic conclusions made in **Chapter 2**, we designed a new photoredox catalyst **3.1**, based on copper and a tridentate bis(phosphino)carbazole ligand **L3.1**, that can serve as an electron donor upon irradiation by blue LED or Hg lamps. We demonstrated that the new photocatalyst features a highly-reducing excited state that can elicit a mesolytic cleavage of an unactivated secondary alkyl bromide. Upon one-electron oxidation, **3.1** forms a metastable radical **3.7** which thermally decomposes to the diamagnetic

cation **3.8** via a formal hydrogen atom transfer. The decomposition product **3.8** can be recycled to give the starting material **3.1** under cross-coupling conditions. We also articulated that **3.1** can catalyze the C–N coupling reaction between *t*-butyl carbamate and 2-bromo-4-phenylbutane. The design embodied in complex **3.1** is crucial in eliciting the observed photochemical transformation, as copper, bis(phosphino)carbazole, and light are all required for the formation of C–N bonds. The methodological development of this carbamate alkylation using complex **3.1** or ligand **L3.1** is discussed in detail in **Chapter 4**.

3.4. Experimental section

3.4.1. General information

Unless otherwise noted, materials were either purchased from commercial suppliers and used as received, or prepared via literature procedures. **L3.1** was synthesized according to a literature procedure[15] and recrystallized from a cold, saturated solution in Et_2O/CH_3CN for use in photoinduced cross-couplings. **L3.2**[16] and **L3.8**[17] were prepared following reported procedures. Solvents were deoxygenated and dried by thoroughly sparging with argon, followed by passage through an activated column in a solvent purification system.

All manipulations of air-sensitive materials were carried out in oven-dried glassware using standard Schlenk, or glovebox techniques, under an N_2 atmosphere. Silicycle *Silia*Flash® P60 silica gel (particle size 40–63 μm) was used for flash chromatography. Analytical thin layer chromatography was conducted with glass TLC plates (silica gel 60 F254), and spots were visualized under UV light or after treatment with standard TLC stains.

X-band EPR measurements were made with a Bruker EMX spectrometer at 77 K. Simulation of EPR data was conducted using the software EasySpin.[18]

IR measurements were recorded on a Bruker ALPHA Diamond ATR or using a Perkin Elmer Paragon 1000 spectrometer using thin films deposited on KBr plates.

^{1}H, ^{13}C, and ^{31}P NMR spectra were recorded on a Bruker Ascend 400 MHz, a Varian 300 MHz, a Varian 400 MHz, a Varian 500 MHz, or a Varian 600 MHz spectrometer with $CHCl_3$ (^{1}H, δ = 7.26) and $CDCl_3$ (^{13}C, δ = 77.0) as internal references and with 85% H_3PO_4

(^{31}P) as an external reference. Multiplicity and qualifier abbreviations are as follows: s = singlet, d = doublet, t = triplet, q = quartet, m = multiplet, br = broad, app = apparent). GC analyses were carried out on an Agilent 6890 Series system with an HP-5 column (length 30 m, I.D. 0.25 mm).

X-ray crystallography studies were carried out at the Beckman Institute Crystallography Facility either Bruker Kappa Apex II diffractometer or a Bruker D8 Venture kappa duo photon 100 CMOS instrument (Mo Kα radiation). Structures were solved using SHELXT and refined against F^2 by full-matrix least squares with SHELXL and OLEX2. Hydrogen atoms were added at calculated positions and refined using a riding model. The crystals were mounted on a glass fiber or a nylon loop with Paratone N oil.

Steady-state fluorimetry was performed in the Beckman Institute Laser Resource Center (BILRC; California Institute of Technology). Steady-state emission spectra were collected on a Jobin S4 Yvon Spec Fluorolog-3-11 with a Hamamatsu R928P photomultiplier tube detector with photon counting. Absorbance spectra were acquired on a Cary 50 UV-Vis spectrophotometer with a Unisoku Scientific Instruments cryostat to maintain temperature.

Measurements of the excited-state lifetimes were conducted in BILRC. A Q-switched Nd:YAG laser (SpectraPhysics Quanta-Ray PRO-Series; 355 nm) was used as the source of the excitation pulse Transmitted light from the sample was detected with a photomultiplier tube (Hamamatsu R928). All instruments and electronics in these systems were controlled by software written in LabVIEW (National Instruments).

Electrochemical measurements were carried out in a thick-walled one-component electrochemical cell fitted with a Teflon stopcock and tungsten leads protruding from the top of the apparatus in a nitrogen-filled glovebox. A CH Instruments 600B electrochemical analyzer or a CHS-3600B potentiostat was used for data collection. A freshly-polished glassy carbon electrode was used as the working electrode, and platinum wire was used as the auxiliary electrode. Solutions (THF) of electrolyte (0.1 M tetra-*n*-butylammonium hexafluorophosphate) contained ferrocene (~1 mM, post measurement), to serve as an internal reference, and analyte (~1 mM).

Mass spectral data were collected on a Thermo LCQ or LTQ ion trap mass spectrometer, or on an Agilent 5973 mass spectrometer.

Photolytic reactions were performed using 34 W Kessil H150 Blue LED lamps, a 100 W Blak-Ray Long Wave Ultraviolet Lamp (Hg), or a 100-W Blak-Ray B-100Y High Intensity Inspection Lamp (Hg). If required, the temperature was maintained with an isopropanol bath cooled by an SP Scientific cryostat.

Elemental analyses were performed by Midwest Microlab (Indianapolis, IN).

3.4.2. Preparation of ligands

General procedure for the preparation of ligands

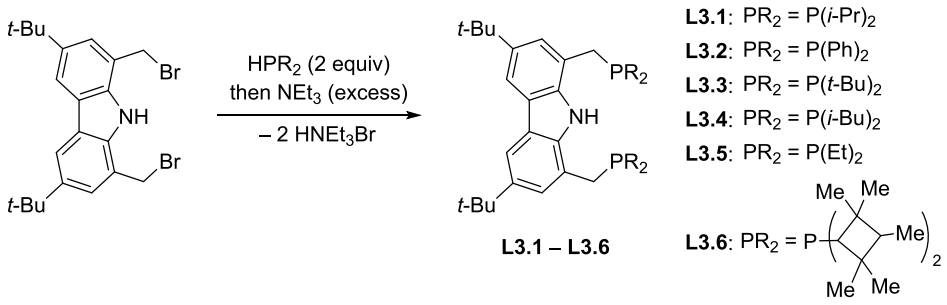

Procedures have been adapted from literature protocols.[15] To a suspension of 1,8-bis(bromomethyl)-3,6-di-*t*-butylcarbazole[16] (1 equiv) in CH_2Cl_2, a solution of secondary phosphine (2 equiv) in CH_2Cl_2 was added dropwise. The resulting clear solution was stirred at room temperature for at least 4 h. Then, volatiles were removed in vacuo, and the resulting residue was washed with *n*-pentane before it was re-suspended in CH_2Cl_2. After excess NEt_3 (1 mL) was added, the solution was stirred for another 30 min. Next, volatiles were removed in vacuo, and the resulting mixture was extracted in Et_2O and filtered. The filtrate was concentrated in vacuo to yield spectroscopically pure target compounds, which can be recrystallized in cold Et_2O/CH_3CN mixture to remove colored impurities.

Preparation of PNP-*t*Bu (L3.3)

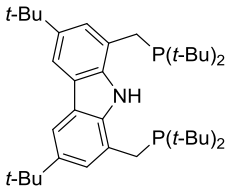

Following the general procedure, **L3.3** can be prepared from the reaction of 1,8-bis(bromomethyl)-3,6-di-*t*-butylcarbazole (604 mg, 1.30 mmol) and di-*t*-butylphosphine (396 mg, 2.71 mmol) in 57% yield (440 mg) as colorless solid. Spectral data matched those reported in the literature.[19]

Preparation of PNP-*i*Bu (L3.4)

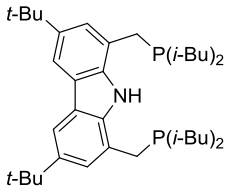

Following the general procedure, **L3.4** can be prepared from the reaction of 1,8-bis(bromomethyl)-3,6-di-*t*-butylcarbazole (465 mg, 1.00 mmol) and di-*i*-butylphosphine (292 mg, 2.00 mmol) in 67% yield (410 mg) as colorless solid.

^{1}H NMR (400 MHz, C_6D_6) δ 9.18 (s, 1H), 8.17 (s, 2H), 7.37 (s, 2H), 2.99 (s, 4H), 1.64–1.57 (m, 4H), 1.49 (s, 18H), 1.41–1.36 (m, 4H), 1.33–1.26 (m, 4H), 0.97–0.92 (m, 24H).

^{31}P NMR (162 MHz, C_6D_6) δ –42.8.

Preparation of PNP-Et (L3.5)

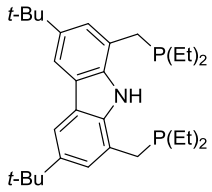

Following the general procedure, **L3.5** can be prepared from the reaction of 1,8-bis(bromomethyl)-3,6-di-*t*-butylcarbazole (465 mg, 1.00 mmol) and diethylphosphine (198 mg, 2.20 mmol) in 95% yield (460 mg) as colorless solid.

^{1}H NMR (400 MHz, C_6D_6) δ 9.13 (s, 1H), 8.21 (s, 2H), 7.38 (s, 2H), 2.97 (s, 4H), 1.48 (s, 18H), 1.29 (q, J = 7.7 Hz, 8H), 0.95 (dt, J = 7.7 Hz, 12H).

^{31}P NMR (162 MHz, C_6D_6) δ –24.3.

Preparation of PNP-PMP (L3.6)

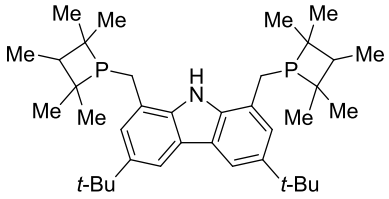

Following the general procedure, **L3.6** can be prepared from the reaction of 1,8-bis(bromomethyl)-3,6-di-*t*-butylcarbazole (465 mg, 1.00 mmol) and 2,2,3,4,4-pentamethylphosphetane[20] (290 mg, 2.01 mmol) in 20% yield (120 mg) as colorless solid.

^{1}H NMR (400 MHz, C_6D_6) δ 9.30 (s, 1H), 8.16 (s, 2H), 7.53 (s, 2H), 3.28 (s, 4H), 2.24–2.17 (m, 2H), 1.48 (s, 18H), 1.23–1.17 (m, 24H), 0.70 (s, 3H), 0.67 (s, 3H).

^{31}P NMR (162 MHz, C_6D_6) δ 22.2.

Preparation of SNS-Ar (L3.7)

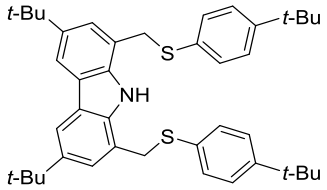

A 4 mL vial was charged with sodium 4-(*t*-butyl)-benzenethiolate[21] (38 mg, 0.20 mmol), 1,8-bis(bromomethyl)-3,6-di-*t*-butylcarbazole (47 mg, 0.10 mmol), and a magnetic stir bar. Then, 1 mL of THF was added, and the mixture was allowed to stir at room temperature overnight. The reaction was quenched by the addition of 1 mL of saturated $NaHCO_3$(aq), and the mixture was extracted with EtOAc (5 mL). The organic layer was collected, concentrated in vacuo, and purified by column chromatography (10% EtOAc in hexanes) to give the title compound (**L3.7**) as white solid in 47% yield (30 mg).

^{1}H NMR (300 MHz, $CDCl_3$) δ 8.67 (s, 1H), 7.92 (d, J = 1.6 Hz, 2H), 7.23 (br, 8H), 7.07 (d, J = 1.7 Hz, 2H), 4.38 (s, 4H), 1.34 (s, 18H), 1.26 (s, 18H).

^{13}C NMR (101 MHz, $CDCl_3$) δ 150.4, 142.3, 137.3, 131.8, 126.3, 126.0, 124.8, 124.2, 119.2, 115.6, 38.0, 34.7, 34.6, 32.1, 31.4.

FT-IR (film): 2956, 2873, 2817, 1491, 1455, 1193, 1027, 849 cm^{-1}.

MS (ESI) m/z $(M)^+$ calcd for $C_{42}H_{53}NS_2$: 635.4, found: 635.4.

Preparation of ONO-Ar (L3.9)

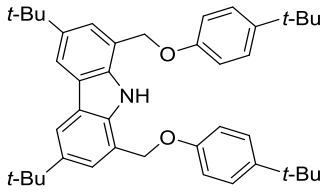

A 4 mL vial was charged with lithium 4-(*t*-butyl)-phenolate[22] (32 mg, 0.20 mmol), 1,8-bis(bromomethyl)-3,6-di-*t*-butylcarbazole (47 mg, 0.10 mmol), and a magnetic stir bar. Then, 1 mL of THF was added, and the mixture was allowed to stir at room temperature overnight. The reaction was quenched by the addition of 1 mL of saturated $NaHCO_3$(aq), and the mixture was extracted with EtOAc (5 mL). The organic layer was collected, concentrated in vacuo, and purified by column chromatography (5→10% Et_2O in hexanes) to give the title compound (**L3.9**) as off white solid in 66% yield (40 mg).

^{1}H NMR (300 MHz, $CDCl_3$) δ 9.46 (s, 1H), 8.28 (d, J = 1.6 Hz, 2H), 7.36–7.35 (m, 3H), 7.19 (s, 2H), 7.03–6.97 (m, 4H), 6.96 (br, 1H), 5.14 (s, 4H), 1.45 (s, 18H), 1.24 (s, 18H).

^{13}C NMR (101 MHz, $CDCl_3$) δ 156.4, 144.0, 142.2, 137.3, 126.4, 124.0, 122.8, 119.0, 116.4, 114.6, 70.1, 34.7, 34.3, 32.2, 31.7.

FT-IR (film): 3466, 2954, 2869, 1512, 1363, 1108, 1004, 828 cm^{-1}.

MS (ESI) m/z $(M+Na)^+$ calcd for $C_{42}H_{53}NO_2Na$: 626.4, found: 626.4.

3.4.3. Preparation of copper complexes

General procedure for the preparation of copper complexes (CuPNP)

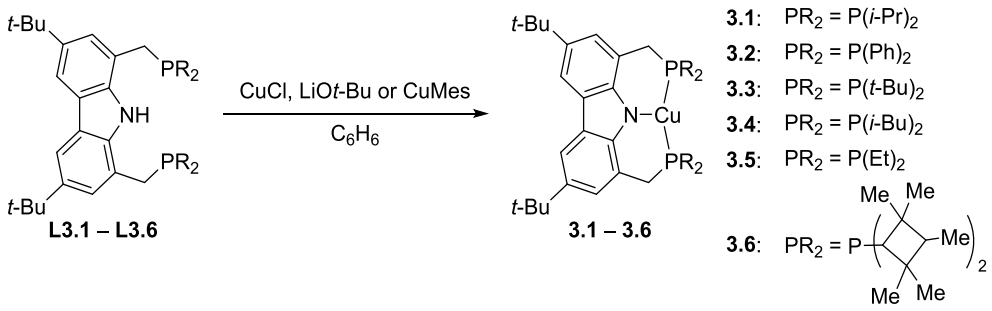

To a 20 mL scintillation vial, bis(phosphino)carbazole (1 equiv), CuCl (1 equiv), LiO*t*-Bu (1 equiv), a magnetic stir bar, and dry, degassed benzene were added. The mixture was vigorously stirred overnight at room temperature. Next, the mixture was filtered through a pad of Celite, and the filtrate was concentrated in vacuo. The ^{1}H NMR spectrum of the residue showed the clean formation of the target compound, which can be further purified by recrystallization from a mixture of benzene/*n*-hexanes, Et_2O or CH_3CN at –35 °C to afford colorless crystals of copper complexes.

CuPNP-*i*Pr (3.1)

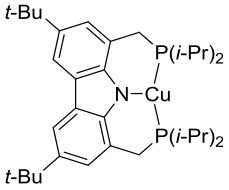

Following the general procedure, 3,6-di-*tert*-butyl-1,8-bis((di-*i*-propylphosphanyl)methyl)-9*H*-carbazole (**L3.1**) (310 mg, 0.57 mmol, 1.0 equiv), CuCl (55 mg, 0.56 mmol, 1.0 equiv), LiO*t*-Bu (48 mg, 0.60 mmol, 1.0 equiv), were used to give

colorless crystals of the target complex after recrystallization in a mixture of benzene/*n*-hexanes at –35 °C (260 mg, 76% yield). Crystals suitable for single-crystal X-ray diffraction were grown by slow evaporation of a concentrated sample in Et_2O at room temperature.

^{1}H NMR (400 MHz, C_6D_6) δ 8.49 (s, 2H), 7.39 (s, 2H), 3.19 (s, 4H), 1.65 (s, 18H), 1.63–1.57 (m, 4H), 0.89 (dq, J = 26.9, 7.1 Hz, 24H).

^{13}C NMR (101 MHz, C_6D_6) δ 148.0, 137.5, 125.5, 123.1, 119.8, 115.7, 34.8, 32.8, 26.4 (t, J = 8.8 Hz, 23.1 (t, J = 7.4 Hz), 19.7 (t, J = 3.8 Hz), 18.8 (t, J = 2.0 Hz).

^{31}P NMR (162 MHz, C_6D_6) δ 21.8.

Anal. Calcd for $C_{34}H_{54}CuNP_2$: C, 67.80; H, 9.04; N, 2.33. Found: C, 68.16; H, 9.38; N, 2.22.

CuPNP-Ph (3.2)

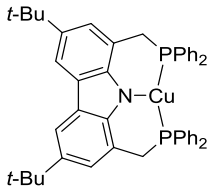

Mesitylcopper (18.3 mg, 0.100 mmol, 1 equiv), and **L3.2** (67.6 mg, 0.100 mmol, 1 equiv) was added to a 20 mL vial containing a magnetic stir bar. Benzene (4 mL) was then added, and the solution was allowed to stir overnight. The resulting precipitate was collected and washed with benzene (3 × 1 mL) to afford the target complex (55 mg, 74%). Crystals suitable for single-crystal X-ray diffraction were grown by vapor diffusion of pentane into a concentrated sample in benzene at room temperature.

^{1}H NMR (500 MHz, CD_2Cl_2) δ 7.95 (s, 2H), 7.61 (br, 8H), 7.35–7.39 (m, 12H), 7.19 (s, 2H), 3.97 (s, 4H), 1.39 (s, 18H).

^{31}P NMR (202 MHz, CD_2Cl_2) δ –0.7.

CuPNP-*t*Bu (3.3)

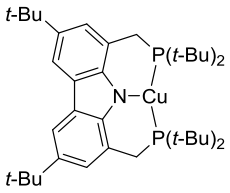

Following the general procedure, **L3.3** (60 mg, 0.10 mmol, 1 equiv), CuCl (9.9 mg, 0.10 mmol, 1 equiv), Li*O*t-Bu (9.0 mg, 0.11 mmol, 1.1 equiv), were used to give colorless crystals of the target complex (57 mg, 87% yield). Crystals suitable for single-crystal X-ray diffraction were grown by slow evaporation of a concentrated sample in Et_2O at room temperature.

^{1}H NMR (400 MHz, C_6D_6) δ 8.47 (s, 2H), 7.44 (s, 2H), 3.36 (s, 4H), 1.65 (s, 18H), 1.06–1.03 (m, 36H).

^{31}P NMR (162 MHz, C_6D_6) δ 38.3.

CuPNP-*i*Bu (3.4)

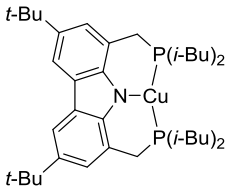

Following the general procedure, **L3.4** (12 mg, 0.020 mmol, 1 equiv), CuCl (2 mg, 0.020 mmol, 1 equiv), LiO*t*-Bu (4.0 mg, 0.050 mmol, 2.5 equiv), were used to give colorless crystals of the target complex (12 mg, 91% yield). Crystals suitable for single-crystal X-ray diffraction were grown by vapor diffusion of pentane into a concentrated sample in THF at room temperature.

^{1}H NMR (400 MHz, C_6D_6) δ 8.49 (s, 2H), 7.36 (s, 2H), 3.13 (s, 4H), 1.64 (s, 18H), 1.62–1.50 (m, 4H), 1.38–1.30 (m, 8H), 0.83 (d, J = 6.6 Hz, 12H) 0.83 (d, J = 6.6 Hz, 12H).

^{31}P NMR (162 MHz, C_6D_6) δ –19.5.

CuPNP-Et (3.5)

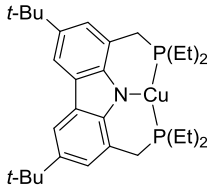

Following the general procedure, **L3.5** (330 mg, 0.68 mmol, 1 equiv), CuCl (6.7 mg, 0.68 mmol, 1 equiv), LiO*t*-Bu (8.5 mg, 0.11 mmol, 1.6 equiv), were used to give colorless crystals of the target complex after recrystallization in a mixture of benzene/*n*-hexanes at –

35 °C (150 mg, 40% yield). Crystals suitable for single-crystal X-ray diffraction were grown from a saturated solution in CH_3CN at –35 °C.

^{1}H NMR (400 MHz, C_6D_6) δ 8.46 (s, 2H), 7.32 (s, 2H), 3.12 (s, 4H), 1.64 (s, 18H), 1.21 (s, 8H), 0.82 (s, 12H).

^{31}P NMR (121 MHz, C_6D_6) δ –2.08.

CuPNP-PMP (3.6)

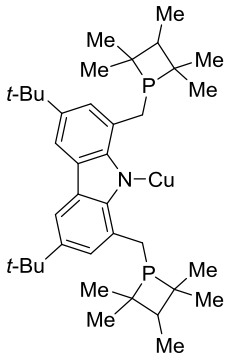

Following the general procedure, **L3.6** (12 mg, 0.020 mmol, 1 equiv), CuCl (2.0 mg, 0.020 mmol, 1 equiv), LiO*t*-Bu (1.6 mg, 0.20 mmol, 1 equiv), were used to give the target product (10 mg, 76% yield). Crystals suitable for single-crystal X-ray diffraction were grown by slow evaporation of a concentrated sample in Et_2O at room temperature.

^{1}H NMR (300 MHz, C_6D_6) δ 8.36 (s, 2H), 7.42 (s, 2H), 3.52 (s, 4H), 2.22 (q, J = 6.7 Hz, 2H), 1.64 (s, 18H), 1.16–1.06 (m, 24H), 0.64 (d, J = 7.2 Hz, 6H).

^{31}P NMR (121 MHz, C_6D_6) δ 41.7.

[CuPNHP][PF_6] (3.8-PF_6)

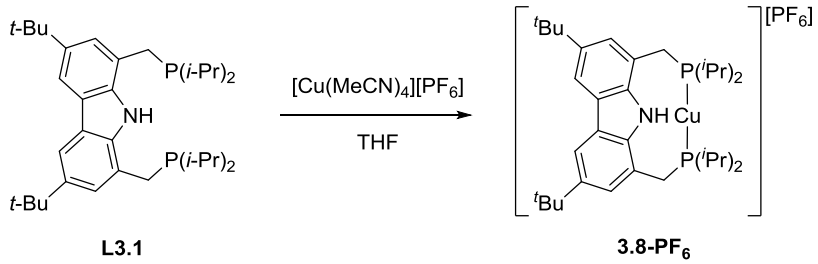

L3.1 **3.8-PF_6**

To a 20 mL scintillation vial, **L3.1** (110 mg, 0.2 mmol, 1 equiv) and [$Cu(CH_3CN)_4$][PF_6] (74 mg, 0.2 mmol, 1 equiv) were added. A magnetic stir bar and 5 mL of THF were then added, and the mixture was vigorously stirred at room temperature overnight. The solution was concentrated to dryness in vacuo and the residue was washed with *n*-hexane to give white solid (110 mg, 73% yield). Crystals suitable for single crystal X-ray diffraction were grown by vapor diffusion of pentane into a concentrated sample in THF at room temperature.

^{1}H NMR (400 MHz, CD_3CN) δ 8.31 (s, 1H), 8.04 (s, 2H), 7.45 (s, 2H), 3.66–2.96 (m, 4H), 1.90 (br, 4H), 1.43 (s, 18H), 1.29–1.07 (m, 24H).

^{13}C NMR (101 MHz, CD_3CN) δ 147.1, 139.9, 128.4, 126.1, 122.8, 116.2, 32.0, 27.1, 23.6, 20.0, 19.2.

^{31}P NMR (162 MHz, CD_3CN) δ 14.1, –144.6 (p).

Anal. Calcd for $C_{34}H_{55}CuF_6NP_3 \bullet C_4H_8O$: C, 55.63; H, 7.74; N, 1.71. Found: C, 55.53; H, 7.63; N, 1.69.

[CuPNP][BAr$^{F}_{24}$][Hexane] (3.7-BAr$^{F}_{24}$)

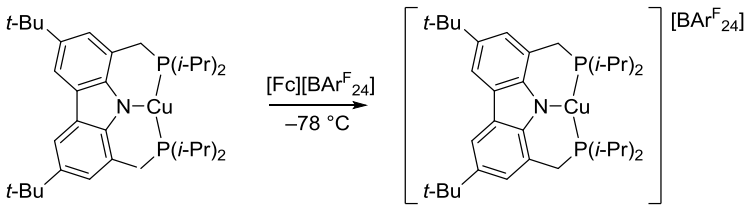

To a 4 mL vial, **3.1** (12.8 mg, 0.020 mmol, 1 equiv), [Fc][BAr$^{F}_{24}$] (20 mg, 0.019 mmol, 1 equiv), and a magnetic stir bar was added. Then, the vial was cooled to –78 °C, and pre-chilled CH_2Cl_2 was added to the vial. The resulting dark mixture was allowed to stir for 30 min, and the volatiles were removed in vacuo at –78 °C. Pre-chilled Et_2O was added to the vial, and the solution was filtered into a new, pre-chilled 4 mL vial. The filtrate was allowed to stand at –35 °C overnight, resulting in an oily residue that contained single crystals of **3.7- BAr$^{F}_{24}$**.

3.4.4. Photoproperties of complexes

Determination of the lifetime of 3.1*

A 1 mg/mL solution was prepared by dissolving 3 mg of **3.1** in 3 mL THF. This solution was then diluted 50-fold, and the diluted solution as transferred to a quartz cuvette. The cuvette was sealed, and the luminescence decays upon 355 nm excitation were measured at various wavelengths. The data are summarized below.

Table 3.1. Luminescence lifetimes of **3.1** at various emission wavelengths in THF

Entry	Emission wavelength	Lifetime	Average lifetime
1	427 nm	7.87 ns	
2	432 nm	7.92 ns	
3	455 nm	8.39 ns	8.12 ns
4	405 nm	8.25 ns	
5	415 nm	8.08 ns	

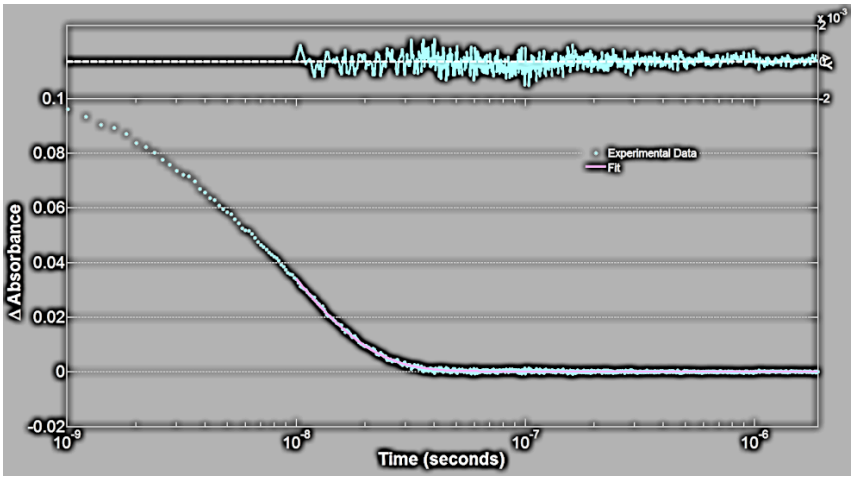

Figure 3.9. Representative fitting of the luminescence decay of copper complex **3.1** at 427 nm.

Quenching of 3.1* by an alkyl bromide

Measured amounts of 2-bromo-4-phenylbutane were added via Hamilton sample locked syringe to a solution of **3.1** in 4 mL THF in a quartz cuvette equipped with a PTFE-

septum cap. Emission spectra were collected at various wavelengths at each concentration of 2-bromo-4-phenylbutane. A representative figure is shown below.

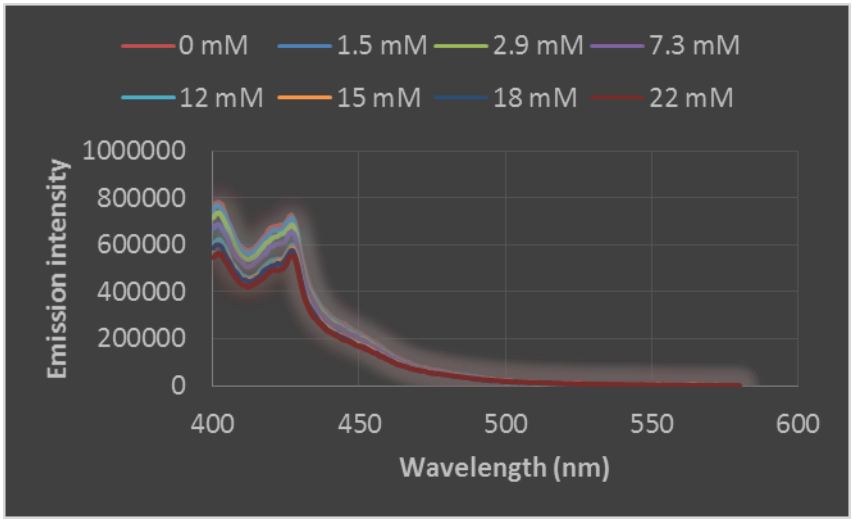

Figure 3.10. The emission spectra of a solution of copper complex **3.1** in THF upon irradiation at 380 nm in the presence of varying amounts of 2-bromo-4-phenylbutane.

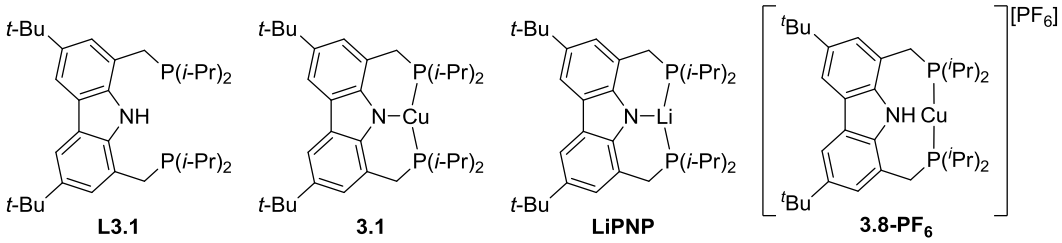

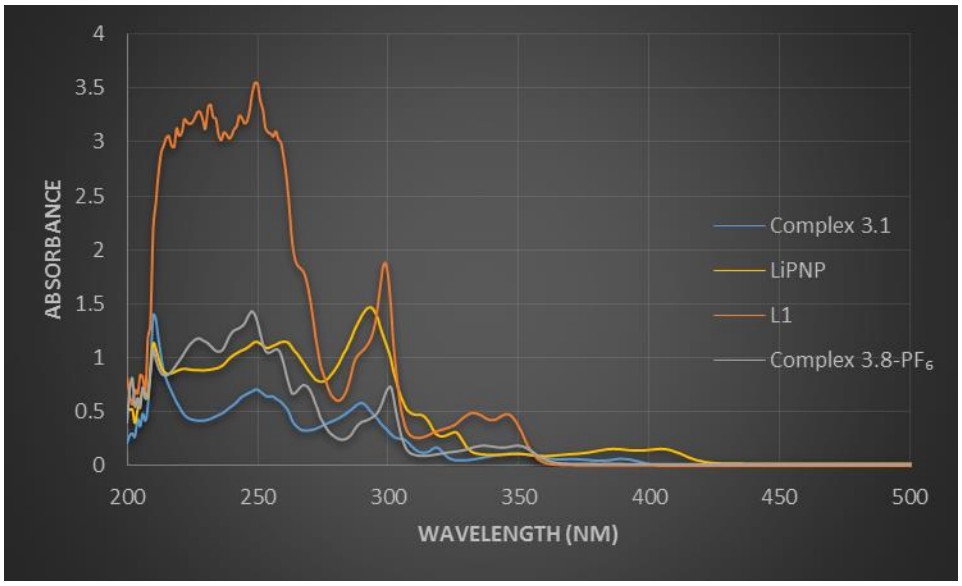

Figure 3.11. UV-vis spectra in THF of **L3.1** and its derivatives.

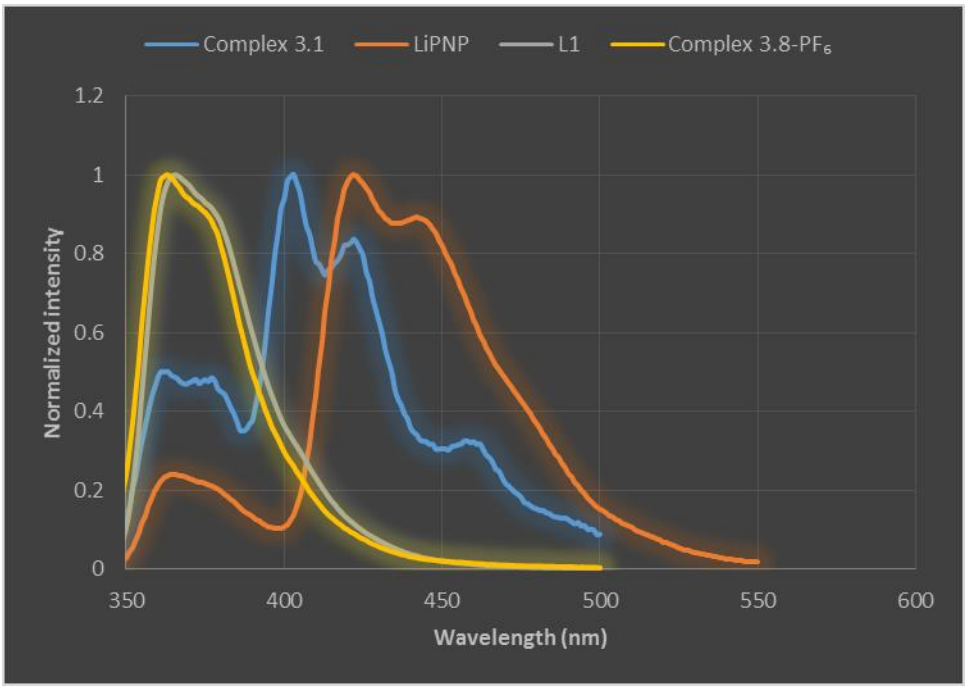

Figure 3.12. Emission spectra in THF of **L3.1** and its derivatives (excitation at 300 nm).

3.4.5. EPR spectroscopy

Oxidation of 3.1 using $FcAcBF_4$

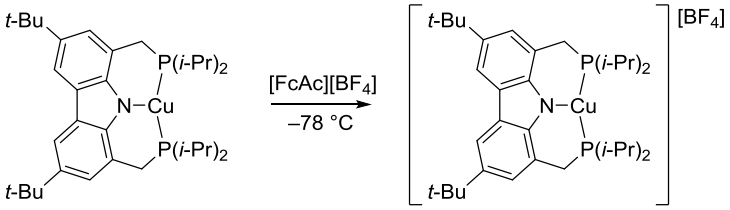

In two separate vials, solutions of **3.1** (4.8 mg, 0.080 mmol, 1 equiv) in 1 mL THF and acetylferrocenium tetrafluoroborate (2.4 mg, 0.076 mmol, 1 equiv) in 1 mL THF were prepared at –78 °C. The solution of **3.1** was then added dropwise to the solution of acetylferrocenium tetrafluoroborate, and the resulting purple mixture was stirred at –78 °C for 2 h, yielding a dark purple mixture. The EPR spectrum of this mixture is provided below. The prolonged storage of the resulting mixture at –35 °C gives twinned crystals of **3.8-BF_4**.

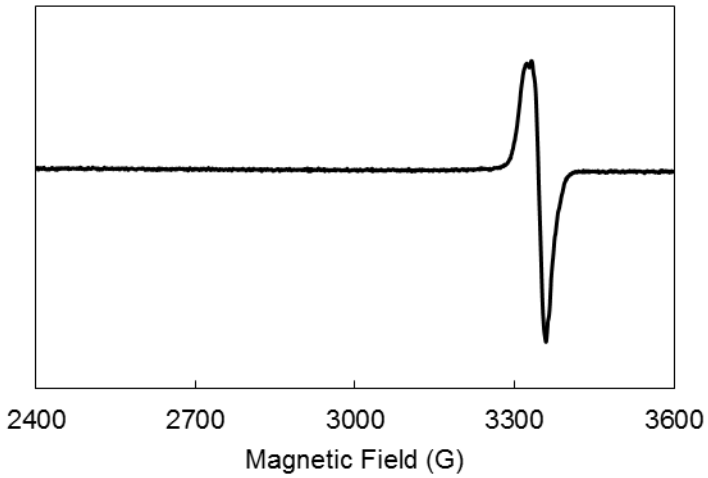

Figure 3.13. X-band EPR spectra of the oxidation product of **3.1** (9.4 MHz, 77 K, THF/2-MeTHF, g = 2.007).

3.4.6. DFT calculations

Geometry optimizations, single-point calculations, frequency calculations, and time-dependent calculations were performed using the Gaussian 09 (Rev B.01) suite of programs with the B3LYP functional and the 6-31G* basis set for all atoms.[23] Frequency calculations were performed on optimized geometries to ensure true minima.

MO	Occupancy	Relative Energy
165		0.02629
164		0.00026
163		-0.01062
162	↿⇂	-0.15466
161	↿⇂	-0.17822
160	↿⇂	-0.17963

Figure 3.14. DFT-generated frontier molecular orbitals (MO = 160, MO = 161, MO = 162, MO = 163, MO = 164, MO = 165) of copper complex **3.1**.

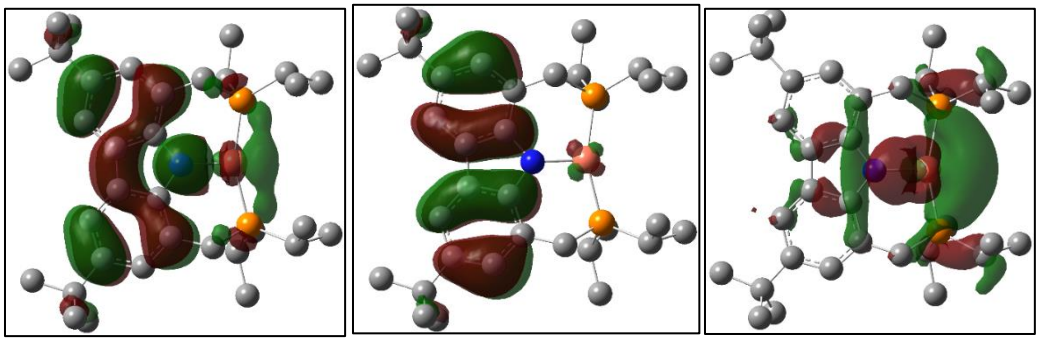

Figure 3.15. HOMO (MO = 162), HOMO-1 (MO = 161), and HOMO-2 (MO = 162) of copper complex **3.1** (H atoms are omitted for clarity).

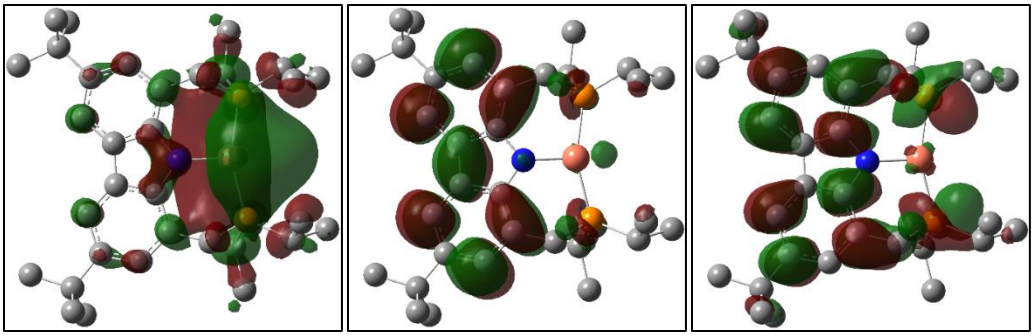

Figure 3.16. LUMO (MO = 163), LUMO+1 (MO = 164), and LUMO+2 (MO = 165) of copper complex **3.1** (H atoms are omitted for clarity).

Excited State 1:				
393 nm (*f* =0.0240)	160 (HOMO-2)	→	163 (LUMO)	(0.19)
	162 (HOMO)	→	**163 (LUMO)**	(0.67)
Excited State 2:				
360 nm (*f* =0.0056)	**160 (HOMO-2)**	→	**163 (LUMO)**	(0.66)
	162 (HOMO)	→	163 (LUMO)	(-0.19)
Excited State 3:				
344 nm (*f* =0.0772)	161 (HOMO-1)	→	165 (LUMO+2)	(-0.11)
	162 (HOMO)	→	**164 (LUMO+1)**	(0.69)

Figure 3.17. TD-DFT results: Orbital compositions of the calculated singlet excitations (first three) of copper complex **3.1**. Transitions of significance are in bold.

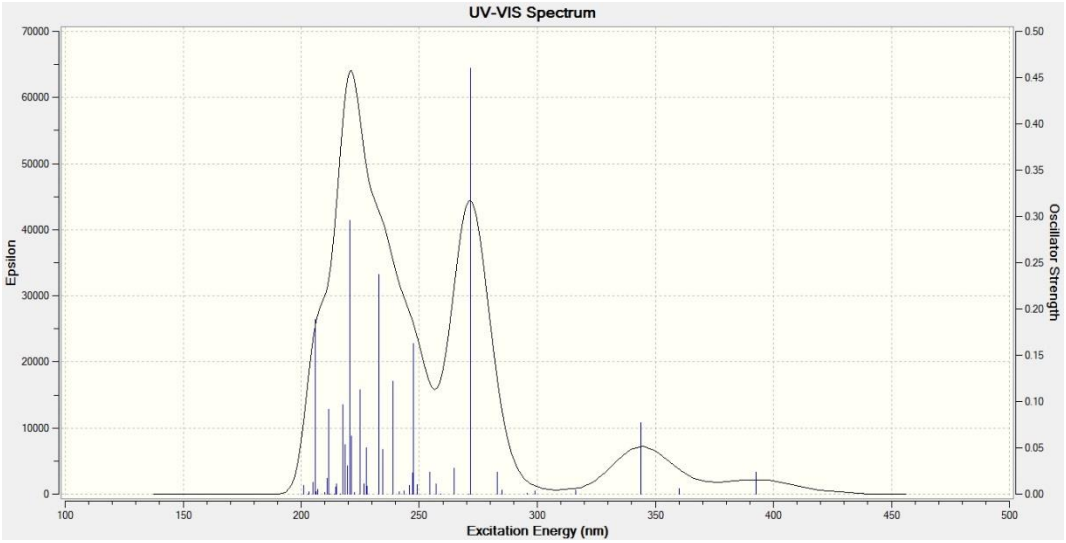

Figure 3.18. Calculated absorption spectrum of copper complex **3.1**.

3.4.7. General procedure for the photoinduced alkylations

Figure 3.19. A typical irradiation setup at room temperature. Shown are three 34-watt blue LED lamps, a reflective Dewar, and a table fan.

A standard reaction mixture was prepared in an 8 mL vial, using either CuBr (10 mg, 0.070 mmol) and **L3.1** (3.8 mg, 0.0070 mmol), or **3.1** (4.2 mg, 0.0070 mmol). Then, LiO*t*-Bu (168 mg, 2.1 mmol), and *t*-butylcarbmate (246 mg, 2.1 mmol), were added to the vial, followed by 2-bromo-4-pheny(149 mg, 0.70 mmol) and DME (8 mL). Next, the vial was capped, and the reaction vial and a magnetic stir bar were submerged in a low-form hemispherical Dewar flask filled with water in a well-ventilated fume hood. Three 34-watt blue LED lamps were placed 3 inches from the vial (as close to the vial as possible, without the lamps being in contact with water), and the vial was irradiated for 16 h. The temperature of the water bath was maintained below 30 °C with a table fan. A typical setup is shown above. After irradiation, a 20 mL vial was charged with a measured quantity of an internal standard (*n*-dodecane). The unpurified reaction mixture was then added to the 20 mL vial that contained the internal standard, ensuring quantitative transfer through EtOAc rinses (2 mL × 3). An aliquot was filtered through a pad of silica gel (eluting with EtOAc) into a GC vial, and the sample was subjected to GC analysis.

3.4.8. X-ray crystallographic data

CuPNP-*i*Pr (3.1)

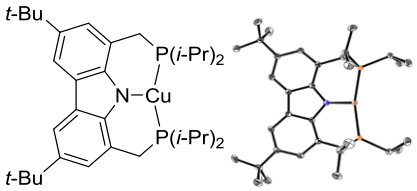

Table 3.2. Crystal data and structure refinement for **3.1**.

Identification code	**3.1**
Empirical formula	$C_{34}H_{54}NP_2Cu$
Formula weight	602.26
Temperature/K	100.05
Crystal system	orthorhombic
Space group	Pbca
a/Å	12.4490(9)
b/Å	22.9148(14)
c/Å	23.1633(14)
α/°	90
β/°	90
γ/°	90
Volume/Å^3	6607.7(7)
Z	8
ρ_{calc}g/cm^3	1.211
μ/mm^{-1}	0.780
F(000)	2592.0
Radiation	MoKα (λ = 0.71073)
2Θ range for data collection/°	3.516 to 66.098
Index ranges	$-18 \leq h \leq 18$, $-34 \leq k \leq 32$, $-28 \leq l \leq 35$
Reflections collected	103697
Independent reflections	11695 [R_{int} = 0.0580, R_{sigma} = 0.0339]
Data/restraints/parameters	11695/0/357
Goodness-of-fit on F^2	1.060
Final R indexes [I>=2σ (I)]	R_1 = 0.0403, wR_2 = 0.1284
Final R indexes [all data]	R_1 = 0.0550, wR_2 = 0.1405
Largest diff. peak/hole / e Å^{-3}	0.76/-0.69

Table 3.3. Fractional Atomic Coordinates ($\times 10^4$) and Equivalent Isotropic Displacement Parameters ($Å^2 \times 10^3$) for **3.1**. U_{eq} is defined as 1/3 of the trace of the orthogonalized U_{IJ} tensor.

Atom	*x*	*y*	*z*	U(eq)	Atom	*x*	*y*	*z*	U(eq)
Cu1	8134.6(2)	3559.3(2)	294.2(2)	12.50(6)	C41	8868.4(14)	5047.2(7)	731.1(7)	24.2(3)
P2	9428.5(3)	2905.6(2)	196.9(2)	12.76(8)	C38	3031.9(13)	4020.1(9)	2166.4(8)	27.9(4)
P3	7233.1(3)	4381.6(2)	205.0(2)	12.32(8)	C42	7096.8(14)	5565.1(6)	568.9(8)	22.6(3)
N1	7194.9(10)	3150.1(5)	848.7(5)	12.0(2)	C8	7105.8(11)	2686.3(5)	1741.8(6)	12.4(2)
C24	8167.6(11)	1844.6(6)	2003.2(6)	13.5(2)	C45	8062.8(13)	4880.5(7)	-786.5(7)	21.4(3)
C26	6469.4(11)	3440.0(5)	1200.3(6)	12.2(2)	C34	8286.5(16)	764.8(7)	2175.6(8)	29.7(4)
C31	8745.3(12)	2222.8(5)	412.9(6)	14.4(2)	C40	7644.0(12)	4981.0(6)	696.4(6)	15.9(3)
C27	6373.7(11)	3171.5(5)	1751.1(6)	12.1(2)	C36	4142.2(12)	4096.6(6)	2444.6(6)	17.0(3)
C28	5640.2(11)	3383.1(6)	2160.4(6)	13.9(2)	C13	5134.5(11)	4132.7(6)	1483.1(6)	14.7(2)
C32	8554.5(13)	1372.6(6)	2423.7(7)	17.2(3)	C35	9771.1(14)	1422.5(7)	2509.7(8)	24.8(3)
C25	7408.6(11)	2263.1(6)	2148.7(6)	14.0(2)	C47	9257.9(14)	2432.7(8)	-898.3(7)	25.5(3)
C23	8594.2(11)	1850.1(5)	1436.6(6)	13.6(2)	C48	10490.3(15)	3291.1(7)	-785.3(7)	25.7(3)
C11	10482.9(12)	2957.7(6)	755.7(6)	16.9(3)	C46	10065.3(13)	2732.3(6)	-500.8(6)	17.8(3)
C22	8308.5(11)	2256.0(5)	1019.2(6)	12.5(2)	C43	6987.5(12)	4709.0(6)	-511.9(6)	15.9(3)
C29	5004.9(11)	3863.9(6)	2031.1(6)	14.0(2)	C44	6380.7(14)	4278.4(7)	-901.0(6)	22.4(3)
C30	5871.9(11)	4205.1(6)	467.6(6)	15.5(3)	C1	11159.6(15)	3512.0(7)	698.6(8)	26.9(3)
C21	7570.0(11)	2691.8(5)	1183.7(6)	11.8(2)	C33	8014.0(15)	1427.5(8)	3013.6(8)	28.0(4)
C20	11192.1(14)	2416.0(7)	810.9(7)	24.6(3)	C39	4340.0(15)	4747.5(7)	2573.0(8)	27.3(4)
C37	4144.0(13)	3773.9(6)	3023.3(7)	20.2(3)	C4	5839.5(11)	3932.0(5)	1061.9(6)	13.1(2)

Table 3.4. Anisotropic Displacement Parameters ($Å^2 \times 10^3$) for **3.1**. The anisotropic displacement factor exponent takes the form: $-2\pi^2[h^2a^{*2}U_{11}+2hka^*b^*U_{12}+\ldots]$.

Atom	U_{11}	U_{22}	U_{33}	U_{23}	U_{13}	U_{12}	Atom	U_{11}	U_{22}	U_{33}	U_{23}	U_{13}	U_{12}
Cu1	14.75(10)	8.87(9)	13.88(10)	1.67(5)	2.58(6)	1.81(5)	C33	30.2(9)	34.8(9)	19.0(8)	14.7(6)	3.5(6)	8.0(7)
P2	15.32(17)	9.46(15)	13.52(17)	0.79(11)	2.63(12)	1.57(11)	C39	40.6(10)	15.6(6)	25.7(8)	-0.7(6)	14.3(7)	4.6(6)
P3	15.15(18)	9.33(14)	12.48(16)	2.07(11)	2.14(12)	1.58(12)	C4	13.8(6)	11.0(5)	14.5(6)	1.8(4)	1.3(5)	-0.5(4)
N1	14.5(5)	8.5(4)	13.0(5)	0.9(4)	1.2(4)	0.4(4)	C41	24.0(8)	20.8(7)	28.0(8)	0.0(6)	-2.7(6)	-1.6(6)
C24	15.7(6)	9.4(5)	15.4(6)	2.4(4)	-0.9(5)	-0.7(4)	C38	17.3(8)	41.2(10)	25.2(8)	5.4(7)	4.2(6)	3.5(6)
C26	13.7(6)	10.1(5)	12.9(6)	-0.2(4)	0.2(5)	-0.5(4)	C42	27.4(8)	13.9(6)	26.4(8)	-3.6(5)	3.6(6)	3.9(5)
C31	19.4(7)	8.6(5)	15.1(6)	-0.9(4)	2.2(5)	0.5(4)	C8	13.7(6)	10.3(5)	13.2(6)	0.6(4)	0.4(5)	-0.7(4)
C27	13.3(6)	9.8(5)	13.2(6)	1.0(4)	-0.1(5)	-1.1(4)	C45	29.9(8)	17.5(6)	16.8(7)	4.0(5)	5.7(6)	-2.1(5)
C28	15.6(6)	12.7(5)	13.3(6)	0.9(5)	1.8(5)	-0.9(4)	C34	41.6(10)	12.8(6)	34.9(10)	8.0(6)	-10.4(8)	-3.2(6)
C32	18.9(7)	14.0(5)	18.6(7)	5.0(5)	-0.7(5)	1.0(5)	C40	19.3(7)	13.5(5)	15.1(6)	-0.7(5)	2.4(5)	-1.0(5)
C25	15.9(6)	12.3(5)	13.9(6)	2.0(4)	-0.1(5)	-1.3(4)	C36	17.3(6)	16.1(6)	17.7(7)	2.0(5)	5.6(5)	2.8(5)
C23	15.8(6)	8.5(5)	16.6(6)	-0.4(4)	0.1(5)	-0.4(4)	C13	14.9(6)	12.6(5)	16.5(6)	1.6(5)	2.3(5)	1.4(4)
C11	17.0(7)	15.9(6)	17.8(7)	0.1(5)	0.0(5)	-1.2(5)	C35	20.0(8)	28.4(8)	26.0(8)	5.9(6)	-4.2(6)	2.6(6)
C22	15.4(6)	8.4(5)	13.7(6)	-0.8(4)	0.8(5)	-1.6(4)	C47	27.3(8)	33.2(8)	16.1(7)	-3.9(6)	3.3(6)	2.3(6)
C29	15.1(6)	12.5(5)	14.4(6)	0.1(4)	2.8(5)	-0.6(4)	C48	31.0(9)	23.9(7)	22.1(8)	5.7(6)	10.6(6)	1.7(6)
C30	16.3(6)	14.5(6)	15.7(6)	4.0(5)	0.5(5)	1.3(5)	C46	21.7(7)	16.5(6)	15.2(7)	2.1(5)	5.2(5)	5.2(5)
C21	13.8(6)	8.5(5)	13.1(6)	0.5(4)	-0.1(4)	-1.2(4)	C43	21.7(7)	12.6(5)	13.3(6)	2.6(5)	1.8(5)	3.4(5)
C20	19.3(7)	24.4(7)	30.1(9)	4.4(6)	-2.3(6)	4.0(6)	C44	27.7(8)	24.3(7)	15.3(7)	-0.9(6)	-0.1(6)	-1.0(6)
C37	22.7(7)	20.2(6)	17.7(7)	1.9(5)	5.9(6)	1.8(5)	C1	25.1(8)	21.7(7)	33.8(9)	0.8(6)	-2.5(7)	-7.7(6)

Table 3.5. Bond Lengths for **3.1**.

Atom	Atom	Length/Å	Atom	Atom	Length/Å
Cu1	P2	2.2112(4)	C32	C34	1.543(2)
Cu1	P3	2.2029(4)	C32	C35	1.532(2)
Cu1	N1	1.9741(11)	C25	C8	1.4039(18)
P2	C31	1.8497(14)	C23	C22	1.3878(18)
P2	C11	1.8474(15)	C11	C20	1.529(2)
P2	C46	1.8434(15)	C11	C1	1.530(2)
P3	C30	1.8452(15)	C22	C21	1.4097(18)
P3	C40	1.8557(14)	C29	C36	1.5347(19)
P3	C43	1.8477(15)	C29	C13	1.4201(19)
N1	C26	1.3857(17)	C30	C4	1.5127(19)
N1	C21	1.3868(16)	C21	C8	1.4162(19)
C24	C32	1.5332(19)	C37	C36	1.531(2)
C24	C25	1.3878(19)	C39	C36	1.541(2)
C24	C23	1.4160(19)	C4	C13	1.3906(19)
C26	C27	1.4214(18)	C41	C40	1.534(2)
C26	C4	1.4103(18)	C38	C36	1.535(2)
C31	C22	1.5080(19)	C42	C40	1.530(2)
C27	C28	1.4028(19)	C45	C43	1.533(2)
C27	C8	1.4379(18)	C47	C46	1.526(2)
C28	C29	1.3889(19)	C48	C46	1.534(2)
C32	C33	1.528(2)	C43	C44	1.535(2)

Table 3.6. Bond Angles for **3.1**.

Atom	Atom	Atom	Angle/°	Atom	Atom	Atom	Angle/°
P3	Cu1	P2	160.224(16)	C22	C23	C24	123.75(12)
N1	Cu1	P2	100.15(3)	C20	C11	P2	114.61(11)
N1	Cu1	P3	99.52(3)	C20	C11	C1	111.31(13)
C31	P2	Cu1	102.15(5)	C1	C11	P2	112.60(11)
C11	P2	Cu1	113.73(5)	C23	C22	C31	121.50(12)
C11	P2	C31	101.06(7)	C23	C22	C21	116.98(13)
C46	P2	Cu1	123.27(5)	C21	C22	C31	121.50(12)
C46	P2	C31	104.64(6)	C28	C29	C36	122.65(12)
C46	P2	C11	108.82(7)	C28	C29	C13	118.17(12)
C30	P3	Cu1	104.45(4)	C13	C29	C36	119.12(12)
C30	P3	C40	102.31(7)	C4	C30	P3	114.53(10)
C30	P3	C43	103.49(7)	N1	C21	C22	127.22(12)
C40	P3	Cu1	115.80(5)	N1	C21	C8	112.35(11)
C43	P3	Cu1	121.06(5)	C22	C21	C8	120.43(12)
C43	P3	C40	107.23(7)	C26	C4	C30	121.52(12)
C26	N1	Cu1	122.75(8)	C13	C4	C26	117.12(12)
C26	N1	C21	104.69(11)	C13	C4	C30	121.23(12)

C21	N1	Cu1	121.61(9)	C25	C8	C27	133.97(13)
C25	C24	C32	123.17(13)	C25	C8	C21	120.63(12)
C25	C24	C23	118.31(12)	C21	C8	C27	105.39(11)
C23	C24	C32	118.52(12)	C41	C40	P3	112.29(10)
N1	C26	C27	112.01(11)	C42	C40	P3	113.97(11)
N1	C26	C4	127.73(12)	C42	C40	C41	111.47(12)
C4	C26	C27	120.23(12)	C29	C36	C39	110.18(12)
C22	C31	P2	112.03(9)	C29	C36	C38	109.18(13)
C26	C27	C8	105.55(11)	C37	C36	C29	112.19(12)
C28	C27	C26	120.77(12)	C37	C36	C39	107.36(13)
C28	C27	C8	133.63(12)	C37	C36	C38	108.27(13)
C29	C28	C27	119.94(12)	C38	C36	C39	109.61(14)
C24	C32	C34	109.40(12)	C4	C13	C29	123.73(12)
C33	C32	C24	111.81(12)	C47	C46	P2	110.03(11)
C33	C32	C34	108.19(14)	C47	C46	C48	110.09(13)
C33	C32	C35	108.24(14)	C48	C46	P2	110.19(10)
C35	C32	C24	109.91(12)	C45	C43	P3	109.42(10)
C35	C32	C34	109.25(13)	C45	C43	C44	110.54(12)
C24	C25	C8	119.80(13)	C44	C43	P3	110.37(10)

CuPNP-Ph[C_6H_6] (3.2-C_6H_6)

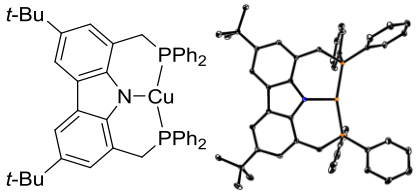

Table 3.7. Crystal data and structure refinement for **3.2-C_6H_6**.

Identification code	**3.2-C_6H_6**
Empirical formula	$C_{52}H_{52}CuNP_2$
Formula weight	738.32
Temperature/K	100.03
Crystal system	triclinic
Space group	P-1
a/Å	12.5805(4)
b/Å	13.8221(4)
c/Å	14.5741(5)
α/°	87.4145(12)
β/°	64.6820(11)
γ/°	67.0504(12)
Volume/Å^3	2086.88(12)
Z	2
ρ_{calc}g/cm^3	1.175
μ/mm^{-1}	0.630
F(000)	776.0
Radiation	MoKα (λ = 0.71073)

2Θ range for data collection/°	4.816 to 72.826
Index ranges	$-20 \le h \le 20$, $-23 \le k \le 23$, $-24 \le l \le 24$
Reflections collected	144242
Independent reflections	20296 [R_{int} = 0.1587, R_{sigma} = 0.0885]
Data/restraints/parameters	20296/0/511
Goodness-of-fit on F^2	1.005
Final R indexes [I>=2σ (I)]	R_1 = 0.0558, wR_2 = 0.1403
Final R indexes [all data]	R_1 = 0.0997, wR_2 = 0.1639
Largest diff. peak/hole / e Å^{-3}	0.93/-1.10

Table 3.8. Fractional Atomic Coordinates ($\times 10^4$) and Equivalent Isotropic Displacement Parameters (Å$^2 \times 10^3$) for **3.2-C$_6$H$_6$**. U_{eq} is defined as 1/3 of the trace of the orthogonalized U_{IJ} tensor.

Atom	*x*	*y*	*z*	U(eq)	Atom	*x*	*y*	*z*	U(eq)
Cu1	7186.1(2)	6763.1(2)	3755.9(2)	8.38(5)	C32	12918.3(15)	6006.1(13)	1969.3(13)	14.2(3)
P2	6168.9(4)	6550.3(3)	2915.6(3)	8.06(7)	C19	6576.2(17)	7978.3(15)	9137.1(13)	17.7(3)
P3	8525.7(4)	7203.3(3)	4066.6(3)	7.18(7)	C24	6899.8(15)	9336.6(13)	4339.8(13)	13.6(3)
N1	6116.3(12)	6565.7(10)	5137.3(10)	8.0(2)	C36	5226.4(18)	8706.8(13)	2781.0(14)	17.5(3)
C20	4899.4(13)	6596.1(11)	5437.1(11)	7.1(2)	C40	3880.0(17)	7860.6(13)	2781.7(13)	16.5(3)
C1	6093.8(14)	6916.7(11)	6024.4(11)	7.9(2)	C31	12464.0(15)	5398.2(13)	2692.3(13)	15.3(3)
C22	8437.4(14)	6678.5(12)	5275.5(11)	8.4(2)	C13	231.4(16)	7245.6(16)	7995.9(14)	18.8(3)
C4	5647.0(14)	7595.2(12)	8011.6(11)	9.0(2)	C26	7311.6(17)	10810.0(13)	4678.1(13)	16.1(3)
C11	4409.6(14)	6306.9(11)	4828.6(11)	7.6(2)	C45	7419.3(19)	4427.9(15)	387.5(13)	19.6(3)
C23	8040.2(14)	8621.1(12)	4351.2(11)	9.8(3)	C15	866.8(17)	5865.7(13)	6605.3(15)	18.1(3)
C2	7096.2(14)	7020.2(11)	6149.0(11)	8.1(2)	C25	6537.3(16)	10423.3(13)	4502.9(14)	16.7(3)
C10	3144.0(14)	6414.7(11)	5316.8(12)	8.6(2)	C18	4249.8(18)	8963.0(15)	9607.4(14)	21.4(4)
C8	2828.4(14)	7051.4(11)	6969.3(12)	9.4(2)	C44	8351.9(18)	4698.1(15)	-364.7(13)	19.2(3)
C3	6838.3(14)	7362.1(12)	7140.8(11)	9.0(2)	C43	8616.8(17)	5507.7(15)	-120.4(13)	19.2(3)
C21	5230.4(14)	5832.8(11)	3713.2(11)	9.0(2)	C39	3009.9(19)	8828.9(15)	2718.6(15)	22.9(4)
C6	4878.6(14)	7164.4(12)	6891.2(11)	8.8(2)	C38	3241(2)	9732.1(15)	2694.6(15)	25.5(4)
C5	4666.3(14)	7493.4(12)	7867.6(11)	9.4(2)	C37	4349(2)	9672.3(14)	2722.6(15)	25.0(4)
C12	929.0(14)	6914.8(12)	6834.0(12)	11.1(3)	C51	8973(2)	95.1(16)	1829.2(17)	31.1(5)
C29	10263.4(14)	6715.9(11)	3261.3(11)	8.9(2)	C52	10267(2)	-422.1(18)	1175.8(18)	31.5(5)
C7	4097.9(14)	6958.6(11)	6502.9(11)	8.4(2)	C47	10700(2)	-1280.6(18)	469.1(16)	33.4(5)
C9	2327.3(14)	6785.6(11)	6381.6(12)	8.8(2)	C48	9830(3)	-1627.7(18)	420.7(17)	36.2(6)
C34	10736.6(15)	7313.0(12)	2515.6(12)	11.7(3)	C50	8097(2)	-238.8(19)	1770.8(17)	34.1(5)
C41	7001.6(15)	5789.7(12)	1635.7(11)	10.2(3)	C49	8531(3)	-1102(2)	1062.4(19)	35.6(5)
C35	4995.9(16)	7789.4(12)	2816.4(12)	11.4(3)	C30	11142.3(15)	5754.1(12)	3332.7(13)	13.7(3)
C16	5411.5(15)	7895.7(13)	9110.6(12)	12.0(3)	C33	12052.0(16)	6962.7(13)	1884.7(12)	13.4(3)
C28	8799.5(16)	9014.8(12)	4552.3(12)	12.0(3)	C42	7953.8(17)	6044.6(14)	871.6(13)	16.3(3)
C27	8433.4(17)	10102.8(13)	4711.8(13)	15.0(3)	C14	221.5(16)	7783.6(14)	6348.0(14)	16.9(3)
C46	6738.9(17)	4970.7(13)	1386.3(13)	14.7(3)	C17	5149.4(18)	7024.3(15)	9749.1(13)	17.7(3)

Table 3.9. Anisotropic Displacement Parameters ($Å^2 \times 10^3$) for **3.2-C_6H_6**. The anisotropic displacement factor exponent takes the form: $-2\pi^2[h^2a^{*2}U_{11}+2hka^*b^*U_{12}+\ldots]$.

Atom	U_{11}	U_{22}	U_{33}	U_{23}	U_{13}	U_{12}	Atom	U_{11}	U_{22}	U_{33}	U_{23}	U_{13}	U_{12}
Cu1	8.72(9)	10.19(9)	7.50(8)	0.89(6)	-3.49(7)	-5.19(7)	C36	22.7(8)	11.8(7)	16.6(8)	3.2(6)	-6.6(7)	-8.1(6)
P2	9.47(16)	7.86(16)	7.71(16)	0.44(12)	-4.32(13)	-3.76(13)	C40	17.5(8)	14.5(7)	16.7(7)	-0.2(6)	-10.8(6)	-2.1(6)
P3	6.78(15)	7.91(15)	6.74(15)	0.63(12)	-2.24(13)	-3.73(13)	C31	9.5(6)	13.7(7)	17.3(7)	1.6(6)	-3.6(6)	-2.2(5)
N1	6.5(5)	10.6(5)	7.0(5)	0.0(4)	-2.6(4)	-4.0(4)	C13	10.5(7)	29.2(9)	15.9(8)	-0.2(7)	-2.1(6)	-11.2(7)
C20	6.4(6)	6.6(5)	8.4(6)	0.3(4)	-3.4(5)	-2.6(5)	C26	20.2(8)	8.7(6)	13.6(7)	-0.8(5)	-2.8(6)	-5.3(6)
C1	6.1(6)	9.0(6)	8.2(6)	-0.2(5)	-2.6(5)	-3.0(5)	C45	26.5(9)	20.6(8)	12.5(7)	-4.0(6)	-6.7(7)	-11.8(7)
C22	7.1(6)	10.1(6)	7.6(6)	1.5(5)	-2.5(5)	-4.0(5)	C15	13.2(7)	13.6(7)	28.3(9)	-0.1(6)	-7.2(7)	-8.2(6)
C4	7.5(6)	12.0(6)	7.5(6)	0.9(5)	-3.2(5)	-4.2(5)	C25	12.2(7)	12.0(7)	19.7(8)	1.0(6)	-4.8(6)	-1.1(6)
C11	7.5(6)	6.5(5)	8.3(6)	0.6(4)	-3.6(5)	-2.4(5)	C18	19.6(8)	23.4(9)	13.7(8)	-7.9(6)	-5.5(7)	-2.5(7)
C23	9.6(6)	9.0(6)	8.4(6)	0.4(5)	-2.4(5)	-3.3(5)	C44	18.4(8)	21.1(8)	11.6(7)	-3.7(6)	-3.9(6)	-4.5(7)
C2	7.8(6)	9.6(6)	7.4(6)	1.7(5)	-3.2(5)	-4.4(5)	C43	17.0(8)	23.9(8)	11.7(7)	0.5(6)	-1.0(6)	-9.4(7)
C10	7.7(6)	8.1(6)	11.1(6)	0.9(5)	-4.9(5)	-3.4(5)	C39	21.4(9)	20.2(8)	19.1(8)	0.0(7)	-11.7(7)	2.6(7)
C8	6.8(6)	9.1(6)	11.0(6)	0.1(5)	-3.6(5)	-2.5(5)	C38	26.9(10)	16.1(8)	15.6(8)	4.2(6)	-5.8(7)	4.0(7)
C3	8.6(6)	10.5(6)	8.8(6)	1.1(5)	-3.9(5)	-4.7(5)	C37	33.9(11)	11.3(7)	20.0(9)	4.1(6)	-5.8(8)	-7.1(7)
C21	10.2(6)	8.6(6)	9.5(6)	-0.2(5)	-4.9(5)	-4.3(5)	C51	41.6(13)	16.9(8)	21.8(10)	4.7(7)	-7.2(9)	-7.7(8)
C6	6.0(6)	11.2(6)	8.5(6)	0.0(5)	-2.5(5)	-3.5(5)	C52	35.1(12)	29.7(11)	30.5(11)	16.3(9)	-15.4(10)	-14.6(9)
C5	5.7(6)	11.6(6)	8.4(6)	-0.8(5)	-1.2(5)	-3.1(5)	C47	28.7(11)	33.4(11)	17.4(9)	10.6(8)	-3.9(8)	-0.8(9)
C12	7.0(6)	11.5(6)	15.2(7)	0.7(5)	-4.8(5)	-4.3(5)	C48	52.3(15)	27.4(11)	19.1(10)	0.6(8)	-16.7(10)	-5.7(10)
C29	8.9(6)	9.1(6)	7.1(6)	-0.3(5)	-1.7(5)	-4.1(5)	C50	26.2(10)	32.9(11)	24.3(10)	9.2(9)	-2.7(8)	-4.0(9)
C7	7.9(6)	9.0(6)	8.9(6)	0.8(5)	-4.1(5)	-3.7(5)	C49	43.5(14)	40.0(13)	33.3(12)	15.3(10)	-22.3(11)	-22.1(11)
C9	7.8(6)	7.9(6)	11.4(6)	1.8(5)	-4.4(5)	-3.9(5)	C46	17.7(7)	15.4(7)	10.8(7)	-0.4(5)	-4.7(6)	-8.4(6)
C34	11.6(6)	11.9(6)	8.8(6)	1.9(5)	-2.2(5)	-4.6(5)	C30	12.2(7)	10.6(6)	14.6(7)	3.2(5)	-3.2(6)	-4.2(5)
C41	11.1(6)	9.8(6)	8.3(6)	0.3(5)	-4.8(5)	-2.3(5)	C33	12.4(7)	15.6(7)	11.3(7)	2.1(5)	-2.5(5)	-8.0(6)
C35	15.5(7)	8.1(6)	8.4(6)	0.4(5)	-5.7(5)	-2.2(5)	C42	15.4(7)	19.3(8)	12.8(7)	-0.4(6)	-2.9(6)	-9.3(6)
C16	9.6(6)	18.8(7)	7.3(6)	-1.1(5)	-2.8(5)	-6.2(6)	C14	9.7(7)	17.1(7)	25.2(9)	5.3(6)	-9.5(6)	-4.9(6)
C28	13.4(7)	11.1(6)	13.3(7)	1.9(5)	-7.8(6)	-4.8(5)	C17	19.6(8)	26.9(9)	12.1(7)	6.1(6)	-7.9(6)	-14.2(7)
C27	20.8(8)	12.2(7)	14.3(7)	1.4(5)	-7.7(6)	-9.2(6)	C32	8.9(6)	17.1(7)	13.1(7)	-1.7(6)	-1.4(5)	-5.5(6)
C24	9.6(6)	12.8(7)	16.8(7)	1.0(5)	-4.7(6)	-4.1(5)	C19	17.9(8)	31.2(9)	11.0(7)	2.8(6)	-7.4(6)	-15.6(7)

Table 3.10. Bond Lengths for **3.2-C_6H_6**.

Atom	Atom	Length/Å	Atom	Atom	Length/Å	Atom	Atom	Length/Å	Atom	Atom	Length/Å
Cu1	P2	2.2113(4)	C12	C15	1.541(2)	C4	C5	1.395(2)	C32	C31	1.387(2)
Cu1	P3	2.2120(4)	C29	C34	1.402(2)	C4	C16	1.544(2)	C24	C25	1.388(2)
Cu1	N1	1.9643(13)	C29	C30	1.393(2)	C11	C10	1.385(2)	C36	C37	1.389(3)
P2	C21	1.8341(15)	C34	C33	1.390(2)	C11	C21	1.507(2)	C40	C39	1.389(2)
P2	C41	1.8245(15)	C41	C46	1.398(2)	C23	C28	1.398(2)	C26	C25	1.390(2)
P2	C35	1.8224(15)	C41	C42	1.397(2)	C23	C24	1.396(2)	C45	C44	1.387(3)
P3	C22	1.8501(15)	C35	C36	1.401(2)	C2	C3	1.400(2)	C44	C43	1.385(3)
P3	C23	1.8190(15)	C35	C40	1.391(2)	C10	C9	1.423(2)	C39	C38	1.384(3)
P3	C29	1.8273(15)	C16	C17	1.540(2)	C8	C7	1.396(2)	C38	C37	1.381(3)
N1	C20	1.3841(18)	C16	C19	1.530(2)	C8	C9	1.392(2)	C51	C52	1.376(3)
N1	C1	1.3865(18)	C16	C18	1.532(2)	C6	C5	1.393(2)	C51	C50	1.385(4)
C20	C11	1.420(2)	C28	C27	1.388(2)	C6	C7	1.440(2)	C52	C47	1.375(3)
C20	C7	1.420(2)	C27	C26	1.389(2)	C12	C9	1.528(2)	C47	C48	1.383(4)
C1	C2	1.408(2)	C46	C45	1.395(2)	C12	C14	1.538(2)	C48	C49	1.378(4)
C1	C6	1.425(2)	C30	C31	1.398(2)	C12	C13	1.527(2)	C50	C49	1.382(3)
C22	C2	1.512(2)	C33	C32	1.388(2)	C4	C3	1.412(2)	C42	C43	1.385(2)

Table 3.11. Bond Angles for **3.2-C_6H_6**.

Atom	Atom	Atom	Angle/°	Atom	Atom	Atom	Angle/°	Atom	Atom	Atom	Angle/°	Atom	Atom	Atom	Angle/°
P2	Cu1	P3	158.689(18)	C13	C12	C14	108.37(14)	C20	C11	C21	122.69(13)	C32	C33	C34	120.59(15)
N1	Cu1	P2	100.36(4)	C13	C12	C15	107.96(14)	C10	C11	C20	117.23(13)	C43	C42	C41	120.84(15)
N1	Cu1	P3	100.36(4)	C34	C29	P3	119.01(11)	C10	C11	C21	119.96(13)	C31	C32	C33	119.54(15)
C21	P2	Cu1	104.72(5)	C30	C29	P3	122.74(12)	C28	C23	P3	121.64(12)	C25	C24	C23	120.61(15)
C41	P2	Cu1	123.25(5)	C30	C29	C34	118.21(14)	C24	C23	P3	119.29(12)	C37	C36	C35	120.50(18)
C41	P2	C21	103.71(7)	C20	C7	C6	105.67(12)	C24	C23	C28	119.04(14)	C39	C40	C35	120.25(17)
C35	P2	Cu1	113.95(5)	C8	C7	C20	121.58(13)	C1	C2	C22	121.84(13)	C32	C31	C30	119.90(15)
C35	P2	C21	105.73(7)	C8	C7	C6	132.75(14)	C3	C2	C1	117.26(13)	C27	C26	C25	119.57(15)
C35	P2	C41	103.87(7)	C10	C9	C12	119.48(13)	C3	C2	C22	120.64(13)	C44	C45	C46	120.51(16)
C22	P3	Cu1	103.40(5)	C8	C9	C10	118.21(13)	C11	C10	C9	123.80(13)	C24	C25	C26	120.10(15)
C23	P3	Cu1	115.40(5)	C8	C9	C12	122.27(14)	C9	C8	C7	119.63(14)	C43	C44	C45	119.72(16)
C23	P3	C22	105.03(7)	C33	C34	C29	120.58(15)	C2	C3	C4	123.87(14)	C44	C43	C42	120.15(16)
C23	P3	C29	102.75(7)	C46	C41	P2	123.51(12)	C11	C21	P2	115.37(10)	C38	C39	C40	120.36(19)
C29	P3	Cu1	125.56(5)	C42	C41	P2	117.66(12)	C1	C6	C7	105.32(12)	C37	C38	C39	120.03(17)
C29	P3	C22	102.36(7)	C42	C41	C46	118.82(14)	C5	C6	C1	121.19(13)	C38	C37	C36	119.98(18)
C20	N1	Cu1	123.44(10)	C36	C35	P2	118.48(13)	C5	C6	C7	133.45(14)	C52	C51	C50	120.1(2)
C20	N1	C1	105.14(12)	C40	C35	P2	122.64(12)	C6	C5	C4	120.20(13)	C47	C52	C51	120.4(2)
C1	N1	Cu1	123.84(10)	C40	C35	C36	118.87(15)	C9	C12	C14	108.34(13)	C52	C47	C48	119.7(2)
N1	C20	C11	128.49(13)	C17	C16	C4	108.65(13)	C9	C12	C15	110.66(13)	C49	C48	C47	120.2(2)
N1	C20	C7	111.97(12)	C19	C16	C4	112.58(13)	C14	C12	C15	109.48(13)	C49	C50	C51	119.5(2)
C7	C20	C11	119.54(13)	C19	C16	C17	107.47(13)	C13	C12	C9	111.98(13)	C48	C49	C50	120.1(2)
N1	C1	C2	128.41(13)	C19	C16	C18	108.18(14)	C2	C22	P3	115.60(10)	C27	C28	C23	120.05(15)
N1	C1	C6	111.90(12)	C18	C16	C4	110.44(13)	C3	C4	C16	123.09(13)	C28	C27	C26	120.61(15)
C2	C1	C6	119.67(13)	C18	C16	C17	109.45(14)	C5	C4	C3	117.79(13)	C45	C46	C41	119.95(16)
C5	C4	C16	119.04(13)	C29	C30	C31	121.16(15)								

CuPNP-*t*Bu [Et_2O]$_{0.25}$ (3.3-Et_2O)

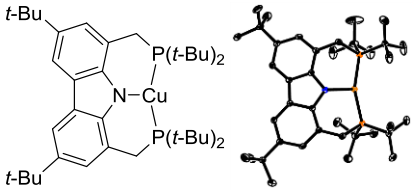

Table 3.12. Crystal data and structure refinement for **3.3-Et_2O**.

Identification code	**3.3-Et_2O**
Empirical formula	$C_{39}H_{64.5}CuNO_{0.25}P_2$
Formula weight	676.95
Temperature/K	99.99
Crystal system	monoclinic
Space group	P2/c

a/Å	25.6250(14)
b/Å	13.0072(7)
c/Å	47.425(3)
α/°	90
β/°	102.731(2)
γ/°	90
Volume/Å^3	15418.7(14)
Z	17
ρ_{calc}g/cm^3	1.166
μ/mm^{-1}	0.676
F(000)	5864.0
Radiation	MoKα (λ = 0.71073)
2Θ range for data collection/°	1.76 to 60.182
Index ranges	-34 ≤ h ≤ 33, -18 ≤ k ≤ 18, -61 ≤ l ≤ 66
Reflections collected	292242
Independent reflections	41022 [R_{int} = 0.0646, R_{sigma} = 0.0527]
Data/restraints/parameters	41022/0/1666
Goodness-of-fit on F^2	1.011
Final R indexes [I>=2σ (I)]	R_1 = 0.0449, wR_2 = 0.0935
Final R indexes [all data]	R_1 = 0.0799, wR_2 = 0.1049
Largest diff. peak/hole / e Å^{-3}	1.18/-0.70

Table 3.13. Fractional Atomic Coordinates (×10^4) and Equivalent Isotropic Displacement Parameters (Å^2×10^3) for **3.3-Et$_2$O**. U_{eq} is defined as 1/3 of the trace of the orthogonalized U_{IJ} tensor.

Atom	*x*	*y*	*z*	U(eq)	Atom	*x*	*y*	*z*	U(eq)
Cu01	2804.7(2)	2960.1(2)	4443.1(2)	13.66(5)	C02R	1343.6(9)	748.5(19)	5774.5(5)	27.3(5)
Cu02	5225.0(2)	6428.2(2)	6865.1(2)	12.80(5)	C02S	-1199.9(9)	8031.0(18)	3148.3(5)	26.0(5)
Cu03	2202.3(2)	3022.7(2)	5657.2(2)	12.72(5)	C02T	4765.3(8)	649.2(18)	5312.4(5)	22.8(5)
Cu04	-88.4(2)	6499.3(2)	3169.8(2)	14.61(5)	C02U	1897.7(9)	2070.6(18)	3895.9(5)	24.6(5)
P005	4881.4(2)	4932.5(4)	6699.6(2)	12.77(10)	C02V	1832.6(9)	180.0(18)	3962.3(5)	26.4(5)
P006	1786.4(2)	4519.9(4)	5654.9(2)	12.97(10)	C02W	2413.5(9)	923.0(18)	6317.8(5)	25.2(5)
P007	3222.0(2)	4434.6(4)	4435.5(2)	15.16(10)	C02X	3390.8(9)	491.2(18)	4789.2(5)	23.3(5)
P008	2363.3(2)	1359.8(4)	5735.3(2)	12.44(10)	C02Y	4031.4(9)	3664(2)	4850.3(5)	26.8(5)
P009	5408.4(2)	8081.4(4)	6856.7(2)	14.24(10)	C02Z	5882.6(9)	8443(2)	6386.9(5)	28.1(5)
P00A	76.3(2)	4846.9(4)	3247.6(2)	15.3(1)	C030	4853.2(8)	9010.5(16)	6710.0(5)	19.9(4)
P00B	2629.3(2)	1320.4(4)	4353.1(2)	13.31(10)	C031	1573.1(9)	628.8(18)	5295.6(5)	25.0(5)
P00C	-452.5(2)	8009.6(4)	3216.8(2)	15.7(1)	C032	4334.3(9)	7328.5(18)	5496.4(6)	30.5(6)
N00D	2208.3(6)	3359.4(12)	4619.0(3)	13.2(3)	C033	4916.9(9)	643.8(17)	5850.8(5)	22.4(5)
N00E	5559.9(6)	6092.0(12)	7269.3(3)	12.8(3)	C034	1519.3(10)	7939.8(17)	4897.9(5)	28.4(5)
N00F	2791.0(6)	3386.0(12)	5470.0(3)	12.6(3)	C035	3133.4(9)	1977.5(17)	6196.5(5)	23.8(5)
O00G	2746.8(6)	8176.3(13)	3603.6(4)	29.8(4)	C036	-135.6(10)	8760.0(18)	3548.0(5)	29.0(5)
N00H	399.4(6)	6854.8(13)	2919.4(4)	15.2(3)	C037	443.3(9)	4483.2(17)	2968.1(5)	25.0(5)
C00I	4263.4(8)	1885.6(15)	5560.1(4)	13.2(4)	C038	6890.9(9)	2189.1(17)	7887.7(5)	26.0(5)
C00J	6344.9(7)	6090.2(14)	7621.5(4)	11.5(4)	C039	1925.0(9)	-691.7(17)	5670.6(5)	27.3(5)
C00K	5955.5(7)	6689.7(15)	7434.1(4)	12.3(4)	C03A	6349.8(9)	9263.5(19)	6855.0(5)	29.8(5)
C00L	3794.1(8)	1297.4(15)	5543.6(4)	13.8(4)	C03B	4584.3(9)	8682.7(19)	6400.4(5)	26.3(5)
C00M	3289.4(8)	1719.6(15)	5515.5(4)	13.2(4)	C03C	7304.8(10)	9294.5(18)	7989.6(5)	30.2(5)
C00N	4215.6(7)	2948.0(15)	5548.7(4)	13.2(4)	C03D	6372.5(9)	7366.0(18)	6789.1(5)	26.5(5)
C00O	3778.3(8)	5402.2(15)	5482.6(4)	13.5(4)	C03E	2289(1)	3684.6(18)	2777.7(6)	32.1(6)
C00P	6177.8(7)	5040.9(15)	7567.7(4)	12.5(4)	C03F	2452.7(9)	5198(2)	3991.1(5)	30.0(5)
C00Q	1082.4(8)	7903.7(15)	2835.9(4)	15.0(4)	C03G	5024.3(10)	10139.6(17)	6712.4(6)	29.2(5)
C00R	1750.3(8)	2779.4(15)	4590.7(4)	12.8(4)	C03H	-42.3(9)	1723.8(19)	4778.8(5)	28.1(5)

C00S	1192.9(8)	1290.9(15)	4548.3(4)	15.0(4)	C03I	962.3(9)	3699.3(19)	5257.9(5)	28.1(5)
C00T	3478.9(8)	6297.4(15)	5449.9(4)	14.7(4)	C03J	2581.3(9)	934.7(19)	3765.9(5)	26.3(5)
C00U	3248.0(7)	2799.0(15)	5501.7(4)	12.4(4)	C03K	5965.2(10)	1515.4(19)	7800.7(6)	34.3(6)
C00V	3523.7(7)	4451.1(15)	5487.5(4)	12.1(4)	C03L	1820.3(10)	4599(2)	6244.2(5)	32.6(6)
C00W	6008.4(8)	7764.9(15)	7431.3(4)	13.7(4)	C03M	3500.2(10)	7919.4(18)	5166.4(6)	32.9(6)
C00X	2961.9(7)	4388.0(15)	5458.8(4)	12.6(4)	C03N	830.4(9)	5538(2)	5354.2(6)	32.5(6)
C00Y	5696.3(7)	5094.8(14)	7352.9(4)	11.8(4)	C03O	-206.3(9)	1771.5(19)	4240.7(5)	29.7(5)
C00Z	6775.8(8)	6561.0(15)	7809.9(4)	13.4(4)	C03P	2799.5(9)	5264(2)	2959.0(6)	32.2(6)
C010	3711.8(8)	3404.9(15)	5518.9(4)	12.6(4)	C03Q	991.8(11)	11382.6(19)	2525.3(5)	33.5(6)
C011	1528.7(8)	6289.6(15)	4623.8(4)	14.8(4)	C03R	1394.8(10)	7963.4(18)	4359.7(5)	27.6(5)
C012	6392.0(8)	4095.0(15)	7674.0(4)	13.7(4)	C03S	3930.9(9)	5817(2)	6698.6(5)	30.2(5)
C013	1700.8(8)	1702.1(15)	4574.4(4)	13.9(4)	C03T	4058.6(10)	5338(3)	6217.6(5)	42.0(7)
C014	552.5(8)	7849.8(16)	2879.2(4)	15.5(4)	C03U	1880.6(10)	10749.4(18)	2784.5(6)	31.8(6)
C015	785.6(8)	2951.5(15)	4547.1(4)	13.7(4)	C03V	3664.8(10)	8594(2)	3669.8(6)	34.8(6)
C016	731.2(8)	1886.7(15)	4536.6(4)	14.8(4)	C03W	3067.0(9)	5113(2)	4080.5(5)	28.0(5)
C017	1793.4(8)	5340.3(16)	2828.7(4)	16.7(4)	C03X	204.5(9)	227.2(17)	4515.4(6)	33.0(6)
C018	1288.1(7)	3399.2(14)	4574.4(4)	12.0(4)	C03Y	1837.5(10)	7683(2)	3575.8(6)	35.4(6)
C019	2918.1(8)	6212.4(15)	5418.6(4)	15.7(4)	C03Z	2324.2(9)	5131.5(19)	2448.8(5)	27.1(5)
C01A	2041.1(8)	4367.6(15)	4626.5(4)	13.0(4)	C040	1660.3(10)	6304.6(19)	5993.5(6)	33.1(6)
C01B	6133.0(8)	3191.9(15)	7571.2(4)	14.7(4)	C041	1250.2(11)	11449.8(19)	3062.4(5)	32.7(6)
C01C	4890.9(8)	4201.3(16)	7034.9(4)	15.3(4)	C042	6459.8(11)	1546.3(19)	7401.2(6)	34.7(6)
C01D	1261.7(8)	6858.3(15)	2844.4(4)	14.9(4)	C043	2550.5(9)	5435(2)	6073.2(5)	29.8(5)
C01E	2087.6(8)	6192.8(15)	4652.9(4)	16.0(4)	C044	3847.7(10)	3997(2)	6558.9(7)	46.3(8)
C01F	1367.6(8)	4759.3(16)	2890.6(4)	18.7(4)	C045	3592.3(10)	7998.0(18)	5700.4(6)	32.4(6)
C01G	1228.1(8)	5394.4(15)	4596.6(4)	14.4(4)	C046	734.0(9)	4193(2)	5719.2(5)	31.6(6)
C01H	1044.1(8)	9753.9(16)	2814.8(4)	17.3(4)	C047	7258.4(11)	7893(2)	8333.2(5)	35.2(6)
C01I	6444.4(8)	8196.8(15)	7618.7(4)	15.1(4)	C048	3239.1(11)	4418(3)	3852.7(5)	42.8(7)
C01J	1734.1(8)	6396.0(16)	2808.6(4)	16.1(4)	C049	5259.1(11)	4632(2)	6198.3(5)	39.1(7)
C01K	1479.8(7)	4437.4(15)	4597.3(4)	12.8(4)	C04A	3179.2(10)	8227(2)	3461.0(6)	35.4(6)
C01L	5418.6(7)	4184.8(15)	7251.0(4)	13.3(4)	C04B	-826.6(10)	4192(2)	2870.3(6)	41.6(7)
C01M	508.8(8)	9682.5(16)	2847.9(4)	18.3(4)	C04C	4171.9(10)	5481(2)	4731.9(7)	41.3(7)
C01N	257.8(8)	8763.6(16)	2881.4(4)	16.8(4)	C04D	4280.8(10)	4048(3)	4390.7(6)	42.4(7)
C01O	833.8(8)	6253.7(16)	2897.6(4)	15.0(4)	C04E	5834.9(10)	4086(2)	6656.7(5)	38.4(7)
C01P	5644.5(8)	3267.1(15)	7363.8(4)	15.6(4)	C04F	7831.6(9)	7714(2)	7974.7(7)	40.2(7)
C01Q	4796.7(8)	1328.2(15)	5580.9(4)	15.4(4)	C04G	-1394.1(10)	7433(3)	2872.5(5)	45.9(8)
C01R	1323.4(8)	8848.5(16)	2806.2(4)	16.6(4)	C04H	2297.1(11)	7704(3)	3429.2(6)	42.9(7)
C01S	2181.1(8)	1011.6(15)	4597.7(4)	15.9(4)	C04I	-276.3(12)	8286(3)	3811.8(6)	54.2(9)
C01T	1047.1(8)	4517.4(17)	5495.0(4)	18.9(4)	C04J	-1387.4(12)	7436(3)	3383.5(6)	58.4(10)
C01U	2801.1(8)	1051.6(15)	5484.8(4)	15.0(4)	C04K	3322.6(12)	6163(2)	4079.3(7)	44.9(7)
C01V	1281.6(8)	7361.4(15)	4617.6(5)	17.5(4)	C04L	264.0(12)	4774(3)	3845.9(6)	66.0(12)
C01W	888.5(8)	5183.3(16)	2924.8(4)	17.1(4)	C04M	5032.3(15)	3035(2)	6427.8(9)	62.6(11)
C01X	6832.8(8)	7619.0(15)	7810.7(4)	14.2(4)	C04N	-857.7(12)	4105(3)	3381.7(7)	68.7(12)
C01Y	2353.2(8)	5266.4(16)	4652.7(4)	15.8(4)	C04O	-345.5(11)	2802(2)	3168.6(9)	63.3(11)
C01Z	6025.2(8)	8336.8(17)	6716.0(5)	21.1(4)	C04Q	464.3(12)	8641(4)	3586.3(6)	78.4(14)
C020	2650.7(8)	5292.8(15)	5424.1(4)	14.3(4)	C04S	640(2)	3394(4)	3694.5(11)	32.1(17)
C021	2772.7(8)	1041.5(15)	6103.6(4)	16.7(4)	C0AA	903(2)	3675(4)	3576.2(12)	29.6(17)
C022	1788.5(8)	446.2(16)	5620.4(5)	19.0(4)	C2AA	-1462(2)	9084(5)	3004(2)	30(2)
C023	7302.5(8)	8127.0(15)	8022.2(4)	17.4(4)	C2AB	-1428.8(19)	9078(4)	3193.9(19)	35.0(18)
C024	2051.3(8)	5279.0(16)	5387.2(4)	16.8(4)	C9	1050(4)	5095(14)	3638.3(15)	30(3)
C025	4151.9(8)	4992.9(17)	6528.5(5)	19.6(4)	C9A	924(4)	5568(9)	3634.0(13)	28.4(17)
C026	6359.2(8)	2125.8(15)	7665.2(5)	19.5(4)	C1	-146.4(19)	9914(4)	3494.4(10)	36.0(14)
C027	5589.7(8)	8430.6(15)	7244.6(4)	17.4(4)	C1A	-456(3)	9813(5)	3577.9(13)	30.0(18)
C028	1290.2(9)	10817.5(16)	2795.1(5)	21.6(4)	C02H	5261.9(8)	2076.2(17)	5595.8(5)	21.4(4)
C029	675.6(8)	7315.9(16)	4583.2(5)	22.4(5)	C02I	-315.6(8)	8755.3(18)	2909.6(5)	22.1(5)
C02A	3958.0(8)	4438.9(18)	4602.5(5)	22.3(5)	C02J	537.5(9)	4583.3(18)	3604.1(5)	25.3(5)
C02B	3724.2(8)	7371.3(16)	5452.1(5)	20.5(4)	C02K	178.2(8)	1405.0(16)	4517.0(5)	19.0(4)
C02C	1946.3(8)	5273.1(17)	6000.0(4)	19.6(4)	C02L	3644.6(8)	656.2(18)	4319.7(5)	24.7(5)
C02D	3183.1(8)	361.7(16)	4462.6(4)	17.4(4)	C02M	-499.3(8)	3922.1(17)	3169.5(5)	20.5(4)
C02E	2294.9(8)	4848.3(17)	2762.3(5)	22.5(5)	C02N	5255.8(9)	4115.7(17)	6486.6(5)	20.7(4)
C02F	3127.7(9)	90.6(17)	6112.7(5)	24.2(5)	C02O	3023.5(9)	-761.9(17)	4396.0(5)	24.7(5)
C02G	2952.3(8)	5248.3(16)	4690.2(5)	17.8(4)	C02P	4437.6(9)	8892.5(18)	6896.2(5)	25.2(5)
C02Q	2219.2(8)	1081.7(16)	3979.6(4)	18.4(4)					

Table 3.14. Anisotropic Displacement Parameters ($Å^2×10^3$) for **3.3-Et₂O**. The anisotropic displacement factor exponent takes the form: $-2\pi^2[h^2a^{*2}U_{11}+2hka^*b^*U_{12}+\ldots]$.

Atom	U_{11}	U_{22}	U_{33}	U_{23}	U_{13}	U_{12}	Atom	U_{11}	U_{22}	U_{33}	U_{23}	U_{13}	U_{12}
Cu01	12.47(11)	14.04(12)	15.64(12)	1.16(9)	5.63(9)	1.50(9)	C03O	19.9(11)	29.4(13)	36.8(14)	-3.2(10)	-0.1(10)	-4.7(10)
Cu02	14.08(11)	11.89(12)	12.02(11)	0.40(9)	1.99(9)	-0.65(9)	C03P	20.5(11)	36.1(14)	37.4(14)	-10.8(11)	0.7(10)	3(1)
Cu03	11.93(11)	11.79(12)	15.47(12)	0.24(9)	5.21(9)	0.45(9)	C03Q	44.2(15)	21.7(12)	30.7(13)	8.8(10)	0.0(11)	-8.0(11)
Cu04	13.62(11)	16.89(13)	14.50(12)	-1.00(9)	5.64(9)	1.05(10)	C03R	29.7(12)	18.2(11)	36.8(13)	8.2(10)	11.6(10)	2.0(9)
P005	13.4(2)	14.1(2)	11.0(2)	-1.03(19)	3.09(18)	-1.78(19)	C03S	20.5(11)	48.3(16)	21.9(12)	2.4(11)	4.4(9)	10.6(11)
P006	11.4(2)	13.8(2)	14.4(2)	0.33(19)	4.25(18)	1.43(19)	C03T	28.8(13)	77(2)	18.6(12)	3.2(13)	1.7(10)	16.6(14)
P007	12.4(2)	17.6(3)	16.6(3)	4.1(2)	5.71(19)	0.1(2)	C03U	30.1(13)	18.2(12)	48.1(16)	0.7(11)	10.7(11)	-5.4(10)
P008	12.0(2)	11.4(2)	14.6(2)	-0.69(19)	4.29(18)	-1.76(19)	C03V	30.4(13)	30.4(14)	43.7(15)	3.4(12)	8.5(11)	0.2(11)
P009	15.0(2)	12.2(2)	14.9(2)	2.53(19)	1.78(19)	0.96(19)	C03W	22.1(11)	36.5(14)	24.9(12)	14(1)	4.2(9)	-2.8(10)
P00A	13.4(2)	15.8(3)	18.1(3)	-3.0(2)	6.37(19)	-2.0(2)	C03X	20.2(11)	15.9(11)	62.1(18)	-5.3(11)	7.5(11)	-5.0(9)
P00B	12.6(2)	13.4(2)	14.2(2)	0.79(19)	3.64(18)	4.04(19)	C03Y	31.1(13)	35.1(15)	39.4(15)	-7.7(12)	6.8(11)	-4.2(11)
P00C	15.7(2)	18.9(3)	13.6(2)	-0.4(2)	5.53(19)	3.4(2)	C03Z	24.5(11)	29.0(13)	30.5(12)	-2.4(10)	11.7(10)	4.4(10)
N00D	12.4(8)	12.5(8)	15.5(8)	-0.2(6)	5.0(6)	-0.7(6)	C040	35.5(14)	28.2(13)	35.1(14)	-10.8(11)	6.7(11)	4.7(11)
N00E	14.0(8)	11.6(8)	12.4(8)	0.1(6)	2.2(6)	-1.0(6)	C041	44.3(15)	20.9(12)	31.1(13)	-8(1)	4.5(11)	-2.1(11)
N00F	12.5(8)	12.3(8)	14.3(8)	0.0(6)	5.4(6)	1.1(6)	C042	46.3(15)	20.5(12)	34.8(14)	-4.4(10)	3.4(11)	13.9(11)
O00G	27.7(9)	28.1(9)	32.2(9)	-4.0(7)	3.6(7)	-1.5(7)	C043	19.9(11)	49.4(16)	18.8(11)	-10.8(10)	1.5(9)	-3.0(11)
N00H	15.3(8)	15.7(9)	16.2(8)	-0.4(7)	6.5(6)	1.4(7)	C044	21.6(13)	36.3(16)	73(2)	3.1(14)	-7.6(13)	-8.2(11)
C00I	13.7(9)	13.3(9)	12.7(9)	0.3(7)	3.4(7)	2.2(7)	C045	33.7(13)	18.2(12)	44.5(15)	-7.0(11)	7.1(11)	-1.2(10)
C00J	13.3(9)	11.3(9)	10.9(9)	-0.3(7)	4.6(7)	-0.2(7)	C046	17.8(11)	53.3(17)	25.6(12)	-2.2(11)	9.0(9)	-7.5(11)
C00K	14.0(9)	12.0(9)	11.1(9)	-0.3(7)	3.2(7)	0.6(7)	C047	46.7(15)	32.3(14)	21.7(12)	-1.1(10)	-3.2(11)	-13.4(12)
C00L	17.7(9)	10.0(9)	14.9(9)	-0.2(7)	6.0(7)	0.6(7)	C048	35.0(14)	73(2)	22.6(13)	11.9(13)	10.7(11)	11.1(14)
C00M	16.1(9)	12.8(9)	12.3(9)	0.3(7)	6.5(7)	-0.6(7)	C049	34.8(14)	67(2)	19.5(12)	1.4(12)	15(1)	13.8(13)
C00N	12.0(9)	14.1(9)	13.8(9)	2.7(7)	3.4(7)	-0.8(7)	C04A	31.0(13)	33.4(14)	42.8(15)	2.9(12)	10.2(11)	-3.1(11)
C00O	13.3(9)	12.5(9)	15.0(9)	1.7(7)	3.8(7)	-0.1(7)	C04B	22.8(12)	54.7(18)	40.8(15)	12.2(13)	-7.5(11)	-13.3(12)
C00P	14.0(9)	11.2(9)	13.3(9)	-0.9(7)	5.1(7)	0.1(7)	C04C	18.4(12)	35.5(15)	64.4(19)	6.5(13)	-2.6(12)	-6.2(11)
C00Q	17.2(10)	16.3(10)	12.2(9)	0.2(7)	4.8(7)	0.7(8)	C04D	25.1(13)	76(2)	31.9(14)	22.1(14)	17.9(11)	20.9(13)
C00R	13.6(9)	13.2(9)	12.1(9)	-1.5(7)	3.9(7)	0.5(7)	C04E	29.3(13)	61.0(19)	27.4(13)	-0.3(12)	11.4(10)	22.0(13)
C00S	18.4(10)	9.4(9)	18.6(10)	-1.2(7)	6.9(8)	0.2(8)	C04F	20.1(12)	39.3(16)	57.3(18)	-21.7(13)	0.4(12)	-2.7(11)
C00T	17.2(9)	11.4(9)	15.8(9)	1.6(7)	4.6(7)	0.3(8)	C04G	25.4(13)	90(2)	22.4(13)	-0.7(14)	4.5(10)	-23.4(14)
C00U	13.1(9)	13.6(9)	11.3(9)	-0.5(7)	4.6(7)	1.7(7)	C04H	37.5(15)	55.8(19)	32.5(15)	0.1(13)	1.8(12)	-10.1(13)
C00V	12.9(9)	11.9(9)	11.8(9)	0.7(7)	3.5(7)	1.3(7)	C04I	42.3(16)	104(3)	17.6(13)	-9.3(15)	9.9(11)	-15.9(17)
C00W	16.6(9)	11.1(9)	13.5(9)	0.1(7)	3.4(7)	1.0(7)	C04J	32.3(15)	118(3)	31.9(15)	-12.6(17)	21.3(12)	-26.1(18)
C00X	14.0(9)	14.2(9)	10.3(9)	1.4(7)	4.3(7)	0.2(7)	C04K	41.8(16)	43.4(17)	47.9(17)	25.5(14)	6.2(13)	-2.7(13)
C00Y	14.0(9)	11.4(9)	10.9(9)	0.7(7)	4.9(7)	0.1(7)	C04L	32.0(15)	145(4)	19.1(13)	26.4(18)	1.7(11)	-9.6(19)
C00Z	15.1(9)	12.6(9)	12.5(9)	1.2(7)	2.9(7)	1.0(7)	C04M	77(2)	28.3(16)	104(3)	-26.6(17)	67(2)	-12.2(15)
C010	15.3(9)	11.4(9)	11.8(9)	1.4(7)	4.7(7)	-0.7(7)	C04N	43.5(17)	121(3)	53.0(19)	-45(2)	35.4(15)	-54(2)
C011	18.5(10)	11.7(9)	15.0(9)	0.0(7)	5.3(8)	1.3(8)	C04O	28.8(15)	19.0(14)	134(3)	13.9(17)	1.0(18)	-8.8(11)
C012	11.7(9)	15.2(10)	14.1(9)	1.7(7)	3.0(7)	0.2(7)	C04Q	44.1(18)	169(4)	20.7(14)	-19(2)	3.6(13)	-53(2)
C013	16.1(9)	12.1(9)	14.7(9)	-0.6(7)	5.8(7)	0.9(7)	C04S	36(3)	32(3)	26(3)	6(2)	2(2)	15(2)
C014	17(1)	18.8(10)	11.3(9)	-0.3(8)	4.2(7)	0.7(8)	C0AA	27(3)	22(3)	36(3)	3(2)	-4(2)	7(2)
C015	12.8(9)	12.8(9)	15.9(9)	-1.6(7)	4.3(7)	1.3(7)	C2AA	18(3)	29(3)	41(6)	4(3)	3(3)	10(2)
C016	13.1(9)	14(1)	17.5(10)	-2.2(8)	3.8(7)	-2.4(8)	C2AB	27(2)	34(3)	49(5)	12(2)	19(2)	14.6(19)
C017	15.4(9)	18.2(10)	17.4(10)	-3.2(8)	5.2(8)	1.8(8)	C9	15(3)	48(7)	22(3)	1(3)	-4(2)	-7(4)
C018	14.4(9)	10.5(9)	11.8(9)	-1.0(7)	4.3(7)	0.9(7)	C9A	25(3)	32(4)	25(3)	3(3)	-2(2)	-4(3)
C019	18.1(10)	11.5(9)	17.7(10)	2.4(7)	4.5(8)	4.3(8)	C02T	17.9(10)	25.3(12)	24.6(11)	-5.7(9)	3.5(8)	5.8(9)
C01A	14.1(9)	14.0(9)	11.8(9)	0.0(7)	5.0(7)	0.0(7)	C02U	23.1(11)	28.3(12)	20.0(11)	0.4(9)	-0.2(9)	10.0(9)
C01B	18(1)	11.1(9)	16(1)	2.1(7)	6.1(8)	1.1(7)	C02V	27.3(12)	26.2(12)	22.5(11)	-5.5(9)	-1.5(9)	-2.1(10)
C01C	15.7(9)	16.8(10)	13.9(9)	-0.4(8)	4.0(7)	-3.8(8)	C02W	31.4(12)	26.5(12)	19.4(11)	2.6(9)	9.5(9)	-1(1)
C01D	15.7(9)	14.6(10)	14.9(9)	-0.7(8)	4.6(7)	0.1(8)	C02X	20(1)	25.3(12)	22.3(11)	4.0(9)	-0.4(9)	7.4(9)
C01E	16.2(10)	11.9(10)	20.7(10)	-0.7(8)	5.7(8)	-4.4(8)	C02Y	19.8(11)	38.8(14)	21.3(11)	5.9(10)	3.6(9)	5.9(10)
C01F	23.8(11)	14.4(10)	19.5(10)	-2.7(8)	8.1(8)	0.6(8)	C02Z	27.9(12)	33.9(13)	25.0(12)	9.1(10)	11.1(9)	-1(1)
C01G	13.6(9)	14.9(10)	15.3(9)	-0.8(7)	4.6(7)	0.3(8)	C030	19(1)	16.6(10)	22.0(11)	3.7(8)	-0.2(8)	2.2(8)
C01H	22.4(10)	16(1)	12.8(9)	2.0(8)	2.0(8)	0.7(8)	C031	19.4(11)	25.5(12)	27.5(12)	-5.3(9)	-0.3(9)	-6.8(9)
C01I	19.7(10)	9.4(9)	16.8(10)	-0.6(7)	5.1(8)	-0.7(8)	C032	23.4(12)	14.7(11)	52.5(16)	2.7(10)	6.3(11)	-3.9(9)
C01J	15.2(9)	17.2(10)	16.9(10)	-1.8(8)	6.0(8)	-1.3(8)	C033	20.6(11)	21.0(11)	24.1(11)	5.3(9)	1.8(9)	5.7(9)
C01K	14.0(9)	12.9(9)	12.4(9)	-2.0(7)	4.7(7)	-0.4(7)	C034	31.0(12)	17.0(11)	33.9(13)	-8.8(10)	-0.1(10)	4.9(10)
C01L	13.4(9)	14.7(10)	12.9(9)	-1.6(7)	5.1(7)	-2.5(7)	C035	27.5(12)	22.8(11)	18.5(11)	-1.0(9)	-0.3(9)	-4.6(9)
C01M	23.7(11)	16.3(10)	14.8(10)	3.3(8)	3.8(8)	7.2(8)	C036	42.3(14)	23.0(12)	17.7(11)	-4.6(9)	-1.8(10)	-0.1(10)
C01N	16.4(10)	22.1(11)	11.9(9)	2.5(8)	3.3(7)	4.3(8)	C037	28.2(12)	21.1(11)	32.3(12)	-12.0(9)	21.2(10)	-8.3(9)
C01O	15.8(9)	17.7(10)	12.7(9)	-2.1(7)	5.5(7)	0.4(8)	C038	25.9(12)	13.1(10)	35.4(13)	4.7(9)	-1(1)	3.5(9)

C01P	19.3(10)	11.2(9)	17(1)	-1.6(7)	5.8(8)	-3.2(8)	C039	25.6(12)	17.8(11)	38.1(14)	-1.7(10)	6(1)	-7.1(9)
C01Q	14.2(9)	13.4(10)	18(1)	0.7(8)	2.5(7)	2.1(8)	C03A	23.8(12)	29.3(13)	35.4(14)	5.8(10)	4.6(10)	-9(1)
C01R	17.6(10)	17.7(10)	14.6(10)	-0.3(8)	3.5(8)	-0.4(8)	C03B	23.1(11)	29.3(13)	23.0(11)	4.2(10)	-2.3(9)	4.3(10)
C01S	16.4(10)	14.2(10)	18.1(10)	1.1(8)	5.8(8)	2.7(8)	C03C	33.0(13)	20.0(12)	32.5(13)	-1.1(10)	-3.9(10)	-8.4(10)
C01T	12.2(9)	24.1(11)	20.6(10)	-2.3(9)	3.9(8)	-0.4(8)	C03D	22.2(11)	29.7(13)	29.8(12)	7.5(10)	10.6(9)	4.8(10)
C01U	16.5(9)	13(1)	17.1(10)	-2.2(8)	7.4(8)	-1.5(8)	C03E	26.5(12)	22.7(12)	50.5(16)	-2.2(11)	15.7(11)	5.8(10)
C01V	19(1)	11.6(10)	21.6(11)	-0.2(8)	3.7(8)	-0.3(8)	C03F	24.8(12)	41.1(15)	23.3(12)	11.8(10)	3.9(9)	6.5(11)
C01W	19.4(10)	15.6(10)	18.7(10)	-5.2(8)	9.7(8)	-2.8(8)	C03G	29.0(12)	17.6(11)	37.2(14)	6.6(10)	-1.1(10)	3.2(10)
C01X	15.9(9)	14(1)	13.1(9)	-1.6(7)	4.0(7)	-1.4(8)	C03H	22.7(11)	27.4(13)	38.1(14)	-1.8(10)	15.3(10)	-8(1)
C01Y	14.9(9)	16.7(10)	16.1(10)	-1.5(8)	4.1(8)	-2.0(8)	C03I	20.8(11)	35.2(14)	27.6(12)	-8.9(10)	3.7(9)	-7(1)
C01Z	18.9(10)	22.8(11)	22.3(11)	5.7(9)	5.9(8)	-1.8(9)	C03J	26.7(12)	35.5(13)	17.0(11)	-0.9(9)	5.2(9)	9.7(10)
C020	15.5(9)	14.4(10)	13.6(9)	2.6(7)	4.7(7)	3.1(8)	C03K	30.4(13)	19.0(12)	53.1(16)	17.2(11)	8.1(12)	-0.4(10)
C021	19.3(10)	14.5(10)	16(1)	0.8(8)	3.6(8)	-0.5(8)	C03L	35.0(13)	45.9(16)	19.6(11)	-3.1(11)	11.9(10)	-1.6(12)
C022	15.8(10)	16.2(10)	25.4(11)	-1.7(8)	5.6(8)	-5.4(8)	C03M	35.2(13)	20.1(12)	40.6(15)	13.3(10)	2.5(11)	-5.4(10)
C023	19.2(10)	12.3(10)	18.9(10)	-1.9(8)	0.2(8)	-0.7(8)	C03N	17.3(11)	33.2(14)	42.6(15)	2.4(11)	-2.9(10)	6(1)
C024	15.1(9)	17.7(10)	18.2(10)	5.8(8)	5.4(8)	3.7(8)	C02G	13.9(9)	16.9(10)	23.3(11)	-3.5(8)	5.7(8)	-3.8(8)
C025	15.2(10)	21.3(11)	20.3(10)	0.3(8)	-0.4(8)	-0.8(8)	C02H	13.3(10)	19.5(11)	31.8(12)	1.5(9)	5.5(9)	2.5(8)
C026	20.5(10)	9.4(10)	27.5(11)	1.7(8)	3.1(9)	0.8(8)	C02I	19.7(10)	29.2(12)	18.2(10)	8.6(9)	6.1(8)	8.4(9)
C027	21.4(10)	11.8(10)	17.6(10)	-1.2(8)	1.3(8)	3.1(8)	C02J	19.2(11)	23.1(12)	29.4(12)	-6.3(9)	-3.3(9)	6.8(9)
C028	27.4(11)	14.5(10)	22.3(11)	0.9(8)	3.9(9)	-1.2(9)	C02K	13.6(9)	14.8(10)	28.4(11)	-3.1(9)	4.0(8)	-3.3(8)
C029	20.9(11)	12.5(10)	34.1(13)	1.2(9)	6.9(9)	3.5(8)	C02L	17.8(10)	28.1(12)	29.5(12)	3.1(10)	8.1(9)	8.9(9)
C02A	13.2(10)	27.6(12)	26.7(12)	7.2(9)	5.7(8)	0.8(9)	C02M	16.8(10)	19.8(11)	25.4(11)	-1.3(9)	6.0(8)	-5.3(8)
C02B	19.6(10)	10.4(10)	30.5(12)	2.7(8)	3.2(9)	-0.2(8)	C02N	24.2(11)	18.7(11)	23.1(11)	-5.7(9)	14.0(9)	-1.7(9)
C02C	17.3(10)	22.0(11)	18.8(10)	-4.6(8)	2.7(8)	2.9(8)	C02O	22.6(11)	19.0(11)	31.8(12)	0.5(9)	4.7(9)	7.7(9)
C02D	16(1)	15.6(10)	20.6(10)	1.9(8)	3.9(8)	7.2(8)	C02P	21.3(11)	25.4(12)	27.8(12)	0.9(9)	2.6(9)	8.8(9)
C02E	16.1(10)	20.1(11)	31.8(12)	-5.1(9)	6.2(9)	1.3(8)	C02Q	17.8(10)	20.8(11)	15.6(10)	-1.9(8)	1.7(8)	4.9(8)
C02F	24.7(11)	21.6(11)	24.7(11)	3.9(9)	2.4(9)	5.9(9)	C02R	17.6(11)	29.8(13)	36.6(13)	-2.9(10)	10.6(9)	-5.7(9)
C02S	15.8(10)	22.8(12)	41.0(14)	-0.2(10)	9.7(9)	6.0(9)							

Table 3.15. Bond Lengths for **3.3-Et$_2$O**.

Atom	Atom	Length/Å	Atom	Atom	Length/Å	Atom	Atom	Length/Å	Atom	Atom	Length/Å
Cu01	P007	2.2001(6)	C01C	C01L	1.506(3)	C00Q	C01D	1.433(3)	C02E	C03Z	1.549(3)
Cu01	P00B	2.2021(6)	C01D	C01J	1.395(3)	C00Q	C01R	1.396(3)	C02J	C04L	1.491(4)
Cu01	N00D	1.9653(16)	C01D	C01O	1.416(3)	C00R	C013	1.408(3)	C02J	C04S	1.612(6)
Cu02	P005	2.2071(6)	C01E	C01Y	1.384(3)	C00R	C018	1.421(3)	C02J	C0AA	1.531(5)
Cu02	P009	2.2033(6)	C01F	C01W	1.388(3)	C00S	C013	1.387(3)	C02J	C9	1.449(7)
Cu02	N00E	1.9691(16)	C01G	C01K	1.402(3)	C00S	C016	1.405(3)	C02J	C9A	1.607(7)
Cu03	P006	2.2188(6)	C01H	C01M	1.418(3)	C00T	C019	1.416(3)	C02K	C03H	1.530(3)
Cu03	P008	2.2177(6)	C01H	C01R	1.383(3)	C00T	C02B	1.531(3)	C02K	C03O	1.532(3)
Cu03	N00F	1.9692(16)	C01H	C028	1.532(3)	C00U	C010	1.413(3)	C02K	C03X	1.534(3)
Cu04	P00A	2.2058(6)	C01I	C01X	1.409(3)	C00V	C00X	1.418(3)	C02M	C04B	1.522(3)
Cu04	P00C	2.2070(6)	C01L	C01P	1.382(3)	C00V	C010	1.440(3)	C02M	C04N	1.523(3)
Cu04	N00H	1.9597(16)	C01M	C01N	1.383(3)	C00W	C01I	1.384(3)	C02M	C04O	1.510(3)
P005	C01C	1.849(2)	C01N	C02I	1.504(3)	C00W	C027	1.505(3)	C02N	C049	1.525(3)
P005	C025	1.868(2)	C01O	C01W	1.402(3)	C00X	C020	1.411(3)	C02N	C04E	1.525(3)
P005	C02N	1.870(2)	C01Q	C02H	1.528(3)	C00Y	C01L	1.410(3)	C02N	C04M	1.520(3)
P006	C01T	1.879(2)	C01Q	C02T	1.537(3)	C00Z	C01X	1.384(3)	C02P	C030	1.534(3)
P006	C024	1.851(2)	C01Q	C033	1.534(3)	C011	C01E	1.414(3)	C02Q	C02U	1.532(3)
P006	C02C	1.874(2)	C01T	C03I	1.528(3)	C011	C01G	1.386(3)	C02Q	C02V	1.526(3)
P007	C02A	1.878(2)	C01T	C03N	1.534(3)	C011	C01V	1.529(3)	C02Q	C03J	1.530(3)
P007	C02G	1.850(2)	C01T	C046	1.526(3)	C012	C01B	1.384(3)	C02S	C04G	1.509(4)
P007	C03W	1.864(2)	C01V	C029	1.526(3)	C013	C01S	1.508(3)	C02S	C04J	1.520(4)
P008	C01U	1.8488(19)	C01V	C034	1.532(3)	C014	C01N	1.410(3)	C02S	C2AA	1.610(7)
P008	C021	1.875(2)	C01V	C03R	1.533(3)	C015	C016	1.392(3)	C02S	C2AB	1.517(5)
P008	C022	1.877(2)	C01W	C037	1.509(3)	C015	C018	1.393(3)	C030	C03B	1.539(3)
P009	C01Z	1.876(2)	C01X	C023	1.536(3)	C016	C02K	1.533(3)	C030	C03G	1.532(3)

P009	C027	1.852(2)	C01Y	C02G	1.506(3)	C017	C01F	1.410(3)	C036	C04I	1.508(4)
P009	C030	1.879(2)	C01Z	C02Z	1.529(3)	C017	C01J	1.382(3)	C036	C04Q	1.516(4)
P00A	C02J	1.869(2)	C01Z	C03A	1.529(3)	C017	C02E	1.529(3)	C036	C1	1.521(5)
P00A	C02M	1.876(2)	C01Z	C03D	1.540(3)	C018	C01K	1.433(3)	C036	C1A	1.620(7)
P00A	C037	1.848(2)	C020	C024	1.507(3)	C019	C020	1.382(3)	C03F	C03W	1.541(3)
P00B	C01S	1.848(2)	C021	C02F	1.530(3)	C01A	C01K	1.417(3)	C03V	C04A	1.488(4)
P00B	C02D	1.874(2)	C021	C02W	1.521(3)	C01A	C01Y	1.406(3)	C03W	C048	1.545(4)
P00B	C02Q	1.876(2)	C021	C035	1.533(3)	C01B	C01P	1.415(3)	C03W	C04K	1.516(4)
P00C	C02I	1.847(2)	C022	C02R	1.535(3)	C01B	C026	1.531(3)	C03Y	C04H	1.494(4)
P00C	C02S	1.871(2)	C022	C031	1.536(3)	C00I	C00N	1.387(3)	C028	C041	1.533(3)
P00C	C036	1.876(2)	C022	C039	1.528(3)	C00I	C01Q	1.531(3)	C02A	C02Y	1.528(3)
N00D	C00R	1.377(2)	C023	C03C	1.527(3)	C00J	C00K	1.415(3)	C02A	C04C	1.538(4)
N00D	C01A	1.383(2)	C023	C047	1.534(3)	C00J	C00P	1.436(3)	C02A	C04D	1.522(3)
N00E	C00K	1.376(2)	C023	C04F	1.521(3)	C00J	C00Z	1.399(3)	C02B	C032	1.532(3)
N00E	C00Y	1.379(2)	C025	C03S	1.524(3)	C00K	C00W	1.405(3)	C02B	C03M	1.527(3)
N00F	C00U	1.378(2)	C025	C03T	1.509(3)	C00L	C00M	1.384(3)	C02B	C045	1.530(3)
N00F	C00X	1.380(2)	C025	C044	1.535(3)	C00M	C00U	1.408(3)	C02C	C03L	1.542(3)
O00G	C04A	1.421(3)	C026	C038	1.531(3)	C00M	C01U	1.504(3)	C02C	C040	1.526(3)
O00G	C04H	1.403(3)	C026	C03K	1.532(3)	C00N	C010	1.400(3)	C02C	C043	1.525(3)
N00H	C014	1.378(3)	C026	C042	1.531(3)	C00O	C00T	1.384(3)	C02D	C02L	1.535(3)
N00H	C01O	1.383(2)	C028	C03Q	1.527(3)	C00O	C00V	1.401(3)	C02D	C02O	1.532(3)
C00I	C00L	1.413(3)	C028	C03U	1.527(3)	C00P	C00Y	1.418(3)	C02D	C02X	1.532(3)
C00Q	C014	1.419(3)	C02E	C03P	1.517(3)	C00P	C012	1.396(3)	C02E	C03E	1.516(3)

Table 3.16. Bond Angles for **3.3-Et$_2$O**.

Atom	Atom	Atom	Angle/°	Atom	Atom	Atom	Angle/°	Atom	Atom	Atom	Angle/°	Atom	Atom	Atom	Angle/°
P007	Cu01	P00B	156.98(2)	C02H	C01Q	C00I	112.18(16)	C00K	C00W	C027	121.36(18)	C04L	C02J	P00A	110.76(17)
N00D	Cu01	P007	101.70(5)	C02H	C01Q	C02T	107.58(17)	C01I	C00W	C00K	117.62(18)	C04L	C02J	C04S	91.8(3)
N00D	Cu01	P00B	101.17(5)	C02H	C01Q	C033	108.65(17)	C01I	C00W	C027	120.92(18)	C04L	C02J	C0AA	126.5(3)
P009	Cu02	P005	157.49(2)	C033	C01Q	C02T	108.80(17)	N00F	C00X	C00V	112.03(16)	C04L	C02J	C9A	100.7(4)
N00E	Cu02	P005	101.80(5)	C01H	C01R	C00Q	120.21(19)	N00F	C00X	C020	128.06(17)	C04S	C02J	P00A	116.7(2)
N00E	Cu02	P009	100.68(5)	C013	C01S	P00B	115.76(14)	C020	C00X	C00V	119.91(18)	C0AA	C02J	P00A	109.9(2)
P008	Cu03	P006	158.17(2)	C03I	C01T	P006	105.38(14)	N00E	C00Y	C00P	112.24(16)	C0AA	C02J	C9A	104.2(5)
N00F	Cu03	P006	101.65(5)	C03I	C01T	C03N	107.64(19)	N00E	C00Y	C01L	127.89(17)	C9	C02J	P00A	113.2(4)
N00F	Cu03	P008	100.17(5)	C03N	C01T	P006	114.21(15)	C01L	C00Y	C00P	119.87(17)	C9	C02J	C04L	113.9(5)
P00A	Cu04	P00C	156.92(2)	C046	C01T	P006	110.96(15)	C01X	C00Z	C00J	120.34(18)	C9	C02J	C04S	108.7(8)
N00H	Cu04	P00A	101.96(5)	C046	C01T	C03I	108.00(19)	C00N	C010	C00U	120.95(17)	C9A	C02J	P00A	100.9(3)
N00H	Cu04	P00C	101.04(5)	C046	C01T	C03N	110.30(19)	C00N	C010	C00V	133.76(18)	C016	C02K	C03X	111.57(17)
C01C	P005	Cu02	102.65(7)	C00M	C01U	P008	114.99(13)	C00U	C010	C00V	105.25(16)	C03H	C02K	C016	109.98(17)
C01C	P005	C025	102.55(9)	C011	C01V	C034	110.33(17)	C01E	C011	C01V	119.30(17)	C03H	C02K	C03O	109.07(18)
C01C	P005	C02N	105.16(10)	C011	C01V	C03R	109.32(17)	C01G	C011	C01E	117.67(18)	C03H	C02K	C03X	107.41(19)
C025	P005	Cu02	113.57(7)	C029	C01V	C011	111.96(17)	C01G	C011	C01V	123.02(17)	C03O	C02K	C016	109.65(18)
C025	P005	C02N	111.88(10)	C029	C01V	C034	108.20(18)	C01B	C012	C00P	120.08(18)	C03O	C02K	C03X	109.11(19)
C02N	P005	Cu02	118.75(7)	C029	C01V	C03R	107.55(18)	C00R	C013	C01S	121.77(17)	C04B	C02M	P00A	106.49(16)
C01T	P006	Cu03	116.17(7)	C034	C01V	C03R	109.41(19)	C00S	C013	C00R	117.40(18)	C04B	C02M	C04N	106.9(2)
C024	P006	Cu03	102.90(7)	C01F	C01W	C01O	117.19(18)	C00S	C013	C01S	120.77(17)	C04N	C02M	P00A	109.37(17)
C024	P006	C01T	102.34(9)	C01F	C01W	C037	119.41(19)	N00H	C014	C00Q	112.17(17)	C04O	C02M	P00A	115.15(16)
C024	P006	C02C	106.11(10)	C01O	C01W	C037	123.27(19)	N00H	C014	C01N	128.43(18)	C04O	C02M	C04B	108.1(2)
C02C	P006	Cu03	116.24(7)	C00Z	C01X	C01I	118.00(18)	C01N	C014	C00Q	119.39(19)	C04O	C02M	C04N	110.4(3)
C02C	P006	C01T	111.12(9)	C00Z	C01X	C023	119.79(17)	C016	C015	C018	120.17(18)	C049	C02N	P005	109.82(16)
C02A	P007	Cu01	116.25(7)	C01I	C01X	C023	122.20(18)	C00S	C016	C02K	122.40(18)	C049	C02N	C04E	106.76(19)
C02G	P007	Cu01	103.60(7)	C01A	C01Y	C02G	122.85(18)	C015	C016	C00S	118.07(18)	C04E	C02N	P005	106.50(15)
C02G	P007	C02A	102.00(10)	C01E	C01Y	C01A	116.97(18)	C015	C016	C02K	119.53(17)	C04M	C02N	P005	114.02(16)
C02G	P007	C03W	106.43(11)	C01E	C01Y	C02G	120.14(18)	C01F	C017	C02E	122.85(19)	C04M	C02N	C049	108.6(2)
C03W	P007	Cu01	114.81(8)	C02Z	C01Z	P009	110.40(15)	C01J	C017	C01F	117.92(18)	C04M	C02N	C04E	110.9(2)
C03W	P007	C02A	111.95(10)	C02Z	C01Z	C03D	107.44(19)	C01J	C017	C02E	119.08(18)	C02U	C02Q	P00B	105.25(14)
C01U	P008	Cu03	102.77(7)	C03A	C01Z	P009	114.05(16)	C00R	C018	C01K	105.24(16)	C02V	C02Q	P00B	113.58(15)

C01U	P008	C021	104.86(9)	C03A	C01Z	C02Z	110.73(19)	C015	C018	C00R	120.68(17)	C02V	C02Q	C02U	109.03(18)
C01U	P008	C022	102.98(9)	C03A	C01Z	C03D	108.48(18)	C015	C018	C01K	134.06(18)	C02V	C02Q	C03J	110.47(18)
C021	P008	Cu03	114.59(7)	C03D	C01Z	P009	105.39(14)	C020	C019	C00T	124.17(18)	C03J	C02Q	P00B	110.54(14)
C021	P008	C022	111.89(9)	C00X	C020	C024	122.62(18)	N00D	C01A	C01K	111.83(17)	C03J	C02Q	C02U	107.66(18)
C022	P008	Cu03	117.63(7)	C019	C020	C00X	117.04(17)	N00D	C01A	C01Y	128.12(17)	C04G	C02S	P00C	105.80(16)
C01Z	P009	Cu02	112.27(7)	C019	C020	C024	120.33(18)	C01Y	C01A	C01K	120.04(18)	C04G	C02S	C04J	106.1(2)
C01Z	P009	C030	112.52(10)	C02F	C021	P008	114.32(14)	C012	C01B	C01P	117.93(18)	C04G	C02S	C2AA	92.5(4)
C027	P009	Cu02	103.26(7)	C02F	C021	C035	108.47(18)	C012	C01B	C026	123.02(18)	C04G	C02S	C2AB	121.5(4)
C027	P009	C01Z	105.26(10)	C02W	C021	P008	110.34(14)	C01P	C01B	C026	119.02(17)	C04J	C02S	P00C	110.02(18)
C027	P009	C030	102.34(9)	C02W	C021	C02F	110.04(18)	C01L	C01C	P005	115.60(13)	C04J	C02S	C2AA	125.1(4)
C030	P009	Cu02	119.15(7)	C02W	C021	C035	107.67(18)	C01J	C01D	C00Q	133.38(19)	C2AA	C02S	P00C	113.7(3)
C02J	P00A	Cu04	112.94(7)	C035	C021	P008	105.70(14)	C01J	C01D	C01O	120.59(18)	C2AB	C02S	P00C	113.7(2)
C02J	P00A	C02M	111.97(10)	C02R	C022	P008	108.49(15)	C01O	C01D	C00Q	106.03(17)	C2AB	C02S	C04J	99.1(3)
C02M	P00A	Cu04	118.60(7)	C02R	C022	C031	107.31(18)	C01Y	C01E	C011	124.42(18)	C02P	C030	P009	106.72(14)
C037	P00A	Cu04	103.78(8)	C031	C022	P008	106.19(14)	C01W	C01F	C017	123.80(19)	C02P	C030	C03B	107.46(18)
C037	P00A	C02J	106.36(11)	C039	C022	P008	115.46(15)	C011	C01G	C01K	119.98(18)	C03B	C030	P009	108.56(15)
C037	P00A	C02M	101.33(10)	C039	C022	C02R	110.04(18)	C01M	C01H	C028	119.16(18)	C03G	C030	P009	114.94(15)
C01S	P00B	Cu01	102.55(7)	C039	C022	C031	109.00(18)	C01R	C01H	C01M	117.83(19)	C03G	C030	C02P	109.01(19)
C01S	P00B	C02D	102.64(9)	C03C	C023	C01X	112.45(17)	C01R	C01H	C028	123.00(19)	C03G	C030	C03B	109.87(18)
C01S	P00B	C02Q	105.10(9)	C03C	C023	C047	107.32(19)	C00W	C01I	C01X	123.62(18)	C04I	C036	P00C	110.10(19)
C02D	P00B	Cu01	118.75(7)	C047	C023	C01X	109.22(17)	C017	C01J	C01D	120.32(19)	C04I	C036	C04Q	106.3(2)
C02D	P00B	C02Q	112.58(9)	C04F	C023	C01X	110.32(17)	C01A	C01K	C018	105.70(16)	C04I	C036	C1	122.9(3)
C02Q	P00B	Cu01	113.04(7)	C04F	C023	C03C	108.2(2)	C01G	C01K	C018	133.38(18)	C04I	C036	C1A	93.1(3)
C02I	P00C	Cu04	103.29(7)	C04F	C023	C047	109.2(2)	C01G	C01K	C01A	120.91(18)	C04Q	C036	P00C	106.70(19)
C02I	P00C	C02S	102.73(10)	C020	C024	P006	116.43(14)	C00Y	C01L	C01C	122.06(17)	C04Q	C036	C1	95.8(3)
C02I	P00C	C036	105.37(11)	C03S	C025	P005	104.64(14)	C01P	C01L	C00Y	117.10(17)	C04Q	C036	C1A	126.6(3)
C02S	P00C	Cu04	115.79(8)	C03S	C025	C044	106.8(2)	C01P	C01L	C01C	120.82(18)	C1	C036	P00C	112.6(2)
C02S	P00C	C036	112.04(11)	C03T	C025	P005	111.39(16)	C01N	C01M	C01H	123.73(19)	C1A	C036	P00C	112.3(3)
C036	P00C	Cu04	115.67(8)	C03T	C025	C03S	108.1(2)	C014	C01N	C02I	122.01(19)	C01W	C037	P00A	117.57(15)
C00R	N00D	Cu01	122.66(13)	C03T	C025	C044	111.6(2)	C01M	C01N	C014	117.66(18)	C03F	C03W	P007	106.49(15)
C00R	N00D	C01A	105.06(15)	C044	C025	P005	113.82(16)	C01M	C01N	C02I	120.30(19)	C03F	C03W	C048	106.3(2)
C01A	N00D	Cu01	122.41(13)	C01B	C026	C03K	110.44(18)	N00H	C01O	C01D	111.52(17)	C048	C03W	P007	108.53(17)
C00K	N00E	Cu02	122.41(13)	C038	C026	C01B	111.97(17)	N00H	C01O	C01W	128.34(18)	C04K	C03W	P007	115.07(18)
C00K	N00E	C00Y	105.05(15)	C038	C026	C03K	107.90(19)	C01W	C01O	C01D	120.14(18)	C04K	C03W	C03F	110.5(2)
C00Y	N00E	Cu02	121.16(12)	C038	C026	C042	107.78(19)	C01L	C01P	C01B	124.05(18)	C04K	C03W	C048	109.5(2)
C00U	N00F	Cu03	122.34(13)	C042	C026	C01B	109.22(18)	C00I	C01Q	C02T	109.61(16)	O00G	C04A	C03V	108.9(2)
C00U	N00F	C00X	104.97(15)	C042	C026	C03K	109.5(2)	C00I	C01Q	C033	109.93(16)	O00G	C04H	C03Y	111.3(2)
C00X	N00F	Cu03	121.68(12)	C00W	C027	P009	115.68(14)	C013	C00R	C018	119.86(17)	C02O	C02D	C02X	109.31(18)
C04H	O00G	C04A	111.4(2)	C01H	C028	C041	109.32(18)	C013	C00S	C016	123.79(18)	C02X	C02D	P00B	106.27(14)
C014	N00H	Cu04	123.01(13)	C03Q	C028	C01H	110.42(18)	C00O	C00T	C019	118.08(18)	C02X	C02D	C02L	106.79(17)
C014	N00H	C01O	105.20(16)	C03Q	C028	C03U	108.5(2)	C00O	C00T	C02B	123.39(17)	C017	C02E	C03Z	108.59(18)
C01O	N00H	Cu04	122.91(13)	C03Q	C028	C041	108.8(2)	C019	C00T	C02B	118.52(17)	C03E	C02E	C017	112.96(18)
C00L	C00I	C01Q	118.94(17)	C03U	C028	C01H	111.94(18)	N00F	C00U	C00M	127.65(18)	C03E	C02E	C03P	110.0(2)
C00N	C00I	C00L	118.07(17)	C03U	C028	C041	107.8(2)	N00F	C00U	C010	112.39(17)	C03E	C02E	C03Z	106.67(19)
C00N	C00I	C01Q	122.96(17)	C02Y	C02A	P007	105.33(14)	C00M	C00U	C010	119.96(17)	C03P	C02E	C017	111.42(18)
C00K	C00J	C00P	105.70(16)	C02Y	C02A	C04C	107.6(2)	C00O	C00V	C00X	121.07(17)	C03P	C02E	C03Z	106.88(19)
C00Z	C00J	C00K	120.52(17)	C04C	C02A	P007	114.03(16)	C00O	C00V	C010	133.59(17)	C01Y	C02G	P007	116.70(14)
C00Z	C00J	C00P	133.78(18)	C04D	C02A	P007	111.22(17)	C00X	C00V	C010	105.34(16)	C01N	C02I	P00C	115.64(14)
N00E	C00K	C00J	112.01(16)	C04D	C02A	C02Y	107.13(19)	C00Y	C00P	C00J	105.00(16)	C040	C02C	P006	115.49(15)
N00E	C00K	C00W	128.11(18)	C04D	C02A	C04C	111.1(2)	C012	C00P	C00J	134.06(18)	C040	C02C	C03L	109.62(19)
C00W	C00K	C00J	119.88(17)	C00T	C02B	C032	111.89(17)	C012	C00P	C00Y	120.92(18)	C043	C02C	P006	106.66(14)
C00M	C00L	C00I	123.80(18)	C03M	C02B	C00T	110.28(18)	C014	C00Q	C01D	105.06(17)	C043	C02C	C03L	106.12(19)
C00L	C00M	C00U	117.33(17)	C03M	C02B	C032	108.14(19)	C01R	C00Q	C014	121.11(18)	C043	C02C	C040	110.0(2)
C00L	C00M	C01U	121.32(17)	C03M	C02B	C045	109.30(19)	C01R	C00Q	C01D	133.78(18)	C02L	C02D	P00B	108.75(14)
C00U	C00M	C01U	121.26(17)	C045	C02B	C00T	109.36(18)	N00D	C00R	C013	127.99(17)	C02O	C02D	P00B	115.23(14)
C00I	C00N	C010	119.88(18)	C045	C02B	C032	107.80(19)	N00D	C00R	C018	112.14(17)	C02O	C02D	C02L	110.10(18)
C00T	C00O	C00V	119.73(17)	C03L	C02C	P006	108.49(16)								

CuPNP-*i*Bu (3.4)

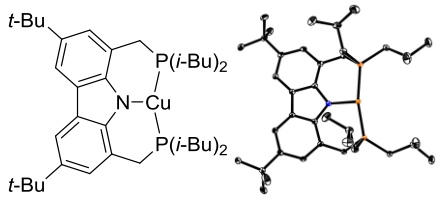

Table 3.17. Crystal data and structure refinement for **3.4**.

Identification code	**3.4**
Empirical formula	$C_{38}H_{62}CuNP_2$
Formula weight	658.36
Temperature/K	100.02
Crystal system	monoclinic
Space group	$P2_1/n$
a/Å	13.4149(7)
b/Å	10.9661(6)
c/Å	24.9005(13)
α/°	90
β/°	93.334(2)
γ/°	90
Volume/Å^3	3656.9(3)
Z	4
ρ_{calc}g/cm^3	1.196
μ/mm^{-1}	0.710
F(000)	1424.0
Crystal size/mm^3	0.39 × 0.35 × 0.33
Radiation	MoKα (λ = 0.71073)
2Θ range for data collection/°	3.276 to 55.098
Index ranges	$-17 \leq h \leq 17$, $-14 \leq k \leq 14$, $-32 \leq l \leq 32$
Reflections collected	92972
Independent reflections	8447 [R_{int} = 0.0229, R_{sigma} = 0.0099]
Data/restraints/parameters	8447/0/393
Goodness-of-fit on F^2	1.053
Final R indexes [I>=2σ (I)]	R_1 = 0.0230, wR_2 = 0.0621
Final R indexes [all data]	R_1 = 0.0239, wR_2 = 0.0628
Largest diff. peak/hole / e Å^{-3}	0.39/-0.27

Table 3.18. Fractional Atomic Coordinates ($\times 10^4$) and Equivalent Isotropic Displacement Parameters ($Å^2 \times 10^3$) for **3.4**. U_{eq} is defined as 1/3 of the trace of the orthogonalized U_{IJ} tensor.

Atom	*x*	*y*	*z*	U(eq)	Atom	*x*	*y*	*z*	U(eq)
Cu01	6829.9(2)	6653.7(2)	3655.8(2)	9.88(4)	C00L	6167.2(8)	3537.4(10)	3536.9(5)	15.1(2)
P002	5887.7(2)	7703.0(2)	4191.3(2)	10.21(6)	C00M	4078.2(8)	8579.5(10)	2280.2(4)	11.20(19)
P003	7775.3(2)	5165.8(2)	3361.0(2)	9.52(6)	C00N	5631.8(9)	4496.2(11)	1074.2(5)	16.0(2)
N004	6362.1(7)	7415.2(8)	2956.4(4)	10.04(17)	C00O	4613.9(8)	7087.5(10)	4198.0(5)	14.1(2)
C005	5503.1(8)	8118.4(9)	2909.4(4)	9.72(19)	C00P	2868.2(8)	10299.5(10)	2485.0(5)	13.9(2)
C006	5464.3(8)	6963.5(10)	2153.8(4)	10.17(19)	C00Q	6900.3(9)	7347.9(11)	5219.0(5)	18.5(2)
C007	6764.5(8)	5157(1)	1878.2(4)	11.8(2)	C00R	5879.6(10)	2194.3(11)	3557.4(6)	23.4(3)
C008	6325.7(8)	6719.6(9)	2490.8(4)	9.86(19)	C00S	5339.6(9)	4273.5(12)	3245.3(6)	24.0(3)
C009	7012.0(8)	5830.5(10)	2337.9(4)	10.66(19)	C00T	4673.6(9)	4866.0(12)	755.0(5)	19.1(2)
C00A	5153.2(8)	8963.9(9)	3281.2(4)	10.37(19)	C00U	9303.4(9)	4682.1(11)	4194.6(4)	16.2(2)
C00B	4939.5(8)	7903.4(9)	2420.5(4)	10.15(19)	C00V	2374.9(9)	10011.3(11)	1930.4(5)	19.3(2)
C00C	5252.0(8)	6291.6(10)	1683.1(4)	11.05(19)	C00W	3780.8(9)	7891.8(11)	4409.0(5)	18.6(2)
C00D	5882.3(8)	5354.4(10)	1547.4(4)	11.6(2)	C00X	2070.5(9)	10174.3(12)	2898.8(5)	20.9(2)
C00E	4292.6(8)	9608.3(10)	3129.6(4)	11.67(19)	C00Y	3234(1)	11627.0(11)	2479.5(6)	22.2(3)
C00F	6272.4(8)	8245.3(10)	4870.0(4)	13.4(2)	C00Z	7230.9(11)	7950.3(14)	5751.5(5)	27.2(3)
C00G	7165.1(8)	3666.2(10)	3272.9(4)	13.4(2)	C010	6350.8(12)	6159.8(13)	5315.6(6)	29.6(3)
C00H	9069.9(8)	4832.1(10)	3590.7(4)	12.7(2)	C011	10423.6(10)	4462.8(15)	4295.9(5)	28.7(3)
C00I	7975.6(8)	5616(1)	2662.8(4)	11.64(19)	C012	8713.2(11)	3649.4(14)	4431.1(5)	27.6(3)
C00J	3755.4(8)	9461.9(10)	2628.1(4)	11.54(19)	C013	3626.2(11)	7645.3(18)	5000.5(6)	36.5(4)
C00K	5678.0(8)	9152.1(9)	3826.1(4)	11.38(19)	C014	5480.8(14)	3203.2(13)	1291.9(7)	37.4(4)
C016	2804.9(10)	7673.2(15)	4080.3(6)	31.5(3)	C015	6476.5(10)	4483.6(18)	689.4(6)	36.0(4)

Table 3.19. Anisotropic Displacement Parameters ($Å^2 \times 10^3$) for **3.4**. The anisotropic displacement factor exponent takes the form: $-2\pi^2[h^2a^{*2}U_{11}+2hka^*b^*U_{12}+\ldots]$.

Atom	U_{11}	U_{22}	U_{33}	U_{23}	U_{13}	U_{12}	Atom	U_{11}	U_{22}	U_{33}	U_{23}	U_{13}	U_{12}
Cu01	10.77(7)	9.00(7)	9.98(7)	-0.45(4)	1.59(5)	1.32(4)	C00N	15.9(5)	18.3(5)	13.6(5)	-5.4(4)	-1.1(4)	5.0(4)
P002	11.55(12)	9.24(12)	9.97(12)	-0.68(9)	1.81(9)	0.18(9)	C00O	13.6(5)	13.0(5)	15.9(5)	-0.7(4)	2.6(4)	-2.2(4)
P003	9.26(12)	9.27(12)	10.05(12)	-0.30(9)	0.79(9)	1.07(9)	C00P	11.8(5)	11.5(5)	18.5(5)	-0.5(4)	0.6(4)	3.1(4)
N004	10.4(4)	9.1(4)	10.8(4)	-0.2(3)	2.2(3)	1.0(3)	C00Q	18.3(5)	22.0(6)	15.0(5)	0.5(4)	-0.6(4)	2.6(4)
C005	9.5(4)	8.1(4)	11.8(5)	2.0(4)	2.0(4)	-0.7(4)	C00R	25.9(6)	14.4(6)	30.7(7)	-1.1(5)	8.8(5)	-6.1(5)
C006	9.9(4)	9.6(4)	11.2(5)	1.7(4)	2.5(4)	0.3(4)	C00S	13.3(5)	21.7(6)	37.0(7)	3.9(5)	0.2(5)	-1.1(5)
C007	12.3(5)	12.4(5)	11.1(5)	0.3(4)	3.0(4)	3.2(4)	C00T	16.0(5)	24.0(6)	16.8(5)	-7.1(5)	-3.0(4)	3.3(4)
C008	10.5(5)	9.2(5)	10.1(5)	1.3(4)	2.2(4)	-0.9(4)	C00U	16.1(5)	20.2(5)	11.9(5)	-1.0(4)	-1.4(4)	3.4(4)
C009	10.4(5)	11.6(5)	10.1(4)	1.9(4)	2.2(4)	1.1(4)	C00V	16.1(5)	19.5(6)	21.7(6)	-0.8(4)	-4.0(4)	6.7(4)
C00A	11.4(5)	8.2(4)	11.6(5)	0.5(4)	1.9(4)	-1.1(4)	C00W	15.3(5)	17.9(6)	23.2(6)	-1.6(5)	6.7(4)	-1.3(4)
C00B	10.6(5)	8.6(4)	11.5(5)	1.1(4)	2.7(4)	-0.9(4)	C00X	14.1(5)	24.6(6)	24.5(6)	-1.0(5)	4.5(4)	6.1(5)
C00C	10.5(5)	12.3(5)	10.5(5)	1.5(4)	0.8(4)	0.3(4)	C00Y	20.7(6)	11.3(5)	34.2(7)	1.8(5)	-2.3(5)	3.2(4)
C00D	12.9(5)	12.5(5)	9.5(5)	0.0(4)	1.7(4)	-0.1(4)	C00Z	27.1(7)	36.5(7)	17.2(6)	-1.8(5)	-5.7(5)	-0.9(6)
C00E	12.2(5)	8.6(4)	14.5(5)	-1.1(4)	3.4(4)	0.7(4)	C010	41.4(8)	21.1(6)	25.3(7)	7.9(5)	-7.0(6)	-2.1(6)
C00F	15.3(5)	13.8(5)	11.3(5)	-2.1(4)	1.5(4)	-0.4(4)	C011	19.0(6)	47.5(9)	18.7(6)	-2.9(6)	-6.3(5)	8.7(6)
C00G	14.1(5)	10.2(5)	15.9(5)	-1.9(4)	1.8(4)	-0.2(4)	C012	33.0(7)	31.1(7)	18.3(6)	9.0(5)	-1.7(5)	-2.9(6)
C00H	11.0(5)	15.3(5)	11.7(5)	-0.7(4)	-0.1(4)	2.3(4)	C013	21.9(7)	64.8(11)	23.9(7)	-6.2(7)	10.9(5)	-1.5(7)
C00I	10.4(5)	14.1(5)	10.5(5)	0.4(4)	1.9(4)	2.5(4)	C014	62.1(11)	14.7(6)	32.8(8)	-5.1(5)	-19.2(7)	1.4(6)
C00J	9.6(5)	9.0(5)	16.1(5)	1.8(4)	2.1(4)	0.3(4)	C015	16.9(6)	71.8(11)	19.3(6)	-22.3(7)	0.4(5)	8.7(7)
C00K	12.5(5)	8.8(4)	12.9(5)	-0.9(4)	1.4(4)	-0.1(4)	C016	16.7(6)	43.7(9)	33.9(7)	-1.2(6)	-0.3(5)	5.2(6)
C00L	15.1(5)	12.1(5)	18.3(5)	-0.7(4)	3.4(4)	-2.2(4)	C00M	10.4(5)	10.7(5)	12.6(5)	1.1(4)	1.0(4)	-0.2(4)

Table 3.20. Bond Lengths for **3.4**.

Atom	Atom	Length/Å	Atom	Atom	Length/Å
Cu01	P002	2.2125(3)	C00C	C00D	1.3852(15)
Cu01	P003	2.2176(3)	C00D	C00N	1.5299(15)
Cu01	N004	1.9992(9)	C00E	C00J	1.4142(15)
P002	C00F	1.8371(11)	C00F	C00Q	1.5324(16)
P002	C00K	1.8443(11)	C00G	C00L	1.5318(15)
P002	C00O	1.8382(11)	C00H	C00U	1.5270(15)
P003	C00G	1.8443(11)	C00J	C00M	1.3849(15)
P003	C00H	1.8335(11)	C00J	C00P	1.5290(14)
P003	C00I	1.8418(11)	C00L	C00R	1.5242(16)
N004	C005	1.3859(13)	C00L	C00S	1.5224(17)
N004	C008	1.3863(13)	C00N	C00T	1.5264(15)
C005	C00A	1.4098(14)	C00N	C014	1.5356(19)
C005	C00B	1.4149(14)	C00N	C015	1.5260(17)
C006	C008	1.4137(14)	C00O	C00W	1.5400(16)
C006	C00B	1.4331(14)	C00P	C00V	1.5292(16)
C006	C00C	1.3996(15)	C00P	C00X	1.5342(16)
C007	C009	1.3863(15)	C00P	C00Y	1.5366(16)
C007	C00D	1.4187(15)	C00Q	C00Z	1.5242(17)
C008	C009	1.4086(14)	C00Q	C010	1.5229(18)
C009	C00I	1.5030(14)	C00U	C011	1.5283(16)
C00A	C00E	1.3870(14)	C00U	C012	1.5200(18)
C00A	C00K	1.5060(14)	C00W	C013	1.5236(18)
C00B	C00M	1.3999(14)	C00W	C016	1.5220(18)

Table 3.21. Bond Angles for **3.4**.

Atom	Atom	Atom	Angle/°	Atom	Atom	Atom	Angle/°
P002	Cu01	P003	160.031(12)	C007	C00D	C00N	119.46(9)
N004	Cu01	P002	98.41(3)	C00C	C00D	C007	118.16(10)
N004	Cu01	P003	100.11(3)	C00C	C00D	C00N	122.30(10)
C00F	P002	Cu01	125.66(4)	C00A	C00E	C00J	123.77(10)
C00F	P002	C00K	101.61(5)	C00Q	C00F	P002	115.44(8)
C00F	P002	C00O	108.79(5)	C00L	C00G	P003	115.09(8)
C00K	P002	Cu01	103.12(4)	C00U	C00H	P003	117.71(8)
C00O	P002	Cu01	112.24(4)	C009	C00I	P003	112.45(7)
C00O	P002	C00K	101.87(5)	C00E	C00J	C00P	119.17(9)
C00G	P003	Cu01	115.91(4)	C00M	C00J	C00E	118.03(10)
C00H	P003	Cu01	126.38(4)	C00M	C00J	C00P	122.78(10)
C00H	P003	C00G	105.36(5)	C00A	C00K	P002	112.09(7)
C00H	P003	C00I	99.23(5)	C00R	C00L	C00G	109.44(9)
C00I	P003	Cu01	103.47(4)	C00S	C00L	C00G	112.19(10)
C00I	P003	C00G	102.41(5)	C00S	C00L	C00R	110.45(10)
C005	N004	Cu01	121.56(7)	C00J	C00M	C00B	119.83(10)
C005	N004	C008	104.29(8)	C00D	C00N	C014	108.89(10)
C008	N004	Cu01	119.52(7)	C00T	C00N	C00D	112.23(9)

N004	C005	C00A	128.13(10)	C00T	C00N	C014	107.74(11)
N004	C005	C00B	112.34(9)	C015	C00N	C00D	110.56(10)
C00A	C005	C00B	119.53(9)	C015	C00N	C00T	108.00(10)
C008	C006	C00B	105.52(9)	C015	C00N	C014	109.35(13)
C00C	C006	C008	121.14(10)	C00W	C00O	P002	119.09(8)
C00C	C006	C00B	133.26(10)	C00J	C00P	C00V	112.11(9)
C009	C007	C00D	123.36(10)	C00J	C00P	C00X	110.71(9)
N004	C008	C006	112.35(9)	C00J	C00P	C00Y	109.06(9)
N004	C008	C009	127.96(10)	C00V	C00P	C00X	107.80(10)
C009	C008	C006	119.67(10)	C00V	C00P	C00Y	108.03(10)
C007	C009	C008	117.58(10)	C00X	C00P	C00Y	109.05(10)
C007	C009	C00I	121.22(9)	C00Z	C00Q	C00F	109.73(10)
C008	C009	C00I	121.20(9)	C010	C00Q	C00F	112.58(10)
C005	C00A	C00K	121.71(9)	C010	C00Q	C00Z	110.63(11)
C00E	C00A	C005	117.38(10)	C00H	C00U	C011	108.84(10)
C00E	C00A	C00K	120.90(9)	C012	C00U	C00H	112.34(10)
C005	C00B	C006	105.44(9)	C012	C00U	C011	110.37(11)
C00M	C00B	C005	121.23(10)	C013	C00W	C00O	111.75(11)
C00M	C00B	C006	133.30(10)	C016	C00W	C00O	110.18(10)
C00D	C00C	C006	119.84(10)	C016	C00W	C013	109.31(11)

CuPNP-Et (3.5)

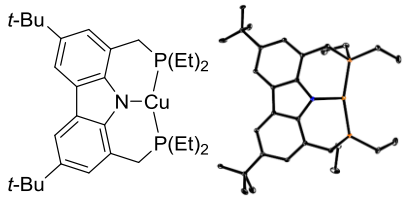

Table 3.22. Crystal data and structure refinement for **3.5**.

Identification code	**3.5**
Empirical formula	$C_{30}H_{46}CuNP_2$
Formula weight	546.20
Temperature/K	294.05
Crystal system	monoclinic
Space group	$P2_1/n$
a/Å	15.141(6)
b/Å	10.413(4)
c/Å	19.344(8)
α/°	90
β/°	90.049(11)
γ/°	90
Volume/Å^3	3050(2)
Z	4
ρ_{calc}g/cm^3	1.171
μ/mm^{-1}	0.838
F(000)	1141.0

Crystal size/mm^3	0.475 × 0.358 × 0.172
Radiation	MoKα (λ = 0.71073)
2Θ range for data collection/°	3.418 to 56.306
Index ranges	-19 ≤ h ≤ 19, -13 ≤ k ≤ 13, -25 ≤ l ≤ 25
Reflections collected	126575
Independent reflections	7139 [R_{int} = 0.0331, R_{sigma} = 0.0148]
Data/restraints/parameters	7139/0/369
Goodness-of-fit on F^2	1.053
Final R indexes [I>=2σ (I)]	R_1 = 0.0477, wR_2 = 0.1357
Final R indexes [all data]	R_1 = 0.0622, wR_2 = 0.1487
Largest diff. peak/hole / e Å^{-3}	0.65/-0.25

Table 3.23. Fractional Atomic Coordinates (×10^4) and Equivalent Isotropic Displacement Parameters (Å^2×10^3) for **3.5**. U_{eq} is defined as 1/3 of the trace of the orthogonalized U_{IJ} tensor.

Atom	*x*	*y*	*z*	U(eq)
Cu01	5305.1(2)	4608.3(3)	6988.3(2)	50.26(12)
P002	4337.4(4)	5878.1(6)	6486.7(3)	47.25(16)
P003	5824.9(4)	2979.9(7)	7586.0(3)	51.24(17)
N004	6411.3(12)	5505.0(18)	6735.9(10)	41.3(4)
C005	6444.8(14)	6367(2)	6198.9(11)	39.0(4)
C006	7231.0(14)	6263(2)	5812.9(11)	39.4(4)
C007	7387.8(15)	7060(2)	5250.4(12)	44.1(5)
C008	8770.4(15)	3557(2)	6338.5(12)	46.2(5)
C009	7192.3(14)	4820(2)	6684.1(11)	39.7(4)
C00A	8262.7(15)	3192(2)	6918.8(13)	48.3(5)
C00B	8493.1(15)	4599(2)	5955.5(12)	43.4(5)
C00C	7488.8(15)	3802(2)	7104.8(12)	44.5(5)
C00D	5794.6(14)	7265(2)	6000.4(12)	41.9(5)
C00E	7713.8(14)	5230(2)	6124.8(11)	39.4(4)
C00F	5976.6(16)	8030(2)	5434.9(13)	46.8(5)
C00G	6765.6(16)	7962(2)	5050.9(13)	47.1(5)
C00H	6988.6(16)	3386(3)	7737.9(12)	52.7(6)
C00I	4941.0(15)	7395(2)	6389.0(13)	47.9(5)
C00J	9598.2(19)	2814(3)	6139.0(15)	64.3(8)
C00K	6920(2)	8869(3)	4449.2(16)	63.6(7)
C00L	4054(3)	5423(3)	5610.2(16)	70.2(8)
C00M	5400(2)	2735(4)	8459.0(16)	70.8(8)
C00N	3300.7(19)	6389(4)	6882.6(19)	72.2(8)
C00O	5854(3)	1352(3)	7244.6(19)	77.0(9)
C00P	3624(4)	6401(4)	5157(2)	118.2(19)
C00Q	6236(3)	1237(5)	6540(3)	112.9(16)
C00R	2671(3)	5285(5)	6998(3)	106.0(15)
C00S	4412(3)	2549(6)	8472(2)	119.6(18)
C00T	9180(9)	1477(11)	5745(8)	75(5)
C00U	9688(7)	1572(8)	6494(4)	109(4)
C1	7101(13)	7983(12)	3799(5)	138(7)
C3	6875(8)	10276(6)	4720(5)	96(4)
C4	6129(5)	8809(15)	3934(5)	116(5)
C4A	6223(7)	9748(12)	4314(7)	79(5)
C3A	7778(8)	9592(12)	4607(9)	155(7)
C1A	7731(7)	8691(12)	4068(6)	90(3)
C00W	10399(3)	3624(8)	6496(6)	164(5)
C0AA	9878(5)	2998(8)	5449(3)	157(4)
C1AA	10121(10)	2380(20)	6701(7)	65(8)

Table 3.24. Anisotropic Displacement Parameters ($Å^2 \times 10^3$) for **3.5**. The anisotropic displacement factor exponent takes the form: $-2\pi^2[h^2a^{*2}U_{11}+2hka^*b^*U_{12}+\ldots]$.

Atom	U_{11}	U_{22}	U_{33}	U_{23}	U_{13}	U_{12}
Cu01	37.79(17)	59.7(2)	53.3(2)	13.02(13)	0.55(12)	4.49(12)
P002	36.3(3)	57.3(4)	48.2(3)	1.9(3)	1.3(2)	8.4(3)
P003	44.4(3)	58.9(4)	50.4(3)	13.5(3)	2.6(3)	3.0(3)
N004	35.0(9)	48(1)	40.8(9)	2.6(7)	-1.7(7)	5.1(7)
C005	36.3(10)	40.2(10)	40.6(10)	-1.1(8)	-2.4(8)	2.9(8)
C006	34.4(10)	41.2(10)	42.5(11)	0.6(8)	-4.3(8)	2.8(8)
C007	38.3(11)	44.2(11)	49.9(12)	4.7(9)	3.3(9)	6.3(9)
C008	36(1)	54.1(13)	48.4(12)	6.9(10)	-0.8(9)	9.4(9)
C009	33.9(10)	46.6(11)	38.5(10)	2.2(9)	-4.0(8)	3.0(8)
C00A	39.8(11)	56.2(13)	48.8(12)	12.1(10)	-2.8(9)	7.1(10)
C00B	36.1(11)	50.3(12)	43.9(11)	7.9(9)	0.8(9)	4.2(9)
C00C	37(1)	54.7(13)	41.8(11)	9.7(10)	-3.1(8)	4.3(9)
C00D	38.3(10)	39.8(10)	47.7(11)	-2.7(9)	-1.1(9)	5.8(8)
C00E	35.5(10)	42.9(11)	39.9(10)	3.3(8)	-4.0(8)	3.4(8)
C00F	43.1(11)	40.8(11)	56.3(13)	3.8(10)	-1.1(10)	11.8(9)
C00G	46.8(12)	40.5(11)	54.0(13)	8.7(9)	2.2(10)	8.4(9)
C00H	43.9(12)	70.7(16)	43.5(12)	15.7(11)	-1.6(9)	6.0(11)
C00I	44.5(12)	48.1(12)	51.1(12)	-3.4(10)	3.6(10)	12.4(10)
C00J	53.5(15)	73.7(18)	65.7(16)	23.5(14)	14.1(12)	26.1(13)
C00K	63.6(16)	59.3(15)	68.0(17)	23.0(13)	12.4(13)	17.2(13)
C00L	96(2)	61.1(17)	53.9(15)	-5.7(13)	-10.0(16)	-3.3(16)
C00M	63.6(17)	89(2)	60.3(16)	23.6(15)	13.0(13)	5.0(15)
C00N	43.3(14)	94(2)	80(2)	-10.1(17)	10.3(13)	9.6(14)
C00O	84(2)	66.5(18)	80(2)	5.2(16)	-11.8(17)	4.0(16)
C00P	183(5)	81(2)	90(3)	4(2)	-74(3)	-12(3)
C00Q	110(3)	116(4)	113(3)	-44(3)	6(3)	-16(3)
C00R	54(2)	135(4)	129(4)	-5(3)	25(2)	-10(2)
C00S	75(2)	185(5)	99(3)	31(3)	27(2)	-12(3)
C00T	67(8)	50(7)	107(12)	-31(7)	25(7)	16(5)
C00U	112(7)	85(5)	129(6)	39(5)	53(5)	54(5)
C1	240(17)	97(7)	76(6)	50(6)	64(8)	62(10)
C3	134(9)	51(4)	104(6)	28(4)	26(6)	1(4)
C4	91(5)	162(12)	94(6)	63(8)	-23(4)	-10(6)
C4A	83(7)	68(7)	87(8)	44(6)	11(6)	22(5)
C3A	99(8)	127(10)	240(17)	124(11)	-25(9)	-45(7)
C1A	91(6)	86(6)	93(6)	49(5)	43(5)	40(5)
C00W	53(3)	137(7)	303(12)	-67(7)	-13(4)	18(3)
C0AA	177(6)	223(8)	70(3)	67(4)	68(4)	170(7)
C1AA	49(8)	91(17)	56(7)	24(7)	-8(5)	35(9)

Table 3.25. Bond Lengths for **3.5**.

Atom	Atom	Length/Å	Atom	Atom	Length/Å
Cu01	P002	2.1988(8)	C00D	C00F	1.381(3)
Cu01	P003	2.1978(9)	C00D	C00I	1.502(3)
Cu01	N004	1.979(2)	C00F	C00G	1.409(3)
P002	C00I	1.835(3)	C00G	C00K	1.517(3)
P002	C00L	1.812(3)	C00J	C00T	1.708(13)
P002	C00N	1.826(3)	C00J	C00U	1.470(6)

P003	C00H	1.835(3)	C00J	C00W	1.631(7)
P003	C00M	1.825(3)	C00J	C0AA	1.413(5)
P003	C00O	1.820(4)	C00J	C1AA	1.418(11)
N004	C005	1.374(3)	C00K	C1	1.583(12)
N004	C009	1.385(3)	C00K	C3	1.558(9)
C005	C006	1.410(3)	C00K	C4	1.559(9)
C005	C00D	1.411(3)	C00K	C4A	1.422(8)
C006	C007	1.389(3)	C00K	C3A	1.532(11)
C006	C00E	1.433(3)	C00K	C1A	1.445(8)
C007	C00G	1.385(3)	C00L	C00P	1.493(5)
C008	C00A	1.413(3)	C00M	C00S	1.509(5)
C008	C00B	1.379(3)	C00N	C00R	1.510(5)
C008	C00J	1.523(3)	C00O	C00Q	1.487(6)
C009	C00C	1.409(3)	C00T	C00U	1.64(2)
C009	C00E	1.407(3)	C1	C4	1.725(18)
C00A	C00C	1.381(3)	C3A	C1A	1.40(2)
C00B	C00E	1.390(3)	C00W	C1AA	1.42(3)
C00C	C00H	1.504(3)			

Table 3.26. Bond Angles for **3.5**.

Atom	Atom	Atom	Angle/°	Atom	Atom	Atom	Angle/°
P003	Cu01	P002	159.13(3)	C00B	C00E	C009	121.0(2)
N004	Cu01	P002	99.85(6)	C00D	C00F	C00G	124.0(2)
N004	Cu01	P003	101.02(6)	C007	C00G	C00F	117.6(2)
C00I	P002	Cu01	103.38(8)	C007	C00G	C00K	122.0(2)
C00L	P002	Cu01	114.37(12)	C00F	C00G	C00K	120.3(2)
C00L	P002	C00I	104.27(15)	C00C	C00H	P003	114.83(16)
C00L	P002	C00N	105.43(17)	C00D	C00I	P002	113.75(16)
C00N	P002	Cu01	124.25(13)	C008	C00J	C00T	102.8(5)
C00N	P002	C00I	102.74(14)	C008	C00J	C00W	104.0(3)
C00H	P003	Cu01	104.45(9)	C00U	C00J	C008	113.8(3)
C00M	P003	Cu01	117.90(11)	C00U	C00J	C00T	61.7(8)
C00M	P003	C00H	102.90(13)	C0AA	C00J	C008	114.7(3)
C00O	P003	Cu01	122.45(12)	C0AA	C00J	C00W	96.0(6)
C00O	P003	C00H	104.45(16)	C0AA	C00J	C1AA	126.8(6)
C00O	P003	C00M	102.37(17)	C1AA	C00J	C008	115.2(6)
C005	N004	Cu01	121.78(14)	C1AA	C00J	C00W	55.0(11)
C005	N004	C009	104.47(18)	C00G	C00K	C1	105.9(4)
C009	N004	Cu01	119.84(15)	C00G	C00K	C3	108.7(4)
N004	C005	C006	112.45(18)	C00G	C00K	C4	110.3(4)
N004	C005	C00D	127.8(2)	C00G	C00K	C3A	106.5(5)
C006	C005	C00D	119.8(2)	C3	C00K	C1	145.4(5)
C005	C006	C00E	105.40(19)	C3	C00K	C4	102.7(8)
C007	C006	C005	120.90(19)	C4	C00K	C1	66.6(9)
C007	C006	C00E	133.7(2)	C4A	C00K	C00G	115.3(4)
C00G	C007	C006	120.5(2)	C4A	C00K	C3A	110.5(8)
C00A	C008	C00J	120.8(2)	C4A	C00K	C1A	128.3(5)
C00B	C008	C00A	118.2(2)	C1A	C00K	C00G	116.3(3)
C00B	C008	C00J	120.9(2)	C1A	C00K	C3A	56.2(8)
N004	C009	C00C	128.1(2)	C00P	C00L	P002	118.2(3)
N004	C009	C00E	112.27(19)	C00S	C00M	P003	112.6(3)
C00E	C009	C00C	119.6(2)	C00R	C00N	P002	112.5(3)
C00C	C00A	C008	123.0(2)	C00Q	C00O	P003	114.6(3)
C008	C00B	C00E	120.2(2)	C00U	C00T	C00J	52.0(5)
C009	C00C	C00H	121.8(2)	C00J	C00U	C00T	66.3(6)
C00A	C00C	C009	117.8(2)	C00K	C1	C4	56.0(5)
C00A	C00C	C00H	120.5(2)	C00K	C4	C1	57.4(7)
C005	C00D	C00I	121.6(2)	C1A	C3A	C00K	58.8(6)
C00F	C00D	C005	117.3(2)	C3A	C1A	C00K	65.0(6)
C00F	C00D	C00I	121.1(2)	C1AA	C00W	C00J	54.9(6)
C009	C00E	C006	105.39(19)	C00W	C1AA	C00J	70.1(8)
C00B	C00E	C006	133.5(2)				

CuPNP-PMP (3.6)

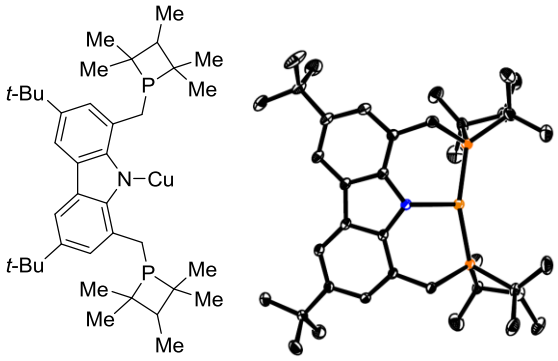

Table 3.27. Crystal data and structure refinement for **3.6**.

Identification code	**3.6**
Empirical formula	$C_{38}H_{58}CuNP_2$
Formula weight	654.33
Temperature/K	100.0
Crystal system	monoclinic
Space group	$P2_1/c$
a/Å	12.8686(5)
b/Å	18.0813(6)
c/Å	16.3204(6)
α/°	90
β/°	102.3660(10)
γ/°	90
Volume/Å^3	3709.3(2)
Z	4
ρ_{calc}g/cm^3	1.172
μ/mm^{-1}	0.700
F(000)	1408.0
Crystal size/mm^3	0.28 × 0.19 × 0.12
Radiation	MoKα (λ = 0.71073)
2Θ range for data collection/°	4.308 to 68.63
Index ranges	$-20 \leq h \leq 19$, $-28 \leq k \leq 27$, $-24 \leq l \leq 25$
Reflections collected	125180
Independent reflections	14571 [R_{int} = 0.0410, R_{sigma} = 0.0365]
Data/restraints/parameters	14571/0/395
Goodness-of-fit on F^2	1.032
Final R indexes [I>=2σ (I)]	R_1 = 0.0488, wR_2 = 0.1164
Final R indexes [all data]	R_1 = 0.0741, wR_2 = 0.1286
Largest diff. peak/hole / e Å^{-3}	1.55/-0.49

Table 3.28. Fractional Atomic Coordinates ($\times 10^4$) and Equivalent Isotropic Displacement Parameters ($Å^2 \times 10^3$) for **3.6**. U_{eq} is defined as 1/3 of the trace of the orthogonalized U_{IJ} tensor.

Atom	*x*	*y*	*z*	U(eq)
Cu01	2672.7(2)	6619.5(2)	4881.4(2)	14.65(5)
P002	4144.1(3)	6956.5(2)	4490.2(2)	15.12(8)
P003	1017.7(3)	6675.1(2)	5049.0(2)	13.43(7)
N004	3239.7(10)	5790.4(7)	5633.3(8)	14.0(2)
C005	1693.2(11)	5623.7(8)	6331.7(9)	13.8(2)
C006	3540.4(11)	5336.4(8)	6996.7(9)	14.2(2)
C007	2194.4(12)	5224.7(8)	7814.1(9)	15.2(3)
C008	3245.8(12)	5151.8(8)	7749.8(9)	15.7(3)
C009	2779.1(11)	5591.2(8)	6293.2(9)	13.5(2)
C00A	5595.4(12)	5213.8(9)	7163.1(10)	17.1(3)
C00B	1436.0(11)	5450.4(8)	7092.9(9)	15.3(3)
C00C	4548.2(11)	5376.5(8)	6752.3(9)	14.5(2)
C00D	5153.3(11)	5812.1(8)	5512.1(9)	15.2(3)
C00E	4317.7(11)	5666.9(8)	5924.4(9)	14.4(2)
C00F	6424.0(12)	5359.0(9)	6767.8(10)	18.2(3)
C00G	-200.7(12)	6891.5(9)	4226.5(9)	17.0(3)
C00H	832.0(11)	5793.7(9)	5567.4(9)	15.8(3)
C00I	1820.7(12)	5075.8(9)	8628.9(10)	19.1(3)
C00J	6179.4(12)	5654.2(9)	5945.4(10)	18.4(3)
C00K	446.0(12)	7456.3(9)	5562.7(9)	17.7(3)
C00L	4967.3(12)	6114.8(9)	4631.3(10)	17.7(3)
C00M	4375.9(14)	7488.9(11)	3559.8(10)	23.1(3)
C00N	7594.2(12)	5234.9(10)	7191.8(11)	22.9(3)
C00O	4902.6(14)	7767.4(9)	5024.8(10)	21.8(3)
C00P	1301.9(15)	5777.2(12)	8896.7(12)	28.2(4)
C00Q	2737.7(14)	4855.8(11)	9351.0(11)	24.7(3)
C00R	3388.7(17)	7625.6(13)	2873.2(13)	33.1(4)
C00S	1000.1(16)	4449.2(12)	8497.5(12)	31.1(4)
C00T	8163.7(16)	5988.1(13)	7263.8(15)	37.7(5)
C00U	7729.2(15)	4924.4(14)	8081.2(14)	36.7(5)
C00V	-249.9(14)	7655(1)	4673.6(11)	23.8(3)
C00W	-0.6(18)	7004.4(14)	3345.8(12)	35.7(5)
C00X	1231.1(17)	8062.0(12)	5917.0(15)	36.4(5)
C00Y	-1327.0(15)	7999.9(12)	4621.0(12)	30.7(4)
C00Z	6059.9(15)	7622.8(11)	5410.5(14)	31.9(4)
C010	-1145.4(16)	6381.3(12)	4185.6(14)	34.8(5)
C011	-183.9(19)	7223.7(13)	6208.0(13)	36.4(5)
C012	4642.9(15)	8183.0(11)	4160.2(12)	26.0(3)
C013	5284.4(18)	7221.0(15)	3183.5(13)	38.1(5)
C014	4374.4(19)	8142.4(13)	5682.6(14)	35.9(4)
C015	5476.7(17)	8711.3(13)	3967.4(14)	37.4(5)
C016	8117.3(16)	4715.4(16)	6666.6(15)	45.2(6)

Table 3.29. Anisotropic Displacement Parameters ($Å^2 \times 10^3$) for **3.6**. The anisotropic displacement factor exponent takes the form: $-2\pi^2[h^2a^{*2}U_{11}+2hka^*b^*U_{12}+\ldots]$.

Atom	U_{11}	U_{22}	U_{33}	U_{23}	U_{13}	U_{12}
Cu01	13.59(8)	14.16(9)	16.27(9)	1.89(6)	3.33(6)	0.82(6)

P002	14.77(16)	15.70(18)	14.75(16)	0.56(13)	2.84(13)	-1.37(13)
P003	13.13(15)	13.48(17)	13.10(16)	1.68(12)	1.51(12)	1.74(12)
N004	12.2(5)	14.5(6)	14.7(5)	0.8(4)	1.8(4)	0.9(4)
C005	11.7(5)	13.3(6)	15.2(6)	2.1(5)	0.0(5)	1.2(5)
C006	13.2(6)	13.1(6)	15.2(6)	-0.5(5)	0.6(5)	2.3(5)
C007	15.3(6)	13.8(6)	15.6(6)	2.8(5)	1.4(5)	0.3(5)
C008	14.9(6)	15.6(7)	15.5(6)	1.9(5)	0.4(5)	2.0(5)
C009	12.7(6)	12.9(6)	14.0(6)	0.3(5)	1.0(5)	1.0(5)
C00A	15.2(6)	17.5(7)	17.2(6)	-3.7(5)	0.2(5)	4.6(5)
C00B	11.8(6)	16.0(6)	17.6(6)	3.3(5)	2.1(5)	0.2(5)
C00C	13.6(6)	13.9(6)	14.9(6)	-2.3(5)	0.6(5)	2.4(5)
C00D	14.0(6)	14.6(6)	17.0(6)	-1.6(5)	3.2(5)	1.4(5)
C00E	13.4(6)	14.0(6)	14.9(6)	-1.6(5)	1.2(5)	1.9(5)
C00F	12.7(6)	18.1(7)	22.4(7)	-4.4(6)	0.4(5)	3.4(5)
C00G	18.6(6)	16.9(7)	13.6(6)	-0.6(5)	-0.4(5)	3.3(5)
C00H	12.5(6)	16.3(7)	17.0(6)	4.0(5)	-0.4(5)	-0.2(5)
C00I	17.1(6)	23.3(8)	16.4(6)	6.0(6)	2.5(5)	-0.9(6)
C00J	14.2(6)	19.0(7)	21.9(7)	-3.0(6)	3.6(5)	1.4(5)
C00K	17.9(6)	19.7(7)	14.0(6)	-2.1(5)	0.0(5)	3.7(5)
C00L	17.0(6)	19.2(7)	17.7(7)	-1.3(5)	5.3(5)	1.6(5)
C00M	22.3(7)	31.9(9)	14.7(7)	3.3(6)	2.8(6)	-4.9(6)
C00N	13.2(6)	30.6(9)	23.1(7)	-3.7(6)	-0.2(5)	5.1(6)
C00O	27.2(8)	18.3(7)	17.4(7)	2.3(6)	-0.8(6)	-5.6(6)
C00P	28.2(8)	35.1(10)	23.2(8)	3.1(7)	10.0(7)	7.8(7)
C00Q	22.5(7)	32.0(9)	18.2(7)	7.5(6)	1.0(6)	0.1(7)
C00R	31.9(9)	38.5(11)	26.0(9)	8.9(8)	-0.2(7)	1.7(8)
C00S	29.4(9)	35.4(10)	26.5(8)	11.3(8)	1.6(7)	-12.7(8)
C00T	22.8(8)	44.2(12)	41.4(11)	-4.0(9)	-4.0(8)	-7.9(8)
C00U	19.9(8)	52.3(13)	34.1(10)	8.5(9)	-2.7(7)	9.5(8)
C00V	24.1(8)	23.3(8)	21.9(7)	-0.2(6)	0.0(6)	4.9(6)
C00W	39.3(11)	49.0(13)	17.7(8)	8.9(8)	3.7(7)	13.7(9)
C00X	32.3(10)	25.8(10)	45.5(12)	-11.2(8)	-4.0(8)	2.2(8)
C00Y	26.9(8)	32.5(10)	28.7(9)	-5.8(7)	-3.3(7)	15.1(7)
C00Z	22.8(8)	27.8(9)	39.6(10)	-0.4(8)	-5.7(7)	-4.3(7)
C010	25.5(9)	29.4(10)	40.7(11)	9.5(8)	-12.4(8)	-6.2(7)
C011	46.7(12)	40.4(12)	26.2(9)	2.8(8)	17.2(9)	11.8(9)
C012	24.7(8)	24.8(8)	26.2(8)	6.5(7)	0.3(6)	-4.2(6)
C013	36.9(11)	53.6(14)	27.4(9)	9.9(9)	14.8(8)	7.9(10)
C014	43.7(12)	30.8(10)	32.2(10)	-8.4(8)	5.8(9)	-0.5(9)
C015	31.5(10)	37.2(11)	38.1(11)	18.2(9)	-4.8(8)	-15.8(8)
C016	22.0(9)	66.6(16)	41.9(12)	-25.2(11)	-4.1(8)	21.4(10)

Table 3.30. Bond Lengths for **3.6**.

Atom	Atom	Length/Å	Atom	Atom	Length/Å
Cu01	P002	2.2096(4)	C00D	C00J	1.388(2)
Cu01	P003	2.2070(4)	C00D	C00L	1.509(2)
Cu01	N004	1.9753(13)	C00F	C00J	1.416(2)
P002	C00L	1.8403(16)	C00F	C00N	1.533(2)
P002	C00M	1.8749(17)	C00G	C00V	1.569(2)
P002	C00O	1.8705(17)	C00G	C00W	1.527(2)
P003	C00G	1.8741(15)	C00G	C010	1.516(3)
P003	C00H	1.8437(15)	C00I	C00P	1.540(3)
P003	C00K	1.8717(16)	C00I	C00Q	1.531(2)
N004	C009	1.3837(19)	C00I	C00S	1.532(2)
N004	C00E	1.3849(18)	C00K	C00V	1.575(2)
C005	C009	1.413(2)	C00K	C00X	1.518(3)
C005	C00B	1.388(2)	C00K	C011	1.520(3)
C005	C00H	1.512(2)	C00M	C00R	1.523(3)
C006	C008	1.402(2)	C00M	C012	1.584(3)
C006	C009	1.4172(19)	C00M	C013	1.512(3)
C006	C00C	1.438(2)	C00N	C00T	1.539(3)
C007	C008	1.386(2)	C00N	C00U	1.531(3)
C007	C00B	1.419(2)	C00N	C016	1.522(3)

C007	C00I	1.532(2)	C00O	C00Z	1.510(3)
C00A	C00C	1.402(2)	C00O	C012	1.570(2)
C00A	C00F	1.384(2)	C00O	C014	1.545(3)
C00C	C00E	1.420(2)	C00V	C00Y	1.506(2)
C00D	C00E	1.410(2)	C012	C015	1.519(3)

Table 3.31. Bond Angles for **3.6**.

Atom	Atom	Atom	Angle/°	Atom	Atom	Atom	Angle/°
P003	Cu01	P002	158.859(17)	C00V	C00G	P003	87.79(9)
N004	Cu01	P002	99.41(4)	C00W	C00G	P003	114.72(12)
N004	Cu01	P003	101.27(4)	C00W	C00G	C00V	110.60(15)
C00L	P002	Cu01	103.98(5)	C010	C00G	P003	116.39(12)
C00L	P002	C00M	109.80(8)	C010	C00G	C00V	116.36(16)
C00L	P002	C00O	111.16(8)	C010	C00G	C00W	109.58(16)
C00M	P002	Cu01	132.10(6)	C005	C00H	P003	114.21(10)
C00O	P002	Cu01	118.38(6)	C007	C00I	C00P	109.72(13)
C00O	P002	C00M	79.50(8)	C007	C00I	C00S	110.10(14)
C00G	P003	Cu01	127.03(5)	C00Q	C00I	C007	112.36(13)
C00H	P003	Cu01	103.93(5)	C00Q	C00I	C00P	107.77(15)
C00H	P003	C00G	109.78(7)	C00Q	C00I	C00S	108.07(14)
C00H	P003	C00K	110.17(7)	C00S	C00I	C00P	108.72(15)
C00K	P003	Cu01	124.91(5)	C00D	C00J	C00F	123.69(14)
C00K	P003	C00G	79.31(7)	C00V	C00K	P003	87.70(10)
C009	N004	Cu01	121.22(10)	C00X	C00K	P003	114.94(13)
C009	N004	C00E	104.81(12)	C00X	C00K	C00V	112.78(15)
C00E	N004	Cu01	123.03(10)	C00X	C00K	C011	110.25(17)
C009	C005	C00H	121.92(13)	C011	C00K	P003	114.88(13)
C00B	C005	C009	117.25(13)	C011	C00K	C00V	114.79(15)
C00B	C005	C00H	120.73(13)	C00D	C00L	P002	112.89(10)
C008	C006	C009	121.19(13)	C00R	C00M	P002	115.26(13)
C008	C006	C00C	133.19(13)	C00R	C00M	C012	111.26(16)
C009	C006	C00C	105.48(13)	C012	C00M	P002	87.52(10)
C008	C007	C00B	118.29(14)	C013	C00M	P002	115.81(14)
C008	C007	C00I	122.84(13)	C013	C00M	C00R	110.42(16)
C00B	C007	C00I	118.87(13)	C013	C00M	C012	114.89(16)
C007	C008	C006	119.71(13)	C00F	C00N	C00T	108.09(15)
N004	C009	C005	128.04(13)	C00U	C00N	C00F	112.50(15)
N004	C009	C006	112.22(12)	C00U	C00N	C00T	107.26(17)
C005	C009	C006	119.74(13)	C016	C00N	C00F	110.25(14)
C00F	C00A	C00C	119.65(15)	C016	C00N	C00T	109.16(18)
C005	C00B	C007	123.64(13)	C016	C00N	C00U	109.48(18)
C00A	C00C	C006	133.51(14)	C00Z	C00O	P002	115.35(13)
C00A	C00C	C00E	121.07(14)	C00Z	C00O	C012	117.29(16)
C00E	C00C	C006	105.39(12)	C00Z	C00O	C014	109.13(16)
C00E	C00D	C00L	122.73(13)	C012	C00O	P002	88.08(10)
C00J	C00D	C00E	117.28(14)	C014	C00O	P002	113.88(13)
C00J	C00D	C00L	119.98(13)	C014	C00O	C012	111.95(16)
N004	C00E	C00C	112.07(13)	C00G	C00V	C00K	98.99(12)
N004	C00E	C00D	128.07(14)	C00Y	C00V	C00G	117.79(15)
C00D	C00E	C00C	119.84(13)	C00Y	C00V	C00K	118.81(15)
C00A	C00F	C00J	118.44(14)	C00O	C012	C00M	98.80(14)
C00A	C00F	C00N	122.82(15)	C015	C012	C00M	116.06(17)
C00J	C00F	C00N	118.72(14)	C015	C012	C00O	117.60(15)

[CuPNP][BAr$^{F}_{24}$][Hexane] (3.7-BAr$^{F}_{24}$)

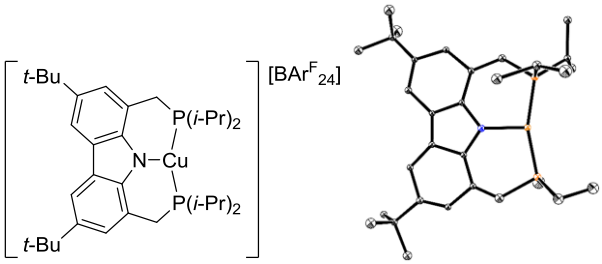

The X-ray diffraction data were of poor quality and hence only sufficient for establishing overall atomic connectivity. Only unit cell parameters are shown below.

Table 3.32. Crystal data for **3.7-BAr$^{F}_{24}$**.

Identification code	**3.7-BAr$^{F}_{24}$**
Empirical formula	$C_{72}H_{80}BNF_{24}P_2Cu$
Formula weight	1551.70
Temperature/K	100.0
Crystal system	monoclinic
Space group	C2/c
a/Å	41.564(6)
b/Å	12.850(2)
c/Å	34.281(5)
α/°	90
β/°	115.347(10)
γ/°	90
Volume/Å^3	16546(5)
Z	12
ρ_{calc}g/cm^3	1.697
μ/mm^{-1}	2.249
F(000)	8604.0
Radiation	CuKα (λ = 1.54178)
2Θ range for data collection/°	5.63 to 122.98
Index ranges	-45 ≤ h ≤ 45, -14 ≤ k ≤ 14, -37 ≤ l ≤ 38
Reflections collected	82784
Independent reflections	12011 [R_{int} = 0.2027, R_{sigma} = 0.1161]

[Fc][BAr$^{F}_{24}$]

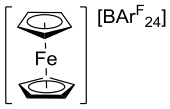

In the attempted crystallization of **3.7**, single crystals of [Fc][BAr^F_{24}] were identified. Only unit cell parameters are shown below.

Table 3.33. Crystal data for [Fc][BAr^F_{24}].

Identification code	[Fc][BAr^F_{24}]
Empirical formula	$C_{42}H_{22}BF24Fe$
Formula weight	1049.26
Temperature/K	99.98
Crystal system	triclinic
Space group	P1
a/Å	12.8562(10)
b/Å	13.1986(9)
c/Å	14.3879(8)
α/°	92.919(4)
β/°	90.196(4)
γ/°	118.691(4)
Volume/Å^3	2137.8(3)
Z	4
ρ_{calc}g/cm^3	2.163
μ/mm^{-1}	2.927
F(000)	1472.0
Radiation	CuKα (λ = 1.54178)
2Θ range for data collection/°	6.154 to 148.534
Index ranges	$-9 \leq h \leq 11$, $-9 \leq k \leq 15$, $-17 \leq l \leq 12$
Reflections collected	5519
Independent reflections	4515 [R_{int} = 0.0600, R_{sigma} = 0.0600]

[CuPNHP][PF_6][THF] (3.8-PF_6)

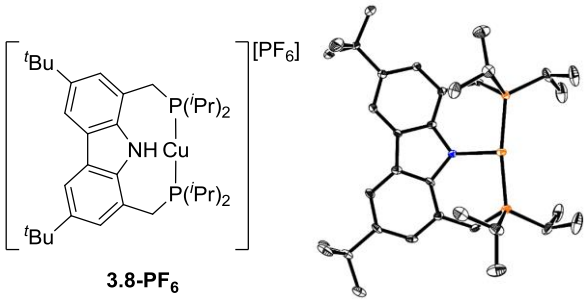

3.8-PF_6

Table 3.34. Crystal data and structure refinement for **3.8-PF$_6$**.

Identification code	**3.8-PF$_6$**
Empirical formula	$C_{38}H_{62}CuF_6NOP_3$
Formula weight	818.83
Temperature/K	100.05
Crystal system	monoclinic
Space group	$P2_1$
a/Å	12.3203(12)
b/Å	14.9319(12)
c/Å	22.797(2)
α/°	90
β/°	99.868(3)
γ/°	90
Volume/Å^3	4131.7(6)
Z	4
ρ_{calc}g/cm^3	1.317
μ/mm^{-1}	0.702
F(000)	1732.0
Crystal size/mm^3	0.362 × 0.057 × 0.055
Radiation	MoKα (λ = 0.71073)
2Θ range for data collection/°	4.324 to 61.164
Index ranges	$-17 \leq h \leq 17$, $-21 \leq k \leq 18$, $-30 \leq l \leq 32$
Reflections collected	128319
Independent reflections	23910 [R_{int} = 0.0618, R_{sigma} = 0.0613]
Data/restraints/parameters	23910/1/930
Goodness-of-fit on F^2	1.040
Final R indexes [I>=2σ (I)]	R_1 = 0.0548, wR_2 = 0.1219
Final R indexes [all data]	R_1 = 0.0776, wR_2 = 0.1308
Largest diff. peak/hole / e Å^{-3}	1.94/-0.56
Flack parameter	0.400(10)

Table 3.35. Fractional Atomic Coordinates (×10^4) and Equivalent Isotropic Displacement Parameters (Å^2×10^3) for **3.8-PF$_6$**. U_{eq} is defined as 1/3 of the trace of the orthogonalized U_{IJ} tensor.

Atom	*x*	*y*	*z*	U(eq)	Atom	*x*	*y*	*z*	U(eq)
Cu01	3579.8(4)	2966.4(3)	5988.7(2)	11.42(11)	C01P	4399(5)	7063(4)	2195(2)	26.0(11)
Cu02	3816.9(4)	5403.6(3)	1037.4(2)	12.68(11)	C01Q	4739(4)	4019(4)	2253(2)	25.2(11)
P003	3309.4(9)	1522.1(7)	5768.8(5)	10.5(2)	C01R	8706(5)	8108(3)	2691(2)	26.8(11)
P004	3411.6(9)	4443.4(7)	6055.1(5)	10.9(2)	C01S	8508(4)	8199(3)	2009(2)	17.3(9)
P005	3598.7(10)	6871.5(8)	987.1(6)	15.3(2)	C01T	2138(4)	402(4)	4869(2)	24.2(10)
P006	3729.2(9)	3922.7(8)	1059.4(5)	11.4(2)	C01U	7698(4)	6601(3)	7084(2)	20.8(10)
P007	5502(1)	3099.3(8)	4172.0(5)	17.1(2)	C01V	8161(4)	302(4)	7666(2)	23.6(10)
P008	5161.5(10)	5421.7(9)	-772.0(5)	19.0(2)	C01W	9595(4)	8045(4)	1786(2)	25.8(11)
F009	4655(3)	2541(2)	3709.9(14)	35.6(8)	C01X	7704(4)	3437(3)	1768(2)	14.2(9)
F00A	5802(3)	6219(2)	-387.4(15)	37.1(8)	C01Y	2037(4)	4716(4)	4971(2)	32.2(13)
F00B	4352(2)	5346(2)	-278.3(13)	34.2(7)	C01Z	7925(4)	4352(3)	1855(2)	13.8(9)

F00C	5256(3)	3961(2)	3761.8(14)	34.0(8)	C020	3691(5)	820(4)	6901(2)	32.0(13)
F00D	6317(3)	3684(2)	4647.5(15)	41.0(9)	C021	8112(4)	5639(3)	7166(2)	15.5(9)
F00E	6491(3)	2840(3)	3846.1(16)	39.2(8)	C022	1728(4)	821(4)	6383(2)	25.8(11)
F00F	5739(4)	2250(2)	4591.8(16)	43.4(10)	C023	3735(5)	5887(3)	6876(2)	27.4(12)
F00G	5965(3)	4713(2)	-390.4(15)	34.7(8)	C024	8113(5)	1784(3)	1954(3)	30.1(13)
F00H	4537(3)	3386(2)	4531.4(15)	39.1(8)	C025	2393(5)	6884(5)	-150(3)	36.7(14)
F00I	4342(3)	6124(2)	-1130.8(15)	38.6(8)	C026	4372(4)	4349(4)	7255(2)	23(1)
F00J	5974(3)	5494(2)	-1237.5(14)	36.6(8)	C027	2434(4)	7313(4)	457(2)	25.6(11)
F00K	4497(3)	4636(2)	-1137.4(16)	44.3(9)	C028	8234(4)	5402(4)	7828.3(19)	25.4(10)
N00L	5619(3)	5439(3)	927.4(15)	12.0(6)	C029	2551(4)	3335(4)	626(2)	23(1)
N00M	5341(3)	2996(2)	5844.1(15)	9.5(6)	C02A	9246(5)	2246(4)	4509(3)	37.3(14)
C00N	5993(3)	3793(3)	1078.8(18)	10.4(8)	C02B	2473(5)	2019(4)	4607(2)	26.5(11)
C00O	5645(3)	1328(3)	5963.3(19)	10.2(8)	C02C	9248(4)	5595(3)	6975(2)	24.2(11)
C00P	6353(3)	690(3)	6268(2)	12.7(8)	C02D	1174(4)	4855(4)	5891(3)	31.7(13)
O00Q	9460(4)	1680(3)	5018(2)	43.2(11)	O02E	787(6)	9242(5)	96(3)	85(2)
C00R	7916(4)	6594(3)	1825(2)	14.8(9)	C02F	9122(6)	3186(4)	4742(3)	44.8(16)
C00S	6744(4)	3180(3)	1383.1(19)	12.8(8)	C02G	3441(6)	8415(4)	1693(3)	33.9(13)
C00T	7602(4)	4056(3)	6840.0(19)	12.6(8)	C02H	8585(5)	2883(4)	2770(2)	34.5(13)
C00U	6893(3)	2460(3)	6472.0(19)	10.4(8)	C02I	2350(5)	3679(5)	-16(3)	41.7(16)
C00V	6903(3)	3436(3)	6502.9(18)	9.6(8)	C02J	1521(4)	3445(5)	904(3)	38.5(15)
C00W	5961(3)	3741(3)	6117.8(18)	9.6(8)	C02K	8787(6)	3027(5)	5351(3)	48.8(16)
C00X	7192(4)	5946(3)	1541(2)	13.5(8)	C02L	9622(4)	2859(4)	1915(3)	34.7(13)
C00Y	5948(4)	2220(3)	6073.4(19)	9.5(8)	C02M	1354(5)	7160(5)	683(3)	42.3(16)
C00Z	4903(4)	3498(3)	727.6(19)	12.0(8)	C02N	8126(5)	9160(3)	1849(2)	23.6(11)
C010	6229(4)	6210(3)	1169(2)	12.6(8)	C02O	1339(7)	9605(6)	-347(4)	65(2)
C011	7352(4)	4969(3)	6796.4(19)	13.3(8)	C02P	1407(7)	10611(6)	-253(3)	66(3)
C012	7696(4)	-763(3)	6815(3)	23.9(11)	C02Q	8869(9)	2063(5)	5447(4)	73(3)
C013	6382(3)	5236(3)	6414.2(18)	11.7(8)	C02R	1191(8)	10743(6)	388(4)	66(2)
C014	7673(4)	7496(3)	1727(2)	14.2(9)	C02S	684(11)	9923(8)	500(5)	101(4)
C015	4566(3)	4936(3)	5739.8(18)	11.5(8)	C01E	7588(4)	1812(3)	6772.2(19)	11.7(8)
C016	7318(4)	905(3)	6662(2)	13.5(9)	C01F	3528(4)	4883(3)	6822(2)	15.6(9)
C017	4584(3)	1070(3)	5557.0(18)	11.5(8)	C01G	2936(4)	710(3)	6311(2)	18.0(9)
C018	2255(4)	1378(3)	5097(2)	18.8(9)	C01H	3484(5)	7405(3)	1711(2)	24.0(11)
C019	6660(4)	7733(3)	1371(2)	15.0(9)	C01I	4812(4)	7374(3)	733(2)	14.7(9)
C01A	2211(4)	5021(3)	5622(2)	17.2(9)	C01J	8487(4)	2739(3)	2098(2)	18.3(10)
C01B	5657(3)	4636(3)	6078.4(18)	10.2(8)	C01K	8085(4)	188(3)	6988(2)	16.3(9)
C01C	7214(4)	4971(3)	1546(2)	11.6(8)	C01L	9249(4)	295(3)	6835(2)	21.5(10)
C01D	6263(4)	4696(3)	1157.8(18)	11.5(8)	C01M	5908(4)	7100(3)	1090(2)	13.6(9)
C01O	4158(5)	2472(4)	1864(3)	29.6(12)	C01N	3899(4)	3465(3)	1819(2)	19.3(10)

Table 3.36. Anisotropic Displacement Parameters ($Å^2 \times 10^3$) for **3.8-PF$_6$**. The anisotropic displacement factor exponent takes the form: $-2\pi^2[h^2a^{*2}U_{11}+2hka^*b^*U_{12}+\ldots]$.

Atom	U_{11}	U_{22}	U_{33}	U_{23}	U_{13}	U_{12}	Atom	U_{11}	U_{22}	U_{33}	U_{23}	U_{13}	U_{12}
Cu01	9.7(2)	10.6(2)	14.0(2)	-0.35(19)	1.85(19)	-0.6(2)	C01P	31(3)	27(3)	22(2)	-3(2)	12(2)	-6(2)
Cu02	15.6(3)	9.2(2)	13.5(2)	-1.5(2)	3.11(19)	1.0(2)	C01Q	25(3)	39(3)	11(2)	0(2)	1.3(18)	4(2)
P003	6.7(5)	12.2(5)	13.0(5)	-1.4(4)	3.0(4)	-1.5(4)	C01R	40(3)	18(2)	23(2)	-7.2(19)	6(2)	-14(2)
P004	8.5(5)	12.4(5)	12.0(5)	2.0(4)	1.9(4)	1.0(4)	C01S	21(2)	12(2)	20(2)	-5.0(16)	4.4(18)	-6.3(16)
P005	13.4(5)	11.5(5)	21.6(6)	-1.1(4)	5.1(4)	3.1(4)	C01T	21(2)	27(2)	24(2)	-12(2)	3.8(18)	-6(2)
P006	11.3(5)	11.7(5)	11.1(5)	-1.5(4)	1.7(4)	-1.1(4)	C01U	22(2)	11(2)	27(2)	-8.7(18)	-0.7(19)	-1.3(18)
P007	22.6(6)	13.1(6)	15.6(5)	-0.1(4)	3.0(4)	-2.6(4)	C01V	23(2)	22(3)	25(2)	5(2)	1.9(19)	4(2)
P008	25.0(6)	11.9(5)	19.1(5)	0.7(5)	0.5(4)	-1.8(5)	C01W	21(2)	25(3)	32(3)	-5(2)	8(2)	-8(2)
F009	34.5(19)	42(2)	28.6(17)	-16.0(14)	0.4(14)	-15.7(15)	C01X	13(2)	11(2)	19(2)	0.9(16)	1.7(17)	-0.4(16)
F00A	48(2)	23.3(17)	39.8(19)	-15.3(14)	8.3(16)	-9.1(15)	C01Y	20(3)	52(4)	21(2)	5(2)	-5(2)	9(3)
F00B	29.2(16)	44.3(19)	28.9(15)	10.6(15)	4.6(12)	1.1(16)	C01Z	13(2)	13(2)	15(2)	1.3(16)	-0.7(16)	-2.6(16)
F00C	52(2)	21.9(16)	27.5(16)	6.7(13)	6.4(15)	7.4(14)	C020	26(3)	48(3)	23(3)	13(2)	9(2)	10(2)
F00D	44(2)	39(2)	34.9(18)	-10.0(15)	-7.7(15)	-11.4(17)	C021	12(2)	15(2)	18(2)	-2.7(16)	0.0(17)	-2.5(16)
F00E	31.5(18)	41(2)	49(2)	-0.6(17)	17.1(16)	7.0(16)	C022	18(2)	31(3)	32(3)	3(2)	14(2)	-3(2)
F00F	76(3)	19.6(16)	33.6(19)	13.6(13)	5.3(19)	0.4(16)	C023	39(3)	20(3)	26(3)	-5.2(19)	13(2)	-2(2)
F00G	37.3(19)	31.3(18)	35.6(18)	10.8(14)	6.0(14)	10.7(15)	C024	24(3)	18(2)	43(3)	10(2)	-9(2)	1(2)
F00H	37.7(19)	52(2)	33.1(18)	-9.3(15)	21.2(15)	-1.4(16)	C025	22(3)	57(4)	27(3)	11(3)	-5(2)	7(3)

F00I	38(2)	35.6(19)	41(2)	19.7(16)	3.6(16)	11.9(16)	C026	24(3)	34(3)	12(2)	4.8(18)	3.3(18)	0(2)
F00J	47(2)	34.7(19)	33.7(17)	5.5(16)	21.7(15)	8.2(17)	C027	20(3)	24(3)	31(3)	10(2)	-1(2)	6(2)
F00K	59(2)	25.9(17)	43(2)	-8.6(15)	-5.6(18)	-12.7(17)	C028	34(3)	25(2)	15(2)	-3(2)	0.4(18)	-6(2)
N00L	12.6(16)	8.5(15)	14.2(16)	-1.1(14)	0.0(13)	1.6(15)	C029	15(2)	25(2)	28(3)	-12(2)	1.6(19)	-6.1(19)
N00M	9.6(15)	7.2(15)	11.4(15)	-0.1(13)	1.6(12)	0.7(14)	C02A	29(3)	39(3)	45(4)	-3(3)	9(3)	5(3)
C00N	11(2)	10.3(19)	10.7(19)	0.2(15)	4.0(15)	1.8(15)	C02B	29(3)	32(3)	17(2)	0(2)	-1(2)	5(2)
C00O	7.9(19)	10.7(19)	13.1(19)	0.5(14)	5.2(15)	-0.1(15)	C02C	13(2)	22(3)	38(3)	-7(2)	4(2)	-6.5(18)
C00P	9(2)	11.7(19)	19(2)	-0.4(15)	5.6(16)	-2.6(15)	C02D	14(2)	46(3)	36(3)	11(3)	8(2)	6(2)
O00Q	46(3)	38(2)	47(3)	2(2)	12(2)	19(2)	O02E	104(5)	91(5)	73(4)	-26(4)	46(4)	-47(4)
C00R	11(2)	14(2)	20(2)	-0.7(17)	4.0(17)	-4.0(17)	C02F	54(4)	29(3)	53(4)	2(3)	14(3)	-16(3)
C00S	11(2)	10(2)	18(2)	0.4(15)	1.7(16)	1.2(14)	C02G	50(4)	22(3)	32(3)	-2(2)	14(3)	8(3)
C00T	11(2)	13(2)	13(2)	0.2(16)	1.2(16)	-1.8(16)	C02H	43(3)	29(3)	27(3)	11(2)	-6(2)	1(3)
C00U	8(2)	10.3(19)	14(2)	-0.2(15)	2.6(15)	-0.4(15)	C02I	26(3)	67(5)	29(3)	-11(3)	-2(2)	-6(3)
C00V	9(2)	10.9(19)	9.8(18)	0.1(14)	3.4(15)	-2.4(15)	C02J	14(3)	60(4)	41(3)	-12(3)	5(2)	-9(3)
C00W	6.6(19)	12.1(19)	10.3(18)	-1.7(15)	2.0(14)	-3.4(15)	C02K	65(4)	34(3)	50(4)	-3(3)	20(3)	-2(3)
C00X	13(2)	11(2)	17(2)	-0.4(16)	7.9(17)	0.6(16)	C02L	19(3)	21(3)	60(4)	12(3)	-3(2)	5(2)
C00Y	8(2)	10.6(19)	10(2)	0.6(14)	2.0(15)	-1.2(14)	C02M	16(3)	71(5)	40(4)	2(3)	5(2)	11(3)
C00Z	16(2)	7.3(19)	13(2)	-1.1(15)	2.4(16)	-1.3(15)	C02N	28(3)	15(2)	29(3)	-5.6(19)	7(2)	-7.1(19)
C010	12(2)	10(2)	17(2)	-4.9(16)	5.3(17)	-4.3(16)	C02O	55(5)	90(7)	53(4)	2(4)	21(4)	-20(5)
C011	13(2)	13(2)	13(2)	-1.5(15)	2.1(16)	-3.1(16)	C02P	70(5)	81(7)	56(5)	25(4)	33(4)	20(5)
C012	21(3)	13(2)	37(3)	8(2)	3(2)	-0.2(19)	C02Q	118(8)	48(5)	67(5)	8(4)	52(6)	34(5)
C013	11.8(19)	11(2)	12.5(19)	1.5(14)	3.0(15)	-1.8(15)	C02R	67(6)	74(6)	60(5)	6(4)	21(4)	-16(4)
C014	14(2)	13(2)	17(2)	-5.5(17)	7.5(17)	-6.8(17)	C02S	147(11)	99(8)	64(6)	-37(6)	41(7)	-33(8)
C015	10.0(19)	15(2)	9.6(19)	3.2(15)	1.9(15)	1.1(15)	C01F	19(2)	16(2)	13(2)	-0.6(15)	6.8(17)	-2.2(17)
C016	10(2)	12(2)	19(2)	3.1(16)	6.3(17)	3.3(16)	C01G	23(2)	15(2)	19(2)	3.2(16)	13.5(19)	0.8(17)
C017	7.6(19)	12.6(19)	15.2(19)	-4.2(15)	4.6(15)	-1.7(15)	C01H	26(3)	20(2)	29(3)	-9(2)	13(2)	-3(2)
C018	13(2)	24(2)	19(2)	-7.7(17)	-0.5(17)	-0.3(18)	C01I	15(2)	9(2)	20(2)	2.5(16)	3.6(18)	3.9(16)
C019	19(2)	8(2)	21(2)	-1.3(16)	12.0(18)	0.0(15)	C01J	16(2)	10(2)	26(2)	7.0(17)	-3.3(19)	-0.6(16)
C01A	14(2)	19(2)	19(2)	4.1(17)	3.2(17)	3.7(17)	C01K	13(2)	15(2)	20(2)	2.9(16)	0.3(17)	-0.9(16)
C01B	9.5(19)	10.3(19)	11.2(18)	1.3(15)	2.8(14)	-0.7(15)	C01L	10(2)	19(2)	34(3)	6(2)	0.5(18)	1.3(18)
C01C	11(2)	8.2(19)	16(2)	-2.2(15)	3.1(16)	-1.1(15)	C01M	12(2)	11(2)	20(2)	1.1(16)	7.5(17)	1.5(16)
C01D	14(2)	9.0(19)	12.3(19)	-2.2(16)	5.1(15)	1.9(16)	C01N	21(2)	24(2)	15(2)	2.4(17)	9.6(18)	-0.1(19)
C01E	9(2)	10.0(19)	16(2)	1.1(15)	3.0(16)	0.5(15)	C01O	36(3)	24(3)	33(3)	14(2)	19(2)	6(2)

Table 3.37. Bond Lengths for **3.8-PF$_6$**.

Atom	Atom	Length/Å	Atom	Atom	Length/Å
Cu01	P003	2.2262(12)	C00X	C010	1.393(6)
Cu01	P004	2.2229(12)	C00X	C01C	1.456(5)
Cu01	N00M	2.250(3)	C010	C01M	1.389(6)
Cu02	P005	2.2088(13)	C011	C013	1.411(6)
Cu02	P006	2.2149(13)	C011	C021	1.523(6)
Cu02	N00L	2.278(3)	C012	C01K	1.528(7)
P003	C017	1.848(4)	C013	C01B	1.398(6)
P003	C018	1.844(5)	C014	C019	1.412(7)
P003	C01G	1.845(4)	C014	C01S	1.532(6)
P004	C015	1.852(4)	C015	C01B	1.499(6)
P004	C01A	1.845(5)	C016	C01E	1.408(6)
P004	C01F	1.849(5)	C016	C01K	1.533(6)
P005	C01H	1.859(5)	C018	C01T	1.545(7)
P005	C01I	1.852(5)	C018	C02B	1.529(7)
P005	C027	1.833(5)	C019	C01M	1.400(6)
P006	C00Z	1.855(4)	C01A	C01Y	1.533(7)
P006	C01N	1.841(5)	C01A	C02D	1.528(7)
P006	C029	1.834(5)	C01C	C01D	1.404(6)
P007	F009	1.586(3)	C01C	C01Z	1.380(6)
P007	F00C	1.589(3)	C01F	C023	1.523(6)
P007	F00D	1.604(3)	C01F	C026	1.530(7)
P007	F00E	1.580(3)	C01G	C020	1.507(7)
P007	F00F	1.585(3)	C01G	C022	1.534(7)
P007	F00H	1.613(3)	C01H	C01P	1.525(8)
P008	F00A	1.604(3)	C01H	C02G	1.509(7)
P008	F00B	1.630(3)	C01I	C01M	1.510(6)

P008	F00G	1.600(3)	C01J	C01X	1.528(6)
P008	F00I	1.583(3)	C01J	C024	1.518(7)
P008	F00J	1.583(3)	C01J	C02H	1.530(7)
P008	F00K	1.584(3)	C01J	C02L	1.537(7)
N00L	C010	1.432(5)	C01K	C01L	1.541(6)
N00L	C01D	1.411(6)	C01K	C01V	1.543(7)
N00M	C00W	1.431(5)	C01N	C01O	1.516(7)
N00M	C00Y	1.429(5)	C01N	C01Q	1.544(7)
C00N	C00S	1.399(6)	C01R	C01S	1.539(7)
C00N	C00Z	1.507(6)	C01S	C01W	1.529(7)
C00N	C01D	1.393(6)	C01S	C02N	1.535(7)
C00O	C00P	1.394(6)	C01U	C021	1.525(6)
C00O	C00Y	1.394(6)	C01X	C01Z	1.401(6)
C00O	C017	1.516(6)	C021	C028	1.532(6)
C00P	C016	1.400(6)	C021	C02C	1.537(7)
O00Q	C02A	1.424(8)	C025	C027	1.517(8)
O00Q	C02Q	1.434(8)	C027	C02M	1.523(8)
C00R	C00X	1.398(6)	C029	C02I	1.531(8)
C00R	C014	1.390(7)	C029	C02J	1.522(7)
C00S	C01X	1.399(6)	C02A	C02F	1.517(9)
C00T	C00V	1.401(6)	O02E	C02O	1.419(9)
C00T	C011	1.397(6)	O02E	C02S	1.393(11)
C00U	C00V	1.458(5)	C02F	C02K	1.533(9)
C00U	C00Y	1.395(6)	C02K	C02Q	1.457(11)
C00U	C01E	1.391(6)	C02O	C02P	1.517(13)
C00V	C00W	1.406(6)	C02P	C02R	1.541(11)
C00W	C01B	1.387(6)	C02R	C02S	1.417(13)

Table 3.38. Bond Angles for **3.8-PF_6**.

Atom	Atom	Atom	Angle/°	Atom	Atom	Atom	Angle/°	Atom	Atom	Atom	Angle/°	Atom	Atom	Atom	Angle/°
P003	Cu01	N00M	95.54(10)	C00N	C00Z	P006	111.7(3)	F00G	P008	F00B	88.48(18)	C024	C01J	C02L	107.9(5)
P004	Cu01	P003	164.67(5)	C00X	C010	N00L	110.0(4)	F00I	P008	F00A	90.1(2)	C02H	C01J	C02L	109.6(5)
P004	Cu01	N00M	95.41(10)	C01M	C010	N00L	126.9(4)	F00I	P008	F00B	89.51(18)	C012	C01K	C016	112.6(4)
P005	Cu02	P006	170.36(5)	C01M	C010	C00X	122.9(4)	F00I	P008	F00G	178.0(2)	C012	C01K	C01L	107.6(4)
P005	Cu02	N00L	94.79(11)	C00T	C011	C013	118.3(4)	F00I	P008	F00J	91.67(19)	C012	C01K	C01V	108.8(4)
P006	Cu02	N00L	94.47(10)	C00T	C011	C021	119.6(4)	F00I	P008	F00K	89.58(19)	C016	C01K	C01L	109.8(4)
C017	P003	Cu01	108.15(14)	C013	C011	C021	122.1(4)	F00J	P008	F00A	90.4(2)	C016	C01K	C01V	109.5(4)
C018	P003	Cu01	110.94(16)	C01B	C013	C011	123.4(4)	F00J	P008	F00B	178.48(19)	C01L	C01K	C01V	108.4(4)
C018	P003	C017	104.5(2)	C00R	C014	C019	118.7(4)	F00J	P008	F00G	90.33(19)	C010	C01M	C019	115.8(4)
C018	P003	C01G	105.0(2)	C00R	C014	C01S	119.1(4)	F00J	P008	F00K	91.6(2)	C010	C01M	C01I	122.6(4)
C01G	P003	Cu01	122.07(15)	C019	C014	C01S	122.2(4)	F00K	P008	F00A	178.0(2)	C019	C01M	C01I	121.6(4)
C01G	P003	C017	104.8(2)	C01B	C015	P004	111.2(3)	F00K	P008	F00B	89.4(2)	C01O	C01N	P006	114.5(4)
C015	P004	Cu01	106.30(14)	C00P	C016	C01E	118.9(4)	F00K	P008	F00G	90.7(2)	C01O	C01N	C01Q	111.8(4)
C01A	P004	Cu01	120.19(16)	C00P	C016	C01K	122.4(4)	C010	N00L	Cu02	115.7(3)	C01Q	C01N	P006	111.0(3)
C01A	P004	C015	101.9(2)	C01E	C016	C01K	118.6(4)	C01D	N00L	Cu02	115.9(3)	C014	C01S	C01R	109.9(4)
C01A	P004	C01F	105.4(2)	C00O	C017	P003	115.5(3)	C01D	N00L	C010	105.3(3)	C014	C01S	C02N	112.6(4)
C01F	P004	Cu01	115.04(15)	C01T	C018	P003	113.6(3)	C00W	N00M	Cu01	114.0(3)	C01W	C01S	C014	108.7(4)
C01F	P004	C015	106.6(2)	C02B	C018	P003	110.3(3)	C00Y	N00M	Cu01	112.9(3)	C01W	C01S	C01R	109.1(4)
C01H	P005	Cu02	113.99(18)	C02B	C018	C01T	111.3(4)	C00Y	N00M	C00W	105.3(3)	C01W	C01S	C02N	108.2(4)
C01I	P005	Cu02	108.72(14)	C01M	C019	C014	122.9(4)	C00S	C00N	C00Z	121.7(4)	C02N	C01S	C01R	108.2(4)
C01I	P005	C01H	107.0(2)	C01Y	C01A	P004	110.2(3)	C01D	C00N	C00S	116.5(4)	C00S	C01X	C01J	121.0(4)
C027	P005	Cu02	117.75(18)	C02D	C01A	P004	111.0(3)	C01D	C00N	C00Z	121.5(4)	C00S	C01X	C01Z	118.7(4)
C027	P005	C01H	105.1(3)	C02D	C01A	C01Y	110.6(4)	C00P	C00O	C017	122.1(4)	C01Z	C01X	C01J	120.3(4)
C027	P005	C01I	103.3(2)	C00W	C01B	C013	116.2(4)	C00Y	C00O	C00P	116.0(4)	C01C	C01Z	C01X	119.3(4)
C00Z	P006	Cu02	106.74(14)	C00W	C01B	C015	122.0(4)	C00Y	C00O	C017	121.9(4)	C011	C021	C01U	112.9(4)
C01N	P006	Cu02	113.22(16)	C013	C01B	C015	121.5(4)	C00O	C00P	C016	123.6(4)	C011	C021	C028	109.9(4)
C01N	P006	C00Z	106.6(2)	C01D	C01C	C00X	106.0(4)	C02A	O00Q	C02Q	105.9(5)	C011	C021	C02C	108.6(4)
C029	P006	Cu02	120.18(18)	C01Z	C01C	C00X	133.0(4)	C014	C00R	C00X	119.6(4)	C01U	C021	C028	108.2(4)
C029	P006	C00Z	102.5(2)	C01Z	C01C	C01D	121.0(4)	C00N	C00S	C01X	123.1(4)	C01U	C021	C02C	107.9(4)
C029	P006	C01N	106.3(2)	C00N	C01D	N00L	127.3(4)	C011	C00T	C00V	119.9(4)	C028	C021	C02C	109.2(4)
F009	P007	F00C	89.86(19)	C00N	C01D	C01C	121.3(4)	C00Y	C00U	C00V	106.7(4)	C025	C027	P005	110.4(4)
F009	P007	F00D	177.7(2)	C01C	C01D	N00L	111.1(4)	C01E	C00U	C00V	132.2(4)	C025	C027	C02M	110.5(5)

F009	P007	F00H	91.07(19)	C00U	C01E	C016	118.4(4)	C01E	C00U	C00Y	121.0(4)	C02M	C027	P005	110.7(4)
F00C	P007	F00D	89.46(19)	C023	C01F	P004	114.3(3)	C00T	C00V	C00U	133.3(4)	C02I	C029	P006	109.8(4)
F00C	P007	F00H	90.09(19)	C023	C01F	C026	112.0(4)	C00T	C00V	C00W	119.5(4)	C02J	C029	P006	111.3(4)
F00D	P007	F00H	86.7(2)	C026	C01F	P004	111.1(3)	C00W	C00V	C00U	107.1(4)	C02J	C029	C02I	110.7(5)
F00E	P007	F009	91.8(2)	C020	C01G	P003	109.8(3)	C00V	C00W	N00M	110.0(4)	O00Q	C02A	C02F	106.2(5)
F00E	P007	F00C	90.3(2)	C020	C01G	C022	110.7(4)	C01B	C00W	N00M	127.1(4)	C02S	O02E	C02O	107.5(7)
F00E	P007	F00D	90.4(2)	C022	C01G	P003	111.0(3)	C01B	C00W	C00V	122.6(4)	C02A	C02F	C02K	103.5(5)
F00E	P007	F00F	90.6(2)	C01P	C01H	P005	109.8(3)	C00R	C00X	C01C	132.8(5)	C02Q	C02K	C02F	105.4(6)
F00E	P007	F00H	177.1(2)	C02G	C01H	P005	114.3(4)	C010	C00X	C00R	119.7(4)	O02E	C02O	C02P	107.4(7)
F00F	P007	F009	90.7(2)	C02G	C01H	C01P	111.9(5)	C010	C00X	C01C	107.5(4)	C02O	C02P	C02R	104.3(6)
F00F	P007	F00C	178.9(2)	C01M	C01I	P005	114.6(3)	C00O	C00Y	N00M	127.0(4)	O00Q	C02Q	C02K	108.8(6)
F00F	P007	F00D	89.9(2)	C01X	C01J	C02H	109.4(4)	C00O	C00Y	C00U	122.1(4)	C02S	C02R	C02P	102.4(8)
F00F	P007	F00H	88.9(2)	C01X	C01J	C02L	108.3(4)	C00U	C00Y	N00M	110.8(4)	O02E	C02S	C02R	114.7(9)
F00A	P008	F00B	88.62(19)	C024	C01J	C01X	113.1(4)	F00G	P008	F00A	89.59(18)	C024	C01J	C02H	108.5(4)

CuNNN-*i*Pr

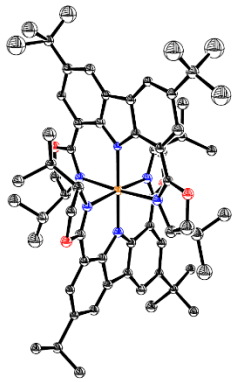

In the attempted preparation of Cu(I) complex of **L3.8**, single crystals of **CuNNN-*i*Pr** were identified. Only unit cell parameters are shown below.

Table 3.39. Crystal data for **CuNNN-*i*Pr**.

Identification code	**CuNNN-*i*Pr**.
Empirical formula	$C_{64}H_{84}N_6O_4Cu$
Formula weight	564.22
Temperature/K	100.05
Crystal system	trigonal
Space group	$P3_1$
a/Å	20.905(8)
b/Å	20.905(8)
c/Å	13.804(8)
α/°	90
β/°	90
γ/°	120

Volume/Å^3	5224(5)
Z	8
ρ_{calc}g/cm^3	1.435
μ/mm^{-1}	1.455
F(000)	2400.0
Crystal size/mm^3	0.16 × 0.04 × 0.02
Radiation	CuKα (λ = 1.54178)
2Θ range for data collection/°	42.054 to 140.09
Index ranges	$1 \leq h \leq 25$, $-18 \leq k \leq 20$, $-10 \leq l \leq 11$
Reflections collected	4574
Independent reflections	4482 [R_{int} = 0.1623, R_{sigma} = 0.2999]

AgPNP-*i*Pr (3.9)

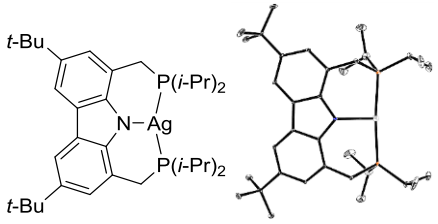

Single crystals of **AgPNP-*i*Pr** were grown from a saturated, equimolar solution of $AgPF_6$ and **LiPNP** in CH_3CN.

Table 3.40. Crystal data and structure refinement for **3.9**.

Identification code	**3.9**
Empirical formula	$C_{34}H_{54}NP_2Ag$
Formula weight	646.59
Temperature/K	99.99
Crystal system	monoclinic
Space group	$P2_1/n$
a/Å	12.5889(5)
b/Å	10.9539(4)
c/Å	24.1553(8)
α/°	90
β/°	99.3740(10)
γ/°	90
Volume/Å^3	3286.5(2)
Z	4
ρ_{calc}g/cm^3	1.307
μ/mm^{-1}	0.733
F(000)	1368.0
Crystal size/mm^3	0.27 × 0.2 × 0.13
Radiation	MoKα (λ = 0.71073)

2Θ range for data collection/°	5.62 to 55.02
Index ranges	$-16 \leq h \leq 16$, $-14 \leq k \leq 14$, $-31 \leq l \leq 31$
Reflections collected	150952
Independent reflections	7548 [R_{int} = 0.0453, R_{sigma} = 0.0123]
Data/restraints/parameters	7548/0/357
Goodness-of-fit on F^2	1.046
Final R indexes [I>=2σ (I)]	R_1 = 0.0356, wR_2 = 0.1195
Final R indexes [all data]	R_1 = 0.0380, wR_2 = 0.1208
Largest diff. peak/hole / e $Å^{-3}$	1.05/-1.42

Table 3.41. Fractional Atomic Coordinates ($\times 10^4$) and Equivalent Isotropic Displacement Parameters ($Å^2 \times 10^3$) for **3.9**. U_{eq} is defined as 1/3 of the trace of the orthogonalized U_{IJ} tensor.

Atom	*x*	*y*	*z*	U(eq)
Ag01	3154.8(2)	4229.7(2)	5908.7(2)	13.09(8)
P002	3972.1(5)	2644.3(6)	5457.7(3)	7.85(14)
P003	2380.8(5)	5976.5(6)	6254.3(3)	6.85(13)
N004	3484.1(16)	3278.1(19)	6765.3(8)	5.1(4)
C005	3670.2(19)	4021(2)	7237.3(10)	4.3(4)
C006	3117.7(19)	5088(2)	7347.3(10)	4.7(4)
C007	4265.5(19)	2380(2)	6861.7(10)	4.5(4)
C008	4892.7(19)	4249(2)	8130.9(10)	4.5(4)
C009	4486.5(19)	1440(2)	6498.5(10)	5.3(4)
C00A	4543.0(18)	3591(2)	7637.5(9)	3.8(4)
C00B	4389.9(19)	5338(2)	8231.6(9)	4.4(4)
C00C	2129.5(19)	5539(2)	6960.1(10)	5.7(4)
C00D	4921.9(18)	2504(2)	7397.4(9)	3.7(4)
C00E	4248(2)	7314(2)	8770.9(11)	11.6(5)
C00F	5748.2(18)	1671(2)	7579.1(10)	4.5(4)
C00G	5415(2)	2789(3)	5390.7(12)	14.4(5)
C00H	3494(2)	5722(2)	7839.4(10)	5.2(4)
C00I	5967.9(19)	732(2)	7227.9(10)	4.7(4)
C00J	5329(2)	646(2)	6691.6(10)	5.8(4)
C00K	3312(2)	2162(3)	4751.4(10)	12.3(5)
C00L	3870(2)	1302(2)	5910.9(10)	7.5(5)
C00M	4778(2)	6058(2)	8770.5(10)	5.9(4)
C00N	1082(2)	6644(2)	5926.1(10)	9.5(5)
C00O	6866.7(19)	-191(2)	7427.8(10)	6.6(4)
C00P	4505(2)	5317(2)	9268.5(10)	11.1(5)
C00Q	6058(3)	3400(3)	5910.2(14)	23.8(7)
C00R	7910(2)	465(3)	7696.5(12)	13.3(5)
C00S	3239(3)	3256(3)	4352.9(12)	21.8(6)
C00T	3038(2)	8271(3)	6750.3(14)	17.7(6)
C00U	1162(3)	7115(3)	5338.6(12)	21.2(6)
C00V	7148(2)	-972(3)	6947.5(12)	12.5(5)
C00W	3325(2)	7284(3)	6353.4(12)	14.4(5)
C00X	6498(2)	-1045(3)	7863.5(13)	16.6(6)
C00Y	6000(2)	6259(3)	8848.4(11)	12.1(5)
C00Z	5941(2)	1586(3)	5255.7(15)	22.6(6)
C010	2190(3)	1660(3)	4771.7(12)	22.0(6)
C011	179(3)	5707(3)	5900.1(16)	26.6(8)
C012	4480(2)	6838(3)	6534.0(17)	26.4(7)

Table 3.42. Anisotropic Displacement Parameters ($Å^2 \times 10^3$) for **3.9**. The anisotropic displacement factor exponent takes the form: $-2\pi^2[h^2a^{*2}U_{11}+2hka^*b^*U_{12}+\ldots]$.

Atom	U_{11}	U_{22}	U_{33}	U_{23}	U_{13}	U_{12}
Ag01	16.79(13)	11.49(12)	10.86(12)	-1.28(7)	1.88(8)	2.84(7)
P002	9.7(3)	8.8(3)	5.1(3)	-1.4(2)	1.4(2)	3.3(2)
P003	6.9(3)	8.4(3)	5.1(3)	2.2(2)	0.6(2)	4.0(2)
N004	5.4(9)	4.2(9)	5.3(9)	-2.5(7)	-0.3(7)	2.3(7)
C005	4.6(10)	5.2(10)	2.8(10)	-1.0(8)	-0.2(8)	0.2(8)
C006	4.7(10)	6.6(11)	2.8(10)	0.5(8)	0.2(8)	2.4(8)
C007	4.6(10)	3.1(10)	5.6(10)	-0.7(8)	0.1(8)	0.7(8)
C008	4(1)	5.4(11)	3.5(10)	0.1(8)	-1.0(8)	0.9(8)
C009	6.5(11)	4.2(10)	4.8(10)	-1.7(8)	-0.2(8)	0.2(8)
C00A	3.6(10)	4.2(10)	3.6(10)	0.3(8)	0.4(8)	1.3(8)
C00B	6.2(10)	4.7(10)	2.0(9)	-0.4(8)	0.0(8)	0.3(8)
C00C	4.5(10)	7.3(11)	4.7(10)	0.0(8)	-0.7(8)	3.3(8)
C00D	4.4(10)	2.7(10)	3.6(10)	-0.1(8)	-0.1(8)	-0.1(8)
C00E	16.3(13)	6.7(11)	10.1(11)	-3.6(9)	-3.1(9)	4.3(10)
C00F	3.4(10)	3.3(10)	6.4(10)	0.9(8)	-0.6(8)	0.7(8)
C00G	12.3(12)	13.8(13)	17.2(13)	-0.4(10)	3.1(10)	-3.5(10)
C00H	7.0(11)	4.8(11)	3.5(10)	-0.1(8)	0.4(8)	2.8(8)
C00I	4.4(10)	1.8(10)	7.7(11)	1.6(8)	0.4(8)	0.5(8)
C00J	7.5(11)	2.7(10)	7.0(11)	-1.8(8)	1.0(9)	0.6(8)
C00K	15.1(13)	16.4(13)	5.5(11)	-0.9(9)	1.9(9)	2.4(10)
C00L	7.9(11)	7.8(11)	6.1(10)	-3.8(9)	-1.1(8)	1.2(9)
C00M	8.2(11)	5.1(10)	3.6(10)	-1.5(8)	-0.9(8)	1.4(9)
C00N	11.6(12)	8.1(11)	7.6(11)	1.5(9)	-2.4(9)	4.2(9)
C00O	5.2(10)	3.5(10)	10.7(11)	0.8(9)	0.1(8)	2.6(8)
C00P	18.7(13)	10.3(12)	4.7(10)	-0.1(9)	2.7(9)	-0.2(10)
C00Q	20.6(15)	21.1(16)	27.1(16)	-1.8(13)	-3.3(12)	-10.6(12)
C00R	6.4(11)	11.1(12)	20.2(13)	-3.5(10)	-4.5(10)	3(1)
C00S	29.0(16)	26.2(16)	9.7(12)	5.7(12)	1.9(11)	0.4(13)
C00T	13.8(13)	9.4(13)	29.4(15)	-2.7(11)	2.4(11)	-3.5(10)
C00U	28.4(16)	23.5(16)	10.3(12)	7.9(11)	-1.0(11)	11.8(13)
C00V	9.7(12)	9.8(12)	17.5(13)	-3.9(10)	1.1(10)	5.2(10)
C00W	11.4(12)	12.2(13)	20.6(13)	2.9(11)	6(1)	-1(1)
C00X	17.1(14)	12.9(13)	21.0(14)	11.6(11)	6.8(11)	6.0(11)
C00Y	9.3(12)	13.7(13)	12.3(12)	-6(1)	-0.7(9)	-1.5(10)
C00Z	12.6(13)	26.0(16)	31.3(17)	-6.2(13)	9.7(12)	3.0(12)
C010	18.8(14)	33.8(18)	10.9(12)	1.9(12)	-5.1(11)	-8.1(13)
C011	12.7(14)	23.1(17)	37.7(19)	13.0(14)	-14.4(13)	-2.8(12)
C012	8.0(13)	24.1(16)	48(2)	-0.6(15)	8.8(13)	-3.2(12)

Table 3.43. Bond Lengths for **3.9**.

Atom	Atom	Length/Å	Atom	Atom	Length/Å
Ag01	P002	2.3720(7)	C00A	C00D	1.439(3)
Ag01	P003	2.3607(7)	C00B	C00H	1.414(3)
Ag01	N004	2.294(2)	C00B	C00M	1.532(3)
P002	C00G	1.856(3)	C00D	C00F	1.400(3)
P002	C00K	1.849(3)	C00E	C00M	1.529(3)
P002	C00L	1.851(3)	C00F	C00I	1.390(3)
P003	C00C	1.847(2)	C00G	C00Q	1.532(4)
P003	C00N	1.848(3)	C00G	C00Z	1.534(4)
P003	C00W	1.852(3)	C00I	C00J	1.412(3)
N004	C005	1.389(3)	C00I	C00O	1.535(3)
N004	C007	1.384(3)	C00K	C00S	1.530(4)

C005	C006	1.408(3)	C00K	C010	1.524(4)
C005	C00A	1.420(3)	C00M	C00P	1.536(3)
C006	C00C	1.512(3)	C00M	C00Y	1.535(3)
C006	C00H	1.391(3)	C00N	C00U	1.528(4)
C007	C009	1.409(3)	C00N	C011	1.526(4)
C007	C00D	1.424(3)	C00O	C00R	1.545(3)
C008	C00A	1.401(3)	C00O	C00V	1.529(4)
C008	C00B	1.390(3)	C00O	C00X	1.535(4)
C009	C00J	1.393(3)	C00T	C00W	1.527(4)
C009	C00L	1.511(3)	C00W	C012	1.528(4)

Table 3.44. Bond Angles for **3.9**.

Atom	Atom	Atom	Angle/°	Atom	Atom	Atom	Angle/°
P003	Ag01	P002	172.21(2)	C00H	C00B	C00M	121.7(2)
N004	Ag01	P002	93.06(5)	C006	C00C	P003	114.09(16)
N004	Ag01	P003	94.23(5)	C007	C00D	C00A	105.3(2)
C00G	P002	Ag01	118.76(10)	C00F	C00D	C007	121.0(2)
C00K	P002	Ag01	118.01(9)	C00F	C00D	C00A	133.7(2)
C00K	P002	C00G	104.06(13)	C00I	C00F	C00D	120.2(2)
C00K	P002	C00L	104.76(12)	C00Q	C00G	P002	111.1(2)
C00L	P002	Ag01	103.48(8)	C00Q	C00G	C00Z	111.1(3)
C00L	P002	C00G	106.44(12)	C00Z	C00G	P002	114.1(2)
C00C	P003	Ag01	104.99(8)	C006	C00H	C00B	123.1(2)
C00C	P003	C00N	103.07(11)	C00F	C00I	C00J	118.0(2)
C00C	P003	C00W	106.51(12)	C00F	C00I	C00O	120.3(2)
C00N	P003	Ag01	123.82(9)	C00J	C00I	C00O	121.7(2)
C00N	P003	C00W	104.72(13)	C009	C00J	C00I	123.7(2)
C00W	P003	Ag01	112.28(9)	C00S	C00K	P002	109.2(2)
C005	N004	Ag01	117.12(16)	C010	C00K	P002	110.66(18)
C007	N004	Ag01	119.59(15)	C010	C00K	C00S	110.0(2)
C007	N004	C005	104.95(19)	C009	C00L	P002	113.65(17)
N004	C005	C006	128.2(2)	C00B	C00M	C00P	108.2(2)
N004	C005	C00A	111.9(2)	C00B	C00M	C00Y	110.6(2)
C006	C005	C00A	119.8(2)	C00E	C00M	C00B	112.6(2)
C005	C006	C00C	122.4(2)	C00E	C00M	C00P	108.8(2)
C00H	C006	C005	117.8(2)	C00E	C00M	C00Y	107.4(2)
C00H	C006	C00C	119.8(2)	C00Y	C00M	C00P	109.1(2)
N004	C007	C009	128.4(2)	C00U	C00N	P003	110.14(19)
N004	C007	C00D	112.1(2)	C011	C00N	P003	110.66(19)
C009	C007	C00D	119.4(2)	C011	C00N	C00U	110.5(3)
C00B	C008	C00A	120.1(2)	C00I	C00O	C00R	111.0(2)
C007	C009	C00L	122.3(2)	C00V	C00O	C00I	112.3(2)
C00J	C009	C007	117.7(2)	C00V	C00O	C00R	107.0(2)
C00J	C009	C00L	119.9(2)	C00V	C00O	C00X	108.2(2)
C005	C00A	C00D	105.7(2)	C00X	C00O	C00I	109.1(2)
C008	C00A	C005	120.7(2)	C00X	C00O	C00R	109.1(2)
C008	C00A	C00D	133.6(2)	C00T	C00W	P003	114.57(19)
C008	C00B	C00H	118.3(2)	C00T	C00W	C012	111.0(3)
C008	C00B	C00M	119.9(2)	C012	C00W	P003	110.6(2)

AuPNP-*i*Pr (3.10)

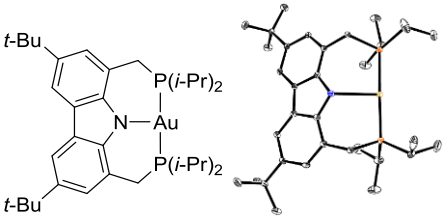

Single crystals of **AuPNP-*i*Pr** were grown from a saturated, equimolar solution of $Au(PPh_3)Cl$ and **LiPNP** in CH_3CN.

Table 3.45. Crystal data and structure refinement for **3.10**.

Identification code	**3.10**
Empirical formula	$C_{34}H_{54}NP_2Au$
Formula weight	735.69
Temperature/K	100.0
Crystal system	monoclinic
Space group	$P2_1/n$
a/Å	12.5670(8)
b/Å	10.9367(7)
c/Å	24.1092(15)
α/°	90
β/°	99.420(2)
γ/°	90
Volume/Å^3	3268.9(4)
Z	4
ρ_{calc}g/cm^3	1.495
μ/mm^{-1}	4.621
F(000)	1496.0
Crystal size/mm^3	0.23 × 0.17 × 0.09
Radiation	MoKα (λ = 0.71073)
2Θ range for data collection/°	5.426 to 55.018
Index ranges	$-16 \leq h \leq 16$, $-14 \leq k \leq 14$, $-31 \leq l \leq 31$
Reflections collected	180370
Independent reflections	7503 [R_{int} = 0.0315, R_{sigma} = 0.0081]
Data/restraints/parameters	7503/0/357
Goodness-of-fit on F^2	1.084
Final R indexes [I>=2σ (I)]	R_1 = 0.0133, wR_2 = 0.0316
Final R indexes [all data]	R_1 = 0.0139, wR_2 = 0.0318
Largest diff. peak/hole / e Å^{-3}	1.07/-0.99

Table 3.46. Fractional Atomic Coordinates ($\times 10^4$) and Equivalent Isotropic Displacement Parameters ($Å^2 \times 10^3$) for **3.10**. U_{eq} is defined as 1/3 of the trace of the orthogonalized U_{IJ} tensor.

Atom	*x*	*y*	*z*	U(eq)
Au01	6830.7(2)	5735.5(2)	4119.7(2)	11.40(2)
P002	7565.7(3)	4074.8(3)	3735.1(2)	9.89(7)
P003	6062.1(3)	7338.5(4)	4527.0(2)	11.75(7)
N004	6557.4(10)	6803.4(12)	3221.4(5)	10.8(2)
C005	5766.9(11)	7689.0(14)	3130.5(6)	10.3(3)
C006	6354.6(11)	6062.3(13)	2751.2(6)	9.7(3)
C007	5545.6(12)	8612.2(14)	3503.3(6)	11.1(3)
C008	6897.0(11)	4984.1(13)	2642.9(6)	9.7(3)
C009	5468.1(11)	6482.6(13)	2351.8(6)	9.5(3)
C00A	5092.6(11)	7569.6(13)	2596.2(6)	9.8(3)
C00B	7867.4(11)	4531.3(14)	3042.6(6)	10.8(3)
C00C	6173.8(12)	8708.7(14)	4092.2(6)	12.4(3)
C00D	3975.7(14)	6600.5(18)	4045.0(8)	25.0(4)
C00E	5214.2(12)	3988.3(14)	1226.7(6)	12.1(3)
C00F	6513.4(12)	4338.4(13)	2153.7(6)	10.8(3)
C00G	6958.6(14)	1770.5(15)	3250.6(8)	20.6(3)
C00H	6620.7(13)	2776.4(15)	3625.1(7)	16.2(3)
C00I	5613.2(12)	4719.5(14)	1763.4(6)	10.2(3)
C00J	5472.7(13)	3220.7(17)	3412.0(9)	25.3(4)
C00K	6732.6(17)	6660.0(19)	5636.4(8)	28.4(4)
C00L	4622.7(13)	7146.5(16)	4581.7(7)	19.5(3)
C00M	8850.8(13)	3436.8(15)	4096.9(7)	15.1(3)
C00N	6725.2(14)	7758.6(16)	5240.0(6)	17.5(3)
C00O	5719.2(14)	2714.0(15)	1236.7(7)	18.0(3)
C00P	5109.4(11)	5814.2(13)	1862.7(6)	10.4(3)
C00Q	5504.0(14)	4704.8(16)	724.7(7)	18.6(3)
C00R	4691.0(12)	9406.2(13)	3318.9(7)	12.0(3)
C00S	8726.2(16)	2918.0(18)	4670.4(7)	25.2(4)
C00T	9734.1(15)	4412.2(18)	4160.7(9)	29.5(4)
C00U	3136.4(12)	10252.2(14)	2589.2(7)	12.6(3)
C00V	4260.2(11)	8400.4(13)	2425.2(6)	10.2(3)
C00W	3983.9(13)	3818.2(16)	1143.6(7)	18.9(3)
C00X	2097.0(13)	9594.9(15)	2315.9(7)	18.3(3)
C00Y	4040.7(12)	9332.1(13)	2786.1(6)	11.4(3)
C00Z	3500.2(14)	11124.6(16)	2156.7(8)	20.8(3)
C010	2850.6(13)	11014.2(15)	3078.0(7)	17.3(3)
C011	4094.1(15)	8322.0(19)	4752.1(9)	30.6(4)
C012	7875.5(15)	8188(2)	5231.5(7)	27.2(4)

Table 3.47. Anisotropic Displacement Parameters ($Å^2 \times 10^3$) for **3.10**. The anisotropic displacement factor exponent takes the form: $-2\pi^2[h^2a^{*2}U_{11}+2hka^*b^*U_{12}+\ldots]$.

Atom	U_{11}	U_{22}	U_{33}	U_{23}	U_{13}	U_{12}
Au01	14.20(3)	9.89(3)	10.13(3)	-1.72(2)	2.00(2)	1.53(2)
P002	11.39(16)	8.77(16)	9.16(16)	0.10(13)	0.64(13)	1.56(13)
P003	13.68(17)	11.36(17)	10.17(17)	-2.52(14)	1.82(13)	1.06(14)
N004	10.5(5)	9.8(6)	11.8(6)	-1.9(5)	1.0(5)	1.2(5)
C005	10.0(6)	9.1(6)	11.8(7)	-0.3(5)	1.8(5)	-0.9(5)

C006	9.7(6)	10.3(7)	9.1(6)	0.1(5)	1.6(5)	-0.4(5)
C007	11.6(6)	9.7(7)	11.7(7)	-1.2(5)	0.8(5)	-1.3(5)
C008	9.1(6)	11.5(7)	8.5(6)	1.1(5)	1.5(5)	1.2(5)
C009	9.8(6)	9.3(6)	9.6(6)	1.3(5)	2.1(5)	0.8(5)
C00A	10.2(6)	8.8(6)	10.6(6)	-0.3(5)	2.1(5)	-1.4(5)
C00B	9.7(6)	12.0(7)	10.3(7)	0.5(5)	0.8(5)	2.5(5)
C00C	14.8(7)	10.7(7)	11.3(7)	-3.0(5)	0.8(5)	0.3(5)
C00D	18.6(8)	23.6(9)	31.5(10)	-1.7(8)	0.7(7)	-5.6(7)
C00E	14.9(7)	11.8(7)	8.8(7)	-1.9(5)	-0.4(5)	2.1(5)
C00F	12.6(6)	10.0(7)	10.0(7)	-0.2(5)	2.9(5)	2.3(5)
C00G	20.5(8)	12.4(7)	29.9(9)	-6.3(7)	7.5(7)	-2.6(6)
C00H	17.5(7)	13.1(7)	18.9(8)	-1.7(6)	6.0(6)	-2.1(6)
C00I	12.5(6)	10.5(7)	7.7(6)	-0.7(5)	1.5(5)	0.2(5)
C00J	13.8(7)	23.6(9)	39.1(11)	-6.7(8)	6.8(7)	-4.0(7)
C00K	40.5(11)	30.7(10)	13.9(8)	3.5(7)	4.1(7)	-1.9(8)
C00L	15.6(7)	19.8(8)	24.1(8)	-1.6(7)	6.7(6)	-1.3(6)
C00M	16.7(7)	13.9(7)	13.3(7)	2.2(6)	-2.2(6)	4.9(6)
C00N	23.5(8)	18.4(8)	10.4(7)	-4.0(6)	2.1(6)	2.5(6)
C00O	23.9(8)	12.9(7)	15.6(7)	-4.4(6)	-1.6(6)	3.6(6)
C00P	9.7(6)	11.2(7)	9.7(6)	1.1(5)	0.0(5)	1.0(5)
C00Q	26.5(8)	18.3(8)	11.1(7)	0.0(6)	3.6(6)	0.7(7)
C00R	13.0(7)	8.2(7)	15.0(7)	-3.0(5)	3.0(6)	-0.2(5)
C00S	31.0(9)	26.4(9)	17.0(8)	8.1(7)	0.2(7)	8.1(7)
C00T	18.9(8)	27.8(10)	36.3(11)	10.8(8)	-11.8(8)	-2.9(7)
C00U	11.6(6)	8.8(7)	17.1(7)	0.4(6)	1.5(6)	1.8(5)
C00V	9.7(6)	8.8(7)	11.7(6)	0.2(5)	0.2(5)	-1.1(5)
C00W	16.2(7)	19.7(8)	19.4(8)	-6.4(7)	-0.7(6)	-0.8(6)
C00X	13.1(7)	15.5(7)	24.6(8)	-2.8(6)	-2.2(6)	2.2(6)
C00Y	10.0(6)	8.7(7)	15.5(7)	1.5(5)	2.5(5)	0.0(5)
C00Z	21.9(8)	15.5(8)	25.5(9)	8.1(7)	5.1(7)	4.8(6)
C010	13.8(7)	14.4(7)	23.7(8)	-3.7(6)	2.9(6)	3.6(6)
C011	21.1(9)	32(1)	41.4(11)	-8.6(9)	13.4(8)	2.9(8)
C012	27.3(9)	36.4(11)	15.0(8)	0.5(7)	-5.6(7)	-9.5(8)

Table 3.48. Bond Lengths for **3.10**.

Atom	Atom	Length/Å	Atom	Atom	Length/Å
Au01	P002	2.3006(4)	C00A	C00V	1.396(2)
Au01	P003	2.2980(4)	C00D	C00L	1.532(2)
Au01	N004	2.4349(13)	C00E	C00I	1.534(2)
P002	C00B	1.8406(15)	C00E	C00O	1.530(2)
P002	C00H	1.8423(16)	C00E	C00Q	1.535(2)
P002	C00M	1.8425(16)	C00E	C00W	1.538(2)
P003	C00C	1.8472(16)	C00F	C00I	1.411(2)
P003	C00L	1.8472(17)	C00G	C00H	1.527(2)
P003	C00N	1.8416(16)	C00H	C00J	1.529(2)
N004	C005	1.3791(19)	C00I	C00P	1.393(2)
N004	C006	1.3828(19)	C00K	C00N	1.534(2)
C005	C007	1.409(2)	C00L	C011	1.534(2)
C005	C00A	1.427(2)	C00M	C00S	1.526(2)
C006	C008	1.408(2)	C00M	C00T	1.529(2)
C006	C009	1.424(2)	C00N	C012	1.523(2)
C007	C00C	1.511(2)	C00R	C00Y	1.407(2)
C007	C00R	1.396(2)	C00U	C00X	1.541(2)
C008	C00B	1.5087(19)	C00U	C00Y	1.534(2)
C008	C00F	1.391(2)	C00U	C00Z	1.537(2)
C009	C00A	1.440(2)	C00U	C010	1.533(2)
C009	C00P	1.398(2)	C00V	C00Y	1.396(2)

Table 3.49. Bond Angles for **3.10**.

Atom	Atom	Atom	Angle/°	Atom	Atom	Atom	Angle/°
P002	Au01	N004	91.58(3)	C008	C00B	P002	113.79(10)
P003	Au01	P002	177.570(14)	C007	C00C	P003	113.58(10)
P003	Au01	N004	90.35(3)	C00I	C00E	C00Q	108.18(13)
C00B	P002	Au01	107.90(5)	C00I	C00E	C00W	110.85(12)
C00B	P002	C00H	107.59(7)	C00O	C00E	C00I	112.59(12)
C00B	P002	C00M	103.73(7)	C00O	C00E	C00Q	109.04(13)
C00H	P002	Au01	112.00(5)	C00O	C00E	C00W	107.31(13)
C00H	P002	C00M	105.70(7)	C00Q	C00E	C00W	108.81(13)
C00M	P002	Au01	119.13(5)	C008	C00F	C00I	122.97(13)
C00C	P003	Au01	107.47(5)	C00G	C00H	P002	113.91(11)
C00L	P003	Au01	115.39(6)	C00G	C00H	C00J	111.63(14)
C00L	P003	C00C	107.40(8)	C00J	C00H	P002	110.72(12)
C00N	P003	Au01	115.57(6)	C00F	C00I	C00E	121.63(13)
C00N	P003	C00C	105.21(7)	C00P	C00I	C00E	119.86(13)
C00N	P003	C00L	105.10(8)	C00P	C00I	C00F	118.46(13)
C005	N004	Au01	118.12(9)	C00D	C00L	P003	111.99(12)
C005	N004	C006	104.48(12)	C00D	C00L	C011	111.08(15)
C006	N004	Au01	115.36(9)	C011	C00L	P003	113.33(12)
N004	C005	C007	127.88(13)	C00S	C00M	P002	110.96(12)
N004	C005	C00A	112.64(13)	C00S	C00M	C00T	110.40(15)
C007	C005	C00A	119.41(13)	C00T	C00M	P002	110.43(11)
N004	C006	C008	127.82(13)	C00K	C00N	P003	109.98(12)
N004	C006	C009	112.58(13)	C012	C00N	P003	110.48(11)
C008	C006	C009	119.59(13)	C012	C00N	C00K	109.92(15)
C005	C007	C00C	121.46(13)	C00I	C00P	C009	120.09(13)
C00R	C007	C005	117.67(13)	C007	C00R	C00Y	123.81(14)
C00R	C007	C00C	120.81(13)	C00Y	C00U	C00X	111.07(12)
C006	C008	C00B	121.45(13)	C00Y	C00U	C00Z	109.24(12)
C00F	C008	C006	118.12(13)	C00Z	C00U	C00X	108.95(13)
C00F	C008	C00B	120.44(13)	C010	C00U	C00X	107.06(13)
C006	C009	C00A	105.20(12)	C010	C00U	C00Y	111.94(13)
C00P	C009	C006	120.68(13)	C010	C00U	C00Z	108.49(13)
C00P	C009	C00A	134.01(13)	C00A	C00V	C00Y	120.39(14)
C005	C00A	C009	105.00(12)	C00R	C00Y	C00U	122.33(13)
C00V	C00A	C005	120.83(13)	C00V	C00Y	C00R	117.79(13)
C00V	C00A	C009	134.13(14)	C00V	C00Y	C00U	119.85(13)

3.5. Notes and References

[1] There are conflicting values of the standard reduction potentials of alkyl halides in the literature. For examples, see (a) Isse, A. A.; Lin, C. Y.; Coote, M. L.; Gennaro, A. *J. Phys. Chem. B.* **2011**, *115*, 678–684. (b) Cleary, J. A.; Mubarak, M. S.; Vieira, K. L.; Anderson, M. R.; Peters, D. G. *J. Electroanal. Chem.* **1986**, *198*, 107–124. (c) Saveant, J.-M. *J. Am. Chem. Soc.* **1987**, *109*, 6788–6795.

[2] Alfassi, Z. B. *In General Aspects of the Chemistry of Radicals*; Alfassi, Z. B., Ed.; Wiley: Chichester, U.K., **1999**; pp 139−173.

[3] (a) Do, H.-Q.; Bachman, S.; Bissember, A. C.; Peters, J. C.; Fu, G. C. *J. Am. Chem. Soc.* **2014**, *136*, 2162–2167. (b) Ratani, T. S.; Bachman, S.; Fu, G. C.; Peters, J. C. *J. Am. Chem. Soc.* **2015**, *137*, 13902–13907.

[4] Pinedo, J. L. V., Mireles, F. G., Ríos, C. M., Quirino, L. L. T., and Dávila, J. I. R. *Geofís. Int.* **2006**, *45*, 263–269.

[5] See the following studies for the competition experiments. (a) Ziegler, D. T.; Choi, J.; Muñoz-Molina, J. M.; Bissember, A. C.; Peters, J. C.; Fu, G. C. *J. Am. Chem. Soc.* **2013**, *135*, 13107–13112. (b) Choi, J. *Fu copper subgroup meeting*, **2013**.

[6] Creutz, S. E.; Lotito, K. J.; Fu, G. C.; Peters, J. C. *Science* **2012**, *338*, 647–651.

[7] Kainz, Q. M.; Matier, C. M.; Bartoszewicz, A.; Zultanski, S. L.; Peters, J. C.; Fu, G. C. *Science* **2016**, *351*, 681−684.

[8] For an example of the deleterious impact of a substitution in the 1 position on the reactivity of the carbazole nitrogen in a photoinduced, copper-catalyzed N–alkylation, see Bissember, A. C.; Lundgren, R. J.; Creutz, S. E.; Peters, J. C.; Fu, G. C. *Angew. Chem., Int. Ed.* **2013**, *52*, 5129−5133.

[9] For an example of reactivity in the absence of a substituent, see Mankad, N. P.; Antholine, W. E.; Szilagyi, R. K.; Peters, J. C. *J. Am. Chem. Soc.* **2009**, *131*, 3878−3880.

[10] Emission spectra of **LiPNP** (lithium salt of **L3.1**) and **L3.1** have been collected and differ from the presented spectrum of **3.1**.

[11] Yin, H.; Jin, Y.; Hertzog, J. E.; Mullane, K. C.; Carroll, P. J.; Manor, B. C.; Anna, J. M.; Schelter, E. J. *J. Am. Chem. Soc.* **2016**, *138*, 16266−16273.

[12] Sattler, W.; Henling, L. M.; Winkler, J. R. Gray, H. B. *J. Am. Chem. Soc.* **2015**, *137*, 1198−1205.

[13] See ref 9.

[14] The coordination of the external nucleophile to species **3.7** to generate a new copper(II)–nucleophile complex is another pathway for the productive bond-formation.

[15] Plundrich, G. T.; Wadepohl, H.; Gade, L. H. *Inorg. Chem.* **2016**, *55*, 353–365.

[16] Grueger, N.; Rodriguez, L.-I.; Wadepohl, H.; Gade, L. H. *Inorg. Chem.* **2013**, *52*, 2050–2059.

[17] Duran-Galvan, M.; Worlikar, S. A.; Connell, B. T. *Tetrahedron* **2010**, *66*, 7707–7719.

[18] Stoll, S.; Schweiger, A. *J. Magn. Reson.* **2006**, *178*, 42–55.

[19] Higuchi, J.; Kuriyama, S.; Eizawa, A.; Arashiba, K.; Nakajima, K.; Nishibayashi, Y. *Dalton Trans.* **2018**, *47*, 1117–1121.

[20] Coleman, D.; Edwards, P.; Kariuki, B. M.; Newman, P. D. *Dalton Trans.* **2010**, *39*, 3842–3850.

[21] Johnson, M. W.; Hannoun, K. I.; Tan, Y.; Fu, G. C.; Peters, J. C. *Chem. Sci.* **2016**, *7*, 4091–4100.

[22] Arnett, E. M.; Moe, K. D. *J. Am. Chem. Soc.* **1991**, *113*, 7288–7293.

[23] Gaussian 09, Revision B.01, M. J. Frisch, G. W. Trucks, H. B. Schlegel, G. E. Scuseria, M. A. Robb, J. R. Cheeseman, G. Scalmani, V. Barone, B. Mennucci, G. A. Petersson, H. Nakatsuji, M. Caricato, X. Li, H. P. Hratchian, A. F. Izmaylov, J. Bloino, G. Zheng, J. L. Sonnenberg, M. Hada, M. Ehara, K. Toyota, R. Fukuda, J. Hasegawa, M. Ishida, T. Nakajima, Y. Honda, O. Kitao, H. Nakai, T. Vreven, J. A. Montgomery, Jr., J. E. Peralta, F. Ogliaro, M. Bearpark, J. J. Heyd, E. Brothers, K. N. Kudin, V. N. Staroverov, T. Keith, R. Kobayashi, J. Normand, K. Raghavachari, A. Rendell, J. C. Burant, S. S. Iyengar, J. Tomasi, M. Cossi, N. Rega, J. M. Millam, M. Klene, J. E. Knox, J. B. Cross, V. Bakken, C. Adamo, J. Jaramillo, R. Gomperts, R. E. Stratmann, O. Yazyev, A. J. Austin, R. Cammi, C. Pomelli, J. W. Ochterski, R. L. Martin, K. Morokuma, V. G. Zakrzewski, G. A. Voth, P. Salvador, J. J. Dannenberg, S. Dapprich, A. D. Daniels, O. Farkas, J. B. Foresman, J. V. Ortiz, J. Cioslowski, and D. J. Fox, Gaussian, Inc., Wallingford CT, **2010**.

Chapter 4. Synthesis of carbamate-protected primary amines via photoinduced, copper-catalyzed N–alkylation reactions of unactivated secondary alkyl bromides

Reproduced in part with permission from:

Ahn, J. M.; Peters, J. C.; Fu, G. C. *J. Am. Chem. Soc.* **2017**, *139*, 18101–18106.

4.1 Introduction

Because primary amines play important roles in many areas of science, including biology, medicinal chemistry, and materials science, the selective synthesis of primary amines is an important challenge in organic chemistry.[1] Perhaps the most obvious route, the nucleophilic substitution of an alkyl electrophile by ammonia (a commodity chemical) can be problematic due to issues such as over-alkylation with powerful electrophiles and insufficient reactivity with weak electrophiles (**Scheme 4.1**, top).[2] Consequently, a number of useful alternative approaches have been developed, including the Gabriel synthesis, which provides direct access to protected primary amines via an S_N2 reaction between phthalimide anion and a suitable alkyl electrophile (**Scheme 4.1**, middle).[3]

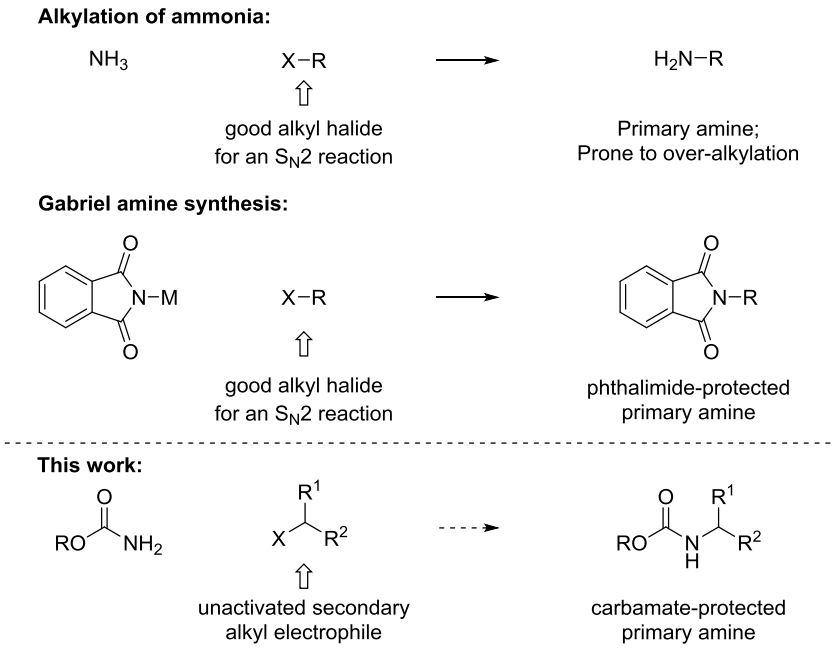

Scheme 4.1. Primary amine synthesis by substitution reactions with alkyl halides. The selective mono-alkylation may be achieved by ammonia surrogates to give protected primary amines.

Carbamates are among the most widely used protecting groups for amines,[4] as well as being important target molecules in their own right (e.g., Ritonavir™ and carbamate insecticides).[5] However, to the best of our knowledge, there are no reports of the N–alkylation of primary carbamates by unactivated secondary alkyl electrophiles (**Scheme 4.1**, bottom).[6] In view of our previous success in achieving the alkylation of primary carboxamides via photoinduced copper catalysis, we envisioned that it might be possible to similarly catalyze the selective mono-alkylation of a primary carbamate.[7,8,9] Unfortunately, the conditions that we developed for the alkylation of carboxamides provide only a modest yield when $BocNH_2$ is used as the nucleophile (**Scheme 4.2**). We therefore sought to develop a method that addresses three key shortcomings: the inefficiency of the alkylation, the need for high-energy ultraviolet irradiation, and the use of an excess of the electrophile (the more valuable coupling partner). Herein, we expand on the catalytic reactivity of a new photocatalyst introduced in **Chapter 3** (complex **3.1**) and disclose the development of a copper-catalyzed method for the selective mono-alkylation of primary carbamates by unactivated secondary alkyl halides induced by irradiation with blue LED lamps.

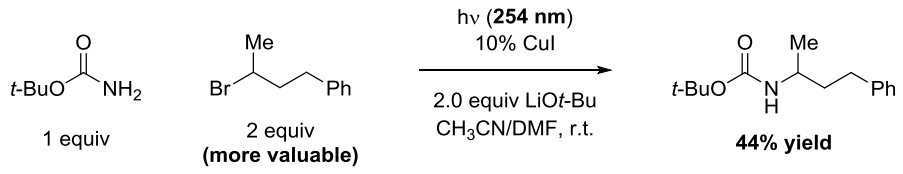

Scheme 4.2. Attempted alkylation of *t*-butyl carbamate under amide alkylation conditions. Deficiencies of the existing conditions are boldfaced.

4.2 Results and Discussions

4.2.1. Optimization

In view of the ubiquity of N-Boc-protected amines in organic synthesis, we focused our initial study on *t*-butyl carbamate as the nucleophile.[10] In **Chapter 3**, complex **3.1** (hereinafter referred to as **4.1**) was shown to serve as a catalyst for the coupling of *t*-butyl carbamate with an unactivated secondary bromide using blue LED lamps as the light source, although the yield is modest (33%, **Scheme 4.3**). On the other hand, in the presence of excess CuBr, the desired alkylation proceeds in excellent yield (96%) with no detectable over-alkylation. In contrast to CuBr, the addition of 10 mol% $CoBr_2$, $NiCl_2$•DME, $Pd(cod)_2Cl_2$, or $Au(PPh_3)Cl$ did not improve the yield of the N–alkylation product.

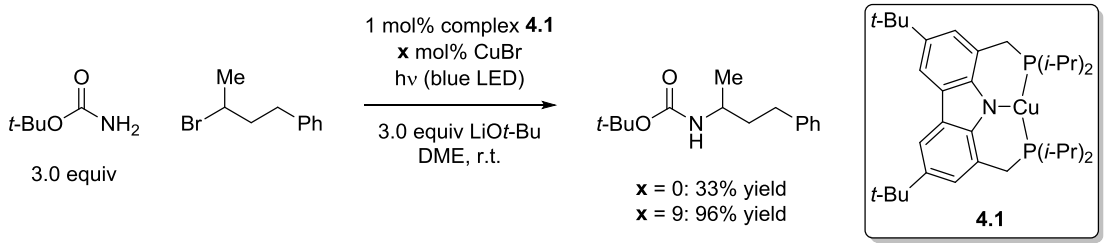

Scheme 4.3. Effect of added CuBr on the photoinduced coupling of *t*-butyl carbamate catalyzed by complex **4.1**

When complex **4.1** is generated in situ from CuBr and **L4.1** (**L3.1** in **Chapter 3**), a similar yield (91%, **Table 4.1**, entry 1) is observed to when the discrete catalyst is used (**Scheme 4.3**, 96%). In the absence of ligand **L4.1**, CuBr, or light, essentially no C–N bond formation occurs (entries 2–4), and the electrophile can be recovered virtually quantitatively. Decreasing the amount of ligand **L4.1** and CuBr, individually or

simultaneously, results in a moderate loss in yield (entries 5–7), as does lowering the quantity of the nucleophile (entry 8). The alkylation is air-sensitive, but not highly water-sensitive (entries 9 and 10). Although commonly used ruthenium and iridium photoredox catalysts cannot be used in place of ligand **L4.1** (entries 11 and 12), a Hg lamp can be employed instead of blue LED lamps (entry 13; in the absence of ligand **L4.1**: <1% yield).

Table 4.1. Effect of reaction parameters.

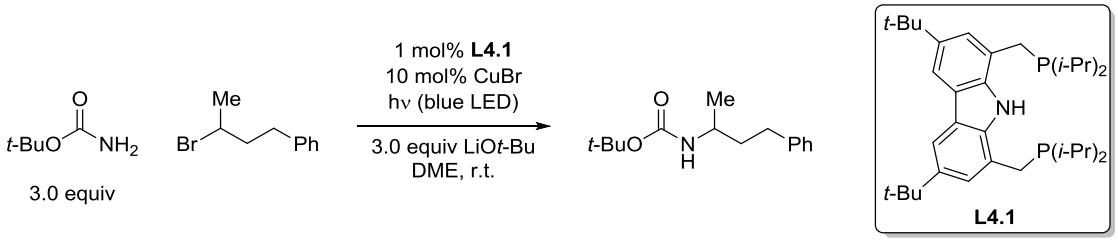

entry	variation from the "standard" conditions	yield (%)[a]
1	none	91
2	no **L4.1**	<1
3	no CuBr	<1
4	no hv	<1
5	0.5 mol% **L4.1**	75
6	5.0 mol% CuBr	81
7	0.5 mol% **L4.1** and 5.0 mol% CuBr	65
8	2.0 equiv carbamate, 2.0 equiv LiO*t*-Bu	52
9	under air (capped vial)	21
10	added H_2O (0.1 equiv)	85
11	1.0 mol% $[Ru(bpy)_3][PF_6]_2$, instead of **L4.1**	<1
12	1.0 mol% $[Ir(dtbbpy)(ppy)_2][PF_6]$, instead of **L4.1**	<1
13	Hg, instead of blue LED, lamp	94
14	THF, instead of DME	90

[a] Average of two runs, based on GC analysis versus an internal standard (*n*-dodecane). bpy = 2,2′-bipyridine; ppy = 2-phenylpyridine; dtbbpy = 4,4′-*t*-butyl-2,2′-bipyridine.

4.2.2. Scope

Under the standard conditions, a variety of carbamates can be N–alkylated in good yield, providing a one-step method for the conversion of an electrophile into a carbamate-protected primary amine (**Table 4.2**). The alkyl group (R) of the carbamate can range in size from methyl to *t*-butyl (entries 1–4). Apart from the *t*-butyl group (entry 4), methyl (entry 1) and (trimethylsilyl)-ethyl (entry 3) groups also serve as amine protecting groups and can be selectively cleaved in the presence of bases or fluoride ions, respectively.[11] When R is benzyl, the alkylation of carbamate does not proceed (<10 % yield), and a significant amount of benzyl alcohol is instead detected; 2,2,2,-trichloroethyl carbamate is also not a suitable nucleophilic coupling partner under our standard conditions. Although we have not detected double alkylation in these reactions, it is possible to achieve C–N bond formation in the case of an unhindered cyclic carbamate (entry 5).

Table 4.2. Scope with respect to the carbamate.

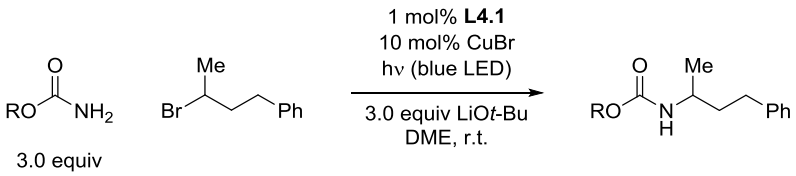

entry	carbamate	yield (%)[a]
1	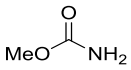	90
2	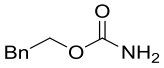	67
3	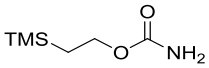	76
4	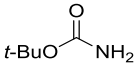	87
5		74

[a] Yield of purified product (average of two experiments).
TMS = trimethylsilyl.

With respect to the electrophile, we have established that a variety of acyclic and cyclic unactivated secondary alkyl bromides are suitable partners in this photoinduced, copper-catalyzed coupling process (**Table 4.3**). When 1-bromo-3-(*t*-butyl)cyclohexane is employed as the electrophile, moderate diastereoselectivity is observed (6.5:1 cis/trans; entry 9).

Table 4.3. Scope with respect to the electrophile.

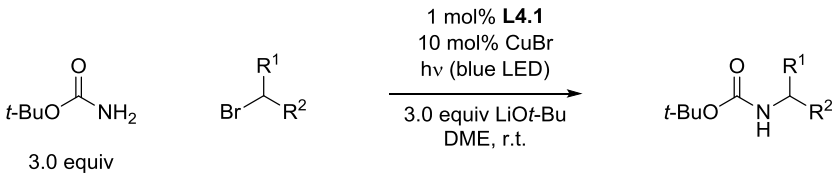

entry	carbamate	yield (%)[a]
1	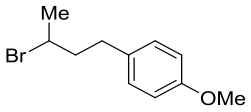	81
2	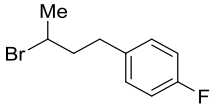	70
3	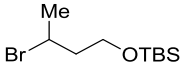	72
4	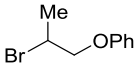	56
5		49 (74)[b]
6	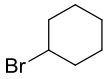	81
7	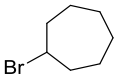	88
8	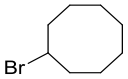	81
9[c]	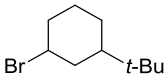	85
10	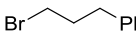	80[b]

[a] Yield of purified product (average of two experiments).
[b] Yield of purified product when a Hg lamp is used.
[c] Starting material: 1:5.4 cis/trans; product: 6.5:1 cis/trans.

The coupling is compatible with the presence of an alkene, an alkyne, a ketone, an N–alkyl indole, a secondary alcohol, a secondary amine, and an unactivated secondary alkyl chloride, whereas it proceeds with significantly lower efficiency in the presence of an N–H indole, an unactivated secondary alkyl iodide, and a pyridine (**Table 4.4**). Under our standard

conditions, essentially no C–N coupling is observed when an unactivated tertiary alkyl bromide or an α-bromo-carbonyl compound is employed as the electrophile.

Table 4.4. Effect of additives.

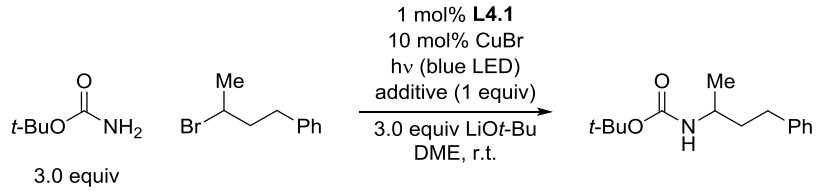

Compatible >70% yield >80% recovery of additive	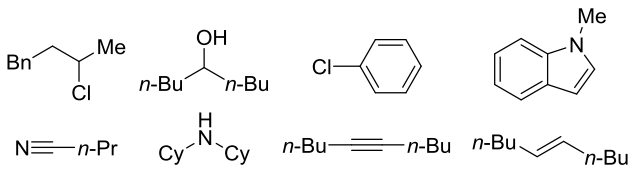
Challenging 30-70% yield >70% recovery of additive	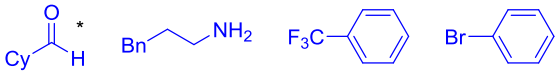
Problematic <30% yield	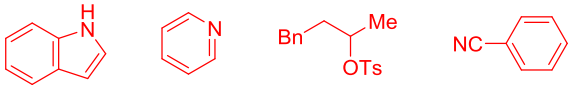

* Only 11% of the additive was recovered.

As indicated in entry 5 of **Table 4.3**, when irradiation by blue LED lamps leads to a modest yield of the desired alkylation product, the use instead of a Hg lamp may be beneficial (49% → 74% yield). Similarly, a primary alkyl bromide can be used as a substrate when a Hg lamp is employed (entry 10); in the absence of irradiation, no coupling is observed. An additional example of a challenging N–alkylation wherein a Hg lamp has proved to be helpful is illustrated in **Scheme 4.4**. In order to suppress the formation of elimination products, the coupling of the sterically demanding substrate requires the lowering of the reaction

temperature, which in turn necessitates the extension of irradiation period and increase in the stoichiometry of reagents, ligand **L4.1**, and CuBr.

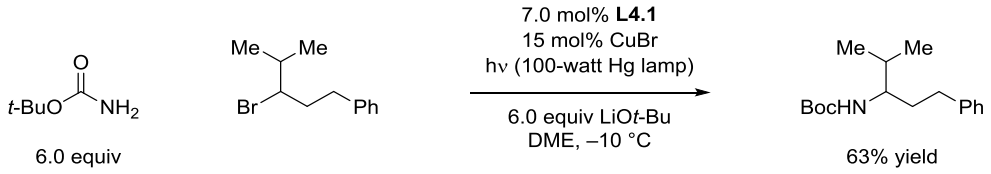

Scheme 4.4. Coupling of a hindered substrate under modified reaction conditions.

The modified condition is also applicable to the derivatization of a complex alkyl bromide (**Scheme 4.5**). For the coupling of the pregnenolone-derived alkyl bromide, the major diastereomer of the product can be isolated as a single isomer (>20:1) via column chromatography followed by recrystallization.

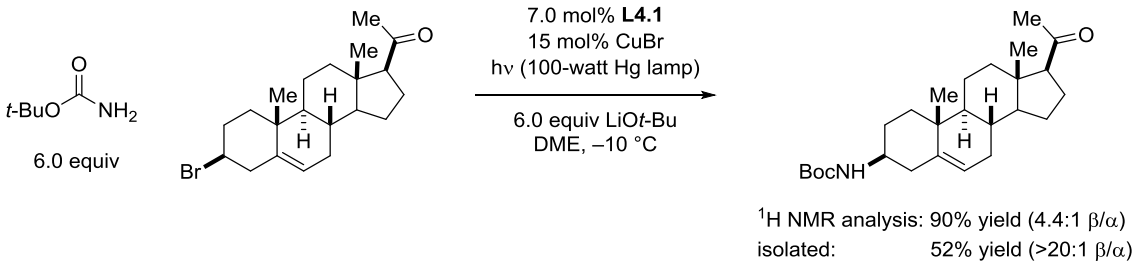

Scheme 4.5. Application of the method to the derivatization of a complex alkyl bromide.

4.2.3. Mechanistic studies

We hypothesize that, under the conditions that include excess CuBr, complex **4.1** may be serving the typical role of photoredox catalysts, i.e., it is a donor and an acceptor of electrons, but it is not directly involved in the key bond-forming process (**Figure 4.1**). This hypothesis stands in contrast to the scenario outlined in the UV-induced alkylation of

carboxamides, wherein a copper–nucleophile complex is proposed to engage in both electron transfer and in bond formation.[7] A ^{31}P NMR study establishes that complex **4.1** does not dissociate ligand **L4.1** or bind *t*-butyl carbamate to a significant extent in the presence of 3.0 equiv of the carbamate/LiO*t*-Bu. The presence of complex **4.1** at the start of the reaction and in a reaction in progress is also supported by ESI-MS analysis.[12]

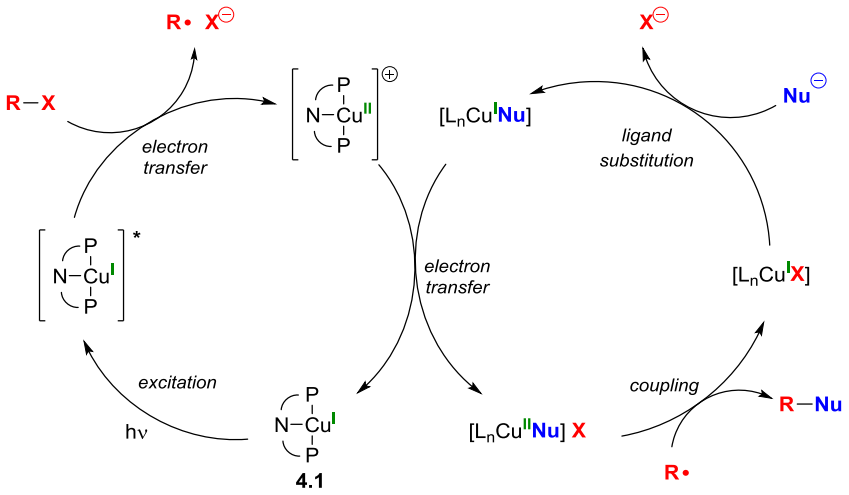

Figure 4.1. Proposed mechanism of photoinduced, copper-catalyzed coupling of carbamates with unactivated secondary alkyl bromides.

The electron transfer from the excited state of complex **4.1** to an alkyl bromide should produce a paramagnetic copper(II) intermediate. The EPR spectrum of the standard reaction mixture (**Table 4.1**, entry 1) reveals an S = 1/2 species with hyperfine coupling to a mononuclear Cu center (I = 3/2) (**Figure 4.2**, black trace). Because the same spectrum is observed when $CuBr_2$ is treated with $BocNH_2$ and LiO*t*-Bu (**Figure 4.2**, red trace), we suggest that this EPR-active species may be $Cu^{II}(NHBoc)_n$, representing the persistent radical that enables efficient cross-coupling.[13]

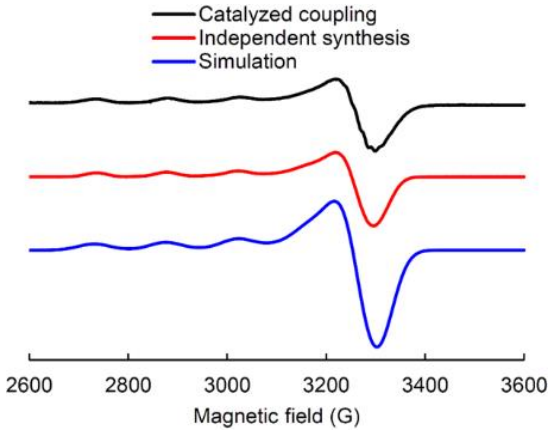

Figure 4.2. EPR spectra (9.4 GHz, 77 K, DME/2-MeTHF). Black trace: catalyzed coupling of $BocNH_2$ with 2-bromo-4-phenylbutane; red trace: mixture of $CuBr_2$, $BocNH_2$ (10 equiv), and Li*O*t-Bu (10 equiv); blue trace: simulation of the spectrum in red (g = [2.276, 2.063, 2.058], A_{Cu} (MHz) = [0, 0, 439], lw = 6.2 MHz).

The current mechanistic proposal in **Figure 4.1** demands the involvement of a free alkyl radical in the coupling step. In reactions of sterically hindered electrophiles (e.g. **Scheme 4.4**), electrophile homocoupling products are detected via the GC analysis of the crude reaction mixtures, consistent with the intermediacy of alkyl radicals.[14] The presence of alkyl radicals is also evident in the stereochemical outcome of the C–N couplings of 3-substituted cyclohexyl bromide (**Table 4.3** entry 9; starting material: 1:5.4 cis/trans; product: 6.5:1 cis/trans) and that of the pregnenolone-derived electrophile (**Scheme 4.5**); the latter predominantly yields the stereoretention product of the substitution reaction.

To gain further insight into the reaction of photo-excited complex **4.1** with an alkyl bromide, we have subjected 6-bromo-1-heptene to our standard coupling conditions, which generates the cyclized product with 3.7:1 cis/trans selectivity (**Scheme 4.6**). Because this is

similar to the stereoselectivity that has been reported for the cyclization of the derived secondary alkyl radical, this observation supports the hypothesis that a secondary alkyl radical is an intermediate in the photoinduced, copper-catalyzed couplings reported herein. Notably, the derived secondary alkyl radical of 6-bromo-1-heptene cyclizes with a rate constant of $1.0 \times 10^5\ s^{-1}$ at 25 °C.[15] Because this is much slower than typical rates of diffusion (generally $>10^8\ s^{-1}$),[16] the radical has sufficient time to diffuse before engaging in the C–N bond formation, as required by the mechanism outlined in **Figure 4.1**.

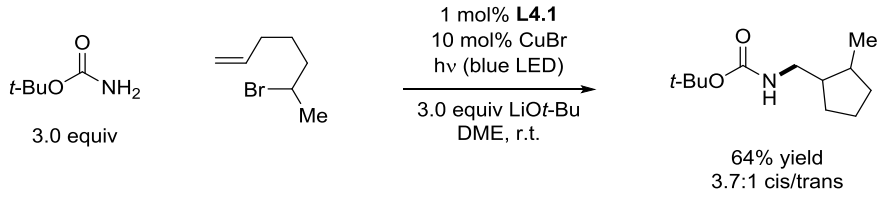

Scheme 4.6. Observation of cyclized alkyl radical coupling products.

Although numerous examples of photoredox processes are thought to follow radical chain pathways,[17] photoinduced, copper-catalyzed C–N coupling reactions likely involve non-chain mechanisms. The quantum yield of the coupling of $BocNH_2$ and 2-bromo-4-phenylbutane under irradiation at 350 nm is 0.06, which, when considered together with the measured lifetime for the excited state of complex **4.1** (8.1 ns), is not suggestive of a chain process. Further corroborating this observation is the light-on-light-off experiment; we have determined that coupling stops when irradiation stops, and that coupling resumes when irradiation resumes. Thus, a variety of data are consistent with the mechanism outlined in **Figure 4.1**.

4.2.4. Stereoselective N–alkylations of ammonia surrogates

In light of successful reactions between carbamates with unactivated secondary alkyl bromides that occur via an out-of-cage radical coupling mechanism, we have sought to extend the strategy to prepare stereoenriched, protected primary amines. To achieve this goal, two stereoconvergent strategies may be targeted: an enantioconvergent synthesis of protected primary amine using a chiral ligand (**Scheme 4.7**, top) and a diastereoselective coupling using a chiral nucleophile (**Scheme 4.7**, bottom).

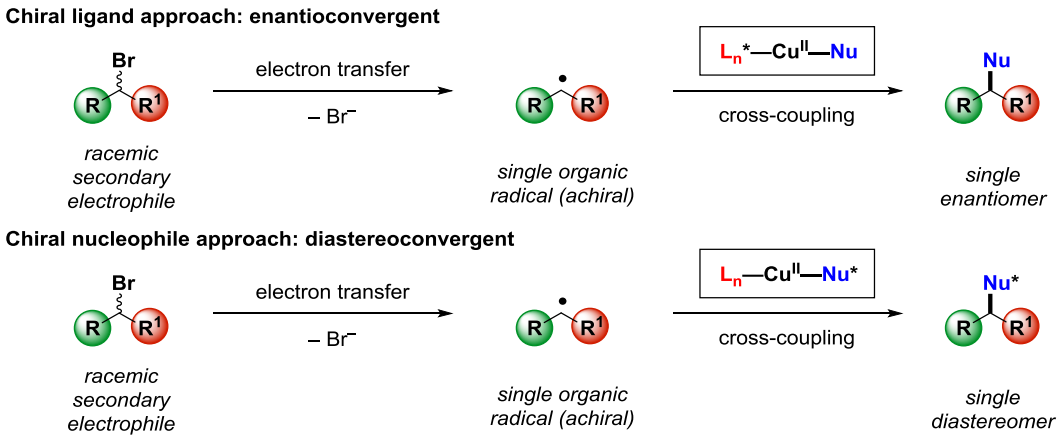

Scheme 4.7. Stereoconvergent coupling of racemic secondary electrophiles. Top: chirality of the coupling catalyst is provided by the substoichiometric chiral ligand; bottom: chirality of the coupling catalyst is provided by the stoichiometric chiral nucleophile.

Unfortunately, we have found that our standard reaction conditions for the racemic coupling of carbamates with unactivated alkyl bromides are not applicable to the coupling of *t*-butyl sulfinamides or 4-phenyloxazolidin-2-one (**Figure 4.3**). Chiral primary carbamates

derived from chiral alcohols such as mentholyl carbamate undergo N–alkylation in good yield but in low diastereoselectivity (generally <2:1; **Figure 4.3**).[18]

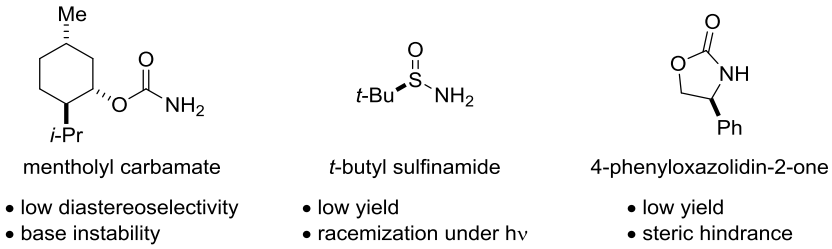

Figure 4.3. Chiral nucleophiles that have been unsuccessful in the synthesis of stereoenriched, protected primary amines and possible reasons for their shortcomings.

In contrast, stereoselectivity has been observed when methyl carbamate is employed in the coupling of an unactivated alkyl bromide with an ether directing group. Specifically, (3-bromo-4-methoxybutyl)benzene reacts in the presence of a chiral diamine ligand **L*** to produce partially stereoenriched C–N coupling product at –20 °C (**Scheme 4.8**).[19,20] In the absence of ligand **L4.1**, no coupling is observed. Although the observed stereoselectivity is only modest, this finding is consistent with the general mechanistic hypothesis of copper-catalyzed C–N couplings (**Figure 3.1** and **Figure 4.1**) and demonstrates the viability of the approach outlined in **Scheme 4.7**.

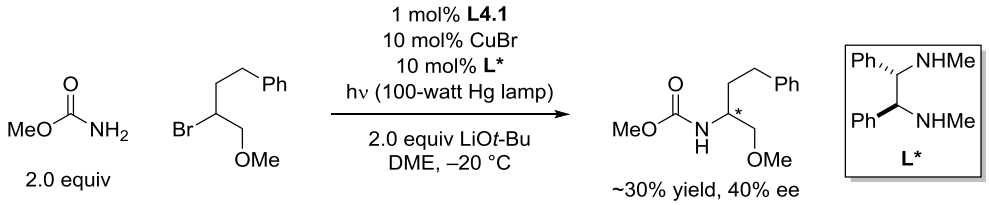

Scheme 4.8. Stereoselective coupling of methyl carbamate in the presence of a chiral diamine ligand.

4.3. Conclusions

We have developed a method for coupling an array of carbamates with unactivated secondary alkyl bromides under mild conditions (room temperature), thereby providing direct access to protected primary amines; to the best of our knowledge, the corresponding uncatalyzed nucleophilic substitution reactions have not been described. To achieve this objective, we designed a photoredox catalyst, based on copper and a tridentate bis(phosphino)carbazole ligand, that can serve as an electron donor upon irradiation by blue LED lamps. Mechanistic studies are consistent with a reaction pathway in which the excited photoredox catalyst reduces the alkyl electrophile, producing an alkyl radical and a copper(II) intermediate; the latter oxidizes a copper(I)–nucleophile complex to a copper(II)–nucleophile intermediate, which then collides in an out-of-cage process with the alkyl radical to generate the C–N coupling product. Furthermore, we have observed that, in the presence of a chiral diamine ligand, a chiral copper(II)–nucleophile intermediate may be formed in situ, leading to the formation of stereoenriched, protected primary amines.

4.4. Experimental Section

4.4.1. General information

Unless otherwise noted, materials were either purchased from commercial suppliers and used as received, or prepared via literature procedures. Ligand **L4.1** was synthesized according to a literature procedure[21] and recrystallized from a cold, saturated solution in Et_2O/CH_3CN for use in photoinduced cross-couplings. Solvents were deoxygenated and dried by thoroughly sparging with argon, followed by passage through an activated column in a solvent purification system.

All manipulations of air-sensitive materials were carried out in oven-dried glassware using standard Schlenk, or glovebox techniques, under an N_2 atmosphere. Silicycle *Silia*Flash® P60 silica gel (particle size 40–63 μm) was used for flash chromatography. Analytical thin layer chromatography was conducted with glass TLC plates (silica gel 60 F254), and spots were visualized under UV light or after treatment with standard TLC stains.

X-band EPR measurements were made with a Bruker EMX spectrometer at 77 K. Simulation of EPR data was conducted using the software EasySpin.[22]

IR measurements were recorded on a Bruker ALPHA Diamond ATR, or using a Perkin Elmer Paragon 1000 spectrometer, using thin films deposited on KBr plates.

^{1}H, ^{13}C, and ^{31}P NMR spectra were recorded on a Bruker Ascend 400 MHz, a Varian 300 MHz, a Varian 400 MHz, a Varian 500 MHz, or a Varian 600 MHz spectrometer with $CHCl_3$ (^{1}H, $\delta = 7.26$) and $CDCl_3$ (^{13}C, $\delta = 77.0$) as internal references and with 85% H_3PO_4

(^{31}P) as an external reference. Multiplicity and qualifier abbreviations are as follows: s = singlet, d = doublet, t = triplet, q = quartet, m = multiplet, br = broad, app = apparent). GC analyses were carried out on an Agilent 6890 Series system with an HP-5 column (length 30 m, I.D. 0.25 mm).

X-ray crystallography studies were carried out at the Beckman Institute Crystallography Facility on either Bruker Kappa Apex II diffractometer or a Bruker D8 Venture kappa duo photon 100 CMOS instrument (Mo Kα radiation). Structures were solved using SHELXT and refined against F^2 by full-matrix least squares with SHELXL and OLEX2. Hydrogen atoms were added at calculated positions and refined using a riding model. The crystals were mounted on a glass fiber or a nylon loop with Paratone N oil.

Mass spectral data were collected on a Thermo LCQ or LTQ ion trap mass spectrometer, or on an Agilent 5973 mass spectrometer.

Photolytic reactions were performed using 34 W Kessil H150 Blue LED lamps, a 100 W Blak-Ray Long Wave Ultraviolet Lamp (Hg), a 100-W Blak-Ray B-100Y High Intensity Inspection Lamp (Hg), or a Luzchem LZC-4V photoreactor equipped with LZC-UVC lamps centered at 254 nm, LZC-UVA lamps centered at 350 nm, or LZC-420 lamps centered at 420 nm. If required, the temperature was maintained with an isopropanol bath cooled by an SP Scientific cryostat.

4.4.2. Photoinduced, copper-catalyzed alkylations

Preparation of a reaction mixture on a Schlenk line (liquid electrophiles)

CuBr, ligand **L4.1**, LiO*t*-Bu, and the carbamate were added to an 8 mL borosilicate glass vial that contained a magnetic stir bar. The vial was capped with a PTFE-lined septum cap, and then it was evacuated and backfilled with nitrogen (3 cycles). Next, DME and the electrophile were added in sequence via syringe, and the mixture was stirred at room temperature until the solids had dissolved (5 min). The vial was then detached from the Schlenk line.

Preparation of a reaction mixture on a Schlenk line (solid electrophiles)

CuBr, ligand **L4.1**, LiO*t*-Bu, the carbamate, and the electrophile were added to an 8 mL borosilicate glass vial that contained a magnetic stir bar. The vial was capped with a PTFE-lined septum cap, and then it was evacuated and backfilled with nitrogen (3 cycles). Next, DME was added via syringe, and the mixture was stirred at room temperature until the solids had dissolved (5 min). The vial was then detached from the Schlenk line.

Note: We recommend that CuBr (white or off-white solid) and LiO*t*-Bu (hygroscopic) be stored in a glovebox. Solutions of $BocNH_2$ and LiO*t*-Bu in DME can be prepared under nitrogen, stirred for 10 min, and filtered through a PTFE syringe filter to remove impurities.

Figure 4.4. A typical irradiation setup at room temperature. Shown are three 34-watt blue LED lamps, a reflective Dewar, and a table fan.

General Procedure: Irradiation of the reaction mixture with blue LED lamps

The reaction vial and a magnetic stir bar were submerged in a low-form hemispherical Dewar flask filled with water in a well-ventilated fume hood. Three 34-watt blue LED lamps were placed 3 inches from the vial (as close to the vial as possible, without the lamps being in contact with water), and the vial was irradiated for 16 h. The temperature of the water bath was maintained below 30 °C with a table fan. A typical setup is shown above.

Workup

After irradiation, the reaction mixture was diluted with EtOAc (5 mL) and then washed with aqueous NH_4Cl (5 mL). The aqueous layer was extracted with EtOAc (5 mL × 3), and the combined organic layers were dried over anhydrous Na_2SO_4, filtered, and

concentrated in vacuo. The residue was purified by flash column chromatography on silica gel.

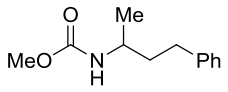

Methyl (4-phenylbutan-2-yl)carbamate. Table 4.2, entry 1 [129830-34-8]. The title compound was synthesized according to the General Procedure, using CuBr (10 mg, 0.070 mmol), ligand **L4.1** (3.8 mg, 0.0070 mmol), LiO*t*-Bu (168 mg, 2.1 mmol), methyl carbamate (158 mg, 2.1 mmol), and 2-bromo-4-phenylbutane (149 mg, 0.70 mmol) in DME (8 mL), and purified by column chromatography (10%→30% Et_2O/hexanes). Colorless oil. First run: 131 mg (90%). Second run: 132 mg (91%).

Spectroscopic data match those previously reported for [129830-34-8].

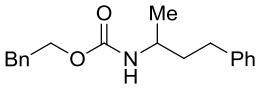

Phenethyl (4-phenylbutan-2-yl)carbamate. Table 4.2, entry 2. The title compound was synthesized according to the General Procedure, using CuBr (10 mg, 0.070 mmol), ligand **L4.1** (3.8 mg, 0.0070 mmol), LiO*t*-Bu (168 mg, 2.1 mmol), phenethyl carbamate (347 mg, 2.1 mmol), and 2-bromo-4-phenylbutane (149 mg, 0.70 mmol) in DME (8 mL), and purified by column chromatography (10%→40% Et_2O/hexanes). White solid. First run: 140 mg (67%). Second run: 141 mg (68%).

^{1}H NMR (400 MHz, $CDCl_3$) δ 7.32–7.28 (m, 4H), 7.23–7.16 (m, 6H), 4.57 (d, J = 7.0 Hz, 1H), 4.29 (t, J = 7.0 Hz, 2H), 3.79–3.72 (m, 1H), 2.93 (t, J = 7.0 Hz, 2H), 2.70–2.58 (m, 2H), 1.73 (q, J = 6.6 Hz, 2H), 1.16 (d, J = 6.5 Hz, 3H).

^{13}C NMR (101 MHz, $CDCl_3$) δ 155.9, 141.8, 138.1, 129.0, 128.51, 128.47, 128.4, 126.5, 125.9, 65.1, 46.9, 39.0, 35.6, 32.5, 21.4.

FT-IR (film): 3322, 2965, 1682, 1548, 1454, 1267, 1111, 699 cm^{-1}.

MS (ESI) m/z $(M+Na)^+$ calcd for $C_{19}H_{23}NO_2Na$: 320.2, found: 320.2.

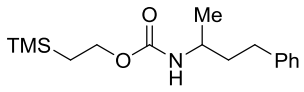

2-(Trimethylsilyl)ethyl (4-phenylbutan-2-yl)carbamate. Table 4.2, entry 3. The title compound was synthesized according to the General Procedure, using CuBr (10 mg, 0.070 mmol), ligand **L4.1** (3.8 mg, 0.0070 mmol), LiO*t*-Bu (168 mg, 2.1 mmol), 2-(trimethylsilyl)ethyl carbamate (339 mg, 2.1 mmol), and 2-bromo-4-phenylbutane (149 mg, 0.70 mmol) in DME (8 mL), and purified by column chromatography (10%→30% Et_2O/hexanes). Colorless oil. First run: 161 mg (78%). Second run: 153 mg (74%).

^{1}H NMR (400 MHz, $CDCl_3$) δ 7.40–7.26 (m, 2H), 7.19–7.17 (m, 3H), 4.50 (br, 1H), 4.20–4.09 (m, 2H), 3.77 (br, 1H), 2.72–2.60 (m, 2H), 1.74 (q, J = 7.1 Hz, 2H), 1.18 (d, J = 6.6 Hz, 3H), 1.01–0.97 (m, 2H), 0.05 (s, 9H).

^{13}C NMR (101 MHz, $CDCl_3$) δ 156.3, 141.9, 128.5, 128.4, 126.0, 62.9, 46.9, 39.2, 32.6, 21.5, 17.9, –1.4.

FT-IR (film): 3326, 2953, 1691, 1534, 1250, 1057, 837, 698 cm^{-1}.

MS (EI) m/z $(M+H)^+$ calcd for $C_{16}H_{28}NO_2Si$: 294.1, found: 294.0.

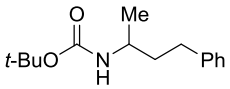

***tert*-Butyl (4-phenylbutan-2-yl)carbamate. Table 4.2, entry 4 [1206464-59-6].** The title compound was synthesized according to the General Procedure, using CuBr (10 mg, 0.070

mmol), ligand **L4.1** (3.8 mg, 0.0070 mmol), LiO*t*-Bu (168 mg, 2.1 mmol), $BocNH_2$ (246 mg, 2.1 mmol), and 2-bromo-4-phenylbutane (149 mg, 0.70 mmol) in DME (8 mL), and purified by column chromatography (10%→35% Et_2O/hexanes). White solid. First run: 150 mg (86%). Second run: 153 mg (88%).

As indicated in **Scheme 4.2**, the title compound was also prepared according to a literature procedure,[7] using CuI (19.5 mg, 0.10 mmol), LiO*t*-Bu (160 mg, 2.0 mmol), $BocNH_2$ (117 mg, 1.0 mmol), and 2-bromo-4-phenylbutane (426 mg, 2.0 mmol) in a mixture of DMF (0.8 mL) and CH_3CN (5.4 mL). Purification by column chromatography (10%→35% Et_2O/hexanes) afforded a pale-yellow solid. First run: 110 mg (44%). Second run: 106 mg (43%).

Spectroscopic data match those previously reported for [1206464-59-6].

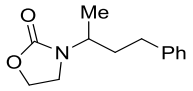

3-(4-Phenylbutan-2-yl)oxazolidin-2-one. Table 4.2, entry 5 [1542235-59-5]. The title compound was synthesized according to the General Procedure, using CuBr (10 mg, 0.070 mmol), ligand **L4.1** (3.8 mg, 0.0070 mmol), LiO*t*-Bu (168 mg, 2.1 mmol), 2-oxazolidinone (183 mg, 2.1 mmol), and 2-bromo-4-phenylbutane (149 mg, 0.70 mmol) in DME (8 mL), and purified by column chromatography (70%→90% Et_2O/hexanes). Pale-yellow oil. First run: 117 mg (76%). Second run: 112 mg (73%).

Spectroscopic data match those previously reported for [1542235-59-5].

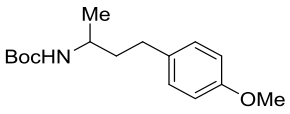

***tert*-Butyl (4-(4-methoxyphenyl)butan-2-yl)carbamate. Table 4.3, entry 1.** The title compound was synthesized according to the General Procedure, using CuBr (10 mg, 0.070 mmol), ligand **L4.1** (3.8 mg, 0.0070 mmol), LiO*t*-Bu (168 mg, 2.1 mmol), $BocNH_2$ (246 mg, 2.1 mmol), and 1-(3-bromobutyl)-4-methoxybenzene (170 mg, 0.70 mmol) in DME (8 mL), and purified by column chromatography (15%→35% Et_2O/hexanes). White solid. First run: 160 mg (82%). Second run: 156 mg (80%).

^1H NMR (300 MHz, $CDCl_3$) δ 7.10 (d, J = 8.6 Hz, 2H), 6.82 (d, J = 8.6 Hz, 2H), 4.32 (br, 1H), 3.78 (s, 3H), 3.69 (br, 1H), 2.74–2.45 (m, 2H), 1.79–1.58 (m, 2H), 1.45 (s, 9H), 1.15 (d, J = 6.6 Hz, 3H).

^{13}C NMR (101 MHz, $CDCl_3$) δ 157.8, 155.4, 134.0, 129.3, 113.9, 79.0, 55.3, 46.4, 39.5, 31.6, 28.5, 21.5.

FT-IR (film): 3353, 2974, 1688, 1612, 1514, 1246, 1175, 1061 cm^{-1}.

MS (ESI) m/z $(M+Na)^+$ calcd for $C_{16}H_{25}NO_3Na$: 302.2, found: 302.1.

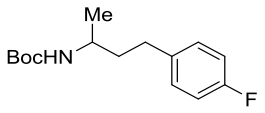

***tert*-Butyl (4-(4-fluorophenyl)butan-2-yl)carbamate. Table 4.3, entry 2.** The title compound was synthesized according to the General Procedure, using CuBr (10 mg, 0.070 mmol), ligand **L4.1** (3.8 mg, 0.0070 mmol), LiO*t*-Bu (168 mg, 2.1 mmol), $BocNH_2$ (246 mg, 2.1 mmol), and 1-(3-bromobutyl)-4-fluorobenzene (162 mg, 0.70 mmol) in DME (8 mL), and purified by column chromatography (10%→35% Et_2O/hexanes). White solid. First run: 135 mg (72%). Second run: 130 mg (69%).

^{1}H NMR (300 MHz, $CDCl_3$) δ 7.13 (dd, J = 8.5, 5.5 Hz, 2H), 6.95 (t, J = 8.8 Hz, 2H), 4.32 (s, 1H), 3.69 (s, 1H), 2.62 (dd, J = 9.6, 6.4 Hz, 2H), 1.77–1.62 (m, 2H), 1.45 (s, 9H), 1.15 (d, J = 6.6 Hz, 3H).

^{13}C NMR (101 MHz, $CDCl_3$) δ 161.2 (d, J = 243.2 Hz), 155.4, 137.5, 129.7 (d, J = 7.8 Hz), 115.1 (d, J = 21.0 Hz), 79.0, 46.2, 39.3, 31.7, 28.5, 21.4.

^{19}F NMR (282 MHz, $CDCl_3$) δ –117.9.

FT-IR (film): 3342, 2976, 1690, 1601, 1511, 1455, 1366, 1223, 1174, 1060, 827 cm^{-1}.

MS (ESI) m/z $(M+Na)^+$ calcd for $C_{15}H_{22}FNO_2Na$: 290.2, found: 290.0.

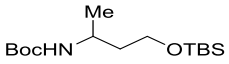

***tert*-Butyl (4-((*tert*-butyldimethylsilyl)oxy)butan-2-yl)carbamate. Table 4.3, entry 3.** The title compound was synthesized according to the General Procedure, using CuBr (10 mg, 0.070 mmol), ligand **L4.1** (3.8 mg, 0.0070 mmol), LiO*t*-Bu (168 mg, 2.1 mmol), $BocNH_2$ (246 mg, 2.1 mmol), and 1 (3-bromobutoxy)(*tert*-butyl)dimethylsilane (187 mg, 0.70 mmol) in DME (8 mL), and purified by column chromatography (10%→30% Et_2O/hexanes). Colorless oil. First run: 157 mg (74%). Second run: 149 mg (70%).

^{1}H NMR (400 MHz, $CDCl_3$) δ 5.12 (s, 1H), 3.80–3.69 (m, 2H), 3.66–3.61 (m, 1H), 1.69 (br, 1H), 1.57–1.51 (m, 1H), 1.39 (s, 9H), 1.12 (d, J = 6.6 Hz, 3H), 0.86 (s, 9H), 0.02 (s, 6H).

^{13}C NMR (101 MHz, $CDCl_3$) δ 155.5, 78.6, 60.5, 45.2, 38.6, 28.5, 26.0, 20.9, 18.2, –5.4.

FT-IR (film): 3350, 2931, 1704, 1506, 1365, 1253, 1177, 1094, 836, 777 cm^{-1}.

MS (ESI) m/z $(M+Na)^+$ calcd for $C_{15}H_{33}NO_3SiNa$: 326.2, found: 326.1.

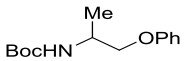

***tert*-Butyl (1-phenoxypropan-2-yl)carbamate. Table 4.3, entry 4 [1824064-92-7].** The title compound was synthesized according to the General Procedure, using CuBr (10 mg, 0.070 mmol), ligand **L4.1** (3.8 mg, 0.0070 mmol), LiO*t*-Bu (168 mg, 2.1 mmol), $BocNH_2$ (246 mg, 2.1 mmol), and (2-bromopropoxy)benzene (151 mg, 0.70 mmol) in DME (8 mL), and purified by column chromatography (10%→30% Et_2O/hexanes). White solid. First run: 103 mg (59%). Second run: 93 mg (53%).

Spectroscopic data match those previously reported for [1824064-92-7].

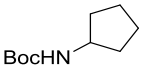

***tert*-Butyl cyclopentylcarbamate. Table 4.3, entry 5 [153789-22-1].** The title compound was synthesized according to the General Procedure, using CuBr (10 mg, 0.070 mmol), ligand **L4.1** (3.8 mg, 0.0070 mmol), LiO*t*-Bu (168 mg, 2.1 mmol), $BocNH_2$ (246 mg, 2.1 mmol), and bromocyclopentane (104 mg, 0.70 mmol) in DME (8 mL), and purified by column chromatography (10%→30% Et_2O/hexanes). White solid. First run: 65 mg (50%). Second run: 63 mg (49%).

Irradiation under 100-watt Hg lamp: First run: 95 mg (73%). Second run: 98 mg (76%).

Spectroscopic data match those previously reported for [153789-22-1].

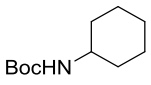

***tert*-Butyl cyclohexylcarbamate. Table 4.3, entry 6 [3712-40-1].** The title compound was synthesized according to the General Procedure, using CuBr (10 mg, 0.070 mmol), ligand

L4.1 (3.8 mg, 0.0070 mmol), LiO*t*-Bu (168 mg, 2.1 mmol), $BocNH_2$ (246 mg, 2.1 mmol), and bromocyclohexane (114 mg, 0.70 mmol) in DME (8 mL), and purified by column chromatography (10%→20% Et_2O/hexanes). White solid. First run: 110 mg (79%). Second run: 116 mg (83%).

Spectroscopic data match those previously reported for [3712-40-1].

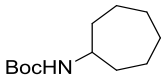

***tert*-Butyl cycloheptylcarbamate. Table 4.3, entry 7 [1005795-57-2].** The title compound was synthesized according to the General Procedure, using CuBr (10 mg, 0.070 mmol), ligand **L4.1** (3.8 mg, 0.0070 mmol), LiO*t*-Bu (168 mg, 0.21 mmol), $BocNH_2$ (246 mg, 2.1 mmol), and bromocycloheptane (124 mg, 0.70 mmol) in DME (8 mL), and purified by column chromatography (10%→30% Et_2O/hexanes). White solid. First run: 131 mg (88%). Second run: 131 mg (88%).

Procedure for gram-scale reaction. A 100 mL Schlenk flask was charged with CuBr (120 mg, 0.84 mmol), ligand **L4.1** (114 mg, 0.21 mmol), LiO*t*-Bu (1.7 g, 21 mmol), $BocNH_2$ (2.5 g, 21 mmol), and a magnetic stir bar. The Teflon plug valve was sealed with a rubber septum, and the vessel was evacuated and backfilled with N_2 (3 cycles). DME (80 mL) was added via syringe, and then the mixture was stirred at room temperature for 5 min. Next, the electrophile (7.0 mmol) was added in one portion via syringe. The rubber septum was quickly replaced under a positive flow of N_2 with a Teflon screw cap. The vessel was sealed and placed in a low-form hemispherical Dewar flask filled with water. Four 34-watt blue LED lamps were placed 2 inches from the flask, which was irradiated for 72 h. The temperature of the water bath was controlled by a standard table fan. Water was refilled occasionally to

prevent warming of the reaction mixture. The Schlenk flask was periodically shaken vigorously to provide even mixing of the material. After 72 h, the reaction mixture was diluted with EtOAc (75 mL) and washed with aqueous NH_4Cl (50 mL). The aqueous layer was extracted with EtOAc (50 mL × 3), and the combined organic layers were dried over anhydrous Na_2SO_4, filtered, and concentrated in vacuo. The residue was purified by flash column chromatography on silica gel.

The title compound was prepared according to the procedure for gram-scale reactions, using bromocycloheptane (1.24 g, 7.0 mmol), and purified by column chromatography (10%→30% Et_2O/hexanes). Pale-yellow solid. First run: 990 mg (66%). Second run: 994 mg (67%). Unreacted bromocycloheptane was recovered by additional purification by flash column chromatography, eluting with hexanes. The combined fractions were concentrated in vacuo with cooling, to minimize the loss of bromocycloheptane. First run: 290 mg (23%). Second run: 270 mg (22%).

Spectroscopic data match those previously reported for [1005795-57-2].

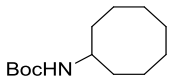

***tert*-Butyl cyclooctylcarbamate. Table 4.3, entry 8 [544478-04-8].** The title compound was synthesized according to the General Procedure, using CuBr (10 mg, 0.070 mmol), ligand **L4.1** (3.8 mg, 0.0070 mmol), Li*O*-*t*-Bu (168 mg, 2.1 mmol), $BocNH_2$ (246 mg, 2.1 mmol), and bromocyclooctane (134 mg, 0.70 mmol) in DME (8 mL), and purified by column chromatography (10%→30% Et_2O/hexanes). Pale-yellow solid. First run: 130 mg (82%). Second run: 126 mg (79%).

Spectroscopic data match those previously reported for [544478-04-8].

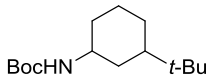

***tert*-Butyl (3-(*tert*-butyl)cyclohexyl)carbamate. Table 4.3, entry 9.** The title compound was synthesized according to the General Procedure, using CuBr (10 mg, 0.070 mmol), ligand **L4.1** (3.8 mg, 0.0070 mmol), Li*O*t-Bu (168 mg, 2.1 mmol), $BocNH_2$ (246 mg, 2.1 mmol), and 1-bromo-3-(*tert*-butyl)cyclohexane (153 mg, 0.70 mmol) in DME (8 mL), and purified by column chromatography (7%→35% Et_2O/hexanes) as a mixture of diastereomers. The relative stereochemistry was determined based on the chemical shifts of the diagnostic methine protons (3.4 ppm = axial = cis isomer; 3.9 ppm = equatorial = trans isomer). Pale-yellow oil. First run: 151 mg (84%), 6.7:1 dr. Second run: 155 mg (87%), 6.4:1 dr. A representative GC trace is shown in **Figure 4.5** (product peaks are at 4.774 and 4.694 min).

^{1}H NMR (400 MHz, $CDCl_3$) δ 4.44 (br, 1H), 3.36 (br, 1H), 2.00–1.81 (m, 2H), 1.77–1.61 (m, 2H), 1.39 (s, 9H), 1.26–1.17 (m, 1H), 1.08–1.02 (m, 1H), 0.93–0.83 (m, 2H), 0.78 (s, 9H), 0.76–0.66 (m, 1H).

^{13}C NMR (101 MHz, $CDCl_3$) δ 155.2, 78.9, 50.4, 47.1, 35.1, 33.8, 32.4, 28.5, 27.6, 26.5, 25.2.

FT-IR (film): 3337, 2942, 1687, 1504, 1366, 1314, 1173, 1047, 734 cm^{-1}.

MS (EI) m/z $(M)^+$ calcd for $C_{15}H_{29}NO_2$: 255.2, found: 255.1.

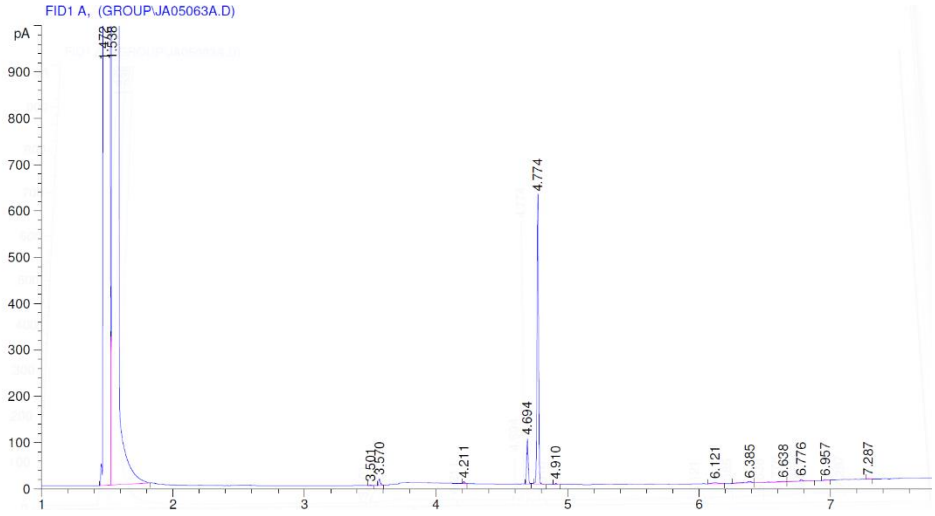

Figure 4.5. Determination of diastereoselectivity by GC.

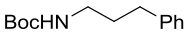

***tert*-Butyl (3-phenylpropyl)carbamate. Table 4.3, entry 10 [147410-39-7].** The title compound was synthesized according to the General Procedure, using a 100-watt Hg lamp, CuBr (10 mg, 0.070 mmol), ligand **L4.1** (3.8 mg, 0.0070 mmol), LiO*t*-Bu (168 mg, 2.1 mmol), $BocNH_2$ (246 mg, 2.1 mmol), and (3-bromopropyl)benzene (139 mg, 0.70 mmol) in DME (8 mL), and purified by column chromatography (10%→30% Et_2O/hexanes). Colorless oil. First run: 135 mg (82%). Second run: 130 mg (79%). In the absence of irradiation, no coupling is observed.

Spectroscopic data match those previously reported for [147410-39-7].

General Procedure 2:

Preparation of a reaction mixture in a nitrogen-filled glovebox. CuBr, ligand **L4.1**, LiO*t*-Bu, and the carbamate were added to an 8 mL borosilicate glass vial that contained a

magnetic stir bar. Next, DME and the electrophile were added in sequence, the vial was capped with a PTFE-lined septum cap, and the mixture was stirred at room temperature until the solids had dissolved (5 min).

Irradiation of the reaction mixture with a Hg lamp; two-portion procedure. A low-form hemispherical Dewar flask was filled with isopropanol in a well-ventilated fume hood. A magnetic stir bar was added to the Dewar flask, and the isopropanol bath was cooled to –10 °C. The reaction vial was submerged in the isopropanol bath and allowed to cool for 5 min. A 100-watt Hg lamp was placed 4 inches from the vial, and the vial was irradiated for 16 h. Then, the vial was transferred to a nitrogen-filled glovebox, and the reaction mixture was filtered through a PTFE-lined syringe filter into a new 8 mL vial that contained CuBr, ligand **L4.1**, LiO*t*-Bu, and the carbamate. The syringe filter was washed with a small amount of DME (0.1 mL). A magnetic stir bar was added to the vial, and the vial was capped and placed in the –10 °C bath. A 100-watt Hg lamp was placed 4 inches away from the vial, and the sample was irradiated for an additional 24 h.

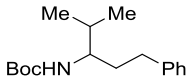

***tert*-Butyl (4-methyl-1-phenylpentan-3-yl)carbamate. Scheme 4.4.** The title compound was synthesized according to General Procedure 2, using CuBr (7.5 mg × 2, 0.052 mmol × 2), ligand **L4.1** (13.5 mg × 2, 0.025 mmol × 2), LiO*t*-Bu (168 mg × 2, 2.1 mmol × 2), $BocNH_2$ (246 mg × 2, 2.1 mmol × 2), and (3-bromo-4-methylpentyl)benzene (168 mg, 0.70 mmol) in DME (8 mL), and purified by column chromatography (5%→30% Et_2O/hexanes). Pale-yellow solid. First run: 128 mg (66%). Second run: 119 mg (61%).

^{1}H NMR (300 MHz, $CDCl_3$) δ 7.30–7.27 (m, 2H), 7.20–7.17 (m, 3H), 4.33 (d, J = 10.4 Hz, 1H), 3.59–3.43 (m, 1H), 2.84–2.46 (m, 2H), 1.89–1.66 (m, 2H), 1.46 (s, 9H), 1.27–1.24 (m, 1H), 0.95–0.83 (m, 6H).

^{13}C NMR (101 MHz, $CDCl_3$) δ 156.1, 142.3, 128.43, 128.41, 125.8, 78.9, 55.5, 34.8, 32.9, 32.4, 28.5, 19.2, 17.7.

FT-IR (film): 3348, 2962, 1694, 1497, 1365, 1247, 1173, 1020, 869, 699 cm^{-1}.

MS (ESI) m/z $(M+Na)^+$ calcd for $C_{17}H_{27}NO_2Na$: 300.2, found: 300.1.

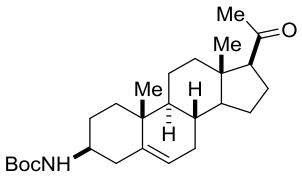

***tert*-Butyl ((3*S*, 8*S*, 9*S*, 10*R*, 13*S*, 14*S*, 17*S*)-17-acetyl-10, 13-dimethyl-2, 3, 4, 7, 8, 9, 10, 11, 12, 13, 14, 15, 16, 17-tetradecahydro-1*H*-cyclopenta[*a*]phenanthren-3-yl)carbamate. Scheme 4.5**. The title compound was synthesized according to General Procedure 2 (except that the method for preparation of a reaction mixture on a Schlenk line for solid electrophiles was used), using CuBr (7.5 mg ×2, 0.052 mmol × 2), ligand **L4.1** (13.5 mg × 2, 0.025 mmol × 2), LiO*t*-Bu (168 mg × 2, 2.1 mmol × 2), $BocNH_2$ (246 mg × 2, 2.1 mmol × 2), and 1-((3*S*,8*S*,9*S*,10*R*,13*S*,14*S*,17*S*)-3-bromo-10,13-dimethyl-2,3,4,7,8,9,10,11,12,13,14,15,16,17-tetradecahydro-1*H*-cyclopenta[*a*]phenanthren-17-yl)ethan-1-one [23, 24] (266 mg, 0.70 mmol) in DME (8 mL), and purified by column chromatography (5%→30% Et_2O/hexanes). The major diastereomer was purified by column chromatography (15%→40% Et_2O/hexanes) and then recrystallization from cold Et_2O/hexanes. White solid. First run: 153 mg (53%; dr before purification: 4.3:1). Second run: 148 mg (51%; dr before purification: 4.6:1). A ^{1}H NMR spectrum of the unpurified

mixture shows 90% conversion of the starting material to the C–N coupled products (**Figure 4.6**). Crystals suitable for X-ray crystallographic analysis were grown by slow evaporation of a saturated solution in Et_2O/hexanes.

Essentially the same results were obtained when the materials were added in a single batch: The title compound was synthesized according to General Procedure 2 (except that the method for preparation of a reaction mixture on a Schlenk line for solid electrophiles was used), using CuBr (15 mg, 0.10 mmol), ligand **L4.1** (27 mg, 0.050 mmol), LiO*t*-Bu (340 mg, 4.2 mmol), $BocNH_2$ (490 mg, 4.2 mmol), and 1-((3*S*, 8*S*, 9*S*, 10*R*, 13*S*, 14*S*, 17*S*)-3-bromo-10,13-dimethyl-2, 3, 4, 7, 8, 9, 10, 11, 12, 13, 14, 15, 16, 17-tetradecahydro-1*H*-cyclopenta[*a*]phenanthren-17-yl)ethan-1-one (266 mg, 0.70 mmol) in DME (8 mL), and purified by column chromatography (5%→30% Et_2O/hexanes). 151 mg (52%). A ^{1}H NMR spectrum of the unpurified mixture shows 90% conversion of the starting material to the C–N coupled products.

^{1}H NMR (400 MHz, $CDCl_3$) δ 5.39–5.33 (m, 1H), 4.40 (br, 1H), 3.36 (br, 1H), 2.53 (t, J = 8.9 Hz, 1H), 2.39–2.28 (m, 1H), 2.23–2.15 (m, 1H), 2.12 (s, 3H), 2.10–1.94 (m, 3H), 1.91–1.81 (m, 2H), 1.72–1.58 (m, 4H), 1.52–1.45 (m, 3H), 1.44 (s, 9H), 1.38–1.08 (m, 4H), 1.06–1.01 (m, 1H), 0.97 (s, 3H), 0.62 (s, 3H).

^{13}C NMR (101 MHz, $CDCl_3$) δ 209.8, 155.3, 140.7, 121.5, 79.2, 63.8, 57.0, 51.0, 50.1, 44.1, 39.8, 39.0, 38.1, 36.7, 32.0, 31.9, 31.7, 29.6, 28.6, 24.6, 23.0, 21.1, 19.5, 13.4.

FT-IR (film): 3371, 2937, 1702, 1514, 1365, 1236, 1172, 733 cm^{-1}.

MS (ESI) m/z $(M+Na)^+$ calcd for $C_{26}H_{41}NO_3Na$: 438.3, found: 438.4.

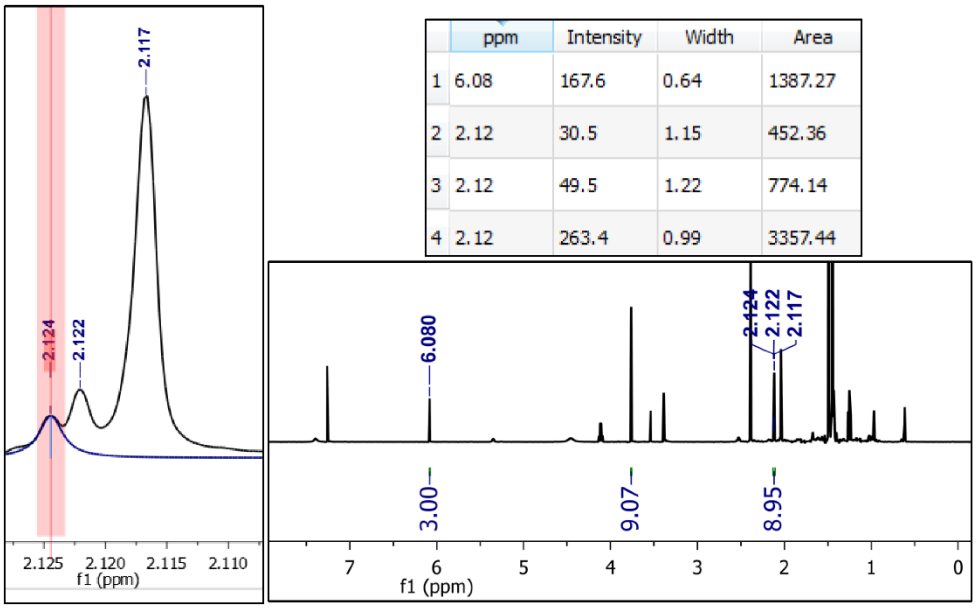

Figure 4.6. ^{1}H NMR spectrum (500 MHz, $CDCl_3$, rt) of the unpurified reaction mixture (pregnenolone-derived electrophile), showing 90% conversion to products (calibrated using 1,3,5-trimethoxybenzene). The relevant resonances are: 1) δ 6.080: 1,3,5-trimethoxybenzene; 2) δ 2.124: remaining starting material; 3) δ 2.122: minor diastereomer of product; 4) δ 2.117: major diastereomer of product.

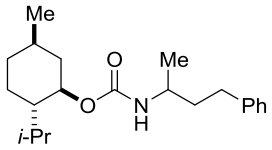

(1R,2S,5R)-2-isopropyl-5-methylcyclohexyl (4-phenylbutan-2-yl)carbamate[25] The title compound was synthesized according to the General Procedure, using CuBr (10 mg, 0.070 mmol), ligand **L4.1** (3.8 mg, 0.0070 mmol), LiO*t*-Bu (168 mg, 2.1 mmol), (1S,2R,5S)-2-isopropyl-5-methylcyclohexyl carbamate (419 mg, 2.1 mmol), and 2-bromo-4-phenylbutane (149 mg, 0.70 mmol) in DME (8 mL), and purified by column chromatography (15%

Et_2O/hexanes). Colorless solid (201 mg, 87% yield). Spectral data for the major diastereomer is shown below.

^{1}H NMR (400 MHz, $CDCl_3$) δ 7.30–7.28 (m, 2H), 7.19–7.17 (m, 3H), 4.67–4.48 (m, 1H), 4.41 (br, 1H), 3.76 (br, 1H), 2.78–2.56 (m, 2H), 2.05 (d, J = 11.8 Hz, 1H), 1.99–1.87 (m, 1H), 1.74 (q, J = 7.4 Hz, 2H), 1.71–1.63 (m, 2H), 1.56–1.45 (m, 1H), 1.30 (t, J = 11.3 Hz, 1H), 1.17 (d, J = 6.5 Hz, 3H), 1.12–0.96 (m, 3H), 0.90 (d, J = 6.6 Hz, 6H), 0.82–0.79 (m, 3H).

^{13}C NMR (101 MHz, $CDCl_3$) δ 156.1, 142.0, 128.54, 128.49, 74.4, 47.6, 41.7, 39.3, 34.5, 32.5, 31.5, 26.6, 23.8, 22.2, 21.6, 20.9, 16.7.

FT-IR (film): 3319, 2951, 1678, 1536, 1251, 1072, 700 cm^{-1}.

MS (EI) m/z $(M)^+$ calcd for $C_{21}H_{33}NO_2$: 331.3, found: 331.3.

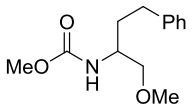

Methyl (1-methoxy-4-phenylbutan-2-yl)carbamate. Scheme 4.8. The title compound was synthesized according to the General Procedure, using CuBr (10 mg, 0.070 mmol), ligand **L4.1** (3.8 mg, 0.0070 mmol), LiO*t*-Bu (168 mg, 2.1 mmol), methyl carbamate (158 mg, 2.1 mmol), and (3-bromo-4-methoxybutyl)benzene (170 mg, 0.70 mmol) in DME (8 mL), and purified by column chromatography (20%→50% Et_2O/hexanes). Colorless oil, 155 mg, 93% yield.

^{1}H NMR (300 MHz, $CDCl_3$) δ 7.30–7.26 (m, 2H), 7.20–7.15 (m, 3H), 4.87 (br, 1H), 3.81 (br, 1H), 3.68 (s, 3H), 3.40 (d, J = 3.5 Hz, 2H), 3.33 (s, 3H), 2.83–2.50 (m, 2H), 1.99–1.68 (m, 2H).

^{13}C NMR (101 MHz, $CDCl_3$) δ 156.8, 141.7, 128.38, 128.36, 125.9, 74.5, 59.1, 52.0, 50.7, 33.9, 32.4.

FT-IR (film): 3327, 2927, 1725, 1653, 1536, 1246, 1125, 1083, 700 cm^{-1}.

MS (EI) m/z $(M)^+$ calcd for $C_{13}H_{19}NO_3$: 237.1, found: 237.1.

4.4.3. Effect of reaction parameters

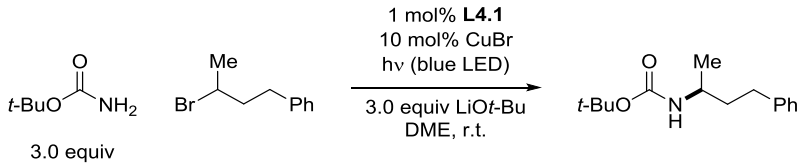

Workup of the irradiated mixture for GC analysis. A 20 mL vial was charged with a measured quantity of an internal standard (*n*-dodecane). The unpurified reaction mixture was then added to the 20 mL vial that contained the internal standard, ensuring quantitative transfer with EtOAc rinses (2 mL × 3). An aliquot was filtered through a pad of silica gel (eluting with EtOAc) into a GC vial, and the sample was subjected to GC analysis. The data are summarized below.

Table 4.5. Effect of reaction parameters – full version.

Entry	Change from the "standard conditions"	Yield[a]
1	None	91%
2	Glovebox-free (Schlenk line)	90%
3	Two 34 W blue LEDs instead of three	80%
4	One 34 W blue LED instead of three	55%
5	100 W Hg lamp instead of blue LED[c]	94%
6	Three 26 W CFLs instead of blue LED[c]	54%
7	2.5 equiv LiO*t*-Bu and $BocNH_2$, instead of 3 equiv	84%
8	2 equiv LiO*t*-Bu and $BocNH_2$, instead of 3 equiv	52%
9	20 mL DME instead of 8 mL	52%
10	4 mL DME instead of 8 mL	73%
11	0.1% **L4.1**, 100 W Hg Lamp[c]	35%
12	$CuBr_2$, instead of CuBr	3%
13	CuI, instead of CuBr	58%
14	CuCl, instead of CuBr	84%
15	5% CuBr instead of 10% CuBr	81%
16	0.5% **L4.1** instead of 1.0%	75%
17	no CuBr	0%
18	no **L4.1**	0%

19	NaO*t*-Bu instead of LiO*t*-Bu	8%
20	KO*t*-Bu instead of LiO*t*-Bu	3%
21	under air	21%
22	THF instead of DME	90%
23	CH_3CN instead of DME	35%
24	Toluene instead of DME	44%
25	2-MeTHF instead of DME	70%
26	no light	0%
27	0.1 equiv H_2O	85%
28	neocuproine instead of **L4.1**	0%
29	1% 3,6-di-*t*-butylcarbazole and 2% P(*t*-Bu)$_3$ instead of **L4.1**	3%
30	1% complex **4.1** instead of 1% **L4.1** and 10% CuBr	33%
31	1% complex **4.1** and 9% CuBr, instead of 1% **L4.1** and 10% CuBr	96%
32	1 equiv H_2O	70%
33	1% $[Ru(bpy)_3][PF_6]_2$ instead of **L4.1**	0%
34	1% $[Ir(dtbbpy)(ppy)_2][PF_6]$ instead of **L4.1**	0%
35	Cu nanoparticle (60–80 nm) instead of CuBr	0%
36	5% CuBr and 0.5% **L4.1** instead of 10% and 1%	65%
37	1% CuBr instead of 10% CuBr	34%
38	0.2% **L4.1**, 100 W Hg Lamp 32 h[b]	59%[c]
39	0.2% **L4.1**, 100 W Hg Lamp 16 h[b]	48%

[a]Average of two runs, based on GC analysis versus an internal standard (*n*-dodecane). [b]Temperature was maintained at 20 °C. [c]38% of 2-bromo-4-phenylbutane remained after the reaction. Bpy = 2,2′-bipyridine; ppy = 2-phenylpyridine; dtbbpy = 4,4′-*t*-butyl-2,2′-bipyridine.

4.4.4. Effect of additives

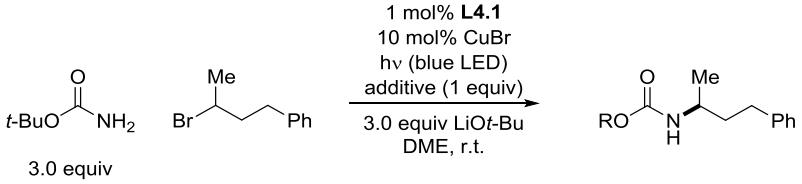

Following General Procedure 2, a standard reaction mixture was prepared in an 8 mL vial, using CuBr (10 mg, 0.070 mmol), ligand **L4.1** (3.8 mg, 0.0070 mmol), LiO*t*-Bu (168 mg, 2.1 mmol), $BocNH_2$ (246 mg, 2.1 mmol), and 2-bromo-4-phenylbutane (149 mg, 0.70 mmol) in DME (8 mL). Next, the additive (0.7 mmol) was added, and the vial was capped and subjected to irradiation with blue LED lamps.

A 20 mL vial was charged with a measured quantity of an internal standard (1,3,5-trimethoxybenzene). The unpurified reaction mixture was then added to the 20 mL vial that contained the internal standard, ensuring quantitative transfer through EtOAc rinses (2 mL ×

3). An aliquot was filtered through a pad of silica gel (eluting with EtOAc) into a GC vial, and the sample was subjected to GC analysis. Another aliquot was concentrated in vacuo, and $CDCl_3$ was added; next, the solids were removed by filtration through a piece of cotton, and the filtrate was subjected to ^1H NMR analysis.

4.4.5. Mechanistic studies

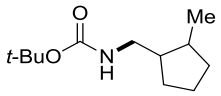

***tert*-Butyl ((2-methylcyclopentyl)methyl)carbamate. Scheme 4.6.** The title compound was synthesized according to the General Procedure, using CuBr (10 mg, 0.070 mmol), ligand **L4.1** (3.8 mg, 0.0070 mmol), Li*O*t-Bu (168 mg, 2.1 mmol), $BocNH_2$ (246 mg, 2.1 mmol), and 6-bromohept-1-ene (124 mg, 0.70 mmol) in DME (8 mL), and purified by column chromatography (7%→30% Et2O/hexanes). Ratio of diastereomers: 4:1, which is consistent with that reported for the cyclization of the derived secondary alkyl radical. Colorless oil. First run: 98 mg (66%). Second run: 94 mg (63%). Spectral data for the major diastereomer is provided below.

^1H NMR (400 MHz, $CDCl_3$) δ 4.52 (s, 1H), 3.18–3.03 (m, 1H), 3.06–2.90 (m, 1H), 2.05–1.99 (m, 1H), 1.93–1.88 (m, 1H), 1.73–1.61 (m, 2H), 1.56–1.45 (m, 2H), 1.39 (s, 9H), 1.32–1.20 (m, 2H), 0.80 (d, J = 7.1 Hz, 3H).

^{13}C NMR (101 MHz, $CDCl_3$) δ 156.1, 79.0, 43.2, 41.7, 35.3, 33.6, 30.4, 28.5, 22.6, 14.9.

FT-IR (film): 3350, 2955, 1694, 1520, 1366, 1250, 1174, 872 cm^{-1}.

MS (ESI) m/z $(M)^+$ calcd for $C_{12}H_{23}NO_2$: 213.2, found: 213.3.

Generation of a Cu(II) complex via independent synthesis

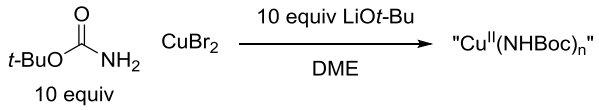

A 4 mL vial was charged with $CuBr_2$ (2.2 mg, 0.0099 mmol), $BocNH_2$ (11.7 mg, 0.10 mmol, 10 equiv), LiO*t*-Bu (8.0 mg, 0.10 mmol, 10 equiv), and a magnetic stir bar. DME (1 mL) was added to the vial, and the mixture was stirred at room temperature for 10 min. An aliquot (0.15 mL) was then transferred to another 4 mL vial that contained 2-MeTHF (0.05 mL), and the mixture was transferred to an EPR tube for X-band EPR measurement at 77 K.

Detection of a Cu(II) intermediate during catalysis

Following General Procedure, a standard reaction mixture was prepared in an 8 mL vial, using CuBr (10 mg, 0.070 mmol), ligand **L4.1** (3.8 mg, 0.0070 mmol), LiO*t*-Bu (168 mg, 2.1 mmol), $BocNH_2$ (246 mg, 2.1 mmol), and 2-bromo-4-phenylbutane (149 mg, 0.70 mmol) in DME (8 mL). The vial was then subjected to irradiation with blue LED lamps. After 4 h, an aliquot (0.2 mL) was transferred via syringe to a 4 mL vial that contained a mixture of DME (0.6 mL) and 2-MeTHF (0.2 mL) under nitrogen. The diluted reaction mixture was then transferred via syringe under nitrogen to an EPR tube for X-band EPR measurement at 77 K.

Generation of a Cu(II) complex via chemical oxidation

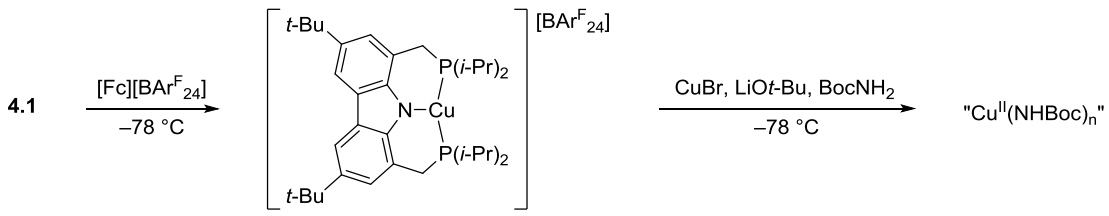

In two separate vials, solutions of complex **4.1** (0.6 mg, 0.001 mmol, 1 equiv) in 2-MeTHF (0.5 mL) and of [Fc][BAr$^F_{24}$] (2.0 mg, 0.0019 mmol, 2 equiv) in 2-MeTHF (0.5 mL) were prepared at –78 °C. The solution of [Fc][BAr$^F_{24}$] was added dropwise to the solution of **4.1** at –78 °C. After stirring for 1 h, the formation of the cation **3.7** was confirmed by EPR spectroscopy (**Figure 4.7**, left). The solution was then transferred to a pre-chilled solution of CuBr (0.6 mg, 0.004 mmol), LiO*t*-Bu (6 mg, 0.08 mmol), and $BocNH_2$ (16 mg, 0.14 mmol) in 2-MeTHF (0.5 mL). The reaction mixture was then transferred to an EPR tube for X-band EPR measurement at 77 K. The EPR signal shows the complete conversion of the cation **3.7** to the Cu(II) intermediate detected during catalysis (**Figure 4.7**, right).

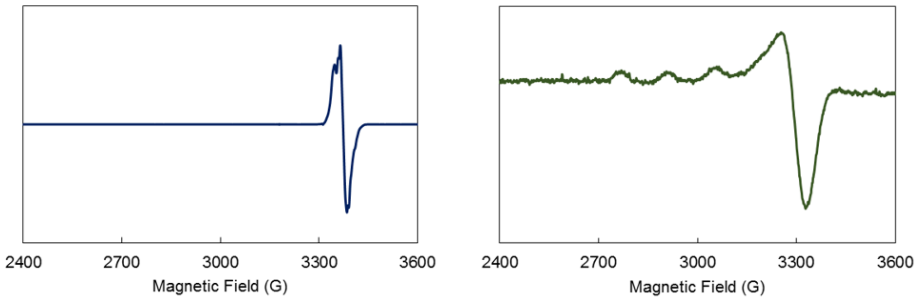

Figure 4.7. EPR spectra (9.4 GHz, 77 K, 2-MeTHF). Left: oxidation product of complex **4.1**. Right: Cu(II) intermediate produced by the chemical oxidation of the mixture of CuBr, LiO*t*-Bu, and $BocNH_2$ by the in situ generated cation **3.7**.

Monitoring the reaction mixture via mass spectrometry

Following General Procedure 2, a standard reaction mixture was prepared in an 8 mL vial, using CuBr (10 mg, 0.070 mmol), ligand **L4.1** (3.8 mg, 0.0070 mmol), LiO*t*-Bu (168 mg, 2.1 mmol), $BocNH_2$ (246 mg, 2.1 mmol), and 2-bromo-4-phenylbutane (149 mg, 0.70 mmol) in DME (8 mL). The reaction mixture was subjected to irradiation with blue LED lamps for 4 h. Next, the vial was then transferred to a nitrogen-filled glovebox, and an aliquot was passed through a PTFE syringe filter into a 4 mL vial. The filtrate was diluted and subjected to ESI analysis. A signal corresponding to copper complex **4.1** (m/z = 601.4) was detected (**Figure 4.8**). The presence of a signal at m/z = 734.3 is consistent with the N–alkylation of complex **4.1**.

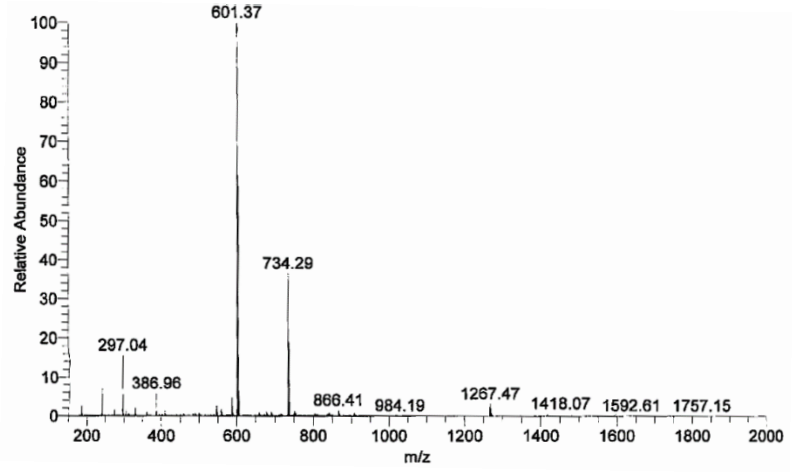

Figure 4.8. ESI-MS trace of a standard reaction mixture after 4 h of irradiation.

Preparation of the N-methyl-substituted variant of L4.1

Yields were not optimized.

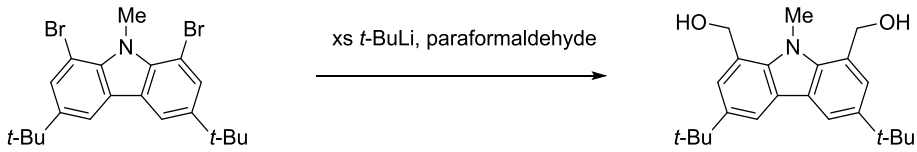

In a 250 mL Schlenk flask, 1,8-dibromo-3,6-di-*t*-butyl-9-methyl-carbazole[26] (2.6 g, 5.8 mmol) was dissolved in 75 mL of dry, degassed Et_2O. The solution was cooled to –78 °C, and *t*-BuLi (1.7 M in pentane, 15 mL, 25 mmol) was added slowly under N_2. The mixture was stirred at –78 °C for 2 h, and paraformaldehyde (0.7 g) was added in one portion at –78 °C. The reaction was allowed to warm to ambient temperature overnight. The organic layer was carefully washed with water (50 mL) and dried over $MgSO_4$. The drying agent was removed by filtration, and the filtrate was concentrated in vacuo. The crude residue was purified by column chromatography (35% → 80 % EtOAc/hexanes) to yield the title compound as white solid (2 g, 93% yield).

^{1}H NMR (300 MHz, $CDCl_3$) δ 8.05 (d, J = 2.0 Hz, 2H), 7.39 (d, J = 2.0 Hz, 2H), 5.11 (s, 4H), 4.45 (s, 3H), 1.45 (s, 18H).

^{13}C NMR (75 MHz, C_6D_6) δ 141.6, 139.0, 124.6, 122.6, 116.5, 62.8, 53.3, 34.5, 32.0.

FT-IR (film): 3263 (br), 2954, 2867, 1489, 1466, 1417, 1363, 1301, 1239, 1069, 1029, 1018, 873 cm^{-1}.

MS (ESI) m/z $(M+H)^+$ calcd for $C_{23}H_{31}NO_2$:354.2, found: 354.2.

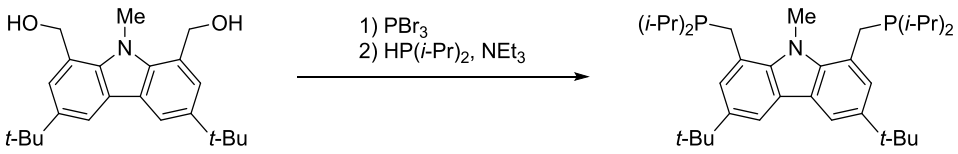

A 100 mL roundbottom flask was charged with (3,6-di-*t*-butyl-9-methyl-carbazole-1,8-diyl)dimethanol (1.9 g, 5.4 mmol) and a magnetic stir bar. Dry, degassed dichloromethane (50 mL) was added to the vessel, and the solution was cooled 0 °C under N_2. At 0 °C, PBr_3 (3 g, 11 mmol) was added slowly via syringe, and the reaction was stirred for 1 h at 0 °C. The reaction was quenched with saturated $NaHCO_{3(aq)}$ (50 mL), and the organic layer was washed with brine (50 mL), dried over MgSO4, and filtered. The filtrate was concentrated in vacuo to give pale yellow solid. A portion of this pale yellow solid (960 mg) was transferred to a 40 mL scintillation vial charged with a magnetic stir bar and dry, degassed dichloromethane (20 mL). HP(*i*-Pr)$_2$ (520 mg, 4.4 mmol) was added slowly to the stirring solution at room temperature, and the solution was allowed to stir for an additional hour. Triethylamine (1 mL) was then added to quench the reaction, and the volatiles were removed in vacuo after 10 min of stirring at room temperature. The solid residue was extracted with Et_2O (15 mL), filtered, and concentrated in vacuo. NMR spectra of the residue show the clean formation of the title compound, which can be further purified by recrystallization in Et_2O/CH_3CN at –30 °C to yield colorless solid (520 mg, 40% yield over two steps).

^{1}H NMR (400 MHz, C_6D_6) δ 8.13 (s, 2H), 7.57 (s, 2H), 4.32 (s, 3H), 3.21 (s, 4H), 1.66 (p, J = 7.1, 6.6 Hz, 2H), 1.48 (s, 18H), 0.99 (ddd, J = 18.9, 11.9, 7.1 Hz, 24H).

^{13}C NMR (101 MHz, C_6D_6) δ 142.4, 141.8, 126.0, 122.7, 122.6, 114.3, 37.6 (t, J = 11.6 Hz), 34.7, 32.1, 28.7 (d, J = 22.6 Hz), 23.8 (d, J = 17.0 Hz), 19.7 (dd, J = 24.1, 12.9 Hz).

^{31}P NMR (162 MHz, C_6D_6) δ 6.99.

FT-IR (film): 2951, 2866, 1488, 1458, 1393, 1363, 1320, 1296, 1237, 867 cm^{-1}.

MS (ESI) m/z $(M+H)^+$ calcd for $C_{35}H_{57}NP_2$: 554.4, found: 554.3.

Monitoring the reaction mixture via ^{31}P NMR spectroscopy. Following General Procedure 2, a standard reaction mixture was prepared in an 8 mL vial, using CuBr (10 mg, 0.070 mmol), ligand **L4.1** (3.8 mg, 0.0070 mmol), LiO*t*-Bu (168 mg, 2.1 mmol), $BocNH_2$ (246 mg, 2.1 mmol), and 2-bromo-4-phenylbutane (149 mg, 0.70 mmol) in DME (8 mL). An aliquot was transferred to an NMR tube under nitrogen, and a ^{31}P NMR spectrum was collected before irradiation (**Figure 4.9**, top). The remaining reaction mixture was subjected to irradiation with blue LED lamps for 4 h. The vial was then transferred to a nitrogen-filled glovebox, and an aliquot was transferred to an NMR tube analysis (**Figure 4.9**, middle).

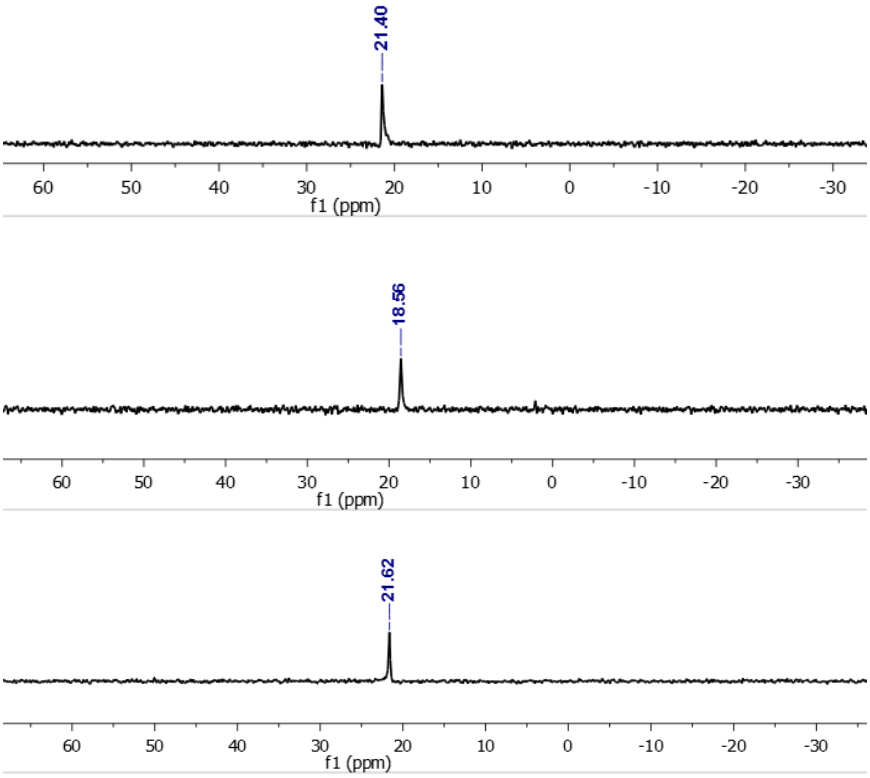

Figure 4.9. ^{31}P NMR spectra (162 MHz, rt). Top: reaction mixture in DME prior to irradiation; middle: reaction mixture in DME after 4 h of irradiation; bottom: complex **4.1** in DME.

Light-on-light-off study. Following General Procedure 2, six standard reaction mixtures in 8 mL vials were prepared, using CuBr (10 mg, 0.070 mmol), ligand **L4.1** (3.8 mg, 0.0070 mmol), LiO*t*-Bu (168 mg, 2.1 mmol), $BocNH_2$ (246 mg, 2.1 mmol), and 2-bromo-4-phenylbutane (149 mg, 0.70 mmol) in DME (8 mL). The six 8 mL vials were then subjected to irradiation with blue LED lamps. After 2 h, the lamps were turned off, and one vial was removed from the irradiation setup for analysis. The remaining five vials were stirred in the absence of light in the water bath for an additional 2 h. Then, one vial was removed for analysis, and the lamps were turned back on to irradiate the remaining four reaction mixtures. After an additional 2 h of irradiation, the lamps were turned off, and one vial was removed for analysis. The remaining three vials were stirred in the absence of light in the water bath for an additional 2 h. Then, a vial was removed for analysis, and the lamps were turned back on to irradiate the remaining two reaction mixtures. After 2 h, the lamps were turned off, and one vial was removed for analysis. The last vial was stirred in the absence of light in the water bath for an additional 2 h, and then it was analyzed.

Workup for ^{1}H NMR analysis. A 20 mL vial was charged with a measured quantity of an internal standard (1,3,5-trimethoxybenzene). The unpurified reaction mixture was then added to the 20 mL vial that contained the internal standard, ensuring quantitative transfer through EtOAc rinses (2 mL × 3). An aliquot was concentrated in vacuo, and $CDCl_3$ was added. Next, the solids were removed by filtration through a piece of cotton, and the filtrate was subjected to ^{1}H NMR analysis.

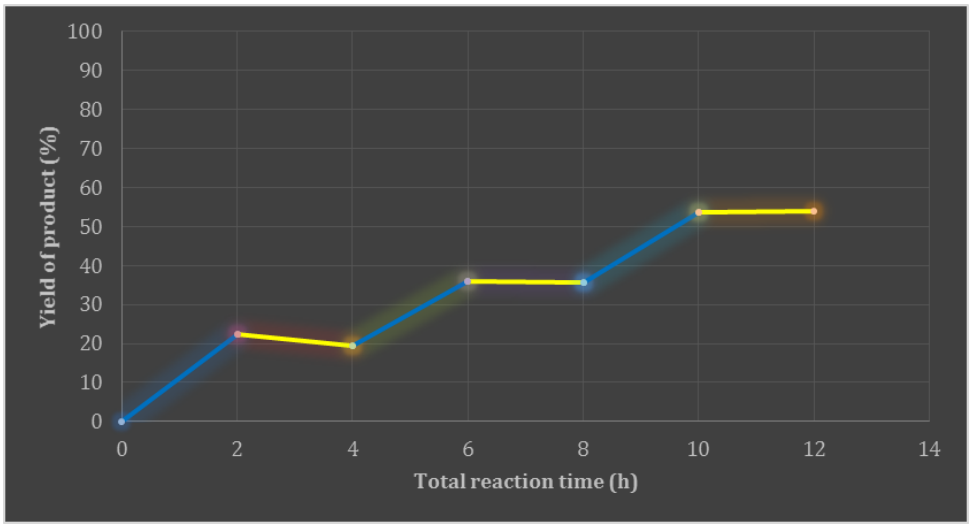

Figure 4.10. Effect of illumination on product formation. Blue lines denote periods during which the blue LED lamps were on, whereas yellow lines denote periods during which the lamps were off.

Table 4.6. Product formation as a function of time. All data are the average of two runs.

Total reaction period (h)	Total illumination period (h)	Yield
2	2	22%
4	2	19%
6	4	36%
8	4	36%
10	6	54%
12	6	54%

Detection of a copper(II) intermediate during catalysis. Following General Procedure 2, a standard reaction mixture was prepared in an 8 mL vial, using CuBr (10 mg, 0.070 mmol), ligand **L4.1** (3.8 mg, 0.0070 mmol), LiO*t*-Bu (168 mg, 2.1 mmol), $BocNH_2$ (246 mg, 2.1 mmol), and 2-bromo-4-phenylbutane (149 mg, 0.70 mmol) in DME (8 mL). The vial was then subjected to irradiation with blue LED lamps. After 4 h, an aliquot (0.2 mL) was transferred via syringe to a 4 mL vial that contained a mixture of DME (0.6 mL) and 2-

MeTHF (0.2 mL) under nitrogen. The diluted reaction mixture was then transferred via syringe under nitrogen to an EPR tube for X-band EPR measurement at 77 K.

Generation of a copper(II) complex via independent synthesis. A 4 mL vial was charged with $CuBr_2$ (2.2 mg, 0.0099 mmol), $BocNH_2$ (11.7 mg, 0.10 mmol, 10 equiv), Li*O*t-Bu (8.0 mg, 0.10 mmol, 10 equiv), and a magnetic stir bar. DME (1 mL) was added to the vial, and the mixture was stirred at room temperature for 10 min. An aliquot (0.15 mL) was then transferred to another 4 mL vial that contained 2-MeTHF (0.05 mL), and the mixture was transferred to an EPR tube for X-band EPR measurement at 77 K. Simulated values are as follows: g = [2.276, 2.063, 2.058], A_{Cu} (MHz) = [0, 0, 439], lw = 6.2 MHz.

4.4.6. Stereoselective N–alkylations of ammonia surrogates

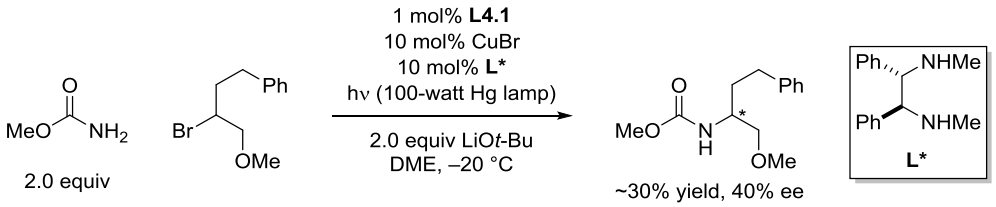

A 4 mL vial was charged with CuBr (1.4 mg, 0.01 mmol), ligand **L4.1** (0.5 mg, 0.0001 mmol), Li*O*t-Bu (16 mg, 0.20 mmol), methyl carbamate (16 mg, 0.21 mmol), and ligand **L*** (2.4 mg, 0.01 mmol), and a magnetic stir bar. Next, DME (4 mL) was added, followed by (3-bromo-4-methoxybutyl)benzene (24 mg, 0.1 mmol). The vial was capped, and subjected to irradiation under 100-watt Hg lamp at –20 °C for 48 h. Then, a 20 mL vial was charged with a measured quantity of an internal standard (*n*-dodecane). The unpurified reaction mixture was then added to the 20 mL vial that contained the internal standard, ensuring quantitative transfer through EtOAc rinses (2 mL × 3). An aliquot was filtered through a pad of silica gel (eluting with EtOAc) into a GC vial, and the sample was subjected to GC analysis. The remainder of the crude mixture was concentrated in vacuo, and the

residue was loaded on a 20 cm × 20 cm TLC plate. Next, the loaded TLC plate was developed using 30% EtOAc/hexanes, and the band containing the target product was isolated and filtered (10% IPA/*n*-hexane). The filtrate was then subjected to HPLC analysis on a chiral IC column.

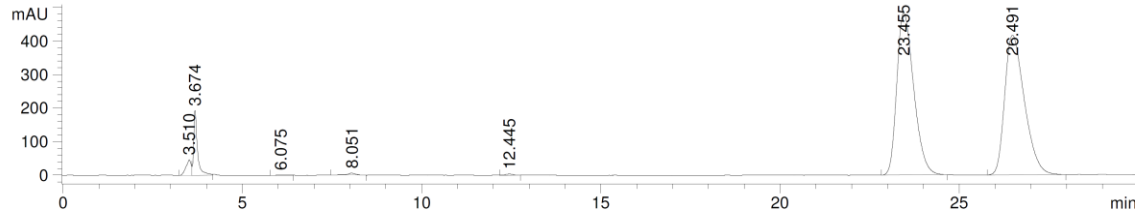

Figure 4.11. HPLC trace of methyl (1-methoxy-4-phenylbutan-2-yl)carbamate (racemate, IC-column, 2% IPA/*n*-hexane).

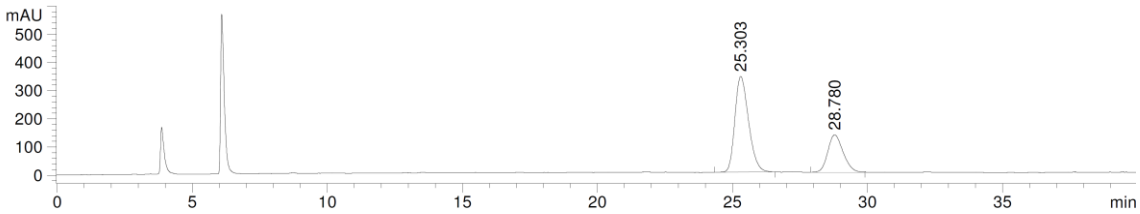

Figure 4.12. HPLC trace of methyl (1-methoxy-4-phenylbutan-2-yl)carbamate (40% ee, IC-column, 2% IPA/*n*-hexane).

4.4.7. X-ray crystallographic data

Starting material of Scheme 4.5

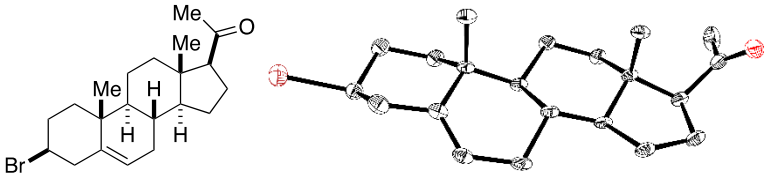

Table 4.7. Crystal data and structure refinement for the starting material of **Scheme 4.5**.

Empirical formula	$C_{21}H_{31}BrO$
Formula weight	379.37
Temperature/K	99.98
Crystal system	orthorhombic
Space group	$P2_12_12_1$
a/Å	7.8610(3)
b/Å	9.0451(4)
c/Å	25.8041(14)
α/°	90
β/°	90
γ/°	90
Volume/Å^3	1834.76(15)
Z	4
ρ_{calc}g/cm^3	1.373
μ/mm^{-1}	2.244
F(000)	800.0
Crystal size/mm^3	0.25 × 0.2 × 0.2
Radiation	MoKα (λ = 0.71073)
2Θ range for data collection/°	4.772 to 54.996
Index ranges	$-10 \leq h \leq 10$, $-11 \leq k \leq 11$, $-33 \leq l \leq 33$
Reflections collected	37018
Independent reflections	4211 [R_{int} = 0.0499, R_{sigma} = 0.0305]
Data/restraints/parameters	4211/0/211
Goodness-of-fit on F^2	1.026
Final R indexes [I>=2σ (I)]	R_1 = 0.0178, wR_2 = 0.0432
Final R indexes [all data]	R_1 = 0.0217, wR_2 = 0.0437
Largest diff. peak/hole / e Å^{-3}	0.20/-0.34
Flack parameter	0.014(3)

Table 4.8. Fractional Atomic Coordinates ($\times 10^4$) and Equivalent Isotropic Displacement Parameters ($Å^2 \times 10^3$) for the starting material of **Scheme 4.5**. U_{eq} is defined as 1/3 of the trace of the orthogonalized U_{IJ} tensor.

Atom	*x*	*y*	*z*	U(eq)
Br01	2873.2(3)	5669.1(2)	3912.8(2)	28.31(6)
O002	8717.5(18)	2250.2(16)	8237.1(6)	31.7(3)
C003	6019.1(19)	4977.8(19)	6132.5(7)	16.1(3)
C004	8859(2)	4720(2)	5713.6(8)	20.9(4)
C005	5895(2)	4900(2)	7129.5(8)	18.8(4)
C006	8578.1(19)	4342(2)	6674.0(7)	16.6(3)
C007	6244(2)	4752.5(19)	5161.3(8)	19.1(4)
C008	7730(2)	4141.5(18)	6151.6(7)	16.7(3)
C009	4036(2)	5884(2)	4588.6(7)	21.1(4)
C00A	7928(2)	4846.8(19)	5212.0(7)	21.0(4)
C00B	7456.4(19)	3901.4(19)	7136.7(7)	16.1(4)
C00C	5037(2)	4654(2)	5625.4(7)	16.5(4)
C00D	8734(2)	4156(2)	7592.5(7)	18.2(4)
C00E	6935(2)	2267.2(19)	7122.4(8)	19.8(4)
C00F	5425(2)	4726(2)	4632.2(8)	24.3(4)
C00G	2742(2)	5762(2)	5023.1(7)	22.7(4)
C00H	3657(2)	5853(2)	5543.2(7)	20.9(4)
C00I	4916(2)	4733(2)	6619.7(7)	19.0(4)
C00J	4197(2)	3111(2)	5632.4(8)	22.6(4)
C00K	8186(2)	3436(2)	8094.3(8)	22.5(4)
C00L	10456(2)	3602(2)	7373.0(8)	21.8(4)
C00M	10266(2)	3548(2)	6779.2(8)	21.7(4)
C00N	6861(3)	4245(3)	8408.8(8)	36.1(5)

Table 4.9. Anisotropic Displacement Parameters ($Å^2 \times 10^3$) for the starting material of **Scheme 4.5**. The anisotropic displacement factor exponent takes the form: $-2\pi^2[h^2a^{*2}U_{11}+2hka^*b^*U_{12}+\ldots]$.

Atom	U_{11}	U_{22}	U_{33}	U_{23}	U_{13}	U_{12}
Br01	32.93(10)	26.75(10)	25.26(10)	-0.08(8)	-4.07(9)	0.64(9)
O002	26.0(7)	25.2(8)	43.8(10)	11.8(7)	-1.6(7)	1.2(7)
C003	10.5(7)	13.3(8)	24.3(10)	0.5(7)	4.0(7)	2.3(6)
C004	12.0(7)	19.2(10)	31.4(11)	4.3(7)	7.7(7)	2.2(7)
C005	13.1(7)	20.6(9)	22.6(10)	-1.2(7)	3.7(7)	4.6(7)
C006	9.9(6)	11.1(7)	28.7(10)	1.2(8)	3.9(6)	-0.2(8)
C007	18.8(8)	14.3(9)	24.1(11)	1.3(7)	6.1(8)	3.0(8)
C008	11.0(6)	13.6(8)	25.5(9)	0.8(7)	4.9(7)	0.0(7)
C009	22.1(8)	18.8(10)	22.5(10)	0.9(7)	-0.8(7)	-1.1(8)
C00A	19.2(8)	17.8(8)	26(1)	3.3(7)	8.9(8)	2.5(9)
C00B	11.3(8)	12.3(8)	24.6(10)	0.0(6)	1.4(6)	0.3(6)
C00C	12.9(7)	14.2(9)	22.3(10)	0.0(6)	4.6(7)	0.0(7)
C00D	13.4(7)	12.2(9)	29.1(10)	-1.0(7)	-1.0(7)	1.0(7)
C00E	17.0(8)	15.0(8)	27.4(10)	1.8(7)	3.2(7)	-3.4(8)
C00F	24.3(9)	23.6(11)	25.1(11)	0.6(7)	6.8(8)	3.4(8)

C00G	17.3(7)	24.7(9)	26.1(9)	-1.7(8)	-0.5(7)	2.9(10)
C00H	15.3(7)	23.3(10)	24(1)	-2.7(8)	1.8(7)	4.5(8)
C00I	11.2(7)	22.6(10)	23.2(11)	0.6(7)	4.0(7)	3.0(7)
C00J	21.9(9)	18.8(10)	27.3(12)	0.1(7)	1.2(7)	-5.3(8)
C00K	16.1(8)	21.5(9)	29.8(11)	0.3(7)	-4.4(7)	-0.7(8)
C00L	11.6(7)	17.7(9)	36.2(12)	-1.0(8)	-1.2(7)	1.0(7)
C00M	10.6(7)	20.2(10)	34.3(12)	1.9(8)	2.5(7)	1.5(7)
C00N	38.9(11)	46.1(13)	23.5(11)	2.9(10)	0.7(8)	14.7(12)

Table 4.10. Bond lengths for the starting material of **Scheme 4.5**.

Atom	Atom	Length/Å	Atom	Atom	Length/Å
Br01	C009	1.9784(19)	C007	C00C	1.531(2)
O002	C00K	1.209(2)	C007	C00F	1.510(3)
C003	C008	1.544(2)	C009	C00F	1.517(2)
C003	C00C	1.547(3)	C009	C00G	1.518(3)
C003	C00I	1.543(2)	C00B	C00D	1.564(2)
C004	C008	1.529(2)	C00B	C00E	1.534(2)
C004	C00A	1.491(3)	C00C	C00H	1.549(2)
C005	C00B	1.524(2)	C00C	C00J	1.543(3)
C005	C00I	1.531(3)	C00D	C00K	1.512(3)
C006	C008	1.515(2)	C00D	C00L	1.550(2)
C006	C00B	1.537(2)	C00G	C00H	1.525(2)
C006	C00M	1.533(2)	C00K	C00N	1.509(3)
C007	C00A	1.333(2)	C00L	C00M	1.540(3)

Table 4.11. Bond angles for the starting material of **Scheme 4.5**.

Atom	Atom	Atom	Angle/°	Atom	Atom	Atom	Angle/°
C008	C003	C00C	111.66(14)	C006	C00B	C00D	100.22(13)
C00I	C003	C008	113.14(15)	C00E	C00B	C006	112.61(15)
C00I	C003	C00C	112.41(13)	C00E	C00B	C00D	109.36(14)
C00A	C004	C008	112.52(15)	C007	C00C	C003	109.94(14)
C00B	C005	C00I	110.89(15)	C007	C00C	C00H	106.63(15)
C008	C006	C00B	114.07(13)	C007	C00C	C00J	109.08(15)
C008	C006	C00M	118.82(15)	C00H	C00C	C003	109.44(14)
C00M	C006	C00B	103.74(15)	C00J	C00C	C003	112.01(15)
C00A	C007	C00C	122.87(19)	C00J	C00C	C00H	109.60(14)
C00A	C007	C00F	120.88(18)	C00K	C00D	C00B	113.42(14)
C00F	C007	C00C	116.25(16)	C00K	C00D	C00L	115.01(15)
C004	C008	C003	108.31(14)	C00L	C00D	C00B	103.79(15)
C006	C008	C003	110.68(14)	C007	C00F	C009	111.28(16)
C006	C008	C004	111.19(14)	C009	C00G	C00H	109.28(15)
C00F	C009	Br01	109.27(13)	C00G	C00H	C00C	114.40(15)
C00G	C009	Br01	109.54(12)	C005	C00I	C003	113.79(14)
C00G	C009	C00F	112.18(16)	O002	C00K	C00D	122.99(18)
C007	C00A	C004	124.59(18)	O002	C00K	C00N	120.3(2)
C005	C00B	C006	107.39(14)	C00N	C00K	C00D	116.66(17)
C005	C00B	C00D	116.06(15)	C00M	C00L	C00D	106.83(14)
C005	C00B	C00E	110.82(14)	C006	C00M	C00L	104.16(15)

Product of **Scheme 4.5**

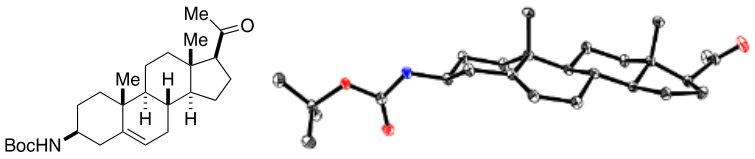

Table 4.12. Crystal data and structure refinement for the product of **Scheme 4.5**.

Empirical formula	$C_{26}H_{41}NO_3$
Formula weight	415.60
Temperature/K	100.02
Crystal system	orthorhombic
Space group	$P2_12_12_1$
a/Å	6.1123(3)
b/Å	19.6726(8)
c/Å	20.4876(8)
α/°	90
β/°	90
γ/°	90
Volume/Å^3	2463.53(18)
Z	4
ρ_{calc}g/cm^3	1.121
μ/mm^{-1}	0.072
F(000)	912.0
Crystal size/mm^3	0.6 × 0.1 × 0.05
Radiation	MoKα (λ = 0.71073)
2Θ range for data collection/°	4.484 to 68.706
Index ranges	$-9 \le h \le 9$, $-30 \le k \le 30$, $-31 \le l \le 30$
Reflections collected	52546
Independent reflections	9627 [R_{int} = 0.0600, R_{sigma} = 0.0711]
Data/restraints/parameters	9627/0/284
Goodness-of-fit on F^2	1.030
Final R indexes [I>=2σ (I)]	R_1 = 0.0562, wR_2 = 0.1152
Final R indexes [all data]	R_1 = 0.0860, wR_2 = 0.1256
Largest diff. peak/hole / e Å^{-3}	0.37/-0.28
Flack parameter	-0.1(3)

Table 4.13. Fractional Atomic Coordinates (×10^4) and Equivalent Isotropic Displacement Parameters (Å^2×10^3) for the product of **Scheme 4.5**. U_{eq} is defined as 1/3 of the trace of the orthogonalized U_{IJ} tensor.

Atom	*x*	*y*	*z*	U(eq)
O(001)	857(2)	8171.2(6)	2159.5(6)	13.8(3)

O(002)	81(2)	8170.0(7)	3250.1(6)	17.5(3)
O(003)	10051(3)	3536.6(7)	6814.1(8)	23.7(3)
N(004)	2602(3)	7454.0(7)	2801.6(7)	14.0(3)
C(005)	1081(3)	7950.1(8)	2784.8(9)	11.7(3)
C(006)	8283(3)	3795.3(9)	6710.5(9)	14.1(3)
C(007)	7807(3)	5795.8(8)	5145.8(8)	9.8(3)
C(008)	7603(3)	4694.7(8)	5816.5(8)	9.6(3)
C(009)	9286(3)	4305.1(9)	5403.7(9)	12.7(3)
C(00A)	7410(3)	6931.2(9)	4587.8(9)	13.7(3)
C(00B)	6174(3)	6661.2(8)	4121.6(9)	10.7(3)
C(00C)	5538(3)	5642.9(8)	4851.6(8)	9.2(3)
C(00D)	5290(3)	4567.4(9)	5568.5(9)	12.1(3)
C(00E)	5265(3)	5939.7(8)	4151.2(8)	9.3(3)
C(00F)	7972(3)	5468.2(8)	5817.5(8)	10.5(3)
C(00G)	4973(3)	4878.6(8)	4887.9(9)	12.2(3)
C(00H)	8022(3)	4544.5(8)	6553.2(8)	11.4(3)
C(00I)	2791(3)	5971.6(9)	3991.7(9)	13.2(3)
C(00J)	2235(3)	6351.2(9)	3361.7(9)	13.9(3)
C(00K)	8114(3)	6565.6(9)	5195.6(9)	13.6(3)
C(00L)	10086(3)	5567.9(9)	6209.2(9)	14.8(3)
C(00M)	3106(3)	7076.6(9)	3397.5(9)	12.9(3)
C(00N)	5580(3)	7073.8(9)	3521.8(9)	13.3(3)
C(00O)	-721(3)	8712.0(9)	2001.6(9)	14.1(3)
C(00P)	6442(3)	5499.4(9)	3637.3(9)	13.0(3)
C(00Q)	10026(3)	4987.5(9)	6725.0(9)	14.6(3)
C(00R)	-3049(3)	8472.5(10)	2128.6(10)	18.8(4)
C(00S)	-171(4)	9357.1(9)	2374.3(10)	19.6(4)
C(00T)	6218(4)	3379.3(10)	6735.3(11)	22.7(4)
C(00U)	-323(4)	8817.4(10)	1277.9(10)	23.2(4)

Table 4.14. Anisotropic Displacement Parameters ($Å^2 \times 10^3$) for the product of **Scheme 4.5**. The anisotropic displacement factor exponent takes the form: $-2\pi^2[h^2a^{*2}U_{11}+2hka^*b^*U_{12}+\ldots]$.

Atom	**U_{11}**	**U_{22}**	**U_{33}**	**U_{23}**	**U_{13}**	**U_{12}**
O(001)	17.0(7)	12.3(5)	12.0(6)	3.4(5)	0.5(5)	4.2(5)
O(002)	21.0(7)	18.2(6)	13.3(6)	1.5(5)	0.8(6)	5.8(6)
O(003)	21.2(8)	21.1(7)	28.9(8)	7.6(6)	-1.8(7)	6.3(6)
N(004)	17.9(8)	14.0(6)	10.1(6)	1.7(5)	0.0(6)	4.7(6)
C(005)	13.2(9)	9.5(7)	12.3(8)	2.0(6)	-2.1(7)	-1.5(6)
C(006)	17.8(9)	15.7(8)	8.8(7)	1.4(6)	0.8(7)	1.2(7)
C(007)	10.4(8)	9.6(7)	9.5(7)	0.5(5)	-0.7(6)	-2.1(6)
C(008)	9.2(8)	9.8(7)	9.6(7)	1.0(5)	0.2(6)	-0.1(6)
C(009)	12.3(8)	12.7(7)	13.0(8)	-1.9(6)	1.5(6)	0.5(6)
C(00A)	16.4(9)	10.1(7)	14.6(8)	2.0(6)	-0.7(7)	-1.7(6)
C(00B)	9.8(8)	9.7(7)	12.5(8)	0.6(6)	2.1(6)	0.3(6)
C(00C)	8.9(8)	9.8(7)	8.8(7)	0.9(5)	-0.6(6)	0.1(6)
C(00D)	9.5(8)	13.3(7)	13.5(8)	4.4(6)	-1.5(7)	-3.3(6)
C(00E)	8.3(8)	10.7(7)	8.9(7)	1.0(5)	0.7(6)	0.1(6)
C(00F)	9.9(8)	11.0(7)	10.5(7)	-0.6(6)	0.5(6)	-0.5(6)
C(00G)	11.1(8)	12.5(7)	13.2(8)	2.9(6)	-2.4(7)	-4.3(6)
C(00H)	11.7(8)	12.0(7)	10.4(7)	1.6(6)	0.1(6)	-0.2(6)
C(00I)	11.0(9)	13.6(7)	15.0(8)	3.6(6)	-0.9(7)	-1.6(6)
C(00J)	11.7(9)	15.0(7)	15.1(8)	3.9(6)	-2.6(7)	0.5(6)
C(00K)	16.8(9)	10.8(7)	13.2(8)	-0.3(6)	-3.2(7)	-2.6(7)

C(00L)	16.4(9)	14.3(7)	13.7(8)	0.3(6)	-3.8(7)	-2.5(7)
C(00M)	13.8(9)	12.9(7)	12.0(8)	2.6(6)	-0.2(7)	1.8(6)
C(00N)	14.7(9)	11.7(7)	13.3(8)	2.6(6)	-0.9(7)	-2.7(6)
C(00O)	16.9(9)	11.8(7)	13.5(8)	2.5(6)	-2.1(7)	2.3(6)
C(00P)	15.8(9)	11.6(7)	11.6(8)	-1.2(6)	1.9(7)	0.6(6)
C(00Q)	14.8(9)	16.9(8)	12.1(7)	0.3(6)	-2.4(7)	-2.4(7)
C(00R)	15.8(10)	18.6(8)	22(1)	-0.2(7)	-3.8(8)	0.4(7)
C(00S)	23.7(10)	11.8(7)	23.4(10)	-0.5(7)	-0.2(9)	-0.7(7)
C(00T)	23.7(11)	16.9(8)	27.5(10)	6.7(8)	-0.9(9)	-2.4(8)
C(00U)	33.3(13)	22.1(9)	14.3(9)	6.1(7)	0.7(8)	4.7(9)

Table 4.15. Bond lengths for the product of **Scheme 4.5**.

Atom	Atom	Length/Å	Atom	Atom	Length/Å
O(001)	C(005)	1.360(2)	C(00B)	C(00E)	1.525(2)
O(001)	C(00O)	1.472(2)	C(00B)	C(00N)	1.517(2)
O(002)	C(005)	1.212(2)	C(00C)	C(00E)	1.558(2)
O(003)	C(006)	1.213(2)	C(00C)	C(00G)	1.544(2)
N(004)	C(005)	1.348(2)	C(00D)	C(00G)	1.535(2)
N(004)	C(00M)	1.462(2)	C(00E)	C(00I)	1.548(3)
C(006)	C(00H)	1.517(2)	C(00E)	C(00P)	1.541(2)
C(006)	C(00T)	1.505(3)	C(00F)	C(00L)	1.533(3)
C(007)	C(00C)	1.542(2)	C(00H)	C(00Q)	1.544(3)
C(007)	C(00F)	1.523(2)	C(00I)	C(00J)	1.529(2)
C(007)	C(00K)	1.529(2)	C(00J)	C(00M)	1.525(2)
C(008)	C(009)	1.537(2)	C(00L)	C(00Q)	1.556(2)
C(008)	C(00D)	1.523(3)	C(00M)	C(00N)	1.533(3)
C(008)	C(00F)	1.538(2)	C(00O)	C(00R)	1.521(3)
C(008)	C(00H)	1.559(2)	C(00O)	C(00S)	1.519(3)
C(00A)	C(00B)	1.329(3)	C(00O)	C(00U)	1.517(3)
C(00A)	C(00K)	1.501(2)			

Table 4.16. Bond angles for the product of **Scheme 4.5**.

Atom	Atom	Atom	Angle/°	Atom	Atom	Atom	Angle/°
C(005)	O(001)	C(00O)	120.29(14)	C(00B)	C(00E)	C(00P)	109.02(14)
C(005)	N(004)	C(00M)	122.28(15)	C(00I)	C(00E)	C(00C)	108.31(14)
O(002)	C(005)	O(001)	125.15(16)	C(00P)	C(00E)	C(00C)	111.62(13)
O(002)	C(005)	N(004)	125.87(16)	C(00P)	C(00E)	C(00I)	109.54(15)
N(004)	C(005)	O(001)	108.97(15)	C(007)	C(00F)	C(008)	114.06(13)
O(003)	C(006)	C(00H)	122.56(17)	C(007)	C(00F)	C(00L)	118.33(15)
O(003)	C(006)	C(00T)	120.88(17)	C(00L)	C(00F)	C(008)	104.52(14)
C(00T)	C(006)	C(00H)	116.56(17)	C(00D)	C(00G)	C(00C)	113.82(14)
C(00F)	C(007)	C(00C)	109.29(14)	C(006)	C(00H)	C(008)	114.01(14)
C(00F)	C(007)	C(00K)	110.53(14)	C(006)	C(00H)	C(00Q)	114.62(15)
C(00K)	C(007)	C(00C)	109.24(14)	C(00Q)	C(00H)	C(008)	104.11(13)
C(009)	C(008)	C(00F)	113.34(14)	C(00J)	C(00I)	C(00E)	114.53(15)
C(009)	C(008)	C(00H)	109.17(14)	C(00M)	C(00J)	C(00I)	109.79(15)
C(00D)	C(008)	C(009)	110.85(14)	C(00A)	C(00K)	C(007)	112.59(14)
C(00D)	C(008)	C(00F)	107.41(14)	C(00F)	C(00L)	C(00Q)	103.99(15)
C(00D)	C(008)	C(00H)	116.36(14)	N(004)	C(00M)	C(00J)	111.19(15)
C(00F)	C(008)	C(00H)	99.33(13)	N(004)	C(00M)	C(00N)	110.37(15)
C(00B)	C(00A)	C(00K)	124.59(16)	C(00J)	C(00M)	C(00N)	110.42(15)
C(00A)	C(00B)	C(00E)	123.41(15)	C(00B)	C(00N)	C(00M)	111.87(15)
C(00A)	C(00B)	C(00N)	120.30(15)	O(001)	C(00O)	C(00R)	110.57(14)
C(00N)	C(00B)	C(00E)	116.29(15)	O(001)	C(00O)	C(00S)	110.38(16)
C(007)	C(00C)	C(00E)	112.54(14)	O(001)	C(00O)	C(00U)	102.03(15)
C(007)	C(00C)	C(00G)	111.84(14)	C(00S)	C(00O)	C(00R)	112.34(17)

C(00G)	C(00C)	C(00E)	112.66(13)	C(00U)	C(00O)	C(00R)	111.07(17)
C(008)	C(00D)	C(00G)	110.75(14)	C(00U)	C(00O)	C(00S)	109.98(16)
C(00B)	C(00E)	C(00C)	110.25(14)	C(00H)	C(00Q)	C(00L)	106.14(15)
C(00B)	C(00E)	C(00I)	108.03(14)				

4.4.8. ^{1}H NMR spectra of selected compounds

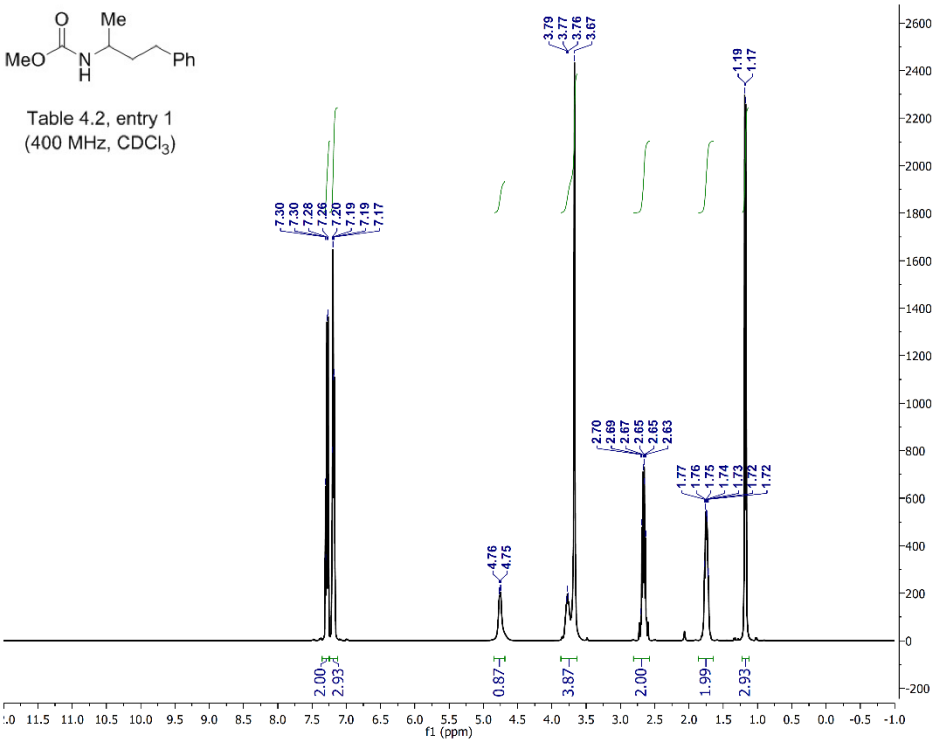

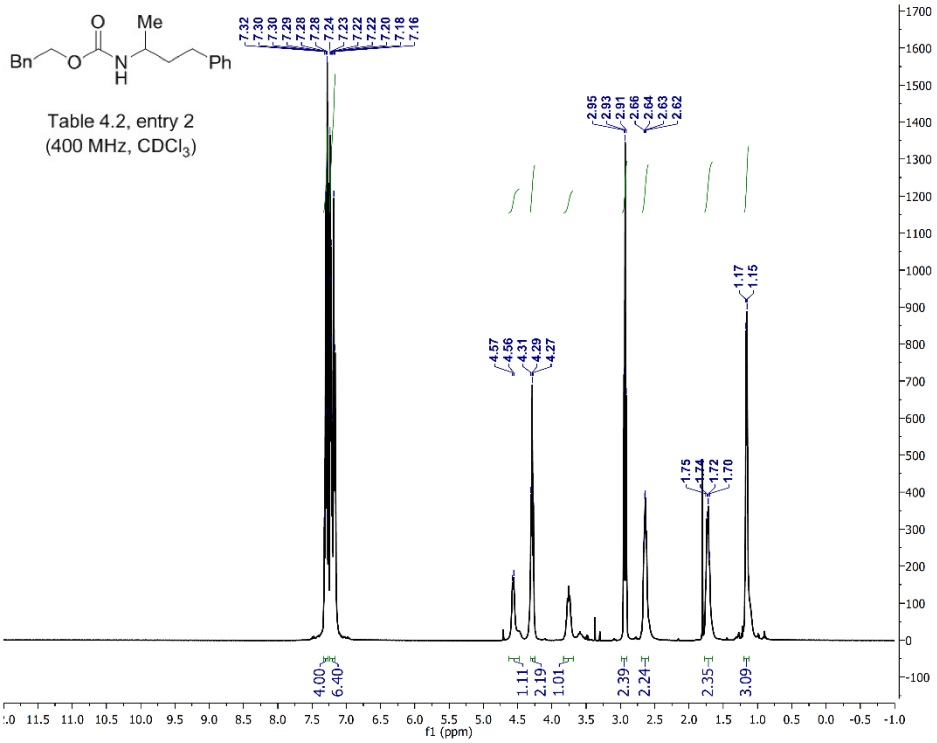

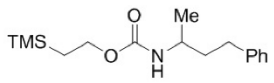

Table 4.2, entry 3
(400 MHz, $CDCl_3$)

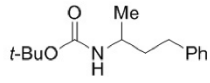

Table 4.2, entry 4
(400 MHz, $CDCl_3$)

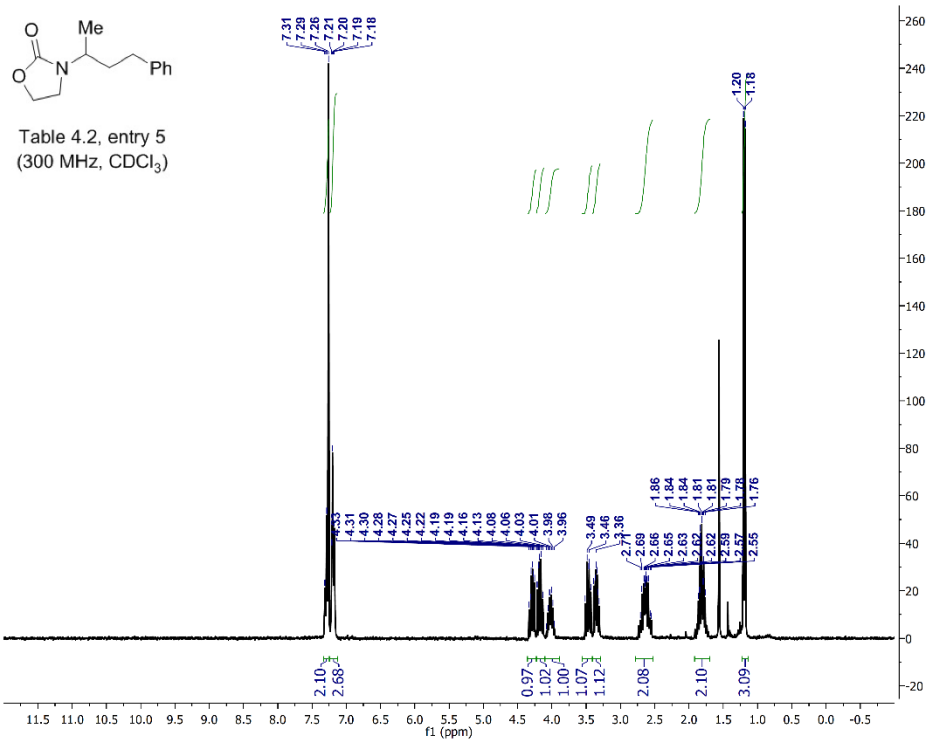
Me
O
N
O
Ph
Table 4.2, entry 5
(300 MHz, CDCl3)
f1 (ppm)

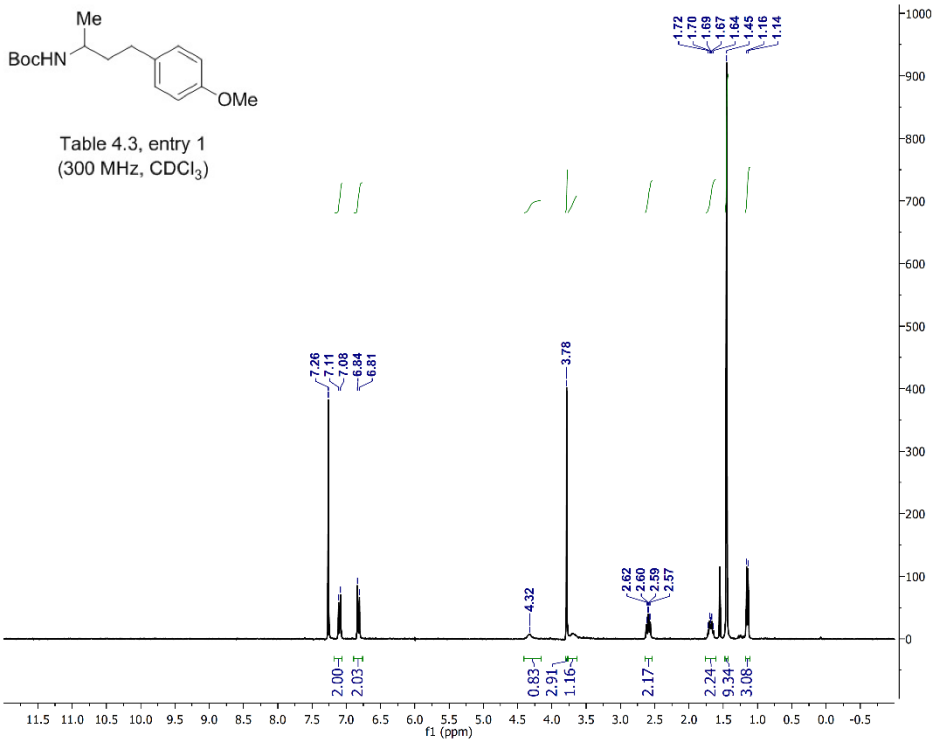
Me
BocHN
OMe
Table 4.3, entry 1
(300 MHz, CDCl3)
f1 (ppm)

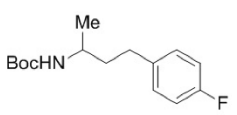

Table 4.3, entry 2
(300 MHz, $CDCl_3$)

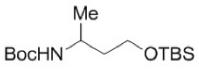

Table 4.3, entry 3
(400 MHz, $CDCl_3$)

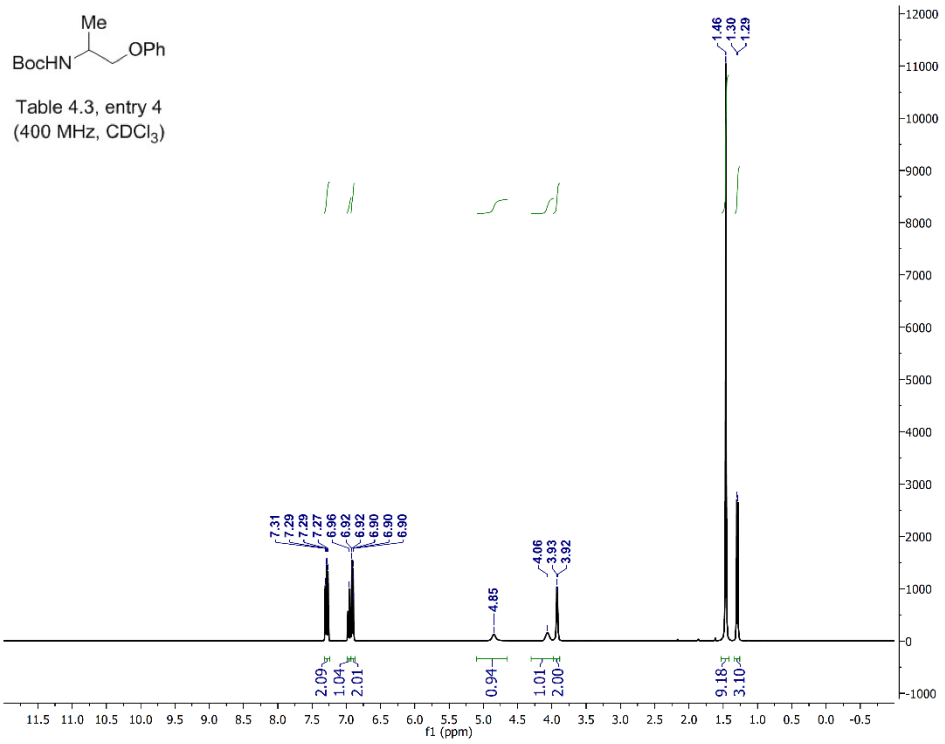
Me
BocHN
OPh
Table 4.3, entry 4
(400 MHz, CDCl3)
1.46
1.30
1.29
7.31
7.29
7.29
7.27
6.96
6.92
6.92
6.90
6.90
6.90
4.85
4.06
3.93
3.92
2.09
1.04
2.01
0.94
1.01
2.00
9.18
3.10
f1 (ppm)

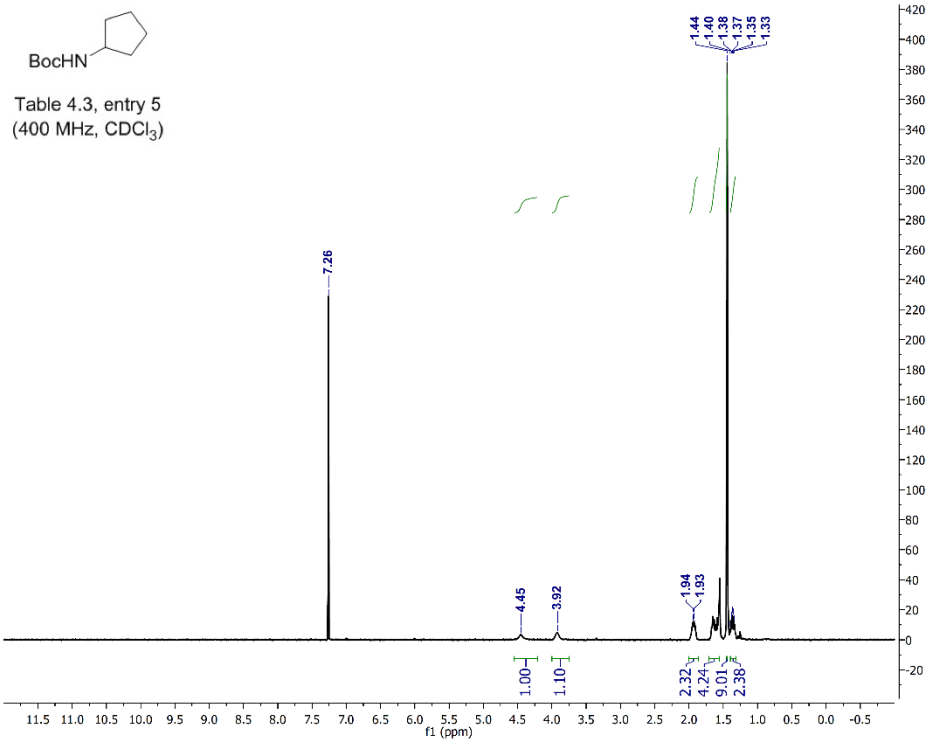
BocHN
Table 4.3, entry 5
(400 MHz, CDCl3)
1.44
1.40
1.38
1.37
1.35
1.33
7.26
4.45
3.92
1.94
1.93
1.00
1.10
2.32
4.24
9.01
2.38
f1 (ppm)

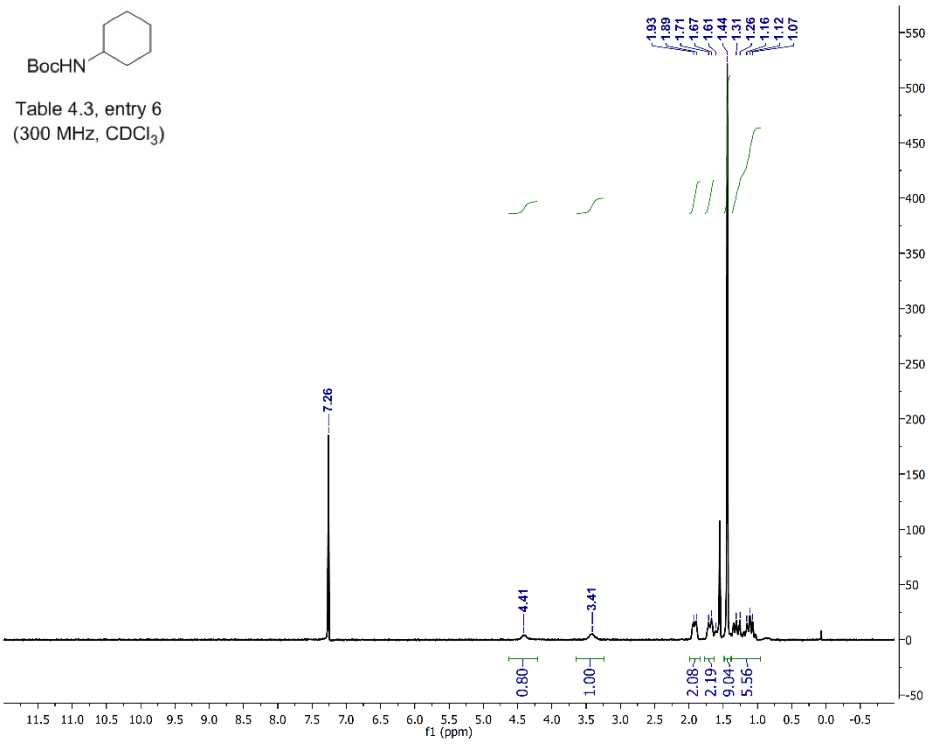
BocHN
Table 4.3, entry 6
(300 MHz, CDCl3)
1.93
1.89
1.71
1.67
1.61
1.44
1.31
1.26
1.16
1.12
1.07
7.26
4.41
3.41
0.80
1.00
2.08
2.19
9.04
5.56
f1 (ppm)

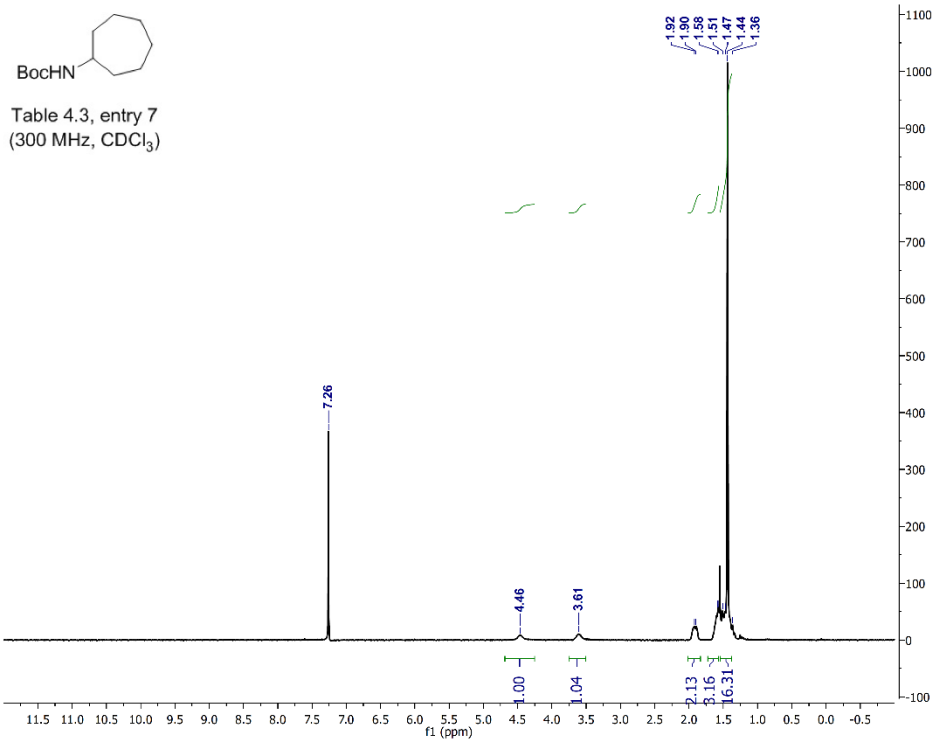
BocHN
Table 4.3, entry 7
(300 MHz, CDCl3)
1.92
1.90
1.58
1.51
1.47
1.44
1.36
7.26
4.46
3.61
1.00
1.04
2.13
3.16
16.31
f1 (ppm)

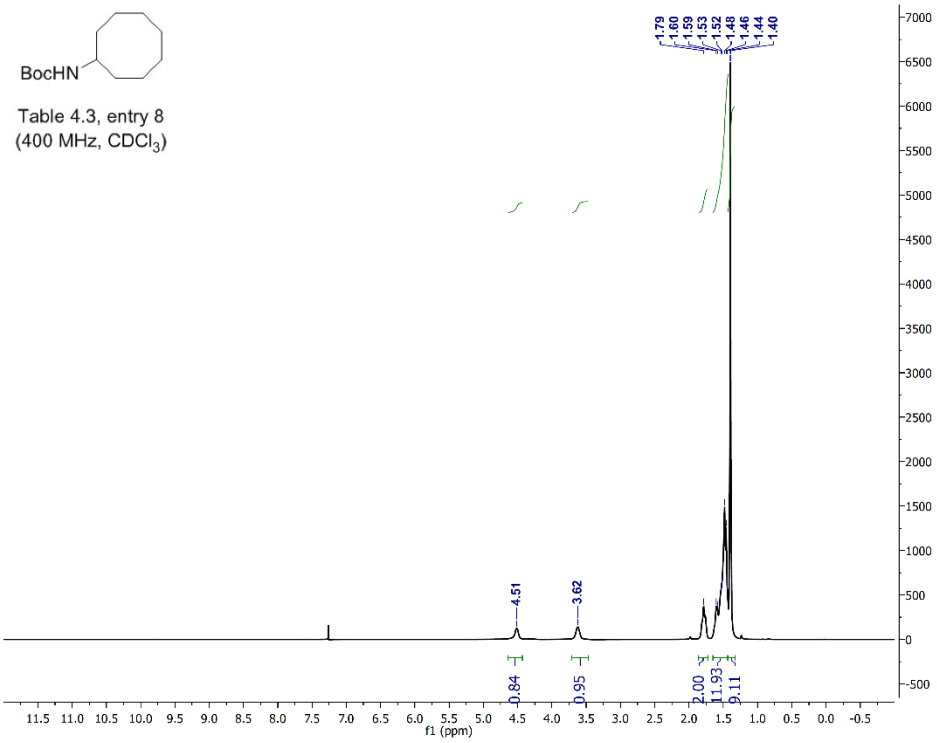
BocHN
Table 4.3, entry 8
(400 MHz, CDCl3)
1.79
1.60
1.59
1.53
1.52
1.48
1.46
1.44
1.40
4.51
3.62
0.84
0.95
2.00
11.93
9.11
f1 (ppm)

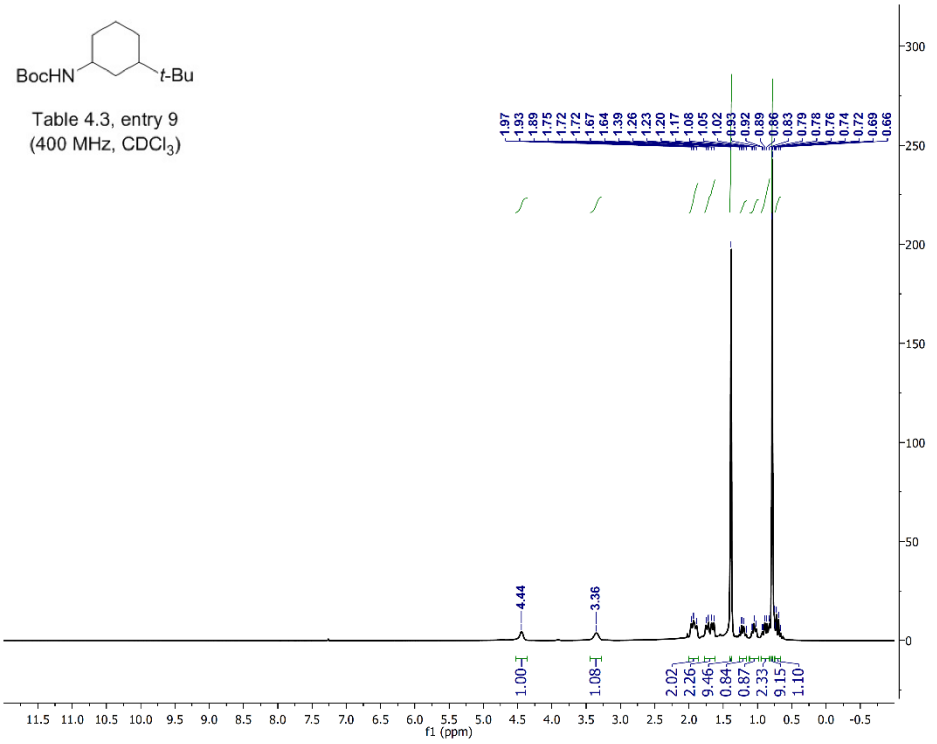
BocHN
t-Bu
Table 4.3, entry 9
(400 MHz, CDCl3)
1.97
1.93
1.89
1.75
1.72
1.67
1.64
1.39
1.26
1.23
1.20
1.17
1.08
1.05
1.02
0.93
0.92
0.89
0.86
0.83
0.79
0.78
0.76
0.74
0.72
0.69
0.66
4.44
3.36
1.00
1.08
2.02
2.26
9.46
0.84
0.87
2.33
9.15
1.10
f1 (ppm)

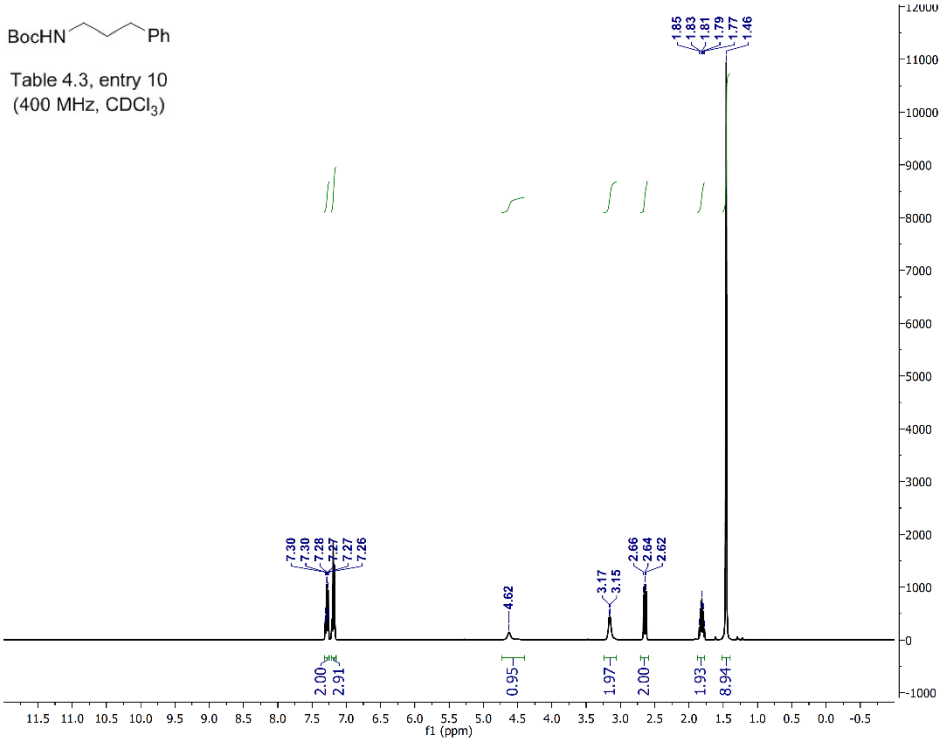
BocHN
Ph
Table 4.3, entry 10
(400 MHz, CDCl3)
f1 (ppm)

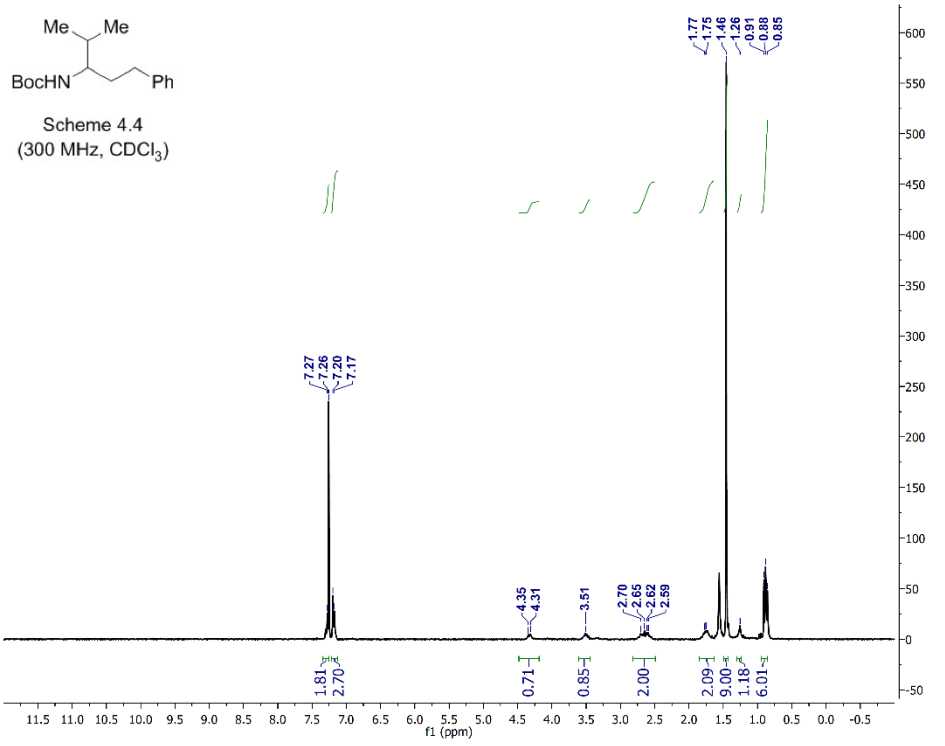
Me
Me
BocHN
Ph
Scheme 4.4
(300 MHz, CDCl3)
f1 (ppm)

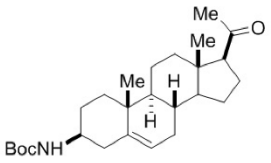

Scheme 4.5
(400 MHz, $CDCl_3$)

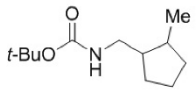

Scheme 4.6
(400 MHz, $CDCl_3$)

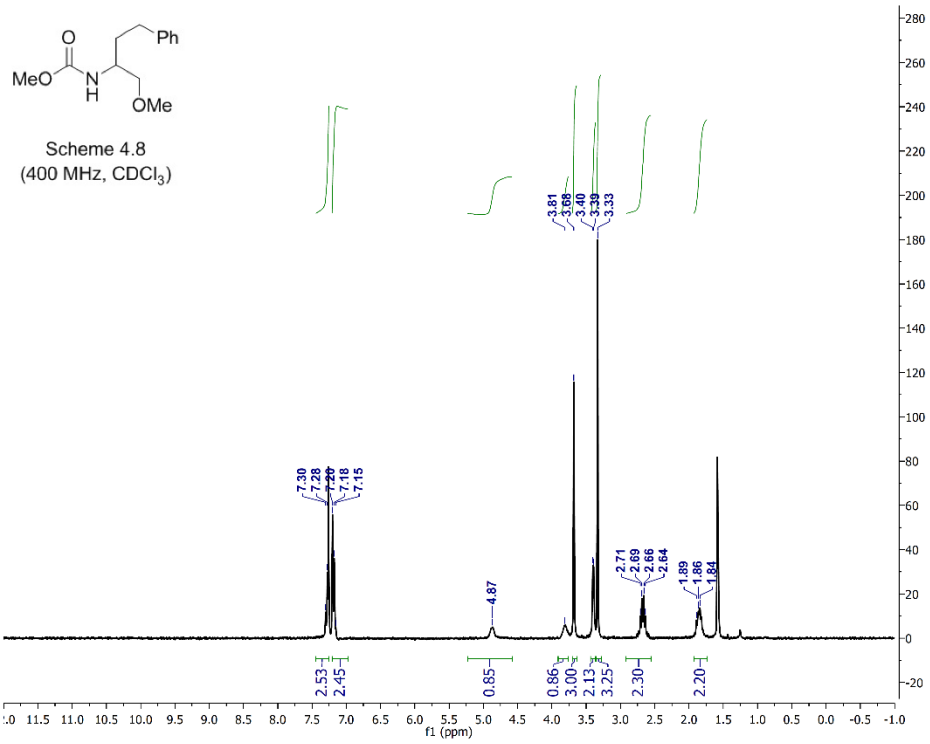

4.5. Notes and References

[1] *Amino Group Chemistry: From Synthesis to the Life Sciences*; Ricci, A., Ed.; Wiley-VCH: Weinheim, Germany, **2008**.

[2] For a discussion and leading references, see: Marvin, C. C. In *Comprehensive Organic Synthesis*; Knochel, P., Molander, G. A., Eds.; Elsevier: Amsterdam, **2015**; Vol. 6, pp 34–99.

[3] For leading references, see: Ahmad, N. M. *Name Reactions for Functional Group Transformations*; Li, J. J., Corey, E. J., Eds.; John Wiley & Sons: Hoboken, NJ, **2007**; pp 438−450.

[4] *Greene's Protective Groups in Organic Synthesis*; Wuts, P. G. M., Ed.; Wiley: Hoboken, NJ, **2014**; Chapter 7.

[5] For reviews, see: (a) Ghosh, A. K.; Brindisi, M. *J. Med. Chem.* **2015**, *58*, 2895–2940. (b) Kuhr, R. J.; Dorough, H. W. *Carbamate Insecticides: Chemistry and Biochemistry*; CRC Press: Cleveland, OH, **1976**.

[6] For examples of other methods that achieve the mono-alkylation of carbamates, see: (a) Palomo, C.; Oiarbide, M.; Halder, R.; Kelso, M.; Gomez-Bengoa, E.; Garcia, J. M. *J. Am. Chem. Soc.* **2004**, *126*, 9188–9189. (Formal hydroamination via 1,4-addition) (b) Das, B. G.; Ghorai, P. *Org. Biomol. Chem.* **2013**, *11*, 4379–4382. (Reductive amination)

[7] Do, H.-Q.; Bachman, S.; Bissember, A. C.; Peters, J. C.; Fu, G. C. *J. Am. Chem. Soc.* **2014**, *136*, 2162–2167.

[8] N–alkylations with alkyl electrophiles are among the most commonly used reactions in medicinal chemistry. For example, see Table 2 in: Roughley, S. D.; Jordan, A. M. *J. Med. Chem.* **2011**, *54*, 3451–3479.

[9] For other reports of transition metal-catalyzed alkylations of nitrogen nucleophiles with unactivated secondary and tertiary alkyl electrophiles, see: (a) Bissember, A. C.; Lundgren, R. J.; Creutz, S. E.; Peters, J. C.; Fu, G. C. *Angew. Chem., Int. Ed.* **2013**, *53*, 5129–5133. (b) Peacock, D. M.; Roos, C. B.; Hartwig, J. F. *ACS Cent. Sci.* **2016**, *2*, 647–652. (c) Matier, C. D.; Schwaben, J.; Peters, J. C.; Fu, G. C. *J. Am. Chem. Soc.* **2017**, *139*, 17707-17710.

[10] Two recent studies have pointed to *N*-Boc as the most commonly used protecting group in medicinal chemistry, accounting for about 30% of all protections/deprotections in the data sets that were analyzed: (a) See Table 3 in ref 8. (b) See Figure 6 in: Schneider, N.; Lowe, D. M.; Sayle, R. A.; Tarselli, M. A.; Landrum, G. A. *J. Med Chem.* **2016**, *59*, 4385–4402.

[11] Isidro-Llobet, A.; Alvarez, M.; Albericio, F. *Chem. Rev.* **2009**, *109*, 2455–2504.

[12] A new species is also detected by ESI-MS of a catalysis mixture after 4 h irradiation that is consistent with the N–alkylation of **L4.1**. If an N–alkylated ligand (that has the N–H

group of **L4.1** replaced by N–Me) is used for the standard reaction, the alkyl bromide is not consumed.

[13] For discussions of persistent radicals, see: (a) Studer, A. *Chem. –Eur. J.* **2001**, *7*, 1159−1164. (b) Fischer, H. *Chem. Rev.* **2001**, *101*, 3581−3610.

[14] Alfassi, Z. B. In *General Aspects of the Chemistry of Radicals*; Alfassi, Z. B., Ed.; Wiley: Chichester, U.K., **1999**; pp 139−173.

[15] Lusztyuk, J.; Maillard, B.; Deycard, S.; Lindsay, D. A.; Ingold, K. U. *J. Org. Chem.* **1987**, *52*, 3509−3514.

[16] Anslyn, E. V.; Dougherty, D. A. *Modern Physical Organic Chemistry*; University Science Books: Sausalito, CA, **2006**; p 156.

[17] Cismesia, M. A.; Yoon, T. P. *Chem. Sci*. **2015**, *6*, 5426–5434.

[18] Under standard conditions (**Table 4.2**), mentholyl carbamate reacts to give 87% isolated yield of C–N coupled product.

[19] At room temperature, this substrate under blue-LED illumination (**Table 4.3**) reacts to give 93% isolated yield of C–N coupled product after 30 h irradiation.

[20] We speculate that the stereoselective C–N bond-forming step may involve the coupling of the alkyl radical with the species [**L***Cu^{II}(Nu)]$^{-}$ such as the one shown below.

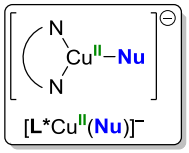

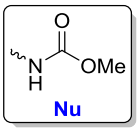

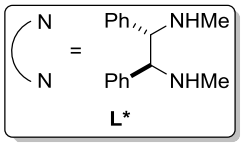

[21] Plundrich, G. T.; Wadepohl, H.; Gade, L. H. *Inorg. Chem.* **2016**, *55*, 353–365.

[22] Stoll, S.; Schweiger, A. *J. Magn. Reson.* **2006**, *178*, 42–55.

[23] Liang, Z.; Xue, W.; Lin, K.; Gong, H. *Org. Lett.* **2014**, *16*, 5620–5623.

[24] The structure was verified by X-ray crystallography, using single crystals grown from a saturated solution in CH_3CN.

[25] Oshikawa, T.; Yamashita, M. *Bull. Chem. Soc. Jpn.* **1989**, *62*, 3177.

[26] Yang, W.; Zhang, Z.; Han, C.; Zhang, Z.; Xu, H.; Yan, P.; Z, Y.; L, S. *Chem. Commun.* **2013**, *49*, 2822–2824.

Chapter 5. Copper complexes supported by bidentate (phosphino)carbazole ligands

5.1. Introduction

In **Chapter 3**, we suggested that the presence of both the phosphine and carbazole moieties is key to conferring the excited-state properties of complex **3.1**, which we exploited in the development of coupling reactions of alkyl bromides with carbamate nucleophiles in **Chapter 4**. As part of our ongoing investigation to examine photoactive copper–carbazolide complexes, we also targeted bidentate (phosphino)carbazole ligands (**Figure 5.1**).

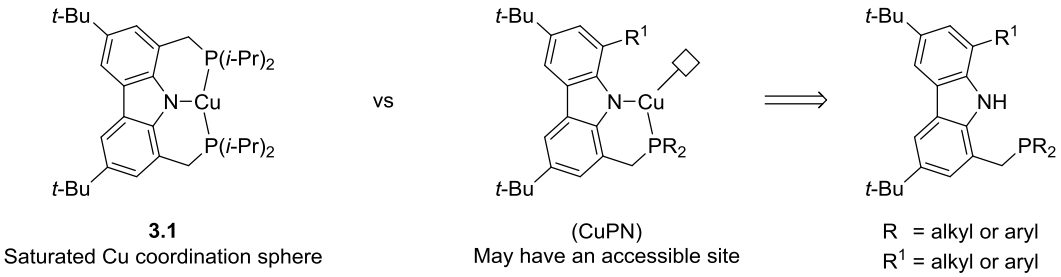

3.1
Saturated Cu coordination sphere

(CuPN)
May have an accessible site

R = alkyl or aryl
R^1 = alkyl or aryl

Figure 5.1. Possible differences between copper complexes supported by tri- and bidentate (phosphino)carbazole ligands.

Our interest in bidentate ligands was initially inspired by the potential modularity in the steric and electronic properties of the corresponding copper(I) complexes through modifications of substituents (R^1) on the carbazole platform. Assuming structural congruence to **3.1**, the third coordination site on the copper center may then be accessible to an approaching substrate in the excited state, or to a nucleophile in the ground state (**Figure 5.2**). Thus, we postulated that bidentate ligands may broaden the scope with respect to coupling partners in photoinduced, copper-catalyzed coupling reactions explored in the Fu and Peters laboratories.

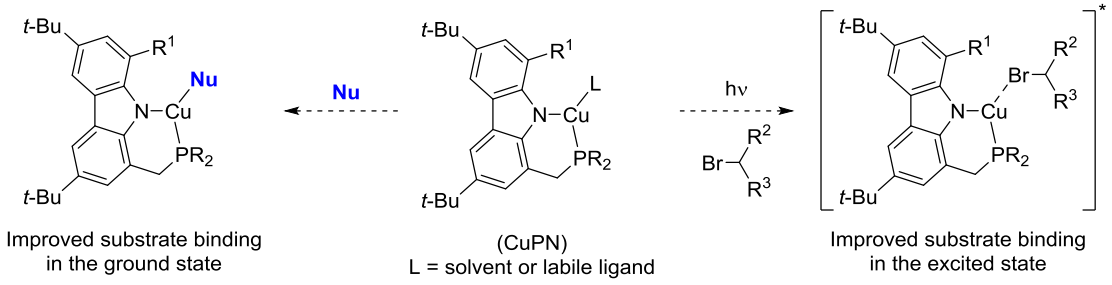

Figure 5.2. Proposed binding of substrates in the ground and excited state of a hypothetical, monomeric copper(I) complex ligated by a bidentate (phosphino)carbazole ligand. R = alkyl or aryl. R^1 = H, alkyl, or aryl. R^2 = alkyl or aryl. R^3 = alkyl or aryl.

Another motivation for the study of bidentate (phosphino)carbazole ligands stemmed from the discovery of the photoinduced, copper-catalyzed enantioconvergent alkylation of carbazole with tertiary α-chloroamides (**Scheme 5.1**).[1] This reaction not only represents the only example reported by the Fu and Peters groups in which optimal results are obtained in a nonpolar solvent (toluene), but it is also highlighted by low loadings of copper (1 mol%) and the chiral ligand (monodentate phosphine, 1.2 mol%).

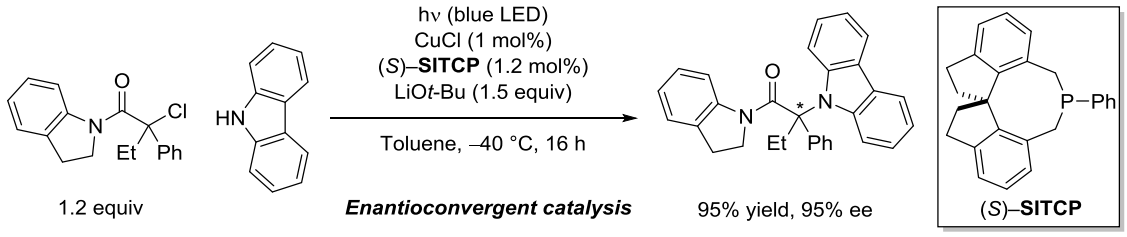

Scheme 5.1. Enantioconvergent copper catalysis: the alkylation of carbazole with a tertiary α-chloroamide.

Initial mechanistic studies on the enantioconvergent N–alkylation reaction confirmed the catalytic and stoichiometric competence of a bis(phosphine) complex, Cu^{I}(**SITCP**)$_2$(carb) (**5.a**) in facilitating the formation of the C–N bond (**Scheme 5.2**). Preliminary investigations also showed that Li(carb) is unlikely to be present in substantial concentration in toluene; stirring a mixture of carbazole and LiO*t*-Bu in toluene does not result in the formation of new species by optical or NMR spectroscopy. This finding is in stark contrast to the behavior observed in CH_3CN, wherein carbazole and LiO*t*-Bu react within minutes to produce Li(carb). Thus, the combined mechanistic data intimated that the irradiation with blue LED lamps results in the photoinduced electron transfer predominantly from the excited state of **5.a** to the alkyl halide, and a catalytic cycle akin to **Figure 2.1** was proposed, which implicates an in-cage C–N coupling process.

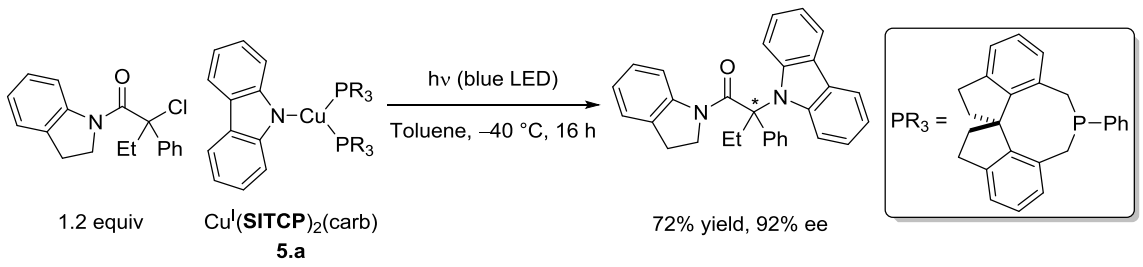

Scheme 5.2. Stoichiometric cross-coupling reaction with isolated complex **5.a**.

However, several key observations suggested that the enantioconvergent alkylation of carbazole may also traverse out-of-cage pathways. For instance, the three-component reaction of carbazole, alkyl iodide, and an α,β–unsaturated amide under related conditions can be achieved in high enantioselectivity (**Scheme 5.3**).[2] In view of the same level of stereoselectivity in both the two- and three-component coupling reactions that yield the same

C–N coupling product, the two reactions likely share a common, chiral, S = 1/2 copper–carbazolide intermediate with sufficient lifetime and concentration in toluene at –40 °C.

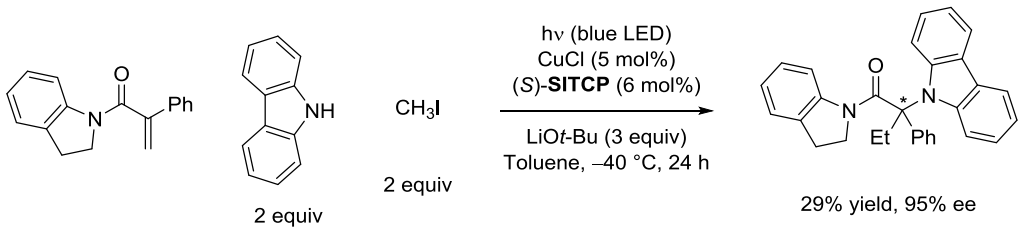

Scheme 5.3. A representative three-component coupling of carbazole, iodomethane, and α,β–unsaturated amide.

Further lending credence to the feasibility of the out-of-cage C–N coupling mechanism is the high enantioselectivity observed using essentially equimolar ratio of CuCl to **SITCP** (1:1.2). This stoichiometry raises the possibility that there may be other copper–carbazolide complexes formed under the standard conditions than complex **5.a** and that only one chiral phosphine may be associated with a copper complex in the stereochemistry-determining step.[3] Assuming that the photoinduced single electron transfer occurs from the bis(phosphine) complex **5.a**, a step-wise dissociation of a phosphine ligand is expected to follow the photo-oxidation of **5.a** in order to yield a paramagnetic copper intermediate with one phosphine ligand.

One plausible structure of a chiral S = 1/2 copper–nucleophile complex that may be accessible under the standard reaction conditions (e.g. **Scheme 5.1**) is the neutral Cu^{II}(**SITCP**)(carb)$_2$ species (**5.b**; **Figure 5.3**).[4] In consideration of the substitutional lability of copper,[5] complex **5.b** is expected to be unstable. We envisioned that a bidentate

(phosphino)carbazole ligand would confer stability against ligand substitution while capturing the geometry and ligand environment at the metal center in **5.b**. Understanding of such species is also of interest in its own right, as it would represent a rare example of a mononuclear $S = 1/2$ copper complex supported by one monophosphine ligand.[6] Herein, we describe the chemistry of a wide array of copper complexes ligated by bidentate (phosphino)carbazoles, including a rare, mononuclear $S = 1/2$ copper–phosphine complex that may serve as a model complex for the elusive copper intermediates of the enantioselective C_{sp^3}–N couplings of carbazoles.

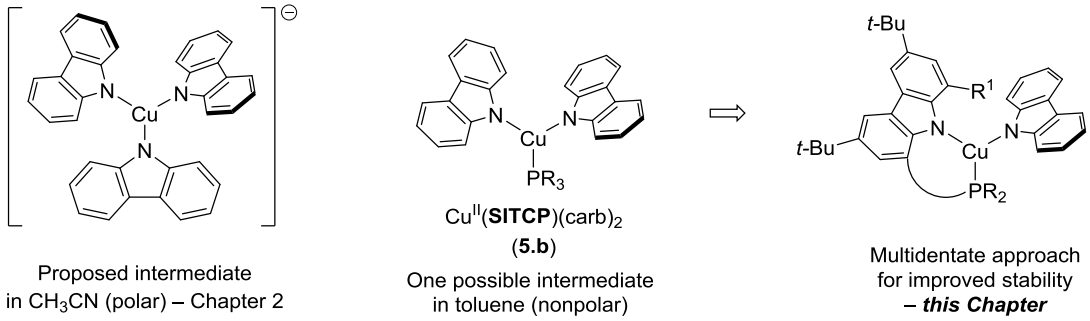

Figure 5.3. Proposed copper(II) intermediates in photoinduced alkylations of carbazoles. PR_3 = **SITCP**. R^1 = H, alkyl, or aryl. R^2 = alkyl or aryl.

5.2. Results and Discussions

5.2.1. Synthesis and characterization of $S = 1/2$ complexes supported by bidentate (phosphino)carbazoles

The preparation of bidentate ligands follows an analogous strategy to that described for the synthesis of tridentate counterparts in **Chapter 3**. Detailed synthetic procedures are

provided in the Experimental Section. Briefly, a hydroxymethyl group in the 1-position of the 3,6,-di-*t*-butylcarbazole backbone is installed and converted to the corresponding benzylic bromide which is then substituted with a secondary phosphine. Molecular structures and labels of (phosphino)carbazole ligands are summarized in **Figure 5.4**.

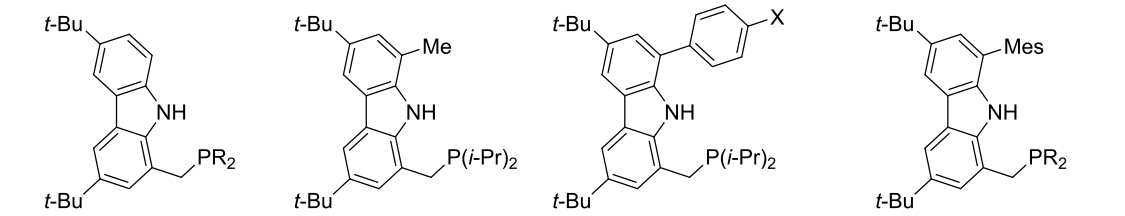

$P_{iPr}N_H$ (**L5.1**): $PR_2 = P(i\text{-Pr})_2$
$P_{Ph}N_H$ (**L5.2**): $PR_2 = P(Ph)_2$

$P_{iPr}N_{Me}$ (**L5.3**)

$P_{iPr}N_{FPh}$ (**L5.4**): X = F
$P_{iPr}N_{tBuPh}$ (**L5.5**): X = *t*-Bu
$P_{iPr}N_{MeOPh}$ (**L5.6**): X = OMe

$P_{iPr}N_{Mes}$ (**L5.7**): $PR_2 = P(i\text{-Pr})_2$
$P_{Ph}N_{Mes}$ (**L5.8**): $PR_2 = P(Ph)_2$
$P_{PhBn}N_{Mes}$ (**L5.9**): PR_2 = PPhBn

Figure 5.4. Bidentate (phosphino)carbazole ligands explored in this study.

With a wide array of bidentate ligands in hand, we attempted to make the mononuclear copper(I) complexes. When CuCl, ligand (**L5.1**–**L5.6**), and a slight excess of LiO*t*-Bu are stirred in benzene, the clean formation of new species is observed by ^{1}H and ^{31}P NMR spectroscopy. These species in general are sparingly soluble in CH_3CN, allowing for their structural characterization in the solid state by single crystal X-ray diffraction. Instead of the initially targeted mononuclear copper(I) complexes, (phosphino)carbazole ligands **L5.1**–**L5.6** support unsymmetrical $S = 0$ dicopper complexes (**5.1–5.6**; **Figure 5.5**). Notably, if the additional substituent (R^1) on the carbazole platform is sterically small, the ligation of a molecule of CH_3CN to the bis(phosphine)copper center is observed (complexes **5.1**–**5.4**).

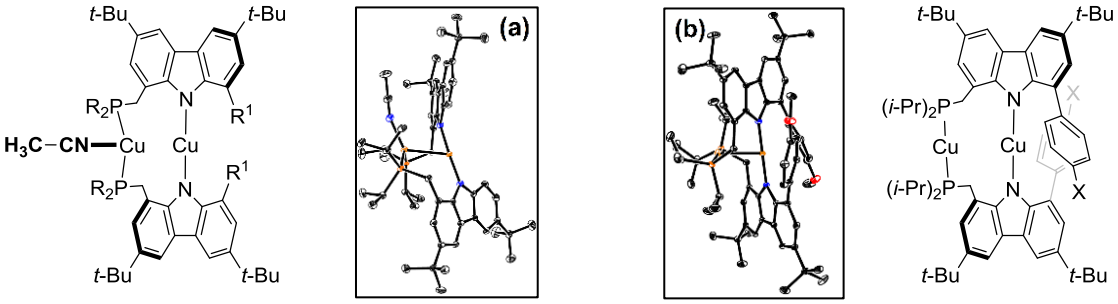

$(CuP_{iPr}N_H)_2$–(CH_3CN) (**5.1–CH_3CN**): R = *i*-Pr; R^1 = H; from **L5.1**
$(CuP_{Ph}N_H)_2$–(CH_3CN) (**5.2–CH_3CN**): R = Ph; R^1 = H; from **L5.2**
$(CuP_{iPr}N_{Me})_2$–(CH_3CN) (**5.3–CH_3CN**): R = *i*-Pr; R^1 = Me; from **L5.3**
$(CuP_{iPr}N_{FPh})_2$–(CH_3CN) (**5.4–CH_3CN**):R = *i*-Pr; R^1 = 4-F-phenyl; from **L5.4**

$(CuP_{iPr}N_{tBuPh})_2$ (**5.5**): X = *t*-Bu; from **L5.5**
$(CuP_{iPr}N_{MeOPh})_2$ (**5.6**): X = OMe; from **L5.6**

Figure 5.5. Unsymmetrical dicopper complexes of bidentate (phosphino)carbazoles. (a) solid-state molecular structure of **5.1–CH_3CN** determined by single crystal XRD depicted at 30 % thermal probability ellipsoids; hydrogen atoms and additional solvent molecules are omitted for clarity. (b) solid-state molecular structure of **5.6** determined by single crystal XRD depicted at 30 % thermal probability ellipsoids; hydrogen atoms and additional solvent molecules are omitted for clarity.

In the solid state, Cu–Cu distances found in the unsymmetrical dicopper complexes vary from 2.5 to 2.7 Å. These values are smaller than the sum of the van der Waals radii of copper (2.8 Å) and close to the sum of the covalent radii of copper and to that observed in the Cu_A center found in several metalloproteins (2.6 Å).[7,8] All complexes are diamagnetic at room temperature and display sharp, single ^{31}P resonances.[9] In pure form, complexes **5.1**–**5.6** are colorless. Thus, various spectroscopic data are consistent with the assignment of the dicopper complexes as a cationic copper(I)–bis(phosphine) unit adjacent to an anionic $[Cu^I(carb)_2]^-$ fragment (i.e. d^{10} electronic configuration at each copper center).

In contrast, the treatment of (phosphino)carbazole ligand **L5.7** or **L5.8**, which contains a sterically encumbering mesityl substituent, with CuCl and LiO*t*-Bu in benzene generates the symmetrical dicopper complexes **5.7** or **5.8** (**Figure 5.6**). As determined by the solid-state structure, Cu–Cu distance in complex **5.7** is 4.9 Å, negating the possibility of a direct Cu–Cu interaction. Under analogous reaction conditions, the attempted metallation of **L5.9** leads to an intractable mixture, suggestive of the formation of multiple isomers of dicopper complexes owing to the presence of a stereogenic P atom.

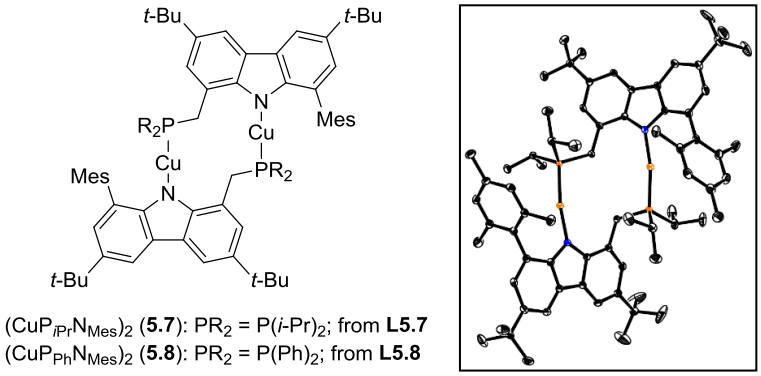

Figure 5.6. Symmetrical dicopper complexes of bidentate (phosphino)carbazoles. Inset: solid-state molecular structure of **5.7** determined by single crystal XRD depicted at 30 % thermal probability ellipsoids; hydrogen atoms and solvent molecules are omitted for clarity.

Because single crystals of **5.1**–**5.8** can be obtained by cooling hot (refluxing CH_3CN), saturated solutions in CH_3CN, the initially targeted monomeric copper(I) adducts of (phosphino)carbazoles (e.g. middle of **Figure 5.2**) do not appear to be accessible. However, the unexpected discovery of unsymmetrical dicopper complexes inspired us to target heterobimetallic variants. In view of the prevalence of photoactive gold–phosphine

complexes in coupling reactions of organohalides,[10] we targeted Au–Cu bimetallic complexes using ligand **L5.1**.

The treatment of **L5.1** with a mixture of Au(PPh_3)Cl (0.5 equiv) and CuCl (0.5 equiv) containing excess LiO*t*-Bu produces a new species according to the ^{31}P spectrum of the crude mixture (δ 56), which differs from that of complex **5.1** (δ 12). The new ^{31}P resonance also does not correspond to the symmetrical digold complex **5.9** (δ 36), which can be prepared by treating Au(PPh_3)Cl with the lithium salt of **L5.1** without CuCl (**Figure 5.7**). As confirmed by XRD, the product instead is the targeted Au–Cu bimetallic complex **5.10** (**Figure 5.7**).[11] Complex **5.10** is colorless and features Au–Cu distance of 2.81 Å, in between the metal–metal distances observed in **5.1–CH_3CN** and **5.9** (2.67 Å and 3.04 Å, respectively). Although the potential interplay of gold and copper in light-driven transformations is of interest, the photochemical applications of complex **5.10** are not described in this Thesis.

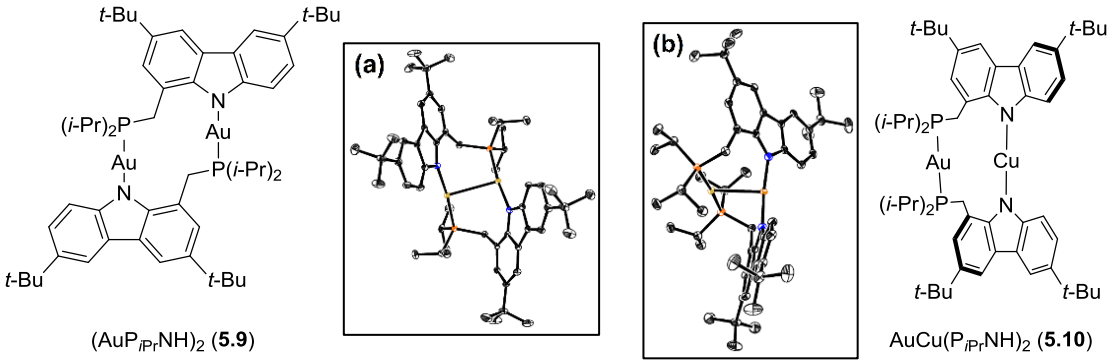

Figure 5.7. Structures of gold complexes supported by ligand **L5.1**. (a) Solid-state molecular structure of **5.9** and (b) solid-state molecular structure of **5.10** determined by single crystal XRD depicted at 30 % thermal probability ellipsoids; hydrogen atoms and additional solvent molecules are omitted for clarity.

5.2.2. Reactivity of *S* = 1/2 complexes supported by bidentate (phosphino)carbazoles

In contrast to our initial hypothesis (e.g. **Figure 5.1** and **Figure 5.2**) that bidentate (phosphino)carbazole platforms may elicit a better catalytic performance in photoinduced copper catalysis, we were unable to find conditions in which ligands **L5.1**–**L5.9** outperform bis(phosphino)carbazole ligand **L3.1** in various attempted coupling reactions of alkyl bromides.[12] During the course of our survey, however, we observed that alkyl bromides are converted to the product of cyanomethylation when CH_3CN is used as the reaction solvent. In view of the binding of CH_3CN to complexes **5.1**–**5.4** in the solid-state, we explored the use of CH_3CN as the nucleophile in photoinduced, copper-catalyzed coupling reactions with unactivated secondary alkyl bromides.

We found that the irradiation of a mixture of CuBr (10 mol%), **L5.1** (4 mol%), LiO*t*-Bu (3 equiv) and a wide range of cyclic or acyclic alkyl bromides (1 equiv) in CH_3CN yields the corresponding products of cyanomethylation. Specifically, under these conditions, 4-phenyl-cyclohexyl bromide is converted in 30% yield to 2-(4-phenylcyclohexyl)acetonitrile (**pdt; Scheme 5.4**). Cyanomethylation is not observed in the absence of CuBr, light, or CuBr and light. In the absence of **L5.1**, the reaction does not proceed.[13]

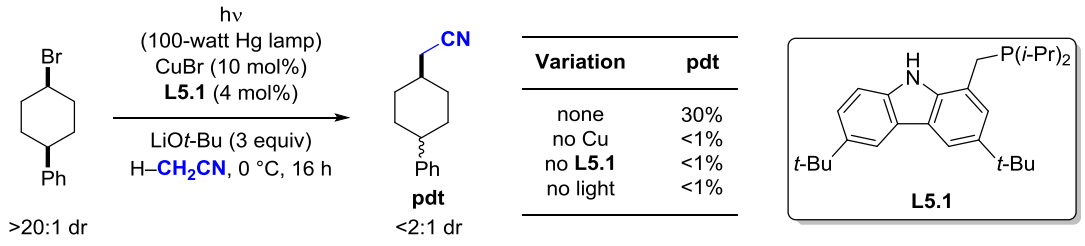

Scheme 5.4. Photoinduced, copper-catalyzed C_{sp^3}–C_{sp^3} cross-coupling: cyanomethylation of 4-phenyl-cyclohexyl bromide.

Although this cyanomethylation reaction represents the first example of a photoinduced, copper-catalyzed C_{sp^3}–C_{sp^3} coupling, we were unable to further improve the yield or address its shortcomings. Namely, the scope of the nucleophilic partner is limited to CH_3CN and heavier nitriles do not participate in the C_{sp^3}–C_{sp^3} coupling. Many acyclic secondary alkyl bromides undergo facile S_N2 substitutions with $LiCH_2CN$,[14] even at 0 °C, in the absence of light. While the cyclic secondary alkyl bromides such as cyclohexyl bromide and 4-phenyl-cyclohexyl bromide do not readily react with $LiCH_2CN$ under analogous conditions, the photoinduced cyanomethylation of 4-phenyl-cyclohexyl bromide (>20:1 dr) proceeds with poor diastereoselectivity (<2:1 dr). The loss of the stereochemical information in the starting material, however, is suggestive of the intermediacy of an alkyl radical, which is likely generated via the photoinduced single electron transfer to the alkyl bromide from the excited state of **5.1** (accessed in situ from CuBr, **L5.1**, and Li*O*t-Bu).

We therefore examined the chemical oxidation of the unsymmetrical dicopper complex **5.1** to gain insight on its photo-oxidation product. Although we were unable to observe well-behaved electrochemistry by cyclic voltammetry on the $S = 0$ dicopper complexes at room temperature in general, the treatment of the colorless complex **5.1–CH₃CN** with an equimolar solution of acetylferrocenium hexafluoroantimonate ([FcAc][SbF_6]) in DCM at –78 °C results in the appearance of a new optical transition at 620 nm which decays within several hours at –35 °C. Consistent with the detection of acetylferrocene (FcAc) by UV-vis spectroscopy, the observed color change is accompanied by the appearance of an EPR signal (**Figure 5.8**). Due to its thermal instability, however, we were unable to structurally confirm this oxidation product of **5.1**.

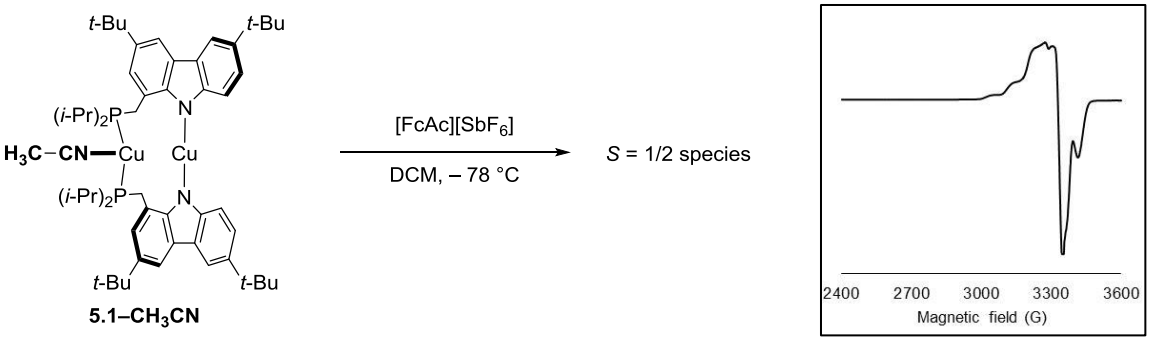

Figure 5.8. Reaction of complex **5.1–CH$_3$CN** with [FcAc][SbF$_6$] at –78 °C in DCM. Inset: EPR spectrum (9.4 GHz, 77 K, DCM/toluene) of the crude mixture. Estimated values are as follows: g = [2.107, 2.033, 1.987]. Similar results are obtained using CH$_3$CN-free **5.1**.

In hopes of improving the stability of the one-electron oxidation product of the unsymmetrical dicopper complex **5.1**, we examined the analogous reactions using structurally related complexes that contain more sterically encumbering aryl substituents on the carbazole ring. In stark contrast to that observed in **5.1**, the oxidation reactions of complexes **5.4**– **5.6** with an equivalent of [FcAc][SbF$_6$] in DCM at –78 °C produce deep purple solutions. The purple color of these mixtures persists for days at –35 °C, although the solution turns pale yellow when warmed to room temperature within hours. Specifically, the oxidation of **5.6** with [FcAc][SbF$_6$] produces an intense absorption at 550 nm, and the EPR spectrum of the purple solution shows a pseudo-isotropic signal, centered near the g-value of the free electron (**Figure 5.9a**). The same EPR spectrum is observed when **5.4** or **5.5** is used in place of **5.6** under analogous reaction conditions.

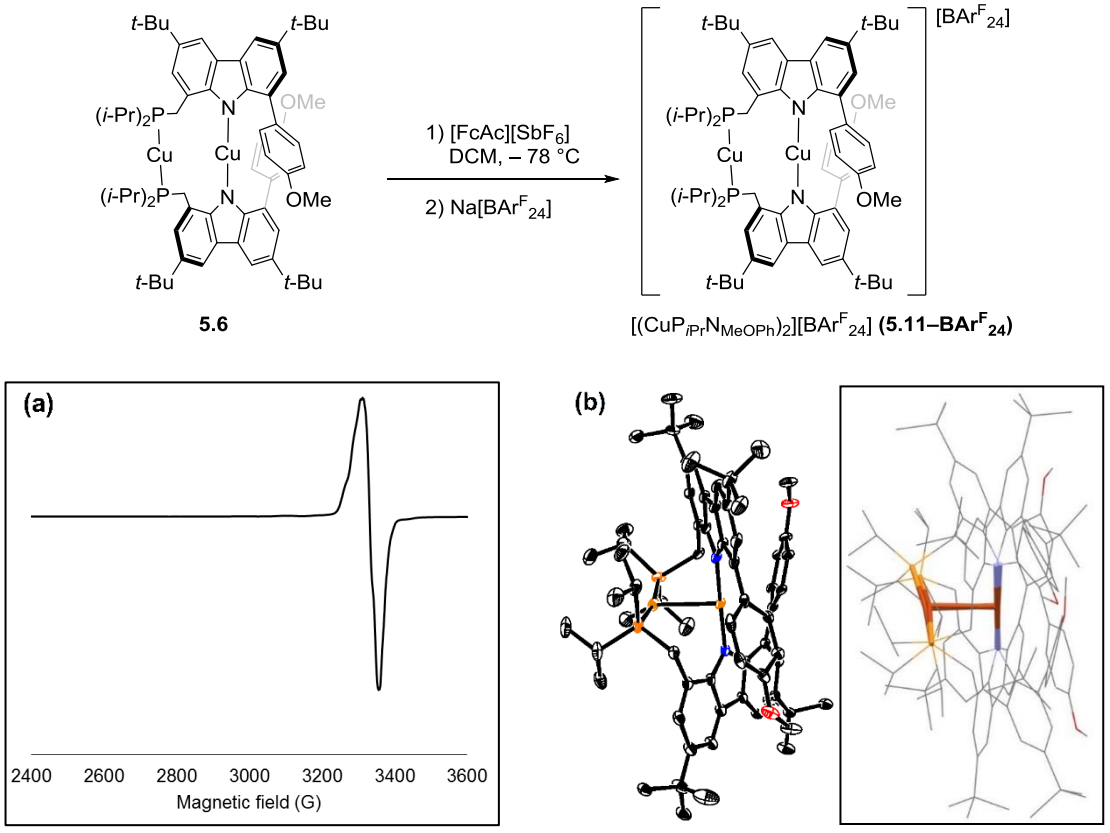

Figure 5.9. Formation and characterization of the cation **5.11**. (a) EPR spectrum (9.4 GHz, 77 K, DCM/toluene) of the crude mixture of the oxidation of **5.6** by [FcAc][SbF_6] . (b) Solid-state molecular structure of the cation **5.11** determined by single crystal XRD depicted at 30 % thermal probability ellipsoids; hydrogen atoms and $[BAr^F{}_{24}]^-$ anion are omitted for clarity; inset: overlay of the dicopper fragments in **5.6** and **5.11** showing the minimal structural reorganization at the $[CuP_2][CuN_2]$ cores between the two redox forms.

We were able to structurally confirm the cation, $[(CuP_{i\text{Pr}}N_{\text{MeOPh}})_2]^+$ (**5.11**), of the one-electron oxidation product of complex **5.6**, as a $BAr^F{}_{24}$ salt by single crystal XRD ($[BAr^F{}_{24}]^-$ = $[B(3,5\text{-}(CF_3)_2\text{-}C_6H_3)_4]^-$; **Figure 5.9b**). The quality of the X-ray diffraction data is modest, and bond metrics should therefore be gleaned with caution. Nonetheless, the solid-state

molecular structure of **5.11**–**BAr$^{F}_{24}$** shows a slight elongation of the Cu–Cu distance from 2.5 Å in **5.6** to 2.7 Å. The dihedral angle between the two carbazolide planes remains essentially unchanged at 56° upon oxidation.[15] The minimal extent of the structural reorganization between the two redox series (**Figure 5.9**, inset) is similar to that exhibited in symmetrical dicopper complexes reported previously by the Peters laboratory (**Figure 5.10**, left),[16] though the latter examples experience an overall contraction of the Cu–Cu distances upon the removal of an electron in general.

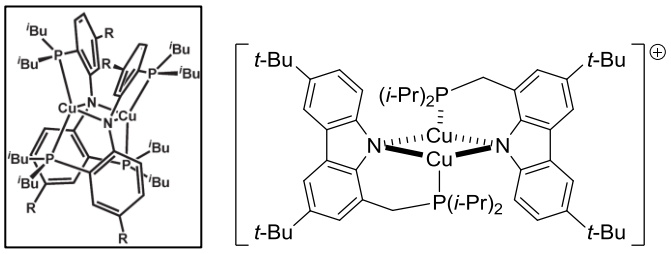

Figure 5.10. Dicopper complexes featuring Cu_2N_2 diamond cores. Left: reported dicopper complex in which the diamond core is preserved across three oxidation states; R = *t*-Bu. Right: one possible structure of the product of the one-electron oxidation of complex **5.1**.

Despite the structural similarity between the unsymmetrical S = 0 dicopper complexes **5.1** and **5.6**, the stark differences between their one-electron oxidation products in terms of λ_{max} and the spread of the *g*-value suggest that the structures of the two paramagnets are significantly different. In consideration of the prevalence of the Cu_2N_2 diamond core in dicopper complexes supported by multidentate arylamido ligands (e.g. **Figure 5.10**, left),[16,17] we speculated that the oxidation of the unsymmetrical dicopper complex **5.1**, which lacks the sterically bulky aryl groups, may induce a structural

rearrangement to a symmetrical dicopper complex (**Figure 5.10**, right), in contrast to the observations made in the conversion of **5.6** to **5.11**. Alternatively, the *g*-anisotropy in the EPR spectrum of the oxidation product of **5.1** may be a result of an increased co-planarity of the two carbazolides in the $S = 1/2$ state that permit a greater degree of spin-delocalization.

To gain more insight into the structure of the oxidation product of **5.1**, we performed the oxidation of the structurally related Au–Cu bimetallic complex **5.10**. We reasoned that the high aurophilicity of phosphines would preserve the "zwitterionic" arrangement in both reduced and oxidized states.[18] Upon the addition of an equimolar solution of [Fc][BAr^F_{24}] in DCM at –78 °C, the colorless solution of **5.10** turns immediately deep purple, similar to the observation made in the oxidation of **5.6**. The EPR spectrum of the resulting solution shows a pseudo-isotropic signal centered near $g = 2$ that closely resembles the spectrum of **5.11**. Although we were unable to ascertain its solid-state molecular structure, we postulate, on the basis of the similarities in spectroscopic observations, that the product of the oxidation of **5.10** is analogous to the cation **5.11**. Thus, we speculate that structural reorganization may ensue upon the oxidation of **5.1**, perhaps to the symmetrical dicopper form (**Figure 5.10**).

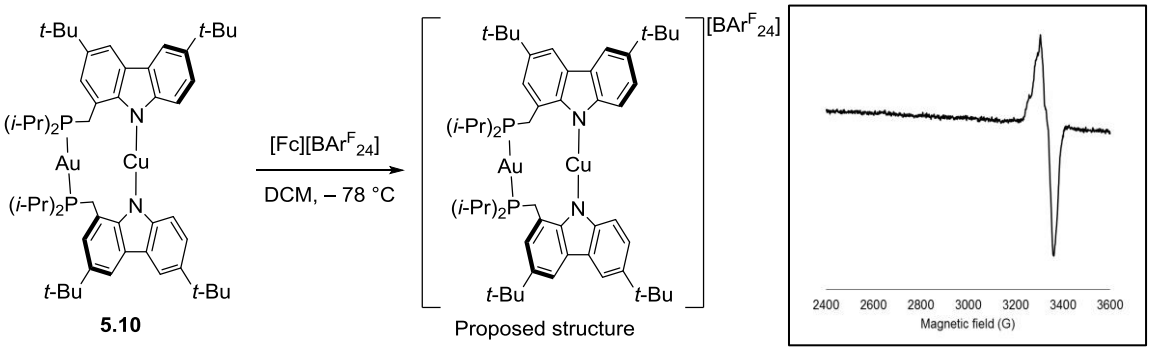

Figure 5.11. Oxidation of **5.10** with [Fc][BAr^F_{24}] at –78 °C in DCM. Inset: EPR spectrum (9.4 GHz, 77 K, DCM/toluene) of the crude mixture.

5.2.3. Investigation of mononuclear *S* = 1/2 copper complexes supported by (phosphino)carbazoles

As illustrated in **Figure 5.3**, we were also interested in targeting mononuclear, paramagnetic copper complexes of (phosphino)carbazole ligands. We found that the attempted substitution reactions of $Cu(OTf)_2$ or $CuBr_2$ at –78 °C using lithium or potassium salts of (phosphino)carbazole ligands do not result in the formation of a new EPR-active species. In contrast, $[Cu^{II}(carb)_3]Li$ or $[Cu^{II}(carb)_3]K$, generated in situ from $CuBr_2$ and Li(carb) or K(carb) (3 equiv) in THF at –78 °C, reacts readily with the lithium or potassium salts of various (phosphino)carbazoles.

Specifically, the addition of the freshly prepared solution of $[Cu^{II}(carb)_3]K$ to a solution of $Li(P_{iPr}N_H)$, the lithiated form of **L5.1**, in 2-MeTHF at –78 °C produces a new *S* = 1/2 species (**Figure 5.12**). The EPR spectrum of the resulting solution differs substantially from that of the oxidation product of the unsymmetrical dicopper complex **5.1** (**Figure 5.8**) or that of $[Cu^{II}(carb)_3]K$ (**Figure 2.7**). Although we were unable to confirm the product structurally, we propose it is $Cu^{II}(P_{iPr}N_H)(carb)$, the neutral mononuclear heteroleptic complex **5.12**, on the basis of the results that are described later in the section. In contrast, the EPR signal of $[Cu^{II}(carb)_3]K$ persists when added to **L5.1** instead of $Li(P_{iPr}N_H)$. Under analogous reaction conditions, the use of $Li(P_{Ph}N_H)$, the lithiated form of **L5.2** which contains a less electron-rich phosphine, produces a reaction mixture that is EPR-silent. The combined results indicate the importance of both an electron-donating phosphine and a basic nitrogen for the stabilization of the putative mononuclear *S* = 1/2 copper–phosphine complex.

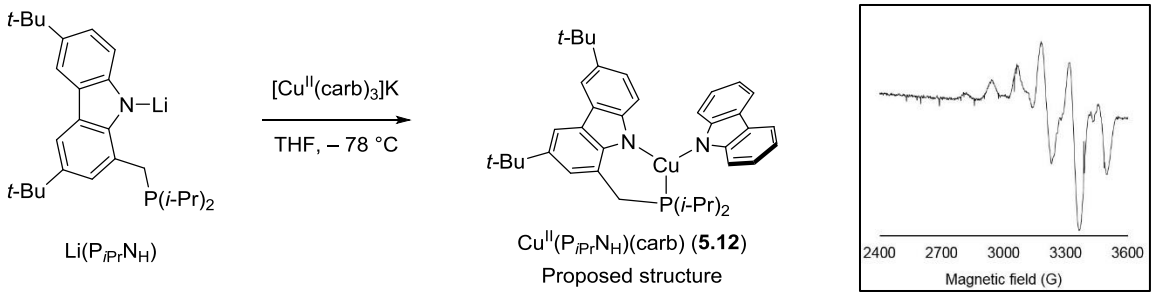

Figure 5.12. EPR spectrum (9.4 GHz, 77 K, THF/2-MeTHF) of a mononuclear S = 1/2 copper complex supported by ligand **L5.1**.

Similarly, the treatment of $[Cu^{II}(carb)_3]K$ with a solution of $Li(P_{iPr}N_{tBuPh})$, the lithium salt of **L5.5**, produces a new S = 1/2 complex as indicated by the EPR spectrum of the resulting mixture (**Figure 5.13**, route a, purple trace). The strong g-anisotropy signifies that the product is unlikely to be the oxidation product of the unsymmetrical dicopper complex **5.5**, which has similar spectral features to the cation **5.11** (pseudo-isotropic). Likewise, the addition of $[Cu^{II}(carb)_3]K$ to a solution of $Li(P_{iPr}N_{Mes})$, the lithium salt of **L5.7**, produces essentially the same EPR spectrum (**Figure 5.13**, route a, blue trace). The observed spectral resemblance is noteworthy in consideration of the structural dissimilarity between **5.5** and **5.7**, which are the S = 0 dicopper complexes supported by **L5.5** and **L5.7**, respectively. Moreover, identical EPR spectra can be acquired upon the addition of $[Fc][PF_6]$ to an equimolar mixture of CuBr, K(carb), and $Li(P_{iPr}N_{tBuPh})$ or $Li(P_{iPr}N_{Mes})$ (**Figure 5.13**, route b); in the absence of K(carb), or the (phosphino)carbazole ligand, the same EPR spectra are not generated, indicating that both the (phosphino)carbazole and carbazole moieties are ligated to the copper(II) complexes. In view of this result, we hypothesized that the products of these reactions may be the neutral, mononuclear heteroleptic complexes **5.13** or **5.14**.

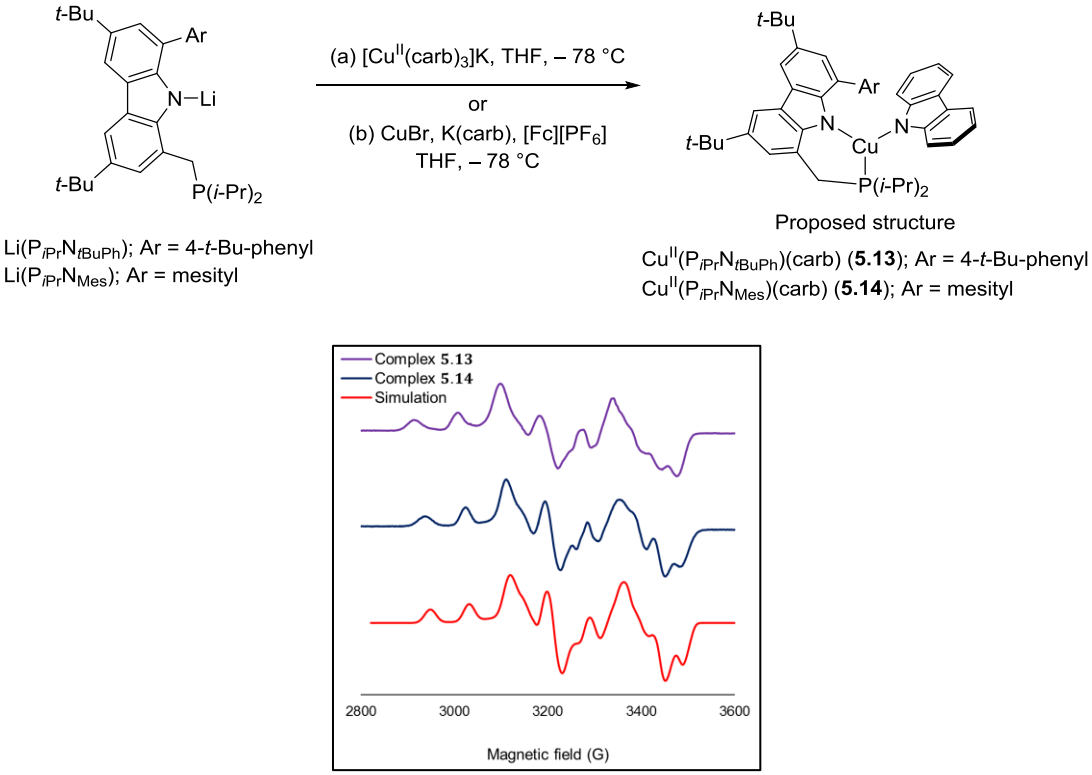

Figure 5.13. EPR spectra (9.4 GHz, 77 K, THF/2-MeTHF) of mononuclear $S = 1/2$ copper complexes supported by (phosphino)carbazole ligands **L5.5** or **L5.7** containing aryl substituents. Purple trace: spectrum of complex **5.13** generated via route a; blue trace: spectrum of complex **5.14** generated via route a; red trace: simulated spectrum of complex **5.14**. Simulation parameters are as follows: g = [2.009, 2.043, 2.126], A_{Cu} (MHz) = [105, 35, 243], A_N (MHz) = [24, 30, 18], A_N (MHz) = [24, 30, 18], A_P (MHz) = [500, 690, 515].

Consistent with our structural assignment, we were able to simulate the EPR spectrum of the putative paramagnetic copper complex **5.14** as a metalloradical (g = [2.009, 2.043, 2.126], A_{Cu} (MHz) = [105, 35, 243]; **Figure 5.13**, red trace) with large hyperfine couplings to one ^{31}P nucleus (A_P (MHz) = [500, 690, 515]).[19] To corroborate our EPR

simulations, we performed density functional theory calculations on complex **5.14**. The DFT computations reveal a significant delocalization of the unpaired spin, with 0.35 e^- on Cu and 0.12 e^- on P (**Figure 5.14a**). The appreciable spin density on the P atom of **5.14** is in line with the degree of spin delocalization observed in mononuclear S = 1/2 copper–bis(phosphine) complex reported by Peters and coworkers (**Figure 5.14b**);[6] however, complex **5.14** displays a more significant copper(II) character.

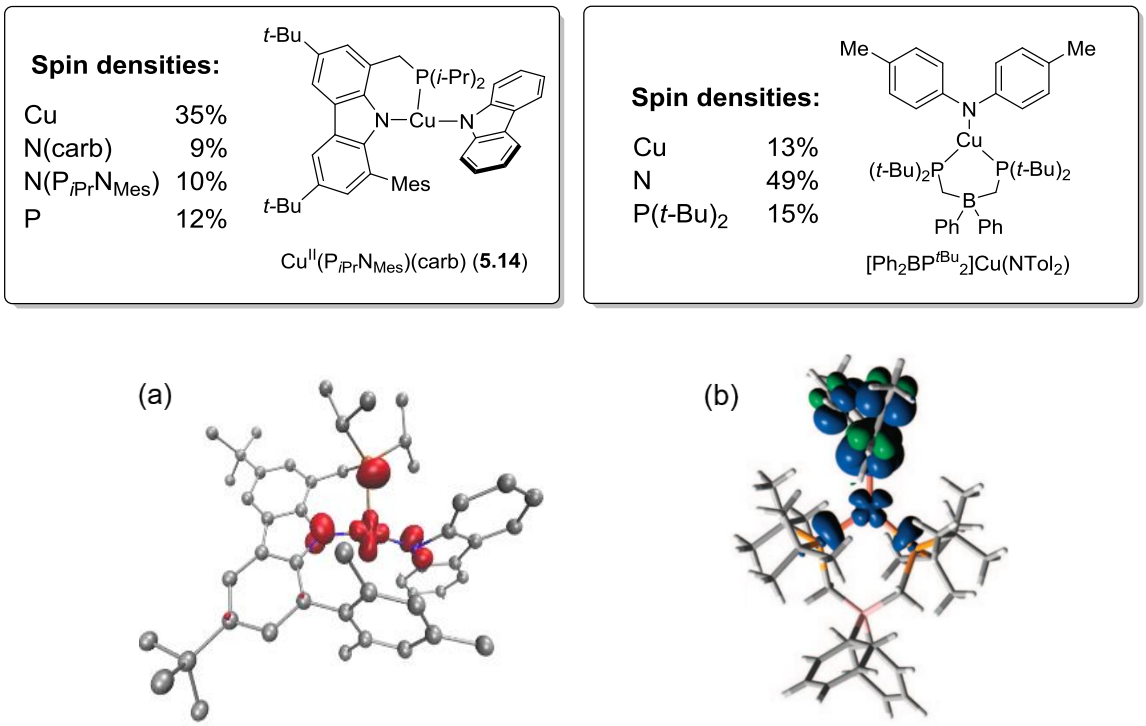

Figure 5.14. DFT-predicted spin densities of S = 1/2 copper–phosphine complexes. (a) Atomic spin density plot (M06-L, def2-TZVP) of complex **5.14**. (b) Atomic spin density plot (B(38HF)P86, GT 6-311+G(d)) of [$Ph_2BP^{tBu}_2$]Cu($NTol_2$) reported by Peters and coworkers; adapted with permission from ref 6. Copyright (2009) American Chemical Society.

Complexes **5.13** and **5.14** are thermally unstable and decompose within several hours at –35 °C. In hopes of improving the thermal stability of the neutral, mononuclear $S = 1/2$ complexes for structural confirmation, we evaluated a wide array of conditions and reagents, including K(carb$_{t\text{Bu}}$), the potassium salt of 3,6-di-*t*-butylcarbazole. We found that the addition of [Fc][PF_6] to an equimolar mixture of CuBr, K(carb$_{t\text{Bu}}$), and Li(P$_{i\text{Pr}}$N$_{\text{Mes}}$) in Et_2O at –78 °C produces a purple solution whose color and EPR spectrum persist for days at –35 °C (**Figure 5.15a**, black trace). The obtained EPR spectrum is essentially identical to that of complex **5.14**, indicating that introducing *t*-Bu groups does not perturb the electronic structure of the paramagnets to a significant degree. Owing to its improved thermal stability, we were able to confirm the identity of this species as complex **5.15**, the expected neutral complex Cu^{II}(P$_{i\text{Pr}}$N$_{\text{Mes}}$)(carb$_{t\text{Bu}}$) by single crystal XRD (**Figure 5.15b**). Although the quality of the X-ray data is modest, it unambiguously establishes the atomic connectivity of **5.15**.

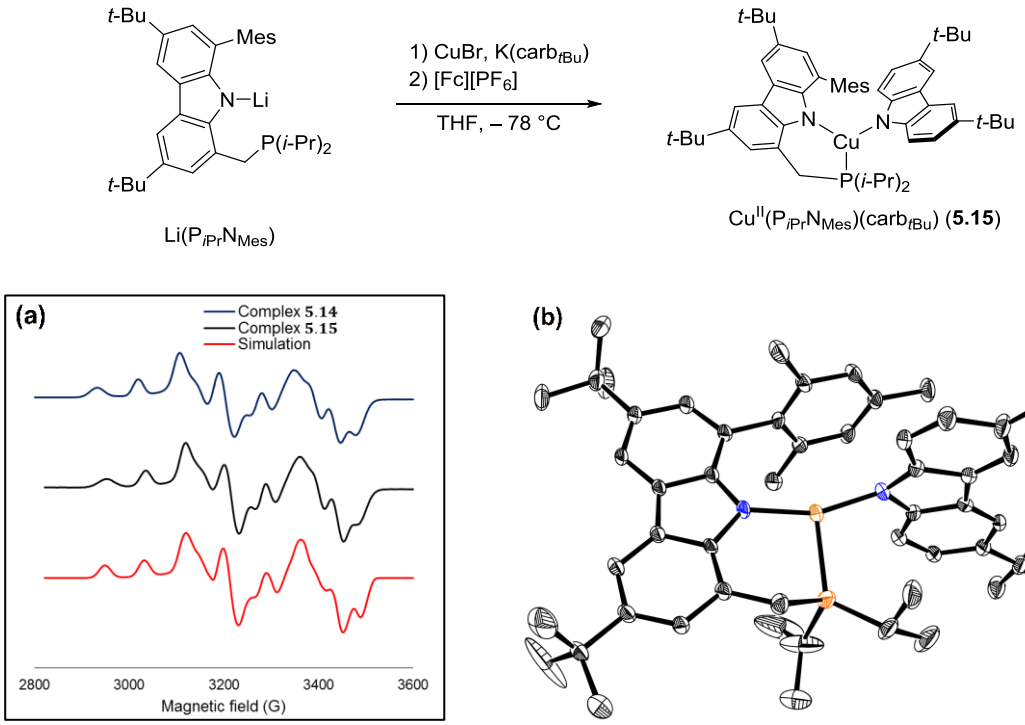

Figure 5.15. Generation of neutral, mononuclear heteroleptic $S = 1/2$ copper complex **5.15**. (a) EPR spectra (9.4 GHz, 77 K, Et_2O/2-MeTHF). Blue trace: complex **5.14**; black trace: complex **5.15**; red trace: simulated spectrum. See **Figure 5.13** for the simulation parameters. (b) Solid-state molecular structure of **5.15** determined by single crystal XRD depicted at 30 % thermal probability ellipsoids; hydrogen atoms and additional solvent molecules are omitted for clarity.

To the best of our knowledge, complex **5.15** is the only example of a structurally confirmed paramagnetic mononuclear copper complex of a monophosphine.[6] This finding is remarkable given the prevalent usage of phosphines as ligands in powerful, copper-catalyzed synthetic transformations.[20] As anticipated for a charge-neutral complex, **5.15** is considerably soluble in nonpolar solvents such as toluene and *n*-pentane even at –78 °C.

Thus, we speculate that the formation of related neutral species such as Cu^{II}(**SITCP**)$(carb)_2$ (**5.b**) may be feasible under the conditions of enantioselective N–alkylations of carbazoles (e.g. **Scheme 5.1**). Consistent with this hypothesis is the detection of a metalloradical in the EPR spectrum of an irradiated sample of the standard reaction mixture described in **Scheme 5.1** (**Figure 5.16**, red trace).[21] The major components of this EPR signal can be seen in the spectrum of the mixture of Cu^{I}(**SITCP**)$_2$(carb) and [Fc][PF_6] in toluene at –78 °C (**Figure 5.16**, black trace). While the observed spectrum is not identical to that of **5.15**, the moderate spread of the *g*-values and the apparent presence of hyperfine couplings to an $I = 1/2$ nucleus are noteworthy. We therefore speculate that the detected paramagnet may be **5.b** and raise the possibility that it may represent the persistent radical involved in an out-of-cage C–N coupling reaction with activated organic radicals in toluene (analogous to the conclusions in **Chapter 2** and **Chapter 4**).

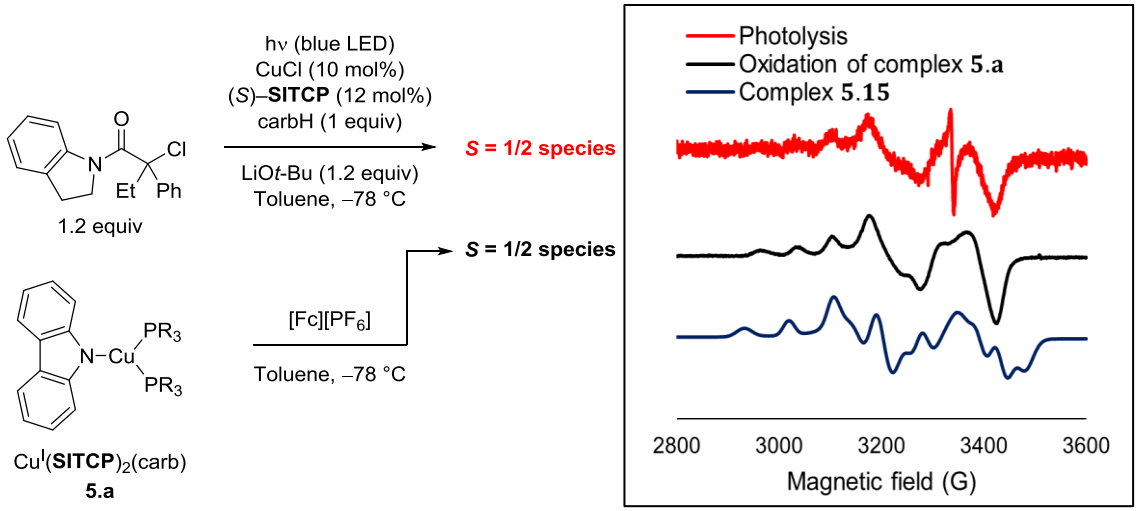

Figure 5.16. Detection of metalloradicals by EPR spectroscopy (9.4 GHz, 77 K). Red trace: EPR spectrum of the photolyzed sample of the standard stereoconvergent carbazole alkylation in toluene; black trace: EPR spectrum of the crude mixture of the chemical oxidation of complex **5.a** in toluene; blue trace: EPR spectrum of complex **5.15** in Et_2O/2-MeTHF. PR_3 = **SITCP**.

5.3. Concluding Remarks

We have prepared new bidentate (phosphino)carbazole ligands that support a diverse family of unusual dicopper complexes both in $S = 0$ and $S = 1/2$ states. We have demonstrated that **L5.1** can facilitate the photoinduced cyanomethylation of unactivated alkyl bromides in the presence of CuBr. The observed reactivity is the first established C_{sp^3}–C_{sp^3} bond-formation under photoinduced copper catalysis explored in the Fu and Peters laboratories. Using the bulky (phosphino)carbazole ligand **L5.7**, we have structurally confirmed a rare example of a mononuclear $S = 1/2$ copper complex containing a monophosphine moiety

(**5.15**). We suggest that it may serve as a model complex for the metalloradical intermediate observed under the conditions of photoinduced, enantioselective alkylations of carbazoles.

5.4. Experimental Section

5.4.1. General information

Unless otherwise noted, materials were either purchased from commercial suppliers and used as received, or prepared via literature procedures. Solvents were deoxygenated and dried by thoroughly sparging with argon, followed by passage through an activated column in a solvent purification system. Tris(4-bromophenyl)ammoniumyl hexachloroantimonate ("Magic Blue") was purchased from Sigma Aldrich and used as received.

All manipulations of air-sensitive materials were carried out in oven-dried glassware using standard Schlenk, or glovebox techniques, under an N_2 atmosphere. Silicycle *Silia*Flash® P60 silica gel (particle size 40–63 μm) was used for flash chromatography. Analytical thin layer chromatography was conducted with glass TLC plates (silica gel 60 F254), and spots were visualized under UV light or after treatment with standard TLC stains.

X-band EPR measurements were made with a Bruker EMX spectrometer at 77 K. Simulation of EPR data was conducted using the software EasySpin.[22]

IR measurements were recorded on a Bruker ALPHA Diamond ATR, or using a Perkin Elmer Paragon 1000 spectrometer, using thin films deposited on KBr plates.

^{1}H, ^{13}C, and ^{31}P NMR spectra were recorded on a Bruker Ascend 400 MHz, a Varian 300 MHz, a Varian 400 MHz, a Varian 500 MHz, or a Varian 600 MHz spectrometer with $CHCl_3$ (^{1}H, δ = 7.26) and $CDCl_3$ (^{13}C, δ = 77.0) as internal references and with 85% H_3PO_4 (^{31}P) as an external reference. Multiplicity and qualifier abbreviations are as follows: s =

singlet, d = doublet, t = triplet, q = quartet, m = multiplet, br = broad, app = apparent). GC analyses were carried out on an Agilent 6890 Series system with an HP-5 column (length 30 m, I.D. 0.25 mm).

X-ray crystallography studies were carried out at the Beckman Institute Crystallography Facility on either Bruker Kappa Apex II diffractometer or a Bruker D8 Venture kappa duo photon 100 CMOS instrument (Mo Kα radiation). Structures were solved using SHELXT and refined against F^2 by full-matrix least squares with SHELXL and OLEX2. Hydrogen atoms were added at calculated positions and refined using a riding model. The crystals were mounted on a glass fiber or a nylon loop with Paratone N oil.

Steady-state fluorimetry was performed in the Beckman Institute Laser Resource Center (BILRC; California Institute of Technology). Steady-state emission spectra were collected on a Jobin S4 Yvon Spec Fluorolog-3-11 with a Hamamatsu R928P photomultiplier tube detector with photon counting. Absorbance spectra were acquired on a Cary 50 UV-Vis spectrophotometer with a Unisoku Scientific Instruments cryostat to maintain temperature.

Measurements of the excited-state lifetimes were conducted in BILRC. A Q-switched Nd:YAG laser (SpectraPhysics Quanta-Ray PRO-Series; 355 nm) was used as the source of the excitation pulse Transmitted light from the sample was detected with a photomultiplier tube (Hamamatsu R928). All instruments and electronics in these systems were controlled by software written in LabVIEW (National Instruments).

Electrochemical measurements were carried out in a thick-walled one-component electrochemical cell fitted with a Teflon stopcock and tungsten leads protruding from the top of the apparatus in a nitrogen-filled glovebox. A CH Instruments 600B electrochemical analyzer or a CHS-3600B potentiostat was used for data collection. A freshly-polished glassy carbon electrode was used as the working electrode, and platinum wire was used as the auxiliary electrode. Solutions (THF) of electrolyte (0.1 M tetra-*n*-butylammonium hexafluorophosphate) contained ferrocene (~1 mM, post measurement), to serve as an internal reference, and analyte (~1 mM).

Mass spectral data were collected on a Thermo LCQ or LTQ ion trap mass spectrometer, or on an Agilent 5973 mass spectrometer.

Photolytic reactions were performed using 34 W Kessil H150 Blue LED lamps, a 100 W Blak-Ray Long Wave Ultraviolet Lamp (Hg), or a 100-W Blak-Ray B-100Y High Intensity Inspection Lamp (Hg). If required, the temperature was maintained with an isopropanol bath cooled by an SP Scientific cryostat.

The Orca 3.0.1 program was used for all calculations.[23] All optimizations and energy calculations were conducted with tight convergence criteria using the M06-L functional[24] and def2-TZVP basis set.[25] Open- and closed-shell species were modeled within the unrestricted and restricted Kohn-Sham formalisms, respectively. All geometry optimizations were conducted without symmetry constraints using gradient methods. Ground state geometries were verified as true minima by the absence of imaginary frequencies.

5.4.2. Synthesis of (phosphino)carbazole ligands

Preparation of $P_{iPr}N_H$ (L5.1)

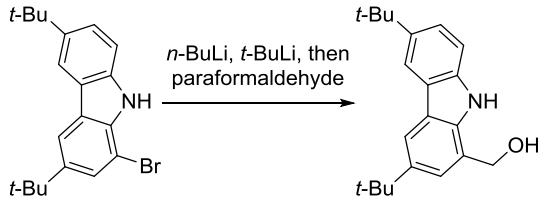

To a suspension of 1-bromo-3,6-di-*t*-butylcarbazole[26] (15 g, 42 mmol, 1 equiv) in 400 mL Et_2O in a 500 mL Schlenk flask, *n*-BuLi in hexanes (42.5 mmol, 1 equiv) was added at 0 °C under nitrogen atmosphere slowly over a period of 5 min. After 30 min, the mixture was cooled to –78 °C, and *t*-BuLi in pentane (84 mmol, 2 equiv) was added slowly over a period of 15 min. The reaction mixture was stirred for an additional 2 h at –78 °C. Next, paraformaldehyde (2 g) was added in one portion under a positive flow of nitrogen, and the suspension was allowed to warm to room temperature overnight. The resulting red solution was carefully quenched with $NH_4Cl_{(aq)}$ (100 mL) under nitrogen atmosphere and transferred to a separatory funnel; and the resulting yellow organic layer was washed with $NaCl_{(aq)}$ (200 mL), dried over Na_2SO_4 and concentrated to yield pale yellow residue which upon washing with cold hexanes gives spectroscopically pure, off-white solid (11 g, 85% yield). This material can be carried forward, but additional purification by column chromatography on silica gel can also be performed, eluting with DCM → 3% DCM/MeOH.

^{1}H NMR (300 MHz, $CDCl_3$) δ 8.58 (br, 1H), 8.07 (d, J = 1.5 Hz, 1H), 8.03 (d, J = 1.6 Hz, 1H), 7.48 (dd, J = 8.5 Hz, 1.9 Hz, 1H), 7.37 (d, J = 8.5 Hz, 1H), 7.28 (d, J = 1.8 Hz, 1H), 5.07 (s, 2H), 1.45 (s, 9H), 1.44 (s, 9H).

^{13}C NMR (151 MHz, $CDCl_3$) δ 142.3, 142.0, 138.3, 137.1, 123.9, 123.8, 123.1, 122.00, 121.95, 116.3, 116.1, 110.5, 64.8, 34.82, 34.78, 32.2.

FT-IR (film): 3332, 2961, 2904, 2867, 1493, 1363, 1241, 1006, 873 cm^{-1}.

MS (ESI) m/z $(M)^+$ calcd for $C_{21}H_{27}NO$: 309.2, found: 309.2.

$P_{iPr}N_H$ (L5.1)

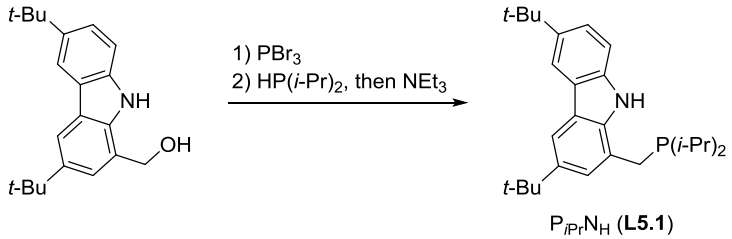

$P_{iPr}N_H$ (**L5.1**)

Note: Aqueous workup was performed under air-free conditions due to the high air-sensitivity of the benzyl bromide intermediate.

A 40 mL scintillation vial was charged with (3,6-di-*t*-butyl-carbazol-1-yl)methanol (400 mg, 1.3 mmol, 1 equiv) and a magnetic stir bar. The vial was capped with a PTFE-lined septum cap, and then evacuated and backfilled with nitrogen (3 cycles). Degassed Et_2O (5 mL) was introduced via syringe, and the resulting suspension was cooled to 0 °C. Phosphorus tribromide (0.12 mL, 1.3 mmol, 1 equiv) was added dropwise, and the resulting solution was stirred for an additional 30 min at 0 °C. Next, degassed $NaHCO_{3(aq)}$ was added via syringe, and the organic layer was transferred to a 20 mL scintillation vial equipped with PTFE-lined septum cap containing $MgSO_4$ and di-*i*-propylphosphine (200 mg, 1.7 mmol, 1.3 equiv) under nitrogen via syringe. The aqueous layer was extracted with Et_2O (5 mL), and the organic layer was added to the vial containing $MgSO_4$ and di-*i*-propylphosphine. The

suspension was stirred overnight and filtered under nitrogen, and the filtrate was concentrated in vacuo to afford yellow residue. The residue was washed with *n*-pentane, re-suspended in Et_2O (5 mL), and stirred for 30 min after adding degassed triethylamine (1 mL). Next, the suspension was filtered and concentrated to afford pale yellow foamy solid (340 mg, 64% yield).

^{1}H NMR (400 MHz, C_6D_6) δ 8.65 (br, 1H), 8.31 (s, 1H), 8.19 (s, 1H), 7.45 (s, 1H), 7.43 (br, 1H), 7.14 (br, 1H), 2.96 (s, 2H), 1.60–1.58 (m, 2H), 1.48 (s, 9H), 1.42 (s, 9H), 1.02–0.84 (m, 12H).

^{13}C NMR (101 MHz, C_6D_6) δ 142.5, 142.4, 138.94, 138.93, 138.20, 138.19, 125.1, 125.0, 124.6, 124.4, 123.9, 121.33, 121.27, 116.7, 114.47, 114.45, 111.1, 34.8, 32.3, 32.2, 28.0, 27.8, 24.0, 23.8, 19.9, 19.7, 19.0, 18.9.

^{31}P NMR (162 MHz, C_6D_6) δ –3.4.

FT-IR (film): 2951, 2902, 2865, 1492, 1459, 1393, 869, 1240, 1202, 809 cm^{-1}.

Preparation of $P_{Ph}N_H$ (L5.2)

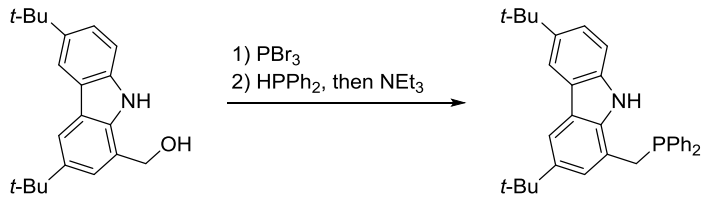

$P_{Ph}N_H$ (**L5.2**)

Note: Aqueous workup was performed under air-free conditions due to the high air-sensitivity of the benzyl bromide intermediate.

A 40 mL scintillation vial was charged with (3,6-di-*t*-butyl-carbazol-1-yl)methanol (800 mg, 2.6 mmol, 1 equiv) and a magnetic stir bar. The vial was capped with a PTFE-lined septum cap, and then evacuated and backfilled with nitrogen (3 cycles). Degassed Et_2O (5 mL) was introduced via syringe, and the resulting suspension was cooled to 0 °C. Phosphorus tribromide (0.24 mL, 2.6 mmol, 1 equiv) was added dropwise, and the resulting solution was stirred for an additional 30 min at 0 °C. Next, degassed $NaHCO_{3(aq)}$ was added via syringe, and the organic layer was transferred to a 20 mL scintillation vial equipped with PTFE-lined septum cap containing $MgSO_4$. The mixture was filtered in the glovebox and concentrated in vacuo, and the residue was dissolved in DCM (5 mL). This solution was added dropwise over 10 min to a solution of diphenylphosphine (1 g, 5.4 mmol, 2 equiv) in DCM (5 mL) in a 20 mL scintillation vial. The solution was stirred overnight and concentrated in vacuo to afford yellow residue. The residue was washed with *n*-pentane, re-suspended in DCM (5 mL), and stirred for 30 min after adding degassed triethylamine (1 mL). Next, volatiles were removed in vacuo and the residue was extracted in Et_2O (5 mL). The resulting white precipitate was removed by filtration and the filtrate was concentrated and washed with *n*-pentane to give off-white solid (550 mg, 44% yield).

^{1}H NMR (400 MHz, C_6D_6) δ 8.28 (s, 1H), 8.13 (s, 1H), 7.51 (d, J = 8.4 Hz, 1H), 7.41 (s, 1H), 7.38–7.26 (m, 4H), 7.12 (s, 1H), 7.06–6.98 (m, 7H), 3.44 (s, 2H), 1.44 (d, J = 1.3 Hz, 9H), 1.34 (d, J = 1.3 Hz, 9H).

^{13}C NMR (101 MHz, C_6D_6) δ 142.3, 141.1, 139.1, 139.0, 138.9, 133.5, 133.3, 129.0, 128.71, 128.65, 125.6, 125.5, 124.5, 123.8, 119.0, 116.7, 114.8, 114.7, 111.0, 111.0, 34.8, 34.7, 33.3, 33.2, 32.3, 32.2.

^{31}P NMR (162 MHz, C_6D_6) δ –19.0.

FT-IR (film): 3433, 2960, 2902, 2866, 1492, 1362, 1241, 869 cm^{-1}.

Preparation of $P_{iPr}N_{Me}$ (L5.3)

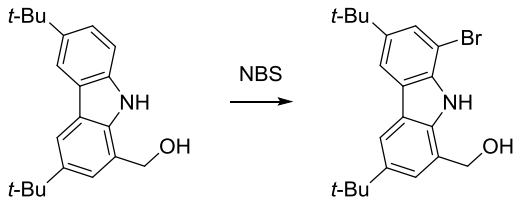

A 250 mL flask was charged with (3,6-di-*t*-butyl-carbazol-1-yl)methanol (7.5 g, 24 mmol, 1 equiv) and a magnetic stir bar, before the addition of chloroform (150 mL). The solution was then cooled to 0 °C and N-bromosuccinimide (4.3 g, 24 mmol, 1 equiv) was added in portions. After warming to room temperature overnight, the white solid was collected by filtration and washed with cold dichloromethane, yielding the title compound in spectroscopically pure form. To recover the target compound in the filtrate, the filtrate was concentrated and the residue was purified by column chromatography, eluting with 10% → 50% EtOAc/hexanes (8.4 g, 90% yield overall).

^{1}H NMR (300 MHz, $CDCl_3$) δ 8.67 (s, 1H), 8.00 (s, 2H), 7.60 (s, 1H), 7.33 (s, 1H), 5.11 (d, J = 6.1 Hz, 2H), 1.44 (s, 18H).

^{13}C NMR (101 MHz, $CDCl_3$) δ 144.2, 142.8, 136.9, 136.8, 126.1, 124.5, 124.3, 122.6, 116.5, 115.6, 104.0, 100.1, 64.9, 35.0, 34.9, 32.1.

FT-IR (film): 3548, 3221, 2958, 1560, 1362, 1007, 950, 875 cm^{-1}.

MS (ESI) m/z $(M)^+$ calcd for $C_{21}H_{26}BrNO$: 387.1, found: 387.1.

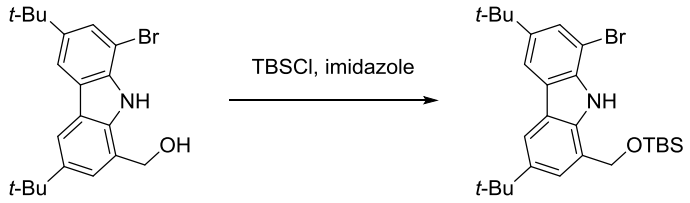

A 40 mL scintillation vial was charged with (8-bromo-3,6-di-*t*-butyl-carbazol-1-yl)methanol (777 mg, 2.0 mmol, 1 equiv), imidazole (272 mg, 4.0 mmol, 2 equiv), DMF (10 mL), and a magnetic stir bar. Next, TBSCl (604 mg, 4.0 mmol, 2 equiv) was added in portions at 0 °C, and the solution was allowed to warm to room temperature overnight. The residue was poured into a separatory funnel containing $NaHCO_{3(aq)}$, (50 mL) and extracted in Et_2O (50 mL). The organic layer was washed with brine (3 × 50 mL). The combined organic layer was dried over Na_2SO_4, filtered, and concentrated in vacuo. The residue was purified by column chromatography eluting with hexanes → 5% Et_2O/hexanes to give the title compound as oily yellow solid (780 mg, 78% yield).

^{1}H NMR (300 MHz, $CDCl_3$) δ 8.82 (s, 1H), 8.01 (s, 1H), 7.96 (s, 1H), 7.60 (d, J = 1.4 Hz, 1H), 7.26 (s, 1H), 5.14 (s, 2H), 1.50–1.37 (m, 18H), 0.99 (s, 9H), 0.16 (s, 6H).

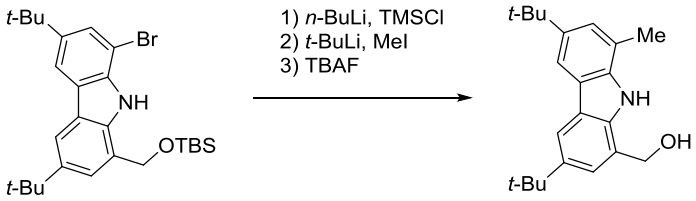

A 250 mL Schlenk flask was charged with 1-bromo-3,6-di-*t*-butyl-8-(((*t*-butyldimethylsilyl)oxy)methyl)-carbazole (1.3 g, 2.6 mmol, 1 equiv) and a magnetic stir bar.

The flask was capped with a rubber septum and placed under nitrogen, and degassed Et_2O (100 mL) was added. The solution was cooled to 0 °C, and *n*-BuLi (2.6 M in hexanes, 2.6 mmol, 1 equiv) was added. After stirring for 30 min, chlorotrimethylsilane (0.33 mL, 2.6 mmol, 1 equiv). After stirring at room temperature for 30 min, the flask was cooled to –78 °C, and *t*-BuLi (1.9 M in pentane, 5.2 mmol, 2 equiv) was added dropwise. After stirring for 1 h, iodomethane (0.4 mL, 6 mmol, 2.3 equiv) was added. The solution was allowed to warm to room temperature overnight. The reaction was quenched with $NH_4Cl_{(aq)}$ (50 mL), and the organic layer was dried over Na_2SO_4, filtered, and concentrated in vacuo. The resulting mixture was dissolved in THF (50 mL), and TBAF (1 M in THF, 6 mmol, 2.3 equiv) was added. The solution was stirred at room temperature overnight and concentrated in vacuo. The residue was extracted in EtOAc (50 mL), and washed with distilled water (50 mL). The organic layer was dried over Na_2SO_4, filtered, and concentrated in vacuo. The residue was purified by column chromatography, eluting with 20% → 50% EtOAc/hexanes to give the target compound as pale yellow solid (330 mg, 39% yield).

^{1}H NMR (300 MHz, $CDCl_3$) δ 8.42 (s, 1H), 8.02 (d, J = 1.6 Hz, 1H), 7.92 (s, 1H), 7.28 (s, 2H), 5.08 (d, J = 6.0 Hz, 2H), 2.56 (s, 3H), 1.44 (s, 18H).

General Procedure 1: the conversion of benzylic alcohols to (phosphino)carbazoles

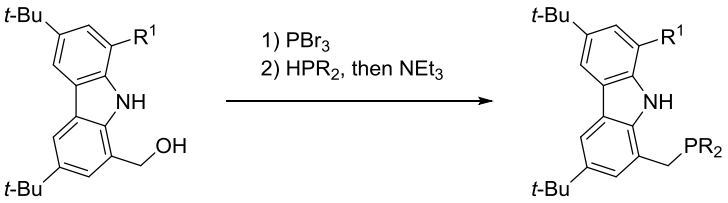

A 100 mL roundbottom flask was charged with the alcohol (1 equiv) and a magnetic stir bar. The flask was placed under nitrogen atmosphere and the starting material was dissolved in degassed DCM (30 mL). After cooling to 0 °C, phosphorus tribromide (1 equiv) was added dropwise, and the resulting solution was stirred for an additional 30 min at 0 °C. Next, the mixture was transferred to a separatory funnel containing $NaHCO_{3(aq)}$ (30 mL). The organic layer was washed with brine (30 mL), dried over Na_2SO_4, filtered, and concentrated in vacuo. The residue was transferred to the glovebox and re-dissolved in DCM (10 mL). To this mixture, a solution of di-*i*-propylphosphine (at least 1 equiv) in DCM was added in one portion. The solution was stirred overnight and concentrated in vacuo to afford yellow residue. The residue was washed with *n*-pentane, re-suspended in DCM (5 mL), and stirred for 30 min after adding degassed triethylamine (1 mL). Next, volatiles were removed in vacuo and the residue was extracted in Et_2O (5 mL). The resulting white precipitate (NH_4Br) was removed by filtration and the filtrate was concentrated and layered with either *n*-pentane or CH_3CN to precipitate the title compound as off-white solid.

$P_{iPr}N_{Me}$ (L5.3)

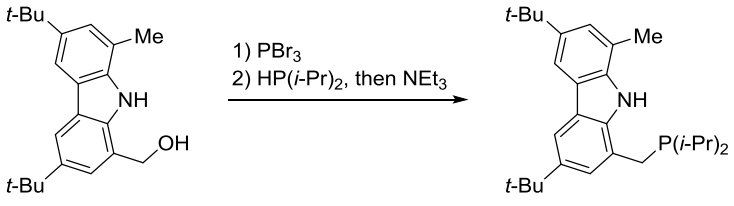

$P_{iPr}N_{Me}$ (**L5.3**)

Following General Procedure 1, the title compound can be obtained from (3,6-di-*t*-butyl-8-methyl-carbazol-1-yl)methanol (320 mg, 1.0 mmol, 1 equiv), phosphorous

tribromide (0.10 mL, 1.1 mmol, 1.1 equiv) and di-*i*-propylphosphine (120 mg, 1.0 mmol, 1 equiv) as pale yellow solid (400 mg, 94% yield).

^{1}H NMR (300 MHz, C_6D_6) δ 8.85 (d, J = 7.9 Hz, 1H), 8.22 (s, 2H), 7.42 (s, 1H), 7.34 (s, 1H), 3.01 (s, 2H), 2.38 (s, 3H), 1.62–1.57 (m, 2H), 1.49 (s, 9H), 1.47 (s, 9H), 1.06–0.85 (m, 12H).

^{13}C NMR (101 MHz, C_6D_6) δ 142.8, 142.6, 138.57, 138.55, 138.29, 138.27, 125.10, 125.09, 124.9, 124.84, 124.82, 124.72, 124.71, 124.17, 124.16, 121.53, 121.47, 119.9, 114.8, 114.5, 110.4, 34.8, 32.33, 32.28, 28.3, 28.1, 24.0, 23.9, 19.9, 19.7, 18.9, 18.8.

^{31}P NMR (121 MHz, C_6D_6) δ –3.9.

FT-IR (film): 3389, 2950, 2903, 2866, 1493, 1383, 1297, 1242, 895 cm^{-1}.

MS (ESI) m/z $(M+Na)^+$ calcd for $C_{28}H_{42}NPNa$: 446.3, found: 446.4.

Preparation of $P_{iPr}N_{FPh}$ (L5.4)

General Procedure 2: Suzuki-Miyaura arylations

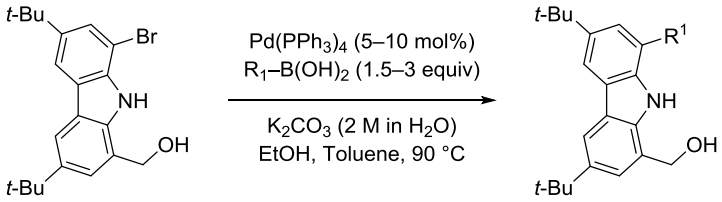

A 40 mL scintillation vial was charged with (8-bromo-3,6-di-*t*-butyl-carbazol-1-yl)methanol (1 equiv), aryl boronic acid (1.5 equiv), and a magnetic stir bar. The vial was capped with a PTFE-lined septum cap, and evacuated and backfilled with nitrogen (3 cycles).

Then, the vial was transported to a nitrogen-filled glovebox, and $Pd(PPh_3)_4$ (0.05 equiv) was added to the vial. Next, degassed toluene (10 mL), ethanol (5 mL), and 2 M $K_2CO_{3(aq)}$ (10 mL) were added to the vial via syringe. After sealing the puncture holes with vacuum grease, the vial was placed on a metal heating block, and the mixture was heated to 90 °C overnight. After cooling to room temperature, the mixture was extracted with EtOAc (3 × 5 mL), and the combined organic layer was dried over Na_2SO_4, filtered, and concentrated. The residue was purified by column chromatography.

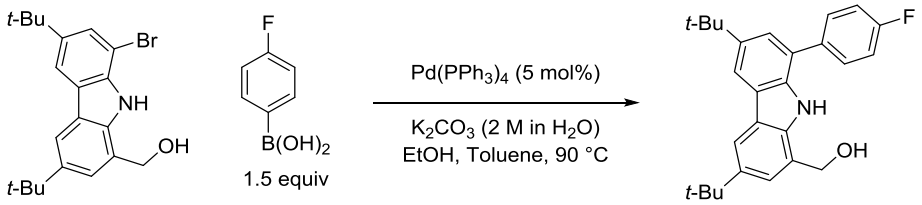

Following General Procedure 2, (8-bromo-3,6-di-*t*-butyl-carbazol-1-yl)methanol (510 mg, 1.3 mmol, 1 equiv) and (4-fluorophenyl)boronic acid (280 mg, 2.0 mmol, 1.5 equiv), were reacted with $Pd(PPh_3)_4$ (75 mg, 0.065 mmol, 0.05 equiv) to give the title compound as off-white solid (510 mg, 97% yield) after purification by column chromatography, eluting with 5% → 30% EtOAc/hexanes.

^{1}H NMR (300 MHz, $CDCl_3$) δ 8.68 (s, 1H), 8.06 (d, J = 3.8 Hz, 2H), 7.67 (dd, J = 8.8, 5.3 Hz, 2H), 7.43 (d, J = 1.8 Hz, 1H), 7.33–7.25 (m, 2H), 7.24 (s, 1H), 5.05 (d, J = 5.6 Hz, 2H), 1.49 (s, 9H), 1.45 (s, 9H).

^{13}C NMR (151 MHz, $CDCl_3$) δ 163.1, 161.5, 142.9, 142.3, 137.2, 136.0, 135.78, 135.76, 130.1, 130.0, 124.1, 123.9, 123.8, 123.6, 122.19, 122.15, 116.23, 116.21, 116.1, 115.7, 64.7, 34.9, 34.8, 32.2, 32.2.

^{19}F NMR (282 MHz, $CDCl_3$) δ –115.1.

FT-IR (film): 3467, 2961, 1606, 1510, 1222, 838 cm^{-1}.

MS (ESI) m/z $(M)^+$ calcd for $C_{27}H_{30}FNO$: 403.2, found: 403.3.

$P_{iPr}N_{FPh}$ (L5.4)

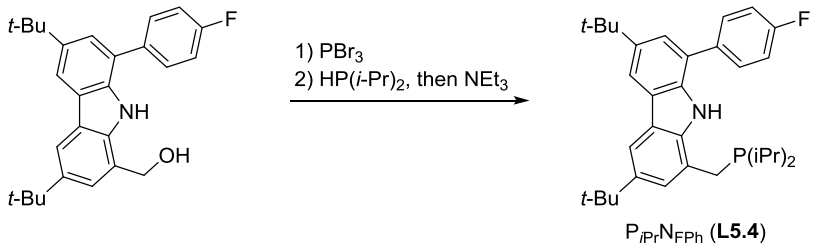

$P_{iPr}N_{FPh}$ (**L5.4**)

Following General Procedure 1, the title compound can be obtained from (3,6-di-*t*-butyl-8-(4-fluorophenyl)-carbazol-1-yl)methanol (510 mg, 1.3 mmol, 1 equiv), phosphorous tribromide (0.12 mL, 1.3 mmol, 1 equiv) and di-*i*-propylphosphine (150 mg, 1.3 mmol, 1 equiv) as white solid (610 mg, 93% yield).

^{1}H NMR (400 MHz, C_6D_6) δ 9.15 (d, J = 6.4 Hz, 1H), 8.35 (s, 1H), 8.24 (s, 1H), 7.64–7.53 (m, 3H), 7.42 (s, 1H), 7.00 (t, J = 8.5 Hz, 2H), 2.89 (s, 2H), 1.60–1.50 (m, 2H), 1.49 (s, 9H), 1.47 (s, 9H), 1.06–0.70 (m, 12H).

^{13}C NMR (126 MHz, C_6D_6) δ 163.7, 161.7, 143.2, 142.9, 138.3, 136.8, 136.3, 130.5, 125.33, 125.2, 125.1, 124.6, 124.2, 123.9, 123.7, 121.9, 116.6, 116.4, 116.2, 115.9, 114.8, 114.5, 34.94, 34.85, 32.5, 32.3, 32.2, 32.0, 27.8, 27.6, 24.1, 24.02, 23.95, 23.9, 19.9, 19.84, 19.80, 19.7, 18.8, 18.7, 18.6.

^{19}F NMR (282 MHz, C_6D_6) δ –115.1.

^{31}P NMR (162 MHz, C_6D_6) δ –2.3.

FT-IR (film): 3377, 3042, 2951, 2866, 1509, 1490, 1266, 1246, 836 cm^{-1}.

MS (ESI) m/z $(M+H)^+$ calcd for $C_{33}H_{43}FNP$: 504.3, found: 504.4.

Preparation of $P_{iPr}N_{tBuPh}$ (L5.5)

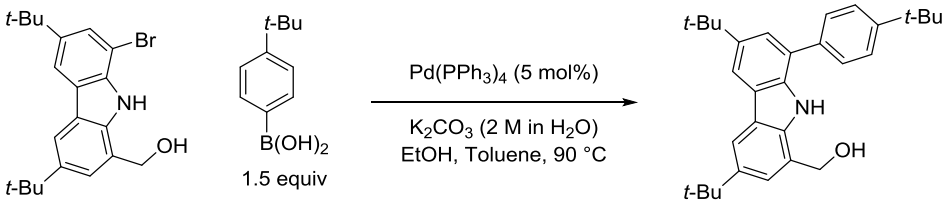

Following General Procedure 2, (8-bromo-3,6-di-*t*-butyl-carbazol-1-yl)methanol (510 mg, 1.3 mmol, 1 equiv) and (4-(*t*-butyl)phenyl)boronic acid (356 mg, 2.0 mmol, 1.5 equiv), were reacted with $Pd(PPh_3)_4$ (75 mg, 0.065 mmol, 0.05 equiv) to give the title compound as pale yellow, foamy solid (500 mg, 87% yield) after purification by column chromatography, eluting with 10% → 30% EtOAc/hexanes.

^{1}H NMR (300 MHz, $CDCl_3$) δ 8.75 (s, 1H), 8.06 (s, 2H), 7.66 (d, J = 8.3 Hz, 2H), 7.58 (d, J = 8.1 Hz, 2H), 7.49 (d, J = 1.9 Hz, 1H), 7.29 (s, 1H), 5.05 (d, J = 5.7 Hz, 2H), 1.48 (s, 9H), 1.45 (s, 9H), 1.42 (s, 9H).

^{13}C NMR (151 MHz, $CDCl_3$) 150.4, 142.9, 142.1, 137.1, 136.9, 136.1, 128.1, 126.3, 124.5, 124.2, 124.1, 123.7, 122.11, 122.07, 116.2, 115.4, 64.8, 34.9, 34.80, 34.77, 32.24, 32.20, 31.5.

FT-IR (film): 3465, 3338, 2950, 1491, 1363, 1234, 1019, 871 cm^{-1}.

$P_{iPr}N_{tBuPh}$ (L5.5)

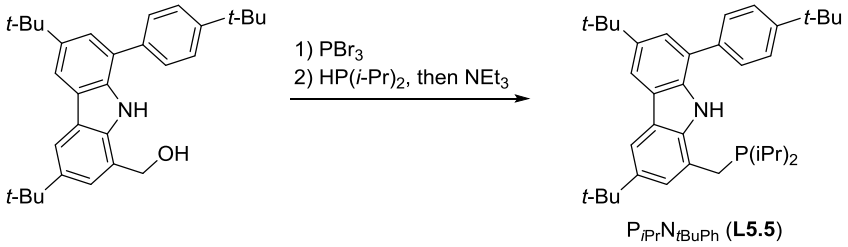

Following General Procedure 1, the title compound can be obtained from (3,6-di-*t*-butyl-8-(4-(*t*-butyl)phenyl)-carbazol-1-yl)methanol (470 mg, 1.1 mmol, 1 equiv), phosphorous tribromide (0.11 mL, 1.2 mmol, 1.1 equiv) and di-*i*-propylphosphine (120 mg, 1.0 mmol, 0.95 equiv) as pale yellow solid (220 mg, 38% yield). Additional purification can be performed by recrystallization from saturated Et_2O solution at –35 °C.

^{1}H NMR (400 MHz, C_6D_6) δ 9.21 (d, J = 5.9 Hz, 1H), 8.36 (d, J = 1.5 Hz, 1H), 8.26 (s, 1H), 7.86 (d, J = 8.5 Hz, 2H), 7.78 (d, J = 1.8 Hz, 1H), 7.48 (d, J = 8.4 Hz, 2H), 7.45 (br, 1H), 2.86 (s, 2H), 1.58–1.55 (m, 2H), 1.50 (s, 9H), 1.49 (s, 9H), 1.31 (s, 9H), 1.03–0.82 (m, 12H).

^{13}C NMR (126 MHz, C_6D_6) δ 150.2, 143.1, 142.6, 138.2, 137.6, 137.0, 126.4, 125.3, 125.1, 124.6, 123.8, 121.8, 116.1, 115.9, 114.8, 114.5, 35.0, 32.6, 32.4, 32.2, 31.7, 31.6, 31.4, 24.1, 19.9, 18.8.

^{31}P NMR (162 MHz, C_6D_6) δ –1.6.

FT-IR (film): 3405, 2951, 2865, 1493, 1459, 1294, 1245, 933 cm^{-1}.

MS (ESI) m/z $(M)^+$ calcd for $C_{37}H_{52}NP$: 541.4, found: 541.3.

Preparation of $P_{iPr}N_{MeOPh}$ (L5.6)

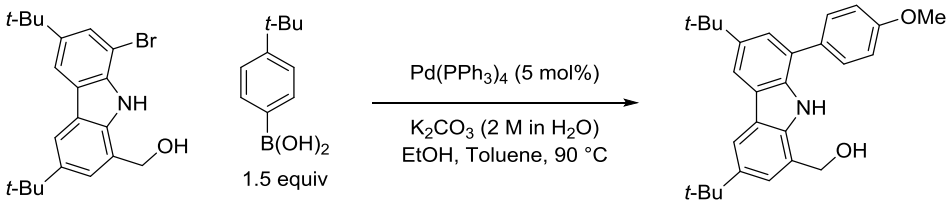

Following General Procedure 2, (8-bromo-3,6-di-*t*-butyl-carbazol-1-yl)methanol (510 mg, 1.3 mmol, 1 equiv) and (4-methoxyphenyl)boronic acid (300 mg, 2.0 mmol, 1.5 equiv), were reacted with $Pd(PPh_3)_4$ (75 mg, 0.065 mmol, 0.05 equiv) to give the title compound as pale yellow, foamy solid (520 mg, 96% yield) after purification by column chromatography, eluting with 5% → 60% EtOAc/hexanes.

^{1}H NMR (300 MHz, $CDCl_3$) δ 8.71 (s, 1H), 8.05 (s, 2H), 7.64 (d, J = 8.4 Hz, 2H), 7.45 (s, 1H), 7.28 (s, 1H), 7.09 (d, J = 8.5 Hz, 2H), 5.04 (d, J = 6.1 Hz, 2H), 3.90 (s, 3H), 1.48 (s, 9H), 1.45 (s, 9H).

^{13}C NMR (151 MHz, $CDCl_3$) δ 159.1, 142.8, 142.1, 137.1, 136.1, 132.2, 129.5, 124.3, 124.2, 123.7, 123.6, 122.21, 122.00, 116.1, 115.1, 114.7, 64.6, 55.4, 34.9, 34.8, 32.20, 32.15.

FT-IR (film): 3460, 2961, 1610, 1513, 1492, 1246, 1034, 833 cm^{-1}.

MS (ESI) m/z $(M+H)^+$ calcd for $C_{28}H_{34}NO_2$: 416.3, found: 416.3.

$P_{iPr}N_{MeOPh}$ (L5.6)

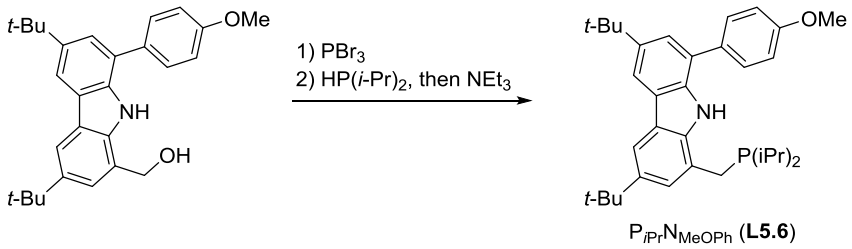

$P_{iPr}N_{MeOPh}$ (**L5.6**)

Following General Procedure 1, the title compound can be obtained from (3,6-di-*t*-butyl-8-(4-methoxyphenyl)-carbazol-1-yl)methanol (520 mg, 1.3 mmol, 1 equiv), phosphorous tribromide (0.12 mL, 1.3 mmol, 1 equiv) and di-*i*-propylphosphine (130 mg, 1.1 mmol, 0.9 equiv) as pale yellow solid (610 mg, 78% yield).

^{1}H NMR (400 MHz, C_6D_6) δ 9.23 (d, J = 5.1 Hz, 1H), 8.36 (s, 1H), 8.26 (s, 1H), 7.79 (d, J = 8.6 Hz, 2H), 7.72 (s, 1H), 7.44 (s, 1H), 6.99 (d, J = 8.8 Hz, 2H), 3.35 (s, 3H), 2.90 (s, 2H), 1.62–1.50 (m, 2H), 1.50 (s, 18H), 1.06 – 0.77 (m, 12H).

^{13}C NMR (101 MHz, C_6D_6) δ 159.6, 143.1, 142.6, 138.3, 136.9, 132.7, 130.0, 125.13, 125.06, 124.7, 123.8, 121.84, 121.77, 115.7, 115.0, 114.6, 54.8, 35.0, 34.9, 32.33, 32.28, 27.8, 27.6, 24.1, 24.0, 19.9, 19.8, 18.8, 18.7.

^{31}P NMR (162 MHz, C_6D_6) δ –2.3.

FT-IR (film): 3382, 2950, 2865, 2836, 1512, 1490, 1246, 812 cm^{-1}.

MS (ESI) m/z $(M)^+$ calcd for $C_{34}H_{46}NOP$: 515.3, found: 515.4.

Preparation of $P_{iPr}N_{Mes}$ (L5.7)

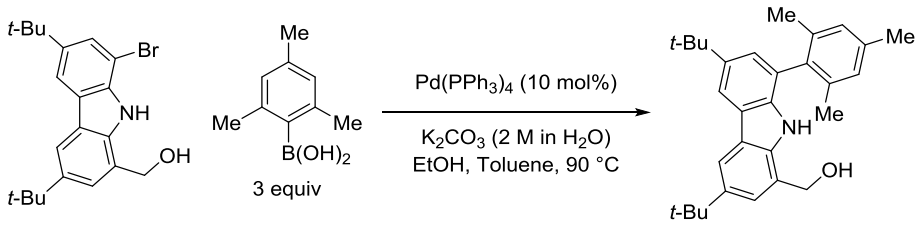

Following General Procedure 2, (8-bromo-3,6-di-*t*-butyl-carbazol-1-yl)methanol (510 mg, 1.3 mmol, 1 equiv) and mesitylboronic acid (490 mg, 3.9 mmol, 3 equiv), were reacted with $Pd(PPh_3)_4$ (150 mg, 0.13 mmol, 0.10 equiv) in four parallel trials to give the title compound as pale yellow, foamy solid (1.8 g, 80% yield) after purification by column chromatography, eluting with 10% → 30% EtOAc/hexanes.

^{1}H NMR (300 MHz, $CDCl_3$) δ 8.08 (d, J = 1.6 Hz, 1H), 8.07 (br, 1H), 8.05 (d, J = 1.7 Hz, 1H), 7.28 (d, J = 1.7 Hz, 1H), 7.23 (d, J = 1.8 Hz, 1H), 7.03 (s, 2H), 4.94 (d, J = 4.6 Hz, 2H), 2.39 (s, 3H), 1.98 (s, 6H), 1.45 (s, 9H), 1.45 (s, 9H).

^{13}C NMR (151 MHz, $CDCl_3$) δ 142.4, 141.6, 137.5, 137.2, 137.1, 136.8, 135.7, 128.2, 124.7, 124.1, 123.1, 123.0, 122.4, 122.2, 116.3, 114.6, 64.2, 34.8, 34.7, 32.2, 32.1, 21.3, 20.3.

FT-IR (film): 3534, 3306, 2961, 1610, 1494, 1362, 1242, 1002, 870 cm^{-1}.

MS (ESI) m/z $(M+Na)^+$ calcd for $C_{30}H_{37}NONa$: 450.3, found: 450.3.

$P_{iPr}N_{Mes}$ (L5.7)

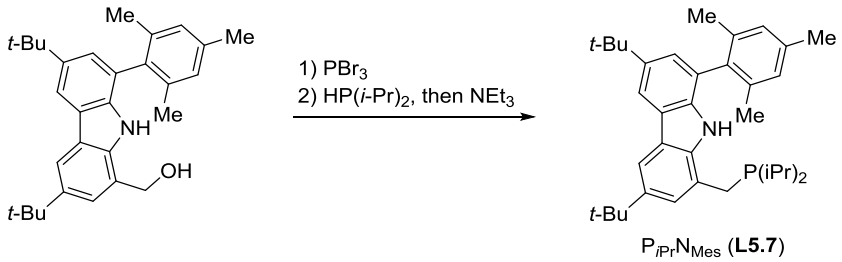

Following General Procedure 1, the title compound can be obtained from (3,6-di-*t*-butyl-8-(mesityl)-carbazol-1-yl)methanol (320 mg, 0.75 mmol, 1 equiv), phosphorous tribromide (0.072 mL, 0.77 mmol, 1 equiv) and di-*i*-propylphosphine (83 mg, 0.7 mmol, 0.9 equiv) as pale yellow solid (360 mg, 78% yield). **Note**: the title compound is only partially soluble in Et_2O, and the removal of NH_4Br was followed by a subsequent extraction in benzene.

^{1}H NMR (300 MHz, C_6D_6) δ 8.46 (d, J = 5.5 Hz, 1H), 8.32 (s, 1H), 8.24 (s, 1H), 7.43 (s, 2H), 6.99 (s, 2H), 2.75 (s, 2H), 2.25 (s, 3H), 2.21 (s, 6H), 1.74–1.25 (m, 20H), 0.99–0.67 (m, 12H).

^{13}C NMR (101 MHz, C_6D_6) δ 142.9, 142.7, 138.2, 137.4, 137.2, 137.1, 135.5, 129.1, 124.9, 124.8, 124.5, 124.0, 121.7, 115.5, 114.6, 34.8, 32.3, 27.7, 27.4, 24.0, 23.9, 21.2, 20.7, 19.7, 19.6, 18.8, 18.7.

^{31}P NMR (121 MHz, C_6D_6) δ –1.2.

FT-IR (film): 3405, 2951, 2865, 1493, 1362, 1294, 1245, 867 cm^{-1}.

MS (ESI) m/z $(M+Na)^+$ calcd for $C_{36}H_{50}NPNa$: 550.4, found: 550.4.

Preparation of $P_{Ph}N_{Mes}$ (L5.8)

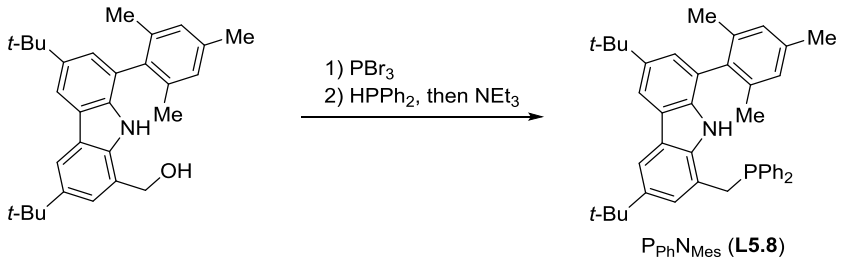

$P_{Ph}N_{Mes}$ (**L5.8**)

A 100 mL roundbottom flask was charged with (3,6-di-*t*-butyl-8-(mesityl)-carbazol-1-yl)methanol (400 mg, 0.93 mmol, 1 equiv) and a magnetic stir bar. The flask was placed under nitrogen atmosphere and the starting material was dissolved in degassed DCM (30 mL). After cooling to 0 °C, phosphorus tribromide (270 mg, 1.0 mmol, 1.1 equiv) was added dropwise, and the resulting solution was stirred for an additional 30 min at 0 °C. Next, the mixture was transferred to a separatory funnel containing $NaHCO_{3(aq)}$ (30 mL). The organic layer was washed with brine (30 mL), dried over Na_2SO_4, filtered, and concentrated in vacuo. The residue was transferred to the glovebox and re-dissolved in DCM (10 mL), and this solution was added to a solution of diphenylphosphine (512 mg, 0.3 mmol, 3 equiv) in DCM (5 mL) in a 20 mL vial dropwise. The resulting solution was stirred overnight and concentrated in vacuo to afford yellow residue. The residue was washed with *n*-pentane, re-suspended in DCM (5 mL), and stirred for 30 min after adding degassed triethylamine (1 mL). Next, volatiles were removed in vacuo and the residue was extracted in Et_2O (5 mL). The resulting white precipitate (NH_4Br) was removed by filtration and the filtrate was concentrated and recrystallized in cold CH_3CN to give the title compound as colorless solid (400 mg, 72%).

^{1}H NMR (400 MHz, C_6D_6) δ 8.28 (s, 1H), 8.17 (s, 1H), 7.87 (s, 1H), 7.42 (s, 1H), 7.27–7.11 (m, 5H), 7.02–6.84 (m, 6H), 3.25 (s, 2H), 2.23 (s, 9H), 1.44 (s, 9H), 1.36 (s, 9H).

^{13}C NMR (101 MHz, C_6D_6) δ 142.9, 142.6, 138.8, 138.7, 137.9, 137.9, 137.31, 137.27, 135.5, 133.3, 133.1, 129.2, 128.8, 125.8, 125.7, 125.0, 124.8, 124.6, 123.9, 119.24, 119.18, 115.5, 114.8, 34.9, 34.7, 33.3, 33.2, 32.24, 32.15, 21.2, 20.8.

^{31}P NMR (162 MHz, C_6D_6) δ –18.3.

FT-IR (film): 2949, 2876, 2817, 1453, 1246, 1193, 1027, 867 cm^{-1}.

MS (ESI) m/z $(M+Na)^+$ calcd for $C_{42}H_{46}NPNa$: 618.3, found: 618.5.

Preparation of $P_{PhBn}N_{Mes}$ (L5.9)

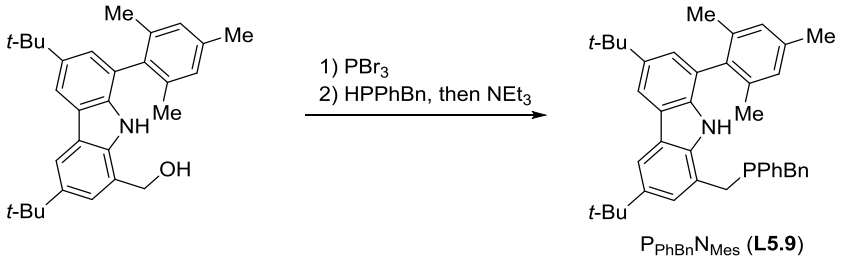

A solution of benzylphenylphosphine was prepared as follows. [27] Dibenzylphenylphosphine (580 mg, 2 mmol, 2 equiv), lithium (500 mg, 71 mmol, 71 equiv), and a magnetic stir bar was added to a 20 mL scintillation vial. The vial was capped with a PTFE-lined septum cap. Next, the vial was evacuated and backfilled with argon (3 cycles), and dry, degassed THF (5 mL) was added to the vial. The suspension was sonicated at ambient temperature for 2 h. The dark red solution was then transferred to a 40 mL vial under nitrogen via syringe. The solution was concentrated in vacuo, and the residue was cooled to

0 °C. Degassed deionized water (20 mL) was slowly added via syringe, and the colorless residue was extracted with degassed Et_2O (2 × 20 mL). The organic layer was dried over Na_2SO_4, filtered, concentrated, and dissolved in DCM (10 mL).

A separate 40 mL scintillation vial was charged with (3,6-di-*t*-butyl-8-(mesityl)-carbazol-1-yl)methanol (428 mg, 1 mmol, 1 equiv) and a magnetic stir bar. The vial was placed under nitrogen atmosphere and the starting material was dissolved in degassed DCM (5 mL). After cooling to 0 °C, phosphorus tribromide (270 mg, 1.0 mmol, 1 equiv) was added dropwise, and the resulting solution was stirred for an additional 30 min at 0 °C. Next, the mixture was transferred to a separatory funnel containing $NaHCO_{3(aq)}$ (30 mL). The organic layer was washed with brine (30 mL), dried over Na_2SO_4, filtered, and concentrated in vacuo. The residue was transferred to the glovebox and added in portions to a stirring solution of freshly prepared benzylphenylphosphine (2 mmol, 2 equiv) in DCM (10 mL) in a 20 mL vial (see previous paragraph). The resulting solution was stirred overnight and concentrated in vacuo to afford yellow residue. The residue was washed with *n*-hexane, re-suspended in DCM (5 mL), and stirred for 30 min after adding degassed triethylamine (1 mL). Next, volatiles were removed in vacuo and the residue was extracted in Et_2O (5 mL). The resulting white precipitate (NH_4Br) was removed by filtration and the filtrate was concentrated. The residue was triturated with *n*-hexane (10 mL), and the precipitates were removed by filtration. The filtrate was concentrated to give the title compound as off white solid (500 mg, 74%).

^{1}H NMR (400 MHz, C_6D_6) δ 8.35–8.22 (m, 2H), 8.17 (s, 1H), 7.81 (s, 1H), 7.40 (s, 1H), 7.11–6.85 (m, 10H), 2.97–2.77 (m, 4H), 2.30 (s, 3H), 2.19 (s, 3H), 2.16 (s, 3H), 1.42 (s, 9H), 1.39 (s, 9H).

^{13}C NMR (101 MHz, C_6D_6) δ 142.9, 142.6, 137.9, 137.4, 137.2, 135.5, 135.4, 133.7, 133.1, 132.9, 132.0, 131.10, 131.05, 129.5, 129.4, 129.3, 129.2, 129.1, 128.51, 128.50, 126.10, 126.08, 125.3, 124.9, 124.6, 123.8, 115.5, 114.8, 34.9, 34.7, 32.24, 32.19, 32.0, 21.3, 20.8, 20.7.

^{31}P NMR (162 MHz, C_6D_6) δ –20.6.

FT-IR (film): 2952, 2903, 2863, 1493, 1362, 1245, 869, 696 cm^{-1}.

MS (ESI) m/z $(M+H)^+$ calcd for $C_{43}H_{49}NP$: 610.4, found: 610.4.

Preparation of Li($P_{iPr}N_H$)

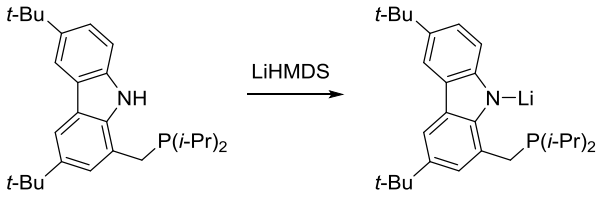

An 8 mL vial was charged with **L5.1** (205 mg, 0.5 mmol, 1 equiv), LiHMDS (84 mg, 0.5 mmol, 1 equiv), and a magnetic stir bar. Next toluene (5 mL) was added, and the vial was capped. The solution was allowed to stir at room temperature overnight and filtered. The filtrate was concentrated in vacuo and washed with cold *n*-pentane to yield the title compound as colorless solid (80 mg, 39% yield).

^{1}H NMR (300 MHz, CD_3CN) δ 7.99 (s, 1H), 7.88 (s, 1H), 7.41 (d, J = 8.3 Hz, 1H), 7.25 (s, 1H), 7.17 (s, 1H), 3.25 (s, 2H), 1.80–1.70 (m, 2H), 1.43 (s, 18H), 1.15–1.04 (m, 6H), 0.99 (dd, J = 12.8, 7.3 Hz, 6H).

^{31}P NMR (121 MHz, CD_3CN) δ –3.5.

Preparation of Li($P_{Ph}N_H$)

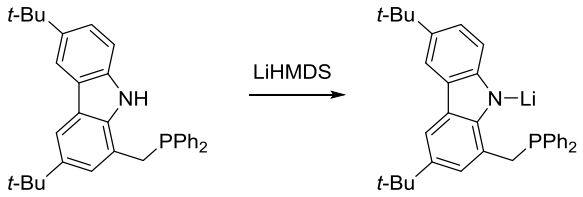

An 8 mL vial was charged with **L5.2** (48 mg, 0.1 mmol, 1 equiv), LiHMDS (20 mg, 0.12 mmol, 1.2 equiv), and a magnetic stir bar. Next *n*-hexane (2 mL) was added, and the vial was capped. The solution was allowed to stir at room temperature for 1 h. The precipitate was collected and washed with cold *n*-hexane to give the title compound as pale yellow solid (45 mg, 93% yield).

^{1}H NMR (400 MHz, CD_3CN) δ 7.98 (s, 1H), 7.84 (s, 1H), 7.61–7.34 (m, 5H), 7.34–7.20 (m, 7H), 6.99 (s, 1H), 3.91 (s, 2H), 1.42 (s, 9H), 1.30 (s, 9H).

^{31}P NMR (162 MHz, CD_3CN) δ –20.2.

Preparation of Li($P_{iPr}N_{tBuPh}$)

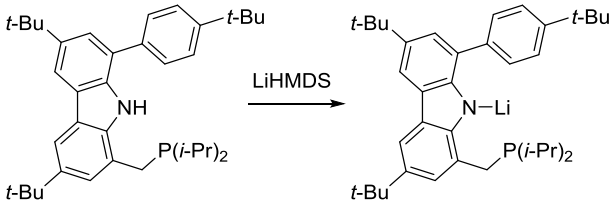

A 20 mL vial was charged with **L5.5** (110 mg, 0.2 mmol, 1 equiv), LiHMDS (37 mg, 0.2 mmol, 1 equiv), and a magnetic stir bar. Next toluene (2 mL) was added, and the vial was capped. The solution was allowed to stir at room temperature for 1 h and layered with *n*-hexane (5 mL). The mixture was kept at –35 °C overnight, and the precipitate was collected to give the title compound as fluorescent yellow solid (100 mg, 91% yield).

^{1}H NMR (300 MHz, CD_3CN) δ 8.17–7.89 (m, 4H), 7.81–7.51 (m, 2H), 7.45–7.17 (m, 2H), 3.23 (s, 2H), 1.87–1.64 (m, 2H), 1.49 (s, 9H), 1.43 (s, 18H), 1.14–0.94 (m, 12H).

^{31}P NMR (121 MHz, CD_3CN) δ 0.5.

Preparation of Li($P_{iPr}N_{Mes}$)

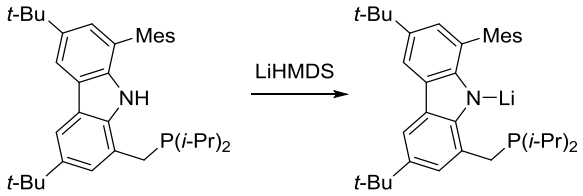

An 8 mL vial was charged with **L5.7** (106 mg, 0.2 mmol, 1 equiv), LiHMDS (33 mg, 0.2 mmol, 1 equiv), and a magnetic stir bar. Next *n*-hexane (3 mL) was added, and the vial was capped. The solution was allowed to stir at room temperature for 1 h and kept at –35 °C

overnight, and the precipitate was collected to give the title compound as fluorescent yellow solid (50 mg, 47% yield).

^{1}H NMR (400 MHz, CD_3CN) δ 8.11 (s, 1H), 7.99 (s, 1H), 7.41 (s, 1H), 7.19 (s, 1H), 7.05 (s, 2H), 3.01 (s, 2H), 2.36 (s, 3H), 1.96 (s, 6H) 1.80–1.63 (m, 2H), 1.44 (d, J = 1.6 Hz, 9H), 1.41 (d, J = 1.7 Hz, 9H), 1.05–0.85 (m, 12H).

^{31}P NMR (162 MHz, CD_3CN) δ 3.2.

Preparation of K(carb$_{t\mathrm{Bu}}$)

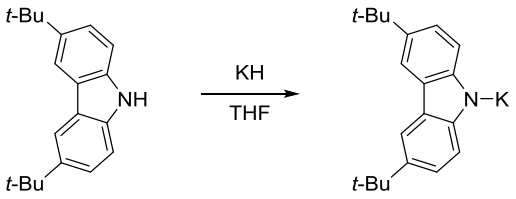

A 20 mL vial was charged with 3,6-di-*t*-butylcarbazole (550 mg, 2 mmol, 1 equiv), KH (84 mg, 2 mmol, 1 equiv), and a magnetic stir bar. Next cold THF (5 mL) was added, and the solution was allowed to stir at room temperature overnight. The solution was filtered and the filtrate was concentrated in vacuo to give the title compound as pale yellow solid (500 mg, 79% yield).

^{1}H NMR (400 MHz, CD_3CN) δ 7.99 (dd, J = 2.1, 0.6 Hz, 2H), 7.32 (dd, J = 8.6, 0.6 Hz, 2H), 7.22 (dd, J = 8.6, 2.1 Hz, 2H), 1.43 (s, 18H).

Preparation of K($P_{iPr}N_{Mes}$)

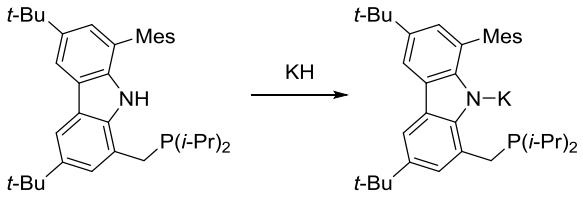

A 20 mL vial was charged with ligands **L5.7** (106 mg, 0.2 mmol, 1 equiv), KH (9 mg, 0.2 mmol, 1 equiv), and a magnetic stir bar. Next cold THF (5 mL) was added, and the solution was allowed to stir at room temperature overnight. The solution was filtered and the filtrate was concentrated in vacuo to give the title compound as yellow solid (100 mg, 88% yield).

^{1}H NMR (400 MHz, CD_3CN) δ 7.92 (s, 1H), 7.80 (s, 1H), 7.19 (s, 1H), 6.99 (s, 2H), 6.87 (s, 1H), 3.14 (s, 2H), 2.36 (s, 3H), 2.02 (s, 6H), 1.73 (td, J = 7.1, 2.6 Hz, 2H), 1.43 (s, 9H), 1.42 (s, 9H), 1.00 (ddd, J = 17.5, 12.0, 7.1 Hz, 12H).

^{31}P NMR (162 MHz, CD_3CN) δ 4.6.

Preparation of K($P_{Ph}N_{Mes}$)

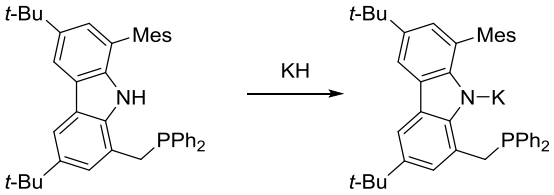

A 20 mL vial was charged with **L5.8** (120 mg, 0.2 mmol, 1 equiv), KH (8.5 mg, 0.2 mmol, 1 equiv), and a magnetic stir bar. Next cold THF (5 mL) was added, and the solution

was allowed to stir at room temperature overnight. The solution was filtered and the filtrate was concentrated in vacuo to give the title compound as yellow solid (100 mg, 88% yield).

^{1}H NMR (400 MHz, CD_3CN) δ 7.94 (s, 1H), 7.81 (s, 1H), 7.59–7.43 (m, 4H), 7.32–7.20 (m, 6H), 6.97 (s, 2H), 6.92 (s, 2H), 3.81 (s, 2H), 2.34 (s, 3H), 2.06 (s, 6H), 1.44 (s, 9H), 1.27 (s, 9H).

^{31}P NMR (162 MHz, CD_3CN) δ –15.3.

5.4.3. Synthesis of bimetallic complexes supported by (phosphino)carbazoles

General Procedure 3: preparation of dicopper complexes

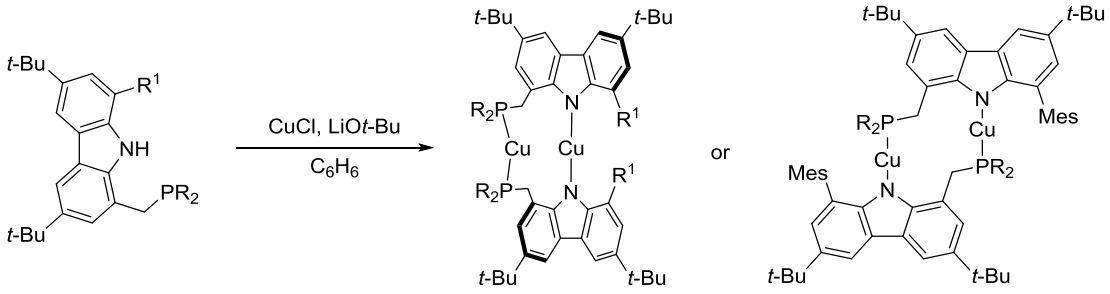

To a 20 mL scintillation vial, (phosphino)carbazole (1 equiv), CuCl (1 equiv), LiO*t*-Bu (1 equiv), a magnetic stir bar, and dry, degassed benzene were added. The mixture was vigorously stirred overnight at room temperature. Next, the mixture was filtered through a pad of Celite, and the filtrate was concentrated in vacuo. The ^{1}H NMR spectrum of the residue showed the clean formation of the target compound, which can be further purified by recrystallization from a mixture of benzene/*n*-hexanes, Et_2O or CH_3CN at –35 °C to afford colorless crystals of copper complexes.

Preparation of $(CuP_{iPr}N_H)_2$–(CH_3CN) (5.1–CH_3CN)

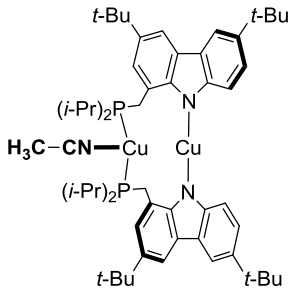

$(CuP_{iPr}N_H)_2$–(CH_3CN) (**5.1–CH_3CN**)

Following General Procedure 3, the title compound was prepared using **L5.1** (250 mg, 0.61 mmol, 1 equiv), CuCl (60 mg, 0.61 mmol, 1 equiv), and LiO*t*-Bu (100 mg, 1.25 mmol, 2 equiv) in 59% yield (170 mg) as colorless solid after recrystallization in CH_3CN. Crystals suitable for single-crystal X-ray diffraction were grown from a saturated solution in CH_3CN at –35 °C.

^{1}H NMR (400 MHz, C_6D_6) δ 8.48 (s, 1H), 8.45 (s, 1H), 8.13 (d, J = 8.7 Hz, 1H), 7.58 (d, J = 8.6 Hz, 1H), 7.25 (s, 1H), 4.37 (d, J = 13.6 Hz, 1H), 3.40–2.91 (m, 1H), 1.59 (s, 9H), 1.58 (s, 9H), 1.52–1.39 (m, 2H), 0.65 (q, J = 7.0 Hz, 6H), 0.58 (s, 1.5H), 0.45 (q, J = 7.3 Hz, 3H), 0.32–0.25 (m, 3H).

^{31}P NMR (162 MHz, C_6D_6) δ 11.5.

Preparation of $(CuP_{Ph}N_H)_2$–(CH_3CN) (5.2–CH_3CN)

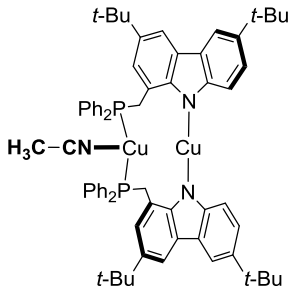

$(CuP_{Ph}N_H)_2$–(CH_3CN) (**5.2–CH_3CN**)

Following General Procedure 3, the title compound was prepared using **L5.2** (191 mg, 0.40 mmol, 1 equiv), CuCl (40 mg, 0.40 mmol, 1 equiv), and LiO*t*-Bu (48 mg, 0.60 mmol, 1.5 equiv) in 60% yield (130 mg) as pale yellow solid. Crystals suitable for single-crystal X-ray diffraction were grown from a saturated solution in Et_2O/CH_3CN at –35 °C or slow evaporation of a saturated solution in Et_2O at –35 °C.

^{1}H NMR (400 MHz, C_6D_6) δ 8.39 (d, J = 1.3 Hz, 1H), 8.30 (s, 1H), 7.55 (d, J = 8.5 Hz, 1H), 7.25 (dd, J = 8.6, 1.7 Hz, 1H), 7.00 (t, J = 7.4 Hz, 1H), 6.91–6.84 (m, 5H), 6.79 (q, J = 5.7 Hz, 2H), 6.67 (t, J = 7.5 Hz, 2H), 6.54 (s, 1H), 4.75 (d, J = 13.0 Hz, 1H), 3.54 (dt, J = 11.7, 5.5 Hz, 1H), 1.53 (s, 9H), 1.32 (s, 9H), 0.69 (s, 1.5H).

^{31}P NMR (162 MHz, C_6D_6) δ –8.5.

Preparation of $(CuP_{iPr}N_{Me})_2$–(CH_3CN) (5.3–CH_3CN)

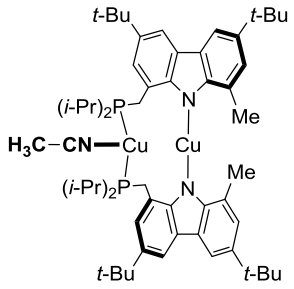

$(CuP_{iPr}N_{Me})_2$–(CH_3CN) (**5.3–CH_3CN**)

Following General Procedure 3, the title compound was prepared using **L5.3** (127 mg, 0.30 mmol, 1 equiv), CuCl (29 mg, 0.29 mmol, 1 equiv), and LiO*t*-Bu (60 mg, 0.75 mmol, 2.5 equiv) in 28% yield (40 mg) as pale pink solid after recrystallization in CH_3CN. Crystals suitable for single-crystal X-ray diffraction were grown from a saturated solution in CH_3CN at –35 °C.

^{1}H NMR (400 MHz, C_6D_6) δ 8.41 (s, 1H), 8.38 (s, 1H), 7.49 (s, 1H), 7.11 (s, 1H), 4.19 (d, J = 13.9 Hz, 1H), 3.56 (s, 3H), 3.26–2.93 (m, 1H), 1.71–1.63 (m, 2H), 1.62 (s, 9H), 1.53 (s, 9H), 0.81–0.65 (m, 6H), 0.59 (1.5 H) 0.40–0.35 (m, 3H), 0.12–0.06 (m, 3H).

^{31}P NMR (162 MHz, C_6D_6) δ 14.0.

MS (ESI) m/z $(M)^+$ calcd for $C_{56}H_{82}Cu_2N_2P_2$: 970.5, found: 970.3.

Preparation of ($CuP_{iPr}N_{FPh}$)$_2$–(CH_3CN) (5.4–CH_3CN)

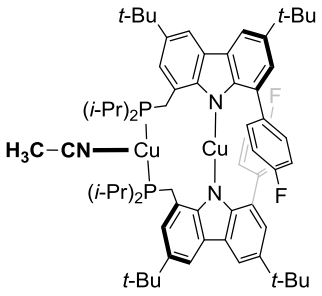

($CuP_{iPr}N_{FPh}$)$_2$–(CH_3CN) (**5.4–CH_3CN**)

Following General Procedure 3, the title compound was prepared using **L5.4** (210 mg, 0.42 mmol, 1 equiv), CuCl (41 mg, 0.41 mmol, 1 equiv), and LiO*t*-Bu (50 mg, 0.63 mmol, 1.5 equiv) in 65% yield (150 mg) as pale yellow solid after recrystallization in CH_3CN. Crystals suitable for single-crystal X-ray diffraction were grown from a saturated solution in CH_3CN at –35 °C.

^{1}H NMR (400 MHz, C_6D_6) δ 8.39 (d, J = 2.0 Hz, 1H), 8.32 (s, 1H), 8.04 (br, 2H), 7.57 (d, J = 2.0 Hz, 1H), 7.11 (s, 1H), 6.82 (t, J = 8.6 Hz, 2H), 3.48 (d, J = 13.0 Hz, 1H), 3.27–2.89 (m, 1H), 1.57 (s, 9H), 1.50 (s, 9H), 1.30–1.14 (m, 1H), 1.07 (dd, J = 12.2, 6.5 Hz, 1H), 0.71–0.59 (m, 3H), 0.59–0.55 (m, J = 7.1 Hz, 6H), 0.09–0.01 (m, 3H).

^{19}F NMR (376 MHz, C_6D_6) δ –115.1.

^{31}P NMR (162 MHz, C_6D_6) δ 14.0.

MS (ESI) m/z $(M)^+$ calcd for $C_{66}H_{86}Cu_2N_2F_2P_2$: 1132.5, found: 1132.0.

Preparation of ($CuP_{iPr}N_{tBuPh}$)$_2$ (5.5)

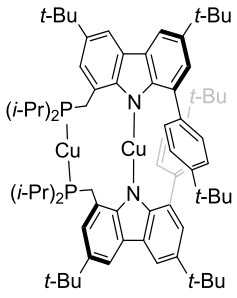

($CuP_{iPr}N_{tBuPh}$)$_2$ (**5.5**)

Following General Procedure 3, the title compound was prepared using **L5.5** (100 mg, 0.18 mmol, 1.1 equiv), CuCl (18 mg, 0.18 mmol, 1.0 equiv), and LiO*t*-Bu (22 mg, 0.28 mmol, 1.5 equiv) in 92% yield (100 mg) as off-white solid. Crystals suitable for single-crystal X-ray diffraction were grown from a saturated solution in CH_3CN at –35 °C.

^{1}H NMR (400 MHz, C_6D_6) δ 8.47 (very br, 2H), 8.44 (s, 1H), 8.35 (s, 1H), 7.78 (s, 1H), 7.41 (d, J = 8.1 Hz, 2H), 7.03 (s, 1H), 3.37 (d, J = 13.6Hz, 1H), 2.87–2.81 (m, 1H), 1.62 (s, 9H), 1.55 (s, 9H), 1.51–1.44 (m, 2H), 0.80 (s, 9H), 0.65–0.53 (m, 9H), 0.07–0.01 (m, 3H).

^{31}P NMR (162 MHz, C_6D_6) δ 13.7.

MS (ESI) m/z $(M)^+$ calcd for $C_{74}H_{102}Cu_2N_2P_2$: 1206.6, found: 1206.3.

Preparation of $(CuP_{iPr}N_{MeOPh})_2$ (5.6)

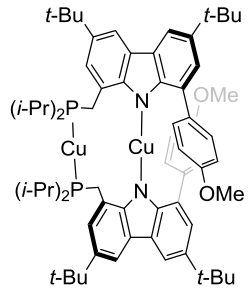

$(CuP_{iPr}N_{MeOPh})_2$ (**5.6**)

Following General Procedure 3, the title compound was prepared using **L5.6** (450 mg, 0.87 mmol, 1 equiv), CuCl (86 mg, 0.87 mmol, 1 equiv), and LiO*t*-Bu (105 mg, 1.3 mmol, 1.5 equiv) in 70% yield (350 mg) as pale yellow solid. Crystals suitable for single-crystal X-ray diffraction were grown from a saturated solution in Et_2O/CH_3CN at –35 °C.

^{1}H NMR (400 MHz, C_6D_6) δ 8.45 (d, J = 1.9 Hz, 1H), 8.40 (br, 2H), 8.38 (d, J = 15.2 Hz, 1H), 7.75 (d, J = 1.8 Hz, 1H), 7.08 (s, 1H), 6.77 (d, J = 7.5 Hz, 2H), 3.44 (d, J = 13.3 Hz, 1H), 2.94–2.82 (m, 1H), 2.70 (s, 3H), 1.60 (s, 9H), 1.54 (s, 9H), 1.53–1.50 (m, 1H), 1.42–1.36 (m, 1H), 0.61 (dq, J = 15.8, 7.1 Hz, 6H), 0.49 (q, J = 7.1 Hz, 3H), 0.17 (q, J = 7.4 Hz, 3H).

^{31}P NMR (162 MHz, C_6D_6) δ 12.7.

MS (ESI) m/z $(M)^+$ calcd for $C_{68}H_{90}Cu_2N_2O_2P_2$: 1154.5, found: 1154.0.

Preparation of $(CuP_{iPr}N_{Mes})_2$ (5.7)

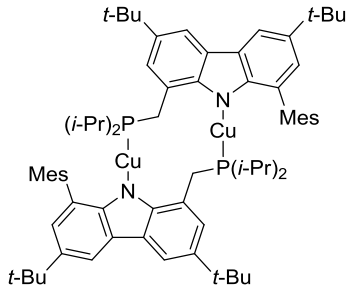

$(CuP_{iPr}N_{Mes})_2$ (**5.7**)

Following General Procedure 3, the title compound was prepared using **L5.7** (106 mg, 0.20 mmol, 1 equiv), CuCl (20 mg, 0.20 mmol, 1 equiv), and LiO*t*-Bu (60 mg, 0.75 mmol, 3.8 equiv) in 85% yield (100 mg) as colorless solid after recrystallization in CH_3CN. Crystals suitable for single-crystal X-ray diffraction were grown from a saturated solution in CH_3CN at –35 °C.

^{1}H NMR (400 MHz, C_6D_6) δ 8.44 (s, 1H), 8.42 (s, 1H), 7.33 (s, 1H), 7.24 (s, 1H), 6.81 (s, 2H), 4.30 (s, 2H), 2.26 (s, 6H), 2.11–2.06 (m, 2H), 2.04 (s, 3H), 1.55 (s, 9H), 1.51 (s, 9H), 0.93 (dd, J = 17.5, 7.0 Hz, 6H), 0.69 (dd, J = 14.9, 7.1 Hz, 6H).

^{31}P NMR (162 MHz, C_6D_6) δ 27.5.

MS (ESI) m/z $(M/2)^+$ calcd for $C_{72}H_{98}Cu_2N_2P_2$: 1178.6, found: 1178.6.

Preparation of $(CuP_{Ph}N_{Mes})_2$ (5.8)

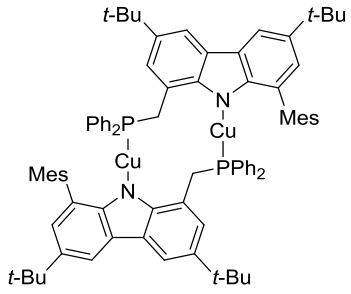

$(CuP_{Ph}N_{Mes})_2$ (**5.8**)

Following General Procedure 3, the title compound was prepared using **L5.8** (60 mg, 0.1 mmol, 1 equiv), CuCl (10 mg, 0.1 mmol, 1 equiv), and LiO*t*-Bu (16 mg, 0.2 mmol, 2 equiv) in 91% yield (60 mg) as colorless solid after recrystallization in CH_3CN. Crystals suitable for single-crystal X-ray diffraction were grown from a saturated solution in CH_3CN at –35 °C.

^{1}H NMR (500 MHz, C_6D_6) δ 8.54 (s, 1H), 8.50 (d, J = 1.9 Hz, 1H), 7.21 (d, J = 1.9 Hz, 1H), 6.97 (br, 3H), 6.81 (br, 7H), 6.55 (s, 1H), 6.02 (br, 1H), 4.77 (br, 1H), 1.83 (s, 6H), 1.51 (s, 9H), 1.38 (br, 12H).

^{31}P NMR (202 MHz, C_6D_6) δ 3.9.

Preparation of $(AuP_{iPr}N_H)_2$ (5.9)

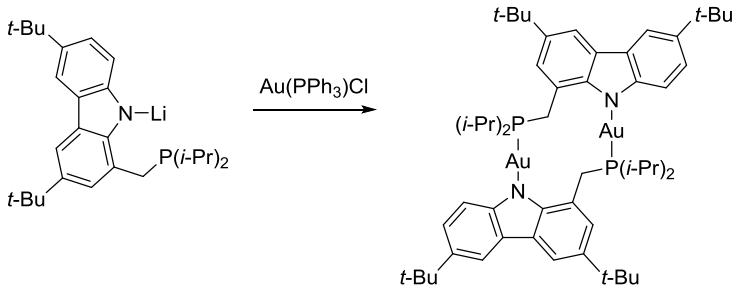

$(AuP_{iPr}NH)_2$ (**5.9**)

A 4 mL vial was charged with $Li(P_{iPr}N_H)$ (42 mg, 0.1 mmol, 1 equiv), $Au(PPh_3)Cl$ (48 mg, 0.1 mmol, 1 equiv), and a magnetic stir bar. After adding CH_3CN (2 mL), the mixture was stirred at room temperature overnight. The resulting precipitate was collected and washed with CH_3CN to give the title compound (50 mg, 83% yield). Crystals suitable for single-crystal X-ray diffraction were grown from a saturated solution in CH_3CN at –35 °C.

^{1}H NMR (400 MHz, C_6D_6) δ 8.49 (s, 1H), 8.43 (d, J = 1.7 Hz, 1H), 7.85 (d, J = 8.6 Hz, 1H), 7.31 (dd, J = 8.6, 1.9 Hz, 1H), 7.20 (s, 1H), 4.06 (d, J = 9.3 Hz, 2H), 1.81–1.66 (m, 2H), 1.61 (s, 9H), 1.42 (s, 9H), 0.90 (d, J = 6.9 Hz, 3H), 0.86 (d, J = 7.1 Hz, 3H), 0.83 (d, J = 7.1 Hz, 3H), 0.79 (d, J = 7.0 Hz, 3H).

^{31}P NMR (162 MHz, C_6D_6) δ 36.1.

MS (ESI) m/z $(M)^+$ calcd for $C_{54}H_{78}Au_2N_2P_2$: 1210.5, found: 1210.4.

Preparation of AuCu($P_{iPr}N_H$)$_2$ (5.10)

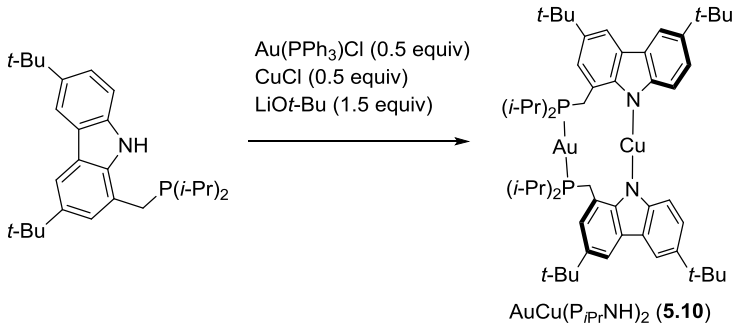

An 8 mL vial was charged with **L5.1** (140 mg, 0.34 mmol, 1 equiv), Au(PPh$_3$)Cl (85 mg, 0.17 mmol, 0.5 equiv), CuCl (17 mg, 0.17 mmol, 0.5 equiv), LiO*t*-Bu (41 mg, 0.51 mmol, 1.5 equiv) and a magnetic stir bar. After adding CH_3CN (4 mL), the mixture was stirred at room temperature overnight. The resulting precipitate was collected and washed with CH_3CN to give the title compound (130 mg, 71% yield) as pale yellow solid. Crystals suitable for single-crystal X-ray diffraction were grown by vapor diffusion of pentane into a concentrated sample in benzene at room temperature.

^{1}H NMR (400 MHz, C_6D_6) δ 8.51 (s, 1H), 8.49 (s, 1H), 8.21 (s, 1H), 7.63 (d, J = 6.7 Hz, 1H), 7.19 (s, 1H), 4.70 (d, J = 13.2 Hz, 1H), 3.64–3.33 (m, 1H), 1.89–1.77 (m, 1H), 1.61 (s, 9H), 1.59 (s, 9H), 1.33–1.22 (m, 1H), 0.78–0.64 (m, 6H), 0.50–0.38 (m, 3H), 0.38–0.29 (m, 3H).

^{31}P NMR (162 MHz, C_6D_6) δ 56.4.

MS (ESI) m/z $(M)^+$ calcd for $C_{54}H_{78}AuCuN_2P_2$: 1076.5, found: 1076.4.

5.4.4. Photoinduced, copper-catalyzed cyanomethylations

General procedure

Preparation of a reaction mixture in a nitrogen-filled glovebox. CuBr, ligand **L5.1**, and LiO*t*-Bu, were added to a 4 mL borosilicate glass vial that contained a magnetic stir bar. Next, CH_3CN and the electrophile were added in sequence, the vial was capped with a PTFE-lined septum cap, and the mixture was stirred at room temperature until the solids had dissolved (5 min).

Irradiation of the reaction mixture with a Hg lamp. A low-form hemispherical Dewar flask was filled with isopropanol in a well-ventilated fume hood. A magnetic stir bar was added to the Dewar flask, and the isopropanol bath was cooled to 0 or –20 °C. The reaction vial was submerged in the isopropanol bath and allowed to cool for 5 min. A 100-watt Hg lamp was placed 4 inches from the vial, and the vial was irradiated for 16 h.

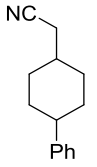

2-(4-phenylcyclohexyl)acetonitrile [1973391-47-7].[28] A 4 mL vial containing CuBr (1.4 mg, 0.01 mmol), **L5.1** (1.6 mg, 0.04 mmol), LiO*t*-Bu (21 mg, 0.3 mmol) 4-phenyl-cyclohexyl bromide (24 mg, 0.1 mmol) CH_3CN (4 mL), and a magnetic stir bar was capped and irradiated following the general procedure at 0 °C. Next, a 20 mL vial was charged with a measured quantity of an internal standard (1,3,5- trimethoxybenzene or *n*-dodecane). The unpurified reaction mixture was then added to the 20 mL vial that contained the internal standard, ensuring quantitative transfer through EtOAc rinses (2 mL × 3). An aliquot was

filtered through a pad of silica gel (eluting with EtOAc) into a GC vial, and the sample was subjected to GC analysis. Another aliquot was concentrated in vacuo, and $CDCl_3$ was added; next, the solids were removed by filtration through a piece of cotton, and the filtrate was subjected to GC or ^1H NMR analysis.

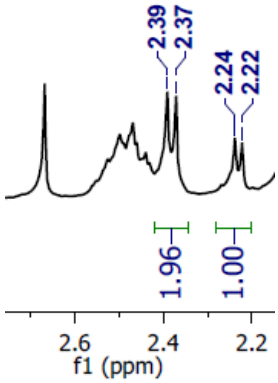

Figure 5.17. ^1H NMR spectrum (400 MHz, $CDCl_3$, rt) of the crude mixture irradiated at –20 °C showing ~2:1 selectivity of cyanomethylation.

5.4.5. Generation of *S* = 1/2 copper complexes supported by (phosphino)carbazoles

Oxidation of complex 5.1–CH_3CN by [FcAc][SbF_6]

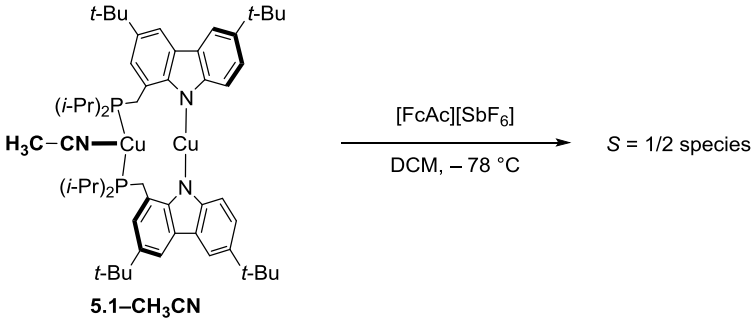

5.1–CH_3CN

A 4 mL vial was charged with **5.1–CH_3CN** (20 mg, 0.02 mmol, 1 equiv), [FcAc][SbF_6] (9 mg, 0.02 mmol, 1 equiv), and a magnetic stir bar in a nitrogen glovebox. The vial was cooled to –78 °C, and pre-chilled DCM (1 mL) was added. After stirring for 30

min, an aliquot was transferred to a pre-chilled cuvette (1 cm path-length) containing DCM. The cuvette was sealed, transferred to a dry ice/acetone bath, then to the pre-chilled spectrometer at –78 °C for measurement. Another aliquot was transferred to a pre-chilled vial containing toluene. The resulting mixture was then transferred to a pre-chilled EPR tube at –78 °C and frozen at 77 K. The UV-vis spectrum the crude reaction mixture is provided below.

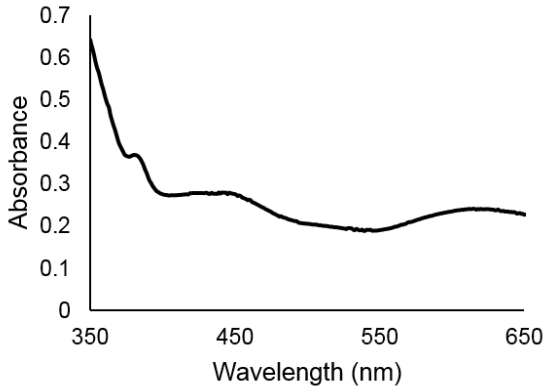

Figure 5.18. UV-vis spectrum of the crude mixture at –78 °C in DCM showing a new transition at 620 nm and the formation of FcAc (λ_{max} = 453 nm).

Oxidation of complex 5.5 by Magic Blue

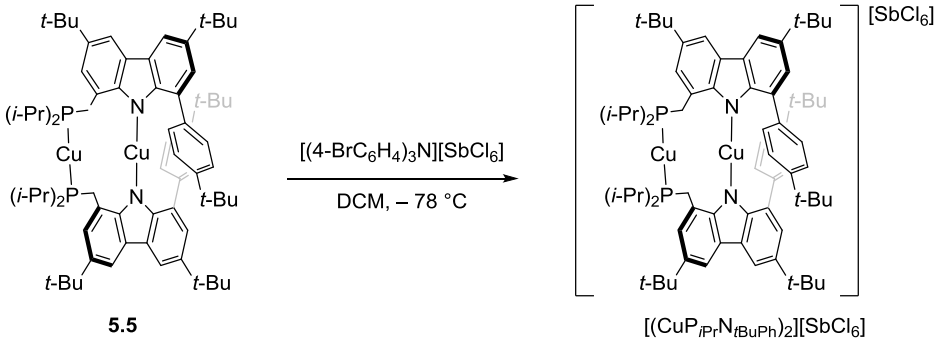

5.5 [(CuP$_{iPr}$N$_{tBuPh}$)$_2$][SbCl$_6$]

A 4 mL vial was charged with **5.5** (2.4 mg, 0.002 mmol, 1 equiv), tris(4-bromophenyl)ammoniumyl hexachloroantimonate ("Magic Blue", 0.8 mg, 0.001 mmol) and a magnetic stir bar in a nitrogen glovebox. The vial was cooled to –78 °C, and pre-chilled DCM (1 mL) was added. After stirring for 30 min, an aliquot was transferred to a pre-chilled vial containing toluene. The resulting mixture was then transferred to a pre-chilled EPR tube at –78 °C and frozen at 77 K. A representative EPR spectrum of the reaction mixture is shown below.

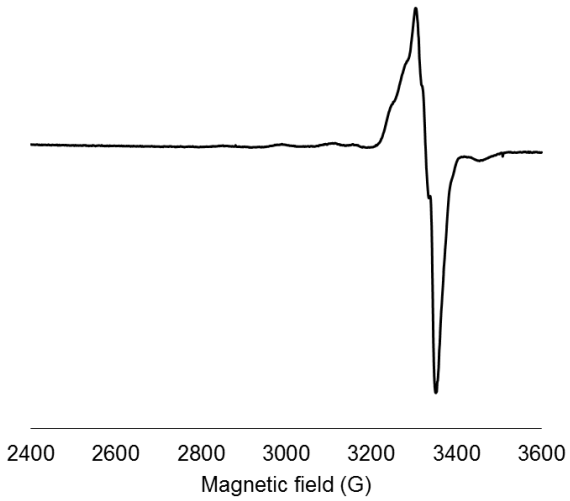

Figure 5.19. EPR spectrum (9.4 GHz, DCM/toluene, 77 K) of the crude mixture of the oxidation of **5.5** by Magic Blue at –78 °C.

Oxidation of complex 5.6 by [FcAc][SbF_6]

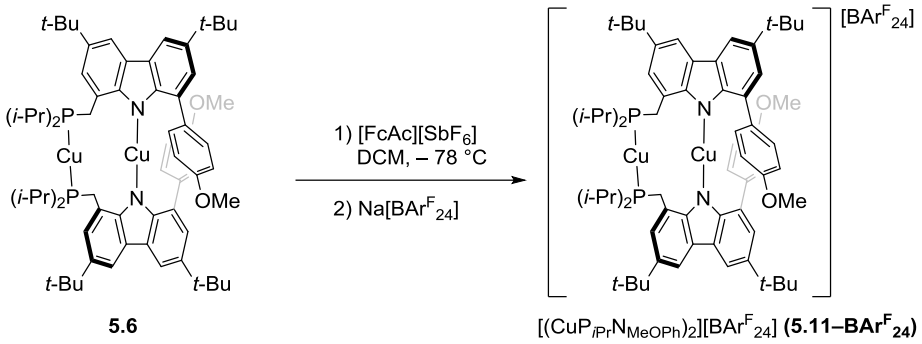

5.6 $[(CuP_{iPr}N_{MeOPh})_2][BAr^F{}_{24}]$ **(5.11–$BAr^F{}_{24}$)**

A 4 mL vial was charged with **5.6** (23 mg, 0.02 mmol, 1 equiv), [FcAc][SbF_6] (9 mg, 0.02 mmol, 1 equiv), and a magnetic stir bar in a nitrogen glovebox. The vial was cooled to –78 °C, and pre-chilled DCM (1 mL) was added. After stirring for 30 min, an aliquot was transferred to a pre-chilled cuvette (1 cm path-length) containing DCM. The cuvette was sealed, transferred to a dry ice/acetone bath, then to the pre-chilled spectrometer at –78 °C for measurement. Another aliquot was transferred to a pre-chilled vial containing toluene. The resulting mixture was then transferred to a pre-chilled EPR tube at –78 °C and frozen at 77 K. The UV-vis spectrum of the crude reaction mixture is provided below.

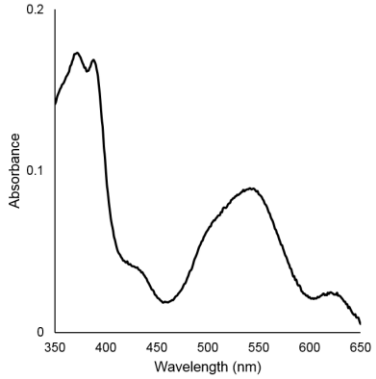

Figure 5.20. UV-vis spectrum of the crude mixture at –78 °C in DCM showing a new transition at 550 nm and the formation of FcAc (λ_{max} = 453 nm).

The remaining purple solution was concentrated in vacuo at –78 °C, and the purple residue was extracted using cold Et_2O at –78 °C and filtered into a pre-chilled 4 mL vial containing Na[BAr^F_{24}] (50 mg, 0.06 mmol, ~3 equiv). The filtrate was layered with cold *n*-hexane at –78 °C and allowed to stand at –35 °C overnight, yielding purple crystals of the target complex.

Oxidation of complex 5.10 by [Fc][BAr^F_{24}]

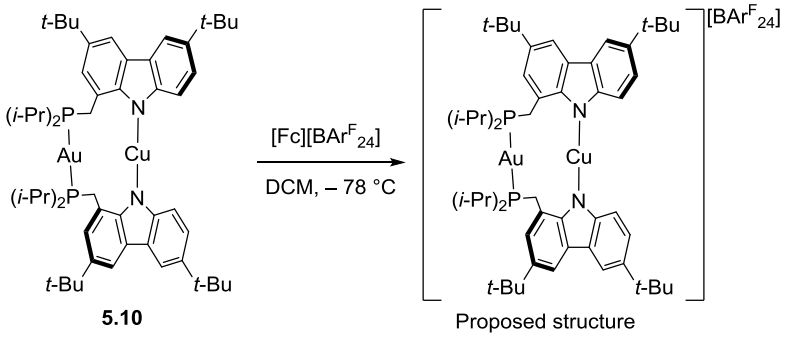

5.10 Proposed structure

A 4 mL vial was charged with **5.10** (2 mg, 0.001 mmol, 1 equiv) and a magnetic stir bar in a nitrogen glovebox. Next, DCM (1 mL) was added and the vial was cooled to –78 °C. After stirring for 30 min, [Fc][BAr^F_{24}] (2 mg, 0.001 mmol, 1 equiv) was added to the vial, and the resulting purple solution was allowed to stir at –78 °C for 30 min. An aliquot was transferred to a pre-chilled vial containing toluene. The resulting mixture was then transferred to a pre-chilled EPR tube at –78 °C and frozen at 77 K. The EPR spectrum of the crude reaction mixture is provided in **Figure 5.11**. Alternatively, the purple solution can also be generated under otherwise identical conditions using **5.10** (22 mg, 0.02 mmol, 1 equiv) and [FcAc][SbF_6] (9 mg, 0.02 mmol, 1 equiv).

Generation of $Cu^{II}(P_{iPr}N_H)(carb)$ (5.12) from $[Cu^{II}(carb)_3]K$

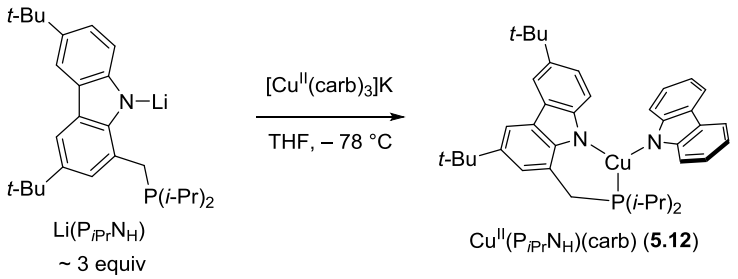

A solution of $[Cu^{II}(carb)_3]K$ (~0.1 M in THF) was freshly prepared by adding a suspension of $CuBr_2$ (6.6 mg, 0.03 mmol, 1 equiv) in THF at –78 °C to a stirring suspension of K(carb) (20 mg, 0.1 mmol, 3.3 equiv) in THF at –78 °C. An aliquot of $[Cu^{II}(carb)_3]K$ (~0.003 mmol, 0.3 mL) was transferred to a stirring suspension of $Li(P_{iPr}N_H)$ (4.2 mg, 0.01 mmol, ~3 equiv) in 2-MeTHF (0.2 mL). After 30 min, the resulting mixture was then transferred to a pre-chilled EPR tube at –78 °C and frozen at 77 K. EPR spectrum of the crude mixture is provided in **Figure 5.12**.

Generation of $Cu^{II}(P_{iPr}N_{tBuPh})(carb)$ (5.13) from $[Cu^{II}(carb)_3]K$

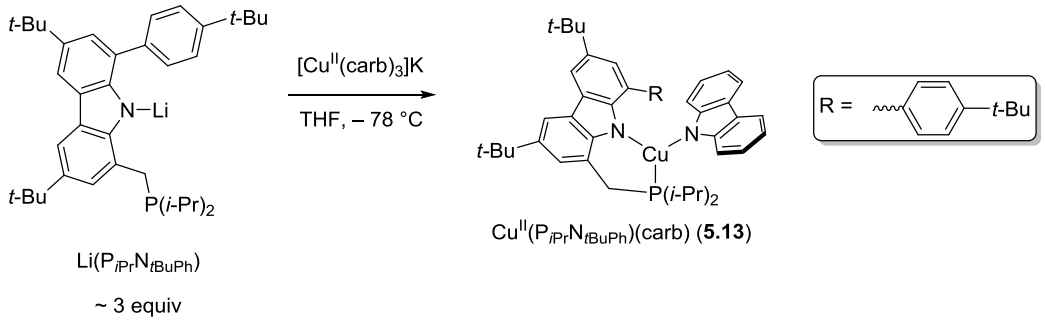

A solution of $[Cu^{II}(carb)_3]K$ (~0.1 M in THF) was freshly prepared by adding a suspension of $CuBr_2$ (6.6 mg, 0.03 mmol, 1 equiv) in THF at –78 °C to a stirring suspension of K(carb) (20 mg, 0.1 mmol, 3.3 equiv) in THF at –78 °C. An aliquot of $[Cu^{II}(carb)_3]K$

(~0.003 mmol, 0.3 mL) was transferred to a stirring suspension of Li($P_{iPr}N_{tBuPh}$) (5.5 mg, 0.01 mmol, ~3 equiv) in 2-MeTHF (0.2 mL). After 30 min, the resulting mixture was then transferred to a pre-chilled EPR tube at –78 °C and frozen at 77 K. EPR spectrum of the crude mixture is provided in **Figure 5.13**.

Generation of $Cu^{II}(P_{iPr}N_{tBuPh})$(carb) (5.13) via oxidation

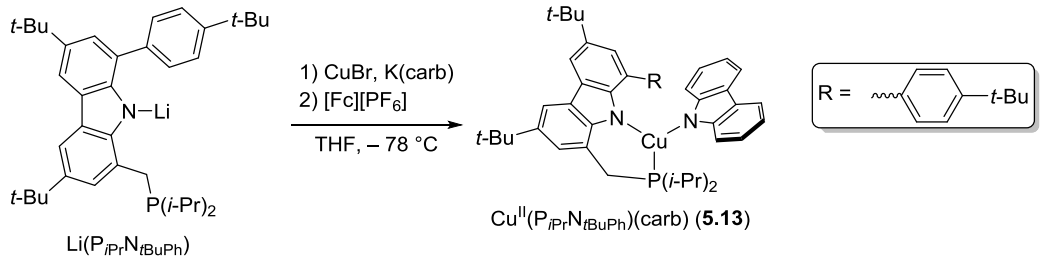

A suspension of CuBr (1.4 mg, 0.01 mmol, 1 equiv) K(carb) (2.2 mg, 0.01 mmol, 1 equiv) and Li($P_{iPr}N_{tBuPh}$) (5.5 mg, 0.01 mmol, 1 equiv) in THF (0.3 mL) was prepared in a 4 mL vial equipped with a magnetic stir bar. The mixture was cooled to –78 °C, and [Fc][PF_6] (3.3 mg, 0.01 mmol, 1 equiv) was added to the stirring suspension. After stirring for 30 min at –78 °C, an aliquot was transferred to a vial containing pre-chilled 2-MeTHF (0.3 mL) at –78 °C. The resulting mixture was then transferred to a pre-chilled EPR tube at –78 °C and frozen at 77 K. EPR spectrum of the crude mixture is provided below.

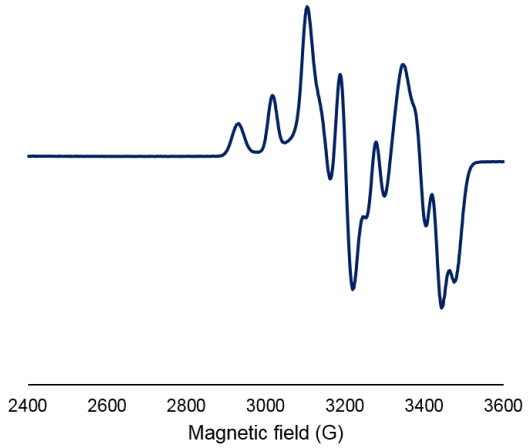

Figure 5.21. EPR spectrum (9.4 GHz, THF/2-MeTHF, 77 K) of **5.13** from the oxidation of an equimolar mixture of CuBr, K(carb), and Li($P_{iPr}N_{tBuPh}$).

Generation of $Cu^{II}(P_{iPr}N_{Mes})$(carb) (5.14) from $[Cu^{II}(carb)_3]K$

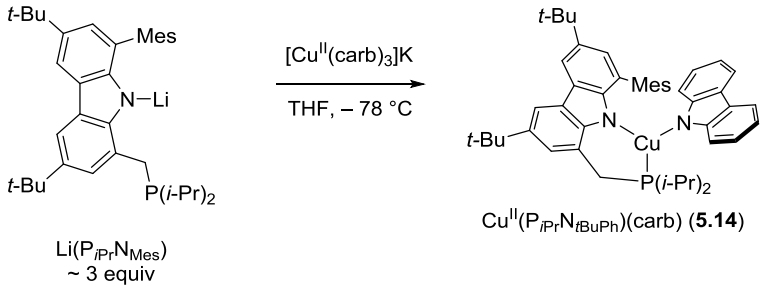

A solution of $[Cu^{II}(carb)_3]K$ (~0.1 M in THF) was freshly prepared by adding a suspension of $CuBr_2$ (6.6 mg, 0.03 mmol, 1 equiv) in THF at –78 °C to a stirring suspension of K(carb) (20 mg, 0.1 mmol, 3.3 equiv) in THF at –78 °C. An aliquot of $[Cu^{II}(carb)_3]K$ (~0.003 mmol, 0.3 mL) was transferred to a stirring suspension of Li($P_{iPr}N_{Mes}$) (5.5 mg, 0.01 mmol, ~3 equiv) in 2-MeTHF (0.2 mL). After 30 min, the resulting mixture was then transferred to a pre-chilled EPR tube at –78 °C and frozen at 77 K. EPR spectrum of the crude mixture is provided below.

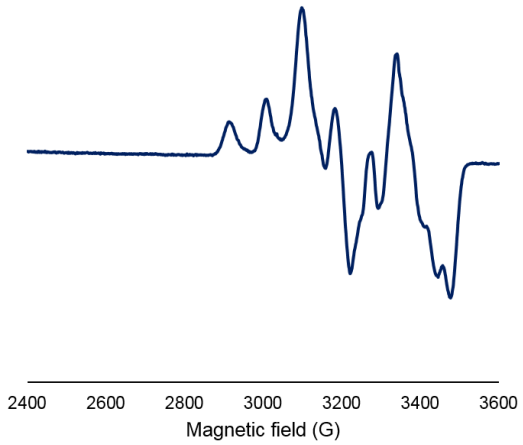

Figure 5.22. EPR spectrum (9.4 GHz, THF/2-MeTHF, 77 K) of **5.14** from the reaction of $[Cu^{II}(carb)_3]K$ with $Li(P_{iPr}N_{Mes})$.

Generation of $Cu^{II}(P_{iPr}N_{Mes})(carb)$ (5.14) from 5.7

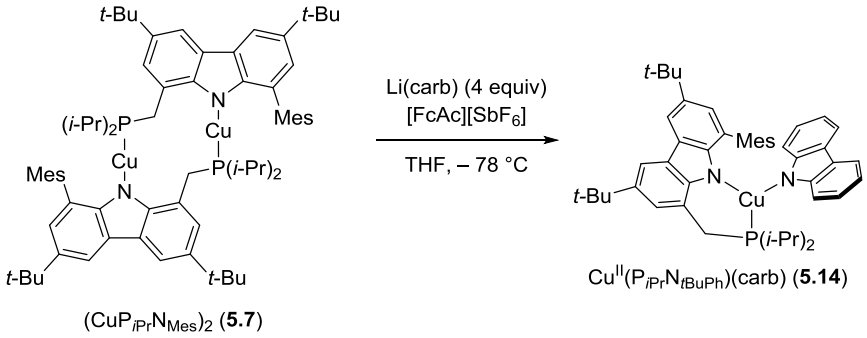

Alternatively, **5.14** can be generated as follows: A suspension of Li(carb) (1.7 mg, 0.01 mmol, 4 equiv) and complex **5.7** (3.0 mg, 0.0025 mmol, 1 equiv) was prepared in THF (0.5 mL) at –78 °C. Then, $[FcAc][SbF_6]$ (1.2 mg, 0.0025 mmol, 1 equiv) was added to the stirring suspension, and the resulting mixture was allowed to stir at –78 °C. After 30 min, an aliquot was transferred to a vial containing pre-chilled 2-MeTHF (0.5 mL) at –78 °C. The

resulting mixture was then transferred to a pre-chilled EPR tube at –78 °C and frozen at 77 K. EPR spectrum of the crude mixture is provided below.

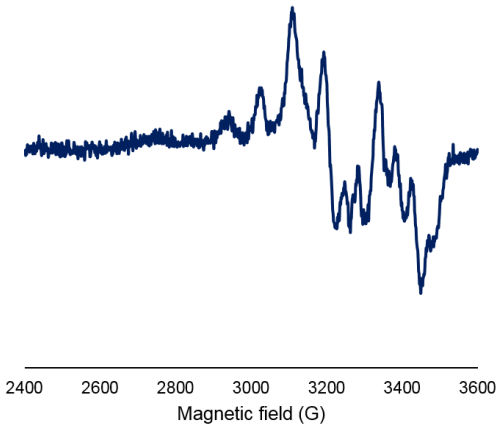

Figure 5.23. EPR spectrum (9.4 GHz, THF/2-MeTHF, 77 K) of **5.14** from the oxidation of **5.7** in the presence of Li(carb).

Table 5.1. DFT-optimized atomic coordinates of **5.14**.

Atom	x	y	z	Atom	x	y	z	Atom	x	y	z
C	0.22639	-4.15882	0.96726	H	0.88143	-4.89857	0.52356	H	3.81237	0.09801	-1.63811
C	-1.05542	-4.53621	1.37765	H	-2.89387	-3.80557	2.22214	H	5.03426	-1.84242	-2.70132
C	-1.88541	-3.55416	1.91229	H	-4.05488	-1.47259	3.08549	H	3.36134	-1.72714	-3.21674
C	-1.43586	-2.25105	2.0417	H	-2.80222	2.61583	3.40243	H	3.84052	-2.94158	-2.03292
C	-0.11538	-1.90265	1.66066	H	2.28576	2.29941	-1.06319	H	5.81593	-0.74241	-0.57193
C	0.72275	-2.86458	1.09117	H	3.71525	3.53745	-2.66888	H	4.65879	-0.40459	0.70592
C	-2.04314	-1.03266	2.49772	H	5.99556	4.22472	-2.04985	H	4.94545	-2.06613	0.18823
C	-1.04948	-0.04208	2.36362	H	6.90918	3.69296	0.18185	H	-0.12377	-1.09748	-1.05746
N	0.14107	-0.56445	1.89934	H	7.27345	2.77605	2.83775	H	0.69314	-3.39024	-1.63586
C	-3.30365	-0.70088	2.97976	H	6.98045	1.73383	5.05698	H	1.50408	-2.73579	-3.05922
C	-3.59086	0.61538	3.31508	H	4.88139	0.594	5.64313	H	-0.23957	-2.64192	-2.91747
C	-2.58211	1.58202	3.15778	H	3.00505	0.4786	4.0251	H	-0.05561	-0.12493	-3.34993
C	-1.31363	1.29146	2.68455	H	2.78926	-2.34547	1.41321	H	0.761	0.90791	-2.18344
Cu	1.65891	0.47606	1.3313	H	2.50276	-3.36982	0.01581	H	1.69891	-0.08427	-3.29599

N	3.18312	1.6112	1.48526	H	-6.895	0.24967	4.32163	H	2.17263	3.99048	4.12291
C	3.80936	2.28018	0.45787	H	-6.11527	-0.58708	2.98695	H	0.96355	4.34711	0.05127
C	5.12203	2.67646	0.82043	H	-5.5765	-0.86838	4.64272	H	-0.7006	2.99211	-0.85673
C	5.31025	2.20462	2.16348	H	-5.76614	2.0335	5.59301	H	-0.98615	1.42847	-0.08387
C	4.09973	1.55287	2.51153	H	-4.13988	2.56542	5.18184	H	-2.05032	2.76694	0.25364
C	3.29703	2.5924	-0.79959	H	-4.38311	0.99009	5.92643	H	-0.5646	2.39011	5.35125
C	4.09838	3.28731	-1.68758	H	-5.68428	1.65878	1.86715	H	0.40657	1.03487	4.83972
C	5.39309	3.67869	-1.33619	H	-6.53234	2.42224	3.2123	H	1.18464	2.44413	5.56487
C	5.90678	3.38004	-0.08512	H	-4.91949	2.96556	2.76386	C	0.69223	-2.57246	-2.35452
C	6.34665	2.27259	3.08621	H	-0.94034	-7.91975	0.58351	C	0.80019	-0.06244	-2.67788
C	6.18017	1.68828	4.33043	H	-0.23815	-6.61287	-0.35784	C	-0.27991	2.33606	2.47897
C	4.98676	1.04154	4.66327	H	0.36945	-6.96336	1.26134	C	0.54197	2.74367	3.53963
C	3.93778	0.96919	3.76589	H	-2.34345	-7.51642	2.55713	C	1.50943	3.7121	3.31032
C	2.09534	-2.53157	0.5865	H	-2.73597	-5.8853	3.08987	C	1.68279	4.2983	2.06398
C	-4.95819	1.05775	3.82892	H	-1.1038	-6.50595	3.30156	C	0.84021	3.90336	1.0337
C	-5.935	-0.10737	3.94926	H	-2.56401	-5.61665	-0.66083	C	-0.12645	2.9238	1.21164
C	-4.80017	1.69943	5.21148	H	-3.19941	-6.99496	0.23832	C	-1.00548	2.51002	0.07058
C	-5.55529	2.08641	2.86169	H	-3.60438	-5.35517	0.73383	C	0.39021	2.12467	4.89374
C	-1.57137	-5.96803	1.24459	C	3.76906	-0.91729	-1.22959	C	2.76442	5.30112	1.82329
C	-0.53124	-6.91169	0.64919	C	4.00153	-1.91253	-2.35725	H	3.6101	5.14042	2.49033
C	-1.96145	-6.49694	2.62904	C	4.8511	-1.03666	-0.1596	H	3.13112	5.24841	0.79852
C	-2.80652	-5.98188	0.33747	C	0.77377	-1.20988	-1.67719	H	2.41039	6.32072	1.98897
P	2.11043	-0.98398	-0.41664								

Generation of $Cu^{II}(P_{iPr}N_{Mes})(carb_{tBu})$ (5.15) via oxidation

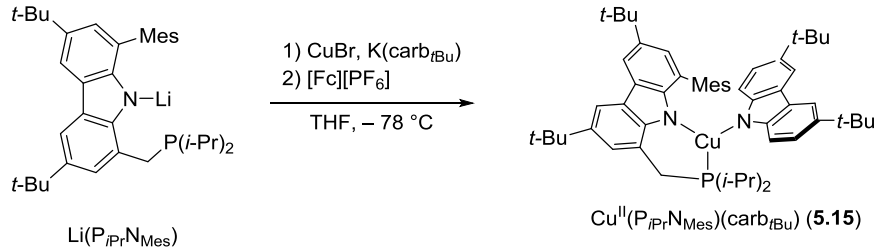

$Li(P_{iPr}N_{Mes})$

$Cu^{II}(P_{iPr}N_{Mes})(carb_{tBu})$ (**5.15**)

A suspension of CuBr (0.7 mg, 0.005 mmol, 1 equiv), $K(carb_{tBu})$ (1.6 mg, 0.005 mmol, 1 equiv) and $Li(P_{iPr}N_{Mes})$ (2.7 mg, 0.005 mmol, 1 equiv) in THF (0.3 mL) was prepared in a 4 mL vial equipped with a magnetic stir bar. The mixture was cooled to –78

°C, and [Fc][PF_6] (1.6 mg, 0.005 mmol, 1 equiv) was added to the stirring suspension. After stirring for 30 min at –78 °C, an aliquot was transferred to a vial containing pre-chilled 2-MeTHF (0.3 mL) at –78 °C. The resulting mixture was then transferred to a pre-chilled EPR tube at –78 °C and frozen at 77 K. EPR spectrum of the crude mixture is provided below. Spectral features are identical to those observed in the EPR spectrum of the analogous crude reaction mixture in Et_2O/2-MeTHF (e.g. **Figure 5.15**).

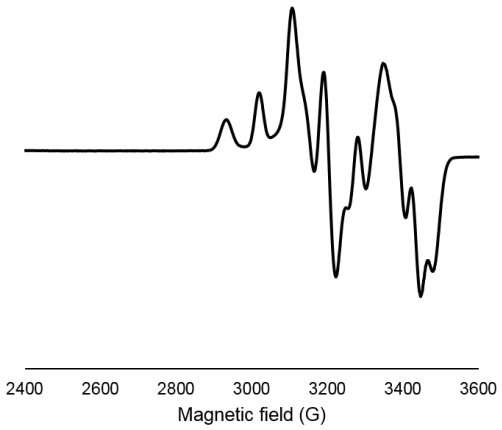

Figure 5.24. EPR spectrum (9.4 GHz, THF/2-MeTHF, 77 K) of **5.15** from the oxidation of an equimolar mixture of CuBr, K(carb$_{t\mathrm{Bu}}$), and Li(P$_{i\mathrm{Pr}}$N$_{\mathrm{Mes}}$).

Isolation of Cu$^{\mathrm{II}}$(P$_{i\mathrm{Pr}}$N$_{\mathrm{Mes}}$)(carb$_{t\mathrm{Bu}}$) (5.15)

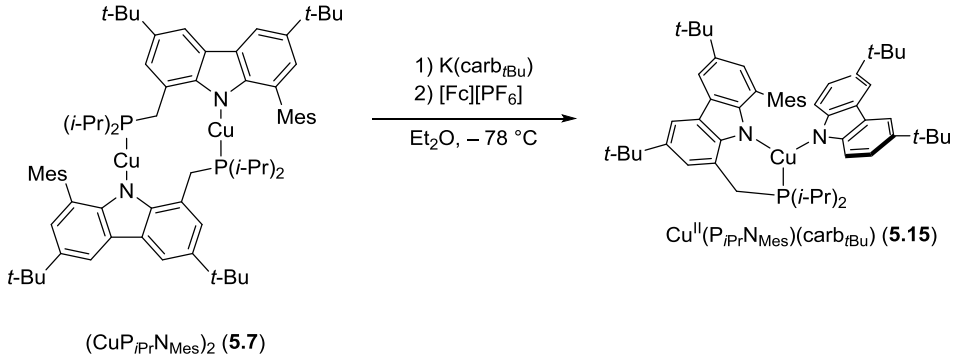

(CuP$_{i\mathrm{Pr}}$N$_{\mathrm{Mes}}$)$_2$ (**5.7**)

Cu$^{\mathrm{II}}$(P$_{i\mathrm{Pr}}$N$_{\mathrm{Mes}}$)(carb$_{t\mathrm{Bu}}$) (**5.15**)

A 4 mL vial was charged with complex **5.7** (118 mg, 0.100 mmol, 1 equiv), K(carb$_{tBu}$) (70 mg, 0.22 mmol, 2.2 equiv), Et_2O (4 mL), and a magnetic stir bar. The suspension was stirred at ambient temperature for 2 h and cooled to –78 °C. Next, [Fc][PF_6] (330 mg, 1.00 mmol, 10 equiv) was added to the stirring suspension at –78 °C, and the mixture was capped with a PTFE-lined septum cap and stirred at –78 °C overnight. The resulting purple suspension was concentrated in vacuo over two days at –78 °C, and the residue was extracted at –78 °C using pre-chilled *n*-pentane (4 mL) and filtered into a pre-chilled 4 mL vial. The filtrate was concentrated in vacuo at –78 °C over several days to give crystals of **5.15** (60 mg, 35% yield). Single crystals suitable for X-ray diffraction were grown by slow evaporation of a saturated solution in *n*-pentane. The simulated EPR spectrum of **5.15** is provided below.

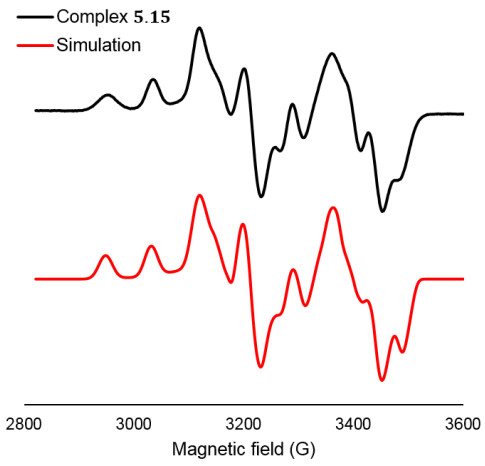

Figure 5.25. EPR spectra of **5.15**. Left: black trace: experimental spectrum (9.4 GHz, THF/2-MeTHF, 77 K); red trace: spectrum. Simulation parameters are as follows: g = [2.009, 2.043, 2.126], H_{strain} (MHz) [30, 30, 40], g_{strain} = [0.001, 0.002, 0.008], A_{Cu} (MHz) = [105, 35, 243], A_N (MHz) = [24, 30, 18], A_N (MHz) = [24, 30, 18], A_P (MHz) = [500, 690, 515].

5.4.6. X-ray crystallographic data

$(CuP_{iPr}N_H)_2$–CH_3CN (5.1–CH_3CN)

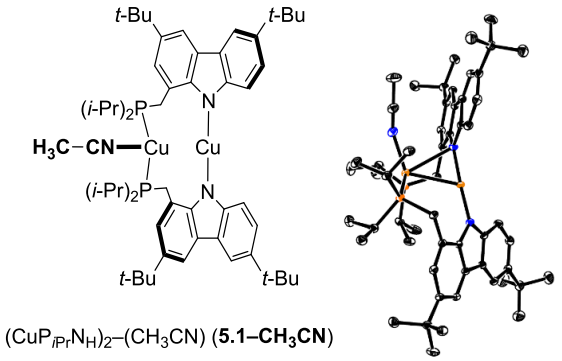

Table 5.2. Crystal data and structure refinement for **5.1–CH_3CN**.

Identification code	**5.1–CH_3CN**
Empirical formula	$C_{57}H_{82.5}Cu_2N_{3.5}P_2$
Formula weight	1005.78
Temperature/K	99.94
Crystal system	monoclinic
Space group	$P2_1/c$
a/Å	31.648(2)
b/Å	12.9087(10)
c/Å	26.762(2)
α/°	90
β/°	93.546(3)
γ/°	90
Volume/Å^3	10912.5(15)
Z	8
ρ_{calc}g/cm^3	1.224
μ/mm^{-1}	0.876
F(000)	4296.0
Crystal size/mm^3	0.23 × 0.1 × 0.07
Radiation	MoKα (λ = 0.71073)
2Θ range for data collection/°	4.626 to 55.048
Index ranges	-41 ≤ h ≤ 41, -16 ≤ k ≤ 16, -34 ≤ l ≤ 34
Reflections collected	238445
Independent reflections	25076 [R_{int} = 0.0651, R_{sigma} = 0.0318]
Data/restraints/parameters	25076/0/1227
Goodness-of-fit on F^2	1.011
Final R indexes [I>=2σ (I)]	R_1 = 0.0347, wR_2 = 0.0800
Final R indexes [all data]	R_1 = 0.0493, wR_2 = 0.0853
Largest diff. peak/hole / e Å^{-3}	1.39/-0.62

Table 5.3. Fractional Atomic Coordinates ($\times 10^4$) and Equivalent Isotropic Displacement Parameters ($Å^2 \times 10^3$) for **5.1–CH_3CN**. U_{eq} is defined as 1/3 of the trace of the orthogonalized U_{IJ} tensor.

Atom	*x*	*y*	*z*	U(eq)	Atom	*x*	*y*	*z*	U(eq)
Cu01	3492.5(2)	7133.8(2)	7430.5(2)	13.43(5)	C022	3829.0(6)	-709.8(17)	6754.5(8)	22.2(4)
Cu02	1726.3(2)	1998.0(2)	5764.4(2)	12.49(5)	C023	2632.0(6)	4526.2(15)	5175.5(8)	19.4(4)
Cu03	1422.0(2)	275.0(2)	5347.0(2)	13.94(5)	C024	1258.9(6)	-2341.4(16)	5997.3(8)	22.9(4)
Cu04	3623.3(2)	5254.0(2)	7827.4(2)	13.81(5)	C025	5001.8(6)	7369.3(16)	9562.8(7)	19.6(4)
P005	3326.0(2)	4400.8(4)	7159.5(2)	13.72(10)	C026	2369.6(6)	-2469.6(16)	5934.8(8)	21.7(4)
P006	1825.4(2)	-696.6(4)	5892.0(2)	13.09(9)	C027	951.8(6)	1692.1(15)	6558.1(7)	17.5(4)
P007	1540.2(2)	979.0(4)	4593.1(2)	14.19(10)	C028	3069.2(6)	4315.4(15)	5139.4(7)	16.9(4)
P008	3345.5(2)	6011.4(4)	8496.5(2)	17.46(10)	C029	2792.0(6)	2625.9(16)	6972.9(8)	21.6(4)
N009	4059.8(5)	7029.6(12)	7663.2(6)	13.6(3)	C02A	229.7(6)	2191.7(15)	6746.5(7)	17.4(4)
N00A	2310.0(5)	2113.4(12)	5817.0(6)	13.6(3)	C02B	1405.3(6)	4436.4(17)	6299.7(8)	23.3(4)
N00B	2920.2(5)	7354.0(12)	7243.1(6)	14.6(3)	C02C	5533.2(6)	6009.3(16)	6620.8(7)	19.5(4)
N00C	1140.0(5)	2023.9(12)	5672.7(6)	13.7(3)	C02D	2202.4(6)	6970.4(14)	7250.0(7)	13.9(4)
N00D	792.8(5)	-79.5(13)	5382.0(6)	19.6(3)	C02E	460.7(6)	-81.7(17)	5521.0(8)	23.3(4)
N00E	4213.6(5)	4707.7(13)	7960.2(6)	17.5(3)	C02F	-10.3(6)	3789.6(16)	4163.9(7)	18.7(4)
C00F	2580.7(5)	418.6(14)	6184.7(7)	13.3(4)	C02G	2015.5(7)	-1998.3(17)	5091.1(8)	24.4(4)
C00G	4050.2(5)	7292.6(14)	8595.6(7)	13.7(4)	C02H	635.4(6)	1785.4(16)	6888.1(7)	19.1(4)
C00H	2604.5(5)	6626.4(14)	7111.2(7)	12.8(4)	C02I	2410.6(6)	700.0(18)	4744.8(8)	23.2(4)
C00I	4247.5(5)	7130.6(14)	8145.5(7)	13.2(4)	C02J	-92.6(6)	2325.6(17)	7146.8(7)	21.4(4)
C00J	3036.0(5)	5227.1(15)	6686.5(7)	14.8(4)	C02K	-414.4(6)	4184.1(17)	4385.6(8)	23.6(4)
C00K	4395.2(5)	6849.7(14)	7362.1(7)	13.7(4)	C02L	1868.9(6)	10335.4(16)	8167.2(8)	21.3(4)
C00L	2170.4(5)	16.3(14)	6366.7(7)	14.0(4)	C02M	3597.2(6)	-1705.4(16)	5977.8(8)	23.2(4)
C00M	3575.3(5)	7307.5(15)	8614.3(7)	15.2(4)	C02N	3347.4(6)	5086.3(16)	4869.5(8)	21.0(4)
C00N	2946.8(6)	-170.2(14)	6265.5(7)	14.7(4)	C02O	2509.0(6)	5437.1(18)	8251.6(8)	24.7(5)
C00O	2707.5(6)	8170.7(14)	7459.8(7)	14.4(4)	C02P	3425.9(8)	5868.2(19)	9574.5(8)	32.5(5)
C00P	1016.5(6)	2634.5(14)	4779.7(7)	14.2(4)	C02Q	84.9(7)	3091.2(18)	7543.6(8)	28.3(5)
C00Q	184.4(6)	3097.2(15)	5044.9(7)	15.9(4)	C02R	1408.7(7)	9955.6(19)	8174.2(10)	33.5(6)
C00R	2930.6(6)	3447.7(15)	7360.3(7)	16.7(4)	C02S	1079.1(6)	5130.6(16)	7049.0(9)	23.4(4)
C00S	897.7(5)	2432.8(14)	5266.5(7)	13.6(4)	C02T	3416.7(8)	5276.7(18)	9079.0(8)	30.6(5)
C00T	2630.6(5)	5675.3(15)	6860.9(7)	13.8(4)	C02U	2768.0(6)	6353.4(19)	8419.7(9)	28.4(5)
C00U	480.8(5)	2663.4(14)	5392.6(7)	13.9(4)	C02V	-129.2(7)	2947.9(18)	3778.5(8)	27.4(5)
C00V	2521.5(5)	2915.1(14)	5591.5(7)	14.2(4)	C02W	3817.5(7)	4792.4(18)	4924.1(9)	29.4(5)
C00W	2618.4(5)	1371.4(14)	5936.1(7)	12.7(3)	C02X	5007.8(6)	4204.8(18)	8005.2(11)	33.9(6)
C00X	4788.2(5)	6806.0(14)	7643.2(7)	13.4(4)	C02Y	1130.8(8)	-641.8(18)	4089.1(9)	35.4(6)
C00Y	2199.3(6)	-1586.5(15)	5596.9(7)	17.1(4)	C02Z	2041.3(7)	10469.7(18)	8712.4(8)	30.2(5)
C00Z	4693.8(5)	7016.1(14)	8154.7(7)	13.5(4)	C030	2587.7(7)	6916.5(19)	8859.9(9)	32.1(5)
C010	2260.5(6)	5109.4(15)	6774.0(7)	15.3(4)	C031	1591.3(7)	3674.7(16)	7151.0(9)	26.0(5)
C011	1861.8(5)	5420.9(14)	6934.7(7)	14.7(4)	C032	36.3(7)	-85(2)	5707.5(11)	39.6(6)
C012	3020.7(5)	1688.4(14)	5783.7(7)	13.4(4)	C033	1864.5(7)	11379.2(17)	7896.2(9)	28.0(5)
C013	4941.6(5)	7093.5(15)	8607.4(7)	15.3(4)	C034	1182.2(8)	992(2)	3575.9(8)	37.2(6)
C014	2269.1(5)	7964.4(14)	7475.2(7)	14.0(4)	C035	2195.2(7)	1778(2)	4007.5(9)	35.0(6)
C015	1449.8(5)	2390.0(14)	4612.7(7)	15.2(4)	N036	934.6(8)	-3188(2)	4415.3(11)	58.5(7)
C016	4308.6(6)	7382.0(14)	9030.3(7)	15.3(4)	C037	5418.9(7)	5128.8(19)	6252.8(9)	31.3(5)
C017	868.5(5)	2005.5(14)	6062.7(7)	14.3(4)	C038	4112.5(6)	-266.7(18)	5933.8(9)	27.4(5)
C018	1526.2(6)	-1545.2(15)	6301.5(7)	17.0(4)	C039	-516.3(7)	2762(2)	6928.7(9)	31.7(5)
C019	713.8(6)	3067.2(15)	4444.4(7)	15.6(4)	C03A	192.6(7)	4704.7(19)	3903.3(10)	34.1(6)
C01A	2067.0(6)	857.3(16)	4327.9(7)	18.3(4)	C03B	1119.7(8)	-3842(2)	4609(1)	35.7(6)
C01B	297.8(6)	3319.2(15)	4565.9(7)	15.7(4)	C03C	-174.6(8)	1271.8(18)	7386.6(9)	32.9(5)
C01C	1247.9(6)	-909.1(16)	6633.6(8)	21.2(4)	C03D	3210.3(8)	5093(2)	4309.6(9)	33.7(5)
C01D	4381.0(6)	6711.5(15)	6845.4(7)	16.4(4)	C03E	3301.1(8)	6176.1(17)	5085.6(10)	33.9(5)
C01E	1837.0(5)	6368.0(15)	7168.4(7)	14.9(4)	C03F	5694.6(8)	6938.1(19)	6331.5(11)	41.0(6)
C01F	3346.1(5)	114.5(15)	6096.4(7)	15.2(4)	C03G	3795.3(9)	4573(2)	9082(1)	49.2(8)
C01G	2152.0(6)	9567.7(15)	7905.6(7)	17.6(4)	C03H	5891.7(7)	5605(2)	6978.5(9)	36.1(6)
C01H	4754.0(6)	7292.4(14)	9052.4(7)	14.9(4)	C03I	1350.6(8)	-4675.6(19)	4869.2(10)	39.6(6)
C01I	3225.4(6)	3392.3(15)	5336.9(7)	16.2(4)	C03J	5472.1(7)	7462(3)	9518.2(10)	54.8(9)

C01J	1997.1(6)	8654.3(15)	7698.0(7)	15.8(4)	C03K	4814(3)	8165(9)	9894(3)	36(2)
C01K	4750.2(6)	6469.3(15)	6620.9(7)	17.4(4)	C03L	4971(4)	6282(7)	9808(4)	35(2)
C01L	5156.6(5)	6534.4(15)	7407.2(7)	15.3(4)	C03M	4844(6)	6620(20)	9941(6)	51(5)
C01M	3076.5(6)	2957.6(16)	7865.0(8)	22.9(4)	C0AA	4968(6)	8521(11)	9772(6)	46(4)
C01N	2361.2(6)	3854.1(15)	5396.5(7)	17.5(4)	C01U	145.7(6)	2480.8(15)	6253.1(7)	16.8(4)
C01O	4562.3(6)	4490.2(15)	7980.5(8)	19.5(4)	C01V	2866.7(6)	9099.0(15)	7666.3(8)	18.7(4)
C01P	3663.0(6)	3661.9(15)	6744.5(8)	18.6(4)	C01W	2956.9(5)	2692.0(14)	5560.8(7)	13.6(4)
C01Q	3717.8(6)	-631.8(15)	6189.6(7)	17.2(4)	C01X	1144.7(7)	539.8(17)	4100.7(8)	23.1(4)
C01R	2590.3(6)	9775.3(16)	7878.8(8)	20.6(4)	C01Y	1486.3(6)	4676.6(15)	6857.2(8)	17.9(4)
C01S	462.5(5)	2388.7(15)	5911.8(7)	14.3(4)	C01Z	3900.8(6)	2771.7(16)	7012.5(8)	24.6(5)
C01T	3378.7(5)	1059.3(15)	5858.7(7)	14.4(4)	C020	5143.1(6)	6339.7(15)	6895.6(7)	16.3(4)
C021	3977.2(7)	4384.6(18)	6509.7(9)	28.1(5)					

Table 5.4. Anisotropic Displacement Parameters ($Å^2×10^3$) for **5.1–CH$_3$CN**. The anisotropic displacement factor exponent takes the form: $-2\pi^2[h^2a^{*2}U_{11}+2hka^*b^*U_{12}+\ldots]$.

Atom	U_{11}	U_{22}	U_{33}	U_{23}	U_{13}	U_{12}	Atom	U_{11}	U_{22}	U_{33}	U_{23}	U_{13}	U_{12}
Cu01	9.51(10)	15.40(11)	15.34(11)	0.36(9)	0.40(8)	0.58(8)	C01U	13.2(8)	18.2(9)	19.1(10)	-1.2(8)	2.1(7)	-0.3(7)
Cu02	8.77(10)	13.51(11)	15.17(11)	0.48(9)	0.64(8)	0.39(8)	C01V	13.4(8)	19.9(10)	22.7(10)	-1.6(8)	1.3(7)	-2.2(7)
Cu03	13.46(10)	14.96(11)	13.32(11)	3.07(9)	0.27(8)	-1.57(9)	C01W	12.6(8)	13.5(9)	14.6(9)	0.7(7)	1.0(7)	-0.4(7)
Cu04	12.11(10)	15.86(11)	13.51(11)	-2.40(9)	1.30(8)	1.30(9)	C01X	25.7(10)	26.1(11)	17.2(10)	-3.0(9)	-2.0(8)	1.5(9)
P005	12.0(2)	14.0(2)	15.0(2)	-2.71(19)	-0.13(17)	3.03(18)	C01Y	14.5(8)	14.1(9)	24.9(10)	-0.2(8)	-0.3(7)	-1.0(7)
P006	11.8(2)	12.9(2)	14.4(2)	2.89(19)	0.27(17)	-1.97(17)	C01Z	22.1(10)	21.9(11)	29.6(12)	-5.7(9)	-1.0(9)	8.9(8)
P007	15.1(2)	14.9(2)	12.9(2)	1.94(19)	3.21(18)	2.05(18)	C020	14.8(8)	15.7(9)	18.8(10)	-0.8(8)	4.9(7)	-0.9(7)
P008	16.9(2)	18.2(2)	18.0(3)	-4.8(2)	7.70(19)	-4.81(19)	C021	24(1)	26.7(11)	34.9(13)	-5.9(10)	11.5(9)	4.3(9)
N009	12.0(7)	15.7(8)	13.2(8)	0.6(6)	1.3(6)	-0.5(6)	C022	19.1(9)	23.5(11)	23.1(11)	1.6(9)	-5.5(8)	3.7(8)
N00A	11.9(7)	12.9(8)	15.8(8)	2.4(6)	0.6(6)	-0.5(6)	C023	22.4(9)	11.9(9)	23.8(10)	3.5(8)	1.6(8)	2.3(7)
N00B	14.7(7)	13.9(8)	15.4(8)	-1.2(6)	1.3(6)	0.1(6)	C024	21.1(9)	18.2(10)	29.0(11)	6.4(9)	-0.9(8)	-7.1(8)
N00C	12.4(7)	15.1(8)	13.8(8)	3.0(6)	1.7(6)	0.3(6)	C025	19.6(9)	24.8(11)	14.1(9)	1.5(8)	-0.6(7)	1.1(8)
N00D	18.9(8)	19.2(9)	20.2(9)	3.2(7)	-1.5(7)	-3.0(7)	C026	19.5(9)	18.7(10)	26.7(11)	4.0(9)	0.5(8)	2.7(8)
N00E	17.3(8)	16.7(8)	18.2(8)	-1.7(7)	-1.0(6)	-1.1(6)	C027	16.4(8)	18.2(10)	17.5(10)	1.3(8)	-1.8(7)	-0.4(7)
C00F	12.6(8)	14.9(9)	12.3(9)	-0.9(7)	0.2(7)	-1.6(7)	C028	19.6(9)	14.9(9)	16.4(9)	1.9(8)	2.8(7)	-4.6(7)
C00G	13.0(8)	10.4(8)	18.0(9)	-1.0(7)	2.6(7)	-1.1(7)	C029	22.4(9)	17.9(10)	24.1(11)	-3.4(8)	-1.1(8)	-1.1(8)
C00H	11.1(8)	14.5(9)	12.7(9)	3.2(7)	-0.2(7)	1.0(7)	C02A	18.6(9)	17.1(9)	16.9(9)	-2.6(8)	4.0(7)	-5.1(7)
C00I	14.5(8)	10.4(8)	14.6(9)	0.4(7)	0.5(7)	-1.5(7)	C02B	16.7(9)	23.2(11)	29.5(12)	-4.3(9)	-2.5(8)	-2.1(8)
C00J	14.0(8)	16.7(9)	13.7(9)	-1.3(7)	1.8(7)	3.2(7)	C02C	18.6(9)	22.6(10)	18(1)	-2.9(8)	6.3(8)	0.9(8)
C00K	12.4(8)	13.3(9)	15.5(9)	1.1(7)	2.6(7)	-1.0(7)	C02D	14.7(8)	12.8(9)	14.2(9)	1.8(7)	1.7(7)	2.9(7)
C00L	12.9(8)	14.7(9)	14.5(9)	2.4(7)	0.1(7)	-2.8(7)	C02E	19.1(10)	23.9(11)	26.5(11)	4.8(9)	-1.5(8)	-1.5(8)
C00M	13.2(8)	16.4(9)	16.5(9)	-2.7(8)	4.5(7)	-0.9(7)	C02F	17.1(9)	20.1(10)	18.5(10)	3.5(8)	-2.6(8)	2.1(8)
C00N	15.1(8)	12.5(9)	16.2(9)	3.8(7)	-1.2(7)	-0.6(7)	C02G	29.1(10)	22.1(11)	22.0(11)	-2.8(9)	1.0(9)	0.9(9)
C00O	14.3(8)	14.9(9)	14.0(9)	2.4(7)	0.8(7)	1.8(7)	C02H	22.8(9)	20.3(10)	14.1(9)	0.9(8)	0.7(8)	-2.6(8)
C00P	14.1(8)	12.0(9)	16.7(9)	1.2(7)	3.1(7)	1.2(7)	C02I	17.1(9)	31.5(12)	21.6(11)	0.8(9)	6.5(8)	1.6(8)
C00Q	13.3(8)	17.0(9)	17.3(9)	-1.3(8)	-0.6(7)	1.4(7)	C02J	22.0(9)	26.0(11)	17(1)	-3.2(8)	8.2(8)	-5.1(8)
C00R	16.2(8)	14.8(9)	19(1)	-2.8(8)	0.1(7)	1.2(7)	C02K	20.1(9)	27.0(11)	22.6(11)	-1.4(9)	-7.2(8)	8.5(8)
C00S	12.4(8)	12.4(9)	16.0(9)	1.5(7)	-0.4(7)	0.0(7)	C02L	21.0(9)	16.1(10)	27.1(11)	-6.1(8)	5.3(8)	2.4(8)
C00T	13.1(8)	15.8(9)	12.3(9)	2.1(7)	-0.3(7)	4.0(7)	C02M	24.1(10)	19.6(10)	25.3(11)	0.6(9)	-3.5(8)	5.8(8)
C00U	13.1(8)	13.6(9)	14.9(9)	-1.7(7)	0.6(7)	0.0(7)	C02N	24.1(10)	16.4(10)	22.9(11)	3.2(8)	5.9(8)	-4.6(8)
C00V	12.5(8)	14.3(9)	15.7(9)	-0.1(7)	0.6(7)	-1.8(7)	C02O	18.0(9)	35.7(13)	20.6(11)	2.4(9)	2.8(8)	0.5(9)
C00W	10.4(8)	14.0(9)	13.5(9)	-1.0(7)	0.5(7)	0.1(7)	C02P	46.9(14)	33.0(13)	18.1(11)	-2.8(10)	6.7(10)	-9.4(11)
C00X	13.0(8)	12.3(9)	14.8(9)	1.3(7)	0.6(7)	-1.5(7)	C02Q	34.7(12)	29.2(12)	21.9(11)	-4.1(9)	9.4(9)	-5.7(10)
C00Y	15.7(8)	15.8(9)	19.9(10)	0.9(8)	1.9(7)	0.0(7)	C02R	24.1(11)	28.1(12)	50.1(15)	-15.0(11)	15.8(10)	1.1(9)
C00Z	13.2(8)	12.8(9)	14.8(9)	0.1(7)	2.4(7)	-1.1(7)	C02S	14.8(9)	22.1(11)	33.7(12)	-1.7(9)	3.9(8)	-3.4(8)
C010	15.9(8)	13.4(9)	16.2(9)	-0.4(7)	-0.6(7)	1.6(7)	C02T	45.7(13)	26.6(12)	19.9(11)	2.0(9)	4.5(10)	-2.3(10)
C011	11.8(8)	15.2(9)	17.0(9)	2.0(7)	-0.7(7)	1.6(7)	C02U	21.9(10)	31.9(12)	31.8(12)	-3.3(10)	5.2(9)	1.1(9)
C012	11.4(8)	14.6(9)	14.2(9)	-0.2(7)	1.8(7)	-1.2(7)	C02V	26(1)	35.9(13)	19.5(11)	-5.3(10)	-5.4(8)	6.5(9)
C013	11.6(8)	16.4(9)	17.7(9)	0.2(8)	0.7(7)	-1.5(7)	C02W	26(1)	28.1(12)	35.2(13)	8.7(10)	9.4(9)	-6.7(9)
C014	14.1(8)	12.9(9)	14.9(9)	1.1(7)	0.2(7)	1.1(7)	C02X	14.8(9)	23.9(12)	62.5(17)	3.6(11)	-2.6(10)	1.8(9)
C015	13.3(8)	14.9(9)	17.7(9)	4.1(8)	4.2(7)	2.3(7)	C02Y	46.3(14)	27.3(12)	31.5(13)	-8.8(11)	-7.3(11)	-3.5(11)
C016	18.3(9)	13.4(9)	14.4(9)	-1.4(7)	4.5(7)	-0.2(7)	C02Z	37.9(12)	27.3(12)	26.0(12)	-6.5(10)	7.2(10)	5.7(10)
C017	13.1(8)	14.5(9)	15.3(9)	-0.4(7)	1.7(7)	-2.2(7)	C030	27.3(11)	34.8(13)	35.0(13)	-9.9(11)	9.4(10)	4.9(10)
C018	14.6(8)	16.6(9)	19.9(10)	5.2(8)	0.7(7)	-2.4(7)	C031	23.3(10)	18.9(10)	35.4(13)	5.4(9)	-1.9(9)	-3.6(8)
C019	18.2(9)	15.6(9)	13.0(9)	2.1(7)	1.8(7)	1.0(7)	C032	19.9(10)	47.5(16)	52.5(17)	6.9(13)	10.6(11)	-1.2(10)
C01A	19.5(9)	19.9(10)	16.2(10)	1.9(8)	7.6(8)	3.1(8)	C033	30.4(11)	21.9(11)	31.7(12)	-2(1)	2.7(9)	6.7(9)
C01B	15.1(8)	14.1(9)	17.5(9)	-0.5(8)	-3.2(7)	1.9(7)	C034	46.0(14)	46.3(15)	18.5(11)	0.7(11)	-4.3(10)	1.9(12)
C01C	18.1(9)	25.0(11)	20.9(10)	5.9(9)	3.6(8)	-2.6(8)	C035	28.6(11)	40.5(14)	38.0(14)	18.7(11)	18.5(10)	10.5(10)

C01D	14.8(8)	17.8(9)	16.4(9)	2.0(8)	−1.4(7)	−0.1(7)	N036	49.6(14)	54.0(16)	69.2(18)	17.5(14)	−17.5(13)	−12.9(13)
C01E	10.8(8)	16.1(9)	17.8(9)	0.5(8)	0.6(7)	1.9(7)	C037	30.4(11)	31.5(13)	32.2(13)	−11.4(10)	5.5(10)	4.3(10)
C01F	11.6(8)	16.5(9)	17.3(9)	−1.0(8)	−1.4(7)	1.0(7)	C038	16.1(9)	29.4(12)	37.0(13)	5.4(10)	5.4(9)	5.9(9)
C01G	19.0(9)	15.9(9)	18.1(10)	−1.0(8)	2.8(7)	3.3(7)	C039	23.8(10)	45.2(15)	27.5(12)	−4.9(11)	12.5(9)	1.7(10)
C01H	16.6(8)	13.1(9)	14.7(9)	0.5(7)	−0.2(7)	−1.7(7)	C03A	25.7(11)	33.5(13)	42.2(14)	21.8(11)	−5.8(10)	2.5(10)
C01I	14.0(8)	17.9(9)	16.7(9)	0.0(8)	1.4(7)	−2.6(7)	C03B	37.3(13)	36.5(14)	32.6(13)	−0.1(11)	−2.6(11)	−11.1(11)
C01J	14.5(8)	15.0(9)	18.1(10)	0.8(8)	2.3(7)	1.9(7)	C03C	39.1(13)	30.8(13)	30.6(13)	−2.7(10)	16.6(10)	−11.1(10)
C01K	21.0(9)	18.4(10)	13.0(9)	0.1(8)	2.0(7)	−1.8(8)	C03D	42.9(13)	33.7(13)	24.6(12)	9(1)	3.6(10)	−10.2(11)
C01L	11.3(8)	17.0(9)	17.4(9)	−0.4(8)	0.6(7)	−2.2(7)	C03E	42.1(13)	17.6(11)	43.6(15)	−0.4(10)	15.4(11)	−8.3(10)
C01M	25.3(10)	19.9(10)	23.3(11)	2.4(9)	−0.5(8)	−1.4(8)	C03F	41.6(14)	30.1(13)	55.1(17)	1.3(12)	34.0(13)	−0.5(11)
C01N	14.2(8)	17.0(9)	21.3(10)	1.0(8)	1.1(7)	2.7(7)	C03G	61.3(18)	63(2)	22.8(13)	9.1(13)	2.0(12)	29.7(15)
C01O	18.9(9)	14.1(9)	25.1(11)	−0.5(8)	−2.5(8)	−1.0(7)	C03H	21.6(10)	58.6(17)	28.7(13)	−9.1(12)	5.3(9)	11.1(11)
C01P	16.3(9)	18.9(10)	20.5(10)	−6.2(8)	1.0(8)	4.3(8)	C03I	47.3(15)	27.3(13)	44.4(15)	−4.5(12)	5.2(12)	2.3(11)
C01Q	13.2(8)	17.0(9)	21.1(10)	1.7(8)	−1.4(7)	2.8(7)	C03J	24.2(12)	117(3)	22.7(13)	−18.9(16)	−3.2(10)	−17.7(15)
C01R	21.1(9)	15.8(10)	24.7(11)	−4.2(8)	1.4(8)	−2.0(8)	C03K	32(3)	53(5)	22(3)	−19(3)	−10(2)	16(3)
C01S	13.2(8)	15.6(9)	14.1(9)	−0.7(7)	0.7(7)	−0.6(7)	C03L	39(4)	39(4)	28(3)	17(2)	−11(3)	−12(2)
C01T	10.1(8)	17.1(9)	15.9(9)	0.5(8)	0.2(7)	−0.1(7)	C03M	45(6)	80(12)	28(6)	26(7)	−10(5)	−20(6)
							C0AA	40(7)	49(6)	45(6)	−25(5)	−27(5)	15(5)

Table 5.5. Bond Lengths for **5.1–CH_3CN**.

Atom	Atom	Length/Å	Atom	Atom	Length/Å	Atom	Atom	Length/Å	Atom	Atom	Length/Å
Cu01	Cu04	2.6707(4)	C013	C01H	1.387(3)	C00F	C00W	1.407(3)	C01Y	C02B	1.530(3)
Cu01	N009	1.8684(15)	C014	C01J	1.397(3)	C00G	C00I	1.406(3)	C01Y	C02S	1.533(3)
Cu01	N00B	1.8711(15)	C014	C02D	1.428(3)	C00G	C00M	1.507(2)	C01Y	C031	1.539(3)
Cu02	Cu03	2.6437(4)	C016	C01H	1.412(2)	C00G	C016	1.385(3)	C020	C02C	1.536(3)
Cu02	N00A	1.8499(15)	C017	C01S	1.412(2)	C00H	C00T	1.404(3)	C023	C028	1.419(3)
Cu02	N00C	1.8568(15)	C017	C027	1.395(3)	C00H	C02D	1.419(2)	C025	C03J	1.506(3)
Cu03	P006	2.2582(5)	C018	C01C	1.528(3)	C00I	C00Z	1.419(2)	C025	C03K	1.503(6)
Cu03	P007	2.2649(5)	C018	C024	1.533(3)	C00J	C00T	1.507(2)	C025	C03L	1.555(7)
Cu03	N00D	2.0509(16)	C019	C01B	1.414(2)	C00K	C00X	1.414(2)	C025	C03M	1.503(11)
Cu04	P005	2.2551(5)	C01A	C02I	1.523(3)	C00K	C01D	1.392(3)	C025	C0AA	1.594(10)
Cu04	P008	2.2650(6)	C01A	C035	1.535(3)	C00N	C01F	1.417(2)	C027	C02H	1.381(3)
Cu04	N00E	2.0080(16)	C01B	C02F	1.532(3)	C00O	C014	1.416(2)	C028	C02N	1.538(3)
P005	C00J	1.8544(19)	C01D	C01K	1.382(3)	C00O	C01V	1.400(3)	C02A	C02H	1.417(3)
P005	C00R	1.858(2)	C01E	C02D	1.400(2)	C00P	C00S	1.402(3)	C02A	C02J	1.534(3)
P005	C01P	1.8512(19)	C01F	C01Q	1.529(2)	C00P	C015	1.502(2)	C02C	C037	1.533(3)
P006	C00L	1.8659(18)	C01F	C01T	1.382(3)	C00P	C019	1.389(3)	C02C	C03F	1.532(3)
P006	C00Y	1.860(2)	C01G	C01J	1.381(3)	C00Q	C00U	1.397(3)	C02C	C03H	1.531(3)
P006	C018	1.8510(19)	C01G	C01R	1.419(3)	C00Q	C01B	1.382(3)	C02E	C032	1.462(3)
P007	C015	1.8449(19)	C01G	C02L	1.534(3)	C00R	C01M	1.536(3)	C02F	C02K	1.530(3)
P007	C01A	1.8586(19)	C01H	C025	1.536(3)	C00R	C029	1.528(3)	C02F	C02V	1.529(3)
P007	C01X	1.849(2)	C01I	C01W	1.400(3)	C00S	C00U	1.414(2)	C02F	C03A	1.533(3)
P008	C00M	1.8438(19)	C01I	C028	1.383(3)	C00T	C010	1.388(3)	C02J	C02Q	1.532(3)
P008	C02T	1.827(2)	C01K	C020	1.415(3)	C00U	C01S	1.439(3)	C02J	C039	1.536(3)
P008	C02U	1.879(2)	C01L	C020	1.390(3)	C00V	C01N	1.402(3)	C02J	C03C	1.533(3)
N009	C00I	1.393(2)	C01N	C023	1.378(3)	C00V	C01W	1.415(2)	C02L	C02R	1.538(3)
N009	C00K	1.391(2)	C01O	C02X	1.455(3)	C00W	C012	1.421(2)	C02L	C02Z	1.536(3)
N00A	C00V	1.390(2)	C01P	C01Z	1.528(3)	C00X	C00Z	1.445(3)	C02L	C033	1.530(3)
N00A	C00W	1.390(2)	C01P	C021	1.527(3)	C00X	C01L	1.404(2)	C02N	C02W	1.533(3)
N00B	C00H	1.400(2)	C01Q	C022	1.534(3)	C00Y	C026	1.532(3)	C02N	C03D	1.534(3)
N00B	C00O	1.396(2)	C01Q	C02M	1.537(3)	C00Y	C02G	1.535(3)	C02N	C03E	1.531(3)
N00C	C00S	1.395(2)	C01Q	C038	1.535(3)	C00Z	C013	1.405(3)	C02O	C02U	1.493(3)
N00C	C017	1.393(2)	C01R	C01V	1.383(3)	C010	C011	1.416(2)	C02P	C02T	1.529(3)
N00D	C02E	1.136(3)	C01S	C01U	1.402(3)	C011	C01E	1.378(3)	C02T	C03G	1.504(3)
N00E	C01O	1.137(2)	C01U	C02A	1.382(3)	C011	C01Y	1.532(3)	C02U	C030	1.525(3)
C00F	C00L	1.507(2)	C01X	C02Y	1.526(3)	C012	C01T	1.398(2)	N036	C03B	1.135(3)
C00F	C00N	1.391(2)	C01X	C034	1.532(3)	C012	C01W	1.435(3)	C03B	C03I	1.454(4)

Table 5.6. Bond Angles for **5.1–CH_3CN**.

Atom	Atom	Atom	Angle/°	Atom	Atom	Atom	Angle/°	Atom	Atom	Atom	Angle/°	Atom	Atom	Atom	Angle/°
N009	Cu01	Cu04	71.34(5)	N00C	C017	C01S	111.86(16)	C00N	C00F	C00W	117.18(16)	C02S	C01Y	C031	108.05(17)
N009	Cu01	N00B	174.06(7)	N00C	C017	C027	128.89(17)	C00W	C00F	C00L	123.66(16)	C01K	C020	C02C	119.38(17)
N00B	Cu01	Cu04	111.61(5)	C027	C017	C01S	119.23(17)	C00I	C00G	C00M	121.80(16)	C01L	C020	C01K	117.57(17)
N00A	Cu02	Cu03	115.84(5)	C01C	C018	P006	111.14(13)	C016	C00G	C00I	117.48(16)	C01L	C020	C02C	123.04(17)
N00A	Cu02	N00C	173.50(7)	C01C	C018	C024	110.50(16)	C016	C00G	C00M	120.63(17)	C01N	C023	C028	122.90(18)
N00C	Cu02	Cu03	67.94(5)	C024	C018	P006	111.60(14)	N00B	C00H	C00T	130.14(16)	C01H	C025	C03L	106.0(3)
P006	Cu03	Cu02	91.014(16)	C00P	C019	C01B	123.99(17)	N00B	C00H	C02D	111.20(16)	C01H	C025	C0AA	109.3(4)
P006	Cu03	P007	132.87(2)	C02I	C01A	P007	110.40(13)	C00T	C00H	C02D	118.62(16)	C03J	C025	C01H	112.80(17)
P007	Cu03	Cu02	87.875(16)	C02I	C01A	C035	108.11(18)	N009	C00I	C00G	128.40(16)	C03J	C025	C03L	101.2(5)
N00D	Cu03	Cu02	119.85(5)	C035	C01A	P007	114.99(14)	N009	C00I	C00Z	111.92(16)	C03J	C025	C0AA	92.4(8)
N00D	Cu03	P006	111.00(5)	C00Q	C01B	C019	117.67(17)	C00G	C00I	C00Z	119.65(16)	C03K	C025	C01H	111.7(3)
N00D	Cu03	P007	110.15(5)	C00Q	C01B	C02F	122.89(16)	C00T	C00J	P005	113.85(13)	C03K	C025	C03J	114.9(5)
P005	Cu04	Cu01	94.691(16)	C019	C01B	C02F	119.40(17)	N009	C00K	C00X	112.08(16)	C03K	C025	C03L	109.3(8)
P005	Cu04	P008	132.40(2)	C01K	C01D	C00K	118.98(17)	N009	C00K	C01D	128.14(16)	C03M	C025	C01H	112.6(5)
P008	Cu04	Cu01	82.187(17)	C011	C01E	C02D	119.61(17)	C01D	C00K	C00X	119.78(16)	C03M	C025	C03J	118.4(8)
N00E	Cu04	Cu01	120.60(5)	C00N	C01F	C01Q	118.49(17)	C00F	C00L	P006	115.43(13)	C03M	C025	C0AA	109.2(15)
N00E	Cu04	P005	107.86(5)	C01T	C01F	C00N	117.99(16)	C00G	C00M	P008	111.50(13)	C02H	C027	C017	118.72(17)
N00E	Cu04	P008	114.46(5)	C01T	C01F	C01Q	123.52(16)	C00F	C00N	C01F	124.00(17)	C01I	C028	C023	117.79(17)
C00J	P005	Cu04	115.13(6)	C01J	C01G	C01R	117.70(17)	N00B	C00O	C014	111.63(16)	C01I	C028	C02N	122.39(17)
C00J	P005	C00R	105.34(8)	C01J	C01G	C02L	122.18(17)	N00B	C00O	C01V	129.73(16)	C023	C028	C02N	119.78(17)
C00R	P005	Cu04	110.46(6)	C01R	C01G	C02L	120.10(17)	C01V	C00O	C014	118.61(17)	C01U	C02A	C02H	118.23(17)
C01P	P005	Cu04	119.98(6)	C013	C01H	C016	117.29(17)	C00S	C00P	C015	122.66(16)	C01U	C02A	C02J	122.69(17)
C01P	P005	C00J	99.56(9)	C013	C01H	C025	123.61(16)	C019	C00P	C00S	117.45(16)	C02H	C02A	C02J	119.05(17)
C01P	P005	C00R	104.82(9)	C016	C01H	C025	119.04(17)	C019	C00P	C015	119.88(17)	C037	C02C	C020	110.42(16)
C00L	P006	Cu03	116.71(6)	C028	C01I	C01W	120.53(17)	C01B	C00Q	C00U	119.92(17)	C03F	C02C	C020	109.13(17)
C00Y	P006	Cu03	114.70(6)	C01G	C01J	C014	120.22(17)	C01M	C00R	P005	110.84(13)	C03F	C02C	C037	109.18(19)
C00Y	P006	C00L	103.46(8)	C01D	C01K	C020	122.69(18)	C029	C00R	P005	115.69(14)	C03H	C02C	C020	112.46(17)
C018	P006	Cu03	114.93(6)	C020	C01L	C00X	120.82(16)	C029	C00R	C01M	111.62(16)	C03H	C02C	C037	106.57(18)
C018	P006	C00L	100.84(8)	C023	C01N	C00V	118.92(17)	N00C	C00S	C00P	128.92(16)	C03H	C02C	C03F	109.01(19)
C018	P006	C00Y	104.37(9)	N00E	C01O	C02X	179.6(3)	N00C	C00S	C00U	111.71(16)	C00H	C02D	C014	106.28(16)
C015	P007	Cu03	109.66(6)	C01Z	C01P	P005	113.03(14)	C00P	C00S	C00U	119.37(16)	C01E	C02D	C00H	122.08(17)
C015	P007	C01A	103.80(9)	C021	C01P	P005	110.25(14)	C00H	C00T	C00J	124.05(16)	C01E	C02D	C014	131.63(17)
C015	P007	C01X	102.92(9)	C021	C01P	C01Z	109.76(16)	C010	C00T	C00H	117.79(16)	N00D	C02E	C032	179.2(2)
C01A	P007	Cu03	120.51(6)	C01F	C01Q	C022	109.23(16)	C010	C00T	C00J	118.16(17)	C01B	C02F	C03A	111.02(16)
C01X	P007	Cu03	111.71(7)	C01F	C01Q	C02M	109.69(15)	C00Q	C00U	C00S	121.57(17)	C02K	C02F	C01B	111.74(16)
C01X	P007	C01A	106.60(9)	C01F	C01Q	C038	111.90(16)	C00Q	C00U	C01S	132.59(17)	C02K	C02F	C03A	107.68(18)
C00M	P008	Cu04	111.01(6)	C022	C01Q	C02M	109.93(17)	C00S	C00U	C01S	105.82(15)	C02V	C02F	C01B	108.15(16)
C00M	P008	C02U	100.15(9)	C022	C01Q	C038	108.44(16)	N00A	C00V	C01N	129.22(16)	C02V	C02F	C02K	108.74(16)
C02T	P008	Cu04	114.66(8)	C038	C01Q	C02M	107.63(17)	N00A	C00V	C01W	111.73(16)	C02V	C02F	C03A	109.46(19)
C02T	P008	C00M	107.38(10)	C01V	C01R	C01G	123.15(18)	C01N	C00V	C01W	119.05(17)	C027	C02H	C02A	122.83(18)
C02T	P008	C02U	106.45(11)	C017	C01S	C00U	105.80(15)	N00A	C00W	C00F	129.17(16)	C02A	C02J	C039	112.25(17)
C02U	P008	Cu04	115.93(7)	C01U	C01S	C00U	132.94(17)	N00A	C00W	C012	111.38(16)	C02Q	C02J	C02A	109.02(16)
C00I	N009	Cu01	130.37(12)	C01U	C01S	C017	121.18(17)	C00F	C00W	C012	119.43(16)	C02Q	C02J	C039	107.52(18)
C00K	N009	Cu01	124.82(12)	C01F	C01T	C012	119.70(16)	C00K	C00X	C00Z	105.68(15)	C02Q	C02J	C03C	110.27(18)
C00K	N009	C00I	104.79(14)	C02A	C01U	C01S	119.76(17)	C01L	C00X	C00K	119.86(17)	C03C	C02J	C02A	109.24(17)
C00V	N00A	Cu02	122.14(12)	C01R	C01V	C00O	118.77(17)	C01L	C00X	C00Z	134.34(17)	C03C	C02J	C039	108.53(18)
C00W	N00A	Cu02	130.21(12)	C00V	C01W	C012	105.79(15)	C026	C00Y	P006	114.76(14)	C01G	C02L	C02R	112.33(17)
C00W	N00A	C00V	105.21(14)	C01I	C01W	C00V	120.81(17)	C026	C00Y	C02G	111.29(17)	C01G	C02L	C02Z	108.86(17)
C00H	N00B	Cu01	129.01(12)	C01I	C01W	C012	133.39(17)	C02G	C00Y	P006	111.83(13)	C02Z	C02L	C02R	107.79(19)
C00O	N00B	Cu01	119.14(12)	C02Y	C01X	P007	109.77(15)	C00I	C00Z	C00X	105.47(15)	C033	C02L	C01G	109.94(17)
C00O	N00B	C00H	104.84(14)	C02Y	C01X	C034	111.43(19)	C013	C00Z	C00I	120.62(16)	C033	C02L	C02R	107.80(18)
C00S	N00C	Cu02	127.34(12)	C034	C01X	P007	116.68(16)	C013	C00Z	C00X	133.89(16)	C033	C02L	C02Z	110.08(18)
C017	N00C	Cu02	123.96(12)	C011	C01Y	C02S	112.08(16)	C00T	C010	C011	123.94(18)	C02W	C02N	C028	112.04(17)
C017	N00C	C00S	104.81(14)	C011	C01Y	C031	108.46(15)	C010	C011	C01Y	118.62(17)	C02W	C02N	C03D	107.97(18)
C02E	N00D	Cu03	159.34(17)	C02B	C01Y	C011	109.92(16)	C01E	C011	C010	117.82(17)	C03D	C02N	C028	109.07(17)
C01O	N00E	Cu04	170.09(17)	C02B	C01Y	C02S	108.09(16)	C01E	C011	C01Y	123.53(16)	C03E	C02N	C028	110.24(17)
C00N	C00F	C00L	119.16(17)	C02B	C01Y	C031	110.23(17)	C00W	C012	C01W	105.89(15)	C03E	C02N	C02W	107.84(18)
C01J	C014	C00O	121.54(17)	C02O	C02U	P008	111.04(15)	C01T	C012	C00W	121.60(17)	C03E	C02N	C03D	109.63(19)
C01J	C014	C02D	132.38(17)	C02O	C02U	C030	112.70(18)	C01T	C012	C01W	132.51(17)	C02P	C02T	P008	118.40(17)
C00P	C015	P007	111.22(13)	C030	C02U	P008	115.80(16)	C01H	C013	C00Z	120.51(16)	C03G	C02T	P008	112.00(17)
C00G	C016	C01H	124.37(17)	N036	C03B	C03I	178.4(3)	C00O	C014	C02D	106.03(16)	C03G	C02T	C02P	108.9(2)

$(CuP_{Ph}N_H)_2$ (5.2)

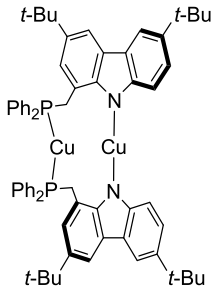

Single crystals were obtained by slow evaporation of a saturated solution in Et_2O. The structure contains severely disordered phenyl groups. Only crystal data are reported here.

Table 5.7. Crystal data for **5.2**.

Identification code	**5.2**
Temperature/K	100.03
Crystal system	monoclinic
Space group	$P2_1/n$
a/Å	20.637(2)
b/Å	23.753(3)
c/Å	27.691(4)
α/°	90
β/°	100.367(6)
γ/°	90
Volume/Å^3	13353(3)
Z	8
ρ_{calc}g/cm^3	1.100
μ/mm^{-1}	0.725
F(000)	4368.0
Crystal size/mm^3	0.343 × 0.218 × 0.184
Radiation	MoKα (λ = 0.71073)
2Θ range for data collection/°	4.25 to 61.206
Index ranges	$-29 \leq h \leq 29$, $-33 \leq k \leq 33$, $-37 \leq l \leq 37$
Reflections collected	398984
Independent reflections	38889 [R_{int} = 0.0697, R_{sigma} = 0.0526]

$(CuP_{Ph}N_H)_2$–CH_3CN (5.2–CH_3CN)

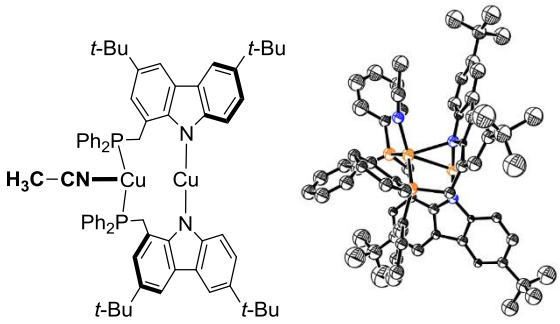

Single crystals obtained in saturated acetonitrile were of poor quality. Only crystal data are reported here.

Table 5.8. Crystal data for **5.2–CH_3CN**.

Identification code	**5.2–CH_3CN**
Temperature/K	99.95
Crystal system	triclinic
Space group	P-1
a/Å	26.607(4)
b/Å	30.104(4)
c/Å	35.544(5)
α/°	105.783(4)
β/°	97.685(4)
γ/°	104.477(4)
Volume/Å^3	25898(6)
Z	19
ρ_{calc}g/cm^3	1.316
μ/mm^{-1}	1.836
F(000)	10792.0
Radiation	CuKα (λ = 1.54178)
2Θ range for data collection/°	4.918 to 93.742
Index ranges	$-24 \leq h \leq 23$, $-27 \leq k \leq 24$, $-33 \leq l \leq 33$
Reflections collected	42113
Independent reflections	30707 [R_{int} = 0.1439, R_{sigma} = 0.2737]

$(CuP_{iPr}N_{Me})_2$–CH_3CN (5.3–CH_3CN)

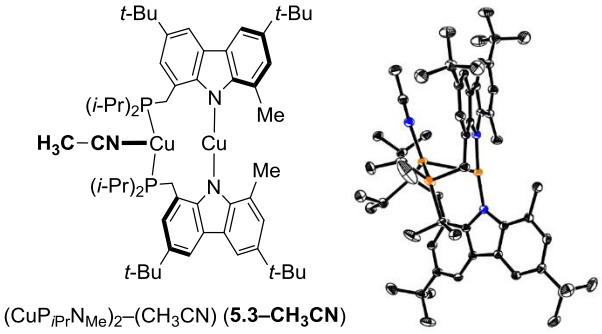

$(CuP_{iPr}N_{Me})_2$–(CH_3CN) (**5.3–CH_3CN**)

Table 5.9. Crystal data and structure refinement for **5.3–CH_3CN**.

Identification code	**5.3–CH_3CN**
Empirical formula	$C_{58}H_{84.55}Cu_2N_3P_2$
Formula weight	1012.85
Temperature/K	100.04
Crystal system	monoclinic
Space group	C2/c
a/Å	31.2892(9)
b/Å	14.6622(4)
c/Å	25.9160(7)
α/°	90
β/°	110.315(2)
γ/°	90
Volume/Å^3	11149.9(6)
Z	8
ρ_{calc}g/cm^3	1.207
μ/mm^{-1}	1.757
F(000)	4332.0
Crystal size/mm^3	0.255 × 0.117 × 0.116
Radiation	CuKα (λ = 1.54178)
2Θ range for data collection/°	6.024 to 158.534
Index ranges	-39 ≤ h ≤ 38, -18 ≤ k ≤ 18, -31 ≤ l ≤ 32
Reflections collected	105031
Independent reflections	11976 [R_{int} = 0.0701, R_{sigma} = 0.0358]
Data/restraints/parameters	11976/0/629
Goodness-of-fit on F^2	1.037
Final R indexes [I>=2σ (I)]	R_1 = 0.0470, wR_2 = 0.1038
Final R indexes [all data]	R_1 = 0.0656, wR_2 = 0.1131
Largest diff. peak/hole / e Å^{-3}	0.78/-0.79

Table 5.10. Fractional Atomic Coordinates ($\times 10^4$) and Equivalent Isotropic Displacement Parameters ($Å^2 \times 10^3$) for **5.3–CH_3CN**. U_{eq} is defined as 1/3 of the trace of the orthogonalized U_{IJ} tensor.

Atom	*x*	*y*	*z*	U(eq)	Atom	*x*	*y*	*z*	U(eq)
Cu01	6263.7(2)	6078.2(2)	6442.4(2)	18.64(9)	C015	5590.0(8)	4668.4(18)	6917.4(10)	23.5(5)
Cu02	6992.3(2)	4970.1(3)	6560.1(2)	19.24(9)	C016	7373.4(9)	5874(2)	9429.2(10)	30.4(6)
P003	6100.6(2)	5415.3(4)	7124.5(2)	18.61(13)	C017	9526.7(9)	5969(2)	8638.9(11)	35.5(7)
P004	6731.7(2)	7208.1(5)	6386.0(3)	25.97(15)	C018	5566.5(9)	1962.7(18)	4508.7(11)	28.0(6)
N005	7416.2(7)	5016.1(15)	7278.8(8)	20.4(4)	C019	5748.8(11)	6875(2)	3453.9(11)	35.3(7)
N006	5723.0(7)	6077.6(15)	5731.7(8)	22.1(4)	C01A	5798.1(9)	5843(2)	8016.3(11)	31.4(6)
N007	6626.9(7)	4883.3(14)	5816.0(8)	18.7(4)	C01B	7941.5(9)	4650(2)	6471.9(10)	29.6(6)
C008	7746.7(8)	5558.0(16)	8172.0(9)	17.1(4)	C01C	7346.4(10)	4977(2)	9721.9(11)	37.2(7)
C009	6375.1(8)	4124.3(16)	5560.8(9)	17.7(5)	C01D	5785.9(10)	7119(2)	7360.7(12)	34.1(6)
C00A	8093.5(8)	5514.8(16)	7926.6(9)	17.2(5)	C01E	6549.8(10)	7436(2)	3764.7(12)	37.0(7)
C00B	7877.8(8)	5183.4(16)	7386.7(9)	17.9(5)	C01F	5104.7(9)	6155(2)	4761.0(11)	36.9(7)
C00C	7761.7(8)	5804.2(17)	8699.8(9)	18.9(5)	C01G	9460.6(10)	6434(2)	7693.5(12)	36.1(7)
C00D	6373.0(8)	3242.8(17)	5773.1(9)	20.5(5)	C01H	7621.2(10)	7701(3)	7075.6(12)	39.7(7)
C00E	8563.3(8)	5677.7(16)	8141.6(9)	17.8(5)	C01I	6955.6(11)	6455(2)	9382.5(13)	40.7(7)
C00F	6116.4(8)	4301.9(17)	5001.7(9)	17.7(5)	C01J	5260.8(11)	2287(2)	3941.9(12)	39.3(7)
C00G	8605.3(8)	5205.0(18)	7276.4(10)	22.7(5)	C01K	5976.0(12)	8191(2)	4093.8(12)	39.4(7)
C00H	8828.1(8)	5523.5(17)	7819.7(10)	20.5(5)	C01L	7801.0(11)	6381(3)	9779.2(12)	47.3(9)
C00I	5848.0(8)	3620.0(18)	4660.8(9)	20.5(5)	C01M	7012.1(12)	7700(2)	7492.6(12)	44.6(8)
C00J	5452.7(8)	6113.5(19)	5305.8(10)	23.9(5)	C01N	9590.9(10)	4795(2)	7975.4(13)	40.7(7)
C00K	6732.6(8)	6417.1(17)	5424.1(9)	19.4(5)	C01O	5249.7(12)	1509(2)	4779.8(13)	47.1(8)
C00L	7348.0(8)	5214.1(17)	7771.4(9)	18.5(5)	C01P	5896.8(12)	1256(3)	4444.2(17)	58.3(11)
C00M	6228.5(8)	5215.9(17)	4898.8(9)	17.6(5)	C01T	7106.8(14)	7885(3)	6951.6(16)	19.3(12)
C00N	6544.1(7)	5540.1(17)	5403.2(9)	16.8(4)	C0AA	6335.4(16)	8142(3)	5907(2)	27.6(13)
C00O	8141.9(8)	5027.3(18)	7049.3(9)	21.3(5)	C01U	7251(2)	7277(5)	7100(2)	21(2)
C00P	6272.6(8)	6627.9(18)	4441.8(9)	20.3(5)	C0AB	6542(3)	8280(5)	6238(3)	20(2)
C00Q	6094.0(8)	5761.2(17)	4425.9(9)	18.8(5)	C1	6648.5(18)	8900(2)	5804.6(19)	71.3(14)
C00R	6102.9(9)	2591.6(18)	5424.7(10)	23.4(5)	C2	6008.5(13)	8433(3)	6102(2)	90.3(19)
C00S	6963.7(8)	5050.7(17)	7925.2(9)	19.6(5)	C00X	7054.4(8)	6828.6(18)	5947.8(9)	20.5(5)
C00T	6597.5(8)	6927.5(18)	4943.4(10)	21.8(5)	C00Y	6137.4(9)	7273.2(18)	3942.4(10)	25.4(5)
C00U	5835.6(8)	2755.1(18)	4867(1)	22.8(5)	C00Z	6998.5(8)	5269.9(18)	8461.2(10)	21.9(5)
C00V	7385.0(8)	5664.6(18)	8853.3(9)	21.8(5)	C010	5664.5(9)	3855.4(19)	6590.1(11)	29.5(6)
C00W	6532.6(8)	4612.0(18)	7553.9(9)	20.7(5)	C011	9345.3(8)	5675(2)	8032.4(11)	27.0(6)
C013	5161.8(8)	5198.4(19)	6585.3(11)	26.7(6)	C012	6678.6(9)	2989.5(18)	6347.5(10)	27.2(6)
C014	6025.2(9)	6241.1(18)	7630.4(10)	24.1(5)					

Table 5.11. Anisotropic Displacement Parameters ($Å^2 \times 10^3$) for **5.3–CH_3CN**. The anisotropic displacement factor exponent takes the form: $-2\pi^2[h^2a^{*2}U_{11}+2hka^*b^*U_{12}+\ldots]$.

Atom	U_{11}	U_{22}	U_{33}	U_{23}	U_{13}	U_{12}	Atom	U_{11}	U_{22}	U_{33}	U_{23}	U_{13}	U_{12}
Cu01	16.48(17)	23.48(19)	16.14(16)	-0.37(13)	5.89(13)	-3.75(14)	C00J	20.5(12)	31.5(14)	21.2(12)	-3.5(10)	9(1)	-1.9(11)
Cu02	16.72(17)	26.8(2)	12.23(16)	-1.40(13)	2.57(12)	0.60(14)	C00K	16.2(11)	25.1(13)	17.0(11)	-3.6(9)	5.8(9)	-1.0(9)
P003	14.4(3)	25.8(3)	16.0(3)	0.4(2)	5.7(2)	-3.1(2)	C00L	17.2(11)	22.5(12)	14.3(10)	0.6(9)	3.6(8)	0.1(9)
P004	25.3(3)	28.7(4)	29.3(3)	-14.7(3)	16.4(3)	-14.2(3)	C00M	15.3(10)	23.4(12)	14.8(10)	-3.1(9)	6.1(8)	-0.1(9)
N005	17.4(9)	29.4(11)	14.8(9)	-1.1(8)	6.0(7)	1.6(9)	C00N	14.6(10)	23.3(12)	13.2(10)	-1.4(9)	5.7(8)	2.1(9)
N006	18.5(10)	27.9(11)	20.3(10)	-1.9(8)	7.4(8)	-2.9(9)	C00O	21.2(11)	27.0(13)	15.7(11)	2.2(9)	6.4(9)	5.2(10)
N007	18.4(9)	21.2(10)	16.4(9)	-1.2(8)	6.0(7)	0.2(8)	C00P	20.6(11)	25.6(13)	15.9(11)	0.3(9)	8.0(9)	1.1(10)
C008	16.6(11)	18.9(12)	15.1(10)	1.3(9)	4.7(8)	0.7(9)	C00Q	16.9(11)	25.4(13)	13.1(10)	-0.3(9)	4.0(8)	2.1(9)

C009	16.9(10)	20.3(12)	15.1(10)	-3.0(9)	4.6(8)	1.1(9)	C00R	27.2(13)	19.2(12)	22.9(12)	-0.8(9)	7.5(10)	0(1)
C00A	18.0(11)	18.5(12)	15.2(10)	1.7(8)	5.8(8)	0.2(9)	C00S	16.9(11)	24.2(13)	16.1(10)	-0.6(9)	3.8(9)	-2.1(10)
C00B	18.2(11)	19.4(12)	15.2(10)	3.2(9)	4.4(9)	2.4(9)	C00T	21.9(12)	22.9(13)	21.0(12)	-1.6(9)	8.0(9)	-2.5(10)
C00C	16.1(11)	24.2(12)	15.6(10)	-2.3(9)	4.4(8)	-2.9(9)	C00U	22.2(12)	23.3(13)	20.1(12)	-4.4(10)	3.7(9)	-0.7(10)
C00D	19.4(11)	23.6(13)	16.8(11)	-0.5(9)	4.2(9)	2.3(10)	C00V	21.2(12)	28.3(13)	16.3(11)	-2.3(9)	7.2(9)	-4(1)
C00E	18.2(11)	18.7(12)	15.4(10)	2.2(9)	4.4(8)	-1.4(9)	C00W	16.7(11)	27.5(13)	16.9(11)	-0.9(9)	4.7(9)	-3.5(10)
C00F	15.7(10)	21.9(12)	15.6(10)	-0.5(9)	5.6(8)	1.8(9)	C00X	16.4(11)	25.9(13)	19.2(11)	-2.3(9)	6.0(9)	-4.6(10)
C00G	20.6(12)	28.2(14)	21.2(11)	4.1(10)	9.7(9)	6.7(10)	C00Y	32.0(14)	23.0(13)	20.8(12)	3.5(10)	8.8(10)	0.0(11)
C00H	16.6(11)	22.8(13)	20.9(11)	4.4(9)	5.1(9)	3.0(9)	C00Z	17.4(11)	30.3(14)	18.8(11)	-0.4(10)	7.2(9)	-4(1)
C00I	16.8(11)	28.8(13)	14.3(10)	-1.6(9)	3.4(9)	1.4(10)	C010	21.0(12)	28.9(14)	31.6(14)	-1.3(11)	0.4(10)	-4.1(11)
C01G	29.3(14)	46.9(19)	35.4(15)	5.5(13)	15.5(12)	-7.4(13)	C011	17.4(12)	37.5(15)	26.2(13)	3.6(11)	7.7(10)	0.1(11)
C01H	30.3(15)	59(2)	24.5(14)	-7.6(13)	3.3(11)	4.4(14)	C012	34.3(14)	23.7(13)	18.2(12)	0.9(10)	2.1(10)	3.3(11)
C01I	40.4(17)	50(2)	38.0(16)	-16.0(14)	22.0(14)	-4.5(15)	C013	16.7(11)	35.9(15)	27.0(13)	-1.7(11)	6.7(10)	-3.3(11)
C01J	42.6(17)	31.7(16)	31.4(15)	-6.7(12)	-2.4(13)	-11.2(14)	C014	22.8(12)	29.3(14)	21.6(12)	-1.9(10)	9.4(10)	-1.2(10)
C01K	52.2(19)	31.6(16)	31.0(15)	5.0(12)	10.3(13)	12.2(14)	C015	17.9(11)	30.8(14)	20.8(11)	2.5(10)	5.7(9)	-3.3(10)
C01L	38.4(17)	80(3)	29.2(15)	-27.2(16)	18.7(13)	-29.3(17)	C016	25.9(13)	48.1(18)	19.7(12)	-11.9(11)	11(1)	-11.0(12)
C01M	59(2)	52(2)	33.2(16)	-22.0(14)	28.6(15)	-27.5(17)	C017	17.2(12)	58(2)	29.1(14)	0.3(13)	5.4(10)	-5.9(13)
C01N	22.0(13)	54(2)	44.4(17)	5.9(15)	8.9(12)	11.3(14)	C018	29.9(13)	22.0(13)	27.1(13)	-3.4(10)	3.9(11)	-3.2(11)
C01O	50(2)	43(2)	38.5(17)	0.9(14)	3.3(14)	-21.1(16)	C019	43.7(17)	33.3(16)	22.0(13)	8.0(11)	2.8(12)	-3.8(13)
C01P	41.6(19)	46(2)	71(2)	-32.8(19)	-0.6(17)	3.0(16)	C01A	27.6(13)	44.2(17)	26.9(13)	-1.5(12)	15.0(11)	-2.6(12)
C01T	20(2)	17(3)	17(2)	-0.4(16)	2.7(16)	-1.1(17)	C01B	24.9(13)	45.9(17)	18.3(12)	-2.7(11)	7.9(10)	5.6(12)
C0AA	35(3)	20(2)	26(3)	-0.2(16)	8(2)	-5.6(17)	C01C	33.4(15)	60(2)	19.1(12)	1.2(13)	9.6(11)	-7.8(15)
C01U	15(3)	28(4)	20(3)	-3(3)	4(2)	-4(3)	C01D	35.3(15)	33.9(16)	33.0(15)	-1.9(12)	11.6(12)	3.0(13)
C0AB	21(4)	25(4)	11(4)	-2(3)	1(4)	-3(3)	C01E	39.3(16)	43.9(18)	32.3(15)	8.9(13)	18.1(13)	-0.7(14)
C1	140(4)	23.6(17)	87(3)	-10.5(18)	86(3)	-21(2)	C01F	26.0(14)	59(2)	21.7(13)	-3.5(13)	3.7(11)	2.0(14)
C2	33(2)	64(3)	148(5)	62(3)	0(2)	-2(2)							

Table 5.12. Bond Lengths for **5.3–CH$_3$CN**.

Atom	Atom	Length/Å	Atom	Atom	Length/Å
Cu01	Cu02	2.7289(5)	C00K	C00T	1.387(3)
Cu01	P003	2.2265(7)	C00K	C00X	1.507(3)
Cu01	P004	2.2493(7)	C00L	C00S	1.412(3)
Cu01	N006	2.023(2)	C00M	C00N	1.419(3)
Cu02	N005	1.8755(19)	C00M	C00Q	1.400(3)
Cu02	N007	1.8739(19)	C00O	C01B	1.512(3)
P003	C00W	1.846(3)	C00P	C00Q	1.383(4)
P003	C014	1.859(3)	C00P	C00T	1.414(3)
P003	C015	1.856(3)	C00P	C00Y	1.539(3)
P004	C00X	1.848(2)	C00R	C00U	1.417(3)
P004	C01T	1.821(4)	C00S	C00W	1.503(3)
P004	C0AA	1.971(5)	C00S	C00Z	1.393(3)
P004	C01U	1.997(6)	C00U	C018	1.542(3)
P004	C0AB	1.676(8)	C00V	C00Z	1.406(3)
N005	C00B	1.394(3)	C00V	C016	1.537(3)
N005	C00L	1.396(3)	C00Y	C019	1.534(4)
N006	C00J	1.135(3)	C00Y	C01E	1.532(4)
N007	C009	1.391(3)	C00Y	C01K	1.536(4)
N007	C00N	1.395(3)	C010	C015	1.527(4)
C008	C00A	1.437(3)	C011	C017	1.536(4)
C008	C00C	1.400(3)	C011	C01G	1.536(4)
C008	C00L	1.410(3)	C011	C01N	1.536(4)
C009	C00D	1.406(3)	C013	C015	1.529(3)
C009	C00F	1.417(3)	C014	C01A	1.530(3)
C00A	C00B	1.412(3)	C014	C01D	1.531(4)
C00A	C00E	1.400(3)	C016	C01C	1.535(4)
C00B	C00O	1.415(3)	C016	C01I	1.529(4)
C00C	C00V	1.384(3)	C016	C01L	1.524(4)
C00D	C00R	1.382(3)	C018	C01J	1.524(4)
C00D	C012	1.510(3)	C018	C01O	1.550(4)
C00E	C00H	1.383(3)	C018	C01P	1.513(4)
C00F	C00I	1.404(3)	C01H	C01T	1.552(5)
C00F	C00M	1.433(3)	C01H	C01U	1.335(7)
C00G	C00H	1.416(3)	C01M	C01T	1.554(5)
C00G	C00O	1.387(3)	C01M	C01U	1.584(7)

C00H	C011	1.534(3)	C0AA	C1	1.564(5)
C00I	C00U	1.382(4)	C0AA	C2	1.357(7)
C00J	C01F	1.454(3)	C0AB	C1	1.568(8)
C00K	C00N	1.408(3)	C0AB	C2	1.598(9)

Table 5.13. Bond Angles for **5.3–CH_3CN**.

Atom	Atom	Atom	Angle/°	Atom	Atom	Atom	Angle/°
P003	Cu01	Cu02	93.69(2)	N007	C00N	C00K	129.6(2)
P003	Cu01	P004	134.99(3)	N007	C00N	C00M	111.1(2)
P004	Cu01	Cu02	84.74(2)	C00K	C00N	C00M	119.3(2)
N006	Cu01	Cu02	120.25(6)	C00B	C00O	C01B	122.7(2)
N006	Cu01	P003	111.90(6)	C00G	C00O	C00B	117.2(2)
N006	Cu01	P004	107.38(6)	C00G	C00O	C01B	120.1(2)
N005	Cu02	Cu01	111.40(6)	C00Q	C00P	C00T	117.8(2)
N007	Cu02	Cu01	74.80(6)	C00Q	C00P	C00Y	123.3(2)
N007	Cu02	N005	173.18(9)	C00T	C00P	C00Y	118.8(2)
C00W	P003	Cu01	115.81(8)	C00P	C00Q	C00M	120.2(2)
C00W	P003	C014	103.66(11)	C00D	C00R	C00U	124.1(2)
C00W	P003	C015	100.05(12)	C00L	C00S	C00W	123.7(2)
C014	P003	Cu01	113.32(9)	C00Z	C00S	C00L	117.6(2)
C015	P003	Cu01	116.08(8)	C00Z	C00S	C00W	118.7(2)
C015	P003	C014	106.33(11)	C00K	C00T	C00P	123.8(2)
C00X	P004	Cu01	108.97(8)	C00I	C00U	C00R	117.6(2)
C00X	P004	C0AA	100.40(15)	C00I	C00U	C018	122.8(2)
C00X	P004	C01U	98.18(19)	C00R	C00U	C018	119.5(2)
C01T	P004	Cu01	126.96(13)	C00C	C00V	C00Z	117.2(2)
C01T	P004	C00X	108.78(15)	C00C	C00V	C016	124.0(2)
C0AA	P004	Cu01	105.74(13)	C00Z	C00V	C016	118.7(2)
C0AA	P004	C01U	132.8(3)	C00S	C00W	P003	114.80(18)
C01U	P004	Cu01	108.43(19)	C00K	C00X	P004	109.71(16)
C0AB	P004	Cu01	121.2(3)	C019	C00Y	C00P	111.6(2)
C0AB	P004	C00X	111.5(3)	C019	C00Y	C01K	107.9(2)
C00B	N005	Cu02	122.10(15)	C01E	C00Y	C00P	109.5(2)
C00B	N005	C00L	104.88(18)	C01E	C00Y	C019	108.7(2)
C00L	N005	Cu02	129.48(16)	C01E	C00Y	C01K	109.0(2)
C00J	N006	Cu01	172.3(2)	C01K	C00Y	C00P	110.0(2)
C009	N007	Cu02	125.88(16)	C00S	C00Z	C00V	124.5(2)
C009	N007	C00N	105.30(18)	C00H	C011	C017	112.2(2)
C00N	N007	Cu02	128.82(16)	C00H	C011	C01G	109.1(2)
C00C	C008	C00A	132.0(2)	C00H	C011	C01N	110.1(2)
C00C	C008	C00L	122.2(2)	C01G	C011	C017	107.8(2)
C00L	C008	C00A	105.6(2)	C01N	C011	C017	108.4(2)
N007	C009	C00D	128.9(2)	C01N	C011	C01G	109.2(2)
N007	C009	C00F	111.5(2)	C01A	C014	P003	114.45(19)
C00D	C009	C00F	119.4(2)	C01A	C014	C01D	110.8(2)
C00B	C00A	C008	106.2(2)	C01D	C014	P003	112.80(18)
C00E	C00A	C008	131.8(2)	C010	C015	P003	109.83(17)
C00E	C00A	C00B	121.9(2)	C010	C015	C013	110.9(2)
N005	C00B	C00A	111.4(2)	C013	C015	P003	111.15(18)
N005	C00B	C00O	129.4(2)	C01C	C016	C00V	109.4(2)
C00A	C00B	C00O	119.2(2)	C01I	C016	C00V	110.0(2)
C00V	C00C	C008	120.0(2)	C01I	C016	C01C	108.9(2)
C009	C00D	C012	121.6(2)	C01L	C016	C00V	111.3(2)
C00R	C00D	C009	117.7(2)	C01L	C016	C01C	108.1(3)
C00R	C00D	C012	120.6(2)	C01L	C016	C01I	109.0(3)
C00H	C00E	C00A	119.9(2)	C00U	C018	C01O	110.6(2)
C009	C00F	C00M	105.8(2)	C01J	C018	C00U	112.0(2)
C00I	C00F	C009	121.1(2)	C01J	C018	C01O	106.5(2)
C00I	C00F	C00M	132.9(2)	C01P	C018	C00U	109.3(2)
C00O	C00G	C00H	124.4(2)	C01P	C018	C01J	109.3(3)
C00E	C00H	C00G	117.5(2)	C01P	C018	C01O	109.0(3)

C00E	C00H	C011	122.5(2)	C01H	C01T	P004	113.8(3)
C00G	C00H	C011	119.9(2)	C01H	C01T	C01M	107.0(3)
C00U	C00I	C00F	120.1(2)	C01M	C01T	P004	111.1(3)
N006	C00J	C01F	179.6(3)	C1	C0AA	P004	107.9(3)
C00N	C00K	C00X	122.7(2)	C2	C0AA	P004	112.0(3)
C00T	C00K	C00N	117.7(2)	C2	C0AA	C1	115.9(4)
C00T	C00K	C00X	119.5(2)	C01H	C01U	P004	114.9(4)
N005	C00L	C008	111.7(2)	C01H	C01U	C01M	117.3(5)
N005	C00L	C00S	129.7(2)	C01M	C01U	P004	101.6(3)
C008	C00L	C00S	118.4(2)	C1	C0AB	P004	124.2(5)
C00N	C00M	C00F	106.2(2)	C1	C0AB	C2	103.0(5)
C00Q	C00M	C00F	132.7(2)	C2	C0AB	P004	116.3(5)
C00Q	C00M	C00N	121.1(2)				

$(CuP_{iPr}N_{FPh})_2$–CH_3CN (5.4–CH_3CN)

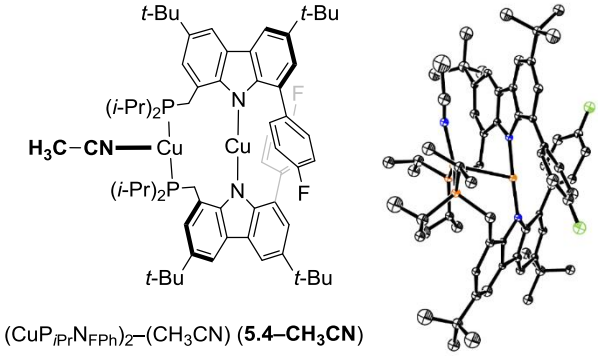

$(CuP_{iPr}N_{FPh})_2$–(CH_3CN) (**5.4–CH_3CN**)

Full data collection was not pursued, and only crystal data are shown below.

Table 5.14. Crystal data for **5.4–CH_3CN**.

Identification code	**5.4–CH_3CN**
Empirical formula	$C_{36}CuFN_{2.5}P$
Formula weight	580.90
Temperature/K	99.98
Crystal system	monoclinic
Space group	$P2_1/c$
a/Å	28.722(2)
b/Å	11.7917(9)
c/Å	22.037(3)
α/°	90
β/°	104.441(5)
γ/°	90
Volume/Å^3	7227.7(12)
Z	8
ρ_{calc}g/cm^3	1.068
μ/mm^{-1}	0.676
F(000)	2292.0

Radiation	MoKα (λ = 0.71073)
2Θ range for data collection/°	4.622 to 50.086
Index ranges	-32 ≤ h ≤ 31, -12 ≤ k ≤ 11, -21 ≤ l ≤ 4
Reflections collected	4985
Independent reflections	4426 [R_{int} = 0.0753, R_{sigma} = 0.1164]

$(CuP_{iPr}N_{tBuPh})_2$ (5.5)

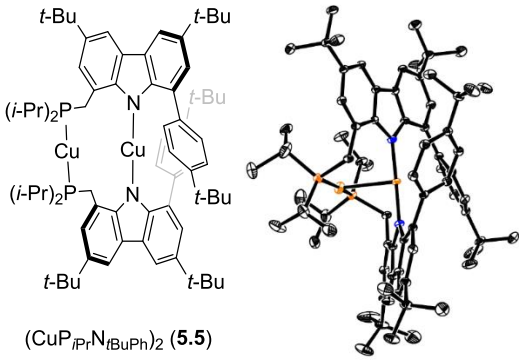

Table 5.15. Crystal data and structure refinement for **5.5**.

Identification code	**5.5**
Empirical formula	$C_{38}H_{47}CuN_{1.5}P$
Formula weight	619.28
Temperature/K	100.01
Crystal system	triclinic
Space group	P-1
a/Å	12.0966(11)
b/Å	17.2552(16)
c/Å	17.7721(16)
α/°	88.239(3)
β/°	76.009(3)
γ/°	75.363(3)
Volume/Å^3	3480.9(6)
Z	4
ρ_{calc}g/cm^3	1.182
μ/mm^{-1}	0.699
F(000)	1318.0
Crystal size/mm^3	0.342 × 0.221 × 0.183
Radiation	MoKα (λ = 0.71073)
2Θ range for data collection/°	4.75 to 55.018
Index ranges	-15 ≤ h ≤ 15, -22 ≤ k ≤ 22, -23 ≤ l ≤ 23
Reflections collected	212201
Independent reflections	15993 [R_{int} = 0.0420, R_{sigma} = 0.0163]
Data/restraints/parameters	15993/0/802
Goodness-of-fit on F^2	1.029
Final R indexes [I>=2σ (I)]	R_1 = 0.0376, wR_2 = 0.0953

Final R indexes [all data]	R_1 = 0.0438, wR_2 = 0.0992
Largest diff. peak/hole / e Å^{-3}	2.22/-0.83

Table 5.16. Fractional Atomic Coordinates (×10^4) and Equivalent Isotropic Displacement Parameters (Å^2×10^3) for **5.5**. U_{eq} is defined as 1/3 of the trace of the orthogonalized U_{IJ} tensor.

Atom	*x*	*y*	*z*	U(eq)	Atom	*x*	*y*	*z*	U(eq)
Cu01	4781.4(2)	7495.8(2)	7416.1(2)	12.07(5)	C01D	2283.2(16)	8814.7(12)	9165.2(11)	22.2(4)
Cu02	3149.5(2)	8730.8(2)	7218.7(2)	20.72(6)	C01E	-184.1(17)	5224.2(12)	7043.1(11)	21.4(4)
P003	2902.1(4)	8338.1(3)	6128.0(3)	16.40(9)	C01F	7952.2(16)	7849.6(12)	9137.2(12)	21.4(4)
P004	3086.9(4)	9275.2(3)	8328.3(3)	15.43(9)	C01G	2548.6(19)	10374.7(12)	8409.6(13)	27.2(4)
N005	3637.7(12)	6934.8(9)	7807.3(8)	13.2(3)	C01H	-269.8(17)	6346.9(12)	6133.3(12)	24.1(4)
N006	5925.6(12)	8040.4(8)	6972.6(8)	13.0(3)	C01I	5800(2)	3885.5(13)	7482.6(13)	31.9(5)
C007	2920.6(14)	6699.1(10)	7395.2(10)	12.5(3)	C01J	7097.2(19)	10958.5(12)	7560.7(12)	24.8(4)
C008	6718.5(14)	7838.2(10)	6249.9(10)	12.8(3)	C01K	2445(2)	5283.2(16)	11137.9(13)	34.8(5)
C009	3293.4(14)	6680.1(10)	8562.3(10)	13.2(3)	C01L	1309.1(18)	5075.3(13)	5788.6(12)	25.4(4)
C00A	3731.3(15)	6732.4(10)	9228.4(10)	14.6(3)	C01M	8418(2)	7427.2(14)	3359.5(11)	29.5(4)
C00B	6604.4(14)	6403.5(10)	6022.5(10)	12.7(3)	C01N	2086(2)	9235.2(15)	9951.8(12)	32.6(5)
C00C	6996.7(14)	7139.5(10)	5773.5(10)	12.9(3)	C01O	513.8(19)	5576.4(15)	10799.5(12)	30.3(5)
C00D	2128.4(14)	6308.8(10)	7880.5(10)	13.1(3)	C01P	9370(2)	8456.3(13)	3660.7(12)	28.9(4)
C00E	5836.6(15)	5297.6(11)	5768.5(10)	16.8(3)	C01Q	6125(2)	3544.3(12)	6087.1(14)	33.2(5)
C00F	5505.7(14)	9248.1(10)	7874.5(10)	14.0(3)	C01S	3105(2)	10736.4(13)	7655.5(15)	35.3(5)
C00G	4794.2(15)	7015.2(10)	9222.2(10)	14.8(3)	C01T	10197.9(18)	7022.1(13)	3901.8(12)	30.5(5)
C00H	6049.0(14)	8778.7(10)	7186.3(10)	13.3(3)	C01U	1153.9(19)	8652.5(16)	9035.5(15)	36.4(5)
C00I	6809.5(15)	7033.5(11)	8612.1(11)	17.4(3)	C01V	4185.6(19)	4398.0(13)	6809.6(15)	33.0(5)
C00J	5861.5(15)	9939.3(11)	7964.3(10)	16.4(3)	C01W	8903.7(19)	7149.4(15)	9325.6(16)	37.7(5)
C00K	6737.0(15)	6061.2(10)	6723.7(10)	14.9(3)	C01X	1345(2)	8445.1(14)	6097.9(18)	42.1(6)
C00L	6837.6(15)	7559.8(11)	9184.5(11)	16.9(3)	C01Y	7348(3)	11427.2(15)	6836.2(14)	42.8(6)
C00M	2898.1(14)	6777.1(10)	6603.0(9)	12.9(3)	C01Z	1205(2)	10651.1(16)	8558.0(17)	43.7(6)
C00N	1356.1(14)	5977(1)	7596.9(10)	13.8(3)	C020	8417(2)	8115.6(17)	8319.9(15)	40.2(6)
C00O	6164.0(15)	5998.2(10)	5539.2(10)	15.4(3)	C021	1105(3)	6660.5(17)	11366.0(14)	43.9(6)
C00P	5940.3(15)	4960.4(10)	6481.8(10)	14.8(3)	C022	7727(2)	8539.0(18)	9710(2)	55.1(9)
C00Q	2344.3(14)	6317.3(10)	8637.6(10)	13.8(3)	C023	8276(3)	10675.8(17)	7817.5(17)	47.7(7)
C00R	6892.8(15)	9048.3(10)	6609.1(10)	15.8(3)	C025	3017(3)	3300.0(18)	8688.0(18)	54.8(8)
C00S	1778.6(15)	6063(1)	9349.9(10)	15.4(3)	N026	2947(4)	2767(2)	8369(2)	85.1(10)
C00T	6416.6(15)	5351.2(10)	6949.4(10)	15.5(3)	C027	6214(3)	11502.0(17)	8204(2)	64.2(10)
C00U	2140.7(15)	6421.9(10)	6343.2(10)	13.9(3)	C028	3121(3)	3964.8(19)	9115(2)	69.6(11)
C00V	3579.1(15)	7250.4(10)	6030.5(10)	14.0(3)	C1	3576(2)	8754.0(13)	5211.9(13)	30.0(4)
C00W	8055.5(16)	8410.2(11)	5250.8(10)	17.6(3)	C2	4876(2)	8416(2)	4951(2)	70.2(11)
C00X	7296.6(15)	8450.5(10)	5991(1)	15.2(3)	C3A	2985(6)	9636(3)	5240(3)	43.2(10)
C00Y	5814.0(15)	6764.1(10)	8630.4(10)	15.6(3)	C3B	3636(6)	9657(3)	5344(4)	43.2(10)
C00Z	561.2(15)	5670.1(10)	6454.9(10)	15.2(3)	C0AA	1079(4)	8250(3)	5416(3)	30.0(11)
C010	4568.9(14)	9035.3(11)	8513.1(10)	14.6(3)	C1AA	576(3)	8395(3)	6756(3)	29.9(12)
C011	3133.3(15)	6478.2(11)	9926.6(10)	17.0(3)	C0AB	892(5)	9305(3)	5661(3)	37.8(13)
C012	5834.3(16)	7779.8(11)	9793.6(11)	18.9(4)	C1AB	488(4)	9175(3)	6607(3)	33.3(12)
C013	7739.3(15)	7130.6(10)	5040.4(10)	14.7(3)	C018	8263.4(15)	7757.8(11)	4755.8(10)	16.3(3)
C014	4831.0(16)	7516.6(11)	9812.3(10)	18.1(3)	C019	5519.6(16)	4203.9(11)	6720.8(11)	17.9(3)
C015	1363.7(14)	6017.9(10)	6818.2(10)	13.5(3)	C01A	9058.9(17)	7668.4(11)	3929.4(11)	20.8(4)
C016	2150.1(15)	6156.6(11)	10011.6(10)	16.8(3)	C01B	1554.8(17)	5921.4(13)	10818.7(11)	22.4(4)
C017	7208.7(16)	9754.9(11)	6717.0(11)	19.7(4)	C01C	6703.3(16)	10212.1(11)	7401.8(11)	18.3(3)

Table 5.17. Anisotropic Displacement Parameters ($Å^2 \times 10^3$) for **5.5**. The anisotropic displacement factor exponent takes the form: $-2\pi^2[h^2a^{*2}U_{11}+2hka^*b^*U_{12}+\ldots]$.

Atom	U_{11}	U_{22}	U_{33}	U_{23}	U_{13}	U_{12}	Atom	U_{11}	U_{22}	U_{33}	U_{23}	U_{13}	U_{12}
Cu01	11.2(1)	14.62(10)	11.74(10)	0.27(7)	-1.27(7)	-7.12(7)	C01D	15.8(8)	27.8(10)	22.5(9)	-3.0(8)	1.8(7)	-10.4(7)
Cu02	22.05(12)	21.06(12)	19.48(12)	-6.91(9)	-7.36(9)	-3.07(9)	C01E	22.4(9)	27.2(10)	21.3(9)	4.4(7)	-8.1(7)	-15.9(8)
P003	19.2(2)	15.4(2)	15.4(2)	-0.95(16)	-4.63(17)	-5.22(17)	C01F	15.5(8)	23.1(9)	29(1)	-2.8(8)	-7.6(7)	-8.3(7)
P004	13.1(2)	17.2(2)	15.5(2)	-5.06(16)	-1.59(16)	-4.23(16)	C01G	31.6(11)	18.2(9)	31.8(11)	-8.0(8)	-13.7(9)	0.2(8)
N005	13.9(6)	17.2(7)	10.4(6)	0.7(5)	-3.4(5)	-7.3(5)	C01H	20.3(9)	28.4(10)	28.8(10)	7.9(8)	-12.6(8)	-9.9(8)
N006	11.9(6)	15.3(7)	12.2(7)	-1.8(5)	-1.2(5)	-5.7(5)	C01I	48.8(13)	29.2(11)	28.5(11)	12.9(9)	-16.1(10)	-24.2(10)
C007	11.8(7)	13.4(7)	13.4(8)	-0.8(6)	-2.7(6)	-5.3(6)	C01J	32.4(10)	19.5(9)	22.4(9)	-6.0(7)	4.1(8)	-16.1(8)
C008	10.6(7)	15.2(8)	12.5(8)	0.5(6)	-2.0(6)	-3.8(6)	C01K	33.2(11)	54.8(15)	27.0(11)	23.6(10)	-15.8(9)	-24.7(11)
C009	12.4(7)	15.0(8)	12.5(8)	0.8(6)	-1.4(6)	-5.5(6)	C01L	23.9(9)	28.7(10)	25.8(10)	-10.7(8)	-2.9(8)	-12.0(8)
C00A	14.5(8)	17.6(8)	13.4(8)	0.2(6)	-3.4(6)	-6.9(6)	C01M	39.5(12)	33.5(11)	15.2(9)	1.2(8)	-0.6(8)	-14.3(9)
C00B	9.8(7)	13.2(7)	13.8(8)	-2.2(6)	0.0(6)	-2.9(6)	C01N	29.1(11)	44.9(13)	20.6(10)	-6.0(9)	5.2(8)	-13.3(10)
C00C	12.6(7)	14.1(8)	12.8(8)	0.8(6)	-3.5(6)	-4.3(6)	C01O	27.6(10)	52.8(14)	18.2(9)	14.9(9)	-6.9(8)	-24(1)
C00D	12.5(7)	14.9(8)	12.3(8)	0.8(6)	-2.1(6)	-5.2(6)	C01P	36.5(11)	26.6(10)	19.3(9)	2.2(8)	7.1(8)	-13.7(9)
C00E	19.0(8)	18.9(8)	15.7(8)	-1.2(6)	-6.7(6)	-7.9(7)	C01Q	47.4(13)	16.9(9)	33.4(12)	-3.8(8)	-3.8(10)	-9.8(9)
C00F	12.7(7)	16.3(8)	13.1(8)	-0.1(6)	-1.8(6)	-5.2(6)	C01S	36.7(12)	24.4(10)	50.7(14)	9.9(10)	-22.2(11)	-8.3(9)
C00G	15.8(8)	18.7(8)	12.7(8)	3.2(6)	-5.8(6)	-7.8(6)	C01T	24.8(10)	31.3(11)	24.7(10)	-0.5(8)	7.5(8)	-0.9(8)
C00H	12.2(7)	13.7(8)	15.3(8)	0.7(6)	-2.8(6)	-5.9(6)	C01U	20.7(10)	50.3(14)	41.3(13)	-1.8(11)	-1.9(9)	-19.7(10)
C00I	12.7(8)	20.7(9)	18.7(8)	-2.2(7)	-2.9(6)	-4.5(6)	C01V	23.7(10)	27.0(11)	51.5(14)	10.3(10)	-8.8(9)	-13.9(8)
C00J	16.2(8)	17.3(8)	15.2(8)	-3.7(6)	-1.4(6)	-5.2(6)	C01W	22(1)	42.2(13)	55.9(15)	12.4(11)	-19(1)	-12.7(9)
C00K	15.3(8)	16.8(8)	13.7(8)	-1.6(6)	-3.3(6)	-6.1(6)	C01X	27.3(11)	26.0(11)	77.5(19)	-17.3(12)	-27.9(12)	2.2(9)
C00L	14.7(8)	18.1(8)	20.6(9)	1.2(7)	-7.6(7)	-6.2(6)	C01Y	79.7(19)	31.8(12)	28.7(12)	4.1(9)	-12.2(12)	-36.9(13)
C00M	12.5(7)	13.8(7)	11.9(7)	0.0(6)	-0.7(6)	-4.7(6)	C01Z	31.5(12)	36.1(13)	51.1(15)	-7.7(11)	-6.6(11)	11.4(10)
C00N	12.2(7)	15.2(8)	15.2(8)	1.2(6)	-2.3(6)	-6.4(6)	C020	36.6(13)	58.0(16)	41.2(13)	16.5(12)	-16.6(10)	-34.2(12)
C00O	17.2(8)	16.7(8)	12.9(8)	0.1(6)	-4.5(6)	-4.6(6)	C021	52.3(15)	52.1(15)	22.2(11)	-7.3(10)	12.6(10)	-23.8(13)
C00P	14.0(8)	14.2(8)	16.1(8)	-1.0(6)	-2.1(6)	-4.7(6)	C022	28.4(12)	54.9(17)	83(2)	-39.9(16)	3.0(13)	-23.2(12)
C00Q	13.2(7)	16.2(8)	13.0(8)	0.8(6)	-3.4(6)	-5.4(6)	C023	63.7(18)	46.0(15)	52.2(16)	4.8(12)	-28.5(14)	-34.2(14)
C00R	15.1(8)	15.3(8)	16.1(8)	-1.0(6)	0.4(6)	-6.1(6)	C025	59.5(18)	41.9(16)	48.6(17)	6.5(13)	4.1(14)	-4.1(13)
C00S	13.8(8)	18.8(8)	15.3(8)	2.6(6)	-3.0(6)	-7.8(6)	N026	122(3)	66(2)	68(2)	-5.7(17)	-24(2)	-23(2)
C00T	17.8(8)	17.5(8)	12.4(8)	1.2(6)	-4.1(6)	-6.1(6)	C027	69(2)	37.2(14)	73(2)	-32.1(14)	34.4(16)	-34.8(14)
C00U	14.6(8)	15.8(8)	11.9(7)	-0.6(6)	-3.1(6)	-5.1(6)	C028	79(2)	40.4(16)	68(2)	-6.5(15)	28.1(18)	-17.7(16)
C00V	14.7(8)	15.8(8)	11.9(7)	0.4(6)	-0.9(6)	-6.9(6)	C1	36.6(12)	26(1)	25.9(10)	6.4(8)	-9.0(9)	-4.8(9)
C00W	17.9(8)	16.1(8)	17.6(8)	1.1(7)	1.8(7)	-8.3(7)	C2	35.0(14)	82(2)	92(3)	64(2)	-12.4(15)	-22.8(15)
C00X	14.2(8)	14.5(8)	16.3(8)	-1.0(6)	-0.5(6)	-5.4(6)	C3A	53(3)	25.0(14)	45(2)	10.1(14)	3(2)	-14(2)
C00Y	16.5(8)	17.0(8)	15.1(8)	-0.6(6)	-5.6(6)	-6.0(6)	C3B	53(3)	25.0(14)	45(2)	10.1(14)	3(2)	-14(2)
C00Z	14.5(8)	18.4(8)	15.2(8)	-0.2(6)	-4.6(6)	-7.8(6)	C0AA	29(2)	35(2)	33(2)	4.0(18)	-19.0(18)	-11.5(17)
C010	13.9(8)	18.9(8)	12.1(8)	-1.2(6)	-1.6(6)	-7.2(6)	C1AA	13.2(19)	26(2)	47(3)	-4.8(19)	-2.2(17)	-2.6(15)
C011	18.0(8)	23.0(9)	12.5(8)	2.0(7)	-5.1(6)	-8.3(7)	C0AB	41(3)	31(3)	40(3)	8(2)	-19(2)	2(2)
C012	20.0(9)	23.1(9)	16.4(8)	-2.9(7)	-7.3(7)	-7.4(7)	C1AB	20(2)	34(2)	40(3)	-0.8(19)	-5.4(17)	2.1(16)
C013	15.7(8)	14.5(8)	13.2(8)	-0.8(6)	-2.2(6)	-3.5(6)	C018	16.6(8)	17.0(8)	13.5(8)	1.6(6)	0.4(6)	-5.2(6)
C014	16.4(8)	25.1(9)	13.7(8)	-1.3(7)	-2.9(6)	-7.6(7)	C019	21.1(9)	15.0(8)	20.0(9)	1.6(7)	-5.3(7)	-8.6(7)
C015	11.4(7)	13.9(8)	16.3(8)	-1.0(6)	-3.3(6)	-5.0(6)	C01A	23.7(9)	19.1(9)	15.3(8)	0.7(7)	4.7(7)	-6.6(7)
C016	16.3(8)	21.1(9)	13.6(8)	2.7(6)	-2.3(6)	-7.3(7)	C01B	24.2(9)	34.8(11)	12.9(8)	5.8(7)	-4.1(7)	-16.8(8)
C017	20.1(9)	17.7(8)	20.1(9)	-1.5(7)	3.8(7)	-10.7(7)	C01C	19.3(8)	15.0(8)	20.5(9)	-2.7(7)	-0.2(7)	-8.5(7)

Table 5.18. Bond Lengths for **5.5**.

Atom	Atom	Length/Å		Atom	Atom	Length/Å	Atom	Atom	Length/Å		Atom	Atom	Length/Å
Cu01	Cu02	2.5930(4)		C00P	C019	1.530(2)	C00B	C00K	1.390(2)		C01B	C01K	1.534(3)
Cu01	N005	1.8723(14)		C00Q	C00S	1.401(2)	C00B	C00O	1.399(2)		C01B	C01O	1.530(3)
Cu01	N006	1.8719(14)		C00R	C00X	1.437(2)	C00C	C013	1.390(2)		C01B	C021	1.529(3)
Cu02	P003	2.1840(5)		C00R	C017	1.398(2)	C00D	C00N	1.404(2)		C01C	C01J	1.537(2)
Cu02	P004	2.1869(5)		C00S	C016	1.384(2)	C00D	C00Q	1.433(2)		C01D	C01N	1.533(3)
P003	C00V	1.8432(18)		C00U	C015	1.412(2)	C00E	C00O	1.385(2)		C01D	C01U	1.532(3)
P003	C01X	1.860(2)		C00W	C00X	1.403(2)	C00E	C00P	1.399(2)		C01F	C01W	1.535(3)
P003	C1	1.847(2)		C00W	C018	1.384(2)	C00F	C00H	1.410(2)		C01F	C020	1.527(3)
P004	C010	1.8424(17)		C00Z	C015	1.530(2)	C00F	C00J	1.392(2)		C01F	C022	1.517(3)
P004	C01D	1.8459(19)		C00Z	C01E	1.531(2)	C00F	C010	1.507(2)		C01G	C01S	1.537(3)
P004	C01G	1.842(2)		C00Z	C01H	1.531(3)	C00G	C00Y	1.395(2)		C01G	C01Z	1.532(3)

N005	C007	1.399(2)	C00Z	C01L	1.537(3)	C00G	C014	1.396(2)		C01J	C01Y	1.508(3)
N005	C009	1.397(2)	C011	C016	1.410(2)	C00H	C00R	1.419(2)		C01J	C023	1.559(4)
N006	C008	1.398(2)	C012	C014	1.392(2)	C00I	C00L	1.396(2)		C01J	C027	1.515(3)
N006	C00H	1.394(2)	C013	C018	1.410(2)	C00I	C00Y	1.389(2)		C01X	C0AA	1.398(5)
C007	C00D	1.417(2)	C016	C01B	1.534(2)	C00J	C01C	1.407(2)		C01X	C1AA	1.323(5)
C007	C00M	1.416(2)	C017	C01C	1.390(2)	C00K	C00T	1.395(2)		C01X	C0AB	1.682(5)
C008	C00C	1.415(2)	C018	C01A	1.537(2)	C00L	C012	1.395(3)		C01X	C1AB	1.560(5)
C008	C00X	1.416(2)	C019	C01I	1.527(3)	C00L	C01F	1.536(2)		C025	N026	1.126(4)
C009	C00A	1.423(2)	C019	C01Q	1.536(3)	C00M	C00U	1.391(2)		C025	C028	1.442(5)
C009	C00Q	1.418(2)	C019	C01V	1.532(3)	C00M	C00V	1.505(2)		C1	C2	1.493(4)
C00A	C00G	1.484(2)	C01A	C01M	1.539(3)	C00N	C015	1.381(2)		C1	C3A	1.506(5)
C00A	C011	1.396(2)	C01A	C01P	1.533(3)	C00P	C00T	1.393(2)		C1	C3B	1.604(6)
C00B	C00C	1.484(2)	C01A	C01T	1.529(3)							

Table 5.19. Bond Angles for **5.5**.

Atom	Atom	Atom	Angle/°	Atom	Atom	Atom	Angle/°	Atom	Atom	Atom	Angle/°	Atom	Atom	Atom	Angle/°
N005	Cu01	Cu02	89.96(5)	C00M	C00V	P003	113.03(12)	N005	C009	C00Q	111.08(14)	C01I	C019	C01V	109.17(17)
N006	Cu01	Cu02	89.76(5)	C018	C00W	C00X	120.08(16)	C00Q	C009	C00A	118.08(15)	C01V	C019	C01Q	108.95(17)
N006	Cu01	N005	177.01(6)	C008	C00X	C00R	105.85(14)	C009	C00A	C00G	124.35(15)	C018	C01A	C01M	109.71(16)
P003	Cu02	Cu01	98.473(16)	C00W	C00X	C008	121.59(16)	C011	C00A	C009	117.29(15)	C01P	C01A	C018	111.56(15)
P003	Cu02	P004	169.66(2)	C00W	C00X	C00R	132.52(16)	C011	C00A	C00G	118.34(15)	C01P	C01A	C01M	107.72(17)
P004	Cu02	Cu01	91.359(16)	C00I	C00Y	C00G	121.09(16)	C00K	C00B	C00C	121.01(15)	C01T	C01A	C018	109.77(16)
C00V	P003	Cu02	105.98(6)	C015	C00Z	C01E	112.04(14)	C00K	C00B	C00O	117.46(15)	C01T	C01A	C01M	109.20(17)
C00V	P003	C01X	104.84(9)	C015	C00Z	C01H	109.67(14)	C00O	C00B	C00C	121.38(15)	C01T	C01A	C01P	108.83(17)
C00V	P003	C1	105.36(9)	C015	C00Z	C01L	109.78(14)	C008	C00C	C00B	124.28(15)	C01K	C01B	C016	109.73(16)
C01X	P003	Cu02	115.18(9)	C01E	C00Z	C01H	108.38(15)	C013	C00C	C008	117.47(15)	C01O	C01B	C016	112.03(15)
C1	P003	Cu02	119.03(8)	C01E	C00Z	C01L	107.92(15)	C013	C00C	C00B	118.16(15)	C01O	C01B	C01K	107.92(17)
C1	P003	C01X	105.19(12)	C01H	C00Z	C01L	108.98(16)	C007	C00D	C00Q	106.24(14)	C021	C01B	C016	109.40(17)
C010	P004	Cu02	110.18(6)	C00F	C010	P004	114.95(12)	C00N	C00D	C007	122.25(15)	C021	C01B	C01K	109.23(19)
C010	P004	C01D	100.90(8)	C00A	C011	C016	124.63(16)	C00N	C00D	C00Q	131.47(15)	C021	C01B	C01O	108.48(19)
C01D	P004	Cu02	112.56(6)	C014	C012	C00L	121.58(16)	C00O	C00E	C00P	122.02(16)	C00J	C01C	C01J	121.08(16)
C01G	P004	Cu02	115.47(7)	C00C	C013	C018	124.23(16)	C00H	C00F	C010	123.22(15)	C017	C01C	C00J	117.28(16)
C01G	P004	C010	106.25(9)	C012	C014	C00G	121.10(16)	C00J	C00F	C00H	117.93(15)	C017	C01C	C01J	121.54(16)
C01G	P004	C01D	110.31(10)	C00N	C015	C00U	117.38(15)	C00J	C00F	C010	118.85(15)	C01N	C01D	P004	114.84(14)
C007	N005	Cu01	126.31(11)	C00N	C015	C00Z	123.65(15)	C00Y	C00G	C00A	120.54(15)	C01U	C01D	P004	113.04(15)
C009	N005	Cu01	128.31(11)	C00U	C015	C00Z	118.96(15)	C00Y	C00G	C014	117.49(16)	C01U	C01D	C01N	112.49(17)
C009	N005	C007	105.37(13)	C00S	C016	C011	117.44(16)	C014	C00G	C00A	121.94(16)	C01W	C01F	C00L	108.49(16)
C008	N006	Cu01	124.35(11)	C00S	C016	C01B	123.31(16)	N006	C00H	C00F	129.83(15)	C020	C01F	C00L	110.69(16)
C00H	N006	Cu01	129.63(11)	C011	C016	C01B	119.25(16)	N006	C00H	C00R	111.45(15)	C020	C01F	C01W	108.20(19)
C00H	N006	C008	105.06(13)	C01C	C017	C00R	120.42(16)	C00F	C00H	C00R	118.68(15)	C022	C01F	C00L	111.73(17)
N005	C007	C00D	111.08(14)	C00W	C018	C013	117.57(16)	C00Y	C00I	C00L	121.72(16)	C022	C01F	C01W	108.7(2)
N005	C007	C00M	130.53(15)	C00W	C018	C01A	123.86(16)	C00F	C00J	C01C	124.15(16)	C022	C01F	C020	109.0(2)
C00D	C007	C00M	118.38(15)	C013	C018	C01A	118.54(15)	C00B	C00K	C00T	121.54(16)	C01S	C01G	P004	109.21(15)
N006	C008	C00C	129.73(15)	C00P	C019	C01Q	109.47(15)	C00I	C00L	C01F	120.01(16)	C01Z	C01G	P004	112.13(16)
N006	C008	C00X	111.54(14)	C00P	C019	C01V	108.73(15)	C012	C00L	C00I	116.92(16)	C01Z	C01G	C01S	109.09(19)
C00C	C008	C00X	118.72(15)	C01I	C019	C00P	112.28(15)	C012	C00L	C01F	123.04(16)	C01C	C01J	C023	108.22(17)
N005	C009	C00A	130.84(15)	C01I	C019	C01Q	108.18(17)	C007	C00M	C00V	125.22(15)	C01Y	C01J	C01C	111.42(17)
C00S	C00Q	C00D	131.38(16)	C1AB	C01X	P003	112.1(2)	C00U	C00M	C007	117.36(15)	C01Y	C01J	C023	106.7(2)
C00H	C00R	C00X	105.98(15)	N026	C025	C028	178.1(4)	C00U	C00M	C00V	117.34(15)	C01Y	C01J	C027	109.8(2)
C017	C00R	C00H	121.49(16)	C2	C1	P003	113.33(16)	C015	C00N	C00D	119.85(15)	C027	C01J	C01C	112.70(17)
C017	C00R	C00X	132.49(16)	C2	C1	C3A	123.8(3)	C00E	C00O	C00B	120.79(16)	C027	C01J	C023	107.7(2)
C016	C00S	C00Q	119.90(16)	C2	C1	C3B	95.8(3)	C00E	C00P	C019	119.89(15)	C0AA	C01X	P003	120.1(3)
C00P	C00T	C00K	121.16(16)	C3A	C1	P003	107.3(2)	C00T	C00P	C00E	116.96(16)	C0AA	C01X	C1AB	118.0(3)
C00M	C00U	C015	124.69(16)	C3B	C1	P003	111.3(2)	C00T	C00P	C019	123.14(16)	C1AA	C01X	P003	118.1(3)
C00S	C00Q	C009	122.44(15)	C0AB	C01X	P003	108.1(2)	C009	C00Q	C00D	106.15(14)	C1AA	C01X	C0AB	110.8(3)

$(CuP_{iPr}N_{MeOPh})_2$ (5.6)

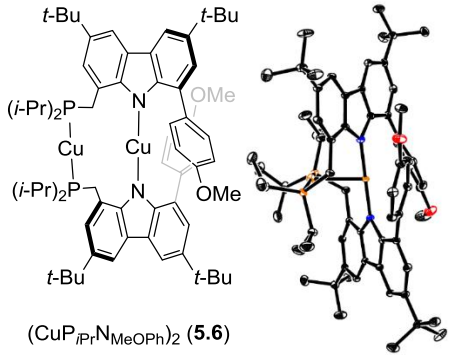

Table 5.20. Crystal data and structure refinement for **5.6**.

Identification code	**5.6**
Empirical formula	$C_{68}H_{90}Cu_2N_2O_2P_2$
Formula weight	1156.43
Temperature/K	100.0
Crystal system	monoclinic
Space group	$P2_1/n$
a/Å	18.1528(12)
b/Å	16.6884(12)
c/Å	20.1620(14)
α/°	90
β/°	91.132(2)
γ/°	90
Volume/Å^3	6106.7(7)
Z	4
ρ_{calc}g/cm^3	1.258
μ/mm^{-1}	0.794
F(000)	2464.0
Radiation	MoKα (λ = 0.71073)
2Θ range for data collection/°	3.168 to 55.16
Index ranges	$-23 \leq h \leq 23$, $-21 \leq k \leq 21$, $-26 \leq l \leq 26$
Reflections collected	343315
Independent reflections	14099 [R_{int} = 0.0620, R_{sigma} = 0.0162]
Data/restraints/parameters	14099/0/707
Goodness-of-fit on F^2	1.018
Final R indexes [I>=2σ (I)]	R_1 = 0.0341, wR_2 = 0.0973
Final R indexes [all data]	R_1 = 0.0400, wR_2 = 0.1011
Largest diff. peak/hole / e Å^{-3}	2.23/-0.66

Table 5.21. Fractional Atomic Coordinates ($\times 10^4$) and Equivalent Isotropic Displacement Parameters ($Å^2 \times 10^3$) for **5.6**. U_{eq} is defined as 1/3 of the trace of the orthogonalized U_{IJ} tensor.

Atom	*x*	*y*	*z*	U(eq)	Atom	*x*	*y*	*z*	U(eq)
Cu01	5935.4(2)	2374.8(2)	7138.5(2)	10.85(6)	C019	2121.1(9)	1685.7(12)	7936.0(8)	17.4(3)
Cu02	5186.0(2)	3580.4(2)	6754.2(2)	17.73(6)	C01A	5296.7(9)	2671.4(10)	10668.4(8)	13.5(3)
P003	4512.1(2)	2845.4(3)	6078.7(2)	13.16(9)	C01B	4784.8(10)	-102.8(11)	6265.7(9)	17.5(3)
P004	5905.9(2)	4444.1(3)	7256.6(2)	14.08(9)	C01C	7675.3(10)	2032.9(11)	7844.9(9)	18.2(3)
O005	4149.1(8)	-366.9(9)	7239.4(7)	24.9(3)	C01D	7979.9(10)	3200.9(12)	8500.1(9)	19.9(4)
N006	6626.1(8)	2426.2(8)	6458.0(7)	11.4(3)	C01E	7972.9(11)	5656.7(11)	5280.7(10)	22.3(4)
O007	8825.1(8)	2616.9(10)	7698.2(8)	29.0(3)	C01F	8168.8(10)	2636.0(12)	8019.7(9)	20.4(4)
N008	5242.1(8)	2313.7(8)	7819.3(7)	11.9(3)	C01G	5707.6(11)	1955.6(12)	10977.9(9)	21.5(4)
C009	7175.6(9)	3832.9(10)	6616.7(8)	11.7(3)	C01H	3624.3(10)	3274.1(11)	5792.6(9)	18.8(3)
C00A	4043.5(9)	1976.8(10)	7183.6(8)	11.8(3)	C01I	9081.5(11)	5185.2(12)	5920.6(10)	24.4(4)
C00B	6783.3(9)	1842(1)	5979.7(8)	11.3(3)	C01J	7317.7(11)	-449.9(11)	4325.5(9)	21.1(4)
C00C	7055.6(9)	3092.3(10)	6288.4(8)	10.8(3)	C01K	8472.1(11)	335.6(13)	4433.7(11)	28.8(4)
C00D	4664.1(9)	2451.9(10)	9539.2(8)	12.3(3)	C01L	5928.1(11)	5441.4(11)	6870.6(10)	22.5(4)
C00E	5299.6(9)	2595.5(10)	9910.6(8)	12.4(3)	C01M	1957.2(11)	856.4(13)	7641.4(10)	27.6(4)
C00F	5965.4(9)	2637.2(10)	9566.4(8)	13.6(3)	C01N	4512.5(10)	2674.4(13)	10940.6(9)	22.3(4)
C00G	7647.8(9)	4382.6(10)	6326.4(8)	13.1(3)	C01O	5044.0(11)	2551.8(12)	5346.1(9)	21.6(4)
C00H	7322.7(9)	898.9(10)	4907.6(8)	13.4(3)	C01P	8833.0(12)	4675.3(12)	4782.1(10)	26.8(4)
C00I	5929.9(9)	659(1)	6266.3(8)	12.1(3)	C01Q	4023.4(11)	-176.9(13)	7919.1(10)	26.4(4)
C00J	4132.0(9)	2200.2(10)	8369.0(8)	11.2(3)	C01R	3043.0(11)	2669.7(12)	5555.4(10)	24.4(4)
C00K	7555.5(9)	1684.9(10)	4993.5(8)	12.8(3)	C01S	5674.2(12)	3449.8(12)	10880.3(9)	23.0(4)
C00L	4700.6(9)	2361.1(10)	8851.7(8)	11.4(3)	C01T	1851.4(11)	1701.0(16)	8648.6(10)	30.4(5)
C00M	6026.3(9)	2548.2(10)	8883.5(8)	12.6(3)	C01U	5773.0(12)	4547.9(13)	8159.9(10)	26.7(4)
C00N	7903.0(9)	3525.3(10)	5417.4(8)	12.0(3)	C01V	5420.5(13)	3285.8(16)	5046.7(11)	33.6(5)
C00O	4482.0(9)	2173.4(10)	7749.1(8)	11.3(3)	C01W	5998.1(12)	5369.1(15)	6119.3(11)	32.3(5)
C00P	6517.6(9)	1049.8(10)	5882.7(8)	11.9(3)	C01X	7462.2(13)	811.4(12)	3677.2(9)	26.5(4)
C00Q	6803.7(9)	607(1)	5352.7(8)	13.8(3)	C01Y	3312.2(12)	3807.8(13)	6339.1(11)	28.4(4)
C00R	3299.2(9)	1828.6(10)	7279.5(8)	13.5(3)	C01Z	4635.8(13)	2060.4(16)	4819(1)	34.4(5)
C00S	8004.9(9)	4261.2(10)	5721.4(8)	12.5(3)	C020	1693.9(11)	2320.8(14)	7534.8(11)	29.4(5)
C00T	5361.5(9)	245.5(11)	5931.1(8)	15.5(3)	C021	5226.1(13)	5911.7(13)	7023.3(13)	34.3(5)
C00U	7291.0(9)	2142.4(10)	5512.6(8)	11.6(3)	C022	6213.2(16)	5240.0(16)	8472.6(11)	40.3(6)
C00V	5315.2(10)	356.2(11)	7300.4(8)	16.3(3)	C023	4965.0(14)	4546.8(16)	8346.9(13)	41.1(6)
C00W	7284.1(10)	3167.0(11)	8779.9(8)	16.6(3)	C024	9285.3(14)	3300.7(18)	7769.8(14)	43.4(6)
C00X	7634.7(10)	396.5(10)	4344.0(9)	16.2(3)	C012	3380.3(9)	2051.5(10)	8444.7(8)	12.5(3)
C00Y	5902.9(9)	679.4(10)	6955.1(8)	13.7(3)	C013	6992.4(9)	2002.4(11)	8137.4(8)	15.1(3)
C00Z	7450.9(9)	2948.5(10)	5704.2(8)	11.0(3)	C014	4336.5(9)	1890.6(10)	6493.2(8)	12.5(3)
C010	5367.4(9)	2412.4(10)	8503.8(8)	11.8(3)	C015	4751.6(10)	-32.9(11)	6954.1(9)	17.0(3)
C011	6849.4(9)	4046.3(10)	7272.7(8)	13.2(3)	C016	2946.5(9)	1861.4(10)	7896.1(8)	13.2(3)
C018	6773.4(9)	2578.3(10)	8598.1(8)	13.2(3)	C017	8468.6(10)	4932.9(10)	5426.8(8)	15.2(3)

Table 5.22. Anisotropic Displacement Parameters ($Å^2 \times 10^3$) for **5.6**. The anisotropic displacement factor exponent takes the form: $-2\pi^2[h^2a^{*2}U_{11}+2hka^*b^*U_{12}+\ldots]$.

Atom	U_{11}	U_{22}	U_{33}	U_{23}	U_{13}	U_{12}	Atom	U_{11}	U_{22}	U_{33}	U_{23}	U_{13}	U_{12}
Cu01	11.84(10)	11.63(10)	9.19(10)	0.76(7)	3.00(7)	-0.12(7)	C00Y	16.2(8)	11.0(7)	13.7(7)	-0.5(6)	-1.1(6)	-1.5(6)
Cu02	14.50(11)	13.83(11)	24.77(12)	-1.44(8)	-2.23(8)	-1.38(8)	C00Z	12.5(7)	10.5(7)	10.1(7)	-0.8(6)	1.5(6)	1.1(6)
P003	13.04(19)	15.7(2)	10.71(18)	2.29(15)	0.41(15)	-0.27(16)	C010	14.5(8)	10.1(7)	11.0(7)	-0.6(6)	2.2(6)	-0.1(6)

P004	13.7(2)	12.3(2)	16.4(2)	-2.85(15)	4.68(16)	-0.75(15)	C011	14.2(7)	14.9(8)	10.6(7)	-2.5(6)	1.5(6)	0.5(6)
O005	22.7(7)	28.6(8)	23.7(7)	1.9(6)	7.7(5)	-11.3(6)	C012	13.3(7)	16.0(8)	8.4(7)	-0.3(6)	2.5(6)	-0.3(6)
N006	13.5(6)	9.9(6)	10.8(6)	-1.1(5)	2.5(5)	0.2(5)	C013	15.9(8)	16.3(8)	13.1(7)	1.7(6)	-2.1(6)	1.6(6)
O007	16.0(7)	35.6(9)	35.8(8)	-4.6(6)	9.1(6)	-4.0(6)	C014	13.7(7)	14.7(8)	9.1(7)	-0.4(6)	1.2(6)	-1.2(6)
N008	11.9(6)	13.4(7)	10.6(6)	-0.8(5)	1.2(5)	-1.7(5)	C015	18.1(8)	14.2(8)	18.9(8)	2.9(6)	3.8(6)	-3.4(6)
C009	12.5(7)	12.2(8)	10.5(7)	-0.6(6)	1.1(6)	2.6(6)	C016	12.9(7)	16.2(8)	10.7(7)	-0.9(6)	1.0(6)	-1.8(6)
C00A	15.5(8)	11.2(7)	8.6(7)	-0.4(5)	1.3(6)	-1.3(6)	C017	17.7(8)	10.6(8)	17.4(8)	0.7(6)	3.9(6)	-3.0(6)
C00B	12.3(7)	11.2(7)	10.4(7)	0.0(6)	1.6(6)	1.4(6)	C018	12.3(7)	16.8(8)	10.4(7)	2.7(6)	-0.5(6)	0.5(6)
C00C	11.6(7)	11.1(7)	9.7(7)	0.8(6)	1.2(6)	1.7(6)	C019	12.5(8)	27.2(10)	12.5(7)	-4.0(7)	0.7(6)	-3.8(7)
C00D	11.9(7)	13.2(8)	11.8(7)	-0.5(6)	1.2(6)	-0.5(6)	C01A	15.6(8)	14.4(8)	10.6(7)	-2.0(6)	-0.8(6)	-0.6(6)
C00E	16.1(8)	10.9(7)	10.3(7)	0.0(6)	-0.6(6)	0.1(6)	C01B	16.3(8)	17.6(8)	18.6(8)	-2.5(6)	0.6(6)	-5.0(6)
C00F	13.0(7)	12.8(8)	15.0(8)	-0.1(6)	-2.5(6)	-1.4(6)	C01C	17.0(8)	21.1(9)	16.4(8)	-0.7(7)	-0.1(6)	6.2(7)
C00G	15.2(7)	11.0(7)	13.1(7)	-2.4(6)	0.1(6)	0.5(6)	C01D	16.2(8)	22.9(9)	20.5(8)	2.3(7)	-2.3(7)	-5.1(7)
C00H	14.8(7)	13.4(8)	12.2(7)	-2.8(6)	1.9(6)	1.4(6)	C01E	26.1(9)	14.0(8)	26.9(9)	6.0(7)	1.6(8)	-1.3(7)
C00I	13.4(7)	9.4(7)	13.7(7)	-0.6(6)	2.0(6)	-0.2(6)	C01F	14.4(8)	26.9(10)	19.9(8)	4.7(7)	2.3(7)	2.3(7)
C00J	13.9(7)	11.6(7)	8.1(7)	-0.6(5)	1.0(6)	0.5(6)	C01G	30.5(10)	21.0(9)	12.9(8)	1.0(7)	-1.4(7)	5.3(8)
C00K	13.5(7)	13.4(8)	11.6(7)	-1.0(6)	3.5(6)	-0.2(6)	C01H	17.9(8)	19.5(9)	18.8(8)	2.3(7)	-1.9(7)	2.8(7)
C00L	11.1(7)	11.4(7)	11.7(7)	0.2(6)	0.8(6)	-0.3(6)	C01I	18.0(9)	23.3(10)	32(1)	-1.7(8)	0.2(8)	-4.9(7)
C00M	11.3(7)	11.1(7)	15.4(8)	0.3(6)	1.2(6)	-0.1(6)	C01J	28.5(10)	14.7(9)	20.4(8)	-7.0(7)	6.0(7)	-2.2(7)
C00N	13.2(7)	12.5(8)	10.3(7)	0.3(6)	3.0(6)	1.1(6)	C01K	20.3(9)	26.5(10)	39.7(11)	-15.8(9)	6.2(8)	2.5(8)
C00O	13.3(7)	10.6(7)	10.2(7)	0.5(6)	3.2(6)	-0.9(6)	C01L	19.9(9)	13.3(8)	34.2(10)	3.8(7)	-0.9(8)	-1.2(7)
C00P	12.6(7)	11.4(7)	11.7(7)	0.1(6)	1.7(6)	-0.3(6)	C01M	23.1(9)	31.4(11)	28.6(10)	-8.7(8)	9.0(8)	-13.8(8)
C00Q	15.1(7)	10.4(7)	15.9(7)	-2.1(6)	1.7(6)	-1.1(6)	C01N	20.4(9)	35.5(11)	10.9(8)	-5.0(7)	1.8(7)	0.2(8)
C00R	15.6(8)	16.0(8)	8.8(7)	-0.9(6)	-1.3(6)	-3.2(6)	C01O	20.5(9)	31.1(10)	13.3(8)	4.1(7)	4.1(7)	6.1(8)
C00S	13.7(7)	10.9(7)	12.9(7)	2.0(6)	1.5(6)	0.1(6)	C01P	36.2(11)	17.7(9)	27.2(10)	-0.8(7)	17.1(8)	-8.6(8)
C00T	17.1(8)	16.6(8)	12.9(7)	-2.4(6)	1.4(6)	-1.8(6)	C01Q	27.7(10)	28.7(11)	23.2(9)	7.4(8)	10.9(8)	-2.9(8)
C00U	12.5(7)	10.8(7)	11.6(7)	0.0(6)	1.6(6)	0.2(6)	C01R	20.8(9)	25.8(10)	26.4(10)	1.9(8)	-7.3(8)	0.2(7)
C00V	21.7(8)	15.2(8)	12.2(7)	2.8(6)	1.6(6)	-1.5(7)	C01S	32.3(10)	19.9(9)	16.6(8)	-5.4(7)	-0.8(7)	-6.5(8)
C00W	16.4(8)	19.0(9)	14.1(7)	-0.4(6)	-1.2(6)	-1.8(7)	C01T	14.1(8)	61.1(15)	16.1(8)	-8.3(9)	4.5(7)	-9.7(9)
C00X	19.8(8)	12.8(8)	16.2(8)	-5.3(6)	4.8(6)	-0.5(6)	C01U	33.4(11)	26.2(10)	20.8(9)	-1.0(8)	10.3(8)	6.9(8)
C022	56.0(15)	40.3(14)	24.7(10)	-17.5(10)	2.3(10)	5.7(12)	C01V	28.9(11)	49.0(14)	23.1(10)	13.3(9)	8.8(8)	-1.3(10)
C023	43.5(14)	41.9(14)	39.0(13)	4.9(10)	25.8(11)	10.7(11)	C01W	25(1)	37.3(12)	34.7(11)	17.7(9)	3.0(9)	8.0(9)
C024	28.7(12)	54.7(16)	47.4(14)	-13.3(12)	15.9(10)	-20.6(11)	C01X	44.7(12)	19.0(9)	15.9(8)	-3.8(7)	4.9(8)	-2.7(8)
C020	16.3(9)	41.1(13)	30.7(11)	1.8(9)	-3.8(8)	2.3(8)	C01Y	25.4(10)	28.7(11)	30.9(10)	-5.8(8)	-3.2(8)	9.9(8)
C021	34.0(12)	20.7(10)	48.3(13)	-0.1(9)	2(1)	9.1(9)	C01Z	38.5(12)	46.3(14)	18.7(9)	-8.2(9)	5.4(9)	3.2(10)

Table 5.23. Bond Lengths for **5.6**.

Atom	Atom	Length/Å	Atom	Atom	Length/Å
Cu01	Cu02	2.5410(3)	C00K	C00U	1.389(2)
Cu01	N006	1.8787(14)	C00L	C010	1.413(2)
Cu01	N008	1.8833(14)	C00M	C010	1.425(2)
Cu02	P003	2.1887(5)	C00M	C018	1.485(2)
Cu02	P004	2.1816(5)	C00N	C00S	1.383(2)
P003	C014	1.8303(17)	C00N	C00Z	1.398(2)
P003	C01H	1.8453(18)	C00P	C00Q	1.407(2)
P003	C01O	1.8467(19)	C00R	C016	1.411(2)
P004	C011	1.8365(17)	C00S	C017	1.529(2)
P004	C01L	1.8380(19)	C00T	C01B	1.384(2)
P004	C01U	1.850(2)	C00U	C00Z	1.428(2)
O005	C015	1.365(2)	C00V	C00Y	1.394(2)
O005	C01Q	1.429(2)	C00V	C015	1.388(2)
N006	C00B	1.405(2)	C00W	C018	1.395(2)
N006	C00C	1.404(2)	C00W	C01D	1.395(2)
O007	C01F	1.368(2)	C00X	C01J	1.525(2)
O007	C024	1.420(3)	C00X	C01K	1.531(3)
N008	C00O	1.404(2)	C00X	C01X	1.539(3)
N008	C010	1.404(2)	C012	C016	1.382(2)
C009	C00C	1.417(2)	C013	C018	1.400(2)
C009	C00G	1.392(2)	C013	C01C	1.384(2)
C009	C011	1.503(2)	C015	C01B	1.395(2)
C00A	C00O	1.416(2)	C016	C019	1.530(2)
C00A	C00R	1.391(2)	C017	C01E	1.531(2)
C00A	C014	1.507(2)	C017	C01I	1.537(2)
C00B	C00P	1.419(2)	C017	C01P	1.532(2)
C00B	C00U	1.422(2)	C019	C01M	1.533(3)
C00C	C00Z	1.412(2)	C019	C01T	1.527(2)

C00D	C00E	1.384(2)	C019	C020	1.534(3)
C00D	C00L	1.397(2)	C01A	C01G	1.534(2)
C00E	C00F	1.407(2)	C01A	C01N	1.536(2)
C00E	C01A	1.533(2)	C01A	C01S	1.526(2)
C00F	C00M	1.391(2)	C01C	C01F	1.388(3)
C00G	C00S	1.407(2)	C01D	C01F	1.399(3)
C00H	C00K	1.388(2)	C01H	C01R	1.530(3)
C00H	C00Q	1.401(2)	C01H	C01Y	1.534(3)
C00H	C00X	1.530(2)	C01L	C01W	1.527(3)
C00I	C00P	1.481(2)	C01L	C021	1.533(3)
C00I	C00T	1.404(2)	C01O	C01V	1.532(3)
C00I	C00Y	1.391(2)	C01O	C01Z	1.523(3)
C00J	C00L	1.430(2)	C01U	C022	1.533(3)
C00J	C00O	1.414(2)	C01U	C023	1.522(3)
C00J	C012	1.398(2)			

Table 5.24. Bond Angles for **5.6**.

Atom	Atom	Atom	Angle/°	Atom	Atom	Atom	Angle/°	Atom	Atom	Atom	Angle/°	Atom	Atom	Atom	Angle/°
N006	Cu01	Cu02	95.87(4)	C00N	C00S	C00G	116.87(15)	C00E	C00D	C00L	120.01(15)	C00W	C018	C013	117.52(16)
N006	Cu01	N008	179.50(6)	C00N	C00S	C017	123.27(15)	C00D	C00E	C00F	117.18(15)	C013	C018	C00M	120.51(15)
N008	Cu01	Cu02	84.47(4)	C01B	C00T	C00I	121.83(15)	C00D	C00E	C01A	122.30(15)	C016	C019	C01M	109.59(15)
P003	Cu02	Cu01	92.024(15)	C00B	C00U	C00Z	106.50(14)	C00F	C00E	C01A	120.47(15)	C016	C019	C020	108.97(15)
P004	Cu02	Cu01	93.981(16)	C00K	C00U	C00B	122.93(15)	C00M	C00F	C00E	124.64(15)	C01M	C019	C020	109.10(16)
P004	Cu02	P003	168.97(2)	C00K	C00U	C00Z	130.56(15)	C009	C00G	C00S	124.58(15)	C01T	C019	C016	112.25(14)
C014	P003	Cu02	107.69(5)	C015	C00V	C00Y	119.57(16)	C00K	C00H	C00Q	117.10(15)	C01T	C019	C01M	108.44(17)
C014	P003	C01H	108.74(8)	C01D	C00W	C018	121.65(17)	C00K	C00H	C00X	119.63(15)	C01T	C019	C020	108.44(17)
C014	P003	C01O	103.46(8)	C00H	C00X	C01K	109.26(14)	C00Q	C00H	C00X	123.27(15)	C00E	C01A	C01G	109.25(14)
C01H	P003	Cu02	116.82(6)	C00H	C00X	C01X	109.28(15)	C00T	C00I	C00P	119.68(15)	C00E	C01A	C01N	112.20(14)
C01H	P003	C01O	108.67(8)	C01J	C00X	C00H	112.37(14)	C00Y	C00I	C00P	123.40(15)	C01G	C01A	C01N	107.69(15)
C01O	P003	Cu02	110.60(7)	C01J	C00X	C01K	108.35(16)	C00Y	C00I	C00T	116.92(15)	C01S	C01A	C00E	109.82(14)
C011	P004	Cu02	108.62(6)	C01J	C00X	C01X	108.98(15)	C00O	C00J	C00L	106.05(14)	C01S	C01A	C01G	109.69(15)
C011	P004	C01L	107.86(8)	C01K	C00X	C01X	108.52(17)	C012	C00J	C00L	130.68(15)	C01S	C01A	C01N	108.15(15)
C011	P004	C01U	98.98(9)	C00I	C00Y	C00V	122.11(15)	C012	C00J	C00O	123.19(15)	C00T	C01B	C015	119.84(16)
C01L	P004	Cu02	114.81(7)	C00C	C00Z	C00U	106.37(14)	C00H	C00K	C00U	120.31(15)	C013	C01C	C01F	119.82(17)
C01L	P004	C01U	109.66(10)	C00N	C00Z	C00C	122.71(15)	C00D	C00L	C00J	130.37(15)	C00W	C01D	C01F	119.27(17)
C01U	P004	Cu02	115.49(7)	C00N	C00Z	C00U	130.91(15)	C00D	C00L	C010	122.93(15)	O007	C01F	C01C	115.24(17)
C015	O005	C01Q	117.26(15)	N008	C010	C00L	110.91(14)	C010	C00L	C00J	106.70(14)	O007	C01F	C01D	124.84(18)
C00B	N006	Cu01	128.12(11)	N008	C010	C00M	131.65(15)	C00F	C00M	C010	117.79(15)	C01C	C01F	C01D	119.91(17)
C00C	N006	Cu01	126.57(11)	C00L	C010	C00M	117.44(15)	C00F	C00M	C018	118.10(15)	C01R	C01H	P003	115.78(13)
C00C	N006	C00B	105.13(13)	C009	C011	P004	116.98(11)	C010	C00M	C018	124.08(15)	C01R	C01H	C01Y	110.20(16)
C01F	O007	C024	116.70(17)	C016	C012	C00J	119.69(15)	C00S	C00N	C00Z	120.17(15)	C01Y	C01H	P003	109.47(13)
C00O	N008	Cu01	127.24(11)	C01C	C013	C018	121.73(17)	N008	C00O	C00A	130.96(15)	C01W	C01L	P004	110.57(14)
C00O	N008	C010	104.98(13)	C00A	C014	P003	114.00(12)	N008	C00O	C00J	111.32(14)	C01W	C01L	C021	108.99(17)
C010	N008	Cu01	127.77(11)	O005	C015	C00V	124.59(16)	C00J	C00O	C00A	117.63(15)	C021	C01L	P004	110.69(15)
C00C	C009	C011	123.94(15)	O005	C015	C01B	115.85(16)	C00B	C00P	C00I	125.75(14)	C01V	C01O	P003	110.32(15)
C00G	C009	C00C	117.94(14)	C00V	C015	C01B	119.56(16)	C00Q	C00P	C00B	117.67(15)	C01Z	C01O	P003	116.50(14)
C00G	C009	C011	118.07(15)	C00R	C016	C019	120.06(14)	C00Q	C00P	C00I	116.48(14)	C01Z	C01O	C01V	111.73(17)
C00O	C00A	C014	124.25(15)	C012	C016	C00R	116.92(15)	C00H	C00Q	C00P	124.52(15)	C022	C01U	P004	113.48(15)
C00R	C00A	C00O	117.47(14)	C012	C016	C019	123.02(15)	C00A	C00R	C016	125.09(15)	C023	C01U	P004	112.88(16)
C00R	C00A	C014	118.24(14)	C00S	C017	C01E	109.10(14)	C00G	C00S	C017	119.85(15)	C023	C01U	C022	113.34(19)
N006	C00B	C00P	131.91(15)	C00S	C017	C01I	110.24(14)	N006	C00C	C009	131.14(14)	C01E	C017	C01P	108.67(15)
N006	C00B	C00U	110.68(14)	C00S	C017	C01P	111.98(14)	N006	C00C	C00Z	111.25(14)	C01P	C017	C01I	107.90(16)
C00P	C00B	C00U	117.39(14)	C01E	C017	C01I	108.88(15)	C00Z	C00C	C009	117.52(15)	C00W	C018	C00M	121.97(15)

$(CuP_{iPr}N_{Mes})_2$ (5.7)

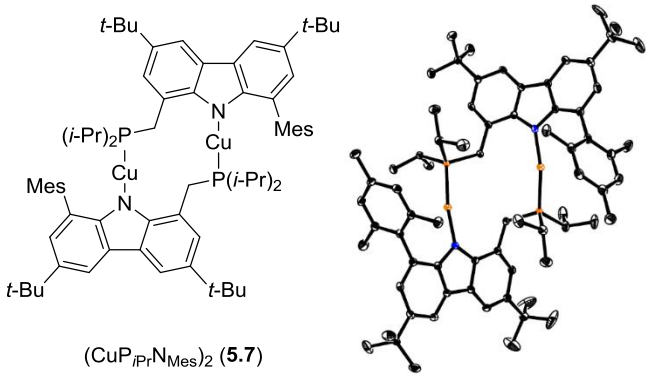

Table 5.25. Crystal data and structure refinement for **5.7**.

Identification code	**5.7**
Empirical formula	$C_{37}H_{50.5}CuN_{1.5}P$
Formula weight	610.80
Temperature/K	100.04
Crystal system	monoclinic
Space group	$P2_1$
a/Å	14.7416(11)
b/Å	11.9929(15)
c/Å	19.3009(17)
α/°	90
β/°	99.519(2)
γ/°	90
Volume/Å^3	3365.3(6)
Z	4
ρ_{calc}g/cm^3	1.206
μ/mm^{-1}	0.722
F(000)	1308.0
Crystal size/mm^3	0.23 × 0.21 × 0.17
Radiation	MoKα (λ = 0.71073)
2Θ range for data collection/°	4.28 to 55.236
Index ranges	$-19 \le h \le 19$, $-15 \le k \le 15$, $-25 \le l \le 25$
Reflections collected	90178
Independent reflections	15582 [R_{int} = 0.0376, R_{sigma} = 0.0337]
Data/restraints/parameters	15582/1/758
Goodness-of-fit on F^2	1.037
Final R indexes [I>=2σ (I)]	R_1 = 0.0238, wR_2 = 0.0611
Final R indexes [all data]	R_1 = 0.0262, wR_2 = 0.0620
Largest diff. peak/hole / e Å^{-3}	0.34/-0.27
Flack parameter	0.016(6)

Table 5.26. Fractional Atomic Coordinates ($\times 10^4$) and Equivalent Isotropic Displacement Parameters ($Å^2 \times 10^3$) for **5.7**. U_{eq} is defined as 1/3 of the trace of the orthogonalized U_{IJ} tensor.

Atom	*x*	*y*	*z*	U(eq)	Atom	*x*	*y*	*z*	U(eq)
Cu01	3035.3(2)	4196.5(2)	6186.3(2)	13.11(6)	C01F	9322(2)	7298(3)	10220.9(17)	44.8(8)
Cu02	4460.4(2)	5542.7(2)	8497.9(2)	14.86(6)	C01G	7290.3(17)	6716(2)	9844.3(12)	20.5(5)
P003	4341.3(4)	3362.2(5)	6551.5(3)	12.48(11)	C01H	6224.6(16)	3415(2)	6332.9(13)	24.1(5)
P004	3001.1(4)	5878.3(5)	8234.1(3)	13.55(11)	C01I	1775.0(18)	7618(2)	7640.1(15)	28.9(6)
N005	5660.2(12)	4989.9(16)	8620.1(9)	13.2(4)	C01J	6169.6(18)	7414(2)	7971.8(12)	22.2(5)
N006	1893.7(12)	4925.7(16)	6049.8(9)	12.2(4)	C01K	5946.5(14)	3944.3(18)	8437.3(10)	12.3(4)
C007	2495.6(15)	4761.6(19)	4588.5(10)	13.6(4)	C01L	3354.8(16)	3388(2)	4058.9(11)	17.6(4)
C008	−566.1(16)	6470(2)	3639.8(11)	17.0(5)	C01M	3768.1(17)	1202(2)	6770.8(13)	22.5(5)
C009	1497.7(14)	4913.8(19)	7278.6(11)	13.0(4)	C01N	7531(2)	139(2)	8686.0(13)	26.7(6)
C00A	2461.7(14)	4738.3(19)	7663.4(11)	13.7(4)	C01P	6787.2(17)	198(2)	7437.0(13)	23.0(5)
C00B	−134.6(15)	5253.9(19)	7326.7(11)	15.8(4)	C01Q	460.0(14)	5510(2)	5495.1(10)	13.2(4)
C00C	6827.7(14)	3677.6(19)	8814.7(10)	12.3(4)	C01R	2729(2)	6910(3)	9466.5(14)	32.6(6)
C00D	1315.7(14)	5053.9(19)	6545.4(11)	12.4(4)	C01S	5365(2)	7316(3)	10427.7(13)	31.5(6)
C00E	4312.4(15)	1877.5(19)	6310.8(11)	14.2(4)	C01T	−980(2)	5513(3)	3161.6(13)	32.5(6)
C00F	6834.0(15)	1932.0(19)	8199.1(11)	13.5(4)	C01U	3260.3(17)	6541(2)	5075.4(13)	20.7(5)
C00G	1597.8(15)	5183.9(19)	4739.9(11)	13.7(4)	C01V	5381(2)	5219(2)	6409.6(16)	31.5(6)
C00H	8004.9(17)	5943(2)	10018.8(12)	21.7(5)	C01W	2530.6(16)	3733(2)	4254.5(11)	16.3(4)
C00I	5606.5(16)	7799(2)	8507.9(12)	18.2(5)	C01X	2768.2(16)	7210(2)	7763.6(12)	19.7(5)
C00J	3286.3(15)	5417(2)	4736.1(10)	14.4(4)	C01Y	2485(2)	4834(3)	9381.4(13)	34.5(7)
C00K	1702.7(18)	2985(2)	4104.7(15)	26.5(6)	C01Z	−43.7(18)	7263(2)	3229.3(14)	27.1(6)
C00L	2385.8(17)	5935(2)	8982.9(12)	21.3(5)	C020	4096.7(15)	5038(2)	4541.3(11)	16.6(4)
C00M	6476.9(16)	6484(2)	9388.1(11)	15.9(4)	C021	−1847(2)	5323(6)	7345.9(16)	76.9(18)
C00N	3889.9(17)	1791(2)	5535.2(12)	20.1(5)	C022	5256.2(17)	7781(2)	9693.5(12)	21.3(5)
C00O	76.0(15)	5977.4(19)	4270.2(11)	14.8(4)	C023	−825(3)	4301(4)	8265(2)	61.2(12)
C00P	5954.2(15)	2207.4(19)	7840.1(11)	13.7(4)	C024	4617.5(18)	8626(2)	9502.8(13)	23.2(5)
C00Q	−897.1(16)	5305(2)	7779.6(12)	19.2(5)	C1	1139(2)	8242(3)	5350.5(19)	40.6(7)
C00R	5508.0(15)	3195.2(19)	7933.7(10)	13.4(4)	C2	8621(2)	6633(3)	11225.3(15)	45.7(9)
C00S	7106.4(15)	4633.9(19)	9244.6(11)	13.9(4)	C3	1904(2)	8941(3)	5258(2)	49.6(9)
C00T	1357.2(15)	5193.8(18)	5411.5(11)	13.6(4)	C4	−785(3)	6339(3)	8228(2)	59.6(12)
C00U	−1347.5(18)	7126(2)	3873.3(13)	26.2(6)	N5	2509(2)	9470(3)	5187(3)	94.4(16)
C00V	6389.2(14)	5412(2)	9097.7(10)	14.0(4)	C6	9583(3)	5357(4)	10633(2)	74.3(15)
C00W	4137.1(15)	4026(2)	4191.7(11)	16.4(5)	C015	3171(2)	7181(2)	7086.2(13)	26.9(6)
C00X	7909.7(16)	4894(2)	9720.4(11)	17.8(5)	C016	5295.8(15)	3997.2(19)	6186.3(11)	17.7(5)
C00Y	7260.8(15)	2687(2)	8692(1)	13.3(4)	C017	4443.6(16)	9044(2)	8826.4(12)	21.5(5)
C00Z	4583.0(15)	3481(2)	7514.6(11)	15.4(4)	C018	−170.9(15)	5908.2(19)	4928.8(11)	14.8(4)
C010	5762.8(16)	7364(2)	9195.8(11)	17.4(5)	C019	419.7(14)	5378.6(18)	6227.2(11)	13.4(4)
C011	763.6(15)	4981.3(19)	7640.1(11)	15.3(4)	C01A	7334.4(16)	873(2)	8033.2(11)	16.5(5)
C012	5017.3(17)	3667(2)	3955.8(13)	23.0(5)	C01B	8244.3(17)	1199(2)	7796.2(14)	24.8(5)
C013	−294.1(14)	5482(2)	6616.1(11)	15.7(4)	C01C	8878.0(19)	6288(3)	10528.1(14)	31.4(6)
C014	4946.2(17)	8621(2)	8337.8(12)	21.0(5)	C01D	3710.7(19)	9916(2)	8617.1(15)	30.1(6)
					C01E	948.6(15)	5581(2)	4188.2(10)	15.5(4)

Table 5.27. Anisotropic Displacement Parameters ($Å^2 \times 10^3$) for **5.7**. The anisotropic displacement factor exponent takes the form: $-2\pi^2[h^2a^{*2}U_{11}+2hka^*b^*U_{12}+\ldots]$.

Atom	U_{11}	U_{22}	U_{33}	U_{23}	U_{13}	U_{12}	Atom	U_{11}	U_{22}	U_{33}	U_{23}	U_{13}	U_{12}

Cu01	11.07(12)	16.03(13)	11.73(11)	-0.76(10)	0.40(9)	2.37(10)	C015	34.9(15)	27.3(14)	18.4(11)	4.7(10)	3.8(10)	-8.4(12)
Cu02	12.76(13)	17.85(14)	13.27(12)	-3.00(11)	0.03(9)	1.19(11)	C016	17.0(11)	19.0(12)	17.1(10)	0.5(9)	2.5(8)	-2.6(9)
P003	11.9(3)	14.1(3)	10.8(2)	-1.8(2)	-0.3(2)	1.1(2)	C017	22.9(12)	14.0(12)	26.2(11)	-2.8(10)	0.0(9)	-3.5(9)
P004	13.4(3)	16.6(3)	10.5(2)	-1.4(2)	1.7(2)	0.7(2)	C018	11.9(10)	15.7(10)	16.7(10)	0.6(8)	1.6(8)	1.7(8)
N005	12.9(9)	14.6(9)	11.6(8)	-2.9(7)	0.7(7)	-1.1(7)	C019	12.3(10)	14.5(11)	13.3(9)	0.3(8)	1.7(8)	0.3(8)
N006	10.5(8)	16.2(9)	9.8(8)	0.2(7)	1.5(7)	0.4(7)	C01A	18.0(11)	17.5(11)	13.3(10)	-0.7(8)	0.2(8)	2.7(9)
C007	16.3(10)	16.2(11)	8.4(9)	2.7(8)	2.3(8)	1.4(9)	C01B	21.2(13)	26.0(14)	28.1(13)	-5.3(10)	6.8(10)	3.8(10)
C008	17.4(11)	19.3(12)	12.7(10)	2.8(9)	-2.1(8)	2.3(9)	C01C	24.1(14)	36.4(16)	29.1(13)	-13.8(12)	-9.4(11)	-3.9(12)
C009	12.9(10)	14.0(11)	12.0(9)	0.3(8)	1.5(8)	0.4(8)	C01D	29.0(14)	22.8(14)	36.5(14)	-3.5(11)	0.1(11)	4.5(11)
C00A	12.6(10)	17.9(11)	10.5(9)	-2.7(8)	2.0(8)	1.1(8)	C01E	18.4(10)	17.8(10)	10.0(9)	-0.8(9)	1.7(8)	-0.8(9)
C00B	13(1)	18.3(12)	17(1)	-1.5(8)	5.1(8)	-0.9(8)	C01F	32.9(16)	61(2)	38.5(16)	-18.7(16)	0.6(13)	-18.4(16)
C00C	11.4(10)	17.2(11)	8.7(9)	1.0(8)	2.8(8)	-2.3(8)	C01G	22.7(12)	20.9(12)	17(1)	-5.9(9)	1.2(9)	-4.4(10)
C00D	11.7(10)	13.2(10)	12.4(9)	-0.9(8)	2.2(8)	-0.7(8)	C01H	16.5(12)	29.8(14)	27.4(12)	2.9(11)	7.3(10)	-1.9(10)
C00E	13.8(10)	13.5(10)	14.6(10)	-2.4(8)	0.0(8)	0.3(8)	C01I	27.1(14)	19.8(13)	37.0(14)	3.3(11)	-3.3(11)	5.2(11)
C00F	15.0(11)	14.8(10)	10.8(9)	0.7(8)	2.3(8)	0.0(8)	C01J	30.4(13)	20.1(12)	17.5(11)	-1.5(9)	7.7(10)	-1.8(10)
C00G	13.4(10)	14.6(10)	12.9(9)	0.6(8)	2.1(8)	0.5(8)	C01K	12.4(10)	15.5(11)	9.2(9)	1.1(8)	2.9(7)	0.3(8)
C00H	18.5(12)	27.4(13)	17.4(11)	-7.1(10)	-2.0(9)	-1.6(10)	C01L	22.9(12)	15.4(11)	14.8(10)	0.0(9)	4.3(9)	4.4(9)
C00I	20.8(12)	15.6(11)	18.3(11)	-3.6(9)	3.6(9)	-6.1(9)	C01M	22.5(12)	21.1(13)	23.3(11)	2.2(10)	2.5(10)	-3.1(10)
C00J	16.6(10)	16.7(11)	10.0(9)	2.3(8)	2.5(8)	-0.2(9)	C01N	38.3(15)	21.4(12)	18.5(11)	2.1(10)	-0.8(10)	6.2(11)
C00K	22.6(13)	23.2(13)	34.4(14)	-9.0(11)	6.9(11)	-5(1)	C01P	25.4(12)	21.2(12)	20.9(11)	-6.2(9)	-0.4(10)	2.6(10)
C00L	24.8(12)	25.4(13)	15.1(10)	-5.4(9)	7.5(9)	-4.4(10)	C01Q	11.9(9)	14.1(10)	13.4(9)	0.2(9)	1.8(7)	0.6(9)
C00M	18.1(11)	18.0(11)	11.8(9)	-1.5(8)	2.6(8)	-0.8(9)	C01R	42.9(17)	35.6(16)	22.5(12)	-14.6(11)	15.1(11)	-10.5(13)
C00N	21.7(12)	20.9(12)	15.9(10)	-4.2(9)	-2.2(9)	2.6(10)	C01S	40.6(16)	38.2(16)	17.4(11)	-0.4(11)	10.0(11)	15.4(13)
C00O	16.4(11)	13.8(10)	12.9(9)	0.4(8)	-1.9(8)	-1.7(9)	C01T	43.6(16)	26.9(13)	21.0(11)	-1.3(11)	-12.3(11)	-1.2(13)
C00P	14.2(10)	16.8(11)	9.5(9)	-1.3(8)	0.1(8)	-3.1(8)	C01U	23.3(12)	16.9(12)	22.8(11)	-2.3(9)	7(1)	-3.1(10)
C00Q	14.7(10)	27.6(14)	17(1)	-0.1(9)	7.2(8)	0.5(9)	C01V	29.0(14)	21.3(14)	44.6(16)	-0.8(11)	6.7(12)	-5.1(11)
C00R	11.9(10)	17.8(11)	9.7(9)	-0.1(8)	-0.2(8)	-1.1(8)	C01W	16.1(11)	20.3(11)	12.7(9)	0.4(8)	3.2(8)	-0.5(9)
C00S	14(1)	17.9(11)	9.9(9)	-1.1(8)	2.1(8)	-2.1(9)	C01X	21.2(12)	16.9(11)	20.0(11)	1.1(9)	0.6(9)	-1.2(9)
C00T	13.1(10)	13.2(10)	14.3(9)	-0.1(8)	2.1(8)	0.1(8)	C01Y	56.4(19)	33.3(16)	15.9(11)	-0.6(11)	12.4(12)	-9.6(14)
C00U	21.7(12)	34.0(15)	21.0(11)	7.2(11)	-1.7(10)	9.3(11)	C01Z	24.1(13)	30.1(14)	26.8(12)	13.3(11)	3.3(10)	4.8(11)
C00V	12.7(10)	20.7(12)	8.8(8)	-3.1(8)	2.3(7)	-2.8(9)	C020	15.0(11)	20.5(12)	13.8(10)	4.0(9)	1.3(8)	-1.4(9)
C00W	16.8(10)	21.8(13)	11.0(9)	4.9(9)	4.0(8)	7.5(9)	C021	15.5(14)	189(6)	28.6(15)	-5(2)	10.3(12)	-8(2)
C00X	14.7(11)	22.9(12)	14.6(10)	-2.4(9)	-0.8(8)	-0.3(9)	C022	26.6(13)	20.3(12)	17(1)	-3.7(9)	3.3(9)	1(1)
C00Y	11.6(10)	19.7(11)	8.2(9)	1.2(8)	0.2(8)	-1.0(8)	C023	57(2)	53(2)	89(3)	39(2)	56(2)	22.3(19)
C00Z	13.2(10)	20.0(12)	11.8(9)	-4.1(8)	-1.5(8)	3.7(9)	C024	28.0(14)	19.4(13)	22.9(11)	-4.3(10)	6.1(10)	2.5(10)
C010	20.1(11)	15.1(11)	16.4(10)	-4.3(9)	1.1(9)	-1.0(9)	C1	38.1(17)	23.9(15)	57(2)	-7.2(14)	-0.6(15)	-0.2(13)
C011	15.9(11)	16.8(11)	13.4(9)	-0.8(8)	2.9(8)	-1.7(9)	C2	50(2)	62(2)	20.3(13)	-7.9(14)	-9.9(13)	-13.5(17)
C012	19.7(12)	28.5(13)	22.4(11)	2.3(10)	8(1)	7.4(10)	C3	30.9(16)	26.5(17)	90(3)	-26.6(17)	5.8(17)	1.9(13)
C013	12.2(10)	17.5(11)	17.2(10)	0.6(9)	1.6(8)	2.1(9)	C4	60(2)	50(2)	83(3)	-36(2)	55(2)	-17.2(19)
C014	25.9(13)	16.4(12)	19.3(11)	0.5(9)	-0.1(9)	-4.7(9)	N5	41.6(18)	43(2)	206(5)	-58(3)	44(2)	-18.7(16)
C6	46(2)	60(3)	95(3)	-36(2)	-53(2)	14.7(18)							

Table 5.28. Bond Lengths for **5.7**.

Atom	Atom	Length/Å	Atom	Atom	Length/Å
Cu01	P003	2.1807(6)	C00J	C01U	1.502(3)
Cu01	N006	1.8761(18)	C00J	C020	1.387(3)
Cu02	P004	2.1649(6)	C00K	C01W	1.504(3)
Cu02	N005	1.8670(18)	C00L	C01R	1.530(3)
P003	C00E	1.839(2)	C00L	C01Y	1.522(4)
P003	C00Z	1.839(2)	C00M	C00V	1.400(3)
P003	C016	1.840(2)	C00M	C010	1.494(3)
P004	C00A	1.851(2)	C00M	C01G	1.393(3)
P004	C00L	1.830(2)	C00O	C018	1.381(3)
P004	C01X	1.841(3)	C00O	C01E	1.405(3)
N005	C00V	1.390(3)	C00P	C00R	1.381(3)
N005	C01K	1.387(3)	C00Q	C021	1.508(4)
N006	C00D	1.391(3)	C00Q	C023	1.519(4)
N006	C00T	1.387(3)	C00Q	C4	1.505(4)
C007	C00G	1.490(3)	C00R	C00Z	1.505(3)
C007	C00J	1.396(3)	C00R	C01K	1.401(3)
C007	C01W	1.397(3)	C00S	C00V	1.403(3)
C008	C00O	1.531(3)	C00S	C00X	1.408(3)
C008	C00U	1.523(3)	C00T	C01Q	1.411(3)
C008	C01T	1.535(4)	C00W	C012	1.507(3)
C008	C01Z	1.526(4)	C00W	C01L	1.372(3)
C009	C00A	1.505(3)	C00W	C020	1.394(3)

C009	C00D	1.406(3)	C010	C022	1.403(3)
C009	C011	1.384(3)	C013	C019	1.395(3)
C00B	C00Q	1.535(3)	C014	C017	1.388(4)
C00B	C011	1.400(3)	C015	C01X	1.523(3)
C00B	C013	1.380(3)	C016	C01H	1.521(3)
C00C	C00S	1.435(3)	C016	C01V	1.527(4)
C00C	C00Y	1.387(3)	C017	C01D	1.510(3)
C00C	C01K	1.417(3)	C017	C024	1.382(3)
C00D	C019	1.416(3)	C018	C01Q	1.397(3)
C00E	C00N	1.527(3)	C019	C01Q	1.433(3)
C00E	C01M	1.524(3)	C01A	C01B	1.538(3)
C00F	C00P	1.405(3)	C01A	C01N	1.525(3)
C00F	C00Y	1.387(3)	C01A	C01P	1.524(3)
C00F	C01A	1.529(3)	C01C	C01F	1.542(5)
C00G	C00T	1.399(3)	C01C	C2	1.514(4)
C00G	C01E	1.393(3)	C01C	C6	1.515(5)
C00H	C00X	1.381(3)	C01I	C01X	1.525(4)
C00H	C01C	1.541(3)	C01L	C01W	1.393(3)
C00H	C01G	1.402(4)	C01S	C022	1.506(3)
C00I	C010	1.409(3)	C022	C024	1.391(4)
C00I	C014	1.386(3)	C1	C3	1.440(5)
C00I	C01J	1.502(3)	C3	N5	1.121(5)

Table 5.29. Bond Angles for **5.7**.

Atom	Atom	Atom	Angle/°	Atom	Atom	Atom	Angle/°	Atom	Atom	Atom	Angle/°	Atom	Atom	Atom	Angle/°
N006	Cu01	P003	169.34(5)	C023	C00Q	C00B	109.6(2)	C00Y	C00C	C00S	133.4(2)	C013	C019	C00D	121.56(19)
N005	Cu02	P004	168.39(6)	C4	C00Q	C00B	109.8(2)	C00Y	C00C	C01K	120.95(19)	C013	C019	C01Q	132.74(19)
C00E	P003	Cu01	112.35(7)	C4	C00Q	C021	108.1(3)	C01K	C00C	C00S	105.51(19)	C00F	C01A	C01B	109.0(2)
C00E	P003	C00Z	108.83(10)	C4	C00Q	C023	108.0(3)	N006	C00D	C009	129.97(19)	C01N	C01A	C00F	109.80(19)
C00E	P003	C016	106.93(11)	C00P	C00R	C00Z	122.24(19)	N006	C00D	C019	111.46(18)	C01N	C01A	C01B	109.7(2)
C00Z	P003	Cu01	107.71(7)	C00P	C00R	C01K	117.76(19)	C009	C00D	C019	118.58(19)	C01P	C01A	C00F	112.67(18)
C00Z	P003	C016	108.82(10)	C01K	C00R	C00Z	120.0(2)	C00N	C00E	P003	107.61(16)	C01P	C01A	C01B	106.82(19)
C016	P003	Cu01	112.12(8)	C00V	C00S	C00C	106.27(18)	C01M	C00E	P003	111.08(16)	C01P	C01A	C01N	108.8(2)
C00A	P004	Cu02	108.36(7)	C00V	C00S	C00X	120.6(2)	C01M	C00E	C00N	111.48(19)	C00H	C01C	C01F	109.2(2)
C00L	P004	Cu02	115.09(8)	C00X	C00S	C00C	133.1(2)	C00P	C00F	C01A	122.00(19)	C2	C01C	C00H	109.6(2)
C00L	P004	C00A	106.08(11)	N006	C00T	C00G	128.8(2)	C00Y	C00F	C00P	117.5(2)	C2	C01C	C01F	108.2(3)
C00L	P004	C01X	106.33(12)	N006	C00T	C01Q	111.61(18)	C00Y	C00F	C01A	120.42(19)	C2	C01C	C6	110.5(3)
C01X	P004	Cu02	111.98(8)	C00G	C00T	C01Q	119.63(19)	C00T	C00G	C007	123.63(19)	C6	C01C	C00H	111.7(2)
C01X	P004	C00A	108.70(10)	N005	C00V	C00M	127.6(2)	C01E	C00G	C007	119.11(19)	C6	C01C	C01F	107.7(3)
C00V	N005	Cu02	124.54(15)	N005	C00V	C00S	111.5(2)	C01E	C00G	C00T	117.3(2)	C00G	C01E	C00O	123.77(19)
C01K	N005	Cu02	127.63(15)	C00M	C00V	C00S	120.85(19)	C00X	C00H	C01C	121.8(2)	C00M	C01G	C00H	123.6(2)
C01K	N005	C00V	105.26(18)	C01L	C00W	C012	121.5(2)	C00X	C00H	C01G	118.8(2)	N005	C01K	C00C	111.40(18)
C00D	N006	Cu01	126.32(14)	C01L	C00W	C020	118.3(2)	C01G	C00H	C01C	119.4(2)	N005	C01K	C00R	129.15(19)
C00T	N006	Cu01	126.81(14)	C020	C00W	C012	120.2(2)	C010	C00I	C01J	120.8(2)	C00R	C01K	C00C	119.4(2)
C00T	N006	C00D	105.13(17)	C00H	C00X	C00S	119.4(2)	C014	C00I	C010	119.0(2)	C00W	C01L	C01W	121.9(2)
C00J	C007	C00G	120.5(2)	C00F	C00Y	C00C	120.5(2)	C014	C00I	C01J	120.1(2)	C00T	C01Q	C019	106.02(17)
C00J	C007	C01W	119.9(2)	C00R	C00Z	P003	122.16(16)	C007	C00J	C01U	120.9(2)	C018	C01Q	C00T	121.19(19)
C01W	C007	C00G	119.5(2)	C00I	C010	C00M	119.6(2)	C020	C00J	C007	119.2(2)	C018	C01Q	C019	132.7(2)
C00O	C008	C01T	108.8(2)	C022	C010	C00I	119.4(2)	C020	C00J	C01U	119.9(2)	C007	C01W	C00K	121.7(2)
C00U	C008	C00O	111.26(19)	C022	C010	C00M	121.0(2)	C01R	C00L	P004	110.64(18)	C01L	C01W	C007	119.2(2)
C00U	C008	C01T	108.6(2)	C009	C011	C00B	123.9(2)	C01Y	C00L	P004	110.38(18)	C01L	C01W	C00K	119.2(2)
C00U	C008	C01Z	107.6(2)	C00B	C013	C019	119.82(19)	C01Y	C00L	C01R	111.1(2)	C015	C01X	P004	109.66(18)
C01Z	C008	C00O	110.76(19)	C00I	C014	C017	122.1(2)	C00V	C00M	C010	122.35(19)	C015	C01X	C01I	111.9(2)
C01Z	C008	C01T	109.8(2)	C01H	C016	P003	117.43(17)	C01G	C00M	C00V	116.7(2)	C01I	C01X	P004	116.84(18)
C00D	C009	C00A	121.38(19)	C01H	C016	C01V	111.0(2)	C01G	C00M	C010	120.9(2)	C00J	C020	C00W	121.6(2)
C011	C009	C00A	120.84(19)	C01V	C016	P003	108.75(17)	C018	C00O	C008	122.1(2)	C010	C022	C01S	121.8(2)
C011	C009	C00D	117.75(19)	C014	C017	C01D	120.7(2)	C018	C00O	C01E	117.95(19)	C024	C022	C010	119.5(2)
C009	C00A	P004	117.90(16)	C024	C017	C014	118.2(2)	C01E	C00O	C008	119.90(19)	C024	C022	C01S	118.7(2)
C011	C00B	C00Q	119.51(19)	C024	C017	C01D	121.1(2)	C00R	C00P	C00F	123.9(2)	C017	C024	C022	121.7(2)
C013	C00B	C00Q	122.5(2)	C00O	C018	C01Q	119.9(2)	C021	C00Q	C00B	112.6(2)	N5	C3	C1	178.9(3)
C013	C00B	C011	118.0(2)	C00D	C019	C01Q	105.67(18)	C021	C00Q	C023	108.5(3)				

$(CuP_{Ph}N_{Mes})_2$ (5.8)

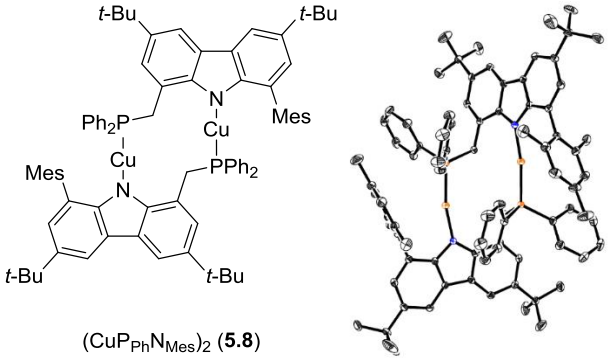

$(CuP_{Ph}N_{Mes})_2$ (**5.8**)

Single crystals obtained in saturated acetonitrile were of poor quality. Only crystal data are reported here.

Table 5.30. Crystal data for **5.8**.

Identification code	**5.8**
Empirical formula	$C_{84}H_{90}Cu_2N_2P_2$
Formula weight	1316.59
Temperature/K	99.96
Crystal system	orthorhombic
Space group	Fdd2
a/Å	23.2174(16)
b/Å	42.857(3)
c/Å	13.9020(11)
α/°	90
β/°	90
γ/°	90
Volume/Å^3	13833.0(18)
Z	8
ρ_{calc}g/cm^3	1.264
μ/mm^{-1}	0.708
F(000)	5568.0
Radiation	MoKα (λ = 0.71073)
2Θ range for data collection/°	5.174 to 55.024
Index ranges	$-29 \leq h \leq 30$, $-55 \leq k \leq 55$, $-18 \leq l \leq 18$
Reflections collected	96353
Independent reflections	7796 [R_{int} = 0.0788, R_{sigma} = 0.0436]

$(AuP_{iPr}N_H)_2$ (5.9)

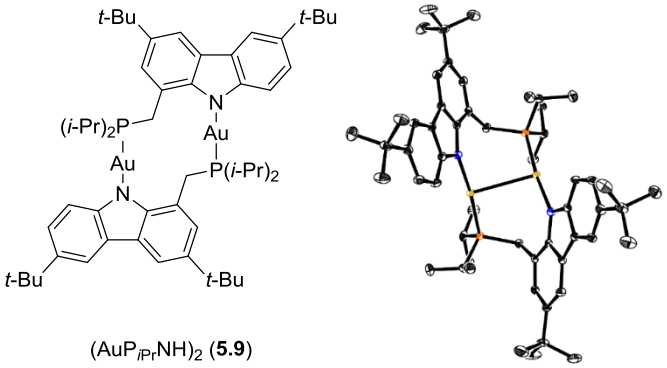

$(AuP_{iPr}NH)_2$ (**5.9**)

Table 5.31. Crystal data and structure refinement for **5.9**.

Identification code	**5.9**
Empirical formula	$C_{58}H_{84}Au_2N_4P_2$
Formula weight	1293.16
Temperature/K	99.99
Crystal system	monoclinic
Space group	$P2_1/c$
a/Å	15.0315(10)
b/Å	13.1932(8)
c/Å	29.6456(18)
α/°	90
β/°	103.410(2)
γ/°	90
Volume/Å^3	5718.8(6)
Z	4
ρ_{calc}g/cm^3	1.502
μ/mm^{-1}	5.219
F(000)	2592.0
Crystal size/mm^3	0.19 × 0.16 × 0.02
Radiation	MoKα (λ = 0.71073)
2Θ range for data collection/°	4.184 to 55.054
Index ranges	-19 ≤ h ≤ 19, -17 ≤ k ≤ 17, -37 ≤ l ≤ 38
Reflections collected	171154
Independent reflections	13134 [R_{int} = 0.0515, R_{sigma} = 0.0187]
Data/restraints/parameters	13134/0/617
Goodness-of-fit on F^2	1.065
Final R indexes [I>=2σ (I)]	R_1 = 0.0215, wR_2 = 0.0428
Final R indexes [all data]	R_1 = 0.0284, wR_2 = 0.0448
Largest diff. peak/hole / e Å^{-3}	1.13/-1.44

Table 5.32. Fractional Atomic Coordinates ($\times 10^4$) and Equivalent Isotropic Displacement Parameters ($Å^2 \times 10^3$) for **5.9**. U_{eq} is defined as 1/3 of the trace of the orthogonalized U_{IJ} tensor.

Atom	*x*	*y*	*z*	U(eq)	Atom	*x*	*y*	*z*	U(eq)
Au01	5910.2(2)	5884.7(2)	6831.3(2)	12.33(3)	C017	4594.8(18)	9861.9(19)	6622.8(9)	14.8(5)
Au02	5856.6(2)	5964.0(2)	5802.0(2)	12.98(3)	C018	4326(2)	7708(2)	5264.0(9)	20.0(6)
P003	6267.0(5)	4231.1(5)	6871.2(2)	12.99(13)	C019	6272.8(18)	7981.9(18)	7186.2(8)	13.4(5)
P004	4415.4(5)	6544.4(5)	5613.8(2)	13.15(13)	C01A	2958(2)	11280(2)	6408.6(12)	31.9(7)
N005	7185.5(14)	5500.9(16)	5903.4(7)	13.0(4)	C01C	7399.0(19)	9436(2)	7732.9(9)	16.9(5)
C006	7827.9(18)	6102.6(19)	5764.5(9)	14.7(5)	C01D	3790(3)	11179(3)	5773.9(13)	39.4(9)
C00B	5359.4(19)	3514.8(19)	7051.5(9)	16.2(5)	C01E	8055(2)	9859(2)	8564.4(10)	26.4(7)
C00C	8672.9(18)	5589.7(19)	5818.2(9)	13.8(5)	C01F	2635(2)	6015(2)	5122(1)	25.6(6)
C00D	7732.3(19)	7090(2)	5589.5(9)	17.8(5)	C01G	7628.9(19)	8395(2)	7752.3(9)	18.9(6)
C00G	9409.4(18)	6067.5(19)	5693.6(9)	15.8(5)	C01H	3799.7(18)	9679.0(19)	6284.7(9)	14.3(5)
C00H	3913.5(18)	6816.7(19)	6115.6(8)	13.5(5)	C01I	8754.5(19)	2864(2)	6257.1(9)	16.7(5)
C00I	6020.8(18)	9013.1(19)	7159.1(8)	13.0(5)	C01J	9098.2(19)	3746(2)	6108.4(9)	16.1(5)
C00J	7269.0(18)	3708.5(19)	6211.0(9)	14.1(5)	C01K	8038(2)	10162(2)	8059.9(10)	21.3(6)
C00K	7340.3(19)	3949(2)	7297.5(9)	17.2(5)	C01L	9022(3)	7133(3)	6869.5(13)	41.6(9)
C00L	8476.0(19)	7548(2)	5472.8(9)	18.6(6)	C01M	5087(2)	8472(2)	5463.5(10)	22.6(6)
C00M	4958.9(18)	8046.5(18)	6661.1(8)	12.0(5)	C01N	9309(2)	1878(2)	6367.6(10)	22.9(6)
C00N	8535.6(18)	4601.0(19)	5997.2(8)	14.1(5)	C01O	9938(2)	8649(2)	5208.3(12)	31.1(7)
C00O	6337.6(19)	3647.4(19)	6313.8(9)	15.7(5)	N01P	6365(2)	10788(2)	6216.4(11)	36.7(7)
C00Q	9324.1(19)	7054(2)	5519.7(9)	17.1(5)	C01Q	8877(2)	1060(2)	6008.0(12)	31.2(7)
C00R	3661(2)	4605(2)	5505.8(11)	26.2(7)	C01S	10131.3(19)	7547(2)	5366.2(10)	20.4(6)
C00S	7086.0(19)	7671(2)	7487.9(9)	17.2(5)	C01T	9014(2)	10090(3)	7986.8(11)	30.4(7)
C00T	7844.2(19)	2874.3(19)	6304.7(9)	16.6(5)	C01U	7200(2)	4050(2)	7790.7(9)	23.8(6)
C00U	3592.6(18)	8668.8(19)	6151.7(8)	13.6(5)	C01V	7289(3)	9110(2)	6397.8(12)	34.5(7)
N00W	5642.9(15)	7393.4(15)	6882.6(7)	13.1(4)	C01X	4353(2)	7460(2)	4761.7(10)	27.5(7)
C00X	5163.1(17)	9061.1(19)	6815.3(8)	13.0(5)	C01Z	10983(2)	7551(2)	5765.6(11)	27.1(7)
C00Y	3617.8(19)	5630(2)	5263.9(9)	18.6(6)	C020	6766(2)	10050(2)	6295.1(11)	28.8(7)
C00Z	6588.2(19)	9734.1(19)	7435.7(9)	15.4(5)	C021	10320(2)	6924(3)	4959.8(11)	30.8(7)
C010	4454(2)	3669(2)	6700(1)	20.4(6)	C022	9595(3)	7981(3)	6823.4(14)	48.6(10)
C011	5567(2)	2389(2)	7139.1(10)	21.4(6)	C024	2336(3)	10232(3)	5723.8(15)	50.6(12)
C012	7616.0(18)	4587.0(19)	6042.0(8)	13.6(5)	C025	9281(3)	1510(3)	6852.3(12)	44.5(10)
C013	3213(2)	10571(2)	6044.3(10)	20.5(6)	N026	10045(3)	8657(4)	6785.0(17)	78.8(13)
C014	7727(2)	11263(2)	7989.5(12)	31.4(8)	C02E	10300(2)	2002(2)	6337.9(13)	34.0(8)
C015	8124(2)	4658(2)	7243.2(10)	22.0(6)	C016	4158.2(18)	7846.9(19)	6322.9(8)	12.5(5)

Table 5.33. Anisotropic Displacement Parameters ($Å^2 \times 10^3$) for **5.9**. The anisotropic displacement factor exponent takes the form: $-2\pi^2[h^2a^{*2}U_{11}+2hka^*b^*U_{12}+\ldots]$.

Atom	U_{11}	U_{22}	U_{33}	U_{23}	U_{13}	U_{12}	Atom	U_{11}	U_{22}	U_{33}	U_{23}	U_{13}	U_{12}
Au01	14.47(5)	9.68(4)	12.24(5)	-0.98(3)	1.89(4)	0.73(4)	C010	18.9(15)	17.3(13)	25.2(14)	0.5(11)	5.7(11)	-2.0(11)
Au02	10.23(5)	15.66(5)	12.64(5)	-1.18(4)	1.85(3)	1.40(4)	C011	22.8(16)	14.6(13)	26.6(15)	3.1(11)	5.4(12)	-0.7(11)
P003	14.7(3)	9.8(3)	14.3(3)	-1.0(2)	3.1(2)	0.4(2)	C012	13.4(13)	16.1(12)	10.9(11)	-2.9(9)	2.1(10)	-0.1(10)
P004	10.7(3)	16.3(3)	11.7(3)	-3.3(2)	1.1(2)	1.2(2)	C013	17.6(15)	16.7(13)	23.7(14)	3.8(11)	-2.6(11)	4.6(11)
N005	6.9(10)	15.2(10)	16.2(10)	-0.9(8)	1.2(8)	0.0(8)	C014	31.4(18)	18.7(14)	34.1(17)	-2.5(12)	-13.1(14)	-5.7(13)
C006	12.2(13)	18.0(12)	13.4(12)	-1.9(9)	2.3(10)	-0.1(10)	C015	18.9(15)	23.4(14)	22.0(14)	-1.5(11)	1.6(11)	-2.9(12)
C00B	17.7(14)	13.7(12)	17.9(13)	-1.2(10)	5.5(11)	-0.2(10)	C016	13.7(13)	13.0(11)	11.1(11)	-1.7(9)	3.3(9)	-1.4(10)
C00C	11.8(13)	15.5(12)	12.5(11)	-1.3(9)	0.0(9)	1.6(10)	C017	14.2(13)	11.5(11)	17.7(12)	-1.2(9)	1.7(10)	-1.5(10)
C00D	15.1(14)	16.2(12)	22.2(13)	1.4(10)	4.3(11)	5.5(10)	C018	21.2(15)	23.9(14)	14.5(12)	4.2(10)	3.5(11)	7.1(12)

C00G	11.5(13)	18.5(13)	16.6(12)	-0.3(10)	1.7(10)	1.6(10)	C019	15.0(13)	12.8(11)	12.0(11)	0.3(9)	2.3(10)	0.8(10)
C00H	12.3(13)	14.9(12)	13.0(12)	-1.4(9)	2.1(10)	-1.5(10)	C01A	31.3(19)	22.6(15)	39.0(18)	3.2(13)	2.4(15)	11.0(13)
C00I	13.4(13)	12.5(11)	12.7(11)	0.2(9)	1.8(9)	0.1(10)	C01C	16.2(14)	16.6(12)	16.1(12)	-0.6(10)	-0.1(10)	-3.2(10)
C00J	13.9(13)	15.9(12)	12.1(11)	-4.5(9)	2(1)	-1.9(10)	C01D	45(2)	35.7(19)	38.8(19)	17.6(15)	13.1(17)	13.1(16)
C00K	17.9(14)	16.0(12)	16.3(12)	0.7(10)	1.3(10)	1.7(10)	C01E	28.0(17)	25.8(15)	20.9(14)	-2.3(11)	-3.3(12)	-4.4(13)
C00L	18.2(14)	15.9(12)	21.6(13)	3.4(10)	4.4(11)	3.1(10)	C01F	15.0(14)	35.0(16)	24.1(14)	-11.7(12)	-1.2(11)	0.3(12)
C00M	12.9(13)	12.5(11)	11.0(11)	0.4(9)	3.5(9)	2.8(9)	C01G	15.2(14)	20.1(13)	18.4(13)	1.6(10)	-2.5(11)	4.4(11)
C00N	13.8(13)	15.8(12)	11.6(11)	-2.3(9)	0.8(10)	-0.6(10)	C01H	11.4(13)	14.4(12)	16.3(12)	0.2(9)	1.6(10)	3(1)
C00O	18.4(14)	13.2(12)	15.9(12)	-2.6(9)	4.7(10)	-1.4(10)	C01I	15.6(14)	17.5(12)	16.1(12)	-1.9(10)	1.9(10)	1.9(10)
C00Q	13.8(13)	19.7(13)	16.9(12)	1.7(10)	1.8(10)	0(1)	C01J	10.9(13)	19.6(12)	16.9(12)	-2.7(10)	1.4(10)	0.7(10)
C00R	24.7(17)	22.9(14)	27.9(15)	-8.2(12)	-0.5(13)	-4.9(12)	C01K	19.1(15)	17.6(13)	22.3(14)	0.4(11)	-4.8(11)	-4.8(11)
C00S	17.9(14)	13.2(12)	18.0(13)	1(1)	-0.7(10)	5(1)	C01L	38(2)	47(2)	36.6(19)	-11.9(16)	2.3(16)	8.3(17)
C00T	21.0(14)	12.8(12)	16.5(12)	-2.0(9)	5.4(10)	-1.5(10)	C01M	22.3(16)	22.9(14)	23.8(14)	3.6(11)	7.7(12)	0.1(12)
C00U	10.6(12)	17.4(12)	12.0(11)	-0.4(9)	0.5(9)	0.2(10)	C01N	23.1(16)	18.2(13)	27.7(15)	4.1(11)	6.8(12)	6.8(11)
N00W	14.4(11)	10.7(10)	13(1)	-1.4(8)	0.5(8)	-0.6(8)	C01O	20.6(16)	27.8(16)	46(2)	18.7(14)	10.4(14)	2.1(13)
C00X	12.8(12)	13.7(11)	12.1(11)	0.1(9)	2.1(9)	-2(1)	N01P	32.7(17)	31.1(15)	48.4(18)	9.9(13)	13.5(14)	-3.7(13)
C00Y	13.8(14)	26.0(14)	15.2(12)	-8.5(10)	1.9(10)	-1.6(11)	C01Q	29.4(18)	17.7(14)	49(2)	-4.8(13)	15.5(15)	0.8(12)
C00Z	16.9(14)	12.2(11)	15.4(12)	0.7(9)	0.6(10)	0.2(10)	C01S	13.6(14)	22.9(14)	24.6(14)	7.6(11)	3.9(11)	1.2(11)
C021	25.7(18)	39.1(18)	32.2(17)	3.3(14)	16.3(14)	-0.5(14)	C01T	20.9(17)	33.3(17)	32.9(17)	7.2(13)	-1.9(13)	-9.5(13)
C022	44(3)	54(3)	43(2)	-14.4(19)	-0.6(18)	6(2)	C01U	25.9(16)	27.6(15)	17.0(13)	-1.0(11)	3.0(11)	-0.7(13)
C024	40(2)	27.1(18)	66(3)	-2.3(17)	-27(2)	8.6(16)	C01V	39(2)	29.5(17)	39.4(18)	1.0(14)	17.1(16)	3.4(15)
C025	59(3)	42(2)	34.0(19)	16.4(16)	13.4(18)	26.6(19)	C01X	33.2(18)	35.7(17)	13.9(13)	1.0(12)	6.0(12)	5.1(14)
N026	72(3)	73(3)	84(3)	-9(3)	2(3)	-14(3)	C01Z	16.7(15)	27.1(15)	34.4(17)	9.3(13)	-0.1(13)	-3.1(12)
C02E	17.2(16)	22.0(15)	59(2)	4.5(15)	0.6(15)	5.1(12)	C020	27.8(18)	28.9(16)	31.8(17)	0.8(13)	11.5(14)	-8.0(13)

Table 5.34. Bond Lengths for **5.9**.

Atom	Atom	Length/Å	Atom	Atom	Length/Å
Au01	Au02	3.0356(3)	C00Q	C01S	1.536(4)
Au01	P003	2.2431(6)	C00R	C00Y	1.525(4)
Au01	N00W	2.043(2)	C00S	C019	1.398(4)
Au02	P004	2.2428(7)	C00S	C01G	1.377(4)
Au02	N005	2.043(2)	C00T	C01I	1.408(4)
P003	C00B	1.838(3)	C00U	C016	1.399(3)
P003	C00K	1.842(3)	C00U	C01H	1.404(4)
P003	C00O	1.848(3)	N00W	C019	1.383(3)
P004	C00H	1.852(3)	C00X	C017	1.395(3)
P004	C00Y	1.842(3)	C00Y	C01F	1.527(4)
P004	C018	1.839(3)	C00Z	C01C	1.385(4)
N005	C006	1.384(3)	C013	C01A	1.544(4)
N005	C012	1.385(3)	C013	C01D	1.536(5)
C006	C00C	1.415(4)	C013	C01H	1.542(3)
C006	C00D	1.397(4)	C013	C024	1.503(4)
C00B	C010	1.523(4)	C014	C01K	1.525(4)
C00B	C011	1.527(4)	C017	C01H	1.391(4)
C00C	C00G	1.396(4)	C018	C01M	1.537(4)
C00C	C00N	1.441(4)	C018	C01X	1.535(4)
C00D	C00L	1.383(4)	C01C	C01G	1.414(4)
C00G	C00Q	1.395(4)	C01C	C01K	1.533(4)
C00H	C016	1.502(3)	C01E	C01K	1.542(4)
C00I	C00X	1.447(3)	C01I	C01J	1.387(4)
C00I	C00Z	1.407(3)	C01I	C01N	1.538(4)
C00I	C019	1.410(3)	C01K	C01T	1.534(4)
C00J	C00O	1.502(4)	C01L	C022	1.438(6)
C00J	C00T	1.387(4)	C01N	C01Q	1.550(4)
C00J	C012	1.410(4)	C01N	C025	1.527(4)
C00K	C015	1.542(4)	C01N	C02E	1.522(4)
C00K	C01U	1.531(4)	C01O	C01S	1.534(4)
C00L	C00Q	1.409(4)	N01P	C020	1.141(4)
C00M	N00W	1.385(3)	C01S	C01Z	1.529(4)
C00M	C00X	1.425(3)	C01S	C021	1.538(4)
C00M	C016	1.401(3)	C01V	C020	1.462(5)
C00N	C012	1.419(4)	C022	N026	1.141(6)
C00N	C01J	1.402(4)			

Table 5.35. Bond Angles for **5.9**.

Atom	Atom	Atom	Angle/°	Atom	Atom	Atom	Angle/°
P003	Au01	Au02	92.106(17)	C019	N00W	C00M	106.3(2)
N00W	Au01	Au02	94.67(6)	C00M	C00X	C00I	106.0(2)
N00W	Au01	P003	172.87(6)	C017	C00X	C00I	133.0(2)
P004	Au02	Au01	93.481(17)	C017	C00X	C00M	121.0(2)
N005	Au02	Au01	92.56(6)	C00R	C00Y	P004	111.41(19)
N005	Au02	P004	173.52(6)	C00R	C00Y	C01F	110.9(3)
C00B	P003	Au01	109.32(9)	C01F	C00Y	P004	113.54(19)
C00B	P003	C00K	106.72(12)	C01C	C00Z	C00I	120.3(2)
C00B	P003	C00O	104.25(12)	N005	C012	C00J	129.4(2)
C00K	P003	Au01	113.16(9)	N005	C012	C00N	111.0(2)
C00K	P003	C00O	107.85(12)	C00J	C012	C00N	119.5(2)
C00O	P003	Au01	114.88(9)	C01D	C013	C01A	108.0(3)
C00H	P004	Au02	114.60(9)	C01D	C013	C01H	108.0(2)
C00Y	P004	Au02	112.42(9)	C01H	C013	C01A	110.3(2)
C00Y	P004	C00H	104.25(12)	C024	C013	C01A	107.4(3)
C018	P004	Au02	111.43(10)	C024	C013	C01D	110.1(3)
C018	P004	C00H	107.49(12)	C024	C013	C01H	112.9(2)
C018	P004	C00Y	106.03(13)	C00M	C016	C00H	123.4(2)
C006	N005	Au02	120.68(17)	C00U	C016	C00H	118.9(2)
C006	N005	C012	106.1(2)	C00U	C016	C00M	117.6(2)
C012	N005	Au02	132.65(18)	C01H	C017	C00X	120.4(2)
N005	C006	C00C	111.2(2)	C01M	C018	P004	112.33(19)
N005	C006	C00D	128.8(2)	C01X	C018	P004	110.7(2)
C00D	C006	C00C	120.0(2)	C01X	C018	C01M	109.2(2)
C010	C00B	P003	109.76(18)	C00S	C019	C00I	120.2(2)
C010	C00B	C011	111.1(2)	N00W	C019	C00I	111.7(2)
C011	C00B	P003	114.4(2)	N00W	C019	C00S	128.0(2)
C006	C00C	C00N	105.8(2)	C00Z	C01C	C01G	118.2(2)
C00G	C00C	C006	120.0(2)	C00Z	C01C	C01K	123.7(2)
C00G	C00C	C00N	134.1(2)	C01G	C01C	C01K	118.0(2)
C00L	C00D	C006	118.7(2)	C00S	C01G	C01C	122.9(2)
C00Q	C00G	C00C	120.6(2)	C00U	C01H	C013	121.9(2)
C016	C00H	P004	113.42(18)	C017	C01H	C00U	117.7(2)
C00Z	C00I	C00X	134.5(2)	C017	C01H	C013	120.3(2)
C00Z	C00I	C019	120.0(2)	C00T	C01I	C01N	118.6(2)
C019	C00I	C00X	105.4(2)	C01J	C01I	C00T	117.8(2)
C00T	C00J	C00O	118.9(2)	C01J	C01I	C01N	123.6(3)
C00T	C00J	C012	117.3(2)	C01I	C01J	C00N	120.1(3)
C012	C00J	C00O	123.7(2)	C014	C01K	C01C	112.4(2)
C015	C00K	P003	112.00(18)	C014	C01K	C01E	108.4(3)
C01U	C00K	P003	110.2(2)	C014	C01K	C01T	108.3(3)
C01U	C00K	C015	109.0(2)	C01C	C01K	C01E	108.6(2)
C00D	C00L	C00Q	122.6(2)	C01C	C01K	C01T	110.6(3)
N00W	C00M	C00X	110.6(2)	C01T	C01K	C01E	108.6(2)
N00W	C00M	C016	130.0(2)	C01I	C01N	C01Q	108.8(2)
C016	C00M	C00X	119.4(2)	C025	C01N	C01I	109.7(2)
C012	C00N	C00C	105.8(2)	C025	C01N	C01Q	109.1(3)
C01J	C00N	C00C	133.2(3)	C02E	C01N	C01I	112.7(2)
C01J	C00N	C012	121.0(2)	C02E	C01N	C01Q	107.2(3)
C00J	C00O	P003	114.10(18)	C02E	C01N	C025	109.2(3)
C00G	C00Q	C00L	118.1(3)	C00Q	C01S	C021	107.9(2)
C00G	C00Q	C01S	119.6(2)	C01O	C01S	C00Q	112.7(2)
C00L	C00Q	C01S	122.3(2)	C01O	C01S	C021	108.9(3)
C01G	C00S	C019	118.3(2)	C01Z	C01S	C00Q	110.4(2)
C00J	C00T	C01I	124.3(2)	C01Z	C01S	C01O	107.4(2)
C016	C00U	C01H	123.9(2)	C01Z	C01S	C021	109.6(3)
C00M	N00W	Au01	135.07(17)	N01P	C020	C01V	179.3(4)
C019	N00W	Au01	118.58(17)	N026	C022	C01L	179.5(6)

AuCu($P_{iPr}N_H$)$_2$ (5.10)

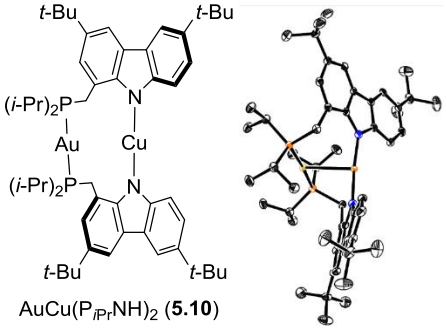

Table 5.36. Crystal data and structure refinement for **5.10**.

Identification code	**5.10**
Empirical formula	$C_{65.03}H_{80.13}Au_{0.98}Cu_{0.95}N_2P_2$
Formula weight	1205.90
Temperature/K	99.97
Crystal system	tetragonal
Space group	$P4_12_12$
a/Å	15.420(2)
b/Å	15.420(2)
c/Å	26.519(4)
α/°	90
β/°	90
γ/°	90
Volume/Å^3	6305(2)
Z	4
ρ_{calc}g/cm^3	1.270
μ/mm^{-1}	2.694
F(000)	2478.0
Crystal size/mm^3	0.19 × 0.16 × 0.02
Radiation	MoKα (λ = 0.71073)
2Θ range for data collection/°	5.312 to 54.994
Index ranges	$-20 \leq h \leq 20$, $-19 \leq k \leq 19$, $-34 \leq l \leq 34$
Reflections collected	121457
Independent reflections	7230 [R_{int} = 0.0492, R_{sigma} = 0.0212]
Data/restraints/parameters	7230/0/359
Goodness-of-fit on F^2	1.069
Final R indexes [I>=2σ (I)]	R_1 = 0.0145, wR_2 = 0.0345
Final R indexes [all data]	R_1 = 0.0162, wR_2 = 0.0349
Largest diff. peak/hole / e Å^{-3}	0.35/-0.34
Flack parameter	0.0072(16)

Table 5.37. Fractional Atomic Coordinates ($\times 10^4$) and Equivalent Isotropic Displacement Parameters ($Å^2 \times 10^3$) for **5.10**. U_{eq} is defined as 1/3 of the trace of the orthogonalized U_{IJ} tensor.

Atom	*x*	*y*	*z*	U(eq)
Au01	4058.8(2)	4058.8(2)	5000	13.40(4)
Cu02	2771.0(2)	2771.0(2)	5000	13.69(13)
P003	3341.7(4)	4869.9(4)	5596.9(2)	14.95(14)
C004	3490.0(16)	1526.7(16)	5654.1(9)	17.6(5)
C006	3870.5(15)	1386.9(15)	6131.6(9)	16.6(5)
N007	3114.0(14)	2345.0(14)	5618.9(8)	18.0(5)
C008	2952.4(16)	3535.5(16)	6268.6(9)	16.3(5)
C009	3527.7(17)	872.3(17)	5290.2(9)	21.5(5)
C00A	4335.2(16)	626.0(16)	6231.0(9)	18.0(5)
C00B	3230.0(16)	2718.9(16)	6090.8(9)	15.9(5)
C00C	3987.1(19)	126.3(15)	5398.0(9)	22.6(5)
C00D	3710.9(18)	3470.8(17)	7651.1(9)	22.8(6)
C00E	3308.9(18)	6405.4(16)	5041.6(13)	30.5(6)
C00F	3641.7(18)	6033.7(19)	6403.2(11)	26.7(6)
C00G	2534.9(15)	4215.0(16)	5939.8(9)	18.1(5)
C00H	4070.3(18)	5322.9(16)	6081.7(9)	20.1(5)
C00I	3543.4(16)	3164.6(16)	7108.1(9)	18.3(5)
C00J	4940.0(17)	5620.7(18)	5858.5(11)	25.6(6)
C00K	4152(3)	2781(2)	7968.3(11)	40.9(8)
C00L	4309(2)	4260(2)	7625.1(11)	38.2(7)
C00N	3677.7(16)	2154.4(16)	6420.5(9)	15.7(5)
C00O	2039.6(17)	5392.6(17)	4955.5(12)	28.4(6)
C00P	3105.8(16)	3723.3(16)	6771.9(9)	18.4(5)
C00Q	4412.1(17)	-9.6(17)	5863(1)	20.3(6)
C00R	4974.9(18)	-823.3(17)	5934.6(11)	25.3(6)
C00S	2719.8(17)	5760.5(15)	5315.9(10)	20.4(5)
C00W	5767(2)	-748(2)	5587.2(13)	41.4(8)
C1	3839.3(16)	2378.8(16)	6924.2(10)	17.9(5)
C2	5294(2)	-914(2)	6478.3(12)	45.0(8)
C3	4461(2)	-1643.8(19)	5801.4(15)	42.6(9)
C4	2863(2)	3729(2)	7912.7(12)	37.4(8)
C0AA	7548(5)	669(5)	6997(3)	120(3)
C1AA	7537(15)	1771(15)	6838(7)	224(11)
C3AA	6469(11)	3642(9)	6492(6)	109(5)
C2AA	6168(7)	2611(9)	6488(6)	85(4)
C5	6799(5)	1178(5)	6768(3)	54(3)
C3AB	5882(8)	3430(9)	6430(4)	121(5)
C1AB	6652(14)	2810(30)	6557(8)	310(20)
C5A	6889(5)	2114(4)	6743(2)	57(3)

Table 5.38. Anisotropic Displacement Parameters ($Å^2 \times 10^3$) for **5.10**. The anisotropic displacement factor exponent takes the form: $-2\pi^2[h^2a^{*2}U_{11}+2hka^*b^*U_{12}+\ldots]$.

Atom	U_{11}	U_{22}	U_{33}	U_{23}	U_{13}	U_{12}
Au01	12.61(4)	12.61(4)	14.99(6)	-1.59(4)	1.59(4)	1.44(5)
Cu02	15.23(16)	15.23(16)	10.6(2)	1.47(14)	-1.47(14)	-0.94(15)

P003	15.5(3)	12.7(3)	16.7(3)	-1.0(2)	1.9(2)	2.3(2)
C004	17.8(12)	15.8(12)	19.2(12)	1.3(10)	2(1)	-3.3(9)
C006	18.5(13)	15.8(12)	15.6(11)	1.1(9)	3.8(9)	-4.0(9)
N007	20.4(11)	16.8(11)	16.7(11)	-0.9(9)	1.0(9)	-0.9(9)
C008	14.8(12)	16.2(12)	18.0(12)	-0.3(9)	3.8(9)	-1.9(9)
C009	27.9(13)	19.7(13)	16.9(12)	-2.0(11)	1.6(10)	-5.3(11)
C00A	21.8(13)	14.8(11)	17.3(12)	3.0(9)	2.8(10)	-2.6(9)
C00B	15.4(12)	16.4(12)	16.0(12)	-0.5(10)	3.5(9)	-3.7(9)
C00C	31.3(15)	15.4(12)	21.0(12)	-4.1(9)	7.2(12)	-4.7(11)
C00D	32.4(14)	19.5(13)	16.5(12)	-4.2(9)	-2(1)	-0.6(11)
C00E	36.5(15)	18.6(12)	36.5(15)	8.1(13)	-2.6(14)	-1.2(11)
C00F	29.1(14)	24.8(15)	26.1(13)	-10.2(12)	0.7(11)	0.8(13)
C00G	17.3(12)	17.0(13)	20.1(11)	0.2(10)	2.8(9)	1.3(9)
C00H	19.7(12)	20.1(12)	20.6(12)	-2.9(10)	0.6(11)	0.7(12)
C00I	21.9(13)	17.0(12)	15.9(12)	-2.9(9)	3.4(10)	-2(1)
C00J	21.3(14)	28.7(14)	26.9(15)	-7.2(12)	0.2(11)	-5.7(11)
C00K	65(2)	32.0(16)	25.2(15)	-6.8(13)	-14.1(16)	4.3(18)
C00L	50(2)	34.6(18)	30.2(15)	-7.3(13)	-1.6(13)	-11.9(13)
C00N	16.5(12)	13.6(11)	17.1(12)	-0.7(10)	2.8(9)	-3.0(9)
C00O	28.2(14)	22.5(13)	34.4(15)	2.6(13)	-12.0(13)	4.9(10)
C00P	22.2(13)	14.0(11)	19.1(13)	-2.6(10)	5(1)	0.3(9)
C00Q	23.6(13)	15.1(12)	22.2(13)	0.5(10)	8.0(11)	-1.6(10)
C00R	30.2(14)	16.2(13)	29.4(14)	0.0(11)	8.4(12)	3.2(11)
C00S	22.0(13)	14.2(13)	25.0(13)	-0.1(10)	1.2(10)	4.8(9)
C00W	34.6(18)	36.2(18)	53(2)	1.2(15)	17.5(15)	6.7(13)
C1	20.6(13)	16.0(12)	17.1(12)	2.3(10)	1.3(10)	-0.3(9)
C2	67(2)	32.7(17)	35.4(17)	3.5(16)	-3.4(16)	26.3(18)
C3	39.4(18)	17.4(15)	71(2)	-0.7(15)	6.6(17)	2.4(13)
C4	42.0(19)	44.9(19)	25.4(16)	-10.8(14)	4.8(14)	-5.7(15)
C0AA	122(6)	135(6)	104(5)	46(4)	44(4)	53(5)
C1AA	200(20)	300(20)	175(15)	-138(16)	37(13)	-11(19)
C3AA	82(10)	87(9)	157(13)	-34(9)	-5(9)	2(7)
C2AA	55(6)	95(8)	104(9)	17(6)	-23(6)	42(6)
C5	57(5)	68(6)	39(4)	5(3)	20(3)	-7(4)
C3AB	90(8)	183(13)	90(7)	-28(7)	19(6)	-11(8)
C1AB	220(20)	570(50)	150(17)	-50(20)	8(15)	260(30)
C5A	57(5)	66(5)	47(4)	-4(3)	6(3)	18(3)

Table 5.39. Bond Lengths for **5.10**.

Atom	Atom	Length/Å	Atom	Atom	Length/Å
Au01	Cu02	2.8081(5)	C00D	C00L	1.529(4)
Au01	P003[1]	2.3007(6)	C00D	C4	1.532(4)
Au01	P003	2.3006(6)	C00E	C00S	1.531(4)
Cu02	N007	1.845(2)	C00F	C00H	1.538(4)
Cu02	N007[1]	1.845(2)	C00H	C00J	1.536(4)
P003	C00G	1.842(2)	C00I	C00P	1.411(3)
P003	C00H	1.845(3)	C00I	C1	1.384(3)
P003	C00S	1.833(3)	C00N	C1	1.402(3)
C004	C006	1.412(3)	C00O	C00S	1.528(4)
C004	N007	1.392(3)	C00Q	C00R	1.537(4)
C004	C009	1.397(3)	C00R	C00W	1.534(4)
C006	C00A	1.400(3)	C00R	C2	1.530(4)
C006	C00N	1.441(3)	C00R	C3	1.534(4)
N007	C00B	1.389(3)	C0AA	C1AA	1.75(2)
C008	C00B	1.411(3)	C0AA	C5	1.522(10)
C008	C00G	1.507(3)	C1AA	C5A	1.16(3)
C008	C00P	1.386(3)	C2AA	C3AB	1.345(16)
C009	C00C	1.381(4)	C2AA	C1AB	0.83(3)
C00A	C00Q	1.388(3)	C2AA	C5A	1.510(11)
C00B	C00N	1.414(4)	C5	C5A	1.452(11)
C00C	C00Q	1.412(4)	C3AB	C1AB	1.56(3)

C00D	C00I	1.537(3)	C1AB	C5A	1.24(4)
C00D	C00K	1.517(4)			

Table 5.40. Bond Angles for **5.10**.

Atom	Atom	Atom	Angle/°	Atom	Atom	Atom	Angle/°
P003[1]	Au01	Cu02	92.555(16)	C008	C00G	P003	112.21(17)
P003	Au01	Cu02	92.556(16)	C00F	C00H	P003	113.24(19)
P003	Au01	P003[1]	174.89(3)	C00J	C00H	P003	112.11(18)
N007	Cu02	Au01	92.81(7)	C00J	C00H	C00F	112.1(2)
N007[1]	Cu02	Au01	92.81(7)	C00P	C00I	C00D	119.0(2)
N007	Cu02	N007[1]	174.37(14)	C1	C00I	C00D	122.9(2)
C00G	P003	Au01	111.48(8)	C1	C00I	C00P	118.0(2)
C00G	P003	C00H	105.96(12)	C00B	C00N	C006	106.1(2)
C00H	P003	Au01	113.13(9)	C1	C00N	C006	132.3(2)
C00S	P003	Au01	112.26(9)	C1	C00N	C00B	121.6(2)
C00S	P003	C00G	104.95(11)	C008	C00P	C00I	124.2(2)
C00S	P003	C00H	108.56(12)	C00A	C00Q	C00C	118.0(2)
N007	C004	C006	111.8(2)	C00A	C00Q	C00R	122.5(2)
N007	C004	C009	128.7(2)	C00C	C00Q	C00R	119.4(2)
C009	C004	C006	119.5(2)	C00W	C00R	C00Q	108.3(2)
C004	C006	C00N	105.4(2)	C2	C00R	C00Q	111.9(2)
C00A	C006	C004	120.6(2)	C2	C00R	C00W	108.5(3)
C00A	C006	C00N	134.0(2)	C2	C00R	C3	107.9(3)
C004	N007	Cu02	120.12(17)	C3	C00R	C00Q	110.7(2)
C00B	N007	Cu02	133.65(18)	C3	C00R	C00W	109.6(2)
C00B	N007	C004	105.2(2)	C00E	C00S	P003	111.68(18)
C00B	C008	C00G	123.8(2)	C00O	C00S	P003	109.59(17)
C00P	C008	C00B	117.1(2)	C00O	C00S	C00E	110.6(2)
C00P	C008	C00G	119.0(2)	C00I	C1	C00N	119.6(2)
C00C	C009	C004	118.7(2)	C5A	C1AA	C0AA	120.3(15)
C00Q	C00A	C006	120.2(2)	C3AB	C2AA	C5A	140.2(12)
N007	C00B	C008	129.2(2)	C1AB	C2AA	C3AB	88(3)
N007	C00B	C00N	111.4(2)	C1AB	C2AA	C5A	55(3)
C008	C00B	C00N	119.4(2)	C5A	C5	C0AA	117.3(8)
C009	C00C	C00Q	122.9(2)	C2AA	C3AB	C1AB	32.0(15)
C00K	C00D	C00I	112.3(2)	C2AA	C1AB	C3AB	59.5(18)
C00K	C00D	C00L	108.2(3)	C2AA	C1AB	C5A	92(4)
C00K	C00D	C4	108.3(3)	C5A	C1AB	C3AB	147(3)
C00L	C00D	C00I	107.7(2)	C1AA	C5A	C2AA	164.7(13)
C00L	C00D	C4	109.2(2)	C1AA	C5A	C1AB	137.6(19)
C4	C00D	C00I	111.1(2)	C1AB	C5A	C2AA	33.2(16)

[(CuP$_{iPr}$N$_{MeOPh}$)$_2$][BAr$^F_{24}$] (5.11–BAr$^F_{24}$)

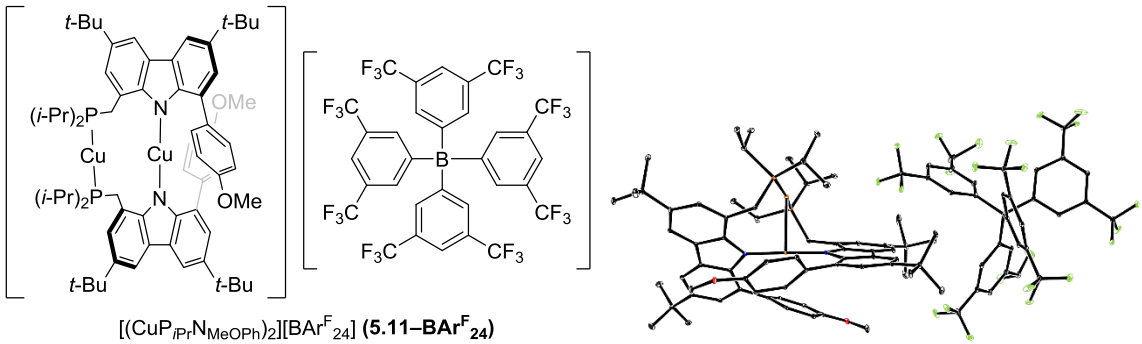

[(CuP$_{iPr}$N$_{MeOPh}$)$_2$][BAr$^F_{24}$] **(5.11–BAr$^F_{24}$)**

The quality of the crystals is modest. Structural information should be viewed with caution.

Table 5.41. Crystal data and structure refinement for **5.11–BAr$^{F}_{24}$**.

Identification code	**5.11–BAr$^{F}_{24}$**
Empirical formula	$C_{100}H_{102}BCu_2F_{24.01}N_2O_2P_2$
Formula weight	2212.02
Temperature/K	100.01
Crystal system	monoclinic
Space group	C2/c
a/Å	41.2206(19)
b/Å	15.5878(7)
c/Å	32.9205(14)
α/°	90
β/°	106.664(2)
γ/°	90
Volume/Å^3	20264.3(16)
Z	8
ρ_{calc}g/cm^3	1.450
μ/mm^{-1}	1.874
F(000)	8641.0
Radiation	CuKα (λ = 1.54178)
2Θ range for data collection/°	4.476 to 161.33
Index ranges	$-52 \leq h \leq 48$, $-19 \leq k \leq 19$, $-42 \leq l \leq 41$
Reflections collected	175259
Independent reflections	21641 [R_{int} = 0.0725, R_{sigma} = 0.0493]
Data/restraints/parameters	21641/0/1331
Goodness-of-fit on F^2	1.033
Final R indexes [I>=2σ (I)]	R_1 = 0.0776, wR_2 = 0.1926
Final R indexes [all data]	R_1 = 0.1016, wR_2 = 0.2057
Largest diff. peak/hole / e Å^{-3}	1.36/-0.84

Table 5.42. Fractional Atomic Coordinates (×10^4) and Equivalent Isotropic Displacement Parameters (Å^2×10^3) for **5.11–BAr$^{F}_{24}$**. U_{eq} is defined as 1/3 of the trace of the orthogonalized U_{IJ} tensor.

Atom	*x*	*y*	*z*	U(eq)	Atom	*x*	*y*	*z*	U(eq)
Cu01	4215.9(2)	6674.6(3)	4648.1(2)	27.99(13)	C02E	4683(1)	4701(3)	5813.9(12)	38.9(9)
Cu02	3622.5(2)	7337.6(4)	4692.2(2)	36.52(15)	C02F	1982.2(10)	7008(3)	589.9(13)	38.2(9)
P003	3451.5(3)	6040.4(7)	4767.9(3)	36.3(2)	C02G	2435.9(12)	6191(3)	1921.3(13)	45.9(10)
P004	3757.1(3)	8679.5(7)	4741.8(3)	39.9(3)	C02H	2986.3(13)	7695(3)	2964.6(12)	46.8(11)
F006	2811.2(7)	8382.6(17)	3023.7(8)	56.2(7)	C02I	4193.7(10)	3581(3)	4604.4(15)	39.2(9)
F008	3278.0(7)	7983(2)	2927.3(8)	65.7(8)	C02J	4760.6(11)	5875(3)	6289.9(11)	41.6(10)
N00A	4032.7(7)	6524.2(19)	4058.0(9)	26.9(6)	C02K	1648.0(11)	7391(3)	570.7(15)	49.4(11)
F00B	3057.4(11)	7265(2)	3334.6(8)	79.4(11)	C02O	4781.9(11)	4998(3)	6231.6(12)	44.2(11)

F00C	4016.5(8)	5250(2)	2265.5(10)	70.0(9)	C02P	3080.5(12)	4156(4)	3024.2(14)	57.2(14)
O00D	4196.0(8)	3408.0(19)	3901.3(10)	51.4(8)	B02Q	2850.3(11)	6484(3)	1456.5(12)	33.0(9)
O00E	5275.3(9)	8888.6(19)	5264.2(9)	51.6(8)	C02S	4600.1(12)	9523(3)	6456.4(12)	45.5(10)
F00F	4065.8(8)	4109(2)	1933.2(11)	75.3(9)	C02T	3608.9(12)	9203(3)	5187.0(16)	51.5(11)
N00H	4407.7(8)	6788(2)	5236.2(9)	32.8(7)	C02U	3868.6(13)	4508(3)	2122.3(15)	52.8(12)
F00J	3873.2(9)	4054(3)	2472.6(11)	93.5(13)	C02V	2848.9(11)	6207(3)	4136.7(17)	55.3(12)
F00M	4116.8(9)	8032(2)	1091.7(15)	96.0(14)	C02W	2810.3(13)	3201(3)	1218.5(16)	51.4(11)
F00N	3873(11)	6840(20)	806(18)	93(16)	C02X	2323.6(13)	6262(3)	2282.2(15)	53.5(12)
C00O	4625.7(9)	7895(2)	4156.2(10)	27.7(7)	C02Y	2503.7(14)	6749(3)	2624.0(14)	53.3(12)
F00P	2829.2(9)	9822(2)	1358.2(16)	102.4(14)	C02Z	4903.2(13)	4391(3)	6613.4(13)	52.0(12)
C00Q	3597.1(9)	5347(2)	4031.2(11)	30.8(8)	C030	2989.1(11)	5895(3)	4593.2(16)	49.7(11)
C00R	4135.3(8)	6940(2)	3736.7(9)	24.8(7)	C031	2950.4(12)	4465(4)	2561.4(13)	55.8(13)
C00S	4382.0(9)	7578(2)	3762.5(10)	26.7(7)	C032	3628.9(12)	5684(3)	5329.2(13)	47.9(11)
C00T	3782.0(8)	5945(2)	3856.4(10)	28.4(7)	C033	5359.0(15)	8382(3)	5645.8(13)	55.8(13)
C00V	3969.2(9)	6998(2)	2963(1)	29.3(7)	C034	4279.2(16)	3730(3)	3542.6(15)	63.5(15)
C00W	4533.6(9)	6111(3)	5520.7(10)	33.2(8)	C035	3611.7(13)	9324(3)	4265.9(14)	51.5(11)
C00X	3107.4(9)	7248(2)	1396.4(10)	29.2(7)	C036	4244.8(13)	9882(4)	6421.5(15)	58.3(13)
C00Y	4201.4(9)	7670(2)	2980.7(10)	27.8(7)	C037	4876.6(14)	3432(3)	6474.4(15)	57.1(13)
C010	3714.4(9)	5984(3)	3410.2(11)	32.2(8)	C038	3737.1(16)	8935(4)	3925.6(17)	66.1(15)
C011	3937.7(9)	6645(2)	3333.1(11)	29.8(7)	C039	3458.2(15)	4885(4)	5442.7(16)	63.2(14)
C012	4401.2(9)	7929(2)	3378.2(10)	27.4(7)	C03B	3656.1(14)	6413(4)	5645.0(15)	61.2(14)
C013	3231.9(9)	8774(2)	1364.2(10)	30.9(8)	C03C	5269.8(14)	4566(4)	6843.3(16)	67.1(15)
C014	3375.8(9)	7093(2)	1225.3(10)	30.7(8)	C03D	4677.3(16)	4489(4)	6901.2(16)	69.2(17)
C015	4471.4(9)	4771(2)	5043.2(11)	31.1(8)	C03E	3649.5(16)	10160(4)	5177.7(17)	67.5(15)
C016	4793.8(9)	7340(2)	4481.1(10)	26.8(7)	C03F	2825.3(14)	6401(4)	4880(2)	72.0(17)
C017	3499.8(10)	8596(3)	1196.6(11)	32.1(8)	C03G	4747.4(17)	9194(4)	6908.8(14)	77.3(19)
C018	3028.9(10)	5540(3)	1513(1)	32.4(8)	C03H	3283(2)	3327(4)	3041(2)	86(2)
C019	5015.1(10)	7638(2)	4855.6(10)	32.5(8)	C03J	3260.2(15)	8907(4)	5183.3(19)	70.5(16)
C01A	3566.7(9)	7753(3)	1127.7(11)	31.3(8)	C03K	3222.2(14)	9416(4)	4115.5(17)	70.4(16)
C01B	4443.7(9)	7531(3)	5480.7(11)	32.7(8)	C03M	4815.5(17)	10245(4)	6374(2)	80.1(18)
C01C	2538.2(10)	6540(2)	1015.3(11)	32.1(8)	F1	2764.7(6)	6164.6(17)	-128.4(7)	44.5(6)
C01D	4585.0(9)	5047(2)	4704.7(11)	27.1(7)	F2	2282.5(8)	6637(2)	-488.8(8)	68.9(9)
C01E	5073.5(11)	8513(3)	4905.8(11)	36.8(9)	F0AA	1389.2(7)	6917(2)	387.3(13)	79.8(14)
C01F	2045.6(10)	6767(3)	218.7(12)	37.1(9)	F1AA	1841.2(9)	6178(2)	2524.6(12)	77.7(10)
C01G	4701.4(10)	8771(2)	4208.7(11)	32.0(8)	F2AA	3233(4)	10213(6)	1177(3)	66(3)
C01H	4375.2(9)	8401(3)	5367.2(10)	32.0(8)	F4	3283.5(14)	9902(2)	1834.2(10)	108(2)
C01I	4229.5(10)	8099(3)	2573.1(11)	33.9(8)	F7	2145(3)	4992(7)	2595(3)	62(3)
C01J	2224(1)	6905(3)	980.0(12)	34.8(8)	F8	2933(6)	2823(17)	972(8)	146(9)
C01K	4443.5(9)	9003(3)	5694.2(11)	34.9(8)	F10	1591.5(10)	8106(3)	339(2)	128(2)
C01L	3362.2(11)	5415(3)	1773.5(11)	37.7(9)	F11	1861(2)	5368(9)	1976(2)	58(4)
C01M	3641.1(9)	5239(2)	4496.9(11)	30.6(8)	F12	2595(4)	3359(6)	834(3)	73(4)
C01N	3042.4(9)	8110(2)	1460.8(10)	29.1(7)	C13	2016.2(19)	5775(5)	2307(2)	84(2)
C01O	4561.7(9)	5224(3)	5454.9(11)	34.2(8)	C14	2797(6)	3842(11)	3190(7)	41(3)
C01P	2357.9(10)	6411(3)	241.8(11)	34.5(8)	C15	3893.4(18)	8540(5)	2361(2)	46(2)
C01Q	4277.5(10)	4009(3)	4982.5(14)	40.5(10)	C1	4509.3(19)	8753(6)	2649.7(19)	46(2)
C01R	2722.0(11)	6618(3)	1882.9(12)	36.5(9)	C2	4298(3)	7396(5)	2274(2)	51(2)
C01S	4582.6(10)	7333(3)	5917.6(11)	36.7(9)	F4AA	2635(5)	2895(13)	1441(5)	96(7)
C01T	4299.7(10)	3879(3)	4267.3(13)	37.6(9)	F3AB	3764.1(13)	7644(6)	540.0(12)	182(4)
C01U	4641.1(10)	7957(3)	6234.2(11)	38.8(9)	F14A	2337.8(8)	5333(2)	-265.5(10)	74.7(13)
C01V	2857.8(11)	4794(3)	1336.8(12)	38.4(9)	F2AB	3369(13)	10275(14)	1380(30)	112(17)
C01W	4503.4(10)	4608(2)	4318.2(11)	31.6(8)	F00O	3987.3(19)	6767(5)	1070(5)	57(3)
C01X	2598.2(10)	6292(3)	633.3(11)	32.6(8)	F11A	1732(4)	5947(13)	1882(3)	106(6)
C01Y	2794.0(12)	7157(3)	2597.7(12)	41.6(10)	F7A	2013(4)	5066(6)	2335(8)	113(8)
C01Z	4227.3(10)	8736(3)	4921.3(11)	33.8(8)	C14A	2730(7)	4220(20)	3174(7)	116(11)
C020	2901.6(10)	7090(3)	2234.8(11)	35.5(8)	C1A	4120(4)	9037(8)	2587(4)	61(4)
C021	2434.9(10)	6132(3)	-156.6(12)	41.9(10)	C2A	4602(3)	8094(9)	2566(3)	42(3)
C022	3488.4(10)	5448(3)	3137.7(12)	39.1(9)	C15A	4025(4)	7693(10)	2179(3)	62(5)
C023	4639.8(10)	6426(3)	5942.2(11)	36.6(9)	F12A	2483(3)	3350(7)	1044(10)	126(10)
C024	3314.7(10)	4826(3)	3305.2(12)	41.3(10)	F8A	2997(3)	2562(8)	1137(7)	89(6)
C025	4568.4(10)	8801(3)	6128.2(11)	38.7(9)	F4AB	2803(6)	2626(10)	1512(6)	98(6)
C026	3336.3(12)	3890(3)	1660.3(13)	43.5(10)	F3AA	1610.2(9)	7624(4)	933.7(13)	133(2)
C028	3377.3(10)	4805(3)	3747.4(12)	36.8(9)	C02B	3852.1(11)	7552(3)	942.7(13)	40.6(9)
C029	3155.4(12)	9678(3)	1445.7(13)	42.8(10)	C02C	3005.9(11)	3986(3)	1407.0(13)	40.2(9)
C02A	4925.7(11)	9079(2)	4575.1(11)	35.7(8)	C02D	3513.4(11)	4615(3)	1843.6(12)	40.8(9)

Table 5.43. Anisotropic Displacement Parameters ($Å^2×10^3$) for **5.11–BAr$^F_{24}$**. The anisotropic displacement factor exponent takes the form: $-2\pi^2[h^2a^{*2}U_{11}+2hka^*b^*U_{12}+\ldots]$.

Atom	U_{11}	U_{22}	U_{33}	U_{23}	U_{13}	U_{12}	Atom	U_{11}	U_{22}	U_{33}	U_{23}	U_{13}	U_{12}
Cu01	29.6(3)	38.2(3)	17.8(2)	9.5(2)	9.43(19)	13.2(2)	C025	29.6(19)	61(3)	24.2(17)	-3.9(17)	5.3(14)	1.8(19)
Cu02	39.5(3)	40.0(3)	33.0(3)	6.3(2)	15.2(2)	16.2(3)	C026	48(2)	42(2)	41(2)	8.1(18)	13.6(19)	-7(2)
P003	34.2(5)	46.8(6)	34.4(5)	18.1(4)	20.2(4)	13.8(4)	C028	29.4(19)	49(2)	33.2(19)	15.8(17)	10.4(15)	-2.2(17)
P004	44.9(6)	35.1(5)	30.1(5)	-7.4(4)	-4.9(4)	19.8(5)	C029	51(3)	42(2)	38(2)	4.6(18)	18.5(19)	2(2)
F006	65.3(18)	53.5(16)	45.4(14)	-10.3(12)	8.9(13)	12.9(14)	C02A	48(2)	30.7(19)	26.5(17)	-2.9(15)	7.5(16)	8.8(17)
F008	52.2(16)	109(2)	32.3(13)	-25.2(14)	6.4(12)	-2.7(17)	C02B	42(2)	48(2)	37(2)	-6.0(18)	19.6(18)	-9(2)
N00A	23.2(14)	35.8(16)	22.9(13)	13.4(12)	8.5(11)	10.4(12)	C02C	45(2)	41(2)	37(2)	-0.7(17)	14.7(18)	-12.6(19)
F00B	150(3)	61.7(18)	21.4(11)	6.2(12)	15.9(16)	24(2)	C02D	45(2)	49(2)	28.8(18)	9.3(17)	11.4(17)	-9(2)
F00C	54.9(18)	68(2)	67.1(19)	0.9(15)	-14.5(14)	-8.9(15)	C02E	41(2)	50(2)	31.2(18)	17.7(17)	18.3(17)	21.6(19)
O00D	47.8(18)	38.6(16)	52.9(18)	-2.1(14)	-9.3(14)	-6.2(14)	C02F	29.4(19)	40(2)	42(2)	-19.0(17)	5.7(16)	-4.4(17)
O00E	74(2)	42.3(16)	25.9(13)	-10.2(12)	-6.5(14)	10.5(16)	C02G	54(3)	52(3)	38(2)	-7.3(19)	25(2)	-11(2)
F00F	46.3(17)	87(2)	83(2)	-6.2(19)	4.1(16)	3.3(17)	C02H	65(3)	53(3)	21.3(17)	-0.5(17)	10.6(18)	14(2)
N00H	34.8(17)	44.2(18)	22.2(13)	9.5(13)	12.4(12)	18.2(14)	C02I	26.1(19)	27.2(18)	63(3)	10.0(18)	10.0(18)	1.9(16)
F00J	75(2)	123(3)	65(2)	58(2)	-7.7(17)	-11(2)	C02J	44(2)	64(3)	19.0(16)	10.6(17)	13.3(15)	21(2)
F00M	60(2)	92(2)	160(4)	-56(3)	69(2)	-33.0(19)	C02K	40(2)	49(3)	55(3)	-31(2)	7(2)	1(2)
F00N	97(19)	83(12)	140(30)	-66(18)	100(20)	-51(13)	C02O	45(2)	62(3)	30.4(19)	18.4(19)	18.6(17)	31(2)
C00O	30.9(18)	34.3(18)	17.7(14)	3.7(13)	6.7(13)	9.6(15)	C02P	48(3)	84(4)	33(2)	13(2)	2.6(19)	-34(3)
F00P	66(2)	63(2)	178(4)	-2(2)	35(3)	26.0(18)	B02Q	37(2)	43(2)	20.8(17)	-4.2(16)	11.2(16)	-10.0(19)
C00Q	26.7(18)	40(2)	26.3(16)	14.0(15)	8.1(14)	8.3(16)	C02S	47(2)	57(3)	26.5(18)	-3.3(18)	0.5(17)	-2(2)
C00R	23.7(16)	36.0(18)	15.7(13)	8.3(13)	7.2(12)	7.9(14)	C02T	43(3)	48(3)	55(3)	-9(2)	1(2)	16(2)
C00S	26.4(17)	34.2(18)	19.4(14)	6.0(13)	6.5(13)	10.5(15)	C02U	58(3)	46(3)	45(2)	16(2)	0(2)	-6(2)
C00T	21.5(16)	40.0(19)	23.3(15)	10.7(14)	5.8(13)	6.1(15)	C02V	31(2)	63(3)	69(3)	18(3)	10(2)	12(2)
C00V	28.3(18)	41(2)	15.7(14)	8.3(14)	1.5(13)	-3.8(16)	C02W	54(3)	51(3)	54(3)	-4(2)	24(2)	-19(2)
C00W	32.7(19)	49(2)	20.6(15)	15.5(15)	11.5(14)	18.9(17)	C02X	65(3)	59(3)	49(3)	-4(2)	36(2)	-14(2)
C00X	30.3(18)	42(2)	13.3(13)	-0.8(13)	2.9(13)	-5.5(16)	C02Y	78(3)	57(3)	39(2)	2(2)	38(2)	-3(3)
C00Y	27.6(17)	37.3(19)	18.9(14)	7.5(14)	6.9(13)	2.9(15)	C02Z	64(3)	67(3)	30.6(19)	24(2)	22(2)	39(3)
C010	27.5(18)	43(2)	25.8(16)	15.3(15)	6.6(14)	0.2(16)	C030	35(2)	58(3)	65(3)	24(2)	28(2)	12(2)
C011	24.0(17)	41(2)	23.5(16)	9.6(14)	5.5(13)	-0.7(16)	C031	45(3)	88(4)	32(2)	5(2)	6.6(18)	-26(3)
C012	26.3(17)	32.6(18)	22.5(15)	5.8(13)	6.0(13)	1.3(15)	C032	47(2)	67(3)	36(2)	18(2)	22.2(19)	16(2)
C013	35.2(19)	38(2)	16.6(14)	-0.4(14)	3.4(13)	-1.6(16)	C033	80(4)	51(3)	24.0(18)	-6.7(18)	-4(2)	14(3)
C014	35.0(19)	36.3(19)	20.3(15)	-4.3(14)	7.1(14)	-5.1(16)	C034	84(4)	52(3)	37(2)	-4(2)	-10(2)	-15(3)
C015	25.0(17)	37.5(19)	32.7(18)	14.5(15)	11.5(14)	12.4(15)	C035	63(3)	47(3)	36(2)	7.2(19)	0(2)	12(2)
C016	34.5(18)	28.9(17)	17.7(14)	0.5(13)	8.4(13)	7.7(15)	C036	62(3)	69(3)	45(2)	-15(2)	16(2)	8(3)
C017	33.3(19)	40(2)	21.9(15)	3.3(14)	6.2(14)	-7.0(17)	C037	77(3)	60(3)	42(2)	22(2)	27(2)	33(3)
C018	37(2)	44(2)	19.7(15)	1.0(14)	12.6(14)	-10.3(17)	C038	87(4)	65(3)	56(3)	29(3)	35(3)	32(3)
C019	40(2)	36.2(19)	18.5(15)	1.5(14)	3.8(14)	14.6(17)	C039	74(4)	76(4)	46(3)	28(3)	27(3)	8(3)
C01A	29.1(18)	42(2)	23.0(15)	-2.6(15)	7.8(14)	-6.0(16)	C03B	70(3)	84(4)	39(2)	11(2)	31(2)	18(3)
C01B	29.5(18)	48(2)	22.7(16)	6.2(15)	10.7(14)	14.6(17)	C03C	63(3)	81(4)	49(3)	34(3)	3(2)	20(3)
C01C	31.5(19)	39(2)	25.7(16)	-6.1(15)	8.0(14)	-9.4(16)	C03D	99(4)	73(4)	49(3)	33(3)	42(3)	39(3)
C01D	22.3(16)	28.7(17)	27.3(16)	12.6(14)	2.2(13)	5.7(14)	C03E	78(4)	64(3)	52(3)	-11(3)	7(3)	26(3)
C01E	45(2)	36(2)	23.9(16)	-8.2(15)	1.4(15)	11.7(18)	C03F	46(3)	100(5)	83(4)	18(3)	41(3)	22(3)
C01F	34(2)	41(2)	30.4(18)	-11.2(16)	-0.3(15)	-4.5(17)	C03G	99(5)	85(4)	29(2)	-13(2)	-12(3)	28(4)
C01G	38(2)	34.7(19)	22.5(15)	1.5(14)	7.0(14)	7.4(16)	C03H	117(6)	50(3)	68(4)	12(3)	-9(4)	-34(4)
C01H	28.7(18)	48(2)	20.2(15)	5.6(15)	8.6(13)	10.4(17)	C03J	65(4)	86(4)	67(3)	-11(3)	31(3)	18(3)
C01I	35(2)	44(2)	19.9(15)	7.0(15)	3.4(14)	-9.4(17)	C03K	61(3)	94(4)	48(3)	10(3)	2(2)	34(3)
C01J	30.8(19)	44(2)	29.0(17)	-14.5(16)	7.1(15)	-9.5(17)	C03M	79(4)	87(4)	66(4)	-11(3)	7(3)	-30(4)
C01K	28.8(18)	48(2)	28.1(17)	4.1(16)	9.3(14)	7.3(17)	F1	40.6(13)	67.3(16)	27.7(10)	-6.5(10)	13.4(10)	-8.5(12)
C01L	43(2)	45(2)	25.8(17)	1.1(16)	11.0(16)	-13.7(19)	F2	59.6(17)	116(3)	23.9(11)	0.8(14)	0.7(11)	19.0(18)
C01M	28.5(18)	39(2)	25.6(16)	15.3(15)	9.7(14)	7.9(16)	F0AA	31.5(16)	76(2)	129(3)	-50(2)	17.5(17)	-3.8(14)
C01N	27.1(17)	43(2)	15.0(13)	1.3(13)	2.9(12)	-2.5(16)	F1AA	79(2)	80(2)	97(2)	2.6(19)	62(2)	-5.2(18)
C01O	29.0(18)	48(2)	29.3(17)	13.1(16)	13.9(15)	17.9(17)	F2AA	122(7)	34(3)	58(5)	10(2)	50(4)	1(3)
C01P	33(2)	44(2)	25.2(17)	-9.8(15)	5.6(15)	-5.9(17)	F4	199(5)	60(2)	44.2(19)	-20.1(15)	2(2)	37(3)
C01Q	27.4(19)	39(2)	61(3)	28(2)	21.8(18)	14.0(17)	F7	58(5)	68(5)	67(6)	32(4)	27(4)	3(4)
C01R	44(2)	41(2)	27.1(17)	0.0(15)	15.3(16)	-3.7(18)	F8	187(18)	159(14)	151(12)	-117(11)	143(13)	-132(13)
C01S	32.8(19)	58(2)	21.2(16)	9.6(16)	10.1(14)	15.3(19)	F10	74(3)	68(3)	266(7)	45(3)	90(4)	31(2)
C01T	25.0(18)	33(2)	47(2)	8.7(17)	-0.8(16)	2.7(16)	F11	45(4)	83(8)	46(4)	6(4)	14(3)	-21(5)
C01U	33(2)	59(3)	22.9(16)	4.9(17)	5.5(15)	13.8(19)	F12	93(9)	59(4)	53(4)	-16(3)	-3(4)	-37(5)
C01V	38(2)	51(2)	30.2(18)	-0.7(17)	15.2(16)	-10.5(19)	C13	105(5)	88(5)	88(5)	-24(4)	76(5)	-35(4)
C01W	34.3(19)	32.3(18)	26.4(16)	9.2(14)	5.5(14)	2.8(16)	C14	37(6)	56(7)	30(6)	7(5)	7(5)	-19(6)
C01X	29.3(18)	41(2)	27.3(17)	-7.4(15)	8.2(14)	-6.8(16)	C15	41(4)	65(5)	27(3)	27(3)	4(3)	6(4)
C01Y	60(3)	45(2)	22.4(17)	3.5(16)	15.7(17)	7(2)	C1	48(4)	65(6)	19(3)	18(3)	0(3)	-27(4)
C01Z	42(2)	39(2)	22.1(16)	2.3(15)	12.2(15)	16.3(17)	C2	77(7)	47(4)	35(4)	9(3)	26(4)	-9(4)
C020	41(2)	44(2)	22.8(16)	3.2(15)	12.0(15)	0.0(18)	F4AA	130(13)	102(13)	82(10)	-42(9)	73(10)	-87(10)
C021	34(2)	60(3)	30.9(18)	-11.7(18)	7.9(16)	-6(2)	F3AB	113(4)	399(11)	53(2)	52(4)	54(2)	122(5)
C022	29.7(19)	60(3)	24.5(17)	14.2(17)	3.6(15)	-9.7(19)	F14A	88(2)	81(2)	73(2)	-50.6(17)	52.6(18)	-44.8(18)
C023	39(2)	53(2)	20.8(16)	10.6(16)	12.4(15)	18.2(19)	F2AB	100(20)	41(7)	230(50)	-25(16)	120(30)	-9(10)

C024	31(2)	60(3)	31.0(19)	17.1(18)	5.7(15)	-6.4(19)	F00O	55(3)	45(3)	84(7)	7(3)	42(4)	9(2)
C15A	70(10)	92(11)	19(5)	15(6)	5(5)	-38(9)	F11A	86(7)	154(14)	93(6)	-2(7)	50(6)	-52(9)
F12A	66(7)	51(5)	210(30)	5(9)	-38(10)	-25(5)	F7A	114(11)	53(5)	210(30)	-4(8)	107(15)	-19(6)
F8A	50(5)	38(5)	172(15)	-37(6)	21(7)	1(4)	C14A	84(15)	220(30)	39(7)	14(15)	14(9)	-93(18)
F4AB	158(17)	54(6)	81(6)	9(5)	33(10)	-49(8)	C1A	99(12)	50(7)	37(6)	20(5)	24(7)	1(8)
F3AA	62(2)	250(6)	80(3)	-75(3)	8.3(19)	58(3)	C2A	50(7)	57(8)	20(4)	7(5)	10(4)	-18(6)

Table 5.44. Bond Lengths for **5.11–BAr$^{F}_{24}$**.

Atom	Atom	Length/Å	Atom	Atom	Length/Å	Atom	Atom	Length/Å		Atom	Atom	Length/Å
Cu01	Cu02	2.6974(7)	C01I	C2A	1.543(12)	C00Y	C012	1.391(5)		C02O	C02Z	1.538(5)
Cu01	N00A	1.886(3)	C01I	C15A	1.472(12)	C00Y	C01I	1.533(4)		C02P	C031	1.540(6)
Cu01	N00H	1.878(3)	C01J	C02F	1.391(5)	C010	C011	1.451(5)		C02P	C03H	1.531(9)
Cu02	P003	2.1791(12)	C01K	C025	1.408(5)	C010	C022	1.375(6)		C02P	C14	1.51(2)
Cu02	P004	2.1582(13)	C01L	C02D	1.384(6)	C013	C017	1.396(5)		C02P	C14A	1.66(3)
P003	C01M	1.835(4)	C01O	C02E	1.405(5)	C013	C01N	1.388(5)		C02S	C036	1.541(7)
P003	C030	1.840(5)	C01P	C01X	1.394(5)	C013	C029	1.484(6)		C02S	C03G	1.527(6)
P003	C032	1.866(4)	C01P	C021	1.499(5)	C014	C01A	1.388(5)		C02S	C03M	1.504(8)
P004	C01Z	1.859(4)	C01Q	C02I	1.367(6)	C015	C01D	1.395(5)		C02T	C03E	1.502(7)
P004	C02T	1.924(5)	C01R	C020	1.392(5)	C015	C01O	1.478(5)		C02T	C03J	1.507(8)
P004	C035	1.812(4)	C01R	C02G	1.392(6)	C015	C01Q	1.413(6)		C02V	C030	1.527(6)
F006	C02H	1.338(5)	C01R	B02Q	1.649(5)	C016	C019	1.387(5)		C02W	F8	1.223(14)
F008	C02H	1.322(6)	C01S	C01U	1.395(6)	C017	C01A	1.375(6)		C02W	F12	1.343(11)
N00A	C00R	1.405(4)	C01S	C023	1.432(6)	C018	C01L	1.409(6)		C02W	F4AA	1.261(12)
N00A	C00T	1.390(5)	C01T	C01W	1.394(5)	C018	C01V	1.397(6)		C02W	F12A	1.328(13)
F00B	C02H	1.347(5)	C01T	C02I	1.385(6)	C018	B02Q	1.632(6)		C02W	F8A	1.333(11)
F00C	C02U	1.329(6)	C01U	C025	1.372(6)	C019	C01E	1.387(6)		C02W	F4AB	1.325(16)
O00D	C01T	1.371(5)	C01V	C02C	1.390(6)	C01A	C02B	1.505(5)		C02X	C02Y	1.384(7)
O00D	C034	1.412(6)	C01Y	C020	1.393(5)	C01B	C01H	1.413(5)		C02X	C13	1.498(7)
O00E	C01E	1.365(4)	C01Y	C02H	1.496(6)	C01B	C01S	1.421(5)		C02Z	C037	1.557(7)
O00E	C033	1.440(5)	C01Y	C02Y	1.379(7)	C01C	C01J	1.388(5)		C02Z	C03C	1.508(8)
F00F	C02U	1.314(6)	C021	F1	1.337(5)	C01C	C01X	1.404(5)		C02Z	C03D	1.515(6)
N00H	C00W	1.408(4)	C021	F2	1.347(5)	C01C	B02Q	1.643(6)		C030	C03F	1.527(7)
N00H	C01B	1.393(5)	C021	F14A	1.327(5)	C01D	C01W	1.398(5)		C032	C039	1.529(7)
F00J	C02U	1.349(5)	C022	C024	1.409(5)	C01E	C02A	1.398(5)		C032	C03B	1.523(7)
F00M	C02B	1.297(5)	C023	C02J	1.402(5)	C01F	C01P	1.384(6)		C035	C038	1.491(7)
F00N	C02B	1.217(17)	C024	C028	1.404(5)	C01F	C02F	1.373(5)		C035	C03K	1.545(7)
C00O	C00S	1.479(5)	C024	C02P	1.538(6)	C01G	C02A	1.379(5)		F1AA	C13	1.314(6)
C00O	C016	1.396(5)	C025	C02S	1.540(6)	C01H	C01K	1.395(5)		F7	C13	1.544(13)
C00O	C01G	1.399(5)	C026	C02C	1.386(6)	C01H	C01Z	1.512(5)		F8	F12	1.57(4)
F00P	C029	1.311(6)	C026	C02D	1.387(6)	C01I	C15	1.525(8)		F11	C13	1.264(10)
C00Q	C00T	1.425(5)	C029	F2AA	1.321(9)	C01I	C1	1.505(8)		C13	F11A	1.568(17)
C00Q	C01M	1.501(4)	C029	F4	1.284(5)	C01I	C2	1.552(9)		C13	F7A	1.110(11)
C00Q	C028	1.387(6)	C029	F2AB	1.35(2)	C01I	C1A	1.536(14)		F8A	F4AB	1.66(4)
C00R	C00S	1.408(5)	C02B	F3AB	1.278(5)	C00V	C011	1.377(4)		C02F	C02K	1.486(6)
C00R	C011	1.422(5)	C02B	F00O	1.360(7)	C00W	C01O	1.409(6)		C02G	C02X	1.397(6)
C00S	C012	1.401(4)	C02C	C02W	1.499(6)	C00W	C023	1.418(5)		C02J	C02O	1.388(7)
C00T	C010	1.416(5)	C02D	C02U	1.498(6)	C00X	C014	1.399(5)		C02K	F0AA	1.296(5)
C00V	C00Y	1.408(5)	C02E	C02O	1.396(6)	C00X	C01N	1.398(5)		C02K	F10	1.333(7)
C00X	B02Q	1.643(6)	C02K	F3AA	1.301(6)							

Table 5.45. Bond Angles for **5.11–BAr$^{F}_{24}$**.

Atom	Atom	Atom	Angle/°	Atom	Atom	Atom	Angle/°	Atom	Atom	Atom	Angle/°		Atom	Atom	Atom	Angle/°
N00A	Cu01	Cu02	90.09(9)	F14A	C021	F1	106.0(4)	C019	C016	C00O	121.9(3)		C14	C02P	C024	114.9(9)
N00H	Cu01	Cu02	91.63(9)	F14A	C021	F2	107.1(3)	C01A	C017	C013	118.3(3)		C14	C02P	C031	111.9(9)
N00H	Cu01	N00A	177.92(13)	C010	C022	C024	119.2(3)	C01L	C018	B02Q	121.6(3)		C14	C02P	C03H	100.6(7)
P003	Cu02	Cu01	88.78(3)	C00W	C023	C01S	106.7(3)	C01V	C018	C01L	115.2(4)		C00X	B02Q	C01C	102.9(3)

P004	Cu02	Cu01	99.09(4)	C02J	C023	C00W	121.7(4)	C01V	C018	B02Q	123.1(3)		C00X	B02Q	C01R	112.7(3)
P004	Cu02	P003	167.23(5)	C02J	C023	C01S	131.6(4)	C016	C019	C01E	118.9(3)		C018	B02Q	C00X	112.4(3)
C01M	P003	Cu02	112.30(12)	C022	C024	C02P	122.3(4)	C014	C01A	C02B	120.0(4)		C018	B02Q	C01C	111.2(3)
C01M	P003	C030	108.2(2)	C028	C024	C022	117.3(4)	C017	C01A	C014	121.1(3)		C018	B02Q	C01R	105.2(3)
C01M	P003	C032	100.24(18)	C028	C024	C02P	120.3(3)	C017	C01A	C02B	118.9(3)		C01C	B02Q	C01R	112.6(3)
C030	P003	Cu02	114.73(16)	C01K	C025	C02S	118.8(4)	N00H	C01B	C01H	131.6(3)		C025	C02S	C036	109.0(4)
C030	P003	C032	110.5(2)	C01U	C025	C01K	117.5(4)	N00H	C01B	C01S	110.5(3)		C03G	C02S	C025	111.6(4)
C032	P003	Cu02	109.99(17)	C01U	C025	C02S	123.7(3)	C01H	C01B	C01S	117.9(4)		C03G	C02S	C036	107.4(4)
C01Z	P004	Cu02	106.97(13)	C02C	C026	C02D	118.5(4)	C01J	C01C	C01X	115.9(3)		C03M	C02S	C025	110.9(4)
C01Z	P004	C02T	105.52(18)	C00Q	C028	C024	125.1(3)	C01J	C01C	B02Q	124.8(3)		C03M	C02S	C036	108.2(5)
C02T	P004	Cu02	109.75(17)	F00P	C029	C013	112.4(4)	C01X	C01C	B02Q	118.9(3)		C03M	C02S	C03G	109.7(5)
C035	P004	Cu02	117.24(17)	F00P	C029	F2AA	100.1(7)	C015	C01D	C01W	121.9(3)		C03E	C02T	P004	110.1(4)
C035	P004	C01Z	107.7(2)	F00P	C029	F2AB	122(2)	O00E	C01E	C019	124.5(3)		C03E	C02T	C03J	114.6(4)
C035	P004	C02T	109.0(2)	F2AA	C029	C013	111.9(5)	O00E	C01E	C02A	115.1(3)		C03J	C02T	P004	112.0(3)
C00R	N00A	Cu01	126.9(2)	F4	C029	F00P	106.0(4)	C019	C01E	C02A	120.4(3)		F00C	C02U	F00J	105.1(4)
C00T	N00A	Cu01	126.6(2)	F4	C029	C013	113.0(4)	C02F	C01F	C01P	118.2(4)		F00C	C02U	C02D	112.9(4)
C00T	N00A	C00R	106.5(3)	F4	C029	F2AA	112.7(7)	C02A	C01G	C00O	121.1(3)		F00F	C02U	F00C	107.3(4)
C01T	O00D	C034	117.1(3)	F2AB	C029	C013	116.3(10)	C01B	C01H	C01Z	125.6(3)		F00F	C02U	F00J	107.3(4)
C01E	O00E	C033	117.0(4)	C01G	C02A	C01E	119.7(4)	C01K	C01H	C01B	117.5(3)		F00F	C02U	C02D	113.1(4)
C00W	N00H	Cu01	125.5(3)	F00M	C02B	C01A	113.4(3)	C01K	C01H	C01Z	116.9(3)		F00J	C02U	C02D	110.7(4)
C01B	N00H	Cu01	128.1(2)	F00M	C02B	F00O	100.1(6)	C00Y	C01I	C2	108.7(4)		F8	C02W	C02C	113.1(7)
C01B	N00H	C00W	106.3(3)	F00N	C02B	F00M	121.8(17)	C00Y	C01I	C1A	106.9(5)		F8	C02W	F12	75.5(19)
C016	C00O	C00S	121.8(3)	F00N	C02B	C01A	119.2(7)	C00Y	C01I	C2A	109.7(4)		F8	C02W	F4AA	128.1(15)
C016	C00O	C01G	117.8(3)	F3AB	C02B	F00M	106.6(5)	C15	C01I	C00Y	108.1(4)		F12	C02W	C02C	111.9(5)
C01G	C00O	C00S	120.4(3)	F3AB	C02B	C01A	112.0(4)	C15	C01I	C2	109.6(5)		F4AA	C02W	C02C	113.5(7)
C00T	C00Q	C01M	124.4(3)	F3AB	C02B	F00O	112.9(9)	C1	C01I	C00Y	113.3(3)		F4AA	C02W	F12	106.5(9)
C028	C00Q	C00T	116.6(3)	F00O	C02B	C01A	111.2(5)	C1	C01I	C15	108.8(5)		F12A	C02W	C02C	113.3(7)
C028	C00Q	C01M	118.9(3)	C01V	C02C	C02W	120.8(4)	C1	C01I	C2	108.3(5)		F12A	C02W	F8A	128.2(13)
N00A	C00R	C00S	130.5(3)	C026	C02C	C01V	120.5(4)	C1A	C01I	C2A	108.0(8)		F8A	C02W	C02C	114.9(7)
N00A	C00R	C011	109.8(3)	C026	C02C	C02W	118.6(4)	C15A	C01I	C00Y	114.6(5)		F4AB	C02W	C02C	111.8(9)
C00S	C00R	C011	119.7(3)	C01L	C02D	C026	120.4(4)	C15A	C01I	C1A	109.7(9)		F4AB	C02W	F12A	101.6(10)
C00R	C00S	C00O	125.9(3)	C01L	C02D	C02U	121.1(4)	C15A	C01I	C2A	107.8(8)		F4AB	C02W	F8A	77.1(17)
C012	C00S	C00O	117.5(3)	C026	C02D	C02U	118.4(4)	C01C	C01J	C02F	121.9(3)		C02G	C02X	C13	119.8(5)
C012	C00S	C00R	116.6(3)	C02O	C02E	C01O	124.7(4)	C01H	C01K	C025	124.5(4)		C02Y	C02X	C02G	120.2(4)
N00A	C00T	C00Q	130.0(3)	C01F	C02F	C01J	121.4(4)	C02D	C01L	C018	122.7(4)		C02Y	C02X	C13	119.9(4)
N00A	C00T	C010	111.4(3)	C01F	C02F	C02K	118.9(4)	C00Q	C01M	P003	118.4(3)		C01Y	C02Y	C02X	118.4(4)
C010	C00T	C00Q	118.6(3)	C01J	C02F	C02K	119.7(4)	C013	C01N	C00X	122.5(3)		C02O	C02Z	C037	111.8(4)
C011	C00V	C00Y	119.8(3)	C01R	C02G	C02X	122.4(4)	C00W	C01O	C015	126.8(3)		C03C	C02Z	C02O	110.0(4)
N00H	C00W	C01O	131.6(3)	F006	C02H	F00B	104.7(3)	C02E	C01O	C00W	117.7(4)		C03C	C02Z	C037	107.3(4)
N00H	C00W	C023	110.0(3)	F006	C02H	C01Y	112.5(4)	C02E	C01O	C015	115.4(4)		C03C	C02Z	C03D	112.0(4)
C01O	C00W	C023	118.3(3)	F008	C02H	F006	106.5(4)	C01F	C01P	C01X	120.5(3)		C03D	C02Z	C02O	109.6(3)
C014	C00X	B02Q	122.4(3)	F008	C02H	F00B	106.6(4)	C01F	C01P	C021	119.7(3)		C03D	C02Z	C037	106.1(4)
C01N	C00X	C014	115.8(3)	F008	C02H	C01Y	113.6(3)	C01X	C01P	C021	119.8(4)		C02V	C030	P003	109.6(3)
C01N	C00X	B02Q	121.3(3)	F00B	C02H	C01Y	112.3(4)	C02I	C01Q	C015	121.6(3)		C02V	C030	C03F	109.5(4)
C00V	C00Y	C01I	120.6(3)	C01Q	C02I	C01T	120.7(4)	C020	C01R	B02Q	123.5(3)		C03F	C030	P003	110.2(4)
C012	C00Y	C00V	117.8(3)	C02O	C02J	C023	120.8(4)	C02G	C01R	C020	116.1(3)		C039	C032	P003	114.1(4)
C012	C00Y	C01I	121.6(3)	F0AA	C02K	C02F	114.9(3)	C02G	C01R	B02Q	120.2(3)		C03B	C032	P003	112.6(3)
C00T	C010	C011	105.4(3)	F0AA	C02K	F10	103.0(5)	C01B	C01S	C023	106.5(3)		C03B	C032	C039	113.0(4)
C022	C010	C00T	123.1(3)	F0AA	C02K	F3AA	106.8(5)	C01U	C01S	C01B	122.5(4)		C038	C035	P004	108.9(3)
C022	C010	C011	131.4(3)	F10	C02K	C02F	111.6(4)	C01U	C01S	C023	131.0(3)		C038	C035	C03K	110.4(4)
C00R	C011	C010	106.8(3)	F3AA	C02K	C02F	115.3(4)	O00D	C01T	C01W	124.6(4)		C03K	C035	P004	112.6(4)
C00V	C011	C00R	121.5(3)	F3AA	C02K	F10	104.1(5)	O00D	C01T	C02I	115.7(4)		C02W	F8	F12	55.7(13)
C00V	C011	C010	131.6(3)	C02E	C02O	C02Z	122.4(4)	C02I	C01T	C01W	119.7(4)		C02W	F12	F8	48.8(8)
C00Y	C012	C00S	124.4(3)	C02J	C02O	C02E	116.8(4)	C025	C01U	C01S	120.0(3)		C02X	C13	F7	106.6(7)
C017	C013	C029	119.6(3)	C02J	C02O	C02Z	120.8(4)	C02C	C01V	C018	122.7(4)		C02X	C13	F11A	107.1(6)
C01N	C013	C017	120.2(4)	C024	C02P	C031	111.3(4)	C01T	C01W	C01D	119.2(3)		F1AA	C13	C02X	113.2(5)
C01N	C013	C029	120.3(3)	C024	C02P	C14A	103.5(11)	C01P	C01X	C01C	122.0(4)		F1AA	C13	F7	100.8(6)
C01A	C014	C00X	122.1(4)	C031	C02P	C14A	100.9(10)	C020	C01Y	C02H	120.6(4)		F1AA	C13	F11A	91.0(7)
C01D	C015	C01O	122.1(3)	C03H	C02P	C024	108.0(4)	C02Y	C01Y	C020	120.9(4)		F11	C13	C02X	115.8(5)
C01D	C015	C01Q	116.9(4)	C03H	C02P	C031	109.4(5)	C02Y	C01Y	C02H	118.4(4)		F11	C13	F1AA	119.2(8)
C01Q	C015	C01O	121.0(3)	C03H	C02P	C14A	123.4(12)	C01H	C01Z	P004	112.7(3)		F11	C13	F7	97.6(8)
F1	C021	F2	105.2(3)	F7A	C13	F11A	102.7(11)	C01R	C020	C01Y	122.0(4)		F7A	C13	C02X	122.7(9)
F2	C021	C01P	112.0(4)	C02W	F8A	F4AB	51.2(10)	F1	C021	C01P	113.2(3)		F7A	C13	F1AA	114.0(7)
F14A	C021	C01P	112.7(4)	C02W	F4AB	F8A	51.7(10)									

$Cu^{II}(P_{iPr}N_{Mes})(carb_{tBu})$ (5.15)

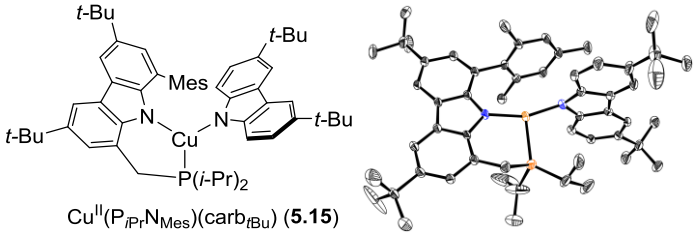

$Cu^{II}(P_{iPr}N_{Mes})(carb_{tBu})$ (**5.15**)

Only crystal data are reported below.

Table 5.46. Crystal data for **5.15**.

Identification code	**5.15**
Empirical formula	$C_{56}H_{73}CuN_2P$
Formula weight	868.67
Temperature/K	100.0
Crystal system	monoclinic
Space group	$P2_1/n$
a/Å	16.022(3)
b/Å	23.988(5)
c/Å	16.035(5)
α/°	90
β/°	100.874(15)
γ/°	90
Volume/Å^3	6052(3)
Z	4
ρ_{calc}g/cm^3	0.953
μ/mm^{-1}	0.977
F(000)	1868.0
Radiation	CuKα (λ = 1.54178)
2Θ range for data collection/°	6.714 to 109.504
Index ranges	$-13 \leq h \leq 14$, $-25 \leq k \leq 24$, $-13 \leq l \leq 16$
Reflections collected	12151
Independent reflections	6007 [R_{int} = 0.0822, R_{sigma} = 0.1349]

AuCu($P_{Ph}N_H$)$_2$

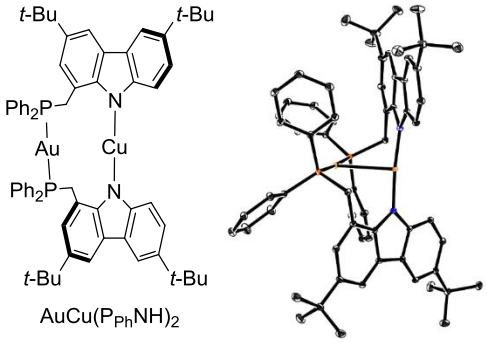

The structure contains severely disordered solvent molecules. Only crystal data are presented.

Table 5.47. Crystal data and structure refinement for **AuCu($P_{Ph}N_H$)$_2$**.

Identification code	**AuCu($P_{Ph}N_H$)$_2$**
Empirical formula	$C_{72.81}H_{77.11}AuCuN_{2.5}O_{1.02}P_2$
Formula weight	1326.11
Temperature/K	100.0
Crystal system	triclinic
Space group	P-1
a/Å	14.2527(4)
b/Å	15.4430(4)
c/Å	29.1548(8)
α/°	83.4845(12)
β/°	88.4338(11)
γ/°	84.6516(11)
Volume/Å^3	6347.0(3)
Z	4
ρ_{calc}g/cm^3	1.388
μ/mm^{-1}	2.739
F(000)	2711.0
Crystal size/mm^3	0.25 × 0.19 × 0.06
Radiation	MoKα (λ = 0.71073)
2Θ range for data collection/°	4.464 to 91.918
Index ranges	$-28 \leq h \leq 28$, $-31 \leq k \leq 31$, $-58 \leq l \leq 58$
Reflections collected	649786
Independent reflections	108838 [R_{int} = 0.0441, R_{sigma} = 0.0382]

5.5. Notes and References

[1] Kainz, Q. M.; Matier, C. M.; Bartoszewicz, A.; Zultanski, S. L.; Peters, J. C.; Fu, G. C. *Science* **2016**, *351*, 681−684.

[2] From Chen, C. *Fu copper subgroup meeting*, **2017**, *7*, 1–10.

[3] Note: increasing the amount of chiral monodentate phosphine was observed to lead to a decrease in enantioselectivity at early conversions (<90% ee).

[4] Multinuclear copper complexes are less likely to be of relevance in view of a) nonpolar reaction medium (toluene) and b) low catalyst loading (generally 1 mol% of copper precatalyst)

[5] Richens, D. T.; *Chem*. *Rev*. **2005**, *105*, 1961–2002.

[6] For the only reported example of an $S = 1/2$ mononuclear copper complex supported by bis(phosphine) ligands, see Mankad, N. P.; Antholine, W. E.; Szilagyi, R. K.; Peters, J. C. *J*. *Am*. *Chem*. *Soc*. **2009**, *131*, 3878–3880.

[7] Cordero, B.; Gomez, V.; Platero-Prats, A. E.; Reves, M.; Echeverria, J.; Cremades, E.; Barragan, F.; Alvarez, S. *Dalton Trans*. **2008**, *0*, 2832–2838.

[8] (a) Iwata, S.; Ostermeier, C.; Ludwig, B.; Michel, H. *Nature* **1995**, *376*, 660–669. (b) Gamelin, D. R.; Randall, D. W.; Hay, M. T.; Houser, R. P.; Mulder, T. C.; Canters, G. W.; de Vries, S.; Tolman, W. B.; Lu, Y.; Solomon, E. I. *J*. *Am*. *Chem*. *Soc*. **1998**, *120*, 5246–5263.

[9] The ^{31}P resonance of complex **5.5** remains essentially unchanged even when heated to 80 °C in C_6D_6.

[10] For a representative account, see McCallum, T.; Rohe, S.; Barriault, L. *Synlett* **2017**, *28*, 289–305.

[11] For examples of related bimetallic complexes of coinage metals, see Koshevoy, I. O.; Shakirova, J. R.; Melnikov, A. S.; Haukka, M.; Tunik, S. P.; Pakkanen, T. A. *Dalton Trans*. **2011**, *40*, 7927–7933.

[12] Various N-nucleophiles have been screened, including aliphatic amines, arylamines, nitrogen heterocycles, etc. However, (phosphino)carbazole ligands appear to be effective only in photoinduced, copper-catalyzed couplings of carboxamides and carbamate nucleophiles under copper photocatalysis.

[13] When **L3.1**, **L5.5**, or **L5.7** is used in place of **L5.1**, a similar yield of the C – C coupling is observed.

[14] Kaiser, E. M.; Hauser, C. R. *J. Org. Chem.* **1968**, *33*, 3402–3404.

[15] The DFT-predicted atomic spin densities (M06-L, def2-TZVP) of the cation **5.11** are as follows Cu: 11%, N: 15%, N: 13%.

[16] Harkins, S. B.; Peters, J. C. *J. Am. Chem. Soc.* **2004**, *126*, 2885–2893.

[17] (a) Mankad, N. P.; Rivard, E.; Harkins, S. B.; Peters, J. C. *J. Am. Chem. Soc.* **2005**, *127*, 16032–16033. (b) Harkins, S. B.; Mankad, N. P.; Miller, A. J. M.; Szilagyi, R. K.; Peters, J. C. *J. Am. Chem. Soc.* **2008**, *130*, 3478–3485.

[18] Gold(I)–phosphine bonds are generally stronger than copper(I)–phosphine bonds. For a representative computation study, see Schwerdtfeger, P.; Hermann, H. L.; Schmidbaur, H. *Inorg. Chem.* **2003**, *42*, 1334–1342.

[19] In the paramagnetic cation, $[(PPh_3)_2Ni(OEt_2)P(OEt)_3]^+$, hyperfine couplings of 550 MHz to ^{31}P have been proposed. See Saraev, V. V.; Kraikivskii, P. B.; Matveev, D. A.; Zelinskii, S. N.; Lammertsma, K. *Inorg. Chim. Acta* **2006**, *359*, 2314–2320.

[20] Alexakis, A.; Krause, N.; Woodward, S. *Copper-Catalyzed Asymmetric Synthesis*. Wiley-VCH, Weinheim, **2014**.

[21] From Yin, H. *Joint Fu and Peters copper subgroup meeting*, **2017**, *7*, 1–20.

[22] Stoll, S.; Schweiger, A. *J. Magn. Reson.* **2006**, *178*, 42–55.

[23] Neese, F. *Wiley Interdiscip. Rev. Comput. Mol. Sci.* **2012**, *2*, 73–78.

[24] Zhao, Y.; Truhlar, D.G. *J. Chem. Phys.* **2006**, *125*, 194101.

[25] Weigend, F.; Furche, F.; Ahlrichs, R. *J. Chem. Phys.* **2003**, *119*, 12753.

[26] Maeda, C.; Todaka, T.; Ueda, T.; Ema, T. *Chem. –Eur. J.* **2016**, *22*, 7508–7513.

[27] Albert, J.; Cadena, J. M.; Granell, J.; Muller, G.; Ordinas, J. I.; Panyella, D.; Puerta, C.; Sanudo, C.; Valerga, P. *Organometallics* **1999**, *18*, 3511–3518.

[28] Spectroscopic data for both diastereomers have been reported: Xin, B.-T.; de Bruin, G.; Huber, E. M.; Besse, A.; Florea, B. I.; Filippov, D. V.; van der Marel, G. A.; Kisselev, A. F.; van der Stelt, M.; Driessen, C.; Groll, M.; Overkleeft, H. S. *J. Med. Chem.* **2016**, *59*, 7177–7187.